THE SYNTHESIS AND ASSESSMENT OF THIOXANTHONE- AND XANTHONE- DERIVED COMPOUNDS AS HOSTS FOR APPLICATION IN HOST-GUEST CHEMISTRY

LIZÉ GREYLING

2019

THE SYNTHESIS AND ASSESSMENT OF THIOXANTHONE- AND XANTHONE- DERIVED COMPOUNDS AS HOSTS FOR APPLICATION IN HOST-GUEST CHEMISTRY

by

LIZÉ GREYLING

Submitted in fulfilment of the requirements for the degree of

PHILOSOPHIAE DOCTOR

in the Faculty of Science to be awarded at Nelson Mandela University

2019

SUPERVISOR: PROF B. BARTON

NELSON MANDELA UNIVERSITY

DECLARATION BY CANDIDATE

NAME: Lizé Greyling

STUDENT NUMBER: 213337665

QUALIFICATION: PhD (Chemistry)

TITLE OF PROJECT: The synthesis and assessment of thioxanthone- and xanthone- derived compounds as hosts for application in host-guest chemistry

DECLARATION:

By Rule G5.6.3, I hereby declare that the above-mentioned treatise/ dissertation/ thesis is my own work and that it has not previously been submitted for assessment to another university or for another qualification.

SIGNATURE: 

DATE: 01 August 2019

ACKNOWLEDGEMENTS

The author wishes to express her sincere thanks to:

- Prof B. Barton for her excellent mentorship, inspiration, insistence on excellence and encouragement throughout this project;
- Dr E.C. Hosten and Dr van Brecht for the running of SCXRD experiments;
- Mr E. Bashman for his assistance in the laboratory;
- My husband and family for moral support and encouragement;
- The National Research Foundation (NRF) for funding; opinions expressed, and conclusions arrived at, are those of the author and are not necessarily to be attributed to the NRF;
- The Nelson Mandela University for financial assistance by way of the postgraduate research scholarship (PGRS); and
- The Dormehl Cunningham Foundation for their scholarship, and hence financial assistance.

PUBLICATIONS AND CONFERENCES

- Chapter 3 (§3.1) of this thesis was presented as an oral at the annual SACI (South African Chemical Institute) conference in October 2017, held at Rhodes University, Grahamstown, South Africa. The presentation title was "*N*,*N'*-Bis(9-phenyl-9-thioxanthenyl)ethylenediamine: highly selective host behaviour in the presence of xylene and ethylbenzene guest mixtures''.

- Chapter 3 (§3.1) of this thesis has been published: Benita Barton, Lize de Jager and Eric C. Hosten, *N*,*N'*-Bis(9-phenyl-9-thioxanthenyl)ethylenediamine: highly selective host behaviour in the presence of xylene and ethylbenzene guest mixtures, *Cryst. Growth Des*., **2017**, 6660–6667.

- Chapter 3 (§3.2) and 4 of this thesis have been published: Benita Barton, Lize de Jager and Eric C. Hosten, Minor modifications afford improved host selectivities in xanthenyl-type host systems, *CrystEngComm,* **2019**, 3000–3013.

- Chapter 5 (§5.1) of this thesis has been published: Benita Barton, Lize de Jager and Eric C. Hosten, Host proficiency of *N*,*N'*-bis(9-phenyl-9-thioxanthenyl)ethylenediamine for pyridine and the methylpyridine guests – a competition study, *Supramol. Chem*., **2017**, 61–71.

- Chapter 6 of this thesis has been accepted for publication: Benita Barton, Lize de Jager, Ulrich Senekal and Eric C. Hosten, Comparing the effect of selected substituent changes on host ability and selectivity in four xanthenyl-type host compounds in the presence of cyclohexanone and methylcyclohexanone isomers, *J. Incl*. *Phenom. Macrocycl. Chem.*, **2019**.

- Chapter 7 of this thesis has been published: Benita Barton, Cedric W. McCleland, Mino R. Caira, Lize de Jager and Eric C. Hosten, Crystal X-ray diffraction and molecular modelling considerations elucidate the factors responsible for the opposing host behaviour of two isostructural xanthenyl- and thioxanthenyl- derived host compounds, *Cryst. Growth Des*., **2019**, 2396–2418.

- Chapter 7 of this thesis will be presented as a poster at the European Symposium on Organic Reactivity (ESOR) in September 2019, held in Dubrovnik, Croatia. The presentation title will be "Host behaviour of *N*,*N'*-bis(9-phenyl-9-thioxanthenyl)ethylenediamine in the

presence of aromatic and aliphatic five-membered heterocyclic guests: selectivity correlations with Hirshfeld surface analyses''.

- Chapter 8 of the thesis has been published: Benita Barton, Lize de Jager and Eric C. Hosten, Host behaviour of *N*,*N'*-bis(9-phenyl-9-thioxanthenyl)ethylenediamine in the presence of aromatic and aliphatic five-membered heterocyclic guests: selectivity correlations with Hirshfeld surface analyses, *Cryst. Growth Des*., **2019**, 1268–1281.

- Chapter 8 of this thesis was presented as a poster at the Frank Warren conference in July 2019, held in the Drakensberg, South Africa. The presentation title was "Host behaviour of *N*,*N'*-bis(9-phenyl-9-thioxanthenyl)ethylenediamine in the presence of aromatic and aliphatic five-membered heterocyclic guests: selectivity correlations with Hirshfeld surface analyses''.

- Chapter 9 and 10 of this thesis have been published: Benita Barton, Lize de Jager and Eric C. Hosten, Comparing the host behaviour of *N*,*N'*-bis(9-phenyl-9-thioxanthenyl)ethylene-diamine and *N*,*N'*-bis(9-phenyl-9-xanthenyl)ethylenediamine in the presence of various alkylated aromatic and aniline guests: crystal engineering considerations, *CrystEngComm,* **2019**, DOI 10.1039/C9CE00823C.

- Chapter 11 (§11.1) of this thesis has been published: Benita Barton, Lize de Jager and Eric C. Hosten, An investigation of the complexation of host *N*,*N'*-bis(9-phenyl-9-thioxanthenyl)ethylenediamine with dihaloalkane guests, *J. Incl. Phenom. Macrocycl. Chem*., **2017**, 105–116.

- Chapter 11 (§11.2) of this thesis has been published: Benita Barton, Lize de Jager and Eric C. Hosten, A comparison of the behaviour of two closely related xanthenyl-derived host compounds in the presence of vaporous dihaloalkanes, *J. Incl. Phenom. Macrocycl. Chem*., **2018**, 181–194.

- Chapter 11 of this thesis was presented as an oral at the annual Studentesimposium vir Natuurwetenskap held at the University of Pretoria, Pretoria, South Africa, on 2–3 November 2017. The presentation title was "*N*,*N'*-Bis(9-feniel-9-tioxanteniel)etileendiamien: 'n selektiewe gasheerverbinding vir dihalo-alkaangaste".

SUMMARY

In this work, the host capabilities of two structurally related compounds, *N*,*N'*-bis(9-phenyl-9-thioxanthenyl)ethylenediamine (**H_1**) and *N*,*N'*-bis(9-phenyl-9-xanthenyl)ethylenediamine (**H_2**) were compared in the presence of a wide variety of guest species. Additionally, the selectivity displayed by these host compounds were examined when exposed to mixtures of guests in order to ascertain whether it would be feasible to employ them in alternative separation strategies for the purification of industrially relevant chemicals.

H_1 and **H_2** were synthesized by reacting thioxanthone and xanthone with phenylmagnesium bromide. The resultant alcohol was then treated with perchloric acid and, finally, two of these molecules were effectively linked by utilizing ethylenediamine to afford the two host compounds.

Initially, **H_1** and **H_2** were investigated for their inclusion abilities by recrystallizing each from a number of potential isomeric and non-isomeric guest compounds such as the xylenes and ethylbenzene, methylanisoles and anisole, methylpyridines and pyridine, methylcyclohexanones and cyclohexanone, heterocyclic five- and six- membered ring compounds, alkyl-substituted benzenes, anilines, and dihaloalkanes. **H_1** displayed excellent inclusion ability when presented with the above-mentioned compounds, and a 1:1 H:G ratio was consistently preferred in each case. **H_2** also proved to be successful in this regard but did not include the methylcyclohexanones and cyclohexanone nor the heterocyclic five-membered ring solvents. Furthermore, varying host:guest ratios were observed for the complexes formed with **H_2**.

Mixed competition experiments were carried out in the presence of either isomeric or related but non-isomeric guest species. When **H_1** and **H_2** were independently recrystallized from mixtures of the former, selectivity orders correlated for both hosts, but it was observed that **H_2** exhibited an enhanced selectivity for the preferred guests in each case, compared with **H_1**. Interestingly, in mixtures of the latter, host behaviours were distinctly opposing (with the exception of the dihaloalkanes).

H_1, and even more so **H_2**, demonstrated very high selectivities for *p*-xylene, aniline and *N*,*N*-dimethylaniline from the xylene and aniline guest series, respectively, where selectivities were

found to be ~90% or higher for host recrystallization experiments from respective mixtures of these guests.

Single crystal X-ray diffraction, Hirshfeld surface and thermal analyses were employed in order to elucidate the reasons for any selectivity observations. The inclusion of these guests was, in most cases, found to be as a result of interactions between host and guest species, which included π···π stacking, C–H···π, hydrogen bonding and various other short contact types. Guest compounds were accommodated in either cavities or channels and this was dependent on the nature of the guest. The host molecule conformations showed **H_1** to adopt a bent tricyclic fused ring system with the N atoms of the linker in a synclinal arrangement, while in complexes with **H_2**, the fused ring system was near-planar and the N atoms adopted an antiperiplanar geometry. These key differences resulted in a very ordered host–host packing for **H_2** as a direct result of the more planar O-containing ring and linear linker; for **H_1**, on the other hand, the buckled S-containing ring and gauche-orientated N atoms resulted in a less ordered packing, which ultimately related to the differences in the behaviour of the two host species. Hirshfeld surface analyses, in general, did not provide much information to explain the host selectivities, with the exception of complexes containing the five-membered ring guest heterocyclics. Thermal analyses were completed on all suitable host-guest complexes and, in most cases but not all, the onset and peak temperatures (terms T_{on} and T_p, respectively) were related to the thermal stability of the complexes, which were used to rationalize the selectivities of these host compounds.

Key Words:

- Host-guest Chemistry
- Inclusion
- Selectivity
- Isomer Separation
- Opposing Behaviour
- Single Crystal X-ray Diffraction
- Thermal Analysis
- Hirshfeld Surface Analysis

ABBREVIATIONS AND SYMBOLS

H	host	ANL	aniline
G	guest	NMA	*N*-methylaniline
π···π	pi···pi	NNDMA	*N*,*N*-dimethylaniline
X–H···π	X–H···pi	ANI	anisole
H_1	*N*,*N'*-bis(9-phenyl-9-thioxanthenyl)ethylenediamine	2MANI	2-methylanisole
H_2	*N*,*N'*-bis(9-phenyl-9-xanthenyl)ethylenediamine	3MANI	3-methylanisole
DCM	dichloromethane	4MANI	4-methylanisole
DBM	dibromomethane	TOL	toluene
DIM	diiodomethane	CU	cumene
o-Xy	*ortho*-xylene	PET ether	petroleum ether (bp 40–60 ˚C)
m-Xy	*meta*-xylene		
p-Xy	*para*-xylene		
EB	ethylbenzene		
CHN	cyclohexanone		
2MCHN	2-methylcyclohexanone		
3MCHN	3-methylcyclohexanone		
4MCHN	4-methylcyclohexanone		
PIP	piperidine		
PYR	pyridine		
MORPH	morpholine		
DIOX	dioxane		
2MP	2-methylpyridine		
3MP	3-methylpyridine		
4MP	4-methylpyridine		
THF	tetrahydrofuran		
THT	tetrahydrothiophene		
H-bonding	hydrogen bonding		
PXRD	powder X-ray diffraction		
SCXRD	single crystal X-ray diffraction		
TG	thermogravimetry		
DSC	differential scanning calorimetry		
DTG	derivative of the thermogram		
^{1}H-NMR	proton nuclear magnetic resonance		
^{13}C-NMR	carbon-13 nuclear magnetic resonance		
IR	infrared		

TABLE OF CONTENTS

1. INTRODUCTION

"Nothing in life is to be feared; it is only to be understood. Now is the time to understand more, so that we may fear less."

-Marie Curie

1.1 Overview of the classification and nomenclature in supramolecular chemistry

1.1.1 History

Supramolecular chemistry may be defined as the "chemistry beyond the molecule".[1] It is the phenomenon in chemistry when two or more molecular components are held together by intermolecular non-covalent forces or other structural factors. The broad term for compounds that are described by this definition is "supramolecules" or "supramolecular compounds".[1,2] This definition is relatively recent. However, the concept and origin of supramolecular chemistry may be traced back to the 19th century when modern chemistry itself was introduced.[3] In 1873, the existence of intermolecular forces was discovered by Johannes Diderik van der Waals and, in 1894, Hermann Emil Fischer first described enzyme–substrate interactions using a "lock-and-key" analogy, anticipating the principles for molecular recognition and host-guest chemistry, which was a fundamental step in establishing supramolecular chemistry as a field of study.[3,4] Jean-Marie Lehn introduced the term "supramolecular chemistry" which he defined as the "chemistry of molecular assemblies and the intermolecular bond'', and for which he won the Nobel Prize in 1987, together with Donald Cram and Charles Pedersen.[2,5]

Figure 1.1 illustrates how molecular chemistry differs from supramolecular chemistry. In the former, molecules are formed by combining molecular precursors by means of a covalent bond while, in the latter, molecules interact to form a supramolecule via non-covalent interactions and/or structural barriers.[6]

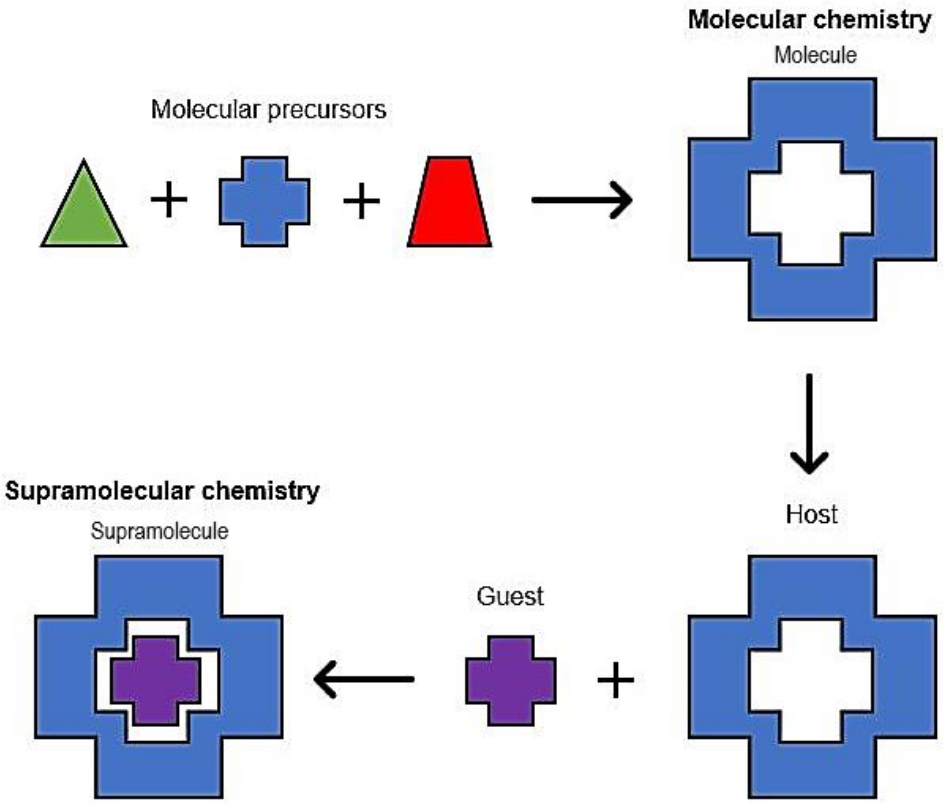

Figure 1.1. Comparison of molecular and supramolecular chemistry.[3]

1.1.2 Subgroups in supramolecular chemistry

Supramolecular chemistry is a vast field of study, and Figure 1.2 is a visual summary of the various categories of compounds that form part of this chemistry field.[7]

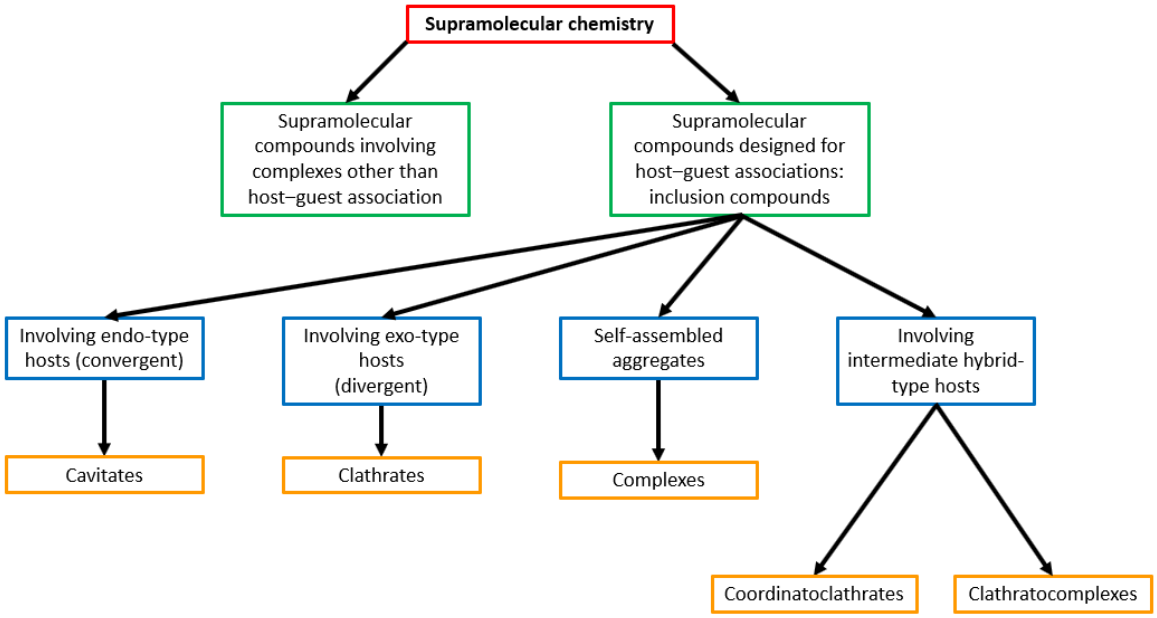

Figure 1.2. Visual summary of the subgroups of supramolecular chemistry.

Supramolecular chemistry may initially be subdivided into two groups, namely those that do not involve host–guest associations, and those that involve these.[7] Most supramolecules fall into the former category, which may be further subdivided into different, but broad, fields that are focused on engineered supramolecular compounds,[6] such as interlocked and interwoven supramolecular systems, liquid crystals, surfactant-type and mono-/multi-layered aggregates, catalytic systems, biological mimics, self-replicating systems and supramolecular devices.[6] The second category that deals with compounds that are designed for host–guest associations[6] is the focus of the present research, and will therefore be discussed in detail. Host-guest chemistry may be defined as molecular associations where two or more different molecules or ions are held together in a unique structural relationship by means of interactions other than full covalent bonds.[6]

Since supramolecular chemistry was influenced by Hermann Emil Fischer's "lock-and-key" mechanism of enzyme–substrate recognition, the host–guest association may be regarded as a synonym for the receptor–substrate principle. The host is often referred to as the receptor, and the guest as the substrate.[6]

Figure 1.3 shows the formation of a supramolecule by means of host–guest association. The guest molecule is enclathrated by the host.

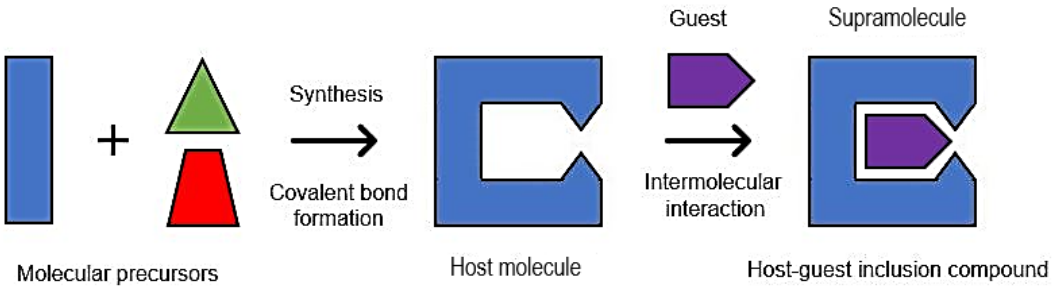

Figure 1.3. The formation of a supramolecule using host–guest association.[6]

When the host provides a hollow space or any non-defined cavity in which a guest can reside, the resultant association is called an inclusion compound.[6] It must be noted that a large number of literature reports refer to inclusion compounds as "complexes" in which one chemical compound (the host) forms a cavity for a second chemical compound (the guest) to reside in. The term "inclusion complex" is commonly used interchangeably with "inclusion compound" and is separate from the subcategory termed "complex" that will be discussed later (see Figure 1.2 for clarity).

1.1.3 Defining inclusion compounds

Inclusion compounds may be divided into four subcategories (Figure 1.2). The first of these involves endo-type receptors/hosts which are single molecules possessing permanent cavities in which the entire guest molecule/molecules reside/s.[3,6] Figure 1.4 illustrates the formation of this type of inclusion compound:

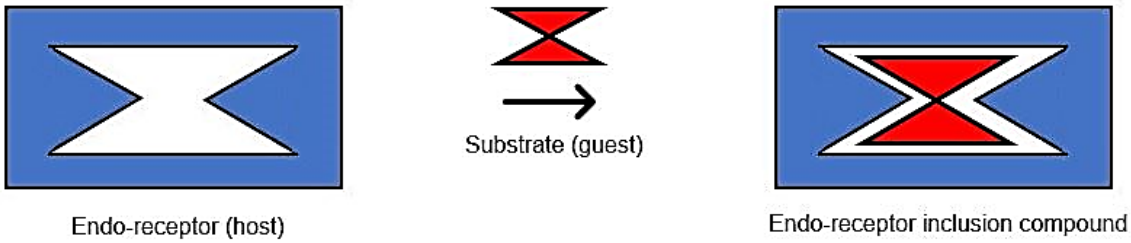

Figure 1.4. Endo-type receptor including a guest entirely and forming an endo-receptor inclusion compound.[6]

A specific example of an endo-receptor inclusion compound is a cavitate. The term “cavitate” (note the suffix “-ate”) refers to the host-guest inclusion compound while cavitand (note the suffix “-and”) refers to the free host.[6] Cavitands may be defined as hosts that are single molecules that possess permanent intramolecular cavities that the guest occupies.[3,6,8] Figure 1.5 is an illustration of the formation of a cavitate inclusion compound.

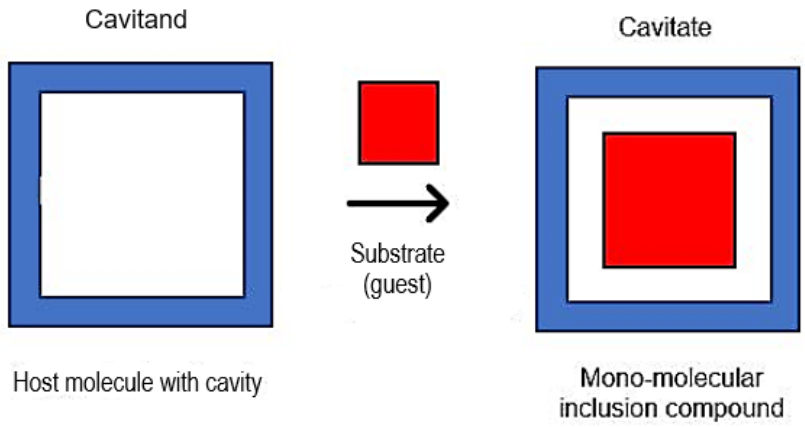

Figure 1.5. Formation of a cavitate inclusion compound.[6]

Since cavitates are mono-molecular species and are limited to a single host–guest entity, they are also referred to as intramolecular, endo-molecular or mono-molecular inclusion compounds.[6] Cavitates may be distinguished from the other subgroups (Figure 1.2) by the fact that the guest is held in place by non-directional interactions only, such as hydrophobic, van der Waals and/or crystal close-packing effects. These exist in both the solid state and solution.[6] Examples of host molecules that form this type of inclusion compound are the crown ethers, cyclodextrins, cyclophanes and cryptands.[5,9]

The second subdivision of inclusion compounds involves receptors/hosts that are of the exo-type (Figure 1.2). These host compounds possess guest binding sites on their surfaces.[3,6] Figure 1.6 illustrates the formation of an exo-receptor/host inclusion compound.

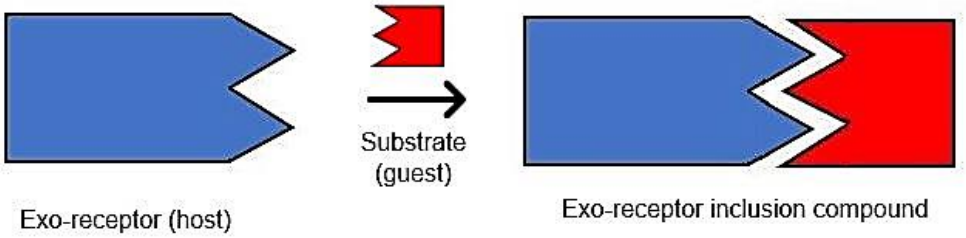

Figure 1.6. Exo-type receptor clathrating a guest to form an exo-receptor inclusion compound.[6]

A specific example of an exo-type receptor/host is a clathrand which comprises more than one host molecule and results in a multi-molecular cavity for the accommodation of the guest compound.[3,6,8] Figure 1.7 illustrates this more clearly.

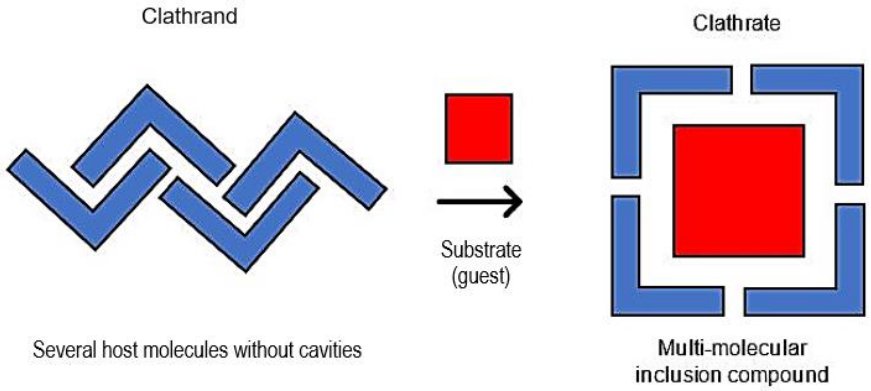

Figure 1.7. Formation of a clathrate inclusion compound.[6]

Clathrates are predominantly formed in the solid state and decompose upon dissolution. They are held together by non-specific and often weak, non-directional interactions.[6,10] Since more than one host molecule is required to trap the guest in multi-molecular cavities, clathrates are referred to as exo-molecular or multi-molecular inclusion compounds.[3] Another common name for this group is “true clathrates”,[10] and examples of host compounds relevant here are urea, helical tabuland diols and MacNicol’s hexa-hosts.[5]

The third subgroup of inclusion compounds is the self-assembled aggregates (Figure 1.2), also known as complexes,[3] which is an umbrella term employed to describe the more general host–guest associations found in supramolecular chemistry. Complexes do not adhere to the classical host-guest description but may still be identified as inclusion compounds since they are formed by non-covalent interactions and are aggregates that are held together primarily

by means of electrostatic forces such as ion-dipole, dipole-dipole and hydrogen bonding interactions, amongst others. Identifying characteristics are that these assemblies retain their identity in solution.[3] Figure 1.8 illustrates the formation of a complex:

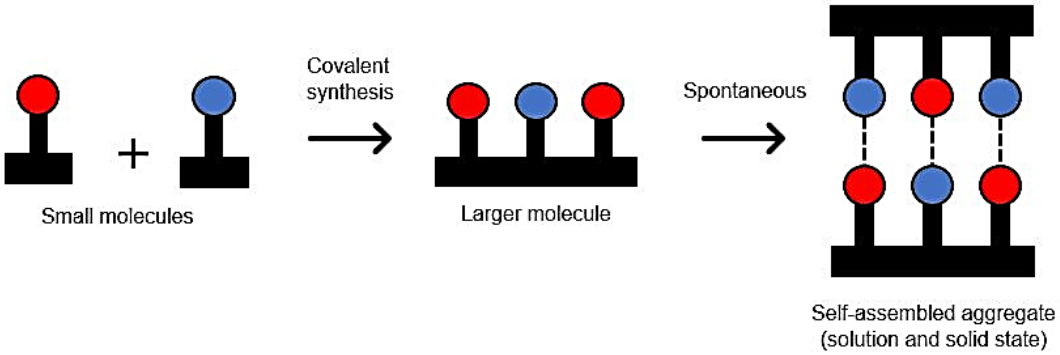

Figure 1.8. Formation of a complex.[3]

The last subgroup of inclusion compounds comprises intermediate hybrids of the other subgroups (Figure 1.2).[6,10]

Clathratocomplexes may be described as inclusion compounds where the host–guest interaction is mainly of the complex-type, but there is also a distinct crystal close-packing effect as observed in both clathrates and cavitates. Furthermore, the interactions present in these species are usually strong, such as hydrogen bonding.[11]

Coordinatoclathrates are associations where the host–guest interaction is mostly due to distinct crystal close-packing, but these also experience some electrostatic forces as observed in complexes. Figure 1.9 illustrates the formation of a hybrid inclusion coordinatoclathrate that uses the crystal packing of the host as well as non-directional interactions to trap the guest compound:

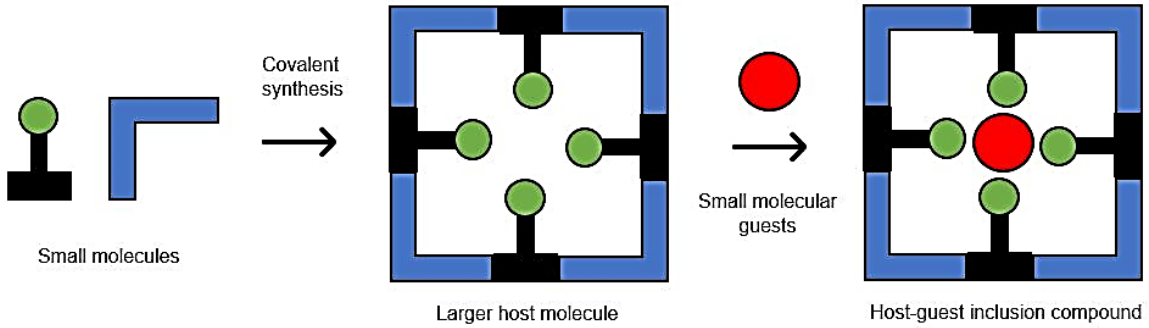

Figure 1.9. Formation of a coordinatoclathrate.[3]

1.1.4 Relationship between host and guest molecules

There exist many additional descriptions to explain the relationship between the host and the guest molecule. The spatial relationship can trivially be defined as either layer-type (two-dimensional, e.g., intercalates), channel-type (one-dimensional open channels, e.g., tubulates), cage-type (enclosed, e.g., cryptates) or hybrids of these.[6] A more specific description of the spatial relationship is shown in Figure 1.10, with the guest represented as a sphere, and includes a) capsular, b) nesting, c) perching, d) tubular, e) wrapping, f) sandwich, g) mono-molecular, h) dinuclear/homonuclear, i) dinuclear/heteronuclear, j) second sphere and k) mononuclear/dihapto relationships between host and guest species.

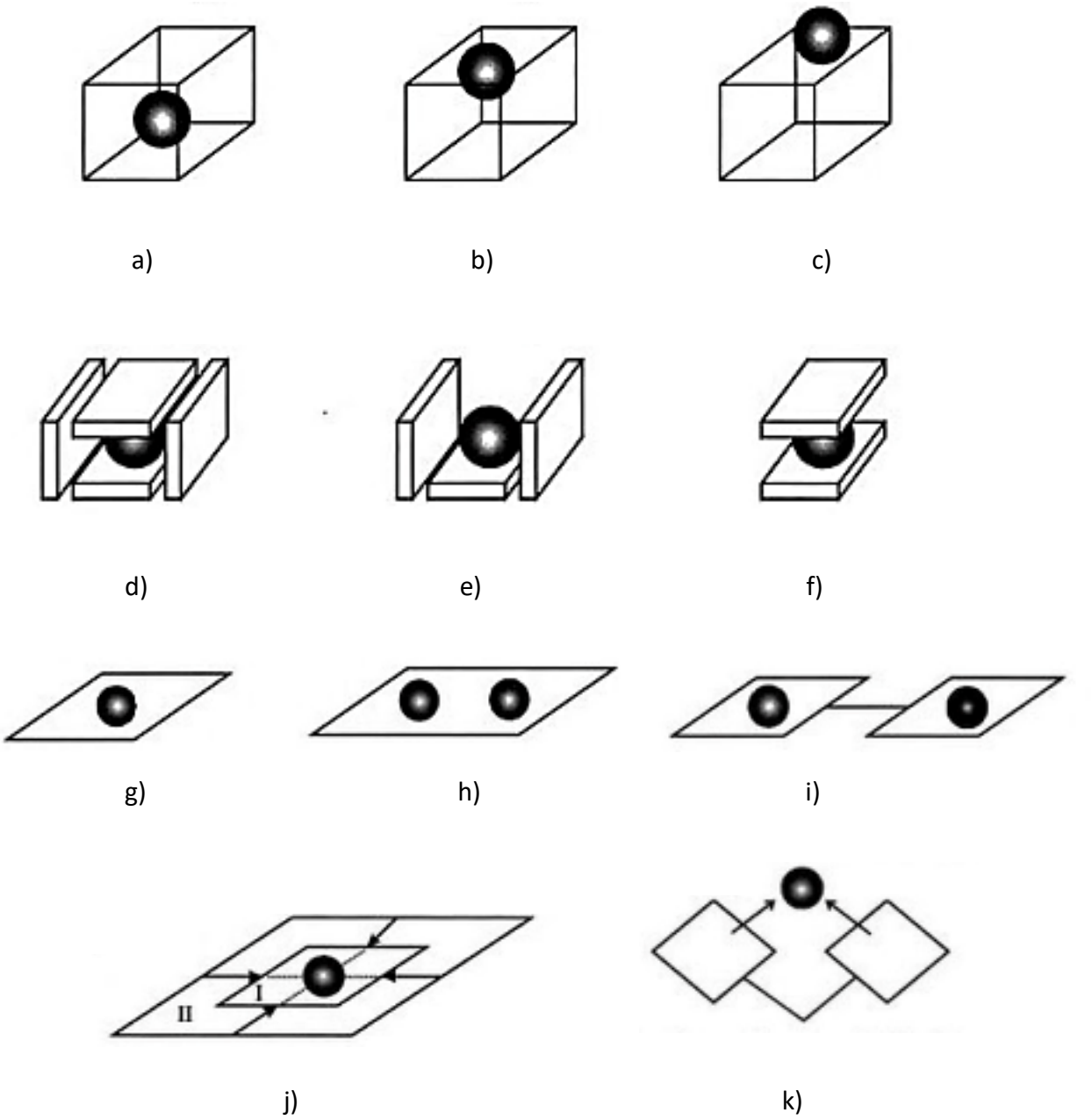

Figure 1.10. The spatial relationships between host and guest compounds.[6]

The nature of bound guests is designated by using the terms homo- or hetero- nuclear, which indicates whether guests are identical or different, respectively. Furthermore, the number of binding units of the host can be described by using the terms mono- or poly- topic. Monotopic associations only have one site at which another compound may form a complex, whereas polytopic ones may have multiple sites.[6]

1.2 Crystal engineering

Crystal engineering is the design and synthesis of molecular solid-state structures with desired properties, based on an understanding of intermolecular interactions.[12,13] In supramolecular chemistry, and specifically host-guest chemistry, many of the bulk properties of molecular materials are dictated by the manner in which the molecules are ordered in the solid state.[14-17] Therefore, crystal engineering and an ability to alter this ordering would afford control over these properties in supramolecular systems. Modern crystal engineering has emerged as an extensive discipline and involves an understanding of the process of synthesis, crystallography, crystal structure analysis, and computational methods.[18] Crystallization is not a trivial process and many factors must be accounted for when attempting to understand the mechanisms that drive the process. This includes the balance between kinetic and thermodynamic features, electrostatic contributions, and crystal packing.[18] Crystallographers have, however, identified key aspects that provide some insight into how these mechanisms may be controlled.

1.2.1 Principles of crystal engineering

1.2.1.1 Non-covalent control of molecular structures

Non-covalent bonding is one of the factors that controls the organization of molecules and ions in the solid state.[19] Many organic supramolecular systems employ hydrogen bonds,[20-22] while inorganic systems centre around the coordination bond.[23] In recent studies, the use of halogen bonds,[24] ion associations,[25-27] π···π,[28] C–H···O[29] and C–H···π[30,31] interactions have proven beneficial in providing additional control in crystal design.

1.2.1.2 Supramolecular synthons

Molecular self-assembly is the process by which molecules adopt a defined arrangement without the influence from an external source.[32] It is a key concept in supramolecular chemistry since it allows the construction of challenging molecular systems.[1,33] Desiraju[34] mimicked the retrosynthetic approach to identify the building blocks that are common to many supramolecular structures and that may be used to order specific groups in the solid state. He termed these groups “supramolecular synthons”, and today these are well

documented at the Cambridge Crystallographic Data Centre (CCDC).[35] Supramolecular synthons have two classes: homosynthons are composed of identical complementary functional groups (dimers, chains, etc.) while heterosynthons are composed of different but complementary functional groups.[36] Some simple examples include carboxylic acid dimers[37] and substituted benzene motifs.[38]

1.2.2 Advances in crystal engineering

1.2.2.1 Design of multi-component cocrystals

A major development in the field of crystal engineering is related to the development of cocrystals, solids that are crystalline materials composed of two or more different molecular or ionic compounds.[39] The design of cocrystals is a difficult task as it involves recognition between different molecules which may possess very different shapes and sizes, and are usually designed by interaction-control[40] or shape-size complementation.[41] The main relevance of multi-component crystals, despite the synthetic challenge, arises from the advantages that may be on offer when modifying a particular property by changing the components (molecular units) of the cocrystals. An industrial application would be the formation of pharmaceutical cocrystals where one of the components enhances or aids the formation or performance of the others.[37,42]

1.2.2.2 Two-dimensional (2D) supramolecular systems

The investigation and synthesis of 2D structures has rapidly developed as a division of crystal engineering.[43] The benefit of understanding the design of 2D molecular layers[44] or networks[45,46] is that a predictable structure may be obtained or a specific architecture may be successfully designed for a particular function. The prediction of the thermodynamic factors that control the formation of these 2D systems are not well understood, but recent contributions from Palma *et al*[44] showed that controlled polymorphism and nanopattern formation of organic systems make it possible to gain semi-quantitative insight into the thermodynamics of physisorption at interfaces.

1.2.2.3 Polymorphism in supramolecular systems

Polymorphism is the phenomenon where the same chemical compound exists in different crystal forms and arises due to the competition between kinetic and thermodynamic factors during crystallization.[47] While long range strong intermolecular interactions dictate the formation of kinetic crystals, the close packing of molecules generally drives the thermodynamic outcome. Understanding this equilibrium between the kinetics and thermodynamics may bring forth information on the mechanism of polymorphism. In organic molecules, three main types of polymorphism are observed.[48] Packing polymorphism arises when molecules pack in different ways to give different structures. Conformational polymorphism, on the other hand, is mostly observed in flexible molecules where moieties have multiple conformational possibilities within a small energy range of the global energy minimum. Finally, synthon polymorphism, the rarest form, arises from the variances in the primary synthon where closely related derivative synthons are cocrystallized and give rise to different polymorphs.

1.2.2.4 Crystal structure prediction (CSP)

CSP is a computational approach to generate energetically feasible crystal structures from a known molecular structure. Many procedures have been proposed and assessed by researchers that have deposited data at the CCDC, but a major development in CSP occurred in 2007 when a hybrid computational method based on tailor-made force fields and density functional theory (DFT) was introduced. In the first step, this method employs force fields to decide upon the ranking of the structures, followed by a dispersion-corrected DFT method to calculate the lattice energies precisely.[49] These calculations offer insights into polymorphism, the design of new structures and also assist in the designing of crystallization experiments.[50]

1.3 Properties of successful guest compounds

In organic host-guest chemistry, the guest is an organic molecule that occupies a cavity, cage or channel within the crystal structure of the host, and is trapped by means of non-covalent interactions and/or steric barriers.[51] Guest molecules are selected according to their

compatibility with the host compound, and this relies upon various characteristics of the host.[5]

Some host molecules depend on the accumulative nature of π···π interactions to form stable inclusion compounds with aromatic guests.[52] Others rely significantly on hydrogen bonding[21] for stability, and therefore guests that are able to hydrogen bond (either as donors or acceptors) are favoured. The crystal packing[53] of the host, furthermore, influences its selectivity towards guests with various shapes and volumes.

1.4 Properties of successful host compounds

In this context, a host may be described as a compound that accommodates the guest in its crystal structure. From a vast number of literature reports involving host-guest chemistry, it was observed that successful host compounds have certain features in common; these may not apply to all hosts but merely serve as a guideline when attempting to design and synthesize novel host materials.[51] The ability of a compound to behave as a host cannot be predicted and may only be ascertained through experiment.[54,55] However, the potential of a compound to behave as a host increases with the presence or absence of specific characteristics inherent within the compound, and these will be discussed now.

1.4.1 Rigidity

Rigidity is the property of a structure that does not bend or flex under an applied force and is usually found in ring, aromatic and fused-ring molecules. This property is regarded as the most important for designing efficient hosts[10,56] since rigidity enhances crystallinity, and the requirement for successful host compounds is that they be solids.[57] Long carbon chains are not rigid compared with, for example, cyclic compounds. As an illustration, compound **1** is a saturated hydrocarbon chain and has free rotation about the single bonds, implying flexibility while, contrastingly, thioxanthone **2** is a fused tricyclic structure in which free rotation about any of the bonds is not possible. Consequently, this molecule displays rigidity.

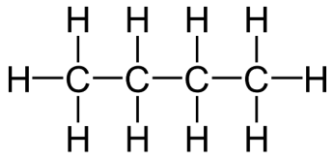

1

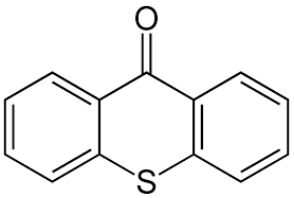

2

1.4.2 Crystallinity

Crystallinity refers to the degree of structural order in a solid. In a crystal, the atoms or molecules are arranged in a regular, periodic manner, and when the crystalline properties of the host are satisfactory, a cavity or channel in which the guest may be trapped is readily formed.[10,58,59]

The requirement that a host be crystalline ensures ease of separation of the inclusion compound from the solution since the host crystallizes out with the entrapped guest in the process. This separation may be achieved through vacuum filtration. Also, only crystalline or solid materials have the ability to possess ordered spaces in their structures into which guests may fit.[10]

1.4.3 Bulkiness

Another characteristic to be considered when designing successful host compounds is to ensure the presence of bulky moieties within the host structure which provide a "surrounding factor" for the guest molecule.[58] Hosts that have larger groups such as phenyl rings, xanthenyl and trityl moieties, or derivatives of these, display improved host properties by facilitating crystallinity and allowing for the formation of cavities or channels in the crystal in which the guests may reside.[60,61] Naturally, this property does not, however, guarantee the success of the compound as a host, and it has previously been shown that some large and bulky mono-molecular species possess channels or cavities that are too immense to successfully entrap any potential guest species.[10]

1.4.4 Non-covalent interactions

Efficient host compounds should be able to either interact non-covalently (coordinatoclathrates), have steric barriers (true clathrates), or a combination of these in order to retain the guest in the host crystal. Many successful host compounds are able to form very strong non-covalent bonds, such as hydrogen bonding,[10] but these interactions are not essential to ensure host efficiency, since a large number of weaker interactions, such as π···π stacking or other short interactions, may function accumulatively, and therefore have a similar stabilizing effect.[62]

1.4.5 Functional groups

Certain functional groups may enhance the ability of a compound to behave as a host by permitting favourable interactions with the guest species or by increasing the crystallinity of the host compound. These groups include -NH, -SH, -CN, -OH, and cyclic sulphite functionalities,[56,63] and often form stabilizing and strong host···guest (H···G) interactions with the guest compounds.

1.4.6 Symmetry

A characteristic of many successful host compounds, but which is less established than the others, is symmetry. There often exists a relationship between host symmetry and successful host behaviour, and it is speculated that this feature improves the crystal packing which positively affects crystallinity.[10]

1.4.7 Chirality

Host chirality can be a valuable tool in host-guest chemistry,[57,64] and some background will be highlighted to understand its application in practice.

Stereoisomers are compounds that have the same molecular formula but differ in the arrangement of their atoms in space. Enantiomers are stereoisomers that are non-superimposable mirror images of one another, and occur only with compounds that have chiral centres.[57]

In Figure 1.11, an example of a pair of enantiomers is shown.

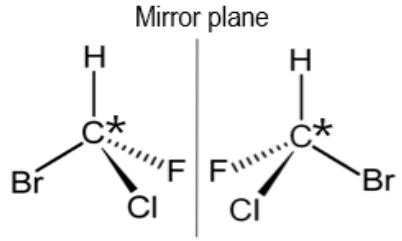

Figure 1.11. A pair of enantiomers.

Chirality is associated with the property of handedness, which is the result of the presence of at least one tetrahedral (sp^3-hybridized) C-atom in the molecule which bears four different groups. The chiral molecule and its mirror image are then related as enantiomers.[57]

Enantiomers have identical physical and chemical properties, except for their optical rotations and interactions in a chiral environment. Optical activity refers to the ability of chiral molecules to rotate/divert the plane of polarization of a transmitted beam of plane-polarized light. When one enantiomer of the pair is isolated, it is said to be optically pure.[57]

A racemic mixture, or racemate, has an equal molar amount of the left- and right-handed enantiomers, which will rotate the plane of polarization by equal amounts but in opposite directions and, overall, no rotation will be observed. Unless specific asymmetric synthetic methods are employed, when chiral compounds are synthesized, the products are usually obtained as a racemic mixture.[57] It is not possible to separate these enantiomers using physical methods such as fractional distillation or crystallization because of their identical physical properties. However, host-guest chemistry where a chiral and optically pure host is employed may permit racemate resolution through preferential inclusion of the one enantiomer only through cocrystallization.[57,64]

1.5 Existing successful host compounds

The structure and mechanism of guest inclusion may be used to categorize host molecules.[57] What follows is a summary of the more prevalent host types that have been reported in the literature.

1.5.1 Cyclodextrins (CD's)

CD's are a family of compounds made up of D-glucopyranose units bound together in a cyclic oligosaccharide ring. These compounds are synthesized by means of enzymatic conversions of D-glucopyranose to form covalent α-1,4-glycosidic bonds. The three main types of these macrocycles possess six, seven or eight of these units, and are respectively named α-, β- or γ-cyclodextrin.[65] These macrocyclic molecules have a cavitated and cylindrical shape, and experience intramolecular hydrogen bonding between the D-glucopyranose units that provide structural rigidity and enable intermolecular interactions (hydrogen bonding, electrostatic interactions) with the guest. These are the factors that are key to the success of these host molecules.[66] Below is the structure of α-cyclodextrin (**3**) displaying some of the intramolecular hydrogen bonds as dotted lines.

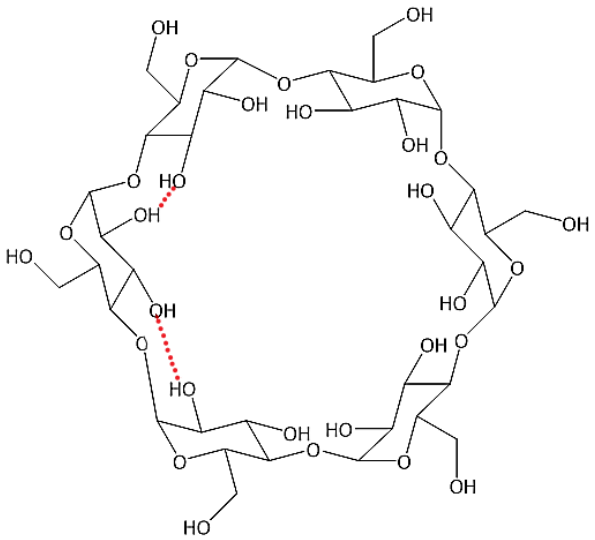

3

Due to their molecular complexation ability, these compounds are widely used in many industrial products, technologies and analytical methods. Their negligible cytotoxic effects are an essential attribute in applications such as their use as drug carriers, in food, cosmetics, packaging, textiles, fermentation, and also in separation science, environmental protection through waste removal, and catalysis.[67]

Recently, Q. Hu *et al*[68] considered the feasibility of employing α- and β- cyclodextrins as hosts in supramolecular nanoparticles with drug actives as guests in drug delivery applications. They investigated the modification of CD's and, consequently, reported improved biocompatibility

of the actives through controlled particle size and biodegradability; the drugs therefore displayed a more controlled response *in vivo*. CD's possess a hydrophilic exterior surface and hydrophobic interior cavity, and these characteristics are responsible for the enhanced biocompatibility. Supramolecular approaches utilizing CD's therefore present advantages with respect to functional delivery systems for medical applications.

1.5.2 Crown ethers, cryptands, spherands, calixarenes and cyclophanes

Crown ethers, cryptands, spherands, calixarenes and cyclophanes are large organic structures that have the ability to facilitate chemical reactions between interacting molecules, ions or radicals.[67]

Crown ethers are cyclic, and the ring is made up of several ether groups. For example, 18-crown-6 (**4**) has regularly-spaced oxygen atoms that are identically bridged, where "18" refers to the number of all atoms and "6" to the number of oxygen atoms in the ring. There also exist derivatives with other heteroatoms such as sulfur (thia-crown ethers, **5**) and amino groups (aza-crown ethers, **6**). These compounds are successful hosts for hydroxyl- and amino-containing guests due to favourable interactions between the guest functional groups and the host heteroatom functionality.[69]

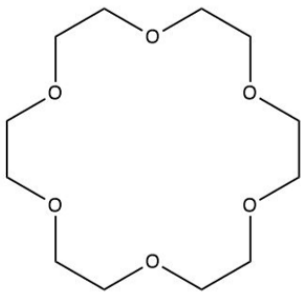

4

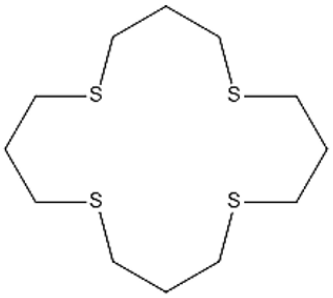

5

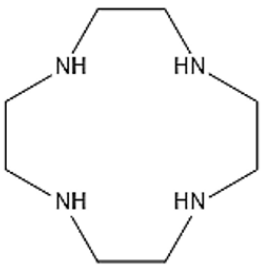

6

R. Kuhn *et al*[70] successfully used chiral crown ethers as a *pseudo*-stationary phase in capillary zone electrophoresis to separate optically active amines from racemic mixtures. These molecules are, furthermore, known to form complexes with biologically-significant cations, and have been widely investigated for their ability to transport pharmacological substrates across membranes. They are also able to function as catalysts.[71] Their ability to form

complexes with heavy metal cations has provided the potential for separation of long-lived radioactive isotopes.[72]

Cryptands are a family of synthetic bi- and poly- cyclic multidentate ligands that have an affinity for a variety of cations. These molecules are three-dimensional (3D) analogues of crown ethers, and are more efficient in their host-guest chemistry.[57] They are, however, more expensive and difficult to prepare, but offer much improved selectivity and strength of binding than many other macrocycles for alkali metals.[73] Cryptands have been shown to enable the synthesis of alkalides and electrides, and may also be used as phase-transfer catalysts for the transfer of ions between phases.[74] An example of these host compounds is 2,2,2-cryptand (**7**).

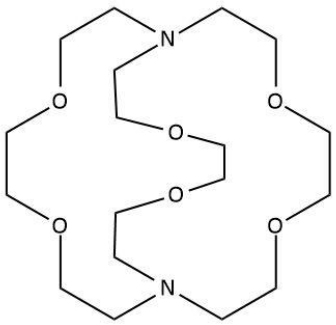

7

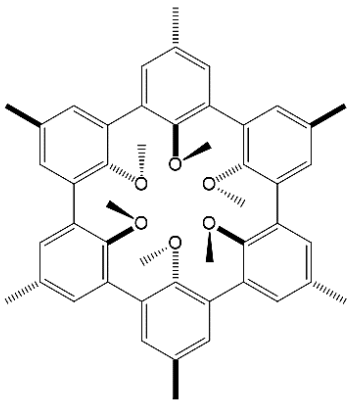

8

Spherands are macrocyclic compounds capable of completely enveloping a cation, having donor atoms (O, N and/or S) arranged such that they provide a solvation sphere to the encapsulated cation. They are usually classified as complex cryptands, and spherand **8** is an example. This host compound has the ability to bind the ammonium cation.[75]

A calixarene is a macrocycle based on a hydroxyalkylation product of a phenol and an aldehyde and has hydrophobic cavities that can encapsulate smaller molecules or ions. Calix[4]arenes have been used extensively as molecular platforms for supramolecular catalysts[76,77] utilizing a process that is based on enzymatic systems; non-covalent interactions dramatically accelerate the rate of reaction and facilitate increased selectivities. These molecules are characterized by a 3D basket, cup or bucket-shaped cavity. Calix[4]arene with

para-tert-butyl substituents (**9**) is shown in molecular (left) and spacefill (right) representation:

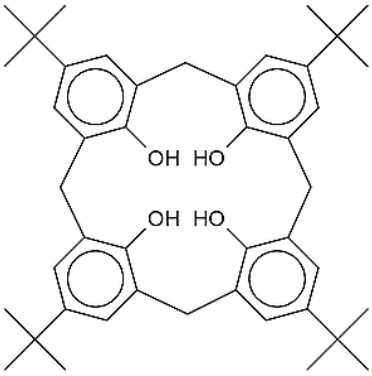

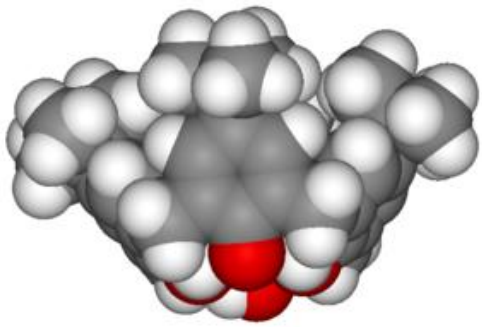

9

A cyclophane is an organic compound consisting of an aromatic unit (typically a benzene ring) and an aliphatic chain that forms a bridge between two non-adjacent positions of the aromatic ring. More complex derivatives with multiple aromatic units and bridges forming cage-like structures are also known.[3] J. Gavin *et al*[78] studied chiral molecular recognition in a tripeptide benzylviologen cyclophane host (**10**) for the inclusion of pharmaceutically-relevant guest molecules, which affect solubility and transport of the guests.

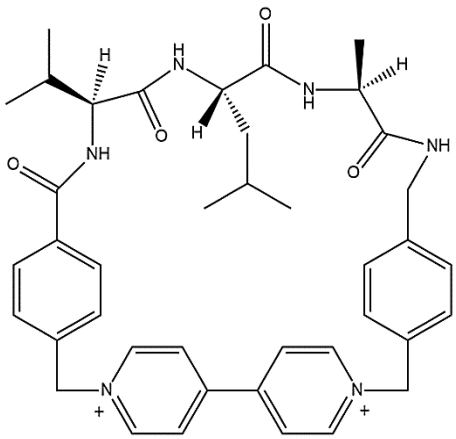

10

1.5.3 Hydroquinones

Hydroquinones are aromatic organic compounds that are a type of phenol, and thus a derivative of benzene. These species are able to enclathrate a variety of solvents[79] and are exceptional in that they possess the ability to include guests from the gas phase.

Unsubstituted hydroquinone **11** is able to include a variety of gas species such as CO_2, N_2, CH_4, Ar, Kr, Xe, SO_2 and H_2.[80-82]

11

1.5.4 TADDOLs

TADDOL is an acronym for α,α,α',α'-tetraaryl-2,2-disubstituted-1,3-dioxolane-4,5-dimethanol (**12**) and represents a family of molecules that is derived from tartaric acid.[83] These compounds are successful as hosts owing to the presence of two hydroxyl groups on the butane backbone which are able to participate in H-bonding with the guest, the bulky aromatic groups that provide a surrounding factor, and the rigidity of the 1,3-dioxolane ring.[83]

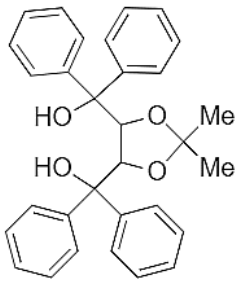

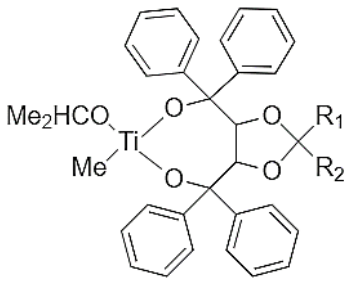

$R_1 = R_2 = Me$
$R_1 = iBu, R_2 = H$

12 **13**

Many successful derivatives of **12** have been synthesized, and compound **13** (which is termed a TADDOLate) is an example, which was found to be highly effective in enantioselective nucleophilic addition reactions.[83] Other derivatives were successfully employed in racemate resolutions by crystallization, and guests included 2-methylpiperidine,[84] 2-(ethysulfinyl)pyridine,[85] 1-benzylpyrrolidin-3-ol,[86] 1-methyl-3-(methylsulfinyl)benzene,[87] 3-methyl-3-phospholene 1-oxide,[88] 1-substituted-3-methyl-3-phospholene 1-oxide,[89] menthol, octan-2-ol, and oct-1-yn-3-ol.[90]

1.5.5 TETROL and derivatives

(+)-(2*R*,3*R*)-1,1,4,4-Tetraphenylbutane-1,2,3,4-tetraol (TETROL) (**14**) is a polyhydric compound that is prepared from tartaric diester using a Grignard reaction.[91] This compound possesses four hydroxyl and four aromatic groups, and is able to stabilize clathrated guests by means of CH···π interactions, both inter- and intra- molecular hydrogen bonds and π···π stacking interactions.[31,92] TETROL and its derivatives have recently demonstrated highly efficient host behaviour by forming complexes with guests pyridine and methylpyridines,[93] cyclohexanone and methylcyclohexanones,[94] and ethylbenzene and xylenes.[95] It was evident from these reports that TETROL has potential to be used for isomeric separations since the host displayed selectivity for one particular guest when recrystallized from a mixture of guests.

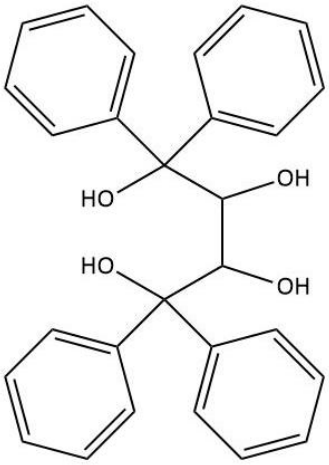

14

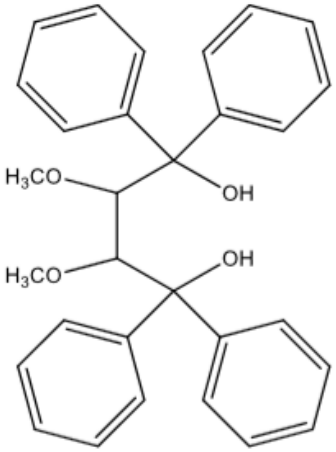

15

A successful derivative of **14** is 2,3-dimethoxy-1,1,4,4-tetraphenylbutane-1,4-diol (DMT, **15**), which may be readily synthesized by deprotonation and subsequent methylation of the internal hydroxyl groups. This host was at first reported by Toda[96] to only have limited host potential, but extensive subsequent investigations have shown this host to be extremely versatile in the presence of a large variety of different guest species.[97,98]

1.5.6 Wheel-and-axle host compounds

Wheel-and-axle hosts are molecules with a central axle, normally comprising triple bonds, to which terminal aryl groups are attached. The presence of the latter moieties prevents close packing of the host molecule, allowing guest molecules to be trapped in the crystal.[99] The molecule 1,1,6,6-tetraphenylhexa-2,4-diyne-1,6-diol (**16**) is an example of this host type and has shown the ability to include di-, tri- and tetra- haloalkanes.[100]

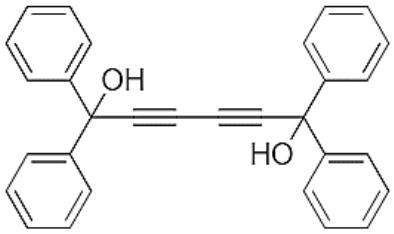

16

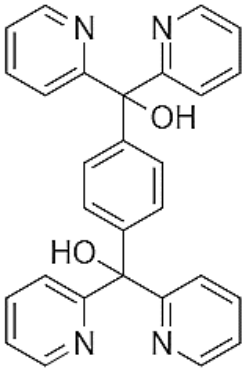

17

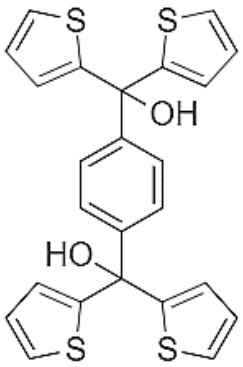

18

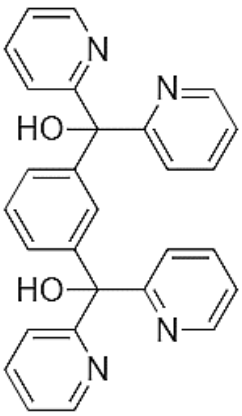

19

More recent wheel-and-axle host derivatives include 1,4-bis[di(pyrid-2-yl)hydroxymethyl]-benzene (**17**), 1,4-bis[di(thien-2-yl)hydroxymethyl]benzene (**18**) and 1,3-bis[di(pyrid-2-yl)hydroxymethyl]benzene (**19**). The sorption measurements of these compounds as sensor films coated on a quartz crystal have been reported, and a variety of solvent vapours were considered, showing potential application as mass sensitive sensor materials.[101]

1.5.7 Metal-organic frameworks (MOF's)

MOF's are synthesized by connecting inorganic metal ions or ion clusters with organic linkers via strong coordination bonds to form one-, two-, or three- dimensional structures with potential voids, and which may be used for various applications.[102] The geometry, size and functionality of these structures may be varied and this has, therefore, led to more than 20 000 different MOF's being reported in the past decade. MOF's are characterized by their robust crystalline structure, permanent porosity (low density), large voids and significant van der Waals interactions that facilitate analyte uptake or release.[103] These aspects have made MOF's ideal candidates for the storage of fuels (hydrogen and methane),[104-106] capture of carbon dioxide,[107,108] and in catalysis,[109,110] sensor[111] and drug delivery[112,113] applications, to mention a few. An example is MOF-76, which combines trivalent lanthanide ions and 1,3,5-benzenetricarboxylate (BTC) linkers to form a 3D lattice. The BTC linker can effectively sensitize the lanthanide emission, resulting in a MOF with variable emission wavelengths depending on the lanthanide identity.[114] Figure 1.12 illustrates the general synthesis of MOF-76.

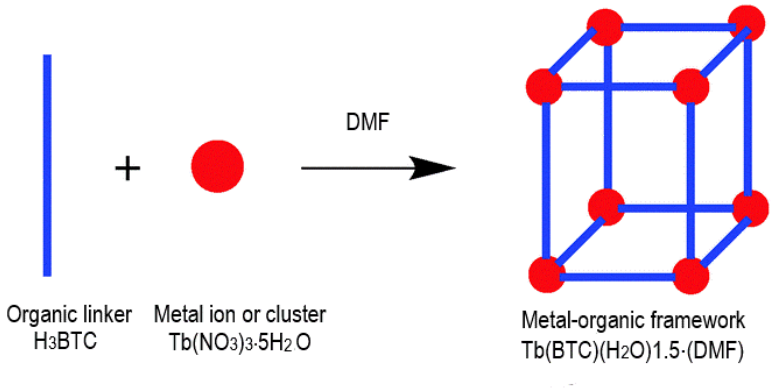

Figure 1.12. The general synthesis of MOF-76.

1.6 Host–guest interactions

The interaction between a host and guest molecule is as a result of what is termed "molecular recognition", where the two molecules have complementary geometric and/or electronic properties.[115] These interactions are non-covalent in nature, and include H-bonding, metal coordination, hydrophobic forces, van der Waals forces, π···π interactions, halogen bonding, electrostatic and/or electromagnetic effects. The association mechanism may be illustrated by means of Equation 1.1:

$H_{\alpha\text{-phase}}$ (*s*) + nG (*l*) → $H{\cdot}Gn_{\beta\text{-phase}}$ (*s*) Equation 1.1

Generally, the host (H, in the non-porous α-phase) is a solid that dissolves in a liquid guest (G), affording a host-guest compound (H·Gn, β phase) of given stoichiometry n.[32]

The process of the interaction occurs via molecular self-assembly, which is the construction of inclusion compounds without guidance or management from an external source other than to provide a suitable environment. The compounds are directed to assemble through the aforementioned non-covalent interactions or steric barriers.[116]

The non-covalent interactions that control the packing of these systems can be classified according to their strength, directional influence and distance-dependence.[5] The stronger these contacts are, the more they stabilize the inclusion compound. Some of the more important of these will now be discussed.

1.6.1 van der Waals forces

van der Waals forces are those attractive and repulsive forces experienced by atoms and molecules that arise as a result of the effect of fluctuating polarizations of nearby species, and are hence different from ionic and covalent bonds.[117] These forces have four significant contributions to the interactions between species: [118]

- They provide a repulsive component resulting from the Pauli exclusion principle that prevents the collapse of molecules;
- They constitute attractive or repulsive electrostatic interactions between permanent charges (in the case of molecular ions), dipoles (in the case of molecules without an inversion centre), quadrupoles (all molecules with symmetry lower than cubic) and, in general, between permanent multipoles; these are sometimes termed Keesom interactions or Keesom forces;
- They allow for induction (also known as polarization) as a result of the attractive interaction between a permanent multipole of one molecule with an induced multipole of another, and this is occasionally termed a Debye force; and

- They provide dispersion or London forces due to the attractive interaction between any pair of molecules, including non-polar atoms, arising from the interactions of instantaneous multipoles.

The main characteristics of van der Waals forces are that they are weaker than regular covalent and ionic bonds, are additive and cannot be saturated, and have no directional properties. These associations are all short range, and hence only interactions between the nearest particles need to be considered (instead of all the particles): van der Waals forces are therefore more significant when species are closer, and are independent of temperature except for those that are dipole–dipole in nature.[118]

1.6.1.1 Dipole–dipole interactions (Keesom forces)

Permanent dipoles occur when two atoms that are bonded together in a molecule have substantially different electronegativities: one atom attracts electron density more than the other, becoming partially-negative, while the other atom becomes partially-positive. A molecule with a permanent dipole moment is termed a polar molecule.[119] Dipole–dipole forces (5–50 kJ·mol^{-1}) result when two dipolar units interact with one another through space and, when this occurs, the partially-negative part of one polar molecule is attracted to the partially-positive part of the second polar molecule. These interactions are the weakest of the non-covalent interactions but are useful to align molecules when specific orientations are required.[120] Figure 1.13 is an example of the two types of arrangements that molecules may have in order to experience a dipole–dipole interaction.

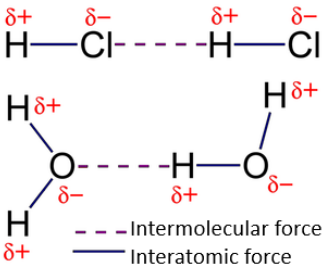

Figure 1.13. A dipole–dipole interaction between HCl, on the one hand, and H_2O on the other.[5]

1.6.1.2 The dipole–induced dipole interaction (Debye force)

These associations occur when one molecule with a permanent dipole repels and disturbs the arrangement of another's electrons, inducing a dipole moment and causing polarization.[121]

1.6.1.3 London dispersion forces

London dispersion forces are weak and arise from the interaction of instantaneous multipoles in molecules without permanent multipole moments. However, these forces dominate the interaction of non-polar molecules and are often more significant than Keesom and Debye forces in polar molecules. These associations are also known as 'dispersion forces', 'London forces' or 'instantaneous dipole–induced dipole forces'. The strength is proportional to the polarizability of the molecule (5–50 $kJ \cdot mol^{-1}$) which, in turn, depends on the total number of electrons and the area over which these extend. Any connection between the strength of the forces and mass is coincidental.[122]

1.6.2 Hydrogen bonding

Hydrogen bonds may be subdivided into three broad categories depending on their strength.[123] Strong hydrogen bonds are formed between a strong acid (donor, D, a highly electronegative atom) and a suitable acceptor (A) with the hydrogen atom close to the centre-point of the donor and acceptor atoms. The D–H···A angles of these interactions are close to linearity (160–180˚).[123] The D–A distance is specified as the difference in the sum of the van der Waals radii of D and A minus ~0.3 Å. Strong bonds (that involve O, N or S) typically measure 2.6 Å, and strong interactions of this type are often termed classical hydrogen bonds.[124] These bonds are generally stronger than ordinary dipole–dipole and dispersion forces, but weaker than true covalent and ionic bonds.[123] For example, phenol can accept and donate in a H-bonding interaction, whereas dioxane is only able to act as an acceptor as it has no hydrogen atoms bonded to the oxygen atom.[123] Moderate-strength hydrogen bonds are formed between donor and acceptor groups through electron lone pairs, and have geometries that are slightly bent (approximately 104˚).[123] Weaker hydrogen bonds are highly non-linear and involve donors and acceptors such as C–H groups, the π systems of aromatic rings and alkynes. The C–H donor hydrogen bonds are weak, but the acidity can be enhanced

if an electronegative atom is in close proximity to the carbon atom. These interactions are commonly known as non-classical hydrogen bonds.[29,125] The larger the D···A distance from the sum of their van der Waals radii, the weaker the H-bond is and, depending on the situation, they are reported up to approximately 3.2 Å (usually when C, H and O atoms are involved). Small angles have also been reported, but these are typically intramolecular in nature.[124]

Figure 1.14 illustrates the types of geometries that may exist in a H-bonding interaction, and include a) linear, b) bent, c) donating bifurcated, d) accepting bifurcated, e) trifurcated, and f) three-centre bifurcated geometries. These are primary hydrogen bond interactions because there is a direct interaction between the donor and acceptor groups. Secondary interactions may exist between neighbouring groups and should also be considered.[126]

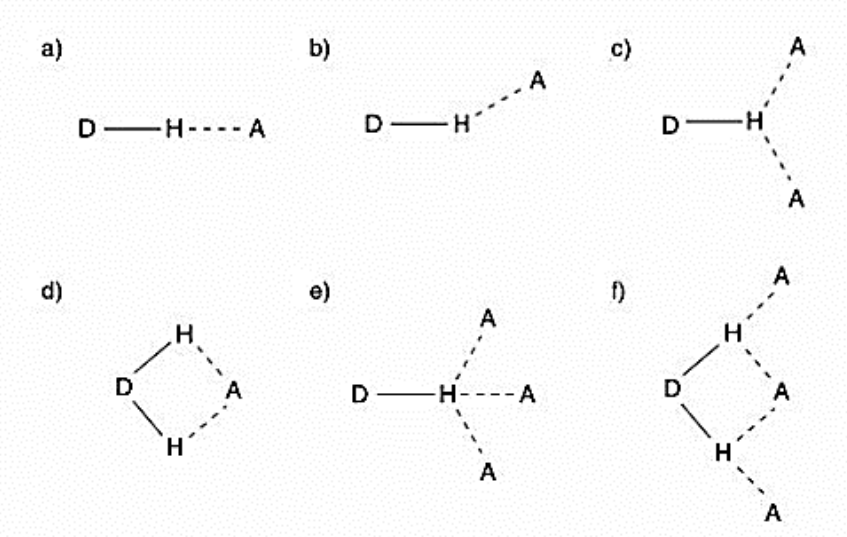

Figure 1.14. Types of geometries for hydrogen bond interactions.[71]

Hydrogen bonding is one of the strongest non-covalent interactions and can therefore play a significant role in inclusion compound formation.[29]

1.6.3 π···π interactions

Pi···pi (π···π) stacking interactions (<5 kJ·mol^{-1}) are non-covalent forces between two aromatic rings as a result of their π bonds, and often occur when one aromatic ring is electron-rich and the other electron-poor.[28] Figure 1.15 illustrates the two general types, namely face-to-face (a, b)

and edge-to-face (c, d) interactions. Specifically, these are termed a) parallel face-to-face, b) parallel face-to-face offset, c) perpendicular T-shaped edge-to-face, and d) perpendicular y-shaped edge-to-face.

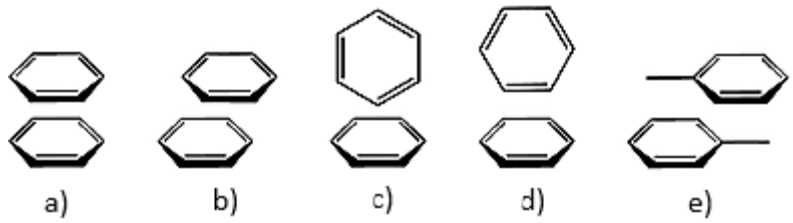

Figure 1.15. Geometries of π···π interactions.[127]

There also exists a wide variety of intermediate geometries.

The benzene dimer is a prototypical system for the study of π···π stacking interactions and is experimentally bound by 8–12 kJ·mol^{-1} (2–3 kcal·mol^{-1}) in the gas phase, with a separation of 4.96 Å between the centres of mass for the T-shaped dimer. Owing to the small binding energy, the benzene dimer is particularly challenging to study experimentally, and other evidence for π···π stacking has emanated from X-ray crystal structures.[128]

The van der Waals radius of a carbon atom is approximately 1.77 Å, and hence the shortest possible π···π interaction is twice that distance (3.54 Å); with zero offset of the aromatic rings, this would correspond to a very significant association. In practice, however, there is generally some offset and the ring planes are not co-planar, and so π···π interactions generally measure greater than 3.54 Å. Distances are usually reported up to ~6 Å, at which point the interaction would be particularly weak, while ~4 Å and less is usually associated with significant interactions.[28]

It must be noted that π···π interactions may have an accumulative effect on the stability of an inclusion compound. In some cases, weak π···π interactions have been reported and, owing to the sheer number of these, the inclusion compounds displayed enhanced stabilities.[129]

1.6.4 X–H···π interactions

The X–H···π interaction is a kind of hydrogen bond operating between a soft acid, X–H, and a soft base π-system. These include double and triple bonds, C6 and C5 aromatic rings, heteroaromatics, and the convex surfaces of fullerenes and nanotubes.[30] The H···π distance is generally reported in the range 2.6–3.0 Å, with distances shorter than <2.6 Å being referred to as strong interactions; these are generally associated with linear X–H···π angles, but large deviations from 180˚ have also been reported.[30]

1.6.5 Other short contacts

Other short contacts not reflected in the previous discussions may also be present between the guest and host when the distance measures less than the sum of the van der Waals radii of the interacting atoms.[1] In practice, significant interactions (<) denote contacts less than the sum of the van der Waals radii and very significant (<<) contacts are this sum minus 0.2 Å. Weak associations of these types may also be accumulative in their stabilizing of the inclusion compound.[129]

1.6.6 Hydrophobic interactions

Hydrophobic interactions describe the association between water-soluble and low water-soluble molecules (hydrophobes). Hydrophobes are non-polar molecules and usually have long carbon chains that do not interact with water molecules. They are excluded from the water matrix when they encounter one another, and the hydrophobes then combine and form one larger hydrophobic region. This combined state is more energetically-favourable than the one in which they were separate, and therefore this combined state will persist.[130,131] Hydrophobic interactions are more correctly termed hydrophobic exclusions.

1.6.7 Crystal close-packing

Crystal close-packing may be described by considering the close-packing theory of Kitaigorodsky,[132] which explains that as molecules pack together, each one fits into the hollows of an adjacent one so that the maximum number of favourable intermolecular contacts may be achieved; this means that molecules tend to pack with maximum density to

minimize free, empty volume. In host-guest chemistry, this “optimal packing” will also occur to form the most stable inclusion compound.[133]

1.7 Preparation of host-guest inclusion compounds

1.7.1 Methods

There are various methods that may be employed to form host-guest inclusion compounds, and these depend largely on whether the guest is in the gas, liquid or solid phase.[54,134,135]

1.7.1.1 Recrystallization

Inclusion compounds may be prepared by dissolving the solid host material in an excess of the guest in the liquid phase. The solution may be heated to assist with host dissolution and, if a minimal amount of the guest is used, crystallization ensues much more rapidly than for a large excess of guest. If both host and guest are solids, a solvent may be employed which dissolves both species, and it is essential that this solvent be, itself, not included by the host.[135] After crystallization, the so-formed solids are usually isolated by vacuum filtration, crushed and thoroughly washed with an appropriate solvent to remove any superficial guest solvent on the host crystal surfaces.[3,71] Owing to its simplicity, this method is the more common one.[136]

1.7.1.2 Gas inclusion

Inclusion compounds may also be formed when the solid host absorbs volatilized guest molecules from the surroundings.[137,138] A memory effect in solid host compounds has recently been observed with calixarenes and vaporous guests,[139] where the host retains its affinity for previously included guest compounds. Inclusion trends from the gas phase are related to both the interactions and structure of the host and guest. Other studies have investigated the structure and kinetics involved in this type of inclusion,[140] guest exchange within systems in the gas phase,[141] using clathrates as gas sensors,[137,138,142] and the possibility of gas storage.[143]

1.7.1.3 Solid-state inclusion complex formation

Inclusion compounds may be prepared from solid host and solid guest compounds by shaking and/or grinding a mixture of the two components.[144,145] In some cases, these solid-state methods have offered advantages relative to other known synthetic approaches to form inclusion complexes:[146] for example, it was observed that mechanochemical reactions may enhance chemical reactivity and produce compounds that have improved solubility.

1.7.2 Solubility

Guest solvents in which the hosts are moderately soluble are ideal in order to form crystals that are large enough for single crystal diffraction analyses.[3] However, host-guest compounds are not always highly crystalline, and resultant complexes may be in the form of powders. If the host compound is too soluble in the guest solvent or if supersaturated solutions are formed, the resulting crystals tend to be small and, in these cases, powder diffraction may be the analytical technique of choice.[147] The solubility may also be manipulated through the addition of co-solvents.[148,149]

1.7.3 Nucleation

Nucleation sites are those sites at which crystallization is initiated from a solution.[3] The manipulation of nucleation is often used to regulate the crystal shape of the resulting inclusion compounds.[150] Dust particles that may be present in the vessel may provide sites of nucleation, and hence it is essential to minimize this and other extrinsic particulate matter in the crystal-growing vessels. It has been reported that all of the host and guest must be completely dissolved to ensure crystallization of the desired material.[151]

1.7.4 Optimization of crystallization

Many methods have been investigated to improve the speed and quality of crystallization, and techniques that have been compared are solvent evaporation, slow cooling of the solution, solvent/non-solvent diffusion, vapour diffusion and sublimation, and many variations of these. It has been reported that when considering the selection of a crystallization method, the preferred one should always be based on the materials that are

being investigated, considering the solubility and ratio of these within the mixture.[152] Naturally, the crystal quality is important when single crystal diffraction is utilized as the analytical technique.

1.7.5 Competition experiments

Host compounds often alter their behaviour when presented with multiple guest species simultaneously.[153,154] Complexation experiments where guests are mixed and the host presented with this mixture provide information regarding host selectivity, that is, whether the host favours any one particular guest species present. These experiments are carried out in much the same manner as the single solvent recrystallizations but the host is recrystallized from equimolar or non-equimolar guest-solvent mixtures in this instance.[155]

1.7.6 Selectivity profiles

Binary competition experiments where the concentration of the two guests is varied beyond equimolar have provided useful information about the selectivity of the hosts in these conditions.[156,157] The procedure requires one to set up a series of samples in which pairs of guest compounds, A and B, can cocrystallize with the host (H). The process may be represented by Equation 1.2:

$$H\ (\alpha, s) + nA\ (l \text{ or } g) + mB\ (l \text{ or } g) \rightarrow H{\cdot}A_n\ (s, \beta) + mB\ (l \text{ or } g) \qquad \text{Equation 1.2}$$

Here, H represents the apohost in its non-porous α-phase which, when mixed with A and B, selects A and forms a solid inclusion compound $H{\cdot}A_n$, and excludes B.[158] However, in practice, when the host is exposed to a mixture of A and B, the crystals that are isolated more usually contain both guests, with one normally being favoured over the other. The amount of guest A (or B) in the resulting crystals (Z) and in the mother liquor from which these formed (X) are analysed and used to plot Z vs. X in order to provide selectivity profiles for each binary experiment. These profiles generally show one of three trends, as illustrated in Figure 1.16.

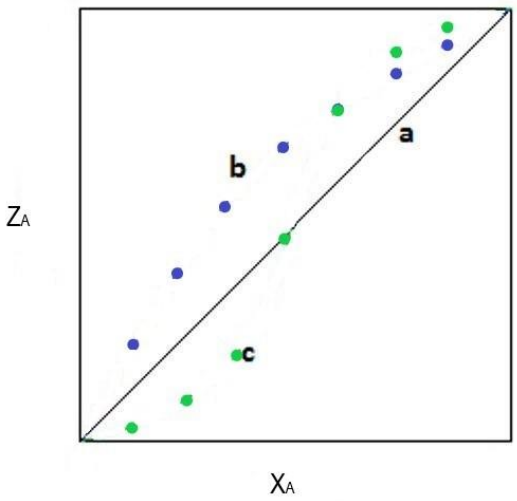

Figure 1.16. General selectivity profiles that may result from non-equimolar guest/guest competition experiments.

The selectivity coefficient may be defined by Equation 1.3:[159]

$$K_{A:B} = Z_A/Z_B \times X_B/X_A, \text{ where } X_A + X_B = 1 \qquad \text{Equation 1.3}$$

X_A represents the mole fraction of guest A in the liquid mixture and Z_A that of guest A enclathrated in the crystal. In Figure 1.16, profile 'a' represents no selectivity and $K_{A:B} = 1$, 'b' results when A is preferentially enclathrated to B over the entire concentration range, while 'c' is obtained when the selectivity is guest-concentration dependent. Co-solvents have been found to alter the shape and position of these selectivity profiles.[159]

1.8 Release of guest from the host cavities/channels

The number of methods that may be employed to release the guest from the host crystal are limited.[3] Here we discuss only the more common strategies to achieve this separation.

1.8.1 Spontaneous release or heating

When a solid inclusion compound (β-phase) is formed between a host and a volatile guest, it may decompose in several ways, either spontaneously or upon heating. Upon decomposition, the guest molecules are released, and the host may return to its original non-porous α-phase. Equation 1.4 represents this process.

$H{\cdot}A_n$ (s, β) → H (*s*, α) + nA (*l* or *g*) Equation 1.4

Alternatively, when the guest is released, the host may not collapse and may retain the features it possessed in the complex, giving rise to an empty cage- or channel- like structure (β_0) (Equation 1.5). This phenomenon is observed in the desorption of zeolites.[160] The process is reversible, and the removal and re-absorption of guests in such solids without the collapse of the cages or channels is a much less common occurrence in molecularly-derived inclusion compounds. Some coordination and hydrogen-bonded networks can rapidly exchange inclusions or counterions while maintaining crystal integrity, and this represents an important step towards a new class of microporous materials.[160]

$H{\cdot}A_n$ (*s*, β) → H (*s*, β_0) + nA (*l* or *g*) Equation 1.5

Inclusion compounds may also release only some of the guest present, thus giving rise to a new γ-phase (Equation 1.6).

$H{\cdot}A_n$ (*s*, β) → HA_m (*s*, γ) + (n-m)A (*l* or *g*) n > m Equation 1.6

Furthermore, the guest may be released by subjecting the inclusion compound to vacuum distillation with gentle heating under reduced pressure. The increased energy provided to the complex in this way mobilizes it and, if sufficient energy has been provided, the guest may escape from the host crystal. The crystal structure may also be disturbed under these conditions, further simplifying the guest release process. The vaporous guest may then be condensed and collected in a collecting vessel.[161] The same mechanism of release through heating is experienced during differential scanning calorimetry and thermogravimetric analysis, but these are not normally conducted under reduced pressure.[162]

1.8.2 Chromatographic techniques

Another procedure often used in order to separate host from guest is column chromatography,[163,164] where the stationary and mobile phase combination affords this separation while in the column, and the host and guest may then be collected as separate fractions. This method usually affords efficient separations, is relatively facile, and depends on the individual interactions of the guest and host molecules (which are dissolved in a mobile

phase) with the stationary phase in the column. The compound that interacts more closely with the stationary phase will be retained and therefore elute last, while the compound that interacts less closely with the stationary phase will elute first. This principle applies to gas chromatography (where the mobile phase is a gas) and high-performance liquid chromatography (HPLC) (where the mobile phase is a liquid).[165] In Figure 1.17, a representative diagram for column chromatography is provided, where the host and guest compounds in the mobile phase are separated from one another by distinct interactions with the stationary phase.

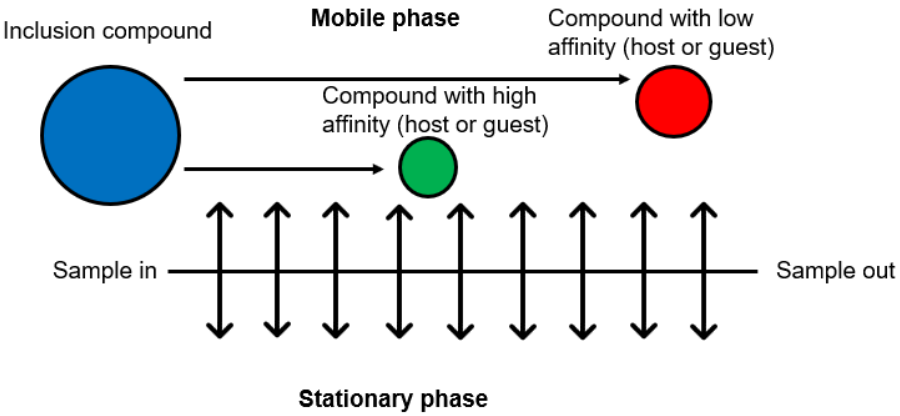

Figure 1.17. Separation of the constituents of inclusion compounds using chromatography.

Other methods involve structural changes in the host or guest molecule, and these include decomposition of the host molecule,[166] photo-induced rearrangements of the inclusion compound,[167,168] and protonation by control of the pH.[169]

1.9 Analysis of host-guest inclusion compounds

Many techniques exist to assist in analysing the hosts and so-formed host-guest inclusion compounds.

1.9.1 Nuclear magnetic resonance (NMR) spectroscopy

NMR spectroscopy is an analytical tool that uses the magnetic properties of specific atomic nuclei (e.g., ^{1}H and ^{13}C) to determine the physical and chemical environment of atoms based on their interaction with an external magnetic field. It can provide detailed information about

the structure, dynamics, reaction state, and chemical environment of atoms. The intramolecular magnetic field around an atom in a molecule changes the resonance frequency applied during these experiments, and this is analysed and interpreted to yield structural information about these compounds.[170]

Proton (^{1}H) and carbon (^{13}C) NMR experiments, and various other related NMR techniques (e.g., COSY, NOESY and HETCOR), may be used to confirm the identity of the host compound.[170] ^{1}H-NMR spectroscopy is also utilized to confirm the inclusion of a guest species and, where complexation was successful, the H:G ratio through integration of relevant host and guest signals.[155,171] This technique may also be employed for the determination of host-guest binding constants by means of titration experiments.[172]

1.9.2 Single crystal X-ray diffraction (SCXRD)

SCXRD is an analytical technique utilized in the phase identification of a crystalline material and can provide information on unit cell dimensions. It remains a conventional technique for the analysis of crystal structures and atomic spacing,[173] and is based on the interaction of monochromatic X-rays and the crystalline sample, which produces constructive interference and a resulting diffracted ray when conditions correlate with Bragg's Law ($n\lambda=2d\sin\theta$). This law is used to relate the wavelength of electromagnetic radiation to the diffraction angle and the lattice spacing in a crystalline sample. The diffracted X-rays are detected, processed, and converted to d-spacings, which allows for the identification of the compound since each has a unique set of d-spacings.[173]

1.9.2.1 Crystal Explorer: Hirshfeld surface analysis

Crystal Explorer[174] is a standard software tool for investigating intermolecular interactions and packing in crystalline materials by means of Hirshfeld surface analysis. Hirshfeld surfaces are generated around molecules by using computational methods based on quantum chemistry. The software maps these surfaces and other distance- and curvature- related metrics to provide unique insights into the in-crystal environment. Furthermore, the software may be used to display and quantify voids in crystal structures, and to accurately and efficiently calculate intermolecular interaction energies and energy frameworks which are

displayed as 2D fingerprint plots.[175] These plots indicate which intermolecular interactions and how much of each are present, and also the relative area of the surface that corresponds to each interaction type, and this is typically related to host behaviour.[176,177,178]

1.9.2.2 Lattice energies

The lattice energies of crystalline organic compounds may be calculated by simple atom–atom potential energy functions using Coulombic terms with point-charge parameters. The software PIXEL® collects these data and obtains Coulombic, polarization, dispersion and repulsion lattice energies.[179] The energies, as measured by the method of atom–atom potentials, have been shown to correlate with the thermodynamics of the guest-release process as well as the selectivity that a given host displays for a particular guest.[180]

1.9.3 Thermal analysis (TA)

TA experiments allow for the measurement of changes in the physical properties of a compound as a function of temperature while the compound is subjected to a controlled temperature programme.[181] Thermogravimetric (TG) analysis measures the mass loss that a sample experiences during the heating process and may be used to confirm complexation, the H:G ratio, the nature of the guest-release process (whether single- or multi- stepped), and also the guest-release onset and peak temperatures (T_{on} and T_p, respectively).[182,183,183] Differential scanning calorimetry (DSC) compares either the heat flow or the power compensation to correct the difference between the sample and reference material as heat is applied. Depending on the method used, this heat flow or power input is related to the enthalpy of the process, which provides information about the thermal event that is taking place.[180] T_{on} and T_p have been related to the relative thermal stability of inclusion compounds,[184] while T_{on}–T_b, where T_b is the boiling point of the pure guest solvent, has been shown to be a useful measure of the relative thermal stabilities of inclusion compounds that possess isostructural host packing.[136]

1.9.4 Infrared (IR) spectroscopy

IR spectroscopy is a technique that measures the absorption of IR radiation by a sample as a function of the wavelength and is used to characterize the inclusion complex or the individual

host or guest species. The resulting spectrum may be used to identify functional groups, confirm inclusion and convey information about the interactions present, both host–guest and host–host in nature.[185]

1.9.5 Gas chromatography-mass spectrometry (GC-MS)

GC-MS is an analytical method that is used to identify different substances within a sample.[186] In GC, the mobile phase is an inert carrier gas such as helium or nitrogen. The stationary phase consists of a microscopic layer of liquid or polymer on an inert solid support inside glass or metal tubing called a column.[187] The compounds being analysed are volatilized and interact with the stationary phase: different compounds interact differently and therefore elute at different times. GC is applicable to host-guest systems when mixed complexes with overlapping guest/guest or host/guest resonance signals on the ^{1}H-NMR spectra prevent quantification through integration of such signals.[187]

MS involves the bombardment of samples with high energy electrons which causes fragmentation of the sample. The resulting fragmentation patterns can be analysed and may allow sample identification. The mass spectrum, obtained from a mass spectrometer, is a plot of the ion signal as a function of the mass-to-charge ratio of the sample fragments.[188] This tool is commonly employed to confirm the structure of the different compounds in mixed inclusion complexes.

1.9.6 Powder X-ray diffraction (PXRD)

PXRD is a scientific technique that utilizes X-ray, neutron or electron diffraction on powders or microcrystalline samples for the structural characterization of materials. A comparison of powder patterns provides information on the packing of the host compound. Powder diffraction is useful when inclusion compounds do not form crystals of suitable quality for SCXRD, and may also be employed to ensure that results from SCXRD experiments are representative of the bulk of the solid since a larger quantity of the sample is analysed.[189]

1.10 Applications of host-guest chemistry

The leading and most relevant applications of host-guest chemistry will now be discussed.

1.10.1 Pharmaceutical applications

1.10.1.1 Chiral resolution

Many pharmaceutical drugs are chiral and are prescribed in their racemic form. However, usually only one enantiomer has the desired therapeutic effect, and the other may have no, some, or harmful effects.[190,191] It would therefore be advantageous to prescribe chiral drugs in optically pure form. However, enantiomers are difficult to separate due to their identical physical properties. Host-guest chemistry may successfully play a resolution role in the presence of such drug racemates, but the host compound itself must be chiral and optically pure. As an example, Kuhn *et al*[70] have successfully resolved the drug (±)-quinagolide by host-guest complexation with CD's and crown ethers using capillary zone electrophoresis.

1.10.1.2 Drug transport and solubility

Another pharmaceutical application of host-guest chemistry is the employment of applicable hosts for complexion with *in vivo* drugs to aid in drug solubility and transport. Caira *et al*[192] showed that complexation of CD's heptakis(2,6-di-*O*-methyl)-β-CD (DIMEB) and heptakis(2,3,6-tri-*O*-methyl)-β-CD (TRIMEB) with the potent anti-cancer agent, 2-methoxyestradiol, improved the aqueous solubility of the drug significantly. Formation of the 2:1 H:G inclusion compound, prepared by two methods, assisted in very rapid dissolution in water at 37 °C relative to untreated 2-methoxyestradiol. The solubility of the antioxidant *R*-(+)-α-lipoic acid was also improved by complexation with permethylated α- and β- CD's.[193] Additionally, local anaesthetics that have a relatively short duration of action may have adverse side-effects such as cardiac and neurological toxicity, and may be accompanied by allergic reactions. Danylyuk *et al*[194] demonstrated that a slow and controlled release of different anaesthetic drugs by supramolecular encapsulation within macrocyclic host molecules such as CD's, *para*-sulfonatocalix[*n*]arenes and cucurbit[7]uril may be achieved, and this alleviates the harmful side-effects. Terpenes and their derivative terpenoids are constituents of essential oils with possible applications in the pharmaceutical industry but,

unfortunately, these are limited due to their high volatility. Complexation with α-, β- and γ-CD's has proven to assist in overcoming this problem as well as to enhance the water solubility and bioavailability of these guest types.[195]

1.10.1.3 Drug stability

The stability of drugs may be manipulated by complexation of the active ingredients with designed host materials. Albendazole (ABZ) is a medication used for the treatment of a variety of parasitic worm infestations. The inclusion compound of cucurbit[7]uril (CB7) with ABZ in the solid state was prepared by freeze drying. X-ray diffraction and thermal analyses showed that this complexation significantly improved both the thermal and physical stabilities of the ABZ drug.[196]

1.10.1.4 Drug resistance

Drug resistance is the reduction in effectiveness of a medication, such as an antimicrobials or antineoplastics, in treating a disease or condition, and is currently a serious worldwide problem.[197] Tuberculosis is an infectious disease caused by various strains of mycobacteria, and the treatment requires a combination of several drugs. Isoniazid (INH) was first introduced for the effective treatment of tuberculosis in 1952, but there is a growing problem with drug resistance to the two most effective drugs, namely INH and rifampicin. Therefore, new pharmaceutical formulations of anti-tubercular antibiotics with prolonged activity and improved properties are crucial. The supramolecular complexation of active pharmaceutical ingredients with macrocyclic host molecules offers the opportunity to manipulate the physicochemical properties of pharmaceutical agents, improve bioavailability and reduce side-effects. Gao *et al*[198] showed that the complexation of INH with the host tetramethyl-cucurbit[6]uril increased the effectivity of the drug.

1.10.2 Isomeric separations

The ability to efficiently separate constitutional isomers remains a significant challenge to industrial chemists because such compounds often have near-identical physical properties. More effective and inexpensive processes are thus always being sought. For example, the separation of positional isomers such as the xylenes (*o*-xylene, bp 144.4 °C, *m*-xylene, bp

139.0 °C and *p*-xylene, bp 138.4 °C) is not trivial.[5] Lusi and Barbour utilized the Werner host, $Ni(NCS)_2$(*para*-phenylpyridine)$_4$, to selectively enclathrate *o*-xylene in preference to *m*- and *p*-xylene from an equimolar ternary mixture, and *m*-xylene in preference to *p*-xylene from a vaporous binary mixture.[199] Effective separations of these isomers are critical in that they serve as chemical building blocks for an array of important commercial products. Not only do the xylenes present a problem with respect to their separation, but other isomers as well, such as the cresols and dihydroxybenzenes,[200] to mention just two. Host-guest chemistry may successfully be applied to address this challenge.

1.10.3 Chemical sensors and the removal of hazardous materials

Host-guest systems have been utilized to remove hazardous materials from the environment. Pyka *et al*[201] demonstrated that the combination of an (−)-isosteviol-derived building block and a 9,9'-spirobifluorenyl or tetraphenylmethyl unit generated a highly effective host with enhanced selectivities for volatile organic compounds, which could be used in their detection. When host molecules are able to include guests from the gas phase, they may be utilized as chemical sensors. Dickert *et al*[142] synthesized *para*-cyclophane hosts that could identify solvent vapours based on different functionalities. With hosts in the solid phase, this principle is also effective to remove carcinogenic aromatic amines and their *N*-nitroso derivatives from water: these waste materials are used in many industrial processes and are found in a variety of products such as pesticides, drugs and cosmetics.[202,203]

1.10.4 The food, cosmetic and toiletry industries

The molecular encapsulation of lipophilic food ingredients by hosts such as the CD's has demonstrated an improvement in the stability of flavourants, vitamins, colourants and unsaturated fats, both in a physical and chemical sense, leading to an extended product shelf-life. Accelerated and long-term storage stability test results showed that the stability of host-entrapped food ingredients surpassed that of the traditionally-formulated ones.[204] Other methods of complexation include spray drying, freeze drying, fluidized-bed coating, extrusion, cocrystallization, molecular inclusion, and co-acervation.[205]

This application of host-guest chemistry is also relevant in cosmetics and toiletries. Enclathration by CD's has been shown to eliminate undesirable odours, stabilize fragrances and dyes, and reduce foaming in these consumables.[206]

1.10.5 Chromatography

Chiral and optically pure host compounds that are able to separate enantiomers through host-guest chemistry also have application in chromatographic techniques such as GC and HPLC. Lynn *et al*[207] employed host-guest complexation for the total optical resolution of amine- and amino- ester salts by GC. The host was applied as the stationary phase which demonstrated selectivity for one of the constituents of the racemic mixture.

1.10.6 Asymmetric synthesis

Asymmetric synthesis can be defined as a chemical reaction or sequence in which one or more new elements of chirality are introduced into in a substrate molecule, producing stereo-isomeric (enantiomeric or diastereoisomeric) products in unequal amounts.[208]

Organic hosts may be used as catalysts in organic synthesis and can also be modified with some transition metals to form new catalysts; furthermore, they are widely used as phase-transfer catalysts for the synthesis of specific products.[208] Host molecules may interact with guest molecules with definite stability, selectivity and kinetic features, react with them and, finally, release the products. The host molecule is thus regenerated in the process.[208]

CD's have been used as chiral "reaction vessels" for the asymmetric oxidation of aryl alkyl sulfides in moderate to poor enantiomeric excesses by Drabowicz[209] and Czarnik.[210] In recent years, Shen *et al*[211] designed and synthesized a series of amino alcohol-modified β-CD's for asymmetric oxidations in water. Park and coworkers[212] investigated the asymmetric reduction of various prochiral ketones with sodium borohydride using β-CD and its derivatives as a chiral template. It was discovered that the enantioselectivity in the asymmetric reduction of ketones to secondary alcohols was dependent on the structures of hosts and ketones, as well as the reaction temperature. CD's have also been employed in asymmetric addition reactions. Pitchumani *et al*[213] studied the asymmetric Michael addition of nitromethane and aliphatic thiols in aqueous media using per-6-amino-β-CD (per-6-ABCD) as a chiral base

catalyst. The better enantiomeric excess was observed in water at room temperature with good yield, and the catalyst could be recovered.

1.10.7 Gas storage

There exists a need for alternative methods of natural gas storage. The most common methods involve the use of underground gas reservoirs which are injected with gas, or naturally-occurring rock and salt formations.[214] These methods are not ideal because of the effect it has on the environment and the economic implications of gas extraction. Host-guest chemistry, however, offers a cost-effective and straightforward method for gas storage. Natural gas hydrates are ice-like structures in which gas, most often methane, is trapped. Gas hydrates are highly flammable, a property that makes these crystalline structures both an attractive future energy source and a storage mechanism. Gas hydrates are possible for methane,[215] ethane and propane,[216] hydrogen,[217] nitrogen and carbon dioxide.[218]

1.11 Feasibility of this research

1.11.1 Host design

Xanthone-derived compounds have been the subject of several investigations for many years.[10,219] Many studies have been conducted using 9-hydroxy-9-phenylfluorene (**20**), which was determined to be a highly efficient host compound, including a wide range of guests such as alcohols (methanol, ethanol, *i*-propanol, *t*-butanol), tetrahydrofuran (THF), acetone, dimethylformamide (DMF), dimethyl sulfoxide (DMSO), and diethyl ether, amongst others.[53]

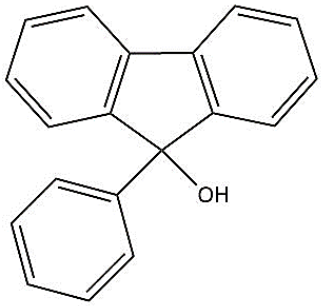

20

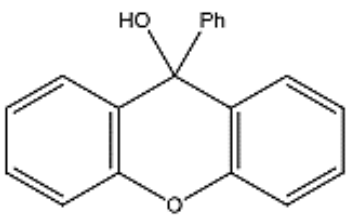

21

Related compounds, 9-phenyl-9-hydroxyxanthene (**21**) and various derivatives thereof (**22**), have also been investigated as hosts.[54,55] The free aromatic moiety in the model compound may readily be derivatized by introducing various substituents.[54] Furthermore, the thioxanthenyl equivalent **23** has also been reported to have highly efficient host behaviour.[10]

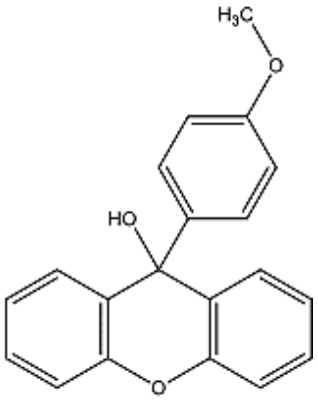

22

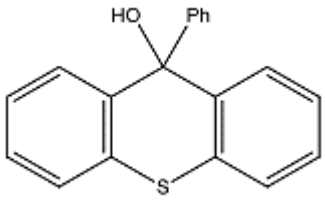

23

From these reports, it was clear that these fused-ring compounds possess structural rigidity that enhances the crystallinity of the compounds and which, in turn, favours host ability.[10] The aromatic rings and hydroxyl group were suggested to increase the possibility of stabilizing intermolecular interactions. Furthermore, the hydroxyl functionality presented further derivatization potential. These considerations thus resulted in the synthesis of compounds **24** and **25**.[10]

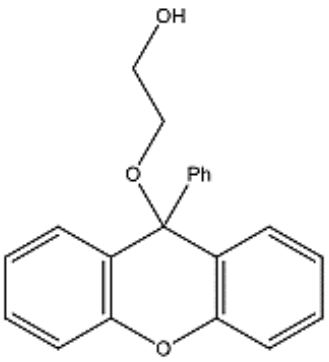

24

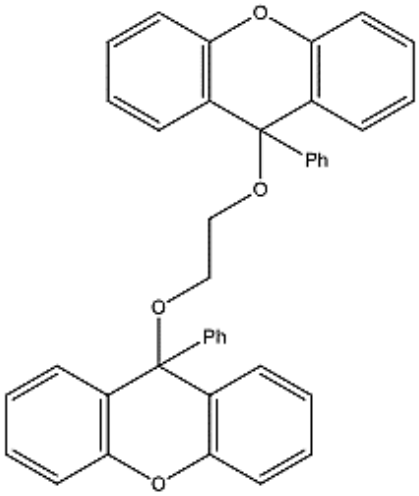

25

However, both **24** and **25** were found to be unsuccessful as host compounds, and no guest inclusion was observed. Subsequently, Barton *et al*[220] successfully synthesized compounds **21**

and **23**, and from these their diamino-bridged analogues **H_1** and **H_2**, respectively[221] [*N*,*N*′-bis(9-phenyl-9-thioxanthenyl)ethylenediamine (**H_1**) and *N*,*N*′-bis(9-phenyl-9-xanthenyl)ethylenediamine (**H_2**)]. Both **H_1** and **H_2** demonstrated significant host ability in the presence of a number of different guest compounds.

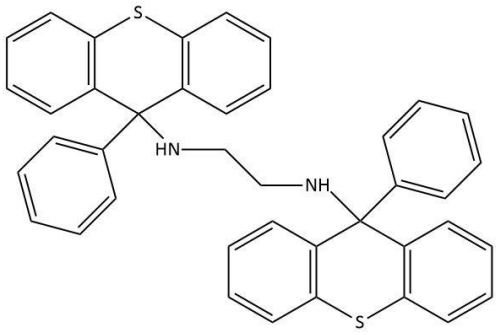

H_1

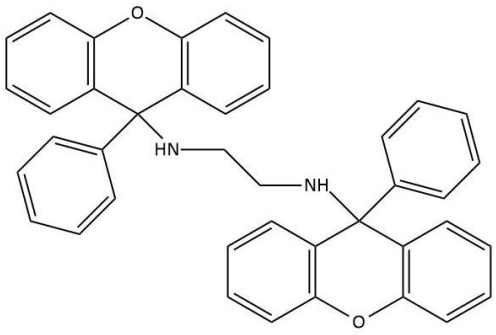

H_2

However, the aptitude of **H_1** and **H_2** for guest separations has never been considered, and this is the focus of the current investigation.

1.11.2 Guest selection

In this work, guests were selected largely based on their industrial relevance, and whether there exists a need to offer alternative separation strategies towards their separation from their isomers or related compounds. Other non-isomeric but related guests were also investigated for the purposes of comparisons in the host behaviour between **H_1** and **H_2**, and it was envisioned that such assessments would increase the knowledge domain of such systems in the host-guest chemistry field.

H_1 and **H_2** will be presented with one or more guests from each of the following guest series', and their host ability will be observed and compared.

- Xylene isomers and ethylbenzene
- Methylanisole isomers and anisole
- Methylpyridine isomers and pyridine
- Methylcyclohexanone isomers and cyclohexanone
- Heterocyclic six-membered ring molecules
- Heterocyclic five-membered ring molecules

- Alkyl-substituted benzene derivatives
- Aniline and *N*-alkyl-substituted derivatives
- Dihaloalkane derivatives
- Miscellaneous guests

1.12 Aims and objectives

Compounds **H_1** and **H_2** have never been assessed for their potential application in isomer and related guest separations. Many relevant organic compounds are found in mixtures that are difficult to separate, and this project therefore centres around alternative separation strategies employing **H_1** and **H_2** using host-guest chemistry principles. This study therefore aims to investigate the feasibility of separating isomers and structurally-related compounds with similar physical and/or chemical properties as provided in the guest series' just listed. Various analytical methods will be employed to analyse any successfully-formed inclusion compounds, and these data will be used to elucidate selectivity and inclusion trends. The inclusion ability of **H_1** will also be compared with that of **H_2** based on the results obtained from comparable guest solvent experiments, and these data related back to host structure and design.

In this work, the extent of host inclusion and guest separation will be examined by means of ^{1}H-NMR spectroscopy and/or GC-MS analyses, as applicable. Host selectivities will be further assessed by constructing selectivity profiles and carrying out guest/guest competition experiments. Any crystalline complexes formed with suitable crystal quality will be analysed using SCXRD to determine the nature of any significant H···G interactions present. Hirshfeld surface analysis of the successfully-formed complexes will additionally be considered. DSC and TG experiments will be employed to provide information on the thermal events experienced by the complexes as they are heated, as well as their relative thermal stabilities. Where applicable, PXRD will be employed to analyse complexes that are formed using guests in the gas phase. The results of this work will therefore provide novel insights into the effect of changes in host structure (**H_1** relative to **H_2**) with host behaviour and will, furthermore, demonstrate whether these hosts have the ability to separate industrially-relevant and other guest mixtures.

2. EXPERIMENTAL

2.1 Instruments

The following instruments and methods were used to complete this research project:

^{1}H-, ^{13}C- and DEPT NMR spectroscopy experiments were carried out by means of a 400 MHz Bruker Ultrashield^{TM} 400 plus spectrometer. Data were analysed using TopSpin3.2 software.

All IR spectra were obtained by means of a Bruker Tensor 27 Fourier Transform Infrared spectrophotometer after data analyses using OPUS software.

Melting points were recorded using a Stuart SMP10 digital melting point apparatus, and these are uncorrected.

Single crystal X-ray diffraction (SCXRD) experiments were conducted using a Bruker Kappa II diffractometer with graphite-monochromated Mo Kα radiation (λ = 0.71073 Å) at 200 K. APEXII[222] and SAINT[222] were used for data collection, and cell refinement and data reduction, respectively. SHELXT-2015[223] was used to solve the structures, and refined by least-squares procedures using SHELXL-2015[224] together with SHELXLE[225] as a graphical interface. All non-hydrogen atoms were refined anisotropically. Carbon-bound hydrogen atoms were added in idealized geometrical positions in a riding model, while nitrogen-bound hydrogen atoms were located on the difference Fourier map. Data were corrected for absorption effects using the numerical method implemented in SADABS.[222] Many of these structures were deposited at the Cambridge Crystallographic Data Centre [CCDC] and the applicable CCDC numbers are provided in the respective chapters.

Powder X-ray diffraction (PXRD) experiments were completed using a Bruker D2 PHASER X-ray diffractometer.

Thermal analyses were carried out by means of a TA SDT Q600 module system or a Perkin Elmer STA 6000, and the data were analysed using TA Universal data analysis or Pyris software, respectively. Samples were placed in open ceramic or platinum pans with an empty

pan functioning as a reference. High purity nitrogen gas was used as purge gas. The ramp rate was 10 °C·min^{-1} from room temperature to approximately 250 °C.

GC-MS experiments were carried out by means of an Agilent 7890A gas chromatograph coupled with an Agilent 5975C VL mass spectrometer. Helium was used as carrier gas. The following programs were used in relevant chapters of this thesis:

Chapter 3: An Agilent J&W DB-WAX column was used. From an initial temperature of 50 °C, a heating rate of 0.5 °C·min^{-1} was employed up to 60 °C, with a final hold time of 1 min.

Chapter 4: An Agilent J&W DB-WAX column was used. From an initial temperature of 65 °C, a heating rate of 2 °C·min^{-1} was employed up to 95 °C, with a final hold time of 1 min.

Chapter 5: An Agilent J&W DB-WAX column was used. An initial temperature of 50 °C was maintained for 5 min, and then a heating rate of 5 °C·min^{-1} was employed up to 60 °C, with a hold time of 5 min. Subsequently, a heating rate of 5 °C·min^{-1} was employed up to 80 °C, with a hold time of 5 min. Thereafter, a heating rate of 5 °C·min^{-1} was employed up to 180 °C, with a hold time of 5 min.

Chapter 6: An Agilent Cyclosil-B column was used. From an initial temperature of 50 °C, a heating rate of 5 °C·min^{-1} was employed up to 60 °C. Subsequently, a heating rate of 5 °C·min^{-1} was employed up to 80 °C, with a hold time of 5 min. Thereafter, a heating rate of 5 °C·min^{-1} was employed up to 105 °C.

Chapter 8: An Agilent Cyclodex-B column was used. From an initial temperature of 60 °C, a heating rate of 3 °C·min^{-1} was employed up to 150 °C, with a final hold time of 2 min.

Chapter 9 and 10: An Agilent ZB-5MSi column was used. From an initial temperature of 50 °C, a heating rate of 15 °C·min^{-1} was employed up to 200 °C, with a final hold time of 1 min.

2.2 Hirshfeld surface analyses

Hirshfeld surface analyses were carried out on relevant inclusion compounds, and surfaces were constructed around the guest species using Crystal Explorer software.[226] These 3D data were translated into 2D fingerprint plots for ease of interpretation. The plots represent the

distances to the nearest atom outside (de) and inside (di) the created surface. Unique plots were also constructed if guests were disordered: each disordered component was considered independently by deleting each in turn and constructing surfaces around the remaining component.

2.3 Stereoviews

All stereoviews of complexes were generated by means of X-seed[227] and POV-ray[228] software.

2.4 Computational methods

The crystal structure .CIF files of the host compounds and their resulting host-guest complexes were converted into Xmol format[229] via Mercury software[230] to enable opening with Spartan '16 molecular modelling software.[231] In Spartan, the guest molecules were removed in each case, and where the unit cells possessed more than one host molecule, each molecule was considered separately. The carbon–carbon bond types in the aromatic rings were corrected from 'single' to 'aromatic'. Initially the coordinates of the heavy (i.e., non-hydrogen) atoms were fixed while the positions of the hydrogen atoms were optimized at the molecular mechanics (MMFF94) level. Next, the frozen atoms were relaxed and further MMFF94 geometry optimization was carried out to a gradient tolerance level of 1×10^{-6}. The MMFF94 structures were further refined at the DFT level, successively applying B3LYP/6-31G*and ωB97X-D/6-31G* methodology, firstly with the heavy atoms frozen, and secondly as fully relaxed systems. Energies were determined through single-point calculations performed on the ωB97X-D/6-31G* geometries at the ωB97X-V/6-311+G(2df,2p) level. Geometry optimizations were also performed on selected structures at the latter level. Conformer distributions for the host compounds were determined at the MMFF94 level, followed by geometry refinement at the DFT levels as previously described. In all cases, the energies and relevant structural features were determined. All torsion angles were assigned according to Newman projections (Figure 2.1) in order to describe the geometric relations of the units in the host compounds.

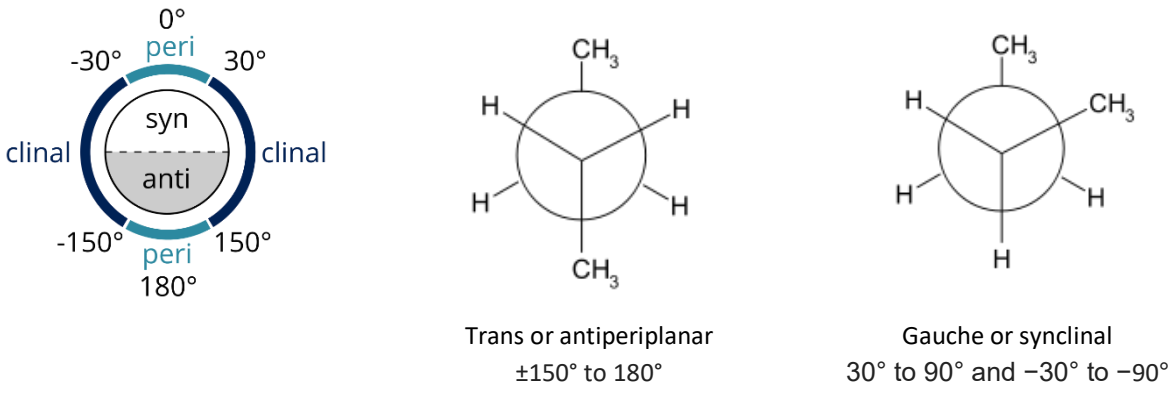

Figure 2.1. Configuration names according to dihedral angle (using the butane molecule as example).

2.5 General synthetic procedures

2.5.1 Grignard reactions to afford alcohols (General Procedure 1)

Magnesium turnings and two iodine crystals were added to a 250 mL round-bottomed flask and these covered with dry THF. A small amount of bromobenzene (1 mL), mixed in dry THF (1 mL), was added to the round-bottomed flask using a dropping funnel. The mixture was stirred until a colour change was observed (from yellow-brown to grey). The remainder of the bromobenzene, diluted with an equal volume of dry THF, was then added dropwise to the flask so as to maintain a steady reflux of the mixture, followed by a 30 min reflux period. The thioxanthone or xanthone, dissolved in THF (30 mL), was added dropwise to the cooled reaction mixture in the round-bottomed flask. After this addition, the mixture was heated under reflux for 1 h, poured into 10% aqueous ammonium chloride (200 mL) and extracted with ethyl acetate (3 x 25 mL). The organic extracts were combined, dried and concentrated to afford a solid product that was purified by recrystallization.

2.5.2 Perchlorate salts from the respective alcohols (General Procedure 2)

Perchloric acid (40%) was added dropwise to a cooled solution of the alcohol (dissolved in dichloromethane, DCM) in an Erlenmeyer flask. Thereafter, diethyl ether was added to the solution whilst cooling in an ice bath to induce crystallization. The highly coloured solid salt product was filtered, washed with diethyl ether and dried under high vacuum.

2.5.3 Reaction of perchlorate salts with ethylenediamine to afford **H_1** and **H_2** (General Procedure 3)

The perchlorate salt, in DCM, was added to a solution of ethylenediamine, also in DCM. The organic layer was washed with water (3 x 100 mL) and dried over sodium sulfate. The product was concentrated using a rotary evaporator, filtered and dried using the high vacuum system. The resulting gum was then crystallized and recrystallized to afford host compounds **H_1** or **H_2**, as applicable.

2.6 Syntheses

2.6.1 9-Hydroxy-9-phenylthioxanthene (**23**) – General Procedure 1

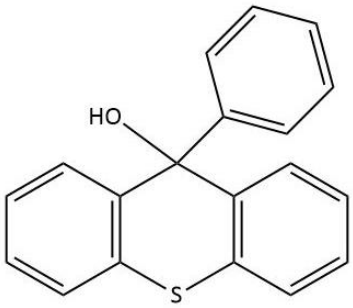

23

Magnesium turnings (1.82 g, 75 mmol), bromobenzene (11.10 g, 71.0 mmol) and thioxanthone (10.00 g, 47.0 mmol) afforded 9-hydroxy-9-phenylthioxanthene (**23**) (11.96 g, 55.0 mmol, 89%) as a cream solid after recrystallization from DCM/PET ether, m.p. 104–106 °C (lit.,[10] 105–106 °C); ν(solid)/cm^{-1} 3294 (OH) and 1439 (Ar); $\delta_H(CDCl_3)$/ppm 2.89 (1H, s, OH), 7.05–7.50 (11H, m, ArH) and 8.05 (2H, d, ArH); $\delta_C(CDCl_3)$/ppm 77.1 (COH), 126.2 (ArC), 126.6 (ArC), 126.7 (ArC), 127.0 (ArC), 127.4 (ArC), 127.8 (ArC), 128.1 (ArC), 131.6 (quaternary ArC), 140.0 (quaternary ArC) and 143.4 (quaternary ArC). (The spectra may be found in the Supplementary Information, Figures S1–3.)

2.6.2 9-Phenylthioxanth-9-ylium perchlorate (**26**) – General Procedure 2

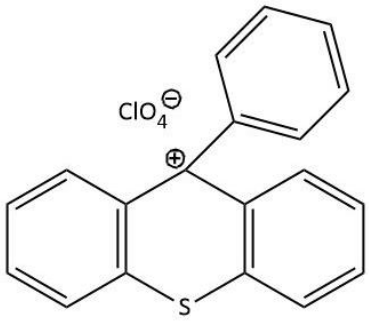

26

Perchloric acid (40%, 4.40 mL) and 9-hydroxy-9-phenylthioxanthene (**23**) (3.00 g, 8.2 mmol) afforded 9-phenylthioxanth-9-ylium perchlorate (**26**) which crystallized from diethyl ether as a bright red solid (3.18 g, 10.0 mmol, 83%), m.p. 230–232 °C (lit.,[10] 239 °C); ν(solid)/cm^{-1} 1449 (Ar); $\delta_H(CDCl_3)$/ppm 7.3–8.8 (13H, m, Ar<u>H</u>). (The spectra may be found in the Supplementary Information, Figures S4–5).

2.6.3 *N*,*N'*-Bis(9-phenyl-9-thioxanthenyl)ethylenediamine (**H$_1$**) – General Procedure 3

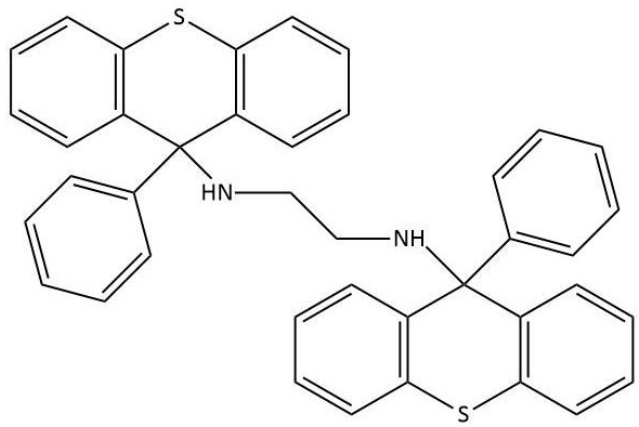

H$_1$

9-Phenylthioxanth-9-ylium perchlorate (**26**) (5.00 g, 14.0 mmol) and ethylenediamine (2.00 g, 33.0 mmol) afforded *N*,*N'*-bis(9-phenyl-9-thioxanthenyl)ethylenediamine (**H$_1$**) which recrystallized from DCM/PET ether as a white solid (2.73 g, 4.5 mmol, 67.5%), m.p. 172–178 °C (lit.,[10] 174–175 ˚C); ν(solid)/cm^{-1} 3365 (weak, NH), 3056 (CH) and 1432 (Ar); $\delta_H(CDCl_3)$/ppm 2.48 (2H, broad s, N<u>H</u>), 2.48 (4H, s, C<u>H</u>$_2$) and 7.19–7.47 (26H, m, Ar<u>H</u>); $\delta_C(CDCl_3)$/ppm 44.4

($\underline{C}H_2$), 65.2 (Ph-$\underline{C}$-NH), 125.8 (Ar$\underline{C}$), 126.0 (Ar$\underline{C}$), 126.8 (Ar$\underline{C}$), 126.9 (Ar$\underline{C}$), 128.0 (Ar$\underline{C}$), 129.8 (Ar$\underline{C}$), 131.6 (quaternary Ar$\underline{C}$), 137.9 (quaternary Ar$\underline{C}$) and 146.5 (quaternary Ar$\underline{C}$). (The spectra may be found in the Supplementary Information, Figures S6–8). Note that two ArC's are overlapping (see DEPT135 experiment in Supplementary Information, Figure S9).

2.6.4 9-Hydroxy-9-phenylxanthene (**21**) – General Procedure 1

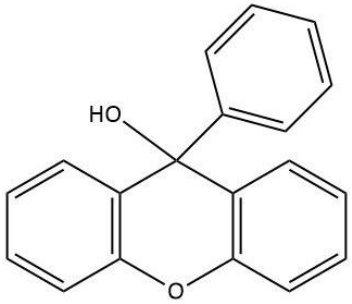

21

Magnesium turnings (0.78 g, 32 mmol), bromobenzene (5.40 g, 34.0 mmol) and xanthone (5.39 g, 27.5 mmol) afforded 9-hydroxy-9-phenylxanthene (**21**) which recrystallized from DCM/PET ether as a cream solid (5.12 g, 25.0 mmol, 74.7%), m.p. 160–162 °C (lit.,[10] 159 °C); ν(solid)/cm^{-1} 3294 (OH) and 1582 (Ar); $\delta_H(CDCl_3)$/ppm 2.67 (1H, s, O$\underline{H}$) and 7.07–7.45 (13H, m, Ar$\underline{H}$); $\delta_C(CDCl_3)$/ppm 70.5 ($\underline{C}$OH), 116.4 (Ar$\underline{C}$), 123.6 (Ar$\underline{C}$), 126.2 (Ar$\underline{C}$), 126.8 (Ar$\underline{C}$), 127.2 (quaternary Ar$\underline{C}$), 128.0 (Ar$\underline{C}$), 129.0 (Ar$\underline{C}$), 129.1(Ar$\underline{C}$), 148.0 (quaternary Ar$\underline{C}$) and 149.7 (quaternary Ar$\underline{C}$). (The spectra may be found in the Supplementary Information, Figures S10–12).

2.6.5 9-Phenylxanth-9-ylium perchlorate (**27**)– General Procedure 2

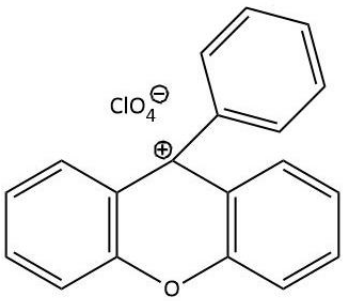

27

Perchloric acid (40%, 6.60 mL) and 9-hydroxy-9-phenylxanthene (**21**) (5.00 g, 8.2 mmol) afforded 9-phenylxanth-9-ylium perchlorate (**27**) which was recrystallized from diethyl ether

as a bright yellow solid (6.08 g, 20.2 mmol, 93.7%), m.p. 284–286 °C (lit.,[10] 280–281 °C); ν(solid)/cm^{-1} 1595 (Ar); δ_H($CDCl_3$)/ppm 7.8–8.5 (13H, m, ArH). (The spectra may be found in the Supplementary Information, Figures S13–14).

2.6.6 *N*,*N*'-Bis(9-phenyl-9-xanthenyl)ethylenediamine (**H_2**) – General Procedure 3

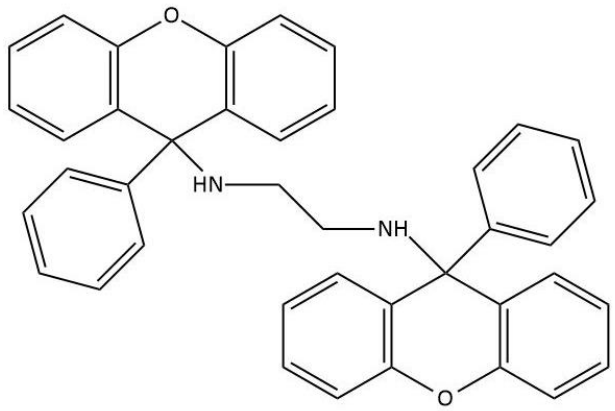

H_2

9-Phenylxanth-9-ylium perchlorate (**27**) (3.00 g, 8.4 mmol) and ethylenediamine (0.30 g, 5.0 mmol) afforded *N*,*N*'-bis(9-phenyl-9-xanthenyl)ethylenediamine **H_2** which recrystallized from DCM/PET ether as a white solid (1.54 g, 2.7 mmol, 58.7%), m.p. 202–203 °C (lit.,[4] 204–206 ˚C); ν(solid)/cm^{-1} 3019 (CH) and 1477 (Ar); δ_H($CDCl_3$)/ppm 2.32 (2H, broad s, NH), 2.25 (4H, s, CH_2) and 7.02−7.43 (26H, m, ArH); δ_C($CDCl_3$)/ppm 43.4 (CH_2), 59.9 (Ph-C-NH), 116.2 (ArC), 123.3 (ArC), 125.7 (quaternary ArC), 126.5 (ArC), 127.2 (ArC), 128.0 (ArC), 128.2 (ArC), 129.0 (ArC), 149.9 (quaternary ArC) and 151.3 (quaternary ArC). (The spectra may be found in the Supplementary Information, Figures S15–17).

2.7 Inclusion compounds

2.7.1 Formation of single solvent inclusion complexes

The guest compounds were purchased from Sigma-Aldrich and were used as received. The host compound (0.3–0.5 mmol) was dissolved in each of the guests (excess, 10–15 mmol), and heat in the form of a hot water bath was used to facilitate complete host dissolution in most cases. These experiments were usually carried out in glass vials that were subsequently left open at ambient temperature and pressure which facilitated the loss of some guest

through evaporation, and this encouraged crystallization. At this point, the vials were closed and left overnight to allow further crystallization. In some cases, especially for high boiling guest solvents, the vials were immediately lidded and left at 0 °C before crystallization was successful. Vacuum filtration was used to recover the crystals, and these were washed well with small quantities of PET ether to rinse off any superficial guest. Recovery of host material from the solutions in this way ranged between 60 and 72%. ^{1}H-NMR spectroscopy was used to determine whether inclusion had occurred, with $CDCl_3$ as the NMR solvent, and the H:G ratio ascertained through the integration of relevant host and guest resonance signals.

Figure 2.1 is a pictorial illustration of this single solvent complexation process.

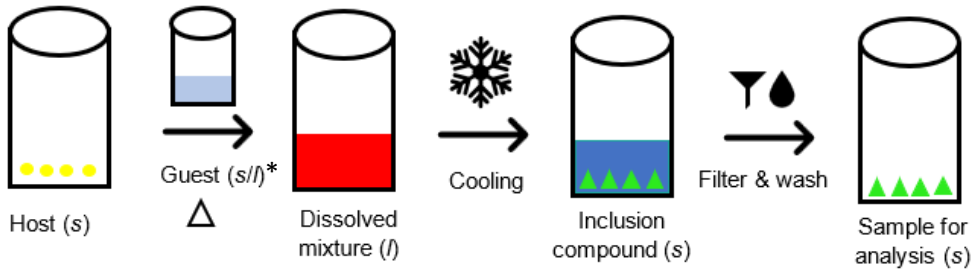

Figure 2.1. Inclusion by recrystallization.

*If the guest was a solid, initial dissolution in a "neutral" co-solvent was required.

2.7.2 Competition experiments

2.7.2.1 Equimolar guest mixtures

In glass vials, the host (0.3–0.5 mmol) was recrystallized from equimolar mixtures of two, three or four of the guests (~5 mmol each): after complete dissolution of the host in these mixtures, facilitated by mild heating, the vials were closed and stored at 0 °C to ensure that the equimolar conditions remained. In this way, crystallization usually occurred within 1−5 days. The crystals were isolated and treated in the same manner as in the single solvent experiments.

Figure 2.2 is an illustration of the process involved for these competition experiments.

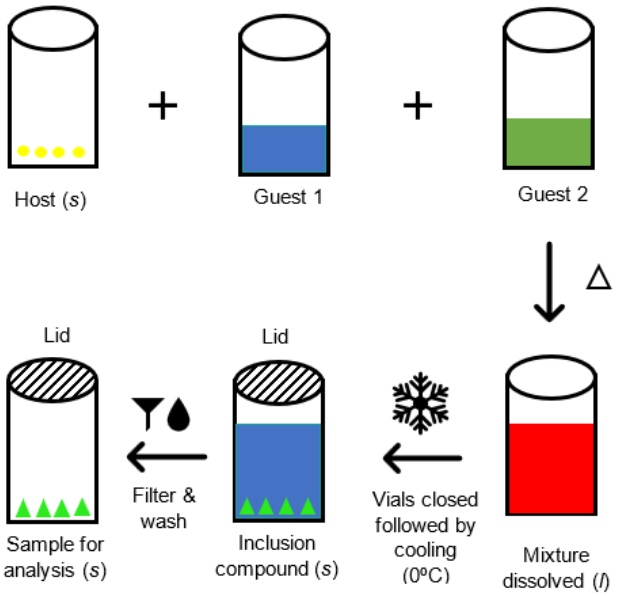

Figure 2.2. Preparation of competition experiments.

^{1}H-NMR spectroscopy was not always suitable for the analysis of the so-obtained mixed complexes owing to host/guest and/or guest/guest resonance signals that overlapped. In such instances, the crystalline samples were analysed by means of GC-MS, with DCM as the dissolution solvent.

2.7.2.2 Varying guest molar quantities

Here, two guests (G1 and G2) were mixed in different molar amounts such that the G1:G2 mol% ratios were approximately 20:80, 40:60, 50:50, 60:40 and 80:20. The host compound (0.3–0.5 mmol) was then recrystallized from each of these mixtures, and the vials treated identically to the equimolar competition experiments. Both the mother liquor from which crystallization occurred and the crystals that were recovered from them were analysed by GC-MS (with DCM as the solvent). It was therefore possible to construct selectivity profiles which provided information on the behaviour of the host compound as the guest concentrations varied. The resulting crystals (Z) and the mother liquors from which these formed (X) were analysed and used to plot Z vs. X, which provided the host selectivity profiles for each experiment. The behaviour of each host compound could therefore be ascertained over the concentration range employed. The selectivity coefficient, also calculated from these profiles, may be defined by Equation 2.1

$K_{A:B} = Z_A/Z_B \times X_B/X_A$, where $X_A + X_B = 1$ Equation 2.1

X_A represents the mole fraction of the preferred guest A in the liquid mixture, and Z_A that of the preferred guest in the crystal. The straight-line plot in each figure represents a hypothetical scenario where the host compound displays no selectivity (and K = 1). Additionally, the average selectivity coefficients for each binary combination were calculated for each binary mixture assessed in this way.

2.7.3 Vapour-phase experiments

These experiments were carried out only on the three xylenes and the dihaloalkanes (see Chapters 3 and 11) in order to determine whether **H_1** and **H_2** possess the ability to absorb these guest types from the gas phase. Hence, in closed glass vials, the crystalline host compound (0.5 mmol) was suspended on filter paper well above each of these liquid-phase guests (30 mmol) or above a mixture of all three guest types (10 mmol each) (Figures 2.3 and 2.4). In this way, the solid host was effectively subjected to the vaporous guest/s. After an allocated time period (the host was suspended for a period between 1 and 31 days), the suspended crystals were then washed with PET ether under vacuum suction and analysed by means of ^{1}H-NMR or GC-MS.

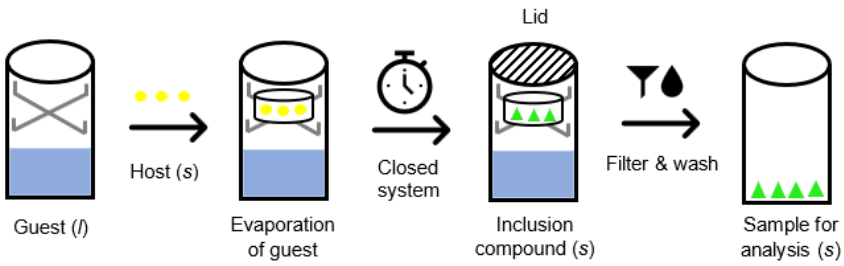

Figure 2.3. Gas inclusion

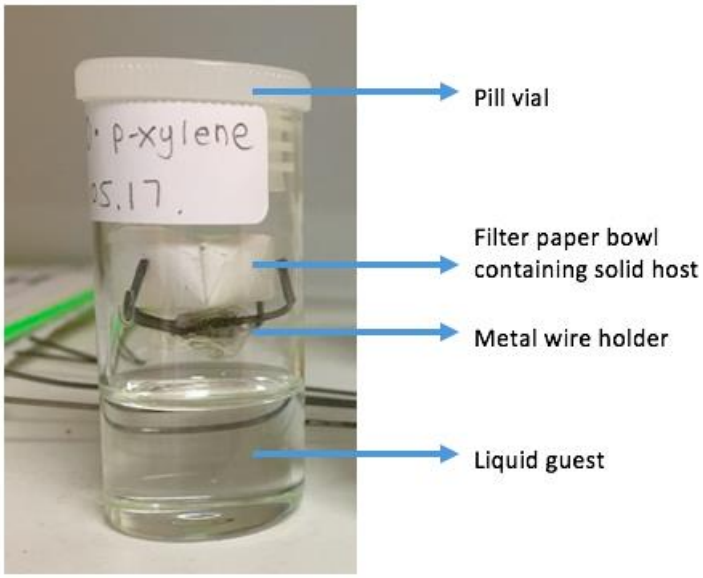

Figure 2.4. Gas inclusion vessel

3. XYLENE ISOMERS AND ETHYLBENZENE

3.1 Inclusion compounds with $\mathbf{H_1}$

3.1.1 Introduction

The three xylenes [*ortho*-, *meta*- and *para*- dimethylbenzene (*o*-Xy, *m*-Xy, *p*-Xy)] are important chemical precursors used in the manufacture of polymers, biocides, and dyes.[199,232-234] Together with ethylbenzene (EB), they are known as the C8 aromatic fraction (Scheme 3.1). These compounds may be isolated from crude oil, or the xylene isomers may be prepared using a naphtha-reforming catalytic process.[235,236] Owing to their similar boiling points, separation of the isomers from one another is not trivial, and distillations are inefficient, time-consuming and costly. As an example, a distillation to retrieve the higher boiling fraction of the four components, *o*-Xy (144 °C), requires 150 theoretical plates, and this number is significantly increased to 360 to separate *m*-Xy (139 °C) from *p*-Xy (138 °C).[199] EB (136 °C) is the lower boiling fraction of the four. Many industrial separations, therefore, rely on the selective adsorption of these isomers onto zeolites.[237] Host-guest chemistry, on the other hand, may provide an alternative means of achieving this separation.[238-240] It has been reported[95] that (*R*,*R*)-(−)-2,3-dimethoxy-1,1,4,4-tetraphenylbutane-1,4-diol, when recrystallized from an equimolar mixture of the three xylenes, displayed some selectivity for the *para* isomer (54.0%), while addition of EB to the ternary mixture had a deleterious effect on this selectivity: *p*-Xy remained preferred but only 40.6% was found in the crystal. The aim of the current investigation was to determine whether $\mathbf{H_1}$ exhibits improved selectivity towards any of the xylene isomers or EB.

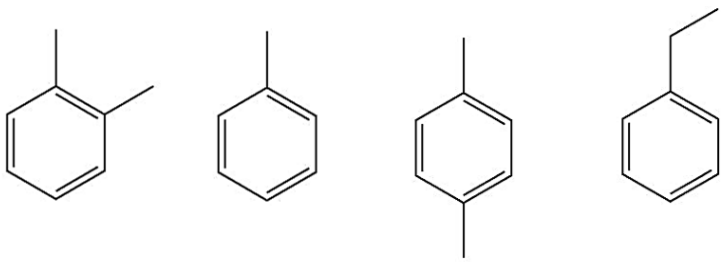

Scheme 3.1. Structures of the xylene isomers and EB guest compounds.

3.1.2 Individual inclusions

Table 3.1 displays the guests that were evaluated for individual inclusion, together with the H:G ratios of successfully formed inclusion compounds.

Table 3.1. H:G ratios of inclusion compounds formed by **H_1**.[a]

Guest (G)	H:G
o-Xy	1:1
m-Xy	[b]
p-Xy	1:1
EB	1:1

[a]Determined using ^{1}H-NMR spectroscopy using $CDCl_3$ as solvent.
[b]No inclusion occurred.

After independent recrystallization of **H_1** from *o*-Xy, *m*-Xy, *p*-Xy and EB, ^{1}H-NMR spectroscopy confirmed that 1:1 H:G inclusion compounds were obtained with *o*-Xy, *p*-Xy and EB, while *m*-Xy was not enclathrated (Table 3.1). [Integrated ^{1}H-NMR spectra of the respective complexes may be found in the Supplementary Information (Figures S18–21)]. These initial results were very encouraging since the separation of *m*-Xy (139 °C) from *p*-Xy (138 °C) is usually the more difficult one to achieve on an industrial scale,[241] and the lack of affinity of **H_1** for *m*-Xy may allow for their separation through host-guest chemistry. Consequently, various competition experiments were carried out to determine the viability of this supposition.

3.1.3 Equimolar competition experiments

Two or more of each of the guests were mixed in equimolar amounts, and the host recrystallized from each mixture. The resulting crystalline compounds were collected and treated using the methods described in § 2.6.1. ^{1}H-NMR analysis was utilized to determine the overall H:G ratios but was not an appropriate analytical technique to determine the G:G ratios due to overlapping G/G resonance signals in the ^{1}H-NMR spectra. [This overlap is evident from the ^{1}H-NMR spectrum of a mixture of the guests and **H_1**, and may be observed in the Supplementary Information (Figure S22); furthermore the resonance peaks that represent the methyl groups of the xylene guests overlap with the bridging ethylenediamine moiety of the host between ~2 and 2.5 ppm]. Table 3.2 provides a summary of the chemical shift values for the various proton resonances of the pure guest compounds.

Table 3.2. ^{1}H-NMR data for pure *o*-Xy, *m*-Xy and *p*-Xy.

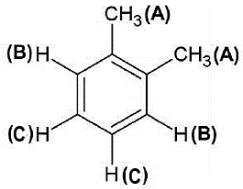		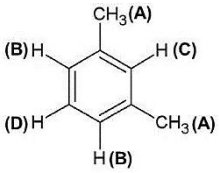		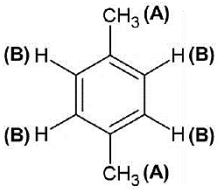	
o-Xy		*m*-Xy		*p*-Xy	
Assignment	**δ(ppm)**	**Assignment**	**δ(ppm)**	**Assignment**	**δ(ppm)**
(A) Methyl	2.33	(A) Methyl	2.43	(A) Methyl	2.36
(B), (C) H	7.15–7.21	(B), (C), (D) H	7.08–7.27	(B) H	7.11

Due to this overlap, GC-MS was selected as a more suitable tool with which to analyse these competition experiments, and traces for each xylene standard and a mixture of these guests are provided in the Supplementary Information (Figures S23–26); chloroform or dichloromethane was employed as the solvent. Table 3.3 summarizes the results obtained. Note that competition experiments were carried out in triplicate, and an average of the three percentages are provided in the table, together with percentage estimated standard deviations (% e.s.d.s). [The triplicate values are provided in the Supplementary Information (Table S27).]

Table 3.3. Results of competitions using **H$_1$** and various equimolar mixtures of the C8 guests.[a,b]

o-Xy	*m*-Xy	*p*-Xy	EB	Average guest ratios	Overall H:G ratio	% e.s.d.s
x		x		2.3:97.7	1:1	(0.5):(0.5)
	x	x		4.5:95.5	1:1	(0.5):(0.5)
x	x			[c]	-	-
x	x	x		0.3:4.8:94.9	1:1	(0.4):(1.6):(1.6)
		x	x	74.2:25.8	1:1	(0.3):(0.3)
x			x	[c]	-	-
	x		x	[c]	-	-
x		x	x	2.4:72.9:24.7	1:1	(0.2):(0.4):(0.3)
	x	x	x	4.2:70.6:25.2	1:1	(0.3):(0.2):(0.3)
x	x		x	[c]	-	-
x	x	x	x	2.5:4.1:68.3:25.1	1:1	(0.3):(0.2):(0.9):(0.4)

[a]G:G ratios were determined using GC-MS with dichloromethane or chloroform as the solvent; overall H:G ratios were obtained by means of ^{1}H-NMR spectroscopy.

[b]Experiments were conducted in triplicate for confirmation purposes; % e.s.d.s are provided in parentheses.

[c]No inclusion occurred.

In the equimolar binary competitions involving the xylene guests, *p*-Xy was virtually exclusively enclathrated at the expense of *o*-Xy (2.3%, despite **H_1** having formed a 1:1 inclusion compound with this guest in the single solvent experiment) and *m*-Xy (4.5%). When *p*-Xy was not present (the *o*-Xy/*m*-Xy experiment), **H_1** failed to enclathrate either one, and only pure host crystallized out. An equimolar ternary experiment involving the three Xy isomers displayed significant discrimination against *o*-Xy (0.3%) and *m*-Xy (4.8%) in favour of *p*-Xy (94.9%). It is interesting that, in some of these recrystallizations, *m*-Xy was found in the host crystals, though in small quantities, despite this isomer not having been enclathrated in the single solvent experiment.

As soon as EB was added to the guest solutions, the host displayed some affinity for this guest in some instances, but the preference for *p*-Xy was retained. An experiment using *p*-Xy/EB showed bias in favour of *p*-Xy (74.2%), while **H_1** did not enclathrate either guests in mixtures of *o*-Xy/EB and *m*-Xy/EB. For equimolar ternary experiments containing EB, *p*-Xy was favoured (70.6−72.9%) whenever present: an *o*-Xy/*p*-Xy/EB mixture resulted in a 2.4%/72.9%/24.7% mixed inclusion compound while, a *m*-Xy/*p*-Xy/EB combination afforded a 4.2%/70.6%/25.2% complex. Once again, in the absence of *p*-Xy, each of *o*-Xy, *m*-Xy and EB were not included, and only apohost crystallized out. Finally, an equimolar quaternary mixture of all four guests led to a 2.5%/4.1%/68.3%/25.1% *o*-Xy/*m*-Xy/*p*-Xy/EB mixed inclusion compound.

Finally, the overall H:G ratio remained 1:1 in all successfully formed complexes.

3.1.4 A gram scale experiment

A gram scale competition experiment was also carried out where the xylene isomers were mixed in larger equimolar portions (10 g, 94 mmol each), and the host (5 g, 8.3 mmol) recrystallized from this mixture, to determine whether results from the small and larger scale experiments correlated. The resulting crystals were treated and analysed as before, together with the mother liquor to ensure that guests were indeed present in equimolar quantities. Satisfyingly, this experiment agreed with the result from the smaller scale, alluding to the feasibility of scale-up for this separation process: the selectivity of the host for *p*-Xy was 93.6% here compared with 94.9% (Table 3.3). Figure 3.1a and b displays the GC traces of the mixed complex and the mother liquor, respectively.

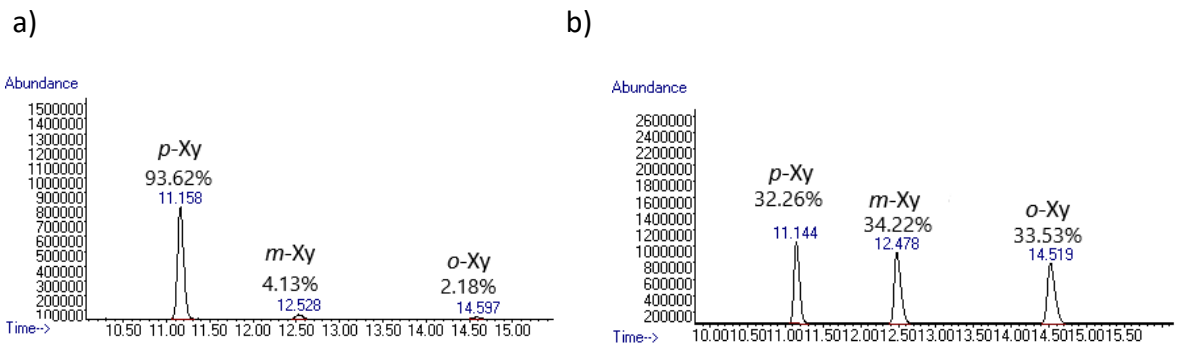

Figure 3.1. GC-MS traces for a) the inclusion compound obtained from the large scale competition experiment, and b) the mother liquor.

3.1.5 Ratio-dependent competition experiments

When the molar ratios of the guests in binary mixtures were varied and the host recrystallized from these mixtures, the resulting solids were treated as before and analysed using GC-MS, together with the mother liquors from which these crystals formed. The average selectivity coefficient, K, was also calculated for each combination (a complete set of the K values are provided in the Supplementary Information, Tables S28–30). Figure 3.2 is the overlaid constructed selectivity profiles for the respective experiments.

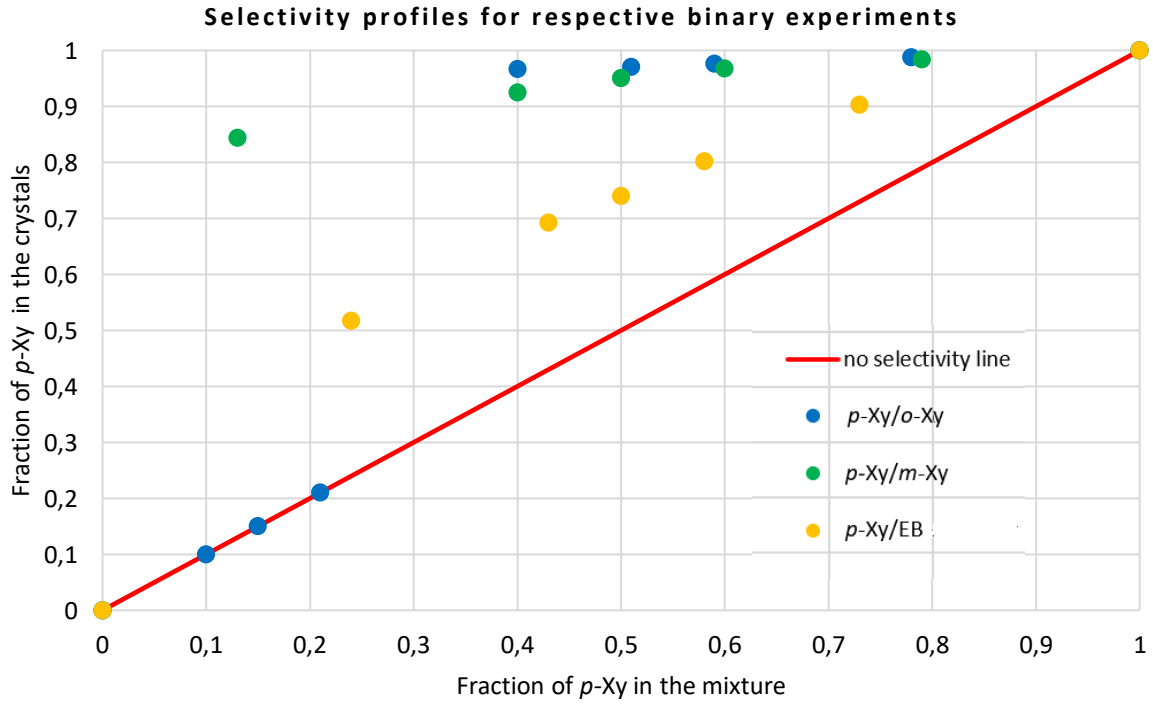

Figure 3.2. Overlaid selectivity profiles of $\mathbf{H_1}$ with the xylene isomers and EB.

Overall, the affinity of **H_1** for *p*-Xy is immediately evident from Figure 3.2, even at low concentrations of this guest in the solution. For example, in the *p*-Xy/*m*-Xy experiment (green plot, K = 22.0), when the solution contained only approximately 13% *p*-Xy, the selectivity of the host for this guest was already 84%, and this increased steadily thereafter as the relative amount of this guest increased in the solution. On the other hand, **H_1** displayed no selectivity in the initial stages (< 21%) of an experiment comprising *p*-Xy/*o*-Xy (blue plot). The selectivity for *p*-Xy, however, increased rapidly after this point, reaching > 94% when the solution contained only 40% of this solvent. The average K value for this experiment was 18.6. In the *p*-Xy/EB experiment (yellow plot, K = 3.1), the host was consistently selective for *p*-Xy, though this selectivity was not as significant as in the previous two experiments. A consideration of these results demonstrated that EB was the only guest to contest, to some extent, the host's preference for *p*-Xy.

3.1.6 Vapour phase inclusion of the Xy isomers

When the host was suspended above each of the xylene solvents, only *p*-Xy was enclathrated, and a 1:1 H:G ratio was attained after only one day. Both *o*-Xy and *m*-Xy, after 20 days of exposure, were not included in this way. Figure 3.3a–c illustrates the ^{1}H-NMR spectra after analysis of each of the suspended solids.

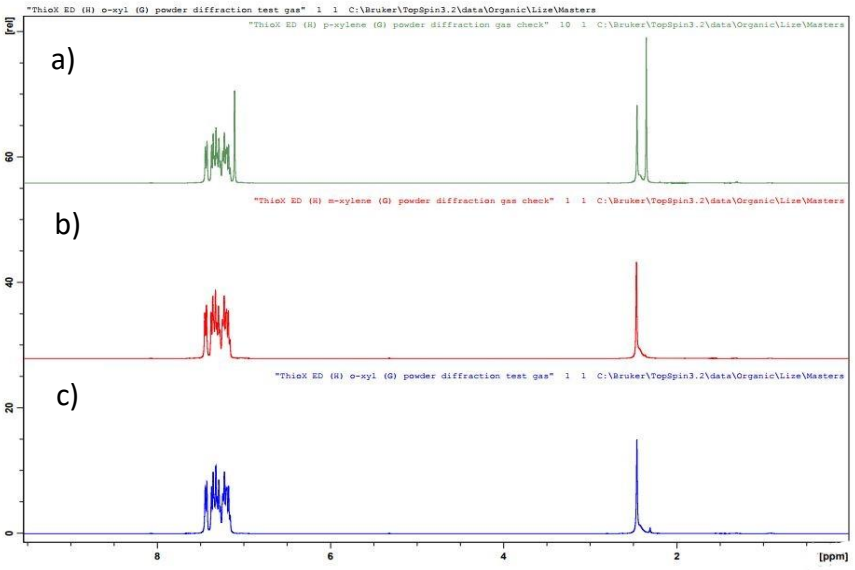

Figure 3.3. ^{1}H-NMR spectra after analysis of the suspended host solid in the presence of vaporous a) *p*-Xy, b) *m*-Xy and c) *o*-Xy.

H_1 was also suspended above an equimolar ternary mixture comprising all three Xy solvents. Once more, the observed selectivity for *p*-Xy was near-complete here (Supplementary Information, Figure S31), but uptake was slow, and a H:G ratio of only 3:1 was obtained after 20 days.

The **H_1**·*p*-Xy inclusion compound obtained by absorption of *p*-Xy from the gas phase was subjected to a powder diffraction experiment (Figure 3.4c), and this result compared to the powder patterns generated by the Mercury software[230] program for the **H_1**·*p*-Xy complex formed from solution (Figure 3.4b) and the host alone (Figure 3.4a). The latter pattern differed from the former two, which were identical, implying that the enclathration of *p*-Xy from the gas phase by apohost **H_1** involves a reorganization of the host atoms in the solid state.

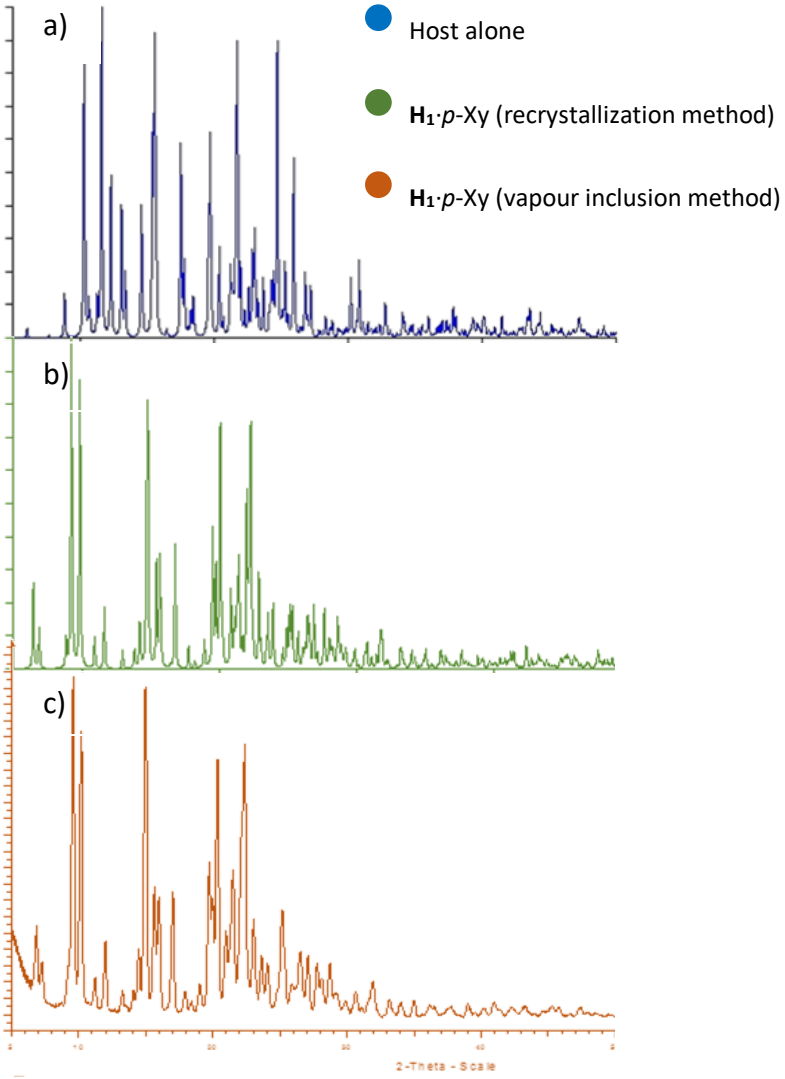

Figure 3.4. Calculated powder patterns (using Mercury software[230]) from SCXRD data for a) **H1** alone and b) **H1**·*p*-Xy formed by recrystallization; c) experimentally-obtained powder pattern for **H1**·*p*-Xy formed by the vapour inclusion method.

The enhanced affinity of **H1** for *p*-Xy was investigated by considering SCXRD data from the three inclusion compounds that successfully formed (**H1**·*o*-Xy, **H1**·*p*-Xy and **H1**·EB).

3.1.7 Single crystal X-ray diffraction (SCXRD)

Table 3.4 summarizes the relevant crystallographic data for the three complexes (**H$_1$**·*o*-Xy, **H$_1$**·*p*-Xy and **H$_1$**·EB). The disfavoured *o*-Xy inclusion compound crystallizes in a different crystal system and space group (monoclinic, $P2_1/n$) compared with the more favoured EB and highly preferred *p*-Xy guests (triclinic, *P*-1) and, in these latter two, the host packing is identical (isostructural). The ethyl group of EB is disordered over two positions but this disorder was successfully modelled.

Table 3.4. Crystallographic data for **H$_1$**·*o*-Xy, **H$_1$**·*p*-Xy and **H$_1$**·EB.

	H$_1$·*o*-Xy	**H$_1$**·*p*-Xy	**H$_1$**·EB
Chemical formula	$C_{40}H_{32}N_2S_2$ ·C_8H_{10}	$C_{40}H_{32}N_2S_2$ ·C_8H_{10}	$C_{40}H_{32}N_2S$ ·C_8H_{10}
Formula weight	710.96	710.96	710.96
Crystal system	Monoclinic	Triclinic	Triclinic
Space group	$P2_1/n$	*P*-1	*P*-1
μ (Mo Kα)/mm^{-1}	0.183	0.182	0.181
a/Å	10.7617(6)	10.5697(7)	10.5909(7)
b/Å	13.2539(8)	13.6135 (10)	13.5528(9)
c/Å	25.7455(13)	13.6984(9)	13.8416(9)
alpha/°	90	84,831 (3)	82.389(3)
beta/°	91.398(2)	88.103 (3)	84.771(3)
gamma/°	90	70.500 (3)	70.772(3)
V/Å^3	3671.1(4)	1850.5 (2)	1857.0(2)
Z	4	2	2
F(000)	1504	752	752
Temp./K	200	200	200
Restraints	0	0	3
Nref	9149	9180	9230
Npar	479	479	492
R	0.0351	0.0371	0.0394
wR2	0.0936	0.1052	0.1086
S	1.04	1.04	1.03
θ min–max/°	1.6, 28.3	1.5, 28.3	1.6, 28.3
Tot. data	102483	80666	130804
Unique data	9149	9180	9230
Observed data [I > 2.0 sigma(I)]	7802	7928	7943
R_{int}	0.019	0.017	0.022
Dffrn measured fraction θ full	1.000	1.000	0.999
Min. resd. dens. (e/Å^3)	–0.30	–0.24	–0.46
Max. resd. dens. (e/Å^3)	0.34	0.47	0.50

Figure 3.5a and b provides views of the unit cells (left) and the voids (dark yellow) present after the guests were removed from the packing calculation (right) for both **H₁**·*o*-Xy and **H₁**·*p*-Xy, respectively (**H₁**·EB is not shown here since the structure is comparable with **H₁**·*p*-Xy). (Voids were calculated using a probe radius of 1.2 Å.)

a)

b)

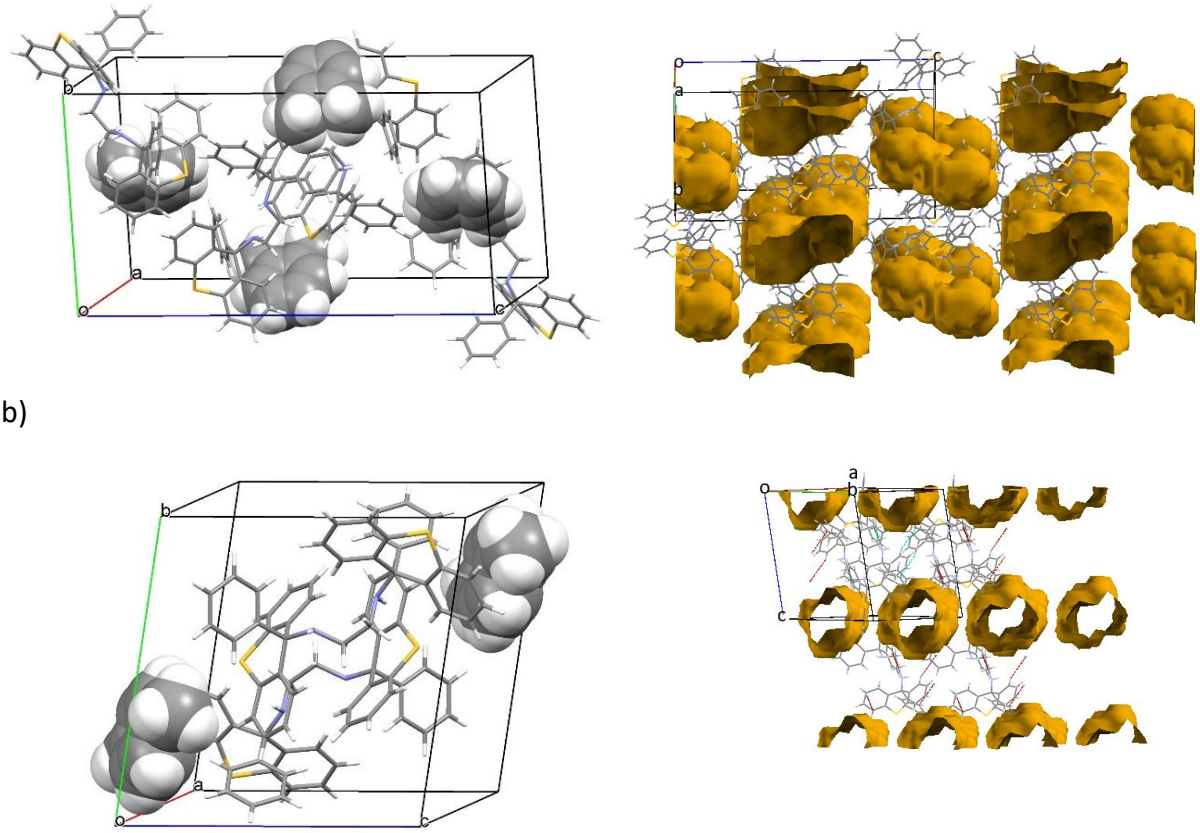

Figure 3.5. The guest packing (left) and voids (right) of a) **H₁**·*o*-Xy and b) **H₁**·*p*-Xy; these diagrams for **H₁**·EB is not provided here since the host packing is isostructural with **H₁**·*p*-Xy.

Guests *p*-Xy and EB occupy somewhat constricted channels in the host crystal while *o*-Xy experiences discrete cavity occupation. It has been reported that guests that occupy discrete cavities often exhibit enhanced thermal stabilities relative to those that are accommodated in channels.[136] This appears counterintuitive here though, since the least preferred guest (*o*-Xy) is found in cavities while the preferred guests (*p*-Xy, EB) are in channels, thus alluding to the relative thermal instability for complexes of the latter two guests. This point will be considered during the thermal analysis investigation.

Table 3.5 summarizes the significant interactions between **H_1** and the guest molecules.

Table 3.5. Significant H···G interactions in **H_1**·*o*-Xy, **H_1**·*p*-Xy and **H_1**·EB.[a,b,c]

Non-covalent interaction	**H_1**·*o*-Xy	**H_1**·*p*-Xy	**H_1**·EB	Symmetry
π···π	5.090(1)–5.893(1) Å [6]	5.010(1)–5.954(1) Å [7]	4.999(1)–5.997(1) Å [7]	
CH···π (H···Cg, C–H···Cg)				
$C_{(G)}$–$H_{(G)}$···$Cg_{(H)}$		2.80 Å, 145°		1+x, y, z
$C_{(G1)}$–$H_{(G1)}$···$Cg_{(H)}$			2.99 Å, 155°	1+x, y, –1+z
$C_{(G2)}$–$H_{(G2)}$···$Cg_{(H)}$			2.88 Å, 163°	1+x, y, –1+z
Other short contacts (X···Z, X–Y···Z)				
$C_{(H)}$–$H_{(H)}$···$H_{(G)}$–$C_{(G)}$	2.38 Å, 164° (<)			3/2–x, –1/2+y, 1/2–z
$C_{(G)}$–$H_{(G)}$···$C_{(H)}$–$C_{(H)}$		2.87 Å, 139° (<)		x, y, z
$C_{(G)}$–$H_{(G)}$···$H_{(H)}$–$C_{(H)}$		2.34 Å, 141° (<)		1–x, 1–y, 2–z

[a]Distances denoted by < are contacts that measure less than the sum of the van der Waals radii of the atoms involved.
[b]Values in square brackets indicate the number of H···G π···π interactions.
[c]Guest 1 (G1) and guest 2 (G2) represent each of the disordered guest components in the host crystal.

Each of the three guests experiences a number of interactions with the host, with π···π stacking being prevalent and comparable in each of the inclusion compounds (though these are all very weak, ~5–6 Å) (Table 3.5). Notable is that the least preferred guest, *o*-Xy, experiences no $C_{(G)}$–$H_{(G)}$···$\pi_{(H)}$ interactions while both *p*-Xy and EB are involved in interactions of this type [2.80 Å (145°) (**H_1**·*p*-Xy), and 2.99 Å (155°), 2.88 Å (163°) (respectively, for both disordered guest components in **H_1**·EB)], the stronger (shorter) of these being associated with the most preferred guest, *p*-Xy. The latter guest also experiences two other short contacts [$C_{(G)}$–$H_{(G)}$···$C_{(H)}$–$C_{(H)}$ and $C_{(G)}$–$H_{(G)}$···$H_{(H)}$–$C_{(H)}$, 2.87 Å (139°), 2.34 Å (141°), respectively], while *o*-Xy is involved in only one $C_{(H)}$–$H_{(H)}$···$H_{(G)}$–$C_{(G)}$ interaction (2.38 Å, 164°), and EB in none. These observations possibly explain the selectivity behaviour of the host. [Table S32 is a summary of the host···host interactions (Supplementary Information)].

It is not a simple task to analyse all the H···G interactions and therefore discern stabilizing interactions from destabilizing ones, and hence we undertook to analyse the Hirshfeld surfaces[175] around the guest molecule in order to obtain at least a quantitative measure of the various interaction types between host and guest.

3.1.8 Hirshfeld surface analyses

Figure 3.6a–d is a depiction of the 2D fingerprint plots that were obtained from the 3D surfaces calculated around each guest molecule, and Figure 3.7 is a graphical comparison of the percentage and type of intermolecular interactions present between the host and the guest (G···H/H···G).

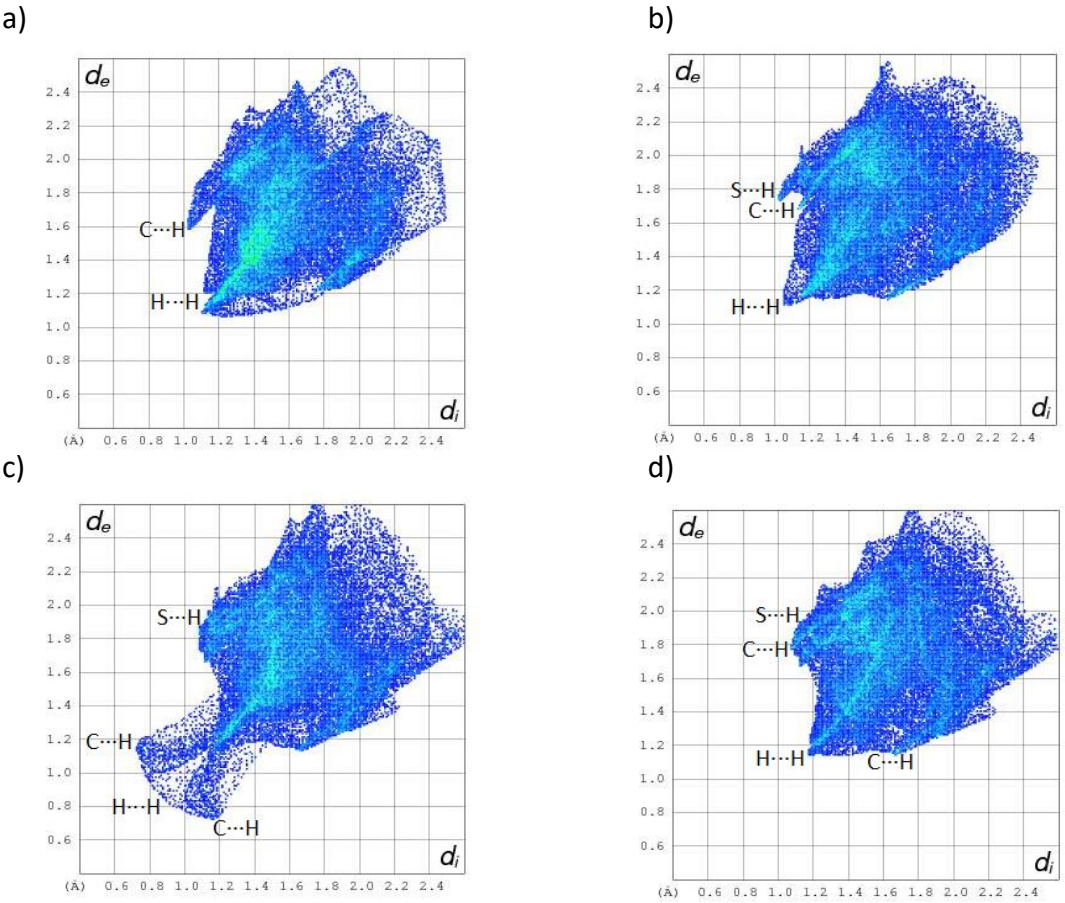

Figure 3.6. 2D fingerprint plots derived from 3D Hirshfeld surfaces around guests in a) **H₁**·*o*-Xy, b) **H₁**·*p*-Xy, c) **H₁**·EB - minor disordered component, and d) **H₁**·EB - major disordered component. The disordered components of EB required careful treatment. Each component was removed from the .cif file in turn, and the remaining guest was manually given a site occupancy factor (s.o.f.) of 1, and the Hirshfeld surfaces were then generated for each component in this way.

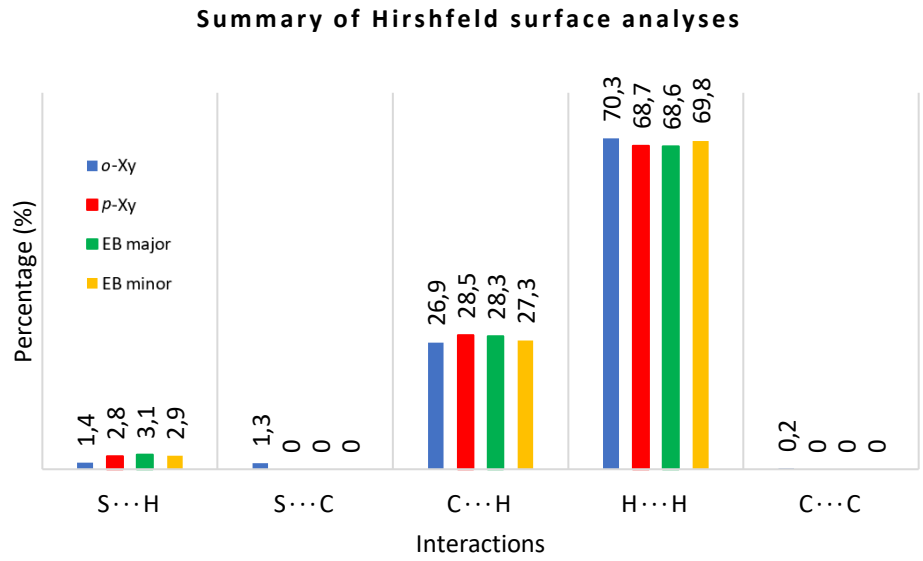

Figure 3.7. Quantitative data for the various H···G interactions in **H₁**·*o*-Xy (blue), **H₁**·*p*-Xy (red), **H₁**·EB - major disordered component (green), and **H₁**·EB - minor disordered component (yellow).

As expected, the most common G···H/H···G interactions are of the hydrogen···hydrogen type since these atoms are found on the periphery of each molecule and are therefore expected to interact more often in close packing environments. It is also clear from this figure that the most preferred guest complex, **H₁**·*p*-Xy, experiences a larger number of C···H/H···C interactions (28.5%), more so than **H₁**·EB [27.3% (minor component), 28.3% (major component)], and that the complex with the least preferred guest, **H₁**·*o*-Xy, is involved in a smaller number of these interaction types (26.9%). However, these differences are not significant, and hence we considered thermal analyses of the three complexes to provide an understanding for the observed host selectivity order.

3.1.9 Thermal analyses (DSC and TG)

The DSC and TG traces (overlaid) are provided in Figures 3.8 and 3.9, respectively.

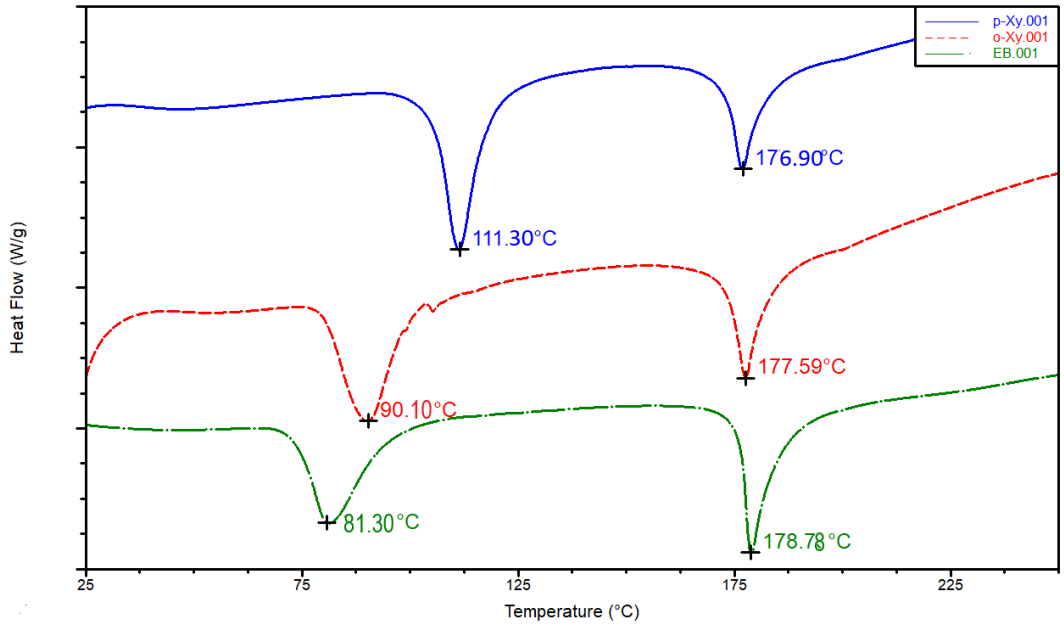

Figure 3.8. Overlaid DSC traces for the **H₁**·*p*-Xy (blue), **H₁**·*o*-Xy (red) and **H₁**·EB (green) complexes.

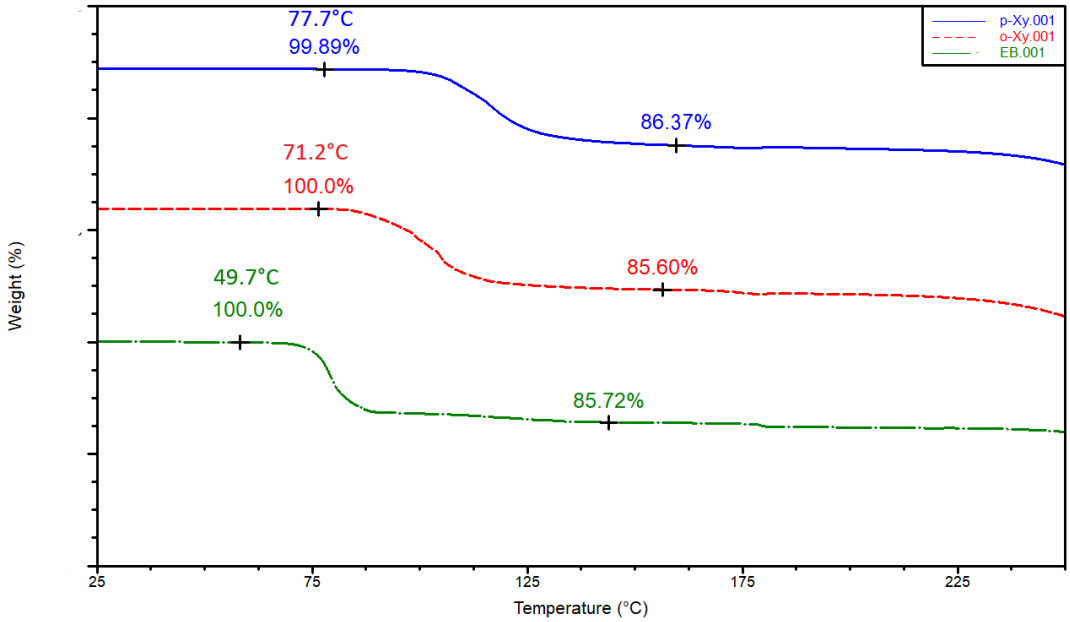

Figure 3.9. Overlaid TG traces for the **H₁**·*p*-Xy (blue), **H₁**·*o*-Xy (red) and **H₁**·EB (green) complexes.

The relevant thermal results obtained from these traces are summarized in Table 3.6.

Table 3.6. Thermal properties of inclusion compounds formed by **H₁**.

Guest (G)	T_{on} /°C	T_p /°C	Mass loss expected /%	Actual mass loss measured /%
o-Xy	71.2	90.1	15.0	14.4
p-Xy	77.7	111.3	15.0	13.5
EB	49.7	81.3	15.0	14.3

The expected mass loss upon complete guest removal through heating is in reasonable agreement (13.5–14.4%) with that expected theoretically (15.0%) for the three inclusion compounds (Figure 3.9, Table 3.6). Furthermore, the DSC traces (Figure 3.8) are rather uneventful, with each displaying a single guest loss endotherm [peak temperatures 90.1 °C (**H₁**·*o*-Xy), 111.3 °C (**H₁**·*p*-Xy) and 81.3 °C (**H₁**·EB)] followed by the melting of **H₁** (176.9−178.8 °C) (a small endotherm immediately after guest removal from **H₁**·*o*-Xy is possibly due to a host phase change; this is absent in **H₁**·*p*-Xy and **H₁**·EB in which the host packing is isostructural and different from that in **H₁**·*o*-Xy). Furthermore, the **H₁**·*p*-Xy complex displays a significantly enhanced relative thermal stability compared with **H₁**·*o*-Xy and **H₁**·EB (T_{on} 77.7 compared with 71.2 and 49.7 °C, respectively). The preferred guest, *p*-Xy, also has the highest T_p value (111.3 °C) when compared with EB (81.3 °C) and *o*-Xy (90.1 °C). [DSC, TG and DTG traces for each inclusion compound can be found in the Supplementary Information (Figures S33−35).]

As alluded to earlier (§ 3.1.7), the complex stability in the present instance is not associated with the nature of the guest occupation (discrete cavities versus channels) since the most thermally stable complex (**H₁**·*p*-Xy) has the guest situated in channels, and not in cavities.

3.1.10 Conclusions

Host compound **H₁** formed inclusion compounds with *o*-Xy, *p*-Xy and EB when recrystallized from these solvents, each with a 1:1 H:G ratio, but failed to include *m*-Xy. Milligram scale competition experiments showed this host to be selective for *p*-Xy when recrystallized from various equimolar mixtures of these guests. Gram scale experiments afforded very similar results, alluding to the feasibility of scaling this process up without altering the selectivity of the host. Varying guest ratios in binary guest competitions showed that the host remained selective for *p*-Xy and usually even at low concentrations of this guest in the solution. The data from gas phase experiments where **H₁** was suspended above each individual guest

revealed that the host rapidly enclathrated *p*-Xy (after one day) but remained uncomplexed in the presence of vaporous *o*-Xy and *m*-Xy (after 20 days). An equimolar gas phase experiment involving the three Xy isomers showed, once more, that the host selectivity for *p*-Xy was near-complete, but uptake was much slower than in the presence of pure gaseous *p*-Xy.

Data from SCXRD experiments on the three complexes (**H$_1$**·*o*-Xy, **H$_1$**·*p*-Xy and **H$_1$**·EB) revealed that the host packing in the **H$_1$**·*p*-Xy and **H$_1$**·EB crystals is isostructural (triclinic, *P*-1), while that comprising *o*-Xy crystallized in a different crystal system altogether (monoclinic, $P2_1/n$). The former crystal packing type, therefore, appears to be associated with the more preferred guests. Furthermore, Hirshfeld surface analyses showed *p*-Xy to be involved in a larger number of C···H (H···G/G···H) interactions relative to EB and *o*-Xy, though differences were not significant. DSC and TG experiments further confirmed that *p*-Xy was held most strongly, having the higher relative thermal stability (as observed by the higher T_{on} and T_p values) compared with *o*-Xy and EB.

3.1.11 Supporting information

Relevant NMR spectra, GC and TG traces, and powder patterns have been deposited in the Supplementary Information for this section, together with the raw data and associated % e.s.d.s that were required to set up relevant tables. The novel crystal structures for each complex were deposited at the Cambridge Crystallographic Data Centre, and CCDC 1542311 (**H$_1$**·*o*-Xy), 1542312 (**H$_1$**·*p*-Xy) and 1542313 (**H$_1$**·EB) contain the crystallographic data for these structures.

3.2 Inclusion compounds with **H$_2$**

3.2.1 Introduction

In the previous section, the validity of employing **H$_1$** for the purpose of effecting the separation of isomers of the C8 aromatic fraction was investigated. This host displayed excellent selectivity for the *para* isomer (94.9%) when recrystallized from a mixture of the three xylene isomers. However, this selectivity was affected significantly and deleteriously when EB was present in the mixture, and only 68.3% of *p*-Xy was found in the host crystal after recrystallization from a mixture of all four solvents. In this present work, we consider

the potential application of **H_2** to effect the same separation, and compare results obtained with that of **H_1**.

3.2.2 Individual inclusions

Table 3.7 is a summary of the results obtained when **H_2** was recrystallized from each solvent. [The ^{1}H-NMR spectra may be found in the Supplementary Information (Figures S36–39).]

Table 3.7. H:G ratios of complexes formed by **H_2**.[a]

Guest (G)	H:G
o-Xy	[b]
m-Xy	[b]
p-Xy	1:1
EB	[b]

[a]Determined using ^{1}H-NMR spectroscopy using $CDCl_3$ as solvent.
[b]No inclusion occurred.

After recrystallization of **H_2** from *o*-, *m*- and *p*- Xy, as well as EB, ^{1}H-NMR spectra of the crystals isolated from each experiment showed that a 1:1 H:G complex was formed with only *p*-Xy, while *o*-Xy, *m*-Xy and EB were not included (Table 3.7). A series of competition experiments were subsequently carried out in which the host was recrystallized from various equimolar combinations of the xylene isomers and EB.

3.2.3 Equimolar competition experiments

In these experiments, the so-formed crystals were treated as usual and subjected to ^{1}H-NMR spectroscopy as well as GC-MS analysis, as before, and the results are provided in Table 3.8 (where the preferred guest is displayed in red, together with % e.s.d.s and overall H:G ratios). In each case, the overall H:G ratio remained 1:1 regardless of the number and type of guest species included. Binary competition experiments comprising the xylenes revealed that **H_2** possesses an extremely high selectivity for *p*-Xy (> 96%), whereas the mixtures where this guest was absent afforded no complexes. A ternary equimolar competition experiment involving all three Xy isomers resulted in *p*-Xy, once more, being included preferentially (96.5%) compared with 1.6% of *o*-Xy and 1.9% of *m*-Xy. A *p*-Xy/EB experiment afforded a

mixed complex which contained only 7.7% EB, a marked improvement compared with **H₁**, where 25.8% EB was found in the crystal. Finally, a quaternary mixture involving all four guest solvents resulted in an astonishing 92.0% *p*-Xy being included, followed by EB (5.2%). Clearly **H₂** is significantly more selective than **H₁**, despite their only difference being the heteroatom (O or S) in the B ring (only 68.3% *p*-Xy was found in the **H₁** crystal in a comparable experiment). (A detailed table of these data may be found in the Supplementary Information, Table S40.)

Table 3.8. Results of competition experiments using **H₂** and various equimolar mixtures of the guests.[a,b]

o-Xy	*m*-Xy	*p*-Xy	EB	Average guest ratios	Overall H:G ratio	% e.s.d.s
x		x		3.3:96.7	1:1	(0.1):(0.1)
	x	x		3.8:96.2	1:1	(0.2):(0.2)
x	x			[c]	-	
x	x	x		1.6:1.9:96.5	1:1	(0.4):(0.3):(0.1)
		x	x	92.3:7.7	1:1	(0.4):(0.4)
x			x	[c]	-	
	x		x	[c]	-	
x		x	x	2.0:92.8:5.2	1:1	(0.0):(0.2):(0.1)
	x	x	x	2.4:91.5:6.1	1:1	(0.5):(0.4):(0.1)
x	x		x	[c]	-	
x	x	x	x	1.5:1.3:92.0:5.2	1:1	(0.6):(0.2):(0.4):(0.0)

[a]G:G ratios were determined using GC-MS with dichloromethane as solvent; overall H:G ratios were obtained by means of ^{1}H-NMR spectroscopy.
[b]Experiments were conducted in duplicate for confirmation purposes; % e.s.d.s are provided in parentheses.
[c]No inclusion occurred.

3.2.4 Ratio-dependent competition experiments

Consequently, **H₂** was subjected to binary guest mixtures in which the guest concentrations were varied in order to ascertain whether this host is capable of discriminating between these C8 aromatic compounds in these conditions. The results obtained are summarized in Figure 3.10, which is an overlay of the obtained selectivity profiles. Note that mixtures where *p*-Xy was absent did not afford any complexes, and therefore no selectivity profiles could be constructed for the affected combinations. The average selectivity coefficients were also calculated for each experiment [the K value of each data point may be found in the Supplementary Information (Tables S41–43)].

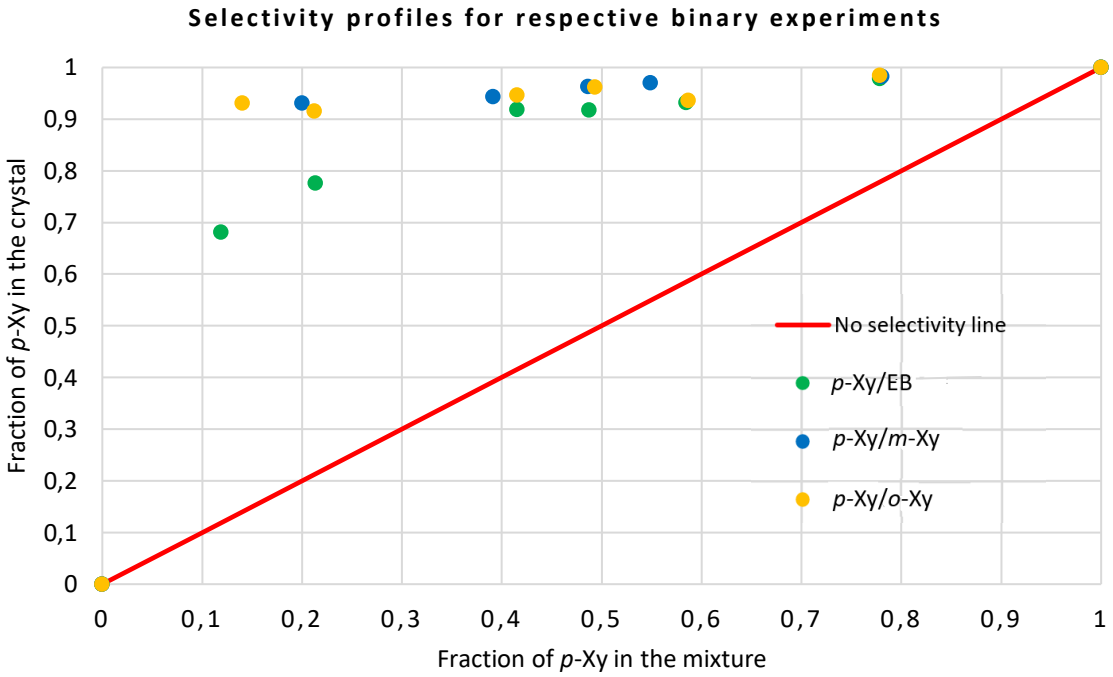

Figure 3.10. Overlaid selectivity profiles for binary mixtures where the concentrations of the guests were varied.

From Figure 3.10, it may be observed that **H₂** has a high selectivity for *p*-Xy even when the guest is present in low concentrations in the solution. When *p*-Xy competed with *m*-Xy (blue plot, K = 29.8) and *o*-Xy (yellow plot, K = 33.6), the host preferentially enclathrated *p*-Xy with a ratio of over 90%, despite the solution only containing approximately ~10–20% of this isomer. For experiments involving EB, the host displayed a lower selectivity for *p*-Xy at low *p*-Xy concentrations, but when the concentration of this isomer was above 40%, the selectivity of **H₂** rapidly increased, and over 90% of *p*-Xy was observed in the crystal (blue plot, K = 13.1). These results are a significant improvement from the analogous experiments with **H₁**, where the introduction of EB affected, negatively, the selectivity for *p*-Xy (K = 3.1).

3.2.5 SCXRD

The inclusion compound of **H₂** with *p*-Xy was further analysed by means of SCXRD, and the crystallographic data indicated that the host framework crystallized in the triclinic *P*-1 crystal system. Table 3.9 lists the relevant crystallographic data, while Figure 3.11 shows the unit cell for this complex. The guest's methyl group displays rotational disorder around an inversion point (Figure 3.12), but this disorder was well modelled over the two positions.

Table 3.9. Crystallographic data for **H₂**·*p*-Xy.

	H₂·*p*-Xy
Chemical formula	$C_{40}H_{32}N_2O_2 \cdot C_8H_{10}$
Formula weight	678.84
Crystal system	Triclinic
Space group	*P*-1
μ (Mo Kα)/mm^{-1}	0.075
a/Å	9.0063(4)
b/Å	9.1151(4)
c/Å	12.6154(5)
alpha/°	92.511(2)
beta/°	106.590(2)
gamma/°	112.306(2)
V/$Å^3$	904.63(7)
Z	1
F(000)	360
Temp./K	200
Restraints	0
Nref	4489
Npar	246
R	0.0425
wR2	0.1115
S	1.03
θ min–max/°	2.5, 28.3
Tot. data	22207
Unique data	4489
Observed data [I > 2.0 sigma(I)]	3531
R_{int}	0.022
Dffrn measured fraction θ full	1.000
Min. resd. dens. (e/$Å^3$)	–0.21
Max. resd. dens. (e/$Å^3$)	0.35

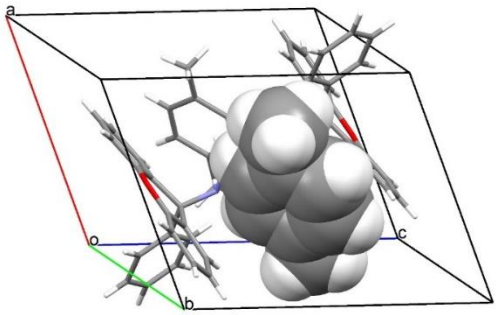

Figure 3.11. Unit cell of **H₂**·*p*-Xy showing only one of the disordered guest components.

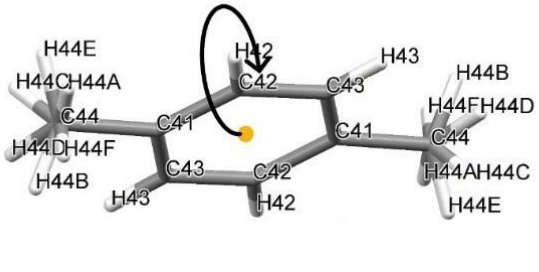

Figure 3.12. The guest in **H₂**·*p*-Xy displays rotational disorder.

After the guest was removed from the packing calculation, constricted channels remained (Figure 3.13). (The guest accommodation in the **H₁**·*p*-Xy complex was also of the constricted channel type.)

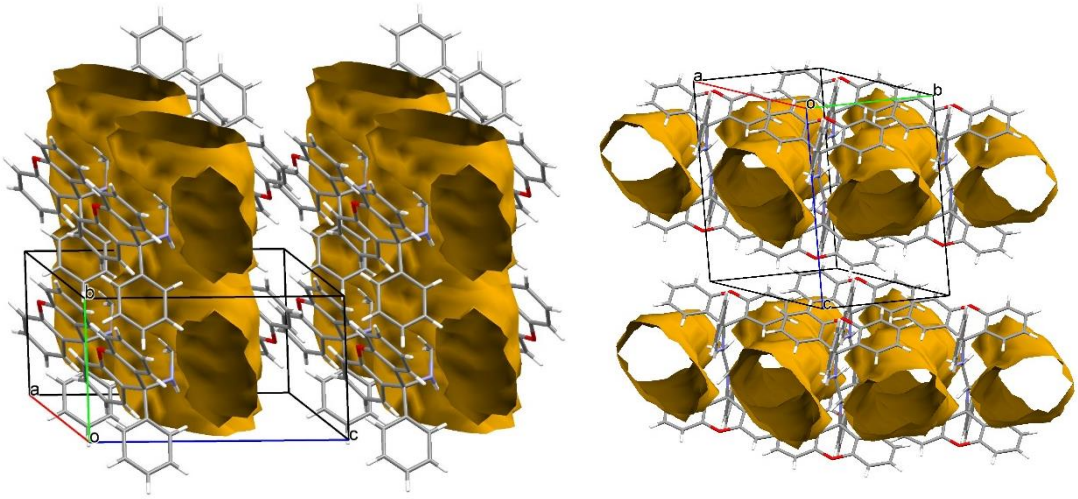

Figure 3.13. Constricted channel occupation of the guest in **H₂**·*p*-Xy.

Table 3.10 is a summary of the significant H···G interactions.

Table 3.10. Significant H···G interactions in **H₂**·*p*-Xy.[a,b]

Non-covalent interaction	**H₂**·*p*-Xy	Symmetry
π···π	4.781(1)–5.926(1) Å [5]	
CH···π (H···Cg, C–H···Cg)		
$C_{(G)}$–$H_{(G)}$···$Cg_{(H)}$	2.76 Å, 145°	x, 1+y, z
H-bonding (H···A, D–H···A)		
$N_{(H)}$–$H_{(H)}$···$C_{(G)}$–$C_{(G)}$	2.77 Å, 159° (<)	1–x, 2–y, 1–z
Other short contacts (X···Z, X–Y···Z)		
$C_{(H)}$–$H_{(H)}$···$H_{(G)}$–$C_{(G)}$	2.33 Å, 130° (<)	x, –1+y, z
$C_{(G)}$–$H_{(G)}$···$C_{(H)}$–$C_{(H)}$	2.87 Å, 139° (<)	x, y, z

[a]Distances denoted by < are contacts that measure less than the sum of the van der Waals radii of the atoms involved.
[b]Values in square brackets indicate the number of H···G π···π interactions.

The **H₂**·*p*-Xy inclusion compound did not display isostructural host packing with any complexes formed with **H₁**. The intermolecular H···G interactions identified were five weak $\pi_{(H)}$···$\pi_{(G)}$ [4.781(1)−5.926(1) Å], one $C_{(G)}$–$H_{(G)}$···$\pi_{(H)}$ (2.76 Å, 145°), one non-classical hydrogen bond (2.77 Å, 159°) and two other short contacts with distances that ranged between 2.33 and 2.87 Å (130–139°) (Table 3.10). (Table S44 of the Supplementary Information provides the host···host interactions.)

Subsequently, the host packing of **H₁** and **H₂** was considered and compared in order to better understand the reasons for the enhanced selectivity displayed by **H₂** relative to **H₁** in the presence of these guests. Figure 3.14 shows the conformations of these hosts in their complexes with *p*-Xy [which is representative for each host (the complete set is provided in the Supplementary Information, Figure S45)]. The angle between the three atoms in the heterocyclic ring, C–Ŝ–C (**H₁**) and C–Ô–C (**H₂**), is provided to indicate any buckling of the ring (where a planar ring would measure 180°). Clearly evident is the more buckled tricyclic fused sulfur-containing ring system (Figure 3.14a, C–Ŝ–C, 100.73 and 101.23°) compared with the near-planar oxygen-containing ring system counterpart (Figure 3.14b, C–Ô–C, 118.59°). The two benzene rings on either side of the heterocyclic in both of the trifused aromatic systems of **H₁** deviate from linearity by between 32.5 and 33.1° (i.e., an angle of 180° between the two benzene rings fused to the S-containing ring that is the central point), while that for **H₂** is significantly closer to linear (the deviation from linearity is only 9.1°)(this was calculated by means of Mercury software[230]). In addition to this fact, the nitrogen atoms in the ethylenediamine

linker of **H₁** adopts a gauche conformation, whereas **H₂** crystallizes with the linker's nitrogen atoms in an antiperiplanar arrangement (Figure 3.14b).

a) b)

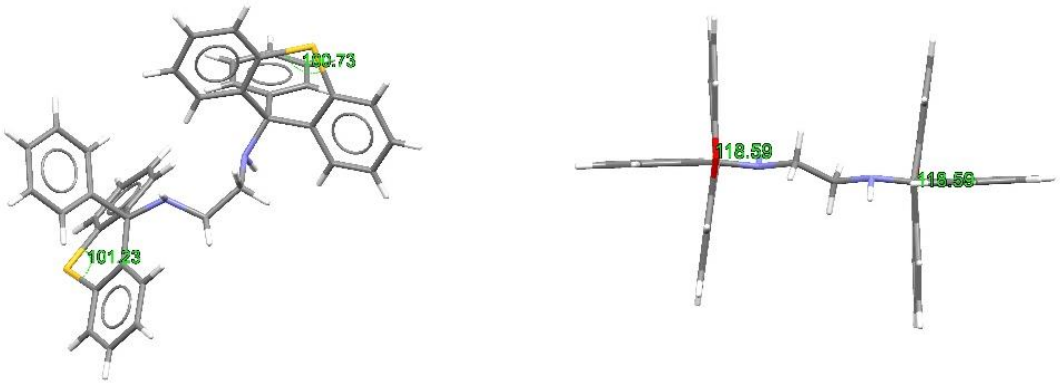

Figure 3.14. The host geometry in respective complexes a) **H₁**·*p*-Xy and b) **H₂**·*p*-Xy.

In this chapter, we have noted that the preferred guests occupied infinite one-dimensional channels. Figure 3.15a and b depicts the packing of the host molecules in **H₁**·*p*-Xy and **H₂**·*p*-Xy after removing the guests from the packing calculations. These figures provide views from different directions, and it is striking how **H₁** and **H₂** differ in this regard. While **H₂** displays a very ordered host–host packing, the opposite is true for **H₁**. The reason for these packing differences is possibly related directly to the geometry of each host molecule, where the buckled S-containing ring of **H₁** prevents an ordered packing with the guest, while the more planar O-containing ring of **H₂** facilitates this order. Since a tighter, more ordered packing is associated with enhanced selectivity based on guest size exclusion in tighter packed systems as reported by Afonso and Uyar *et al*,[242,243] **H₂** behaved more selectively than **H₁**, the latter compound accommodating a larger range of guests owing to the less complementary and less tight packing as a direct result of the buckled S-containing rings. The different host geometries as a result of these heteroatoms may be observed in the stereoviews in Figure 3.16a–c for the relevant complexes of **H₁** and **H₂**.

a)

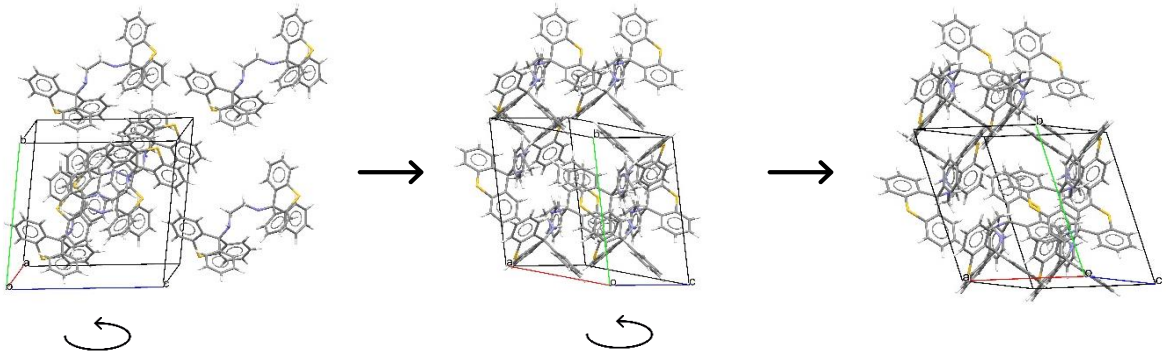

b)

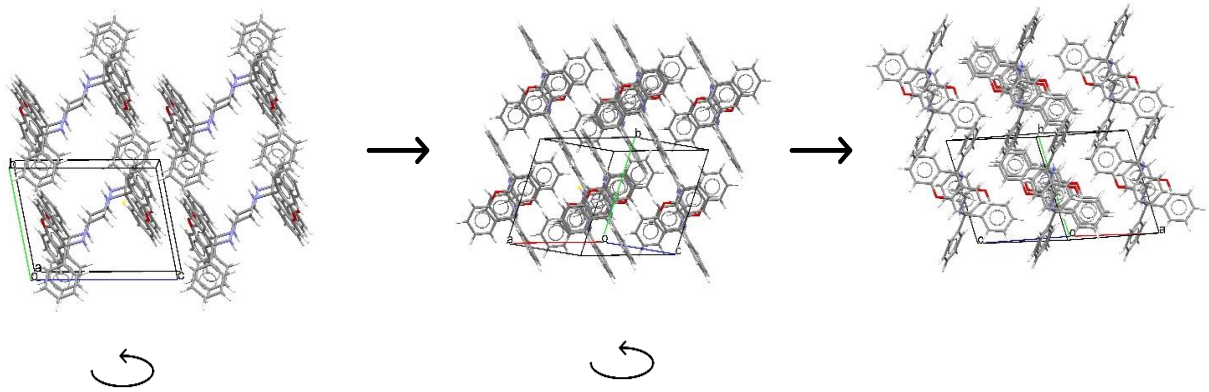

Figure 3.15. Visual representations of the host packing of a) $\mathbf{H_1}$ and b) $\mathbf{H_2}$ in various directions after removal of the *p*-Xy guest from the packing calculation.

a)

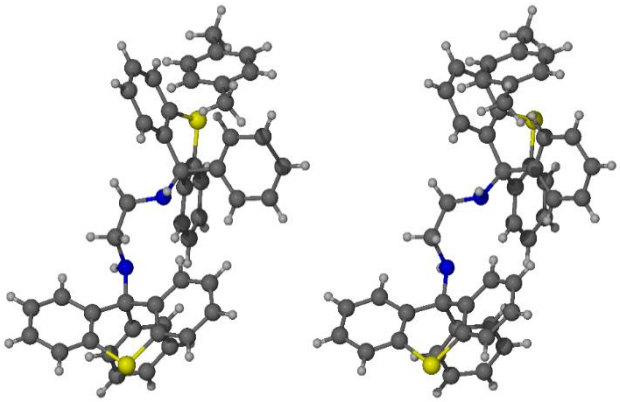

b)

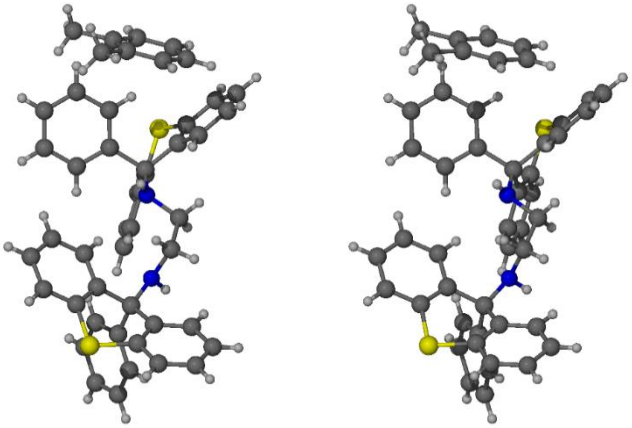

c)

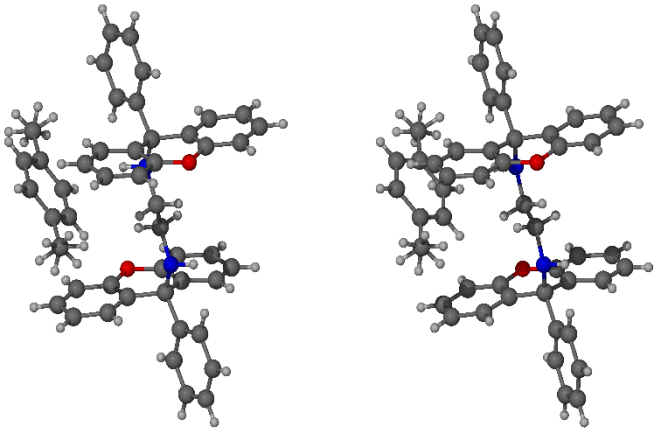

Figure 3.16. Stereoviews of complexes a) **H₁**·*p*-Xy (also representative of **H₁**·EB), b) **H₁**·*o*-Xy and c) **H₂**·*p*-Xy.

3.2.6 Hirshfeld surface analyses

Hirshfeld surfaces around the guest compound were analysed, but the results of these are purely academic and do not add value to these discussions. Hence the relevant diagrams and figures may be found in the Supplementary Information, Figures S46 and S47.

3.2.7. Thermal analyses (DSC and TG)

Thermal analyses were performed on the inclusion compound of **H₂** with *p*-Xy. The overlaid TG, DTG and DSC traces thus obtained are provided in Figure 3.17.

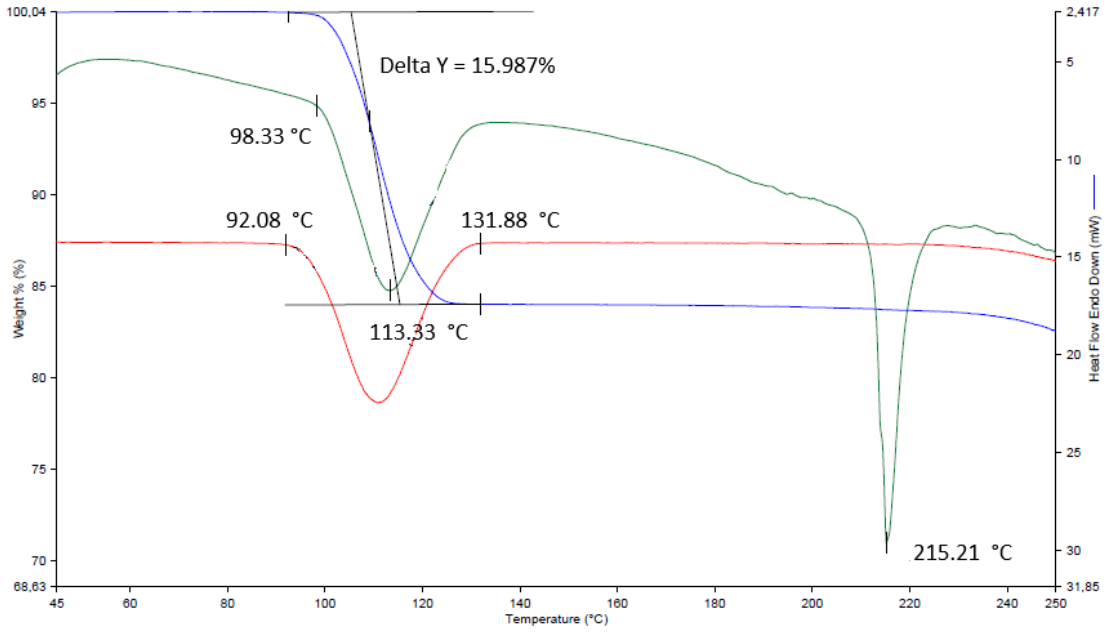

Figure 3.17. Overlaid TG (blue), DTG (red) and DSC (green) traces for **H₂**·*p*-Xy.

The traces in Figure 3.17 allude to an uneventful decomplexation process, with the guest released in a single step, and the host melt occurring after this event. Furthermore, the inclusion compound is stable at room temperature since the guest is released at only 92.1 °C. The expected guest mass loss (15.7%) was in reasonable agreement with that which was obtained experimentally (16.0%). Table 3.11 summarizes the relevant thermal data.

Table 3.11. Thermal properties of complex **H₂**·*p*-Xy.

Guest (G)	T_{on} /°C	T_p /°C	Mass loss expected /%	Actual mass loss measured /%
p-Xy	92.1	113.3	15.7	16.0

3.2.8 Conclusions

H₂, when recrystallized from each of the solvents of the C8 aromatic fraction of crude oil (EB, and *o*-, *m*- and *p*- Xy), clathrated only *p*-Xy and with a 1:1 H:G ratio. When this host was recrystallized from various mixtures of these solvents, it was observed to display a significant preference towards *p*-Xy. In comparison, **H₁** showed considerably reduced selectivities when presented with certain of these mixed guests. Since **H₂** only enclathrated *p*-Xy, SCXRD and Hirshfeld surface analyses could not be employed in a comparative manner to elucidate the reasons for this preference. However, after removing the guest from the packing calculation,

it was observed that *p*-Xy occupied infinite one-dimensional channels within the host crystal, and that **H_2** experienced a very ordered host–host packing, while the opposite was true for **H_1**. The reason for these packing differences is plausibly as a result of differences in the geometry of each host molecule, where the buckled S-containing tricyclic fused ring system of **H_1** prevents an ordered packing with the guest, while the more planar O-containing ring systems of **H_2** enables this. This tighter and more ordered packing was singled out as the factor that enhanced the selectivity of **H_2** compared with **H_1** for this guest series.

In the presence of the three xylene isomers, **H_1** exhibited excellent selectivity for the *para* isomer (94.9%). However, this selectivity was negatively affected when EB was present in the mixture, and only 68.3% of *p*-Xy was found in the host crystal. Employing **H_2** in such experiments, however, showed the selectivity of this host to remain very high when presented with the xylene isomers (96.2–96.7% of *p*-Xy was clathrated) but, and most importantly, the presence of EB did not significantly affect the host's preference for *p*-Xy (91.5–92.8%). This was an important finding and one that provides a distinct advantage of employing **H_2** rather than **H_1** to effect a possible alternative separation strategy for these C8 aromatic compounds.

3.2.9 Supporting information

Relevant NMR spectra, GC and TG traces, and powder patterns have been deposited in the Supporting Information for this section, together with the raw data and associated % e.s.d.s that were required to set up certain of the tables. The novel crystal structure was deposited at the Cambridge Crystallographic Data Centre, and CCDC 1895591 (**H_2**·*p*-Xy) contains the relevant crystallographic data for this structure.

4. METHYLANISOLE ISOMERS AND ANISOLE

4.1. Inclusion compounds with **H_1**

4.1.1 Introduction

Anisole (ANI), 2-methylanisole (2MANI), 3-methylanisole (3MANI) and 4-methylanisole (4MANI) (Scheme 4.1) are aromatic compounds that may be obtained by methylating phenol or the cresol isomers.[244] Anisole is a precursor to perfumes, synthetic pheromones, pharmaceuticals, and various other chemical compounds (e.g., anethole). The methylanisole isomers, on the other hand, are not of significant commercial interest although they do serve as starting materials in the synthesis of the corresponding methoxybenzoic acids, methoxybenzaldehydes,[245] and a variety of naturally occurring chemical compounds that are required to be synthesized on a larger scale.[246-248] In the present work, we assess the host ability of **H_1** for these anisoles, and report here on the findings.

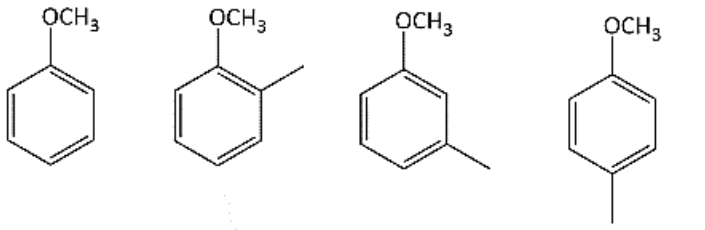

Scheme 4.1. Structures of ANI and the MANI isomers.

4.1.2 Individual inclusions

Following independent recrystallizations of **H_1** from ANI and the isomeric MANIs, the resultant crystals were subjected to ^{1}H-NMR spectroscopy. **H_1** successfully enclathrated ANI, 3MANI and 4MANI, but not 2MANI. All successfully formed complexes crystallized with a 1:1 H:G ratio (Table 4.1). [Integrated ^{1}H-NMR spectra of the respective complexes may be found in the Supplementary Information (Figures S48–50).]

Table 4.1. H:G ratios of inclusion compounds formed by **H₁**.[a]

Guest (G)	H:G
ANI	1:1
2MANI	[b]
3MANI	1:1
4MANI	1:1

[a]Determined using ^{1}H-NMR spectroscopy with $CDCl_3$ as solvent.
[b]No inclusion occurred.

Further competition experiments were carried out to investigate the host selectivity, if any, when exposed to a variety of mixtures of these guests.

4.1.3 Equimolar competition experiments

Various competition experiments were carried out by recrystallizing **H₁** from equimolar mixtures of the guests. GC-MS was selected as an appropriate tool for these analyses, and chromatographs of each anisole standard and a mixture of these guests are provided in the Supplementary Information (Figures S51–54), while Table 4.2 summarizes the results obtained. The experiments were carried out in duplicate, and an average of the percentages are provided in the table, together with percentage estimated standard deviations (% e.s.d.s). [The duplicate values are provided in the Supplementary Information (Table S55).] The binary experiment comprising 2MANI and 4MANI revealed that **H₁** possesses a significant preference for 4MANI (96.2%), and this guest was also preferred when competing with 3MANI (59.7%). In the absence of 4MANI, that is, in the 2MANI/3MANI experiment, **H₁** preferred the latter guest (86.8%), and a ternary competition experiment between only the methylanisoles showed that 4MANI (54.0%) was preferred over 3MANI (42.1%) and 2MANI (3.9%). In the binary experiment involving ANI and 4MANI, 64.2% of 4MANI was enclathrated by the host and, contrastingly, ANI was preferred when guest solvents 3MANI or 2MANI were present (56.1 and 96.2%, respectively). Using an ANI/2MANI/3MANI mixture, 55.2% of 3MANI (preferred here) was included, while the ANI/2MANI/4MANI and ANI/3MANI/4MANI experiments resulted in the preferential inclusion of 4MANI, with 60.2 and 40.2% of this guest being trapped in the crystal, respectively. Finally, a quaternary competition mixture incorporating all four guests resulted in a 29.0%/3.0%/21.9%/46.1% mixed complex

(ANI/2MANI/3MANI/4MANI). In each experiment, the overall H:G ratio remained 1:1 (as shown by ^{1}H-NMR spectroscopy, Table 4.2).

Table 4.2. Results of competitions using **H_1** and various equimolar mixtures of the anisole guests.[a,b]

ANI	2MANI	3MANI	4MANI	Average guest ratios	Overall H:G ratio	% e.s.d.s
x	x			96.2:3.8	1:1	(2.1):(2.1)
x		x		56.1:43.9	1:1	(1.7):(1.7)
x			x	35.8:64.2	1:1	(0.2):(0.2)
	x	x		13.2:86.8	1:1	(1.7):(1.7)
		x	x	40.3:59.7	1:1	(0.2):(0.2)
	x		x	3.8:96.2	1:1	(0.2):(0.2)
x	x	x		36.8:8.0:55.2	1:1	(1.7):(0.1):(1.6)
x		x	x	28.4:31.4:40.2	1:1	(1.1):(1.4):(0.3)
x	x		x	36.0:3.8:60.2	1:1	(0.3):(0.7):(1.1)
	x	x	x	3.9:42.1:54.0	1:1	(0.7):(1.3):(0.6)
x	x	x	x	29.0:3.0:21.9:46.1	1:1	(2.0):(0.1):(2.3):(0.3)

[a]G:G ratios were determined using GC-MS with dichloromethane or chloroform as the solvent; overall H:G ratios were obtained by means of ^{1}H-NMR spectroscopy.
[b]Experiments were conducted in duplicate for confirmation purposes; % e.s.d.s are provided in parentheses.

Interestingly, in both § 3.1.3 and this present work, the overall host selectivity order was according to the guest substitution pattern [*para*-substituted methyl isomer (*p*-Xy and 4MANI) > monosubstituted aromatic (EB and ANI) > *ortho*-substituted methyl isomer (*o*-Xy and 3MANI) > *meta*-substituted methyl isomer (*m*-Xy and 2MANI)]. Perhaps the more linear guest molecules (*p*-Xy, 4MANI, EB, ANI) facilitate a tighter packing in the crystal which has a stabilizing effect on the complex.[132]

4.1.4 Ratio-dependent competition experiments

H_1 was recrystallized from binary guest solutions in which the guest molar fractions were varied, and selectivity profiles were constructed from the data obtained after GC-MS analyses of both the resultant crystals and the mother liquors. Figures 4.1a and b represents the overlaid selectivity profiles of **H_1** that were obtained from these experiments involving ANI and the MANI isomers on one hand, and only the MANIs on the other, respectively. No crystals were formed when the molar ratio was varied beyond equimolar for the

2MANI/4MANI combination, and thus no selectivity profile could be constructed in this case. The average selectivity coefficient, K, was also calculated for each combination.

a)

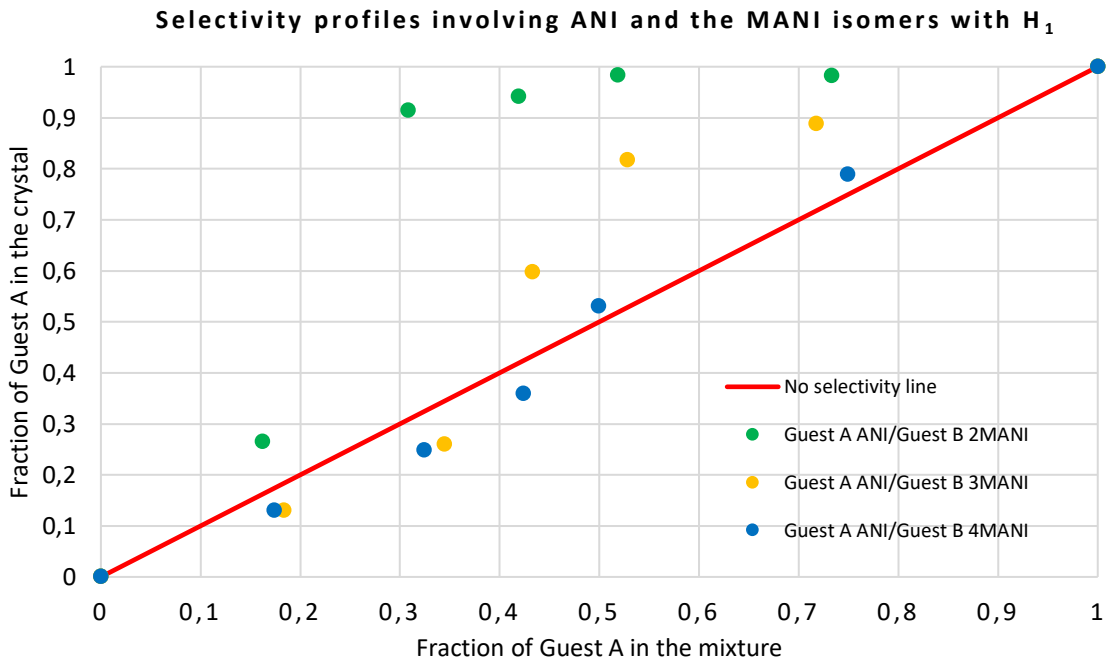

b)

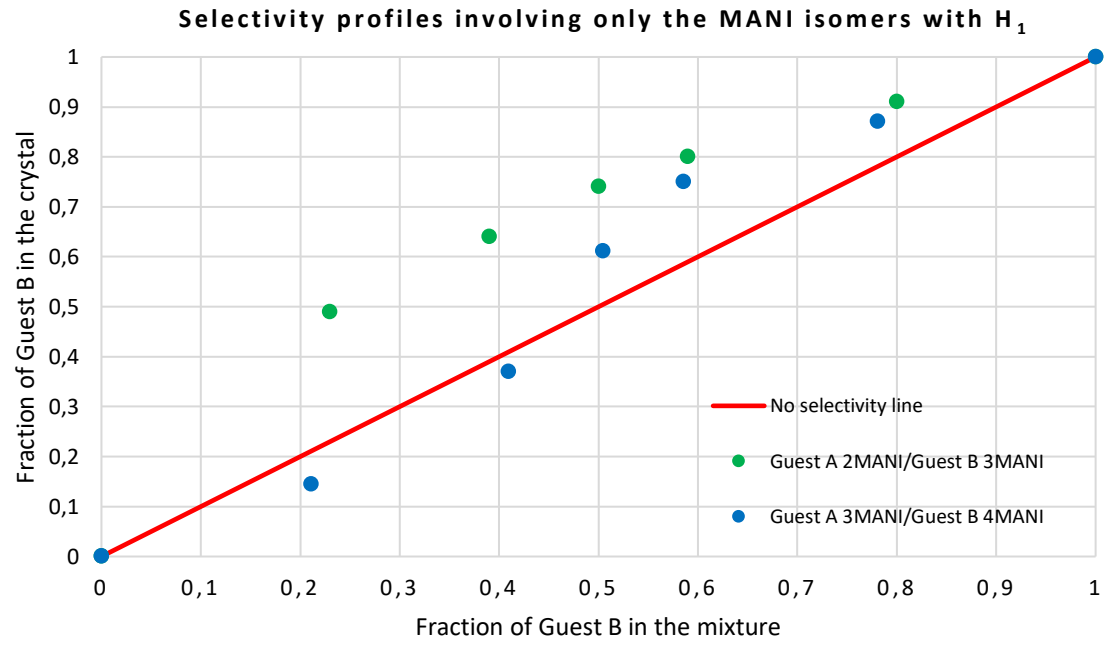

Figure 4.1. Overlaid selectivity profiles of **H_1** when recrystallized from a) binary guest combinations with ANI and b) binary guest combinations in the absence of ANI.

From Figure 4.1a, it is observed that **H_1** preferred ANI above 2MANI across the entire concentration range used, and the selectivity (K = 24.3) was significant, while the preference displayed by this host in the ANI/3MANI and ANI/4MANI experiments was more ambivalent and depended on the guest concentration. The highest selectivity coefficient (K) in the series of ANI/3MANI experiments was calculated to be 4.0, in favour of ANI, and this was when the mother liquor comprised approximately 50% of this guest. Similarly, the highest K value in the ANI/4MANI investigation was 1.5, in favour of 4MANI, obtained when the mother liquor contained 67% 4MANI. Figure 4.1b further supports results from the equimolar experiments (Table 4.2), and 3MANI was consistently preferred in the 2MANI/3MANI experiment (K = 4.7). However, when 3MANI and 4MANI were mixed, the host preference altered as the guest concentrations were varied. These results are in direct accordance with the proposed host selectivity order for these guests (4MANI > ANI > 3MANI > 2MANI). (A complete set of the K values are provided in the Supplementary Information, Tables S56–60.)

4.1.5 SCXRD

The individual inclusion complexes of **H_1** with ANI and the MANI isomers were further analysed by means of SCXRD. Table 4.3 contains a summary of the relevant crystallographic data and refinement parameters for novel complexes **H_1**·ANI, **H_1**·3MANI and **H_1**·4MANI. These inclusion compounds do not display isostructural host packing, despite all solids crystallizing in the triclinic crystal system with *P*-1 symmetry (Table 4.3). Furthermore, 4MANI experienced positional disorder (over two positions) in the **H_1**·4MANI complex, while guests in the **H_1**·ANI and **H_1**·3MANI complexes did not display disorder.

Table 4.3. Crystallographic data for **H₁**·ANI, **H₁**·3MANI and **H₁**·4MANI.

	H₁·ANI	**H₁**·3MANI	**H₁**·4MANI
Chemical formula	$C_{40}H_{32}N_2S_2$ ·C_7H_8O	$C_{40}H_{32}N_2S_2$ ·$C_8H_{10}O$	$C_{40}H_{32}N_2S_2$ ·$C_8H_{10}O$
Formula weight	712.93	726.96	726.96
Crystal system	Triclinic	Triclinic	Triclinic
Space group	*P*-1	*P*-1	*P*-1
μ (Mo Kα)/mm^{-1}	0.187	0.183	0.184
a/Å	10.3730(5)	10.5363(6)	10.5144(6)
b/Å	13.4532(6)	13.6858(7)	13.7009(7)
c/Å	13.9106(6)	13.7100(7)	13.7121(7)
alpha/°	83.333(2)	95.756(2)	84.337(2)
beta/°	84.907(2)	108.128(2)	70.982(2)
gamma/°	70.842 (2)	90.207(2)	87.993(2)
V/Å^3	1831.66(14)	1868.08(17)	1858.38(17)
Z	2	2	2
F(000)	752	768	768
Temp./K	200	200	200
Restraints	0	0	20
Nref	8662	9251	9229
Npar	478	488	544
R	0.0352	0.0354	0.0435
wR2	0.0950	0.0960	0.1252
S	1.03	1.03	1.02
θ min–max/°	1.6, 28.0	2.0, 28.3	2.0, 28.3
Tot. data	78409	66086	82965
Unique data	8662	9251	9229
Observed data [I > 2.0 sigma(I)]	7285	7825	7732
R_{int}	0.024	0.023	0.021
Dffrn measured fraction θ full	0.998	0.999	0.999
Min. resd. dens. (e/Å^3)	–0.36	–0.27	–0.29
Max. resd. dens. (e/Å^3)	0.34	0.32	0.64

The unit cells of the three complexes are provided in Figure 4.2a−c. Additionally, the guests were removed from the packing calculation and the resultant voids (dark yellow, Figure 4.3a−c) calculated in order to determine the nature of the guest accommodation, whether these are located in discrete cavities or continuous channels. Upon close analyses of packing diagrams and voids, it was noted that all guests reside in infinite channels (which was also observed for the complexes with *p*-Xy and EB in § 3.1.7).

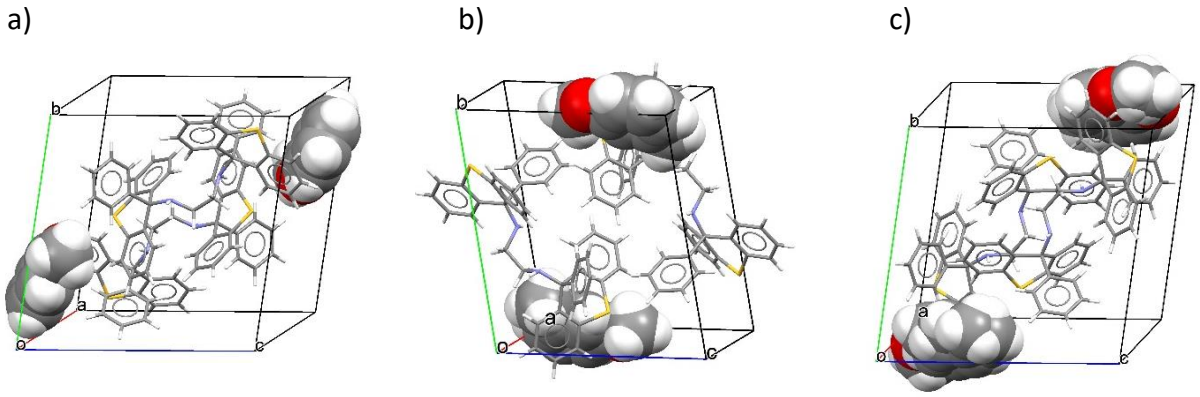

Figure 4.2. Unit cells for a) **H₁**·ANI, b) **H₁**·3MANI and c) **H₁**·4MANI; guests are in spacefill and hosts in stick representation.

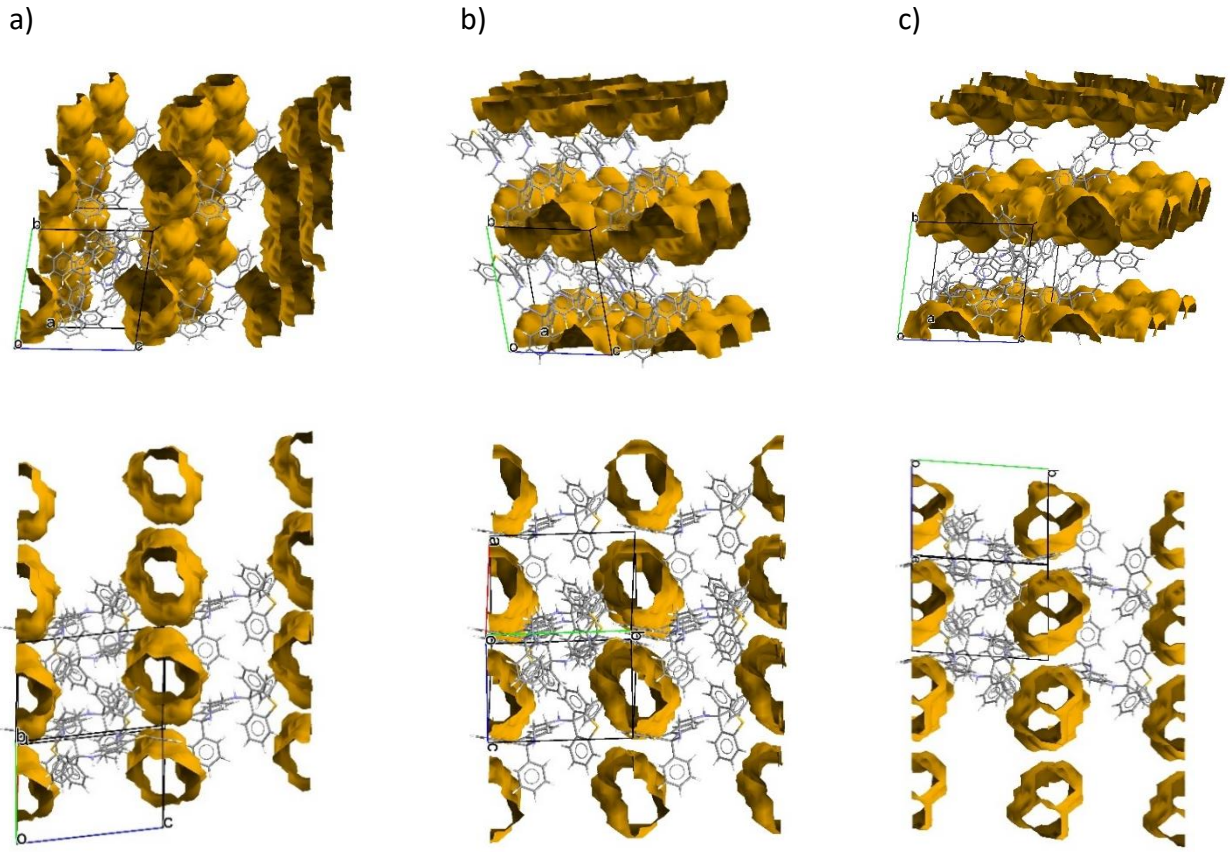

Figure 4.3. Calculated voids (dark yellow) for a) **H₁**·ANI, b) **H₁**·3MANI and c) **H₁**·4MANI after removal of the guests from the packing calculation.

The host geometry appears to be very similar in all three complexes, crystallizing with a buckled sulfur-containing ring. The two fused benzene rings on either side of the heterocyclic in both tricyclic fused aromatic systems deviate from linearity by between 29.04 and 32.82° in the three complexes. Figure 4.4a–c displays the conformations of **H₁** in the complexes with

ANI, 3MANI and 4MANI. Once again, it was observed that the nitrogen atoms of the linker adopted a synclinal (gauche) conformation (Figure 4.4).

a) b) c)

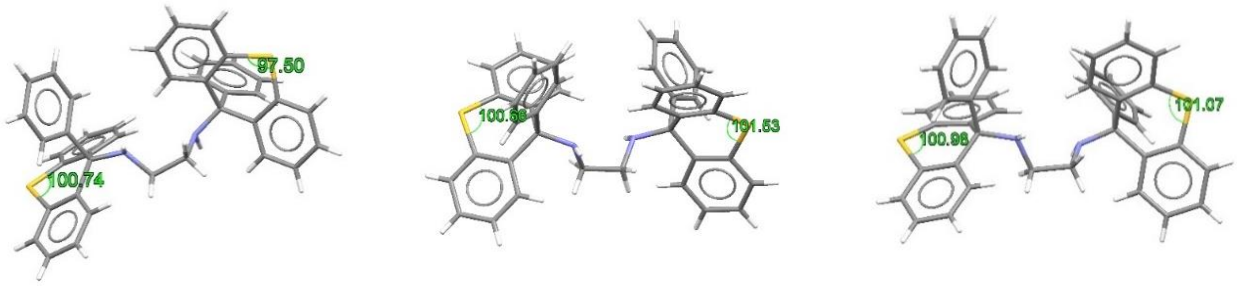

Figure 4.4. Host geometry within the respective complexes a) **H$_1$**·ANI, b) **H$_1$**·3MANI and c) **H$_1$**·4MANI.

In order to ascertain whether the geometry of **H$_1$** within the respective complexes is similar, host molecules from each were overlaid and the guests removed using the Mercury software:[230] **H$_1$** has near identical geometry in each of the complexes and this is depicted in Figure 4.5a–c.

a) b) c)

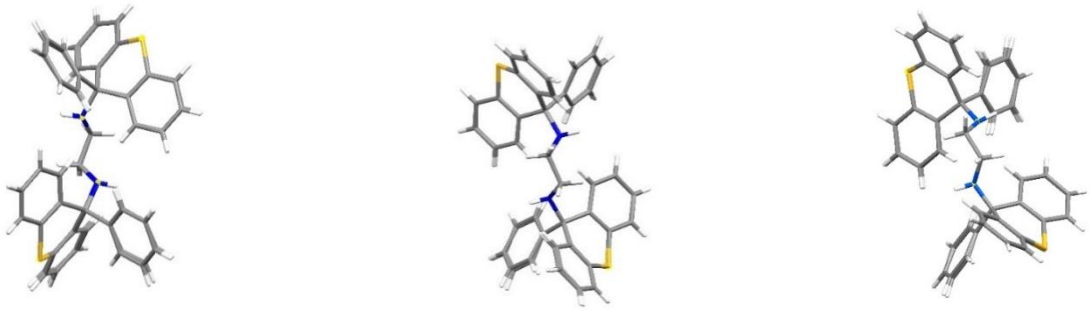

Figure 4.5. H$_1$ overlaid in complexes of a) **H$_1$**·ANI and **H$_1$**·4MANI, b) **H$_1$**·ANI and **H$_1$**·3MANI and c) **H$_1$**·3MANI and **H$_1$**·4MANI, after guest removal.

The relevant H:G interactions were then investigated in order to determine if the guest structure influences the host packing and consequent H···G interactions. Table 4.4 contains a summary of these significant H···G interactions that facilitate retention of the guests within the host crystal for all successfully formed complexes. (A table of all H···G and H···H interactions is provided in the Supplementary Information, Table S61.)

Table 4.4. H···G interactions present in complexes **H₁**·ANI, **H₁**·3MANI and **H₁**·4MANI.[a,b,c,d]

Non-covalent interaction	**H₁**·ANI	**H₁**·3MANI	**H₁**·4MANI	Symmetry
π···π	4.909(1)−5.986(1) Å [7]	5.028(1)−5.765(1) Å [7]	4.571(1)−5.998(1) Å [G1 6], [G2 7]	
C–H···π (H···Cg, C–H···Cg)				
$C_{(G)}$–$H_{(G)}$···$Cg_{(H)}$		2.78 Å, 170°		1–x, 2–y, 1–z
$C_{(G2)}$–$H_{(G2)}$···$Cg_{(H)}$			2.74 Å, 134°	−1+x, y, z
H-bonding (H···A, D–H···A)				
$C_{(H)}$–$H_{(H)}$···$O_{(G)}$	2.70 Å, 127° (<)			x, y, z
$C_{(H)}$–$H_{(H)}$···$O_{(G1)}$		2.87 Å, 160° (<)	2.55 Å, 132° (<)	1–x, –y, –z
$C_{(H)}$–$H_{(H)}$···$O_{(G1)}$		2.74 Å, 148° (<)		1–x, 1–y, 1–z
Other short contacts (X···Z, X–Y···Z)				
$C_{(H)}$–$H_{(H)}$···$C_{(G)}$–$C_{(G)}$	2.87 Å, 141° (<)			1–x, 1–y, 1–z
$C_{(G)}$–$H_{(G)}$···$C_{(H)}$–$C_{(H)}$	2.86 Å, 143° (<)			–x, 1–y, 1–z
$C_{(H)}$–$H_{(H)}$···$H_{(G)}$–$C_{(G)}$		2.36 Å, 143° (<)		1–x, 2–y, 1–z
$C_{(H)}$–$H_{(H)}$···$H_{(G)}$–$C_{(G)}$		2.94 Å, 130° (<)		x, 1+y, z
$C_{(H)}$–$H_{(H)}$···$H_{(G)}$–$C_{(G)}$		2.34 Å, 158° (<)		2–x, 2–y, 1–z
$C_{(H)}$–$H_{(H)}$···$H_{(G2)}$–$C_{(G2)}$			2.25 Å, 141° (<)	1–x, –y, 1–z
$C_{(H)}$–$H_{(H)}$···$H_{(G2)}$–$C_{(G2)}$			2.27 Å, 158° (<)	2–x, –y, –z
$C_{(G1)}$–$H_{(G1)}$···$H_{(H)}$–$C_{(H)}$			2.26 Å, 141° (<)	1–x, 1–y, 1–z

[a] A summary of the H···H and H···G interactions may be found in the Supplementary Information (Table S61).
[b] Guest 1 (G1) and guest 2 (G2) represent the disordered guest components in the host crystal.
[c] Distances denoted by < are contacts that measure less than the sum of the van der Waals radii of the atoms involved.
[d] Values in square brackets indicate the number of H···G π···π interactions.

H₁ experiences no C–H···π interactions with ANI, while both 3MANI and 4MANI are involved in one interaction each of this type [$C_{(G)}$–$H_{(G)}$··· $\pi_{(H)}$ 2.78 Å, 170° and 2.74 Å, 134°, respectively] (Table 4.4). Non-classical hydrogen bonding [$C_{(H)}$–$H_{(H)}$···$O_{(G)}$] is also present in complexes with ANI, 3MANI and 4MANI, and measure between 2.55 and 2.87 Å (127–160°), and 4MANI, the preferred guest, experiences the strongest of these interactions (2.55 Å, 132°) compared to the 3MANI and ANI guests. Other short contacts are also observed, largely of the C–H···H–C and C–H···C–C types, two for ANI (2.87, 2.86 Å and 141, 143°), three for 3MANI (2.34–2.94 Å, 130–158°), and 4MANI also experiences three of these (2.25–2.27 Å, 141–158°). Here too, 4MANI experiences the stronger of these short contacts, and this is conceivably the reason for the enhanced selectivity of **H₁** for this guest. All π···π interactions are comparable when considering distance and number of contacts for all the complexes, and these are all very weak.

4.1.6 Hirshfeld surface analyses

Subsequently, Hirshfeld surfaces were considered in order to acquire a quantitative measure of the applicable G···H/H···G interactions present in the anisole complexes with **H_1**. The 2D fingerprint plots are depicted in Figure 4.6a–c, while Figure 4.7 summarizes the quantity and types of interactions obtained from these 2D plots.

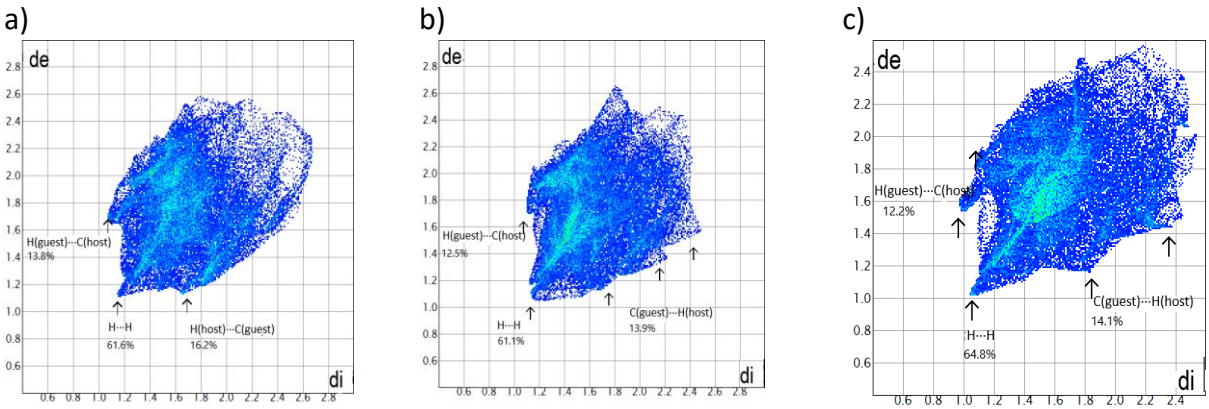

Figure 4.6. 2D fingerprint plots for the inclusion compounds a) **H_1**·ANI, b) **H_1**·3MANI and c) **H_1**·4MANI.

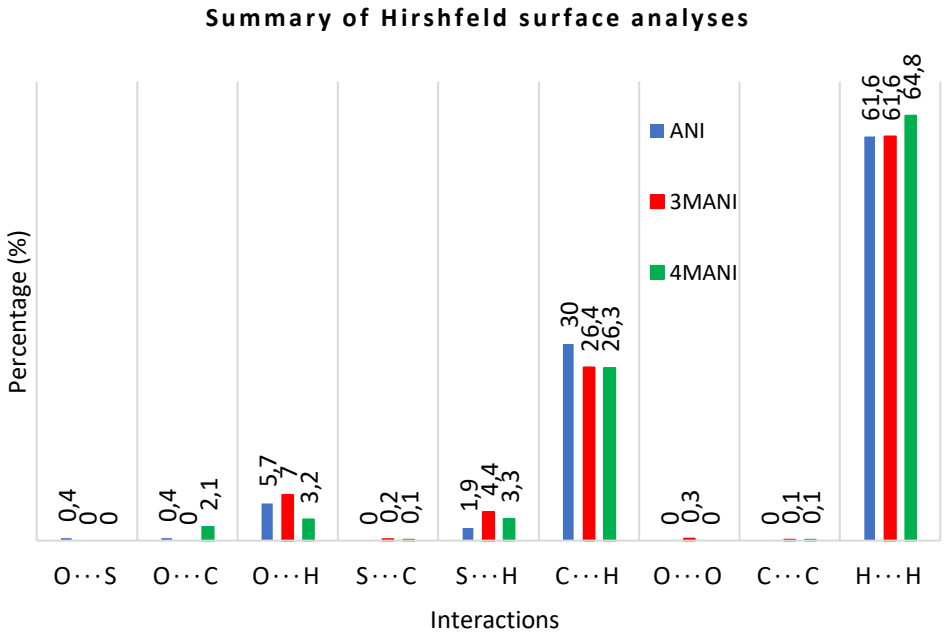

Figure 4.7. A graphical representation of the percentage and types of G···H/H···G interactions in complexes of **H_1** with ANI, 3MANI and 4MANI.

From Figures 4.6 and 4.7, the most prevalent interactions of the guest with the host involves hydrogen atoms (H···H), as expected. More interesting is the observation that 4MANI experiences more of these interaction types (64.8%) compared with ANI and 3MANI (both 61.6%).

4.1.7 Thermal analyses (DSC and TG)

The thermograms for each complex are provided in Figure 4.8a–c, and the relevant thermal data are summarized in Table 4.5.

a)

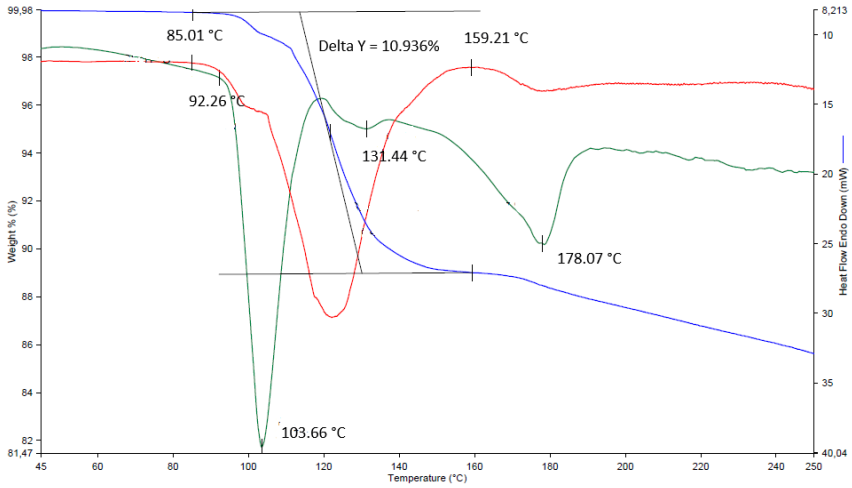

b)

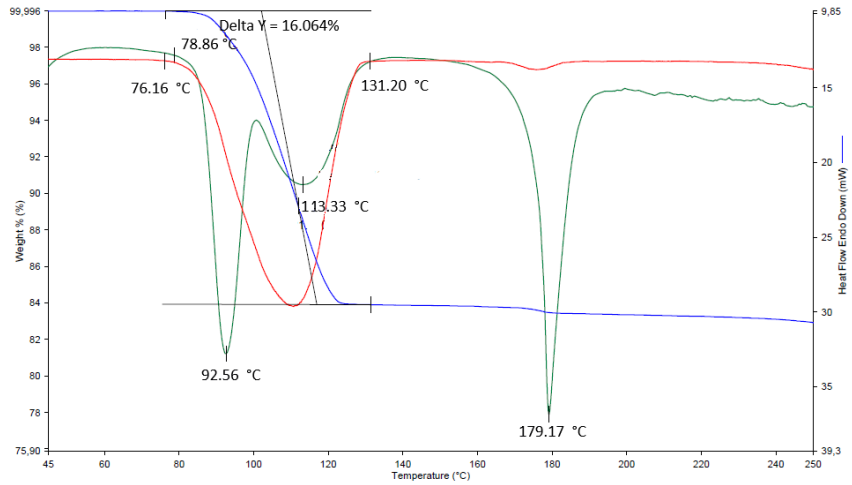

c)

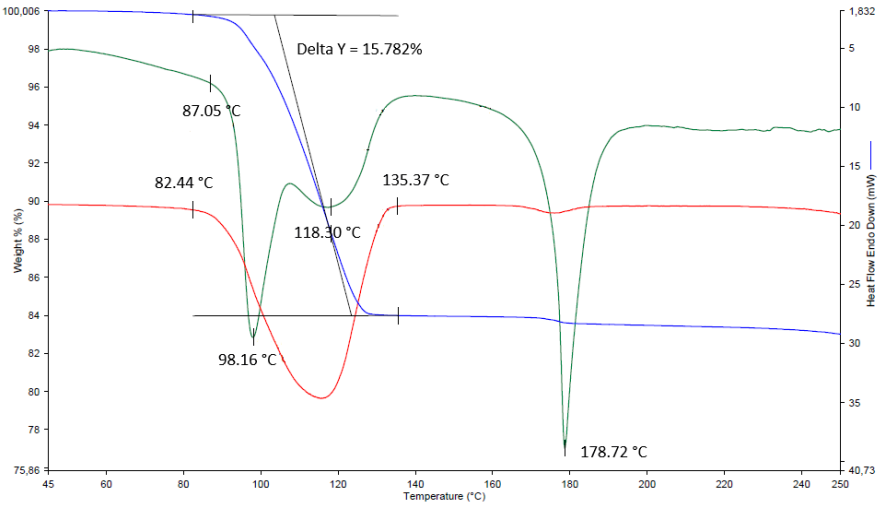

Figure 4.8. Thermal plots [DSC (green), TG (blue)and DTG (red)] for a) **H$_1$**·ANI, b) **H$_1$**·3MANI, and c) **H$_1$**·4MANI.

Table 4.5. Thermal data for complexes **H$_1$**·ANI**,** **H$_1$**·3MANI, and **H$_1$**·4MANI.

Complex	T_{on} /°C	T_p /°C	Mass loss expected /%	Actual mass loss measured /%
H$_1$·ANI	85.0	103.7, 131.4	15.2	10.9
H$_1$·3MANI	76.2	92.6, 113.3	16.8	16.1
H$_1$·4MANI	82.4	98.2, 118.3	16.8	15.8

From these thermograms, it is clear that mass loss is experienced by complexes **H$_1$**·ANI (Figure 4.8a), **H$_1$**·3MANI (Figure 4.8b) and **H$_1$**·4MANI (Figure 4.8c) in more than one step, followed by the host melt process (178.1–179.2 °C). The mass losses expected for all the complexes correlate well with the mass losses obtained experimentally, with the exception of the **H$_1$**·ANI complex (expected 15.2%, obtained 10.9%, Table 4.5). The reason for this discrepancy is quite possibly as a result of the continual mass loss observed from the TG that is also concomitant with the host melt, alluding to more guest release, but which could not be measured accurately since no point of inflection was clearly evident on this trace. Additionally, the complexes were stable at room temperature. Furthermore, the preferred guests (4MANI and ANI) are bound more strongly in the host crystal, as indicated by their greater T_{on} values (82.4, 85.0 °C, respectively), while the less preferred guest, 3MANI, is less tightly bound (76.2 °C), in accordance with the host selectivity order. [The small inflection on the DTG during the host melt that is observed around ~178 °C may be due to some host decomposition, since the complexes' physical state changed from white crystals to a yellow liquid at this temperature.]

4.1.8 Conclusions

With consistent H:G ratios of 1:1, **H_1** formed complexes with ANI, 3MANI and 4MANI, but failed to include 2MANI in the single solvent experiments. This host was recrystallized from various mixtures of these solvents and so was observed to display a significant preference towards 4MANI whenever this guest was present. Collectively, these experiments provided a host selectivity order of 4MANI > ANI > 3MANI > 2MANI, which mimicked that of the analogous guest series in § 3 (*p*-Xy > EB > *o*-Xy ≈ *m*-Xy) with respect to guest substitution pattern. SCXRD was employed to elucidate the reasons for the host preference for 4MANI, and it was found that this guest was involved in stronger interactions with the host when compared to the other guests. Hirshfeld surfaces were also considered, and 4MANI experienced the larger number of H···H interactions with the host, which also correlates with the host selectivity. After removing the guests from the packing calculation, it was observed that these occupied infinite one-dimensional channels within the host crystal. The host in all three complexes crystallized with a buckled sulfur-containing ring, and it was determined that **H_1** had near indistinguishable geometrical differences within each of the three complexes. Thermal experiments provided data, based on T_{on}, that correlated with the host selectivity behaviour.

4.1.9 Supporting information

NMR spectra, and GC and TG traces relevant to this work have been deposited in the Supplementary Information for this section. The raw data and associated % e.s.d.s that were required to set up relevant tables are also provided. The novel crystal structures for each complex were deposited at the Cambridge Crystallographic Data Centre, CCDC 1895446 (**H_1**·ANI), 1895447 (**H_1**·3MANI) and 1895448 (**H_1**·4MANI).

4.2. Inclusion compounds with **H_2**

4.2.1 Introduction

In the previous chapter, it was demonstrated that **H_2** is significantly more selective in the presence of the C8 aromatic fraction than **H_1**. Consequently, the selectivity of **H_2** in the presence of the anisole guests was investigated in order to determine whether this holds true here as well, in comparison with **H_1**.

4.2.2 Individual inclusions

After recrystallizing **H_2** independently from anisole and the methylanisole isomers, the resultant crystals were subjected to ^{1}H-NMR spectroscopy in order to determine whether inclusion had occurred. It was observed that **H_2** forms 1:1 H:G complexes with 4MANI and ANI, but 2MANI and 3MANI were not clathrated in this way (Table 4.6). **H_2** is, therefore, a more discerning host compound compared with **H_1** (which included three of the four guests), and this observation motivated an investigation where **H_2** was presented with multiple guest mixtures in order to observe any host selectivity in these conditions. [Integrated ^{1}H-NMR spectra of the respective complexes may be found in the Supplementary Information (Figures S62–63).]

Table 4.6. H:G ratios of inclusion compounds formed by **H_2**.[a]

Guest (G)	H:G
ANI	1:1
2MANI	[b]
3MANI	[b]
4MANI	1:1

[a]Determined using ^{1}H-NMR spectroscopy using $CDCl_3$ as solvent.
[b]No inclusion occurred.

4.2.3 Equimolar competition experiments

When **H_2** was recrystallized from the various equimolar combinations of the guests, the crystals that were collected from these experiments were subjected to ^{1}H-NMR spectroscopy as well as GC-MS analysis, and the averaged percentages are provided in Table 4.7 (where the

preferred guest is displayed in red; % e.s.d.s are in parentheses). In each case, the overall H:G ratio remained 1:1 regardless of the number and types of guest species included. From these results involving the MANIs, it is clear that **H_2** displays a significant selectivity for 4MANI, where this guest was preferentially included over 3MANI with a 93.6%:6.4% ratio, whereas 2MANI was discriminated against, in favour of 4MANI, with a 96.3%:3.7% ratio. When 4MANI was absent, no inclusion occurred from the 2MANI/3MANI mixture. These binary competition experiments therefore indicate a host selectivity order of 4MANI >> 3MANI > 2MANI, and this was confirmed through a ternary competition experiment between all three isomers (1.7%:4.8%:93.5% for 2MANI/3MANI/4MANI, respectively).

After ANI was introduced into the mixtures, the overall host selectivity order was modified to 4MANI > ANI > 3MANI > 2MANI which, once again, correlates closely with the alkyl aromatic guest experiments if one considers the guest substitution patterns. **H_2** fared exceptionally well as a selective host compared with **H_1** in the same conditions. The selectivity of **H_2** for 4MANI was nearly doubled to 82.6% (Table 4.7) from 46.1% for **H_1** (§ 4.1, Table 4.2) in the quaternary solvent experiment. The introduction of ANI to these experiments therefore decreased the selectivity of **H_1** towards 4MANI but, in comparison, this effect was much reduced for **H_2**. This was evident also when considering the ternary experiments that involved ANI, where the ANI/2MANI/4MANI and ANI/3MANI/4MANI solutions produced mixed complexes containing significant amounts of 4MANI (87.0 and 85.0%, respectively). The ANI/2MANI/3MANI experiments, however, yielded no crystals. Finally, a quaternary experiment with all four solvents resulted in a 4MANI (82.6%) > ANI (11.3%) > 3MANI (4.6%) > 2MANI (1.5%) mixed complex which correlates exactly with all of the prior binary and ternary competitions of **H_2** with this guest series. (All experiments were carried out in duplicate, and all duplicate values are provided in the Supplementary Information, Table S64.)

Table 4.7. Results of competition experiments using **H_2** and equimolar mixtures of the ANI and MANI guests.[a,b]

ANI	2MANI	3MANI	4MANI	Guest ratios	Overall H:G ratio	% e.s.d.s
x	x			96.3:3.7	1:1	(1.2):(1.2)
x		x		90.9:9.1	1:1	(1.0):(1.0)
x			x	14.3:85.7	1:1	(0.2):(0.2)
	x	x		[c]	-	-
		x	x	6.4:93.6	1:1	(0.2):(0.2)
	x		x	3.7:96.3	1:1	(0.2):(0.2)
x	x	x		[c]	-	-
x		x	x	10.5:4.5:85.0	1:1	(0.7):(0.3):(1.0)
x	x		x	10.9:2.1:87.0	1:1	(0.8):(0.3):(1.1)
	x	x	x	1.7:4.8:93.5	1:1	(0.5):(0.9):(1.3)
x	x	x	x	11.3:1.5:4.6:82.6	1:1	(0.3):(0.3):(0.7):(0.6)

[a]G:G ratios were determined using GC-MS with dichloromethane or chloroform as the solvent; overall H:G ratios were obtained by means of ^{1}H-NMR spectroscopy.
[b]Experiments were conducted in duplicate for confirmation purposes; % e.s.d.s are provided in parentheses.
[c]Crystallization did not occur, and a gel remained.

4.2.4 Ratio-dependent competition experiments

Figure 4.9a and b represent the overlaid selectivity profiles of **H_2** obtained from binary competition experiments between the anisole and the methylanisole isomers, and only the methylanisoles, respectively, where the G:G ratios varied. A selectivity profile could not be constructed for the 2MANI/3MANI experiment since no crystallization occurred from any of these solvent mixtures (Table 4.7).

a)

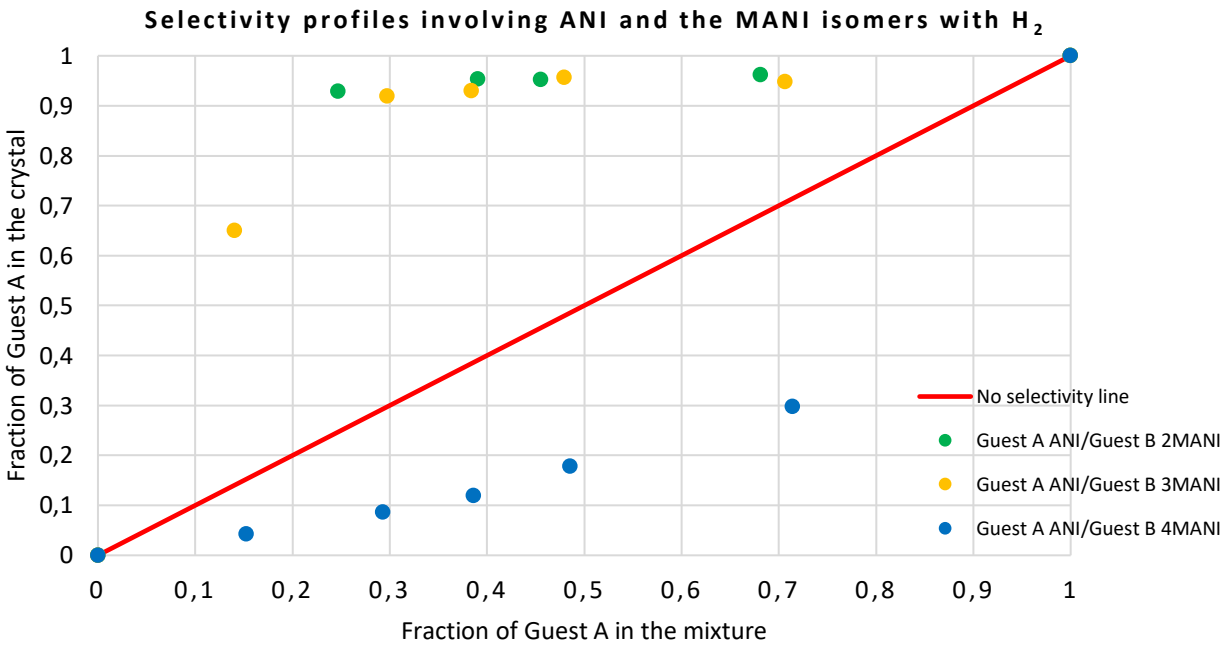

b)

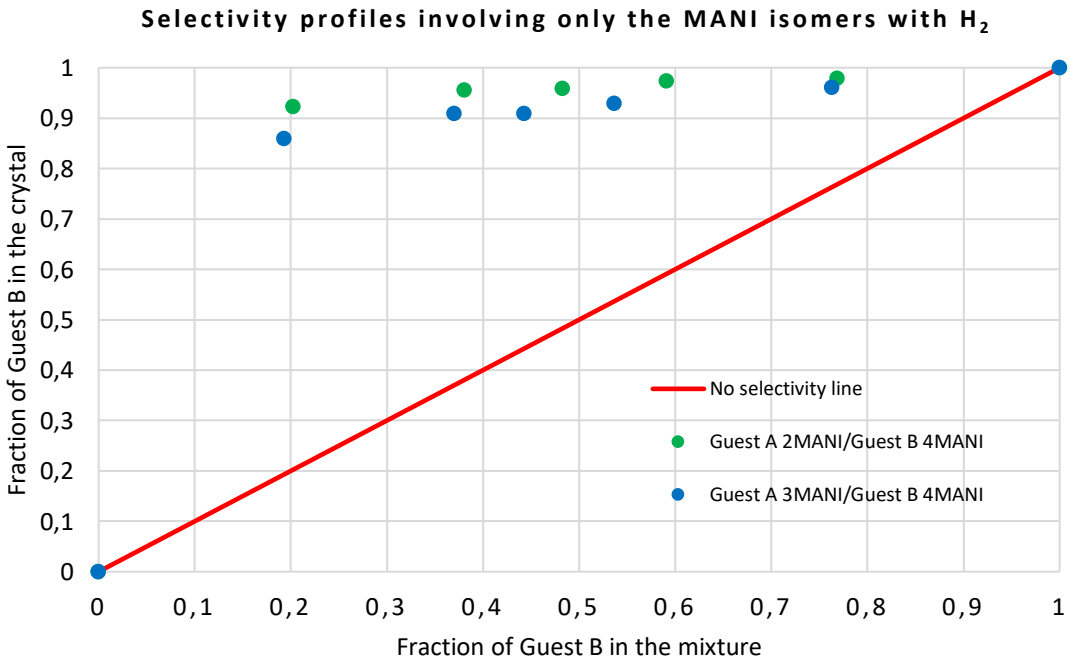

Figure 4.9. Overlaid selectivity profiles of **H_2** when recrystallized from a) binary guest combinations with ANI and the MANIs and b) binary guest combinations of the MANIs in the absence of ANI.

Figure 4.9a indicates that **H_2**, whether recrystallizing from ANI/2MANI or ANI/3MANI mixtures, consistently preferred the unsubstituted ANI guest (K = 26.8 and 18.2, respectively). However, when ANI was combined with 4MANI, the selectivity of the host shifted entirely towards the latter guest (K = 4.7). This was confirmed by results observed in Figure 4.9b, where 4MANI was preferentially enclathrated above the other isomers and across the complete concentration range (selectivity coefficients for the 2MANI/4MANI and 3MANI/4MANI experiments were 29.3 and 14.8, respectively, in favour of 4MANI). These results correspond to the host selectivity order for the four anisole guests (4MANI > ANI > 3MANI > 2MANI). (A complete set of the K values is provided in the Supplementary Information, Tables S65–69.)

4.2.5 SCXRD

The two successfully formed complexes of **H_2** were subjected to SCXRD to ascertain the reasons for the observed selectivity of the host. Table 4.8 thus contains crystallographic data for the 1:1 H:G complexes, **H_2**·ANI and **H_2**·4MANI. Both guests displayed rotational disorder around an inversion point. (Note that the formed species with ANI cocrystallized with a small amount of water, see Table 4.8.) Both complexes shared an isostructural host packing, crystallizing in a triclinic *P*-1 crystal system.

In both **H_2**·ANI and **H_2**·4MANI, the tricyclic fused ring system is near planar, and Figure 4.10a and b display the geometry of **H_2** in these complexes (together with the angle between the three atoms where the "bending" occurs in the heterocyclic, C–Ô–C), while Figure 4.10c is an overlay of the two structures. Clearly, **H_2** possesses near-identical geometries in the two complexes. The two benzene rings on either side of the heterocyclic in both trifused aromatic systems of **H_2** deviate from linearity by between 6.19° and 8.01° in the two complexes. The nitrogen atoms in the ethylenediamine linker of **H_2** crystallized in an antiperiplanar arrangement (Figure 4.11).

a)

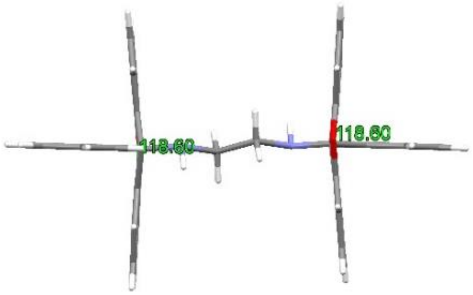

b)

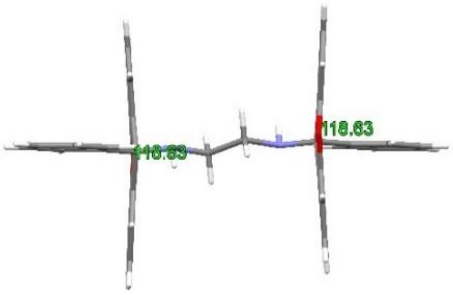

c)

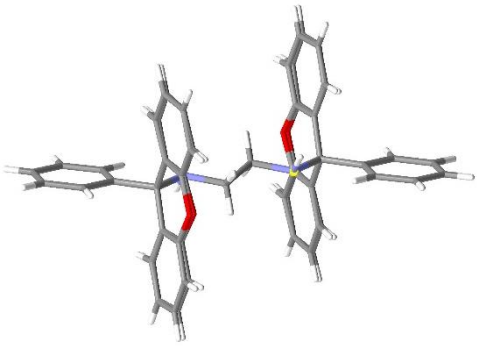

Figure 4.11. Host geometry within the respective complexes a) **H_2**·ANI and b) **H_2**·4MANI, and c) an overlay of the host molecule from each complex.

Subsequently, the host–host packing of **H_2** in its complexes with the anisoles was compared by removing the guests from the packing calculations. Figure 4.11a and b illustrates the result of this exercise.

a)

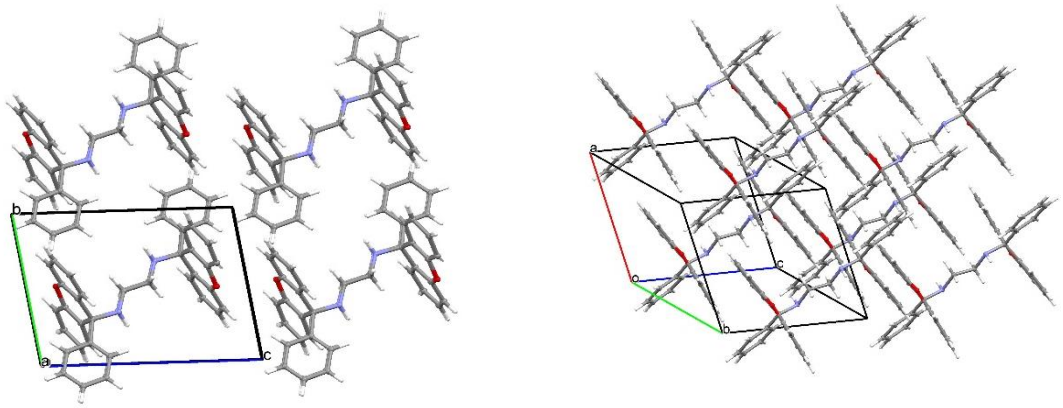

b)

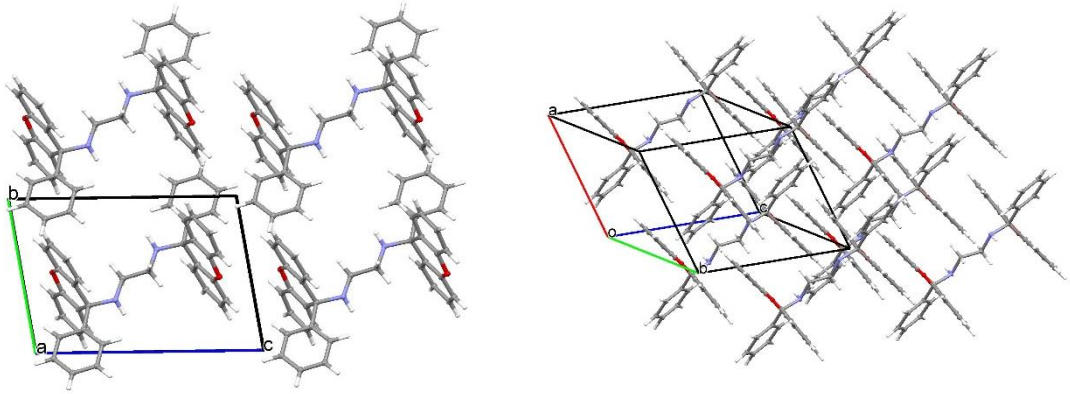

Figure 4.11. Host packing within the respective complexes of a) **H₂**·ANI and b) **H₂**·4MANI.

Clearly, **H₂** displays a very ordered host–host packing compared with **H₁**, and the reason for these packing differences may, once more, be related directly to the geometry of each host molecule, where the buckled S-containing ring of **H₁** prevents an ordered packing with the guest, while the more planar O-containing tricyclic fused ring system of **H₂** facilitates an ordered packing. The enhanced selectivity of **H₂** relative to **H₁**, therefore, may again be attributed to the tighter packing of the **H₂** molecules in the crystal.

The guest molecules were then removed from the packing calculation and the subsequent voids visualized in Mercury.[230] It is clear that the guest molecules occupy infinite channels within the host crystal, and this is displayed in Figure 4.12a and b.

a) b)

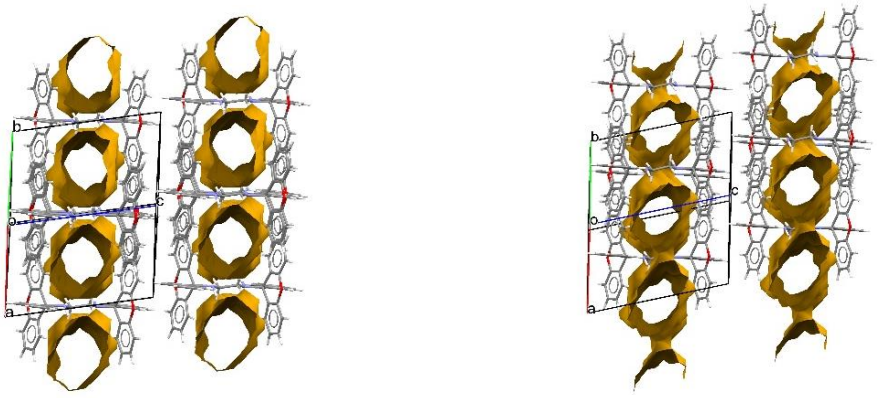

Figure 4.12. Calculated voids (dark yellow) for a) **H₂**·ANI and b) **H₂**·4MANI after removal of the guests from the packing calculation.

Table 4.8. Crystallographic data for **H₂**·ANI and **H₂**·4MANI

	H₂·ANI	**H₂**·4MANI
Chemical formula	$C_{40}H_{32}N_2O_2$ ·C_7H_8O·0.22(O)	$C_{40}H_{32}N_2O_2$ ·$C_8H_{10}O$
Formula weight	687.69	694.84
Crystal system	Triclinic	Triclinic
Space group	*P*-1	*P*-1
μ (Mo Kα)/mm^{-1}	0.079	0.079
a/Å	8.9198(5)	8.9125(5)
b/Å	9.1073(5)	9.0807(5)
c/Å	12.6511(7)	13.0222(6)
alpha/°	92.046(3)	90.729(2)
beta/°	107.834(2)	109.691(2)
gamma/°	111.184(2)	111.869(2)
V/$Å^3$	899.75(9)	909.28(9)
Z	1	1
F(000)	363	368
Temp./K	200	200
Restraints	0	0
Nref	4473	4523
Npar	256	274
R	0.0415	0.0416
wR2	0.1083	0.1107
S	1.04	1.04
θ min–max/°	2.4, 28.4	2.4, 28.3
Tot. data	22995	24571
Unique data	4473	4523
Observed data [I > 2.0 sigma(I)]	3429	3572
R_{int}	0.022	0.022
Dffrn measured fraction θ full	0.999	0.998
Min. resd. dens. (e/$Å^3$)	–0.21	–0.23
Max. resd. dens. (e/$Å^3$)	0.26	0.29

Table 4.9 contains a summary of the significant H···G interactions that facilitate retention of the guests within the host crystal for the two complexes of **H₂**. [A detailed table with H···G and H···H interactions is provided in the Supplementary Information (Table S70).] Interestingly, the **H₂**·4MANI inclusion compound did not experience any π···π contacts, while five very weak interactions of this type were identified in **H₂**·ANI. The latter guest is, furthermore, entrapped in the crystal of **H₂** by means of a $C_{(G)}$–$H_{(G)}$···$\pi_{(H)}$ [2.90 Å (137°)] and $N_{(H)}$–$H_{(H)}$···$C_{(G)}$ [2.68 Å (159°)] interaction while 4MANI experiences a greater number and variety of interaction types, including one $C_{(G)}$–$H_{(G)}$···$\pi_{(H)}$ (2.78 Å, 135°), two $N_{(H)}$–$H_{(H)}$···$C_{(G)}$–$C_{(G)}$ hydrogen bonds [2.63–2.70 Å (156–160°)] and one $C_{(H)}$–$H_{(H)}$···$H_{(G)}$–$C_{(G)}$ (2.30 Å, 127°) contacts.

Table 4.9. Significant H···G interactions present in complexes of **H_2** with the respective guests.[a,b,c]

Non-covalent interaction	**H_2**·ANI	**H_2**·4MANI	Symmetry
π···π	4.725(1)–5.920(1) Å [5]		
CH···π (H···Cg, C–H···Cg)			
$C_{(G)}$–$H_{(G)}$···$Cg_{(H)}$	2.90 Å, 137°		x, y, z
$C_{(G1)}$–$H_{(G1)}$···$Cg_{(H)}$		2.78 Å, 135°	−1+x, −1+y, z
H-bonding (H···A, D–H···A)			
$N_{(H)}$–$H_{(H)}$···$C_{(G1)}$	2.68 Å, 159° (<<)		1−x, −y, 1−z
$N_{(H)}$–$H_{(H)}$···$C_{(G2)}$–$C_{(G2)}$		2.63 Å, 156° (<<)	1−x, −y, 1−z
$N_{(H)}$–$H_{(H)}$···$C_{(G2)}$–$C_{(G2)}$		2.70 Å, 160° (<)	1+x, y, z
Other short contacts (X···Z, X–Y···Z)			
$C_{(H)}$–$H_{(H)}$···$H_{(G2)}$–$C_{(G2)}$		2.30 Å, 127° (<)	1+x, 1+y, z

[a]Values in square brackets indicate the number of H···G π···π interactions.
[b]Guest 1 (G1) and guest 2 (G2) represent the disordered guest components in the host crystal.
[c]Distances denoted by < are contacts that measure less than the sum of the van der Waals radii of the atoms involved, while those denoted by << is this sum minus 0.2 Å.

4.2.6 Hirshfeld surface analyses

Hirshfeld surface analyses could not be carried out on the **H_2**·ANI and **H_2**·4MANI complexes owing to the nature of the disorder displayed by the guests, that is, rotational disorder around an inversion point.

4.2.7 Thermal analyses (DSC and TG)

The thermal stability of the two successfully formed inclusion complexes was investigated, and the overlaid TG, derivative of the TG (DTG) and DSC traces thus obtained are provided in Figure 4.13a and b, and the relevant thermal data are summarized in Table 4.10.

a)

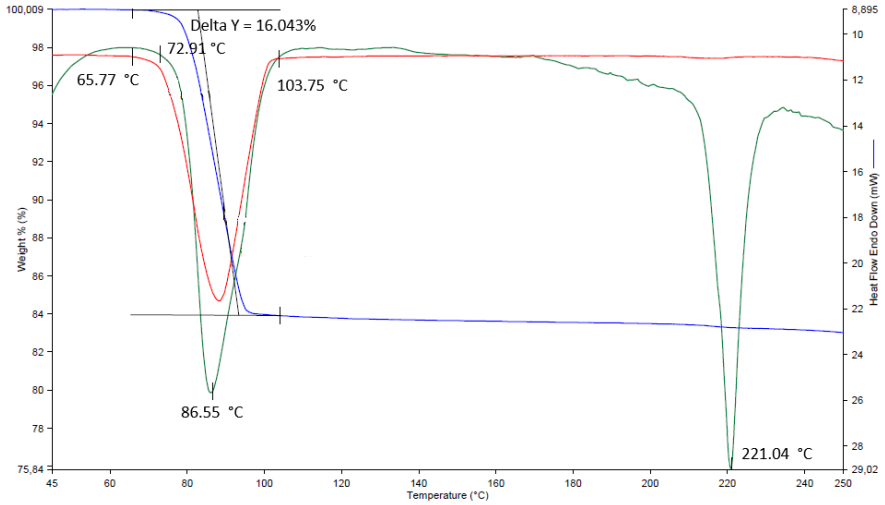

b)

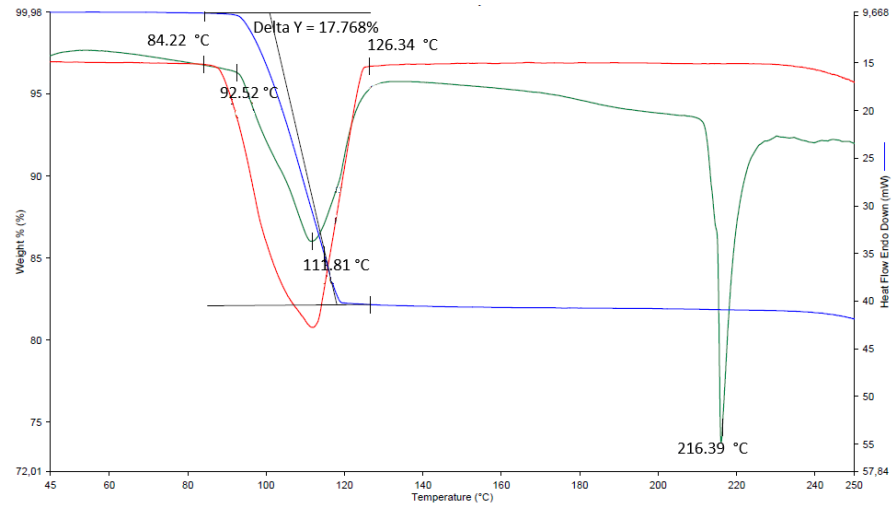

Figure 4.13. Thermal traces [DSC (green) , TG (blue) and DTG (red)] for a) **H₂**·ANI and b) **H₂**·4MANI.

Table 4.10. Thermal data for complexes **H₂**·ANI and **H₂**·4MANI.

Guest (G)	T_{on} /°C	T_p /°C	Mass loss expected /%	Actual mass loss measured /%
ANI	65.8	86.6	16.4	16.0
4MANI	84.2	111.8	17.6	17.8

For both samples, the expected mass loss upon release of the guest is in reasonable agreement with that expected theoretically (Table 4.10). Each trace showed a guest loss endotherm followed by the melting of **H₂** (221.0, 216.4 °C), and appears significantly less convoluted than the complexes of **H₁** with these guest types. The T_{on} and T_p values indicate a higher relative thermal stability for the **H₂**·4MANI complex (84.2, 111.8 °C) compared with **H₂**·ANI (65.8, 86.6 °C), which correlated exactly with the selectivity preference displayed by **H₂** for these guests.

4.2.8 Conclusions

H_2 proved to be an efficient host compound for ANI and 4MANI, including these guests in a 1:1 H:G ratio. When this host was recrystallized from various mixtures of the anisole guests, a high selectivity towards 4MANI (82.6% from the quaternary guest mixture) was observed, and an overall host selectivity order of 4MANI >> ANI > 3MANI > 2MANI was noted. SCXRD revealed that 4MANI experienced a greater number of stabilizing interactions in the host crystal compared with ANI, in accordance with this host's selectivity order. Hirshfeld surface analyses could not be carried out on the complexes owing to the guests displaying disorder around an inversion point, and thermal analyses showed that ANI was not as tightly bound in the crystal as 4MANI (based on T_{on} and T_p values) (this was also in direct accordance with the host selectivity order). **H_2** proved to be significantly more selective than **H_1**, and this is, once more, possibly as a result of the more ordered and tighter host packing displayed by **H_2** relative to **H_1** as a result of the near-planar oxygen-containing tricyclic fused moiety of **H_2** versus the buckled sulfur-containing one. These same observations were also noted in the work with the C8 aromatic fraction with these hosts.

4.2.9 Supporting information

All relevant spectra, traces and raw data have been placed in the Supplementary Information for this section. The novel crystal structures for each complex were deposited at the Cambridge Crystallographic Data Centre, CCDC 1895593 (**H_2**·ANI) and 1895592 (**H_2**·4MANI).

5. METHYLPYRIDINE ISOMERS AND PYRIDINE

5.1 Inclusion compounds with $\mathbf{H_1}$

5.1.1 Introduction

The focus on methylpyridine separations is of significant industrial importance. The boiling points of the three isomers are very similar and, consequently, their separation and purification by means of fractional distillation is a difficult, expensive and time-consuming process.[249] These compounds have extensive industrial application as solvents, colourants and as precursors to countless pharmaceutical and agrochemical compounds, as well as in the preparation of various polymers and textiles.[249] Therefore, a simplistic and inexpensive method of separating them from one another, based on host-guest chemistry, may provide an attractive alternative to current methodologies. There have been many advances in the design of highly selective host species for these guest types: for example, the wheel-and-axle compound, 1,1,6,6-tetraphenylhexa-2,4-diyne-1,6-diol, was observed to display selectivity for 4-methylpyridine when recrystallized from an equimolar binary mixture of this guest and pyridine.[250] Furthermore, the team of Nassimbeni *et al.* carried out competition experiments where their host compound, comprising both rigid fluorenyl and binaphthyl units, exhibited a selectivity preference for these guests in the order 4- > 3- > 2- methylpyridine.[158] More recently, Tiffin *et al.*[251] studied the preferences of three TADDOL-derived host compounds towards the methylpyridine isomers, and all three hosts displayed different preferences towards these isomers. This was rationalized by analysis of the resulting crystal structures and crystal packing, and their results correlated with thermal analysis. In this present work, the use of $\mathbf{H_1}$ for the inclusion and possible separation of mixtures of pyridine (PYR) and 2- (2MP), 3- (3MP) and 4- methylpyridine (4MP) (Scheme 5.1) is reported.

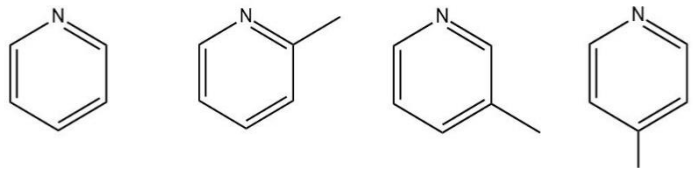

Scheme 5.1. Structures of the MP isomers and PYR guest compounds.

5.1.2 Individual inclusions

Table 5.1 summarizes the results of the H:G ratios that were obtained through the integration of relevant host and guest resonance signals from ^{1}H-NMR experiments on successfully formed complexes when **H$_1$** was recrystallized independently from each potential guest solvent. (Spectra of the respective complexes may be found in the Supplementary Information, Figures S71–74.)

Table 5.1. H:G ratios of inclusion compounds formed by **H$_1$**.[a]

Guest (G)	H:G
PYR	1:1
2MP	1:1
3MP	1:1
4MP	1:1

[a]Determined using ^{1}H-NMR spectroscopy with $CDCl_3$ as solvent.

These experiments have shown that **H$_1$** is a capable host species for the individual enclathration of PYR, 2-, 3- and 4- MP, including each of these consistently with a 1:1 H:G ratio (Table 5.1).

5.1.3 Equimolar competition experiments

Table 5.2 provides a summary of the chemical shifts for the proton resonance signals of the pure guests. From these data and an overlaid ^{1}H-NMR spectrum of the complexes (Supplementary Information, Figure S75), it was concluded that NMR would not be a suitable method of analysis for mixed complexes (guest resonances overlap with that of the host, and of other guests, making accurate integration not possible). GC-MS was therefore selected as the analysis technique, and a chromatograph of each guest standard and a mixture of guests may be found in the Supplementary Information (Figures S76–80). ^{1}H-NMR spectroscopy, however, was used to determine overall H:G ratios.

Table 5.2. ^{1}H-NMR-data for pure PYR, 2MP, 3MP and 4MP.

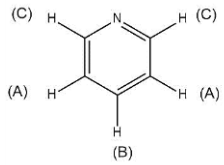		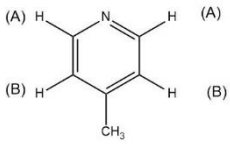		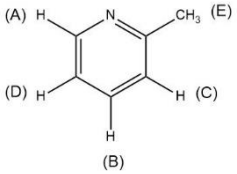		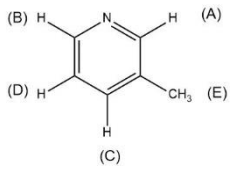	
Assignment	**δ(ppm)**	**Assignment**	**δ(ppm)**	**Assignment**	**δ(ppm)**	**Assignment**	**δ(ppm)**
(A) H	6.88–6.91	(A) H	8.46	(A) H	8.48	(A) H	8.44
(B) H	7.27–7.31	(B) H	7.10	(B) H	7.54	(B) H	8.42
(C) H	8.24–8.25	(C) Methyl	2.35	(C) H	7.12	(C) H	7.46
				(D) H	7.08	(D) H	7.16
				(E) Methyl	2.55	(E) Methyl	2.32

Since **H$_1$** possesses the ability to individually include PYR and the isomeric MPs, we subsequently conducted competition experiments to ascertain whether the host shows selectivity in the presence of any of these guests in mixtures. Mixed equimolar binary, ternary and quaternary variations of the guests were considered, and hence Table 5.3 was populated with the average of the obtained GC-MS data. The preferred guest is shown in red font for ease of examination. [Experiments were conducted in triplicate and these values are provided in the Supplementary Information (Table S81).]

Table 5.3. Results of competition experiments using **H$_1$** and various guest mixtures.[a,b]

PYR	2MP	3MP	4MP	Average guest ratios	Overall H:G ratio	% e.s.d.s
	x	x		16.8:83.2	1:1	(0.8):(0.8)
	x		x	24.2:75.8	1:1	(1.1):(1.1)
		x	x	69.9:30.1	1:1	(0.5):(0.5)
	x	x	x	9.3:63.5:27.2	1:1	(0.6):(0.2):(0.7)
x	x			77.1:22.9	1:1	(2.4):(2.4)
x		x		38.8:61.2	1:1	(3.0):(3.0)
x			x	62.4:37.6	1:1	(0.8):(0.8)
x	x	x		35.0:10.8:54.2	1:1	(0.4):(1.5):(1.2)
x	x		x	56.5:12.3:31.2	1:1	(0.6):(1.5):(2.1)
x		x	x	21.2:50.7:28.1	1:1	(1.7):(0.3):(1.6)
x	x	x	x	25.3:6.9:47.0:20.8	1:1	(0.6):(3.3):(1.9):(3.2)

[a]G:G ratios were determined using GC-MS with dichloromethane as solvent; overall H:G ratios were obtained by means of ^{1}H-NMR spectroscopy.
[b]Experiments were conducted in triplicate for confirmation purposes; % e.s.d.s are provided in parentheses.

The overall H:G ratio remained 1:1 in all of these competitions, which was also the favoured ratio in the single solvent experiments (Table 5.1). From this table, it is evident that **H_1** consistently favours 3MP whenever it is present. In the equimolar binary experiments involving the MPs, 83.2 and 69.9% of 3MP was included by the host when recrystallized from mixtures of 2MP/3MP and 3MP/4MP, respectively. In the absence of 3MP, **H_1** remained preferential in its behaviour, and selected significantly more of 4MP (75.8%) than 2MP (24.2%) (in the 2MP/4MP experiment). A ternary experiment involving the three MP isomers, once again, highlighted the host's preference for 3MP, and the selectivity was revealed to be in the order 3MP (63.5%) >> 4MP (27.2%) > 2MP (9.3%), in accordance with that which might have been expected when considering results from the binary experiments alone.

Addition of PYR to these competitions did not alter the selectivity order of the host for the MPs other than to insert, as its preference, this guest over 4- and 2- MP. 3MP remained the favoured guest in all instances. Equimolar binary experiments with PYR/2MP, PYR/3MP and PYR/4MP resulted in the preferential inclusion of PYR (77.1%), 3MP (61.2%) and PYR (62.4%), respectively. The three ternary experiments where PYR was present, PYR/2MP/3MP, PYR/2MP/4MP and PYR/3MP/4MP, showed selective enclathration of 3MP (54.2%), PYR (56.5%) and 3MP (50.7%), correspondingly. An experiment where the host was recrystallized from an equimolar mixture of all four guests, and a consideration of the results of all binary and ternary experiments, therefore allowed us to conclude that the overall selectivity of this host compound may be written as in the order 3MP > PYR > 4MP > 2MP. The only experiment which is not in agreement with this summary is when the recrystallizing mixture contained PYR/3MP/4MP, where 4MP was slightly favoured over PYR (28.1 versus 21.2%); however, here 3MP remained the preferred guest solvent.

5.1.4 Ratio-dependent competition experiments

Experiments in which the host compound was recrystallized from binary mixtures of any two guest species were conducted while the ratio of each guest in the mixture was varied systematically. After consideration of the so-obtained data, the following overlaid selectivity profiles [Figure 5.1a (MP combinations) and b (PYR/MP combinations)] were thus constructed. Additionally, the average selectivity coefficients were calculated, and a complete set of these K values are provided in the Supplementary Information, Tables S82–87.

a)

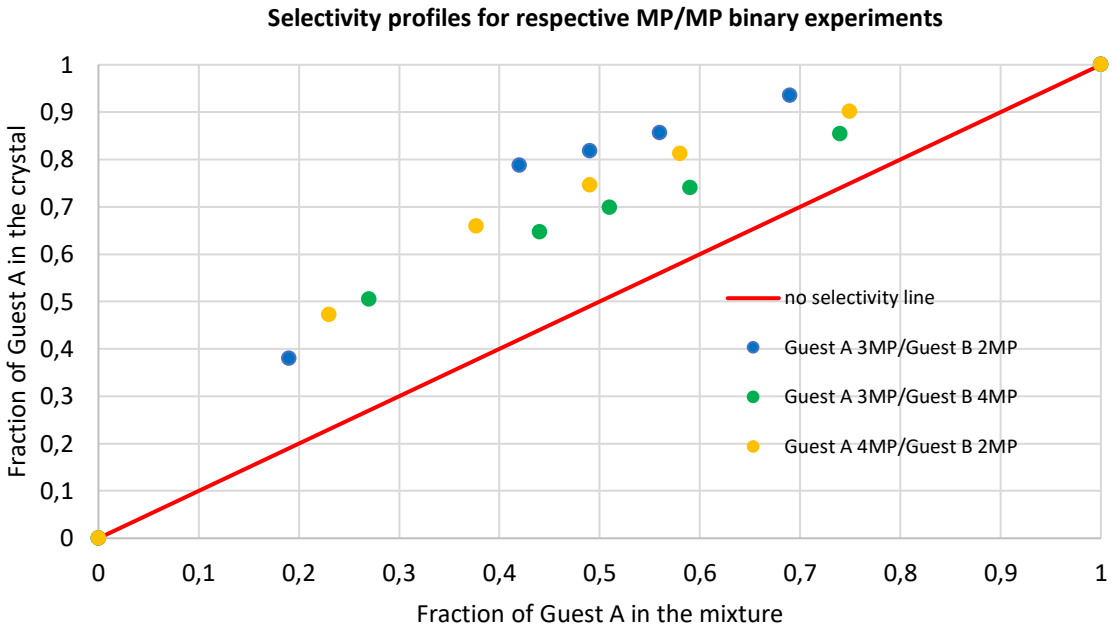

b)

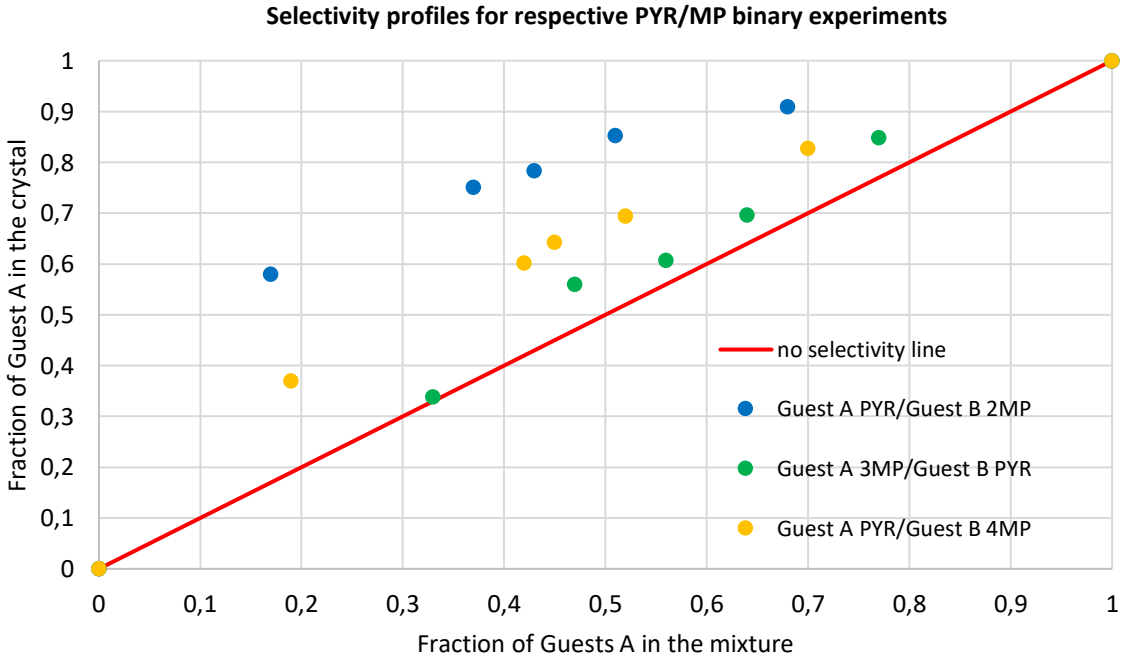

Figure 5.1. Selectivity profiles for G/G combinations in the a) absence of PYR and b) presence of PYR.

It is clear from Figure 5.1a that **H_1** has a considerable preference for 3MP whenever it is present: analyses of the 3MP/2MP and 3MP/4MP experiments showed that the amount of 3MP in each crystalline inclusion compound was always greater than the amount present in the solution from which the crystals had formed (K = 4.7 and K = 2.3, respectively). The 4MP/2MP experiment revealed that the selectivity for 4MP was significant (K = 3.5) in these conditions. In the 3MP/PYR experiment (Figure 5.1b), the host displayed some ambivalence in its selectivity but only at low concentrations of 3MP: K = 1 (i.e., there was no selectivity) when the solution contained approximately 33% 3MP, after which point the host displayed some selectivity in favour of 3MP once more (K = 1.3). In the absence of 3MP and presence of PYR, the host's selectivity was consistently for PYR, regardless of this guest's concentration in the solution [PYR/4MP (K = 2.2) and PYR/2MP (K = 5.2)]. These selectivity experiments further confirm the preference of the host for these guests to be in the order 3MP > PYR > 4MP > 2MP.

5.1.5 SCXRD

After SCXRD analyses, it was observed that each of the four complexes crystallizes in the monoclinic crystal system and $P2_1/n$ space group (Table 5.4), and all of them are isostructural with respect to the host packing, as observed in the depiction of the unit cells in Figure 5.2a–d. 4MP displayed disorder over several positions, to the extent that this disorder could not be modelled fittingly. Each of the other guest molecules, however, assumed only one orientation in their respective crystals.

Table 5.4. Crystallographic data for **H₁**·PYR, **H₁**·2MP, **H₁**·3MP and **H₁**·4MP.

	H₁·PYR	**H₁**·2MP	**H₁**·3MP	**H₁**·4MP
Chemical formula	$C_{40}H_{32}N_2S_2$ ·C_5H_5N	$C_{40}H_{32}N_2S_2$ ·C_6H_7N	$C_{40}H_{32}N_2S_2$ ·C_6H_7N	$C_{40}H_{32}N_2S_2$ ·C_6H_7N
Formula weight	683.90	697.92	697.92	697.92
Crystal system	Monoclinic	Monoclinic	Monoclinic	Monoclinic
Space group	$P2_1/n$	$P2_1/n$	$P2_1/n$	$P2_1/n$
μ (Mo Kα)/mm^{-1}	0.195	0.189	0.191	0.190
a/Å	10.1347(3)	10.5651 (6)	10.3996 (4)	10.4008 (8)
b/Å	13.3006(3)	13.0737(7)	13.3612 (6)	13.2791(10)
c/Å	25.3821(7)	25.7522(15)	25.3108 (11)	25.5934(19)
alpha/°	90	90	90	90
beta/°	91.964(2)	92.053(3)	91.310 (2)	90.039(3)
gamma/°	90	90	90	90
V/Å^3	3419.44(2)	3554.7 (3)	3516.1 (3)	3534.8 (5)
Z	4	4	4	4
F(000)	1440	1472	1472	1472
Temp./K	200	200	200	200
Restraints	0	0	0	0
Nref	8508	8847	8747	8822
Npar	459	469	469	436
R	0.0343	0.0381	0.0368	0.0569
wR2	0.0970	0.1041	0.0999	0.1648
S	1.06	1.06	1.03	1.03
θ min–max/°	1.6, 28.3	1.6, 28.3	1.6, 28.3	1.6, 28.4
Tot. data	74142	160065	78757	84737
Unique data	8508	8847	8747	8822
Observed data [I > 2.0 sigma(I)]	6832	7654	7099	7448
R_{int}	0.035	0.019	0.023	0.018
Dffrn measured fraction θ full	1.000	0.998	1.000	0.999
Min. resd. dens. (e/Å^3)	–0.25	–0.28	–0.26	–1.02
Max. resd. dens. (e/Å^3)	0.31	0.35	0.36	0.93

a) b)

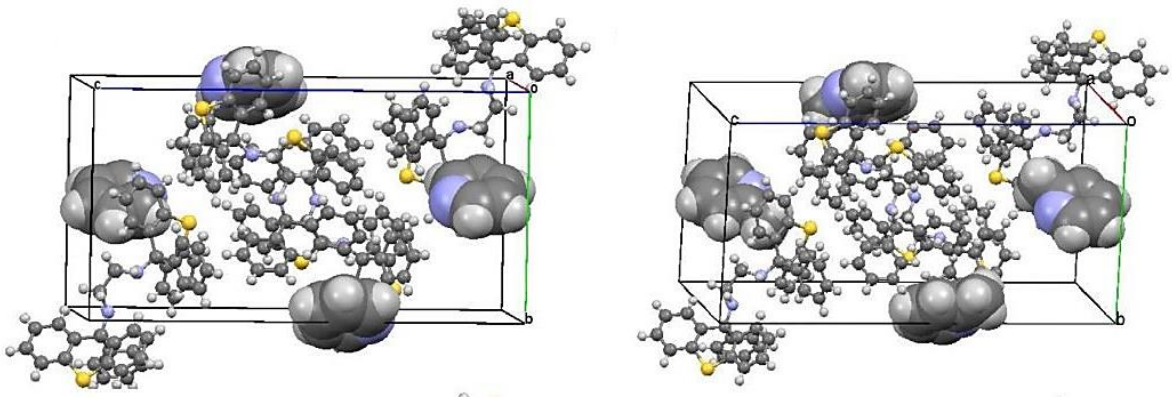

c) d)

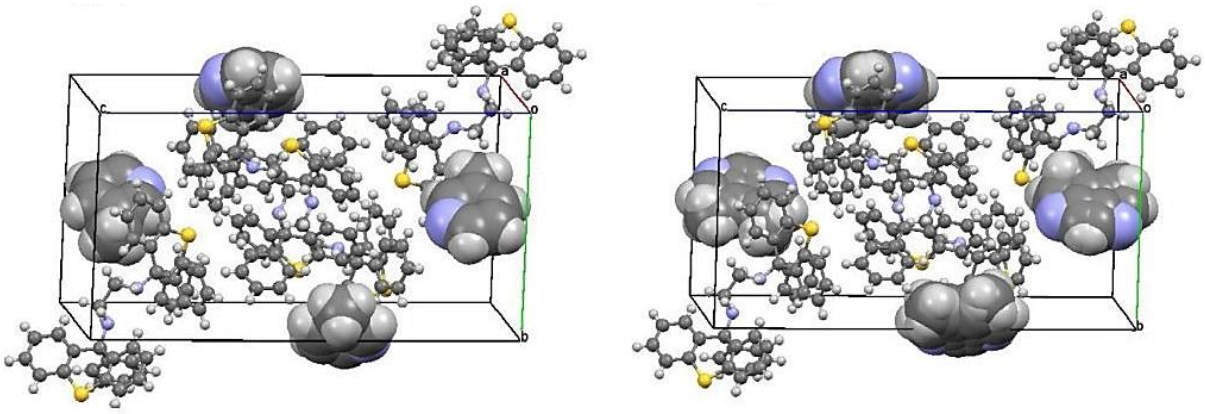

Figure 5.2. Unit cells for a) **H₁**·PYR, b) **H₁**·2MP, c) **H₁**·3MP and d) **H₁**·4MP; host molecules are shown in ball-and-stick representation and guests in space-fill form; only the 4MP guests are disordered.

Consequently, the H···G interactions were considered in each of these complexes to attempt to establish the reasons for the host's obvious bias towards 3MP. Note that due to the difficulty in modelling, adequately, the significant disorder in the 4MP guest, the resultant H···G bond distances and angles were discounted in this present investigation. Consequently, only the interactions present in the other three inclusion compounds have been summarized in Table 5.5. (The H···H interactions are provided in the Supplementary Information, Table S88.)

Table 5.5. Crystallographic data for **H₁**·PYR, **H₁**·2MP and **H₁**·3MP.[a,b,c]

Non-covalent interaction	**H₁**·PYR	**H₁**· 2MP	**H₁**·3MP	Symmetry
π···π	4.782(1)–5.975(1) Å [9]	4.960(1)–5.950(1) Å [8]	5.008(1)–5.987(1) Å [9]	
C–H···π (H···Cg, C–H···Cg) $C_{(G)}$–$H_{(G)}$···$Cg_{(H)}$			2.76 Å, 138°	–1+x, y, z
Other short contacts (X···Z, X–Y···Z) $C_{(H)}$–$H_{(H)}$···$H_{(G)}$–$C_{(G)}$			2.32 Å, 158° (<)	1–x, 1–y, 1–z

[a]Distances denoted by < are contacts that measure less than the sum of the van der Waals radii of the atoms involved.
[b]4MP experienced significant disorder which could not be modelled satisfactorily, and hence the H···G interactions for this complex are not included here.
[c]Values in square brackets indicate the number of H···G π···π interactions.

A close analysis of the intermolecular H···G interactions revealed that there exists more π···π contacts in the case of the 3MP and PYR inclusion compounds, the more favoured guests [9 contacts each, ranging overall from 4.782(1) to 5.987(1) Å] compared with the complex containing 2MP [8 contacts, 4.960(1)–5.950(1)]; however, this is not significant since all interactions are very weak and comparable. More significantly, the most preferred guest (3MP) is the only one to experience $C_{(G)}–H_{(G)}\cdots\pi_{(H)}$ (2.76 Å, 138°) and a $C_{(H)}–H_{(H)}\cdots H_{(G)}–C_{(G)}$ (2.32 Å, 158°) interaction (Figure 5.3a and b, respectively), and this observation may explain the observed affinity of **H_1** for 3MP. Surprisingly, any intermolecular H-bonds present are non-classical and host···host in nature, despite the H-bond acceptor and donor capabilities of the guest and host species, respectively.

a) b)

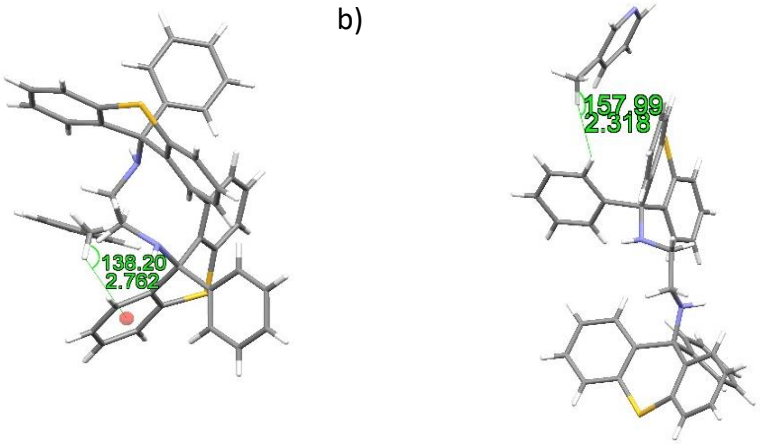

Figure 5.3. The preferred guest, 3MP, is involved in a) $C_{(G)}–H_{(G)}\cdots\pi_{(H)}$ and b) $C_{(H)}–H_{(H)}\cdots H_{(G)}–C_{(G)}$ interactions.

The guest molecules were omitted from the packing calculation using the Mercury CSD software package. Figure 5.4 is representative of the four resultant void diagrams (using the **H_1**·PYR inclusion complex in the calculation).

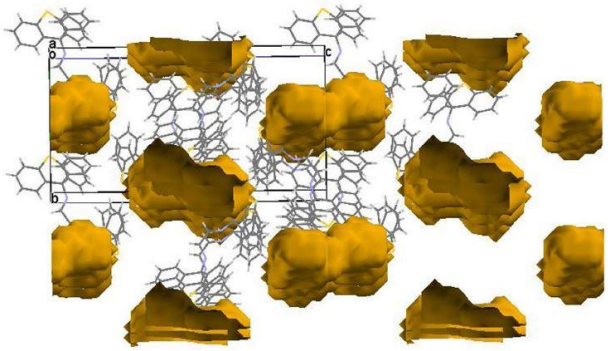

Figure 5.4. Discrete voids are present in the host crystal in all four complexes after guest removal (using **H_1**·PYR as the representative example).

In each complex, the guests occupy discrete voids, with two of these molecules contained in each. Once again it was found that the host molecule adopted a "buckled" geometry in all of its complexes here with respect to the tricyclic fused aromatic ring system (deviating from linearity by 29.03–33.93°). Furthermore, and in previous complexes, the ethylenediamine linker in this host has the two nitrogen atoms in a gauche conformation. This host geometry, once more, is possibly responsible for the nature of the host packing observed in these complexes (diagrams of the packing in all four complexes are provided in the Supplementary Information, Figure S89).

5.1.6 Hirshfeld surface analyses

Subsequently, Hirshfeld surface analyses of the guests within each H/G complex were considered, but no correlation between the host selectivity order that was established from equimolar and binary non-equimolar competition experiments as well as the crystal structures, could be observed: the relative percentages of interactions are very similar in all of these complexes (Figure 5.5). Note that the N···H and C···H interactions are common here because of the nature of both host and guest. (The 2D fingerprint plots for the complexes are provided in the Supplementary Information, Figure S90.) (Due to the nature of the disorder of the 4MP guest, Hirshfeld surface analyses could not be carried out on the **H$_1$**·4MP complex.)

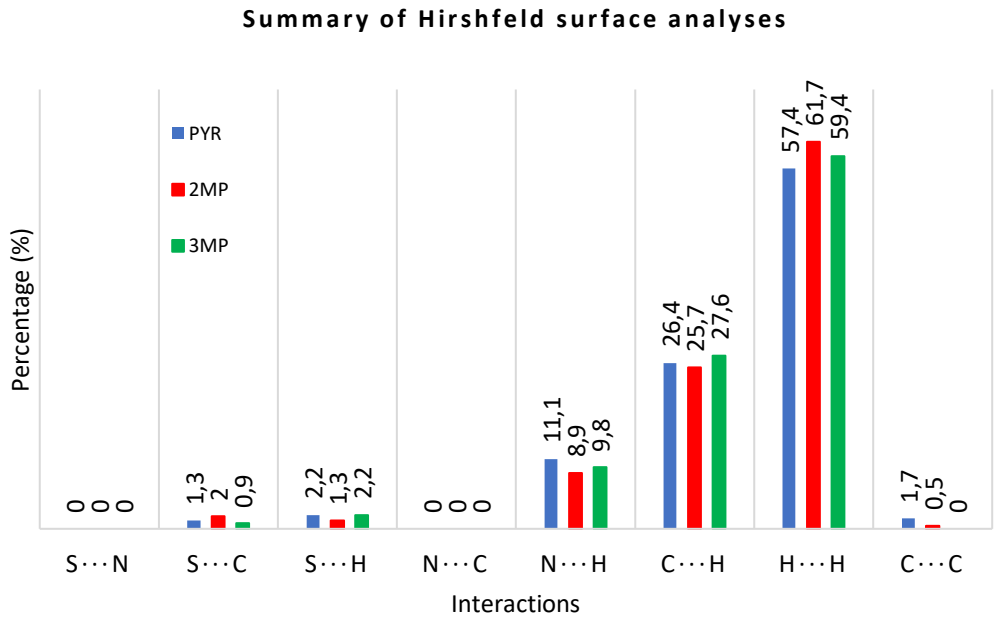

Figure 5.5. Quantitative interactions after Hirshfeld surface analyses.

5.1.7 Thermal analyses (DSC and TG)

After heating the complexes at 10 °C·min^{-1} under thermal analysis conditions, the traces (DSC, TG and DTG) provided in Figure 5.6a–d were obtained, and the relevant thermal data are summarized in Table 5.6. The thermal events observed for each inclusion compound were not unexpected: each DSC is characterized largely by two endotherms, the first representing guest release, and the second the melting of the host compound (176.8–178.7 °C, endotherm peak temperatures). After closer analysis of the guest release process for the PYR-containing complex (Figure 5.6a), two overlapping endotherms are observed, the first peaking at 137.2, and the second at 142.0 °C, which is similar to that for the release of 3MP (133.5 °C). We noted from an earlier selectivity profile that PYR alone competed at least to some extent with 3MP (Figure 5.1b, green profile), and these similar T_p values may reflect this fact. The remaining values follow an identical trend to the selectivity order for this host: these decrease in the order 3MP (133.5 °C) > 4MP (119.1 °C) > 2MP (95.3 °C). The T_{on} values are in the order PYR (91.1 °C) > 3MP (83.4 °C) > 4MP (77.7 °C) > 2MP (64.5 °C) (Table 5.6). The mass loss that was measured for complexes containing PYR (12.4%) and 3MP (14.0%) upon complete guest removal is in reasonable agreement with that expected (11.7 and 13.4%, respectively, Table 5.6). The 2MP and 4MP complexes, however, experienced mass losses of only 11.2 and 10.8%, respectively (expected 13.4%). In the former instance, this may be as a result of the uncertainty in assessing the guest release end point owing to the continual downward slope of the TG; however, in the latter case, this observation cannot be explained with certainty.

a)

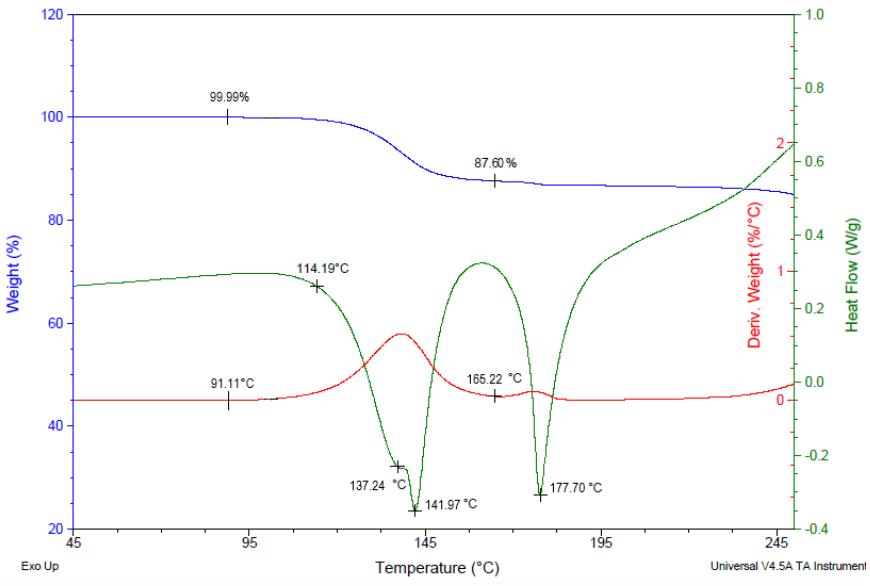

b)

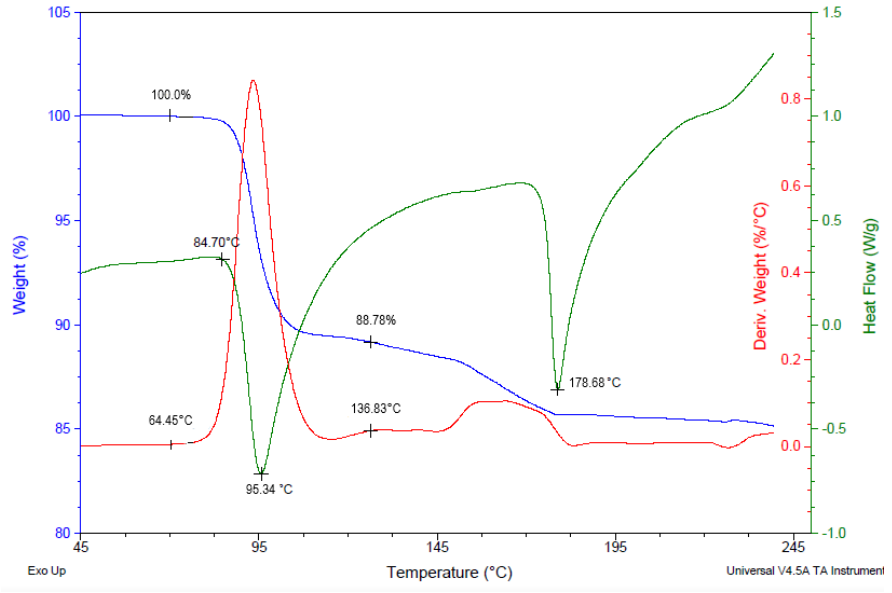
100.0%
84.70°C
88.78%
64.45°C
95.34 °C
136.83°C
178.68 °C
Weight (%)
Deriv. Weight (%/°C)
Heat Flow (W/g)
Temperature (°C)
Exo Up
Universal V4.5A TA Instrument

c)

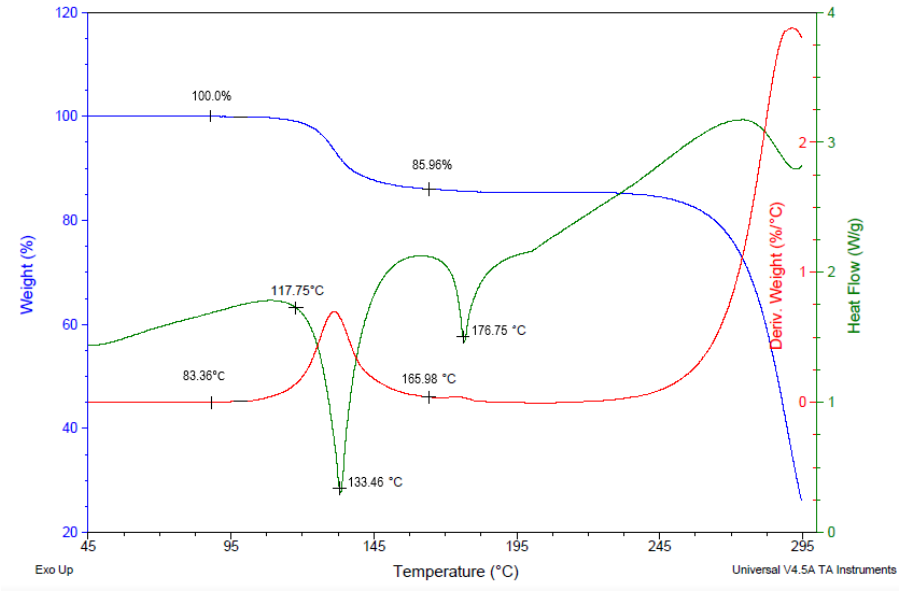
100.0%
85.96%
117.75°C
83.36°C
176.75 °C
165.98 °C
133.46 °C
Weight (%)
Deriv. Weight (%/°C)
Heat Flow (W/g)
Temperature (°C)
Exo Up
Universal V4.5A TA Instruments

d)

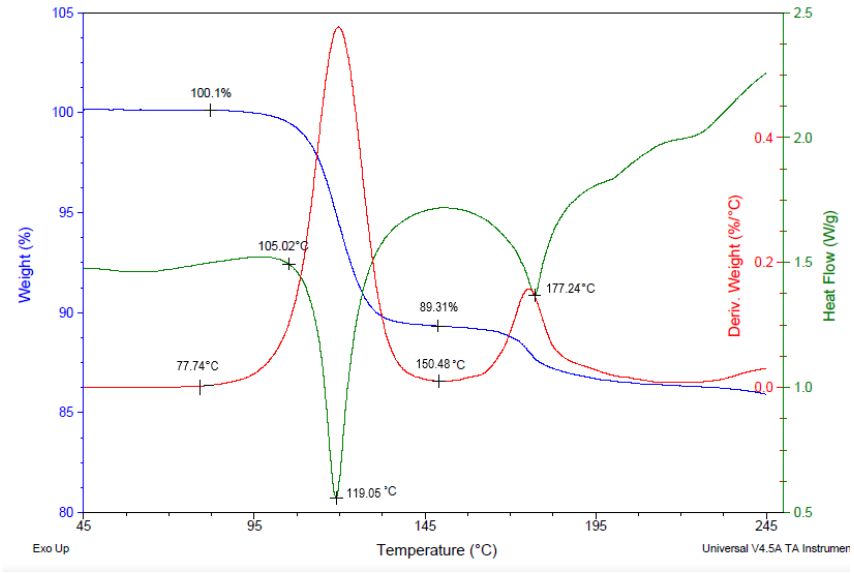

Figure 5.6. The overlaid DSC (green), TG (blue) and DTG (red) traces for **H_1** in its complexes with a) PYR, b) 2MP, c) 3MP and d) 4MP.

Table 5.6. Thermal properties of complexes formed by **H_1**.

Guest (G)	T_{on} /°C	T_p /°C	Mass loss expected /%	Mass loss measured /%
PYR	91.1	137.2, 142.0	11.7	12.4
2MP	64.5	95.3	13.4	11.2
3MP	83.4	133.5	13.4	14.0
4MP	77.7	119.1	13.4	10.8

5.1.8 Conclusions

H_1 was recrystallized from each of PYR and the MP isomers, and each one was enclathrated with a 1:1 H:G ratio. Recrystallization of this host from various equimolar binary mixtures of these guests showed **H_1** to favour 3MP significantly. From an equimolar ternary mixture of the three MPs, a host selectivity order of 3MP (63.5%) >> 4MP (27.2%) > 2MP (9.3%) was obtained, while from a similar mixture with added PYR, the preference was in the order 3MP (47.0%) > PYR (25.3%) > 4MP (20.8%) > 2MP (6.9%). Binary G:G ratios were also varied, and the host recrystallized from such mixtures: **H_1** remained consistently selective for 3MP, even at low concentrations of this guest. One exception was noted: when these experiments were carried out between 3MP and PYR (the first and second favoured guests, respectively), the host showed ambivalence when the solution contained 33% 3MP, and K = 1 here. At higher concentrations of 3MP, the host returned to its usual bias in favour of 3MP. SCXRD

experiments revealed that the four inclusion compounds of **H_1** experienced isostructural host packing (monoclinic, $P2_1/n$). Furthermore, the 4MP guest displayed significant disorder, and much of this could not be modelled. In each inclusion compound, guests resided in discrete cavities, and each void accommodated two of these molecules. A study of the H···G interactions obtained from SCXRD analyses was useful for establishing the reasons for the observed preference for 3MP: this guest experienced both a $C_{(G)}–H_{(G)}\cdots\pi_{(H)}$ (2.76 Å, 138°) and a $C_{(H)}–H_{(H)}\cdots H_{(G)}–C_{(G)}$ (2.32 Å, 158°) interaction, which are absent in the other two inclusion compounds. Finally, thermal analyses correlated reasonably well with the host selectivity order for these guests with respect to both T_p and T_{on} values.

5.1.9 Supporting information

All relevant spectra and detailed tables are provided in the Supplementary Information. The crystal structures were deposited at the Cambridge Crystallographic Data Centre, and CCDC numbers 1549682 (**H_1**·PYR), 1549683 (**H_1**·2MP), 1549684 (**H_1**·3MP) and 1549685 (**H_1**·4MP) contain the supplementary crystallographic data for this chapter.

5.2. Inclusion compounds with **H_2**

5.2.1 Introduction

The host capabilities of **H_2** in the presence of these pyridines were investigated, and the results will now be reported.

5.2.2 Individual inclusions

When **H_2** was independently recrystallized from PYR and each of the three MP isomers and the crystals isolated, washed and subjected to ^{1}H-NMR spectroscopy, it was observed that, with the exception of 2MP, each solvent was complexed, PYR and 4MP with 1:2 H:G ratios, and 3MP with a H:G ratio of 3:5 (Table 5.7). The latter complex crystallized with some water. (The integrated ^{1}H-NMR spectra of the respective complexes may be found in the Supplementary Information, Figures S91–94.)

Table 5.7. H:G ratios of inclusion compounds formed by **H_2**.[a]

Guest (G)	H:G
PYR	1:2
2MP	[b]
3MP	3:5
4MP	1:2

[a]Determined using ^{1}H-NMR spectroscopy with $CDCl_3$ as solvent.
[b]No inclusion occurred.

5.2.3 Equimolar competition experiments

As considered for **H_1**, a series of competition experiments were carried out in which **H_2** was recrystallized from various equimolar combinations of PYR and the MP isomers. The crystals that were collected from these vials were subjected to ^{1}H-NMR spectroscopy as well as GC-MS analysis, and the averaged results are provided in Table 5.8 (where the preferred guest is displayed in red for ease of examination). Experiments were conducted in duplicate, and all of these values are provided in the Supplementary Information, Table S95. In each case, the overall H:G ratio remained 1:2 regardless of the number and type of guest species included. From these results, it is clear that **H_2** also displays selectivity for 3MP whenever this guest is present (as was the case for **H_1**). In particular, 3MP was preferentially included over 2MP with a 70.4%:29.6% ratio, whereas 4MP was discriminated significantly against, in favour of 3MP (91.6%:8.4%). When 3MP was absent (2MP/4MP), no crystallization occurred, and a gel remained. These binary competition experiments therefore indicated a host selectivity order of 3MP > 4MP > 2MP (which was also the case for **H_1**). The ternary competition experiment involving these guests demonstrated a host selectivity order of 57.3% (3MP) > 22.0% (4MP) ≈ 20.7% (2MP) and, in these conditions, the host was somewhat more ambivalent in its selection between 2MP and 4MP.

When PYR was introduced to these experiments, it was favoured over 2MP (PYR/2MP, 70.6%:29.4%) but not when 3MP or 4MP were present (PYR/3MP and PYR/4MP, 20.0%:80.0% and 40.1%:59.9%, respectively). Ternary experiments that involved PYR resulted in mixed complexes that comprised 17.2%:21.2%:61.6% (PYR/2MP/3MP), 36.3%:20.5%:43.2% (PYR/2MP/4MP) and 14.8%:55.6%:29.6% (PYR/3MP/4MP) of the relevant guests. The quaternary equimolar competition experiment involving all four guest solvents gave a

PYR/2MP/3MP/4MP complex with a 12.0%:19.2%:48.8%:20.0% ratio. Notably, the host preference for either PYR or 2MP interchanged depending on the other guests that were present. This was interesting since 2MP was not included by **H_2** in the single solvent experiment.

Table 5.8. Results of competition experiments using **H_2** and equimolar mixtures of PYR and the MP isomers.[a,b]

PYR	2MP	3MP	4MP	Average guest ratios	Overall H:G ratio	% e.s.d.s
	x	x		29.6:70.4	1:2	(0.1):(0.1)
	x		x	[c]	1:2	-
		x	x	91.6:8.4	1:2	(0.4):(0.4)
	x	x	x	20.7: 57.3: 22.0	1:2	(0.1):(2.5):(2.6)
x	x			70.6:29.4	1:2	(1.9):(1.9)
x		x		20.0:80.0	1:2	(0.7):(0.7)
x			x	40.1:59.9	1:2	(2.5):(2.5)
x	x	x		17.2:21.2:61.6	1:2	(0.5):(0.4):(0.7)
x	x		x	36.3:20.5:43.2	1:2	(0.3):(0.6):(0.9)
x		x	x	14.8:55.6:29.6	1:2	(0.9):(0.4):(0.5)
x	x	x	x	12.0:19.2:48.8:20.0	1:2	(0.3):(0.4):(0.4):(0.5)

[a]G:G ratios were determined using GC-MS with dichloromethane as solvent; overall H:G ratios were obtained by means of ^{1}H-NMR spectroscopy.
[b]Experiments were conducted in duplicate for confirmation purposes; % e.s.d.s are provided in parentheses.
[c]No crystallization occurred and a gel remained.

The host selectivity was then further investigated in the presence of varying molar ratios of these guests in binary mixtures.

5.2.4 Ratio-dependent competition experiments

After recrystallizing **H_2** from binary G/G mixtures in which the molar ratios of the guests were varied, and assessing both the mother liquor and resultant crystals for the guest's content by means of GC-MS, the selectivity profiles in Figure 5.7 were constructed. The average selectivity coefficients were also calculated for each G/G combination, and the complete set of these values for each data point is provided in the Supplementary Information, Tables S96–100. (Note that all 2MP/4MP combinations resulted in a gel, and hence a selectivity profile could not be constructed here.)

a)

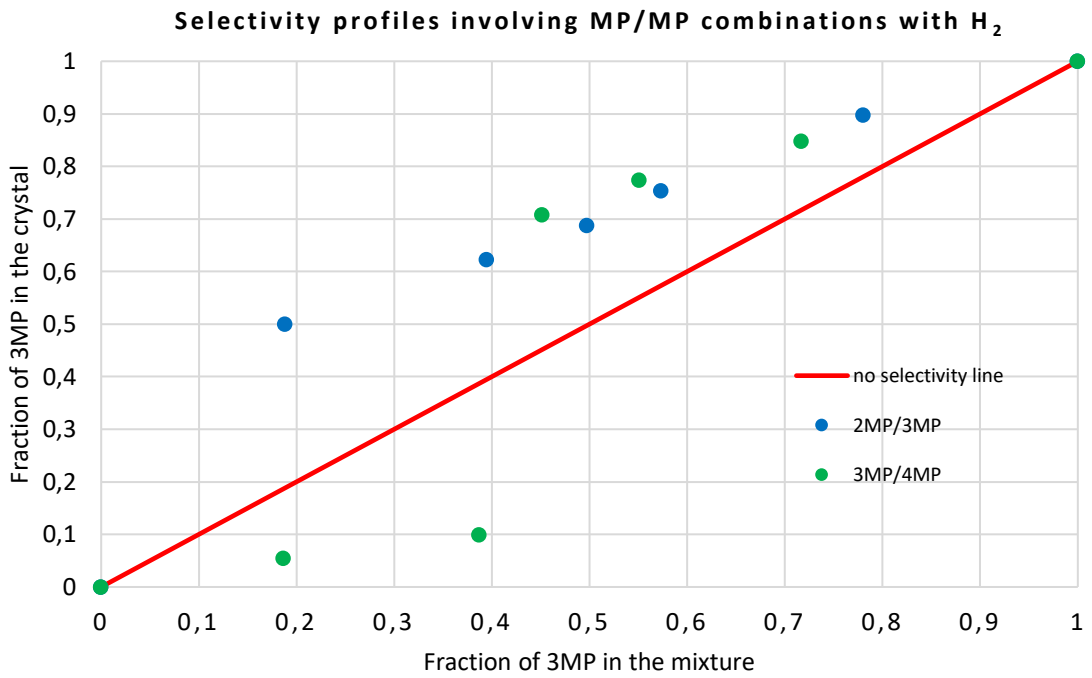

b)

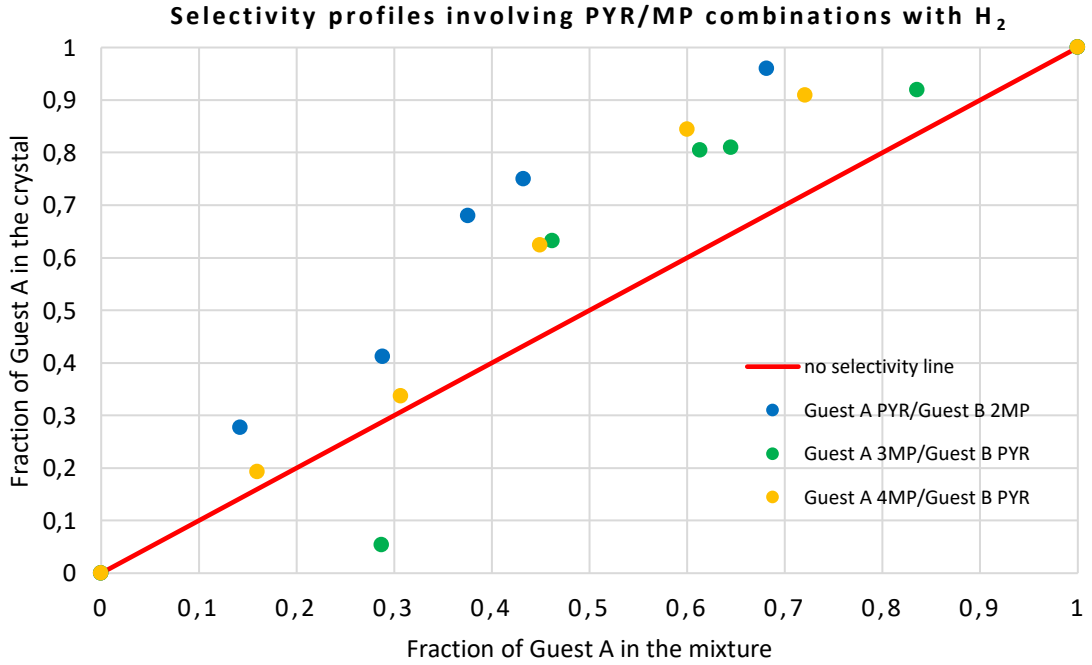

Figure 5.7. Selectivity profiles for G/G combinations in the a) absence of PYR and b) presence of PYR.

For binary combinations that only involved the MP isomers, it was observed that 3MP was consistently preferred by **H_2** over 2MP (Figure 5.7a, blue profile, K = 2.8), but the host selectivity was ambivalent in the 3MP/4MP experiment (Figure 5.7a, green profile), and the host preference depended largely on the concentration of the two guests present in the mother liquor. The highest recorded K value in the latter experiment was determined to be 5.7 (where 4MP was favoured) with the guests mixed in a ~39%(3MP):61%(4MP) ratio.

In the presence of PYR, 4MP was preferred across the entire concentration range (Figure 5.7b, yellow profile, K = 2.4), as was PYR in the PYR/2MP experiment (Figure 5.7b, blue profile, K = 4.6). Unexpectedly, in the PYR/3MP experiment, the host preferred PYR at high concentrations of this guest (71.3%) but reverted to selecting 3MP at higher 3MP concentrations.

5.2.5 SCXRD

Single crystals of the successfully formed inclusion complexes of **H_2** with the PYR, 3MP and 4MP guests were subjected to X-ray diffraction experiments. The data from these (Table 5.9) indicate that all three complexes crystallize in the triclinic *P*-1 crystal system and do not display isostructural host packing. In the 3(**H_2**)·5(3MP) complex, the MP guest molecules were found to be disordered. The unit cell is quite large and contains two complete and two half hosts that are symmetry generated. Two guests are hydrogen bonded to the host molecule and, do not display disorder, while three guests display disorder over two positions. Furthermore, the complex crystallized with some water. Additionally, 4MP and PYR were disordered over two positions but this was modelled satisfactorily.

Table 5.9. Crystallographic data for **H₂**·2(PYR), 3(**H₂**)·5(3MP)·0.268(O) and **H₂**·2(4MP).

	H₂·2(PYR)	3(**H₂**)·5(3MP)·0.268(O)	**H₂**·2(4MP)
Chemical formula	$C_{40}H_{32}N_2O_2$ ·2(C_5H_5N)	3($C_{40}H_{32}N_2O_2$) ·5(C_6H_7N)·0.268(O)	$C_{40}H_{32}N_2O_2$ ·2(C_6H_7N)
Formula weight	730.88	2187.95	758.93
Crystal system	Triclinic	Triclinic	Triclinic
Space group	*P*-1	*P*-1	*P*-1
μ (Mo Kα)/mm^{-1}	0.078	0.076	0.075
a/Å	9.3906(4)	14.5824(7)	9.0363(4)
b/Å	13.9667(7)	18.1825(8)	10.3497(4)
c/Å	15.8401(8)	24.2594(12)	11.8943(4)
alpha/°	112.772(2)	78.841(2)	76.273(2)
beta/°	92.849(2)	82.304(2)	82.691(2)
gamma/°	93.679(2)	68.564(2)	73.318(2)
V/$Å^3$	1905.05(16)	5860.0(5)	1033.05(8)
Z	2	2	1
F(000)	772	2316	402
Temp./K	200	200	200
Restraints	0	45	0
Nref	8482	29198	5095
Npar	513	1425	267
R	0.0397	0.0693	0.0434
wR2	0.1052	0.2075	0.1218
S	1.02	1.03	1.05
θ min–max/°	1.7, 28.4	0.9, 28.4	1.8, 28.3
Tot. data	68864	264398	45828
Unique data	9492	29198	5095
Observed data [I > 2.0 sigma(I)]	7634	17235	4207
R_{int}	0.021	0.043	0.018
Dffrn measured fraction θ full	0.998	0.998	0.998
Min. resd. dens. (e/$Å^3$)	–0.25	–0.83	–0.19
Max. resd. dens. (e/$Å^3$)	0.33	1.04	0.28

Figure 5.8 shows the unit cells for the complexes that involve PYR and 4MP and, due to the nature of the guest disorder in the 3(**H₂**)·5(3MP)·0.268(O) complex, an illustration of the unit cell was not informative and thus not included here. Additionally, Figure 5.9 is a depiction of the resultant voids after removal of the guests from the packing calculation. These guests occupy constricted channels in the host crystal.

a) b)

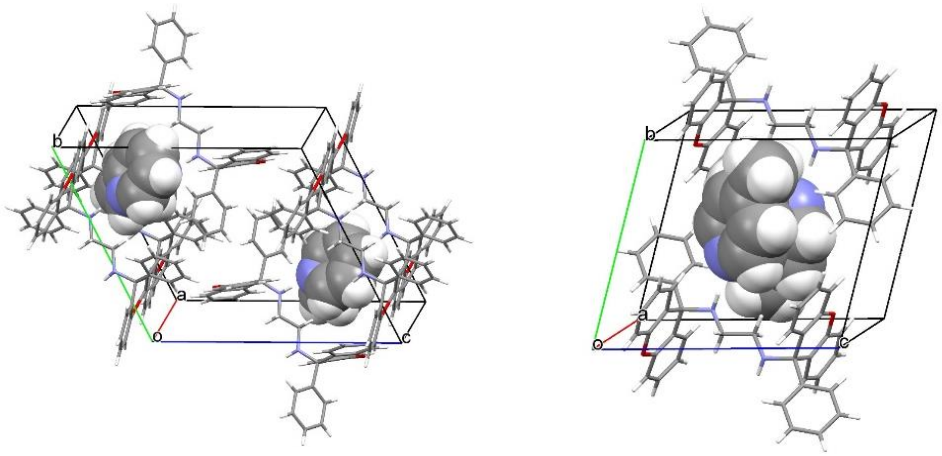

Figure 5.8. Unit cells of complexes a) **H_2**·2(PYR) and b) **H_2**·2(4MP).

a) b)

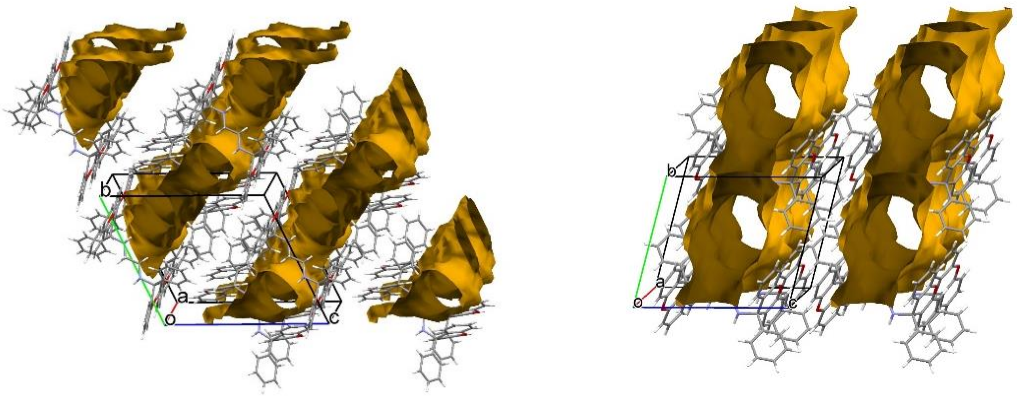

Figure 5.9. Voids in complexes a) **H_2**·2(PYR) and b) **H_2**·2(4MP) after guest removal.

Subsequently, the geometry of the host compound in each of the complexes was examined. Figure 5.10 is a depiction of these host molecules after removal of the guests. The deviation from planarity within the xanthone moiety was calculated to range between 2.9 and 16.9°, with the increased deviation being observed in the PYR-containing complex (16.9 and 13.9°). The C–Ô–C angles were also calculated for each xanthone B ring and these ranged between 117.6–118.9°. (These angles for each complex are provided in the Supplementary Information, Figure S101.) The nitrogen atoms of the ethylenediamine linker in **H_2** crystallized in an antiperiplanar arrangement.

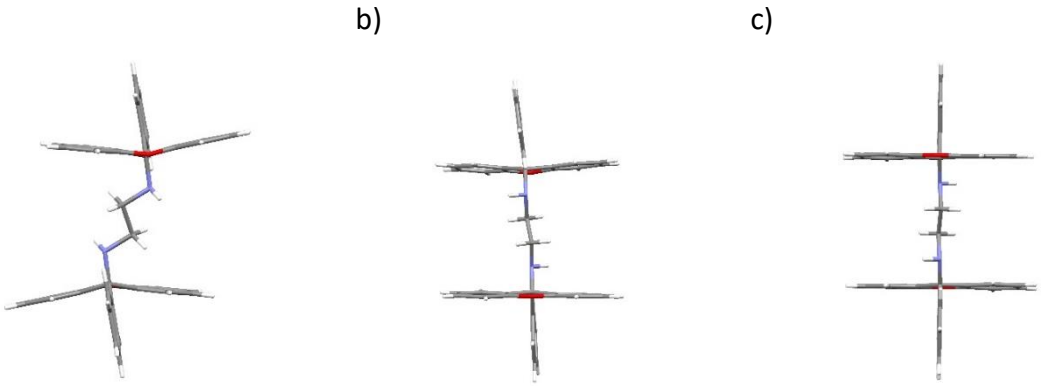

Figure 5.10. Host geometry in complexes a) **H₂**·2(PYR) b) 3(**H₂**)·5(3MP)·0.268(O) and c) **H₂**·2(4MP).

Tables 5.10 [**H₂**·2(PYR) and **H₂**·2(4MP)] and 5.11 [3(**H₂**)·5(3MP)·0.268(O)] contain a summary of the significant H···G interactions measured in these complexes in order to identify those interactions that contribute to the selective behaviour of **H₂** towards these guests. (Since the disorder was so significant in the 3(**H₂**)·5(3MP)·0.268(O) complex, these H···G interactions for all disordered components are provided here in a separate table. The detailed set H···H and H···G interactions may be found in the Supplementary Information, Table S102.) The π···π interactions in the **H₂**·2(PYR) and **H₂**·2(4MP) complexes are comparable and very weak [with distances ranging between 4.081(1) and 5.987(1) Å]. The PYR guest also experiences one $C_{(G)}$–$H_{(G)}$···$\pi_{(H)}$ interaction (2.70 Å, 124°) while 4MP is not involved in such interaction types. For the preferred guest, 3MP, the disordered component G1 experiences two C–H···π interactions [2.87 Å (144°) and 2.85 Å (148°)], one with **H₂** and the other with a second guest molecule while the G2 component is involved in a much shorter interaction of this type [2.52 Å (155°)] compared to the others. PYR was additionally enclathrated by one $C_{(H)}$–$H_{(H)}$···$C_{(G2)}$–$C_{(G2)}$ interaction (2.87 Å, 139°) while 4MP, once again, did not experience any of these kinds of contacts. Furthermore, most of the guest components of 3MP experience at least one other short contact which may explain the selectivity of **H₂** for this guest. Also, one classical H···G hydrogen bond could be identified in each complex with 3MP {G1 [2.52 Å, 161.7(19)°] and G2 [2.36 Å, 165(2)°]}, PYR {G1 [2.36 Å, 173°] and G2 [2.38 Å, 161.7°]}, and 4MP {G1 [2.53 Å, 175.5(13)°]}, and Figure 5.11 is a visual representation of these interactions. A complete table of the H···G and H···H interactions for **H₂**·2(PYR) and **H₂**·2(4MP) is provided in the Supplementary Information (Table S103).

a)

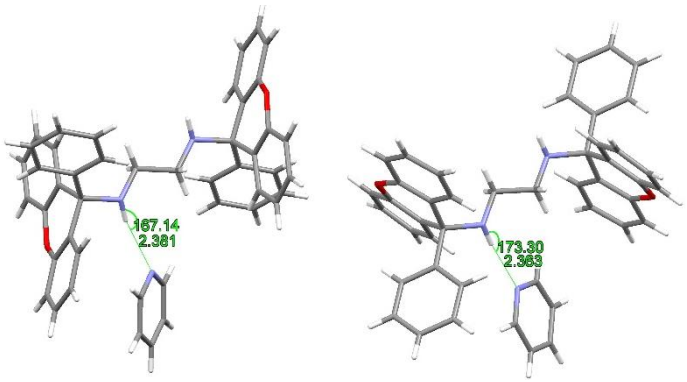

b)

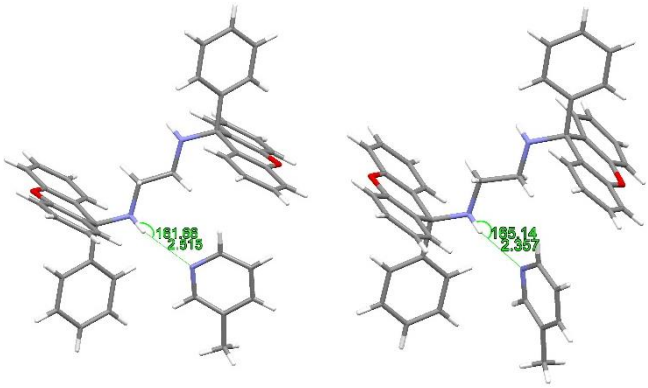

c)

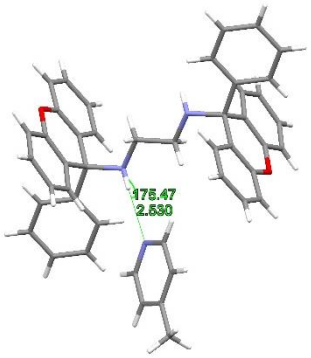

Figure 5.11. The classical H···G H-bonding in complexes a) **H₂**·2(PYR) b) 3(**H₂**)·5(3MP)·0.268(O) [note that the water was removed in Mercury] and c) **H₂**·2(4MP).

Table 5.10. H···G interactions present in complexes **H₂**·2(PYR) and **H₂**·2(4MP).[a,b,c]

Non-covalent interaction	**H₂**·2(PYR)	**H₂**·2(4MP)	Symmetry
π···π H···G G1 H···G G2	 4.947(1)–5.987(1) Å [9] 4.402(1)–5.512(1) Å [7]	 4.081(1)–5.898(1) Å [10]	
C–H···π (H···Cg, C–H···Cg) $C_{(G2)}$–$H_{(G2)}$···$Cg_{(H)}$	 2.70 Å, 124°		 –x, 1–y, –z
H-bonding (H···A, D–H···A) $N_{(H)}$–$H_{(H)}$···$N_{(G2)}$–$C_{(G2)}$ $N_{(H)}$–$H_{(H)}$···$N_{(G1)}$–$C_{(G1)}$ $N_{(H)}$–$H_{(H)}$···$N_{(G1)}$–$C_{(G1)}$	Non-classical 2.38 Å, 167° (<) 2.36 Å, 173° (<)	Non-classical 2.53 Å, 175.5(13)° (<<)	 –x, 1–y, –z x, y, z x, y, z
Other short contacts (X···Z, X–Y···Z) $C_{(H)}$–$H_{(H)}$···$C_{(G2)}$–$C_{(G2)}$	 2.87 Å, 139° (<)		 1+x, –1+y, z

[a]Distances denoted by < are contacts that measure less than the sum of the van der Waals radii of the atoms involved, while those denoted by << is this sum minus 0.2 Å.
[b]Number of π···π interactions are indicated in square brackets.
[c]Guest 1 and 2 (G1 and G2) represents the two disordered guest components in the crystal.

Table 5.11. H···G interactions present in the complex 3(**H₂**)·5(3MP)·0.268(O).[a,b,c]

Non-covalent interaction	3(**H₂**)·5(3MP)·0.268(O)	Symmetry
π···π		
G1	4.455(4)–5.908(2) Å [8]	
G2	4.7414(16)–5.887(2) Å [8]	
G3	4.0633(16)–5.7847(16) Å [7]	
G4	4.9038(19)–5.887(2) Å [10]	
G5	4.779(2)–5.908(2) Å [9]	
G6	4.389(4)–5.949(4) Å [9]	
G7	5.073(4)–5.874(4) Å [8]	
G8	4.346(4)–5.647(4) Å [6]	
CH···π (H···Cg, C–H···Cg)		
$C_{(G1)}$–$H_{(G1)}$···$Cg_{(H2)}$	2.87 Å, 144°	1–x, 2–y, 1–z
$C_{(G1)}$–$H_{(G1)}$···$Cg_{(G1)}$	2.85 Å, 148°	2–x, 2–y,1–z
$C_{(G4)}$–$H_{(G4)}$···$Cg_{(H4)}$	2.89 Å, 138°	1–x, 1–y, 1–z
$C_{(H3)}$–$H_{(H3)}$···$Cg_{(G6)}$	2.89 Å, 114°	x, y, z
$C_{(H4)}$–$H_{(H4)}$···$Cg_{(G2)}$	2.52 Å, 155°	2–x, 1–y,1–z
$C_{(H2)}$–$H_{(H2)}$···$Cg_{(G5)}$	2.78 Å, 142°	1–x, 2–y, 1–z
$C_{(H2)}$–$H_{(H2)}$···$Cg_{(G8)}$	2.98 Å, 150°	1–x, 2–y, 1–z
H-bonding (H···A, D–H···A)	Non-classical and classical	
$N_{(H2)}$–$H_{(H2)}$···$N_{(G1)}$–$C_{(G1)}$	2.52 Å, 161.7(19)° (<<)	x, y, z
$N_{(H3)}$–$H_{(H3)}$···$N_{(G2)}$–$C_{(G2)}$	2.36 Å, 165(2)° (<<)	x, y, z
$C_{(G3)}$–$H_{(G3)}$···$O_{(H1)}$–$C_{(H1)}$	2.25 Å, 169° (<<)	x, y, z
Short contacts (X···Z, X–Y···Z)\		
$C_{(H1)}$–$H_{(H1)}$···$H_{(G6)}$–$C_{(G6)}$	2.83 Å, 145° (<)	x, y, z
$C_{(H1)}$–$H_{(H1)}$···$H_{(G8)}$–$C_{(G8)}$	2.24 Å, 153° (<)	–1+x, y, z
$C_{(H1)}$–$H_{(H1)}$···$N_{(G1)}$–$C_{(G1)}$	2.69 Å, 150° (<)	–1+x, y, z
$C_{(H3)}$–$H_{(H3)}$···$H_{(G3)}$–$C_{(G3)}$	2.39 Å, 144° (<)	x, y, z
$C_{(H4)}$–$H_{(H4)}$···$C_{(G2)}$–$N_{(G2)}$	2.75 Å, 176° (<)	2–x, 1–y, 1–z
$C_{(H4)}$–$H_{(H4)}$···$C_{(G3)}$–$N_{(G3)}$	2.84 Å, 148° (<)	1–x, 2–y, 1–z
$C_{(G4)}$–$H_{(G4)}$···$C_{(H4)}$–$C_{(H4)}$	2.77 Å, 152° (<)	1–x, 1–y, 1–z
$C_{(G5)}$–$H_{(G5)}$···$C_{(H4)}$–$O_{(H4)}$	2.82 Å, 165° (<)	2–x, 2–y, 1–z
$C_{(G5)}$–$H_{(G5)}$···$H_{(H3)}$–$C_{(H3)}$	2.25 Å, 159° (<)	x, y, z

[a]Distances denoted by < are contacts that measure less than the sum of the van der Waals radii of the atoms involved while those denoted by << is this sum minus 0.2 Å.
[b]Number of π···π interactions are provided in square brackets.
[c]Host 1–4 (H1–H4) and Guest 1–8 (G1–8) represent the disordered host and guest components in the crystal.

5.2.6 Hirshfeld surface analyses

Due to the extent of the disorder in the 3(**H₂**)·5(3MP)·0.268(O) complex, Hirshfeld surface analysis could not be carried out on this H:G complex. The 2D fingerprint plots, together with a graphical representation of the percentage and types of interactions in the complexes with PYR and 4MP are provided in the Supplementary Information, Figures S108 and S109, respectively, since these data could not be utilized to explain the host behaviour.

5.2.7 Thermal analyses (DSC and TG)

Thermal analysis was carried out on the complexes of **H_2** with the successfully included guests. TG (and DTG) and DSC were used to determine the temperatures at which the significant thermal events occurred upon heating. The thermal traces thus obtained are provided in Figure 5.12.

a)

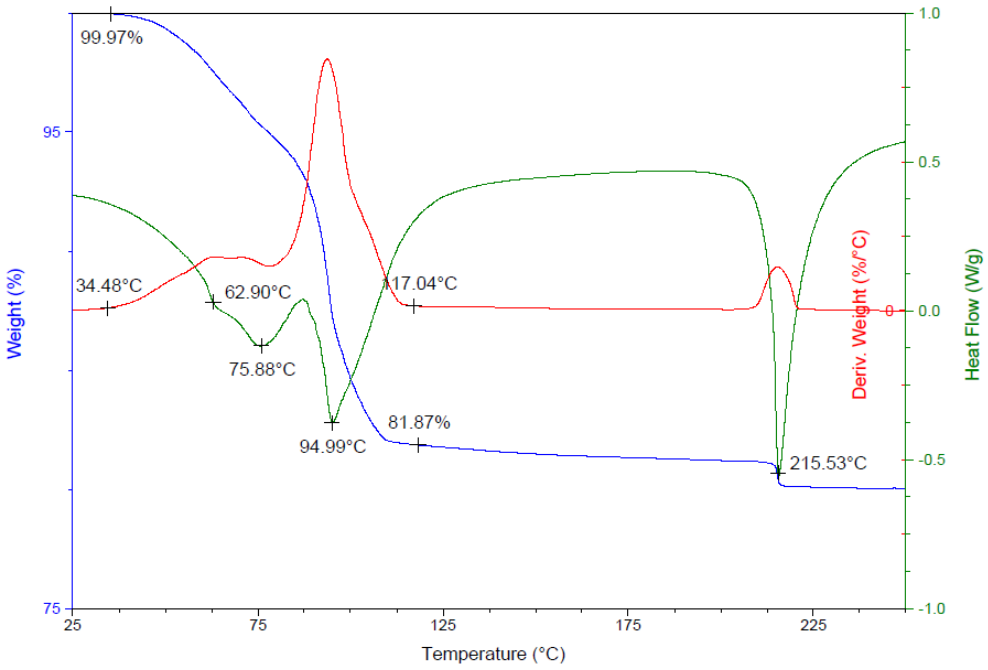

b)

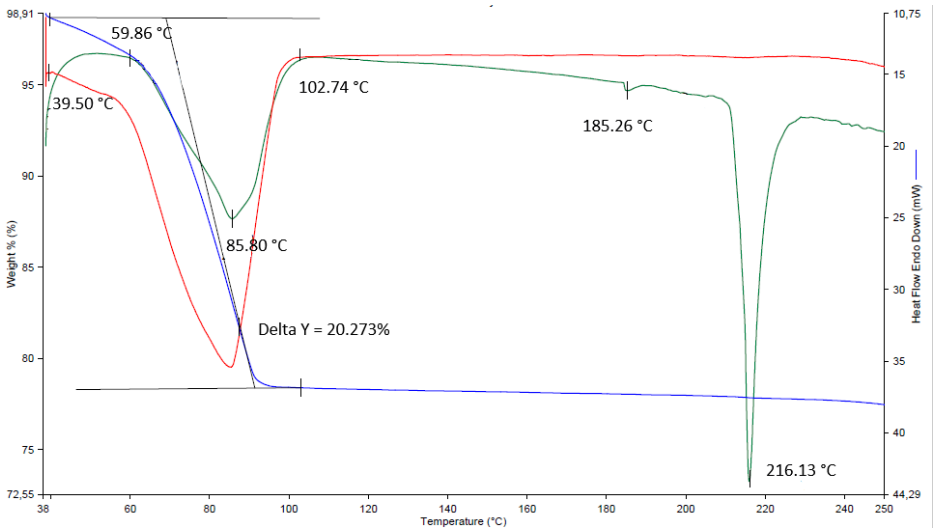

c)

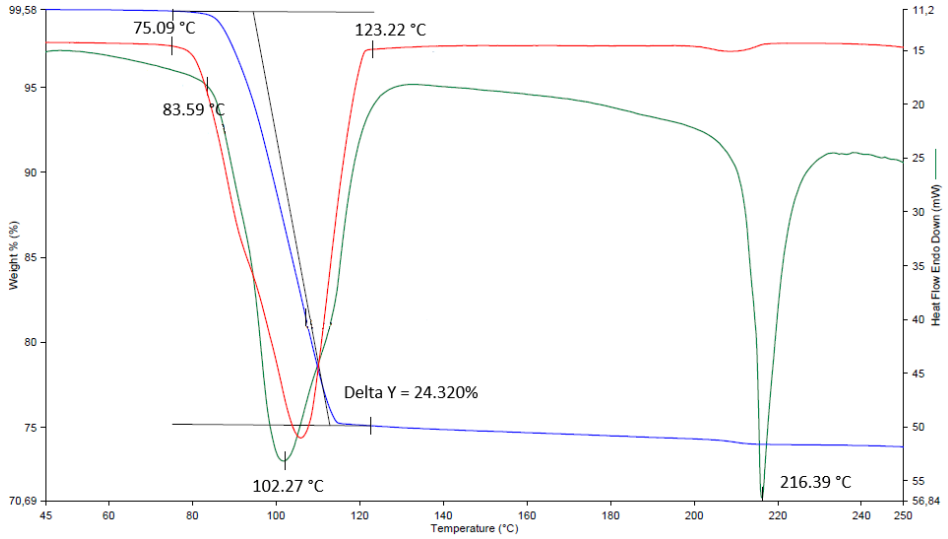

Figure 5.12. DSC (green), TG (blue) and DTG (red) traces for **H_2** in complexes with guests a) PYR, b) 3MP and d) 4MP.

Table 5.12 provides a summary of the temperatures at which the significant thermal events occurred during these thermal experiments. The thermal stability of the complexes could not be correlated to the host selectivity preference since the most preferred guest (3MP) was unstable even from the outset of the experiment (~39.5 °C). PYR, however, demonstrated a T_{on} of 34.5 °C, while the least preferred guest (4MP), usually, proved to be the most thermally stable based on both T_{on} and T_p values (75.1 and 102.3 °C, respectively). The measured mass loss was in reasonable agreement with that expected for 3(**H_2**)·5(3MP)·0.268(O) and **H_2**·2(4MP) (with 21.5 and 24.6% expected, while 20.3 and 24.3% were measured, respectively). The mass loss expected for **H_2**·2(PYR) (21.7%), however, was significantly higher than that measured (18.1%) and, at this stage, we are uncertain as to the reason for this discrepancy.

Table 5.12. Thermal properties of complexes formed by **H_2**.

Complex	T_{on} /°C	T_p /°C	Mass loss expected /%	Mass loss measured /%
H_2·2(PYR)	34.5	62.9, 75.9, 95.0	21.7	18.1
3(**H_2**)·5(3MP)·0.268(O)	[a]	85.8	21.5	20.3
H_2·2(4MP)	75.1	102.3	24.6	24.3

[a]Could not be determined due to the instability of the complex at low temperatures.

5.2.8 Conclusions

In this work, **H_2** demonstrated the ability to include PYR, 3MP and 4MP. The H:G ratio was 1:2, 3:5 and 1:2, respectively. **H_2** displayed selective behaviour in the presence of mixed guests, and 3MP was always preferred relative to PYR and 2MP. Furthermore, the host showed ambivalent selectivity in binary and ternary experiments involving PYR and 2MP, which depended on which other guests were present. The host selectivity order, obtained from the quaternary experiment, was determined to be 3MP > 4MP > 2MP ≈ PYR. Thermal analyses of the complexes were considered but were not in accordance with the selectivity of the host. Additionally, Hirshfeld surface analysis could not be carried out on the complex containing the preferred guest, and this analytical tool could therefore not be utilized to ascertain the reasons for the selectivity of **H_2** for 3MP. The SCXRD data, however, did correlate with the host behaviour, and 3MP was found to experience the stronger and greater number of C–H···π and other short interactions. All three guests also experienced one classical hydrogen bond. These data therefore explain the preference of **H_2** for 3MP.

5.2.9 Supporting information

All relevant spectra, figures and detailed tables may be found in the Supplementary Information. The crystal structures were deposited at the Cambridge Crystallographic Data Centre, and CCDC numbers 1587302 [**H_2**·2(PYR)], 1909509 [3(**H_2**)·5(3MP)·0.268(O)], and 1909510 (**H_2**·4MP) contain the supplementary crystallographic data for this chapter.

6. METHYLCYCLOHEXANONE ISOMERS AND CYCLOHEXANONE

6.1. Inclusion compounds with **H_1**

6.1.1 Introduction

Cyclohexanone and the methylcyclohexanone isomers are synthesized by the catalytic oxidation or hydrogenation of the appropriate precursors:[252] cyclohexane may be oxidized in air to form cyclohexanone, while the hydrogenation of phenol and the respective cresols produces the corresponding cyclic ketones. The methylcyclohexanone isomers serve as intermediates in the synthesis of various flavours, fragrances and pharmaceuticals,[252] and a large quantity of unsubstituted cyclohexanone is produced annually for use as a precursor to nylon.[253]

Barton *et al*[254] reported that (+)-(2*R*,3*R*)-1,1,4,4-tetraphenylbutane-1,2,3,4-tetraol (TETROL) is a highly efficient host for the inclusion of cyclohexanone and 2-, 3-, and 4-methylcyclohexanone. The 3- and 4- methyl isomers were unexpectedly included with their methyl groups in the higher energy axial orientation, while this group in 2-methylcyclohexanone preferred the more usual equatorial position. The host also displayed some preference for the (*R*)-enantiomer, which was attributed to a much stronger hydrogen bond between a hydroxyl group of TETROL and the carbonyl group of this stereoisomer. They also noted that the host selectivity was in the order 2- ≫ 3- > 4- methylcyclohexanone and that the addition of unsubstituted cyclohexanone to these competitions prompted a complete reversal of this order.[255]

Here, the host ability and selectivity of **H_1** is reported in the presence of these compounds [2- (2MCHN), 3- (3MCHN), 4- methylcyclohexanone (4MCHN) and cyclohexanone (CHN), Scheme 6.1]. This investigation is merely an academic exercise since the MCHN isomers do not ordinarily occur as mixtures in industry, but this study will add to the knowledge base with respect to these particular xanthenyl-type host systems and their behaviour in the presence of these cyclic ketone guest solvents.

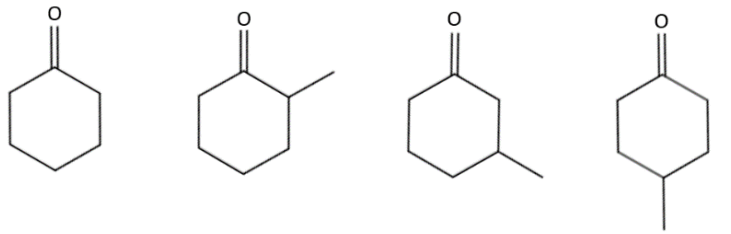

Scheme 6.1. Structures of CHN and the MCHN isomers.

6.1.2 Individual inclusions

Recrystallization experiments of **H_1** from each guest afforded crystalline complexes in each case (Table 6.1), and ^{1}H-NMR analysis of the crystals indicated the H:G ratio was consistently 1:1. (The ^{1}H-NMR spectra are provided in the Supplementary Information, Figures S110–113.)

Table 6.1. H:G ratios of inclusion compounds formed by **H_1**.[a]

Guest (G)	H:G
CHN	1:1
2MCHN	1:1
3MCHN	1:1
4MCHN	1:1

[a]Determined using ^{1}H-NMR spectroscopy using $CDCl_3$ as solvent.

6.1.3 Equimolar competition experiments

Competition experiments were carried out between these guest solvents to establish if **H_1** would be able to discriminate between these guests. The resultant crystals were analysed by means of ^{1}H-NMR spectroscopy (to obtain the overall H:G ratios) and GC-MS (to determine the G:G ratios). Table 6.2 is a summary of the data thus obtained from the recrystallization experiments of **H_1** from the various equimolar binary, ternary and quaternary combinations of CHN, 2-, 3- and 4- MCHN. The preferred guest species is presented in red font. These experiments were conducted in duplicate, and the averaged values are provided in the table. [Duplicate values may be found in the Supplementary Information (Table S114), together with a GC trace of a mixture of the pure guests to show the suitability of GC as analytical tool in these conditions (Figure S115).]

Table 6.2. Results of competition experiments using **H_1** and various equimolar mixtures of the guests.[a,b]

CHN	2MCHN	3MCHN	4MCHN	Average guest ratios	Overall H:G ratio	% e.s.d.s
x	x			52.4:47.6	1:1	(1.2):(1.2)
x		x		81.5:18.5	1:1	(2.1):(2.1)
x			x	89.4:10.6	1:1	(0.4):(0.4)
	x	x		74.5: 25.5	1:1	(0.3):(0.3)
	x		x	83.4:16.6	1:1	(1.1):(1.1)
		x	x	70.6:29.4	1:1	(1.0):(1.0)
x	x	x		39.3:47.3:13.4	1:1	(0.7):(0.6):(0.2)
x	x		x	42.5:49.5:8.0	1:1	(0.9):(0.1):(0.9)
x		x	x	64.9:23.0:12.1	1:1	(0.8):(0.4):(0.5)
	x	x	x	67.6:23.1:9.3	1:1	(2.2):(1.2):(1.0)
x	x	x	x	39.2:41.7:13.5:5.6	1:1	(0.2):(0.2):(0.3):(0.2)

[a]G:G ratios were determined using GC-MS with dichloromethane or chloroform as the solvent; overall H:G ratios were obtained by means of ^{1}H-NMR spectroscopy.

[b]Experiments were conducted in duplicate for confirmation purposes; % e.s.d.s are provided in parentheses.

From experiments involving the isomeric MCHNs, it is clear that 2MCHN was significantly preferred in binary mixtures whenever it was present [Table 6.2, 74.5% (2MCHN/3MCHN) and 83.4% (2MCHN/4MCHN)]. In the absence of 2MCHN, 3MCHN was favoured above 4MCHN (70.6%:29.4%). The equimolar ternary competition of all three MCHNs agreed with these observations, and a mixed complex containing 67.6% 2MCHN, 23.1% 3MCHN and 9.3% 4MCHN was formed. In the equimolar binary competition studies conducted in the presence of CHN, this guest (CHN) was the only one to compete significantly with 2MCHN: a 52.4%:47.6% CHN/2MCHN complex was obtained in this instance. The other binary combinations afforded 81.5%:18.5% (CHN/3MCHN) and 89.4%:10.6% (CHN/4MCHN) mixed complexes, with significant quantities of CHN clathrated in each case. The ternary competitions afforded 39.3%(CHN):47.3%(2MCHN):13.4%(3MCHN), 42.5%(CHN):49.5%(2MCHN):8.0%(4MCHN) and 64.9%(CHN):23.0%(3MCHN):12.1%(4MCHN) mixed complexes, while the equimolar quaternary experiment confirmed a host selectivity order of 2MCHN (41.7%) ≈ CHN (39.2%) > 3MCHN (13.5%) > 4MCHN (5.6%).

6.1.4 Ratio-dependent competition experiments

Further binary competitions were conducted but in the presence of varying molar ratios of CHN and the three MCHN isomers, and the selectivity of **H_1** evaluated in these conditions by the construction of selectivity profiles (Figure 6.1). The G:G ratios of the mother liquors and mixed complexes were determined through GC-MS as before. The average selectivity coefficients (K) were also calculated and the complete data set is provided in the Supplementary Information, Tables S116–121.

Binary experiments in the absence of CHN (Figure 6.1a) indicated that 2MCHN, when present, was preferred, and at all evaluated concentrations [2MCHN/3MCHN (green profile), K = 2.8 and 2MCHN/4MCHN (yellow profile), K = 5.2]. In the 3MCHN/4MCHN experiment (blue profile), **H_1** displayed selectivity for 3MCHN over the entire concentration range (K = 2.2). Based on the K values, the host selectivity order in these experimental conditions was determined to be 2MCHN > 3MCHN > 4MCHN, in accordance with data from the equimolar experiments. In the presence of CHN, the profiles obtained for the CHN/2MCHN (green profile, K = 1.4), CHN/3MCHN (yellow profile, K = 5.0) and CHN/4MCHN (blue profile, K = 8.6) experiments (Figure 6.1b) showed that **H_1** preferred CHN consistently, with only 2MCHN providing some competition once more.

a)

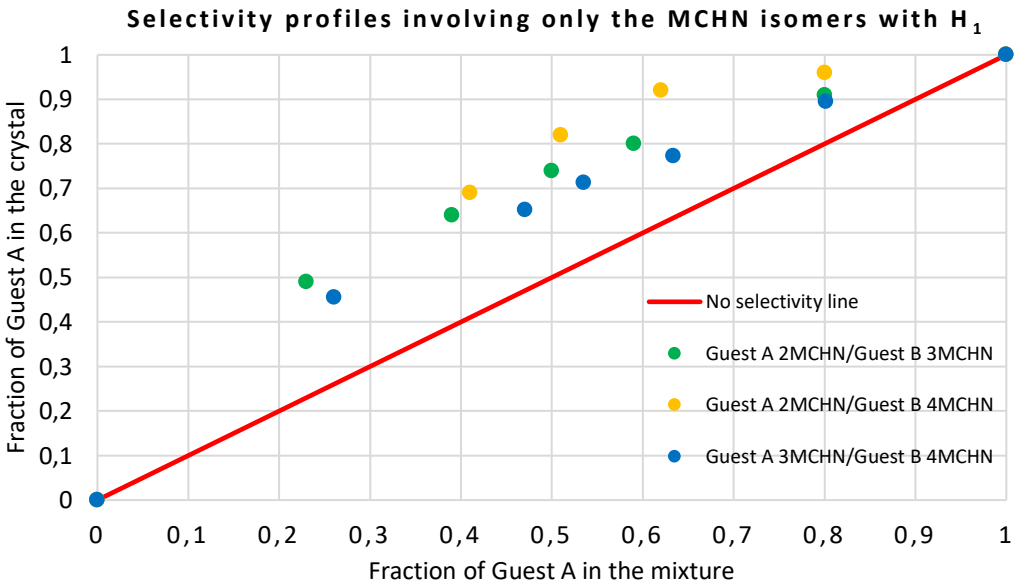

b)

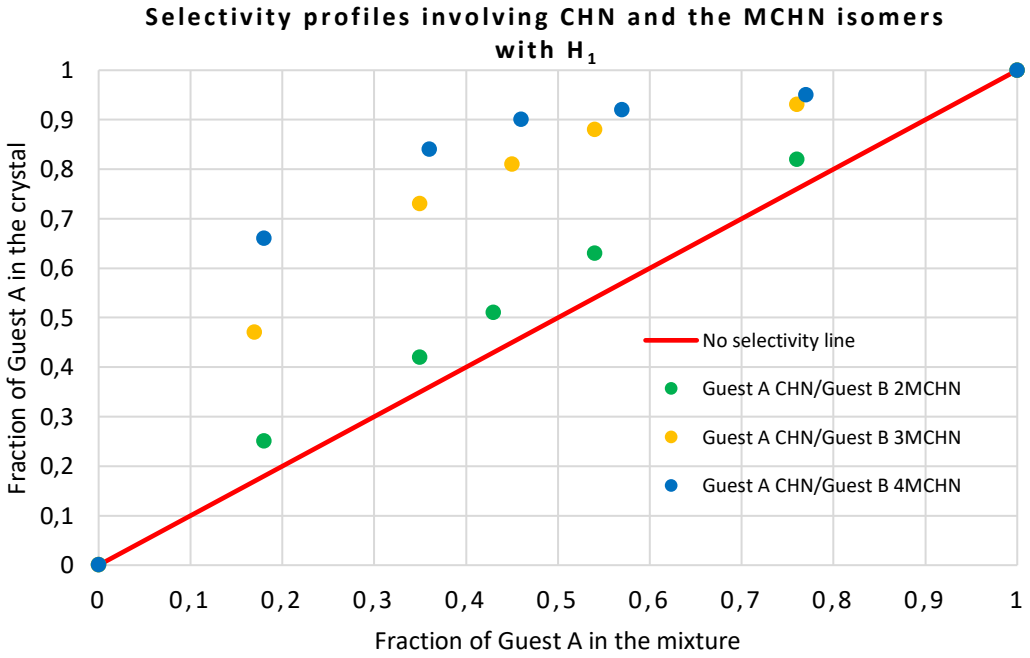

Figure 6.1. Overlaid selectivity profiles of **H_1** when recrystallized from a) binary guest combinations in the absence of CHN, and b) binary guest combinations with CHN present.

6.1.5 SCXRD

The relevant crystal data and refinement parameters of the four complexes are provided in Table 6.3. **H₁**·CHN, **H₁**·2MCHN and **H₁**·3MCHN are isostructural and crystallize in the monoclinic $P2_1/n$ crystal system, while the host packing differed in the **H₁**·4MCHN complex (triclinic *P*-1). Figure 6.2 shows the unit cells for the four complexes, and guests in each displayed disorder, but this was satisfactorily modelled over two positions.

Table 6.3. Crystallographic data for **H₁**·CHN, **H₁**·2MCHN, **H₁**·3MCHN and **H₁**·4MCHN.

	H₁·CHN	**H₁**·2MCHN	**H₁**·3MCHN	**H₁**·4MCHN
Chemical formula	$C_{40}H_{32}N_2S_2$ $\cdot C_6H_{10}O$	$C_{40}H_{32}N_2S_2$ $\cdot C_7H_{12}O$	$C_{40}H_{32}N_2S_2$ $\cdot C_7H_{12}O$	$C_{40}H_{32}N_2S_2$ $\cdot C_7H_{12}O$
Formula weight	702.94	716.96	716.96	716.96
Crystal system	Monoclinic	Monoclinic	Monoclinic	Triclinic
Space group	$P2_1/n$	$P2_1/n$	$P2_1/n$	*P*-1
μ (Mo Kα)/mm^{-1}	0.190	0.186	0.184	0.186
a/Å	10.5340(8)	10.8200(4)	11.0347(7)	10.6126(5)
b/Å	13.391(1)	13.4654(6)	13.4709(8)	13.6304(6)
c/Å	25.279(2)	25.1070(1)	24.973(2)	13.7297(6)
alpha/°	90	90	90	83.815(2)
beta/°	91.476(4)	90.892(2)	91.342(3)	85.819 (2)
gamma/°	90	90	90	69.913 (2)
V/Å^3	3564.8(5)	3657.5(3)	3711.1(4)	1853.0(2)
Z	4	4	4	2
F(000)	1488	1520	1520	760
Temp./K	200	200	200	200
Restraints	15	24	0	18
Nref	8878	9126	9233	9229
Npar	502	522	496	466
R	0.0428	0.0511	0.0425	0.0528
wR2	0.1144	0.1372	0.1186	0.1510
S	1.02	1.08	1.03	1.04
θ min–max/°	1.6, 28.3	1.6, 28.4	1.6, 28.3	1.6, 28.4
Tot. data	110345	79487	78389	54602
Unique data	8878	9126	9233	9229
Observed data [I > 2.0 sigma(I)]	7527	7659	7530	7768
R_{int}	0.024	0.021	0.023	0.021
Dffrn measured fraction θ full	1.000	1.000	1.000	0.997
Min. resd. dens. (e/Å^3)	–0.36	–0.37	–0.35	–1.01
Max. resd. dens. (e/Å^3)	0.51	0.97	0.56	1.05

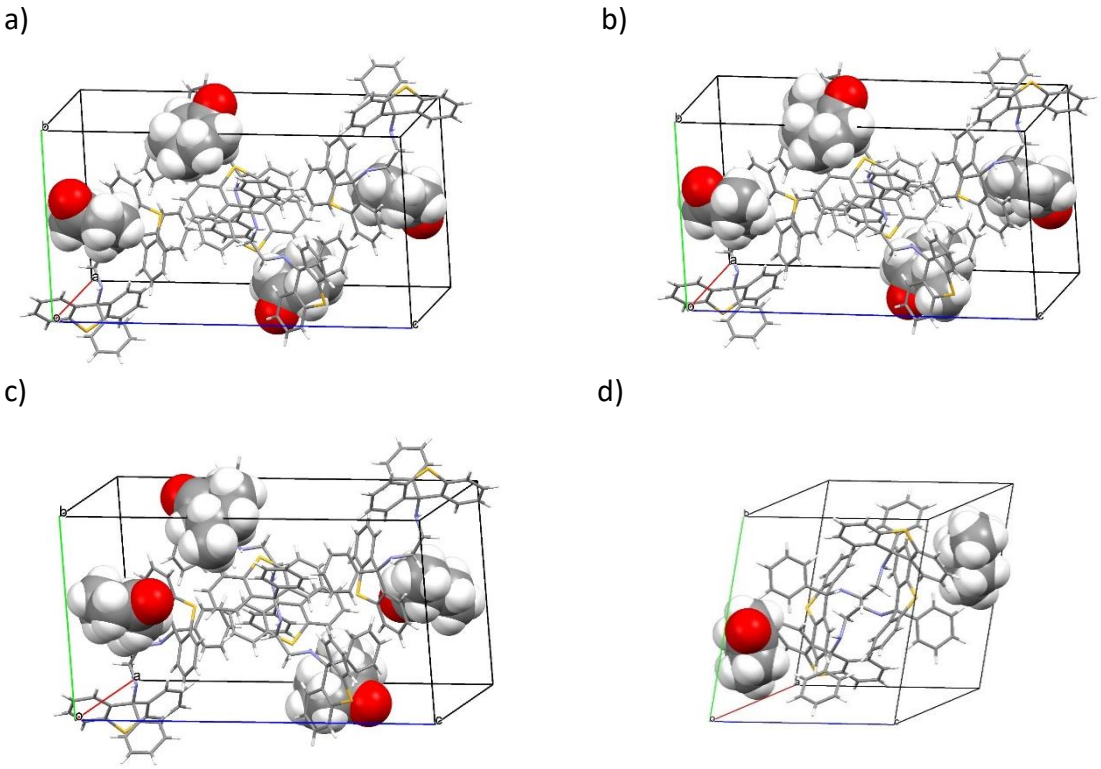

Figure 6.2. Unit cells for a) **H₁**·CHN, b) **H₁**·2MCHN, c) **H₁**·3MCHN and d) **H₁**·4MCHN; guests are in spacefill and the hosts in stick representation.

Subsequently, the guests were removed from the packing calculation and the resultant voids determined using Mercury software.[230] In Figure 6.3, the voids in **H₁**·2MCHN (as representative of the three isostructural complexes) are depicted as well as those in **H₁**·4MCHN. Within the isostructural complexes (**H₁**·CHN, **H₁**·2MCHN and **H₁**·3MCHN), the guests occupy discrete cavities (one guest per cavity), while in **H₁**·4MCHN, guests reside in infinite and constricted channels.

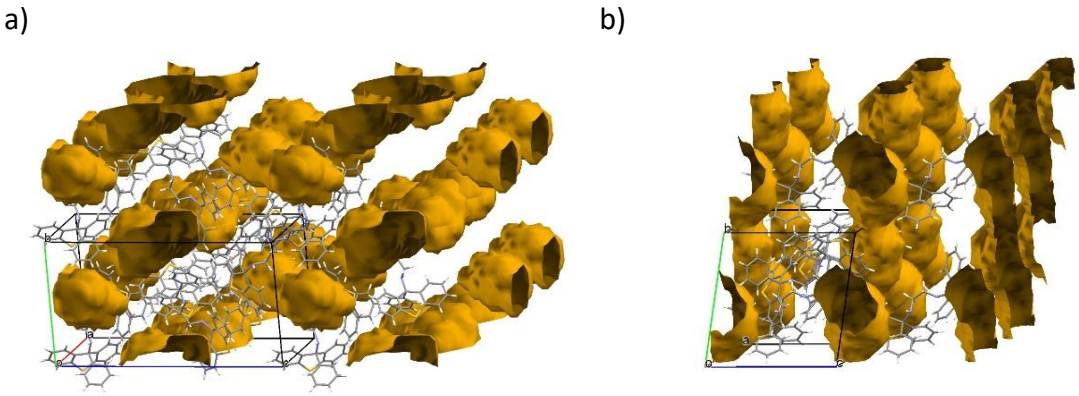

Figure 6.3. Calculated voids (dark yellow) for a) **H₁**·2MCHN (as representative of the isostructural complexes of **H₁** with CHN and 3MCHN) and b) **H₁**·4MCHN, after removal of the guests from the packing calculation.

All the noteworthy H···G interactions obtained from SCXRD experiments for the four complexes are summarized in Table 6.4 for ease of comparison. (All H···H interactions are summarized in Table S122 in the Supplementary Information.) All guests experienced non-classical $C_{(H)}$–$H_{(H)}$···$O_{(G)}$–$C_{(G)}$ H-bonds. In the **H_1**·CHN complex, each disordered guest component experiences two of these interaction types, with one being particularly strong [$C_{(H)}$–$H_{(H)}$···$O_{(G1)}$–$C_{(G1)}$ and $C_{(H)}$–$H_{(H)}$···$O_{(G2)}$–$C_{(G2)}$, 2.40 Å (167°) and 2.51 Å (125°), respectively]. Similarly, both disordered guest components in **H_1**·2MCHN are also involved in such interactions, with the one involving G2 also being particularly stabilizing (2.49 Å, 130°). On the other hand, 3MCHN in its complex with **H_1**, has only the one disordered guest component (G1) experiencing this interaction, while both guest components in **H_1**·4MCHN are involved similarly, but interactions are not as strong as in the complexes containing CHN and 2MCHN. These observations explain the affinity of **H_1** for CHN and 2MCHN. Analysis of the other short contacts further elucidates the reasons for this preference: preferred guests are held in the host crystal by an increased number of interactions compared with 3MCHN and 4MCHN; furthermore, 2MCHN experiences the shorter of these, and interactions ranged between 2.21 and 2.67 Å (141–162°).

Analysis of the host geometry revealed that in all four complexes, **H_1** crystallized with its characteristic “buckled” thioxanthenyl tricyclic fused moiety, and deviation from planarity ranged between 26.9° and 33.0°. (This is depicted in Figure S123 which may be found in the Supplementary Information.) Contrary to findings using TETROL as host compound in the presence of these guests,[254] all methylcyclohexanones adopted their more stable conformation, with the methyl groups occupying the more usual equatorial positions (Supplementary Information, Figure S124).

Table 6.4. H···G interactions present in complexes **H₁**·CHN, **H₁**·2MCHN, **H₁**·3MCHN and **H₁**·4MCHN.[a,b,c]

Non-covalent interaction	**H₁**·CHN	**H₁**·2MCHN	**H₁**·3MCHN	**H₁**·4MCHN	Symmetry
H-bonding (H···A, D–H···A)	Non-classical	Non-classical	Non-classical	Non-classical	
$C_{(H)}$–$H_{(H)}$···$O_{(G1)}$–$C_{(G1)}$	2.62 Å, 148° (<)				3/2–x, –1/2+y, 1/2–z
$C_{(H)}$–$H_{(H)}$···$O_{(G2)}$–$C_{(G2)}$	2.61 Å, 172° (<)				1+x, y, z
$C_{(H)}$–$H_{(H)}$···$O_{(G1)}$–$C_{(G1)}$	2.40 Å, 167° (<<)				1/2–x, –1/2+y, 1/2–z
$C_{(H)}$–$H_{(H)}$···$O_{(G2)}$–$C_{(G2)}$	2.51 Å, 125° (<<)				x, y, z
$C_{(H)}$–$H_{(H)}$···$O_{(G2)}$–$C_{(G2)}$		2.49Å, 130° (<<)			1/2–x, –1/2+y,1/2–z
$C_{(H)}$–$H_{(H)}$···$O_{(G1)}$–$C_{(G1)}$		2.66 Å, 165° (<)			x, –1+y, z
$C_{(H)}$–$H_{(H)}$···$O_{(G1)}$–$C_{(G1)}$		2.53 Å, 154° (<)			1+x, –1+y, z
$C_{(H)}$–$H_{(H)}$···$O_{(G1)}$–$C_{(G1)}$			2.49Å, 159° (<<)		1+x, y, z
$C_{(H)}$–$H_{(H)}$···$O_{(G1)}$–$C_{(G1)}$			2.50Å, 131° (<<)		1/2–x, 1/2+y, 1/2–z
$C_{(H)}$–$H_{(H)}$···$O_{(G1)}$–$C_{(G1)}$			2.54Å, 125° (<)		x, y, z
$C_{(H)}$–$H_{(H)}$···$O_{(G2)}$–$C_{(G2)}$				2.67Å, 131° (<)	1–x, 2–y, 2–z
$C_{(G1)}$–$O_{(G1)}$···$H_{(H)}$–$C_{(H)}$				2.69Å, 135° (<)	1–x, 1–y, 1–z
Other short contacts (X···Z, X–Y···Z)					
$C_{(G1)}$–$H_{(G1)}$···$C_{(H)}$–$C_{(H)}$	2.86 Å, 161° (<)				3/2–x, –1/2+y, 1/2–z
$C_{(G2)}$–$H_{(G2)}$···$C_{(H)}$–$S_{(H)}$	2.87 Å, 121° (<)				3/2–x, –1/2+y, 1/2–z
$C_{(G2)}$–$H_{(G2)}$···$H_{(H)}$–$C_{(H)}$	2.27 Å, 161° (<)				1/2+x, 3/2–y, –1/2+z
$C_{(G2)}$–$H_{(G2)}$···$H_{(H)}$–$C_{(H)}$	2.34 Å, 169° (<)				3/2–x, 1/2+y, 1/2–z
$C_{(H)}$–$H_{(H)}$···$H_{(G2)}$–$C_{(G2)}$		2.21 Å, 150° (<)			x, –1+y, z
$C_{(H)}$–$H_{(H)}$···$H_{(G1)}$–$C_{(G1)}$		2.34 Å, 162° (<)			3/2–x, –1/2+y,1/2–z
$C_{(G2)}$–$H_{(G2)}$···$H_{(H)}$–$C_{(H)}$		2.21 Å, 141° (<)			1–x, 1–y, 1–z
$C_{(G2)}$–$H_{(G2)}$···$H_{(H)}$–$S_{(H)}$		2.67Å, 157° (<<)			–1+x, y, z
$C_{(G2)}$–$H_{(G2)}$···$H_{(H)}$–$C_{(H)}$			2.29Å, 161° (<)		–1/2+x, 1/2–y, –1/2+z
$C_{(G1)}$–$H_{(G1)}$···$H_{(H)}$–$C_{(H)}$			2.24Å, 144° (<)		3/2+x, 1/2+y, 1/2–z
$C_{(G1)}$–$H_{(G1)}$···$C_{(H)}$–$S_{(H)}$				2.69Å, 157° (<<)	1+x, y, z
$C_{(G2)}$–$H_{(G2)}$···$H_{(H)}$–$S_{(H)}$				2.83Å, 137° (<)	1+x, y, z

[a]A summary of the H···H interactions may be found in the Supplementary Information (Table S122).

[b]Guest 1 (G1) and guest 2 (G2) represent the disordered guest components in the host crystal.

[c]Distances denoted by < are contacts that measure less than the sum of the van der Waals radii of the atoms involved while those denoted by << is this sum minus 0.2 Å.

6.1.6 Hirshfeld surface analyses

In order to visualize and quantify the multiple intermolecular H···G interactions that are present in these complexes, Hirshfeld surface analysis was carried out on each guest. The 2D fingerprint plots are provided in the Supplementary Information (Figure S125), while a summary of the percentage of each interaction type is displayed graphically in Figure 6.4.

a)

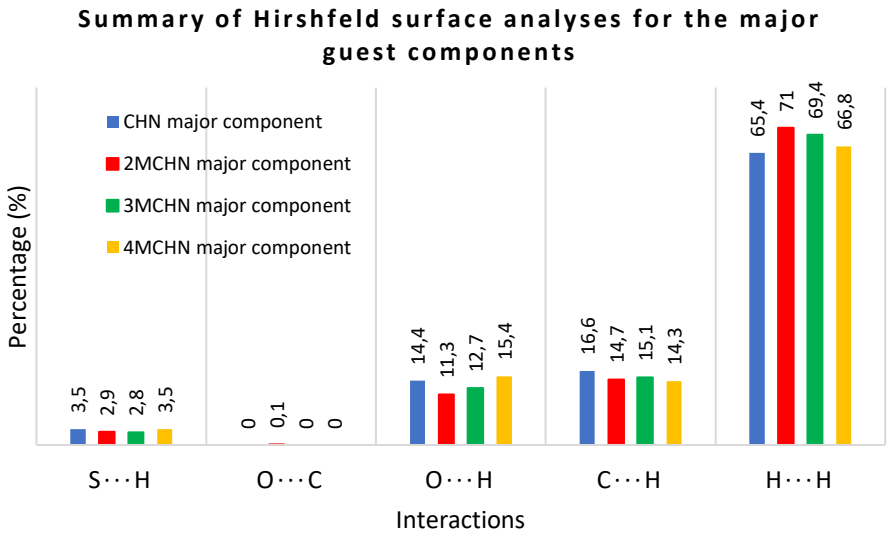

b)

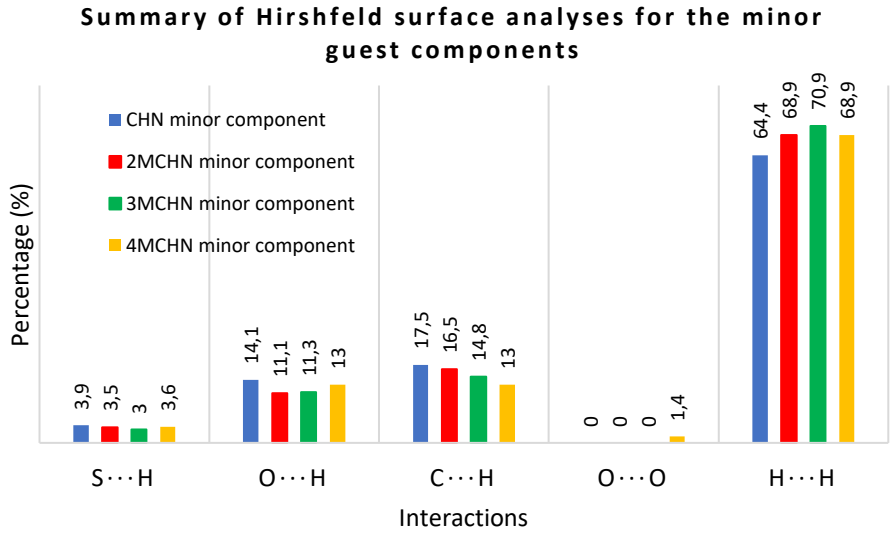

Figure 6.4. A graphical representation of the percentage and types of interactions in complexes of **H₁** with CHN, 2MCHN, 3MCHN and 4MCHN for the a) major components and b) minor components.

Due to the nature of the host and guests, all complexes with **H_1** are predominantly stabilized by H···H (64.4–71.0%), C···H (13.0–17.5%) and O···H (11.1–15.4%) interactions (Figure 6.4), and the reasons for the host selectivity order is not clearly evident from these data.

6.1.7 Thermal analyses (DSC and TG)

Simultaneous TG and DSC experiments were carried out on each of the four complexes of **H_1**. Figure 6.5 depicts the resultant TG, DTG and DSC traces obtained upon heating the solids at 10 °C·min^{-1} under high purity nitrogen as purge gas, while Table 6.5 summarizes the relevant thermal data.

a)

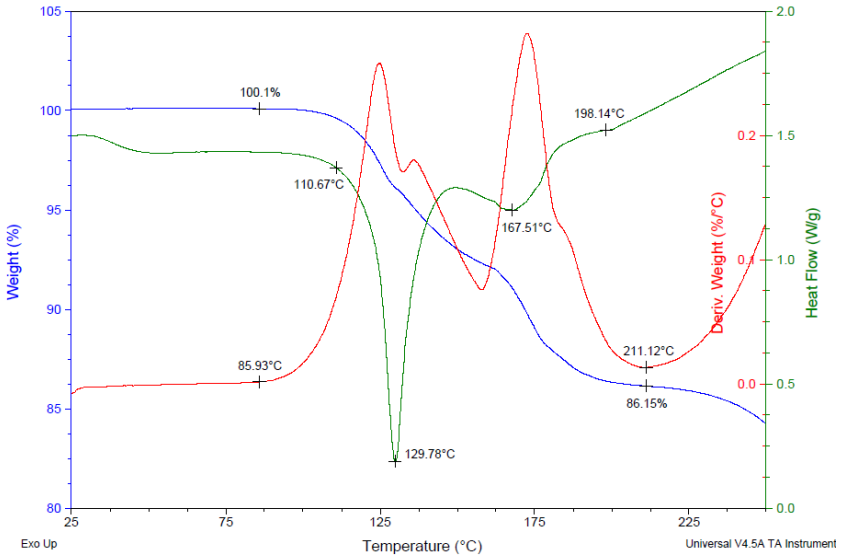

b)

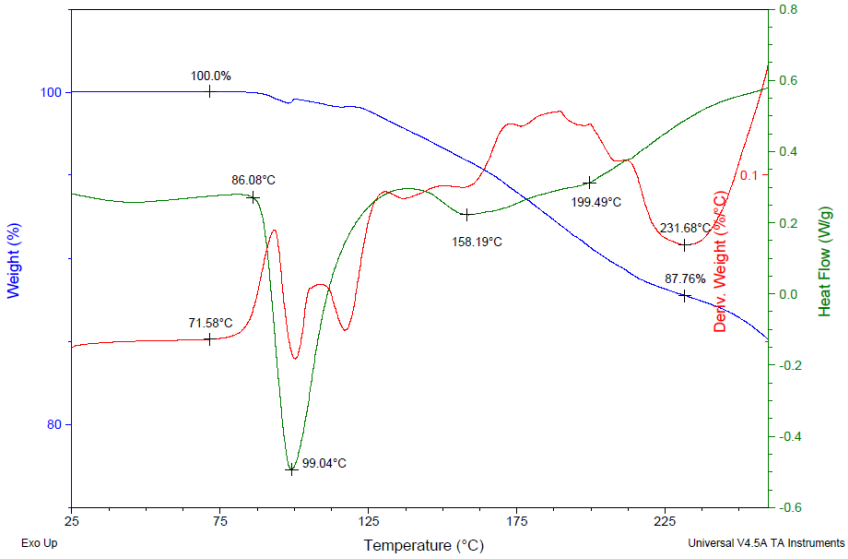

c)

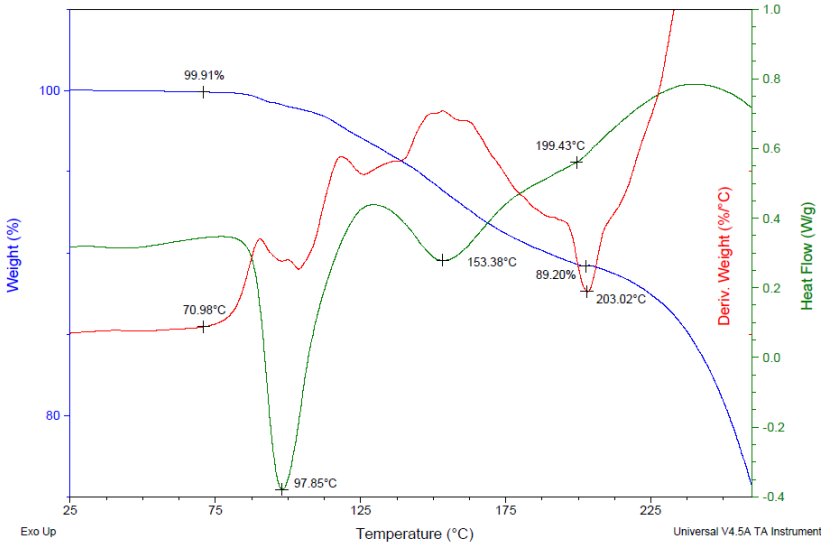

d)

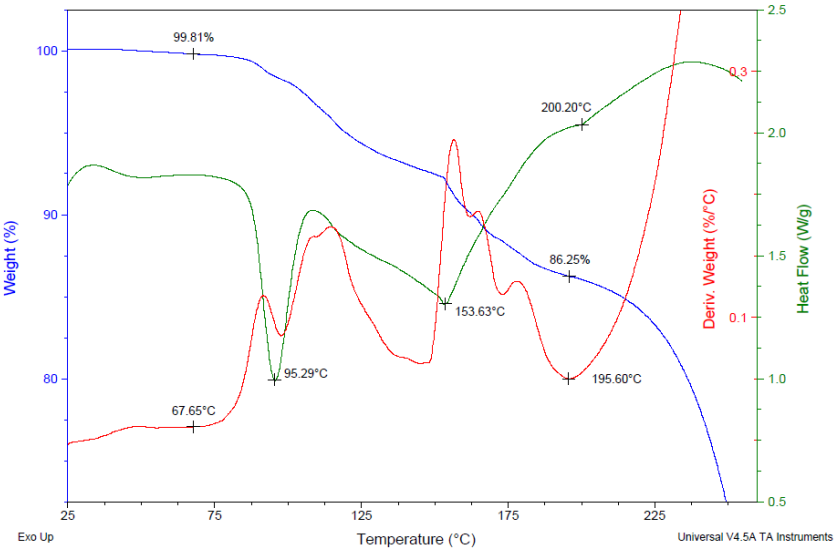

Figure 6.5. DSC (green), TG (blue) and DTG (red) traces for **H_1** in complexes with guests a) CHN, b) 2MCHN, c) 3MCHN and d) 4MCHN.

In each case, guest release is especially convoluted (Figure 6.5a–d). The measured mass loss for the 1:1 **H_1**·CHN complex 14.0% (Table 6.5), which is exactly as expected (14.0%). The MCHN complexes, however, experienced mass losses of only 12.2% (2MCHN), 10.7% (3MCHN) and 13.6% (4MCHN), significantly lower than that calculated (15.7%): in each case, the TG has a continual downward slope, ensuring difficulty in determining the end point of the guest release process, and this may explain these mass loss discrepancies. However, the CHN complex did demonstrate higher T_{on} and T_p values (85.9 and 129.8°C), followed by

2MCHN (71.6 and 99.0°C), and these observations agree with the host selectivity order obtained from the binary competition experiments (CHN > 2MCHN > 3MCHN > 4MCHN). Considering only the MCHN isomers, the T_{on} (71.6 °C > 71.0 °C > 67.7 °C) and T_p (99.0 °C > 97.9 °C > 95.3 °C) values were also found to be in accordance with results from these competitions (2MCHN > 3MCHN > 4MCHN).

Table 6.5. Thermal data for complexes **H_1**·CHN, **H_1**·2MCHN, **H_1**·3MCHN and **H_1**·4MCHN.

Guest (G)	T_{on} /°C	T_p /°C	Mass loss expected /%	Actual mass loss Measured /%
CHN	85.9	129.8	14.0	14.0
2MCHN	71.6	99.0	15.7	12.2
3MCHN	71.0	97.9	15.7	10.7
4MCHN	67.7	95.3	15.7	13.6

6.1.8 Conclusions

The host **H_1** successfully included CHN and the MCHN isomers with a 1:1 H:G ratio. Competition experiments demonstrated that the selectivity order of the host for the three isomeric MCHNs was in the order 2MCHN (67.6%) > 3MCHN (23.1%) > 4MCHN (9.3%), while in the presence of added CHN, this was modified to 2MCHN (41.7%) ≈ CHN (39.2%) >> 3MCHN (13.5%) > 4MCHN(5.6%) (from the quaternary mixtures). 2MCHN was also the preferred isomer at all evaluated guest concentrations in the non-equimolar binary recrystallization experiments. SCXRD analysis indicated that complexes with CHN, 2-, and 3- MCHN experienced isostructural host packing (monoclinic, $P2_1/n$), while the **H_1**·4MCHN complex crystallized in a triclinic *P*-1 crystal system with completely different cell parameters. All four guests experienced non-classical $C_{(H)}$–$H_{(H)}$···$O_{(G)}$–$C_{(G)}$ H-bonding interactions, with the CHN-containing complex (CHN a co-preferred guest) experiencing the shortest of these (2.40 Å, 167°). Based on the analysis of additional short contacts present, the favoured CHN and 2MCHN guests were held in the host crystal by stronger and a greater number of interactions when compared with the other two guests. Hirshfeld surface analyses were considered but did not add to the investigation. Thermal analyses further confirmed the observation that complexes with both CHN and 2MCHN possess enhanced thermal stabilities relative to the inclusion compounds with the other two cyclic ketones.

6.1.9 Supporting information

All spectra and detailed tables that were relevant to this chapter are provided in the Supplementary Information. The crystal structures were deposited at the Cambridge Crystallographic Data Centre, and CCDC numbers 1910105 (**H_1**·CHN), 1910106 (**H_1**·2MCHN), 1910107 (**H_1**·3MCHN) and 1910108 (**H_1**·4MCHN) contain the supplementary crystallographic data for this chapter.

6.2. Inclusion compounds with **H_2**

Surprisingly, no crystallization occurred when **H_2** was introduced to CHN and the MCHN isomers, and a gel remained behind in the crystallization vessels. From previous sections, it was shown that **H_2** is a much more discerning host compound than **H_1**, and this is apparent here too and, at this stage, the reason for this behaviour of **H_2** cannot be explained with confidence.

7. HETEROCYCLIC SIX-MEMBERED RING COMPOUNDS

7.1 Inclusion compounds with $\mathbf{H_1}$

7.1.1 Introduction

Pyridine (PYR), piperidine (PIP), morpholine (MORPH) and 1,4-dioxane (DIOX) are six-membered ring heterocyclic compounds (Scheme 7.1) that have a wide range of important applications. They are used in the manufacture of pharmaceuticals, insecticides, herbicides, food preservatives, food additives, and also in the production of inks and adhesives.[40,256]

Historically, PYR was extracted from coal tar or obtained as a by-product of coal gasification. The process was labour intensive and inefficient and, currently, most PYR is preferably produced using improved synthetic reactions (such as the Chichibabin pyridine synthesis, dealkylation of alkylpyridines, Bönnemann cyclization and the Kröhnke pyridine synthesis, to name a few).[257]

PIP is a common organic compound, and its structural motif is present in numerous natural alkaloids and pharmaceuticals.[258,259] PIP is commonly used as a solvent and as a base,[260] and to produce dipiperidinyl dithiuram tetrasulfide, which is used as an accelerator in the sulfur vulcanization of rubber.[261] Industrially, PIP is produced by the catalytic hydrogenation or reduction (via a modified Birch reaction) of PYR.[261]

MORPH is often produced industrially by the dehydration of diethanolamine with sulfuric acid.[262] It is a common additive for pH adjustment in both fossil fuel and nuclear power plant steam systems, is widely used in organic synthesis as a solvent or building block, and has application in the agricultural industry (as a fruit coating or component of fungicides).[263-265]

DIOX is used as a solvent, a stabilizer for chlorinated hydrocarbons,[244] and also serves as an internal standard in NMR spectroscopy in deuterium oxide.[266] This compound is produced by the catalytic dehydration of diethylene glycol.[267]

In this present work, we report on the behaviour of $\mathbf{H_1}$ in the presence of these guest types and, later, compare the results with those obtained for $\mathbf{H_2}$.

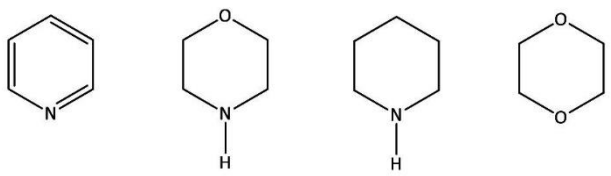

PYR	MORPH	PIP	DIOX
115 °C	129 °C	106 °C	101 °C

Scheme 7.1. Structures of the four heterocyclic six-membered ring guests.

7.1.2 Individual inclusions

The feasibility of this study was first evaluated by determining whether the four proposed guests, with their unique structural features, form cocrystals with **H_1** in single solvent experiments. This was achieved by growing crystals of **H_1** from each of these guests, and the analysis of the resultant ^{1}H-NMR spectra confirmed that the host successfully included each one with a 1:1 H:G ratio (Table 7.1). (^{1}H-NMR spectra of all four complexes are provided in the Supplementary Information, Figures S126–129.)

Table 7.1. H:G ratios of inclusion compounds formed by **H_1**.[a]

Guest (G)	H:G
PYR	1:1
MORPH	1:1
PIP	1:1
DIOX	1:1

[a]Determined using ^{1}H-NMR spectroscopy with $CDCl_3$ as solvent.

7.1.3 Equimolar competition experiments

Since each of the four solvents was successfully enclathrated, the host selectivity was investigated when **H_1** was recrystallized from equimolar binary, ternary and quaternary mixtures of these guests. ^{1}H-NMR spectroscopy was found to be a suitable method of analysis for the so-formed mixed inclusion compounds (to obtain the G:G ratios) since one resonance signal for each guest is available for integration and did not overlap with either the host or the other guests present (Table 7.2). A ^{1}H-NMR spectrum of a quaternary mixed inclusion compound is provided in the Supplementary Information (Figure S130), and the peaks that were used for integration are clearly labelled.

Table 7.2. ^{1}H-NMR data for pure PYR, MORPH, PIP and DIOX.

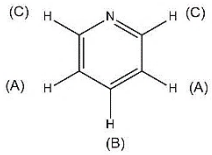		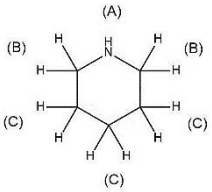		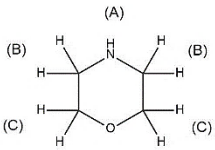		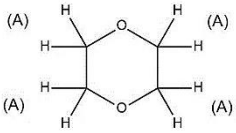	
Assignment	**δ(ppm)**	**Assignment**	**δ(ppm)**	**Assignment**	**δ(ppm)**	**Assignment**	**δ(ppm)**
(A) H	6.88–6.91	(A) NH	1.55	(A) NH	2.09	(A) H	3.55
(B) H	7.27–7.31	(B) H	2.42–2.43	(B) H	2.68		
(C) H	8.24–8.25	(C) H	1.15–1.17	(C) H	3.50		

Table 7.3 summarizes the averaged data from these equimolar mixed experiments, together with the % e.s.d.s for each combination. The H:G ratios were, once more, determined through ^{1}H-NMR spectroscopy, and the preferred guest is indicated in red. These experiments were conducted in duplicate, and the complete set of data may be found in the Supplementary Information, Table S131.

Table 7.3. Results of competitions using **H$_1$** and various equimolar mixtures of the heterocyclic guests.[a,b]

PYR	MORPH	PIP	DIOX	Average guest ratios	Overall H:G	% e.s.d.s
x			x	81.8:18.2	1:1	(0.7):(0.7)
x		x		81.4:18.6	1:1	(0.5):(0.5)
x	x			75.6:24.4	1:1	(1.1):(1.1)
		x	x	53.8:46.2	1:1	(0.9):(0.9)
	x		x	49.9:50.1	1:1	(0.7):(0.7)
	x	x		52.0:48.0	1:1	(1.3):(1.3)
x	x	x		65.8:18.2:16.0	1:1	(0.2):(0.6):(0.4)
x		x	x	69.4:16.7:13.9	1:1	(0.3):(0.6):(0.3)
x	x		x	61.3:16.9:21.8	1:1	(0.4):(0.2):(0.2)
	x	x	x	33.3:34.2:32.5	1:1	(0.5):(0.4):(0.9)
x	x	x	x	57.1:16.1:14.5:12.3	1:1	(0.1):(0.1):(0.2):(0.1)

[a]G:G and overall H:G ratios were determined using ^{1}H-NMR spectroscopy with $CDCl_3$ as solvent.
[b]Experiments were conducted in duplicate for confirmation purposes; % e.s.d.s are provided in parentheses.

From Table 7.3, it is clear that **H$_1$** favours the aromatic heterocyclic compound, PYR, over any of the saturated heterocyclics whenever it is present. Furthermore, the selectivity for this guest is significant in all instances: from the equimolar binary experiments PYR/MORPH,

PYR/PIP and PYR/DIOX, 75.6%, 81.4% and 81.8% of PYR was observed in the host crystal, respectively. Ternary experiments involving this guest (PYR/MORPH/PIP, PYR/PIP/DIOX and PYR/MORPH/DIOX) resulted in a slight decline in the host selectivity, but PYR remained highly favoured (61.3−69.4%). An equimolar mixture of all four solvents resulted in a mixed inclusion compound containing 57.1% of the aromatic guest.

More remarkable is the observation that **H_1** is unusually ambivalent towards all the saturated heterocyclic compounds, regardless of whether PYR is present or not, and regardless of how many guests were used in the competition experiment. PIP/DIOX, MORPH/DIOX and MORPH/PIP binary mixtures produced complexes with only 53.8% PIP, 50.1% DIOX and 52.0% MORPH, respectively. This ambivalence is also noted in the ternary experiment involving MORPH, PIP and DIOX: the mixed complex contained 33.3%, 34.2% and 32.5% of each of these guests. Furthermore, in those ternary and quaternary experiments where PYR was present, the host selectivity was never overwhelmingly different for any of the remaining saturated heterocyclics. The host selectivity may therefore be written in the order PYR >> PIP ≈ MORPH ≈ DIOX.

Another observation is that the overall H:G ratio was consistently 1:1, which was also the preferred ratio in the single solvent experiments.

To determine whether the selectivity of **H_1** remains consistent even when the molar amounts of these guests in binary competition experiments are varied, ratio-dependent competition experiments were subsequently conducted.

7.1.4 Ratio-dependent competition experiments

The host was dissolved in a mixture of known amounts of any two of the four relevant solvents and, upon crystallization, both the mother liquor and the crystalline material (after washing) were analysed using ^{1}H-NMR spectroscopy. Selectivity profiles were set up which display the behaviour of the host across each guest concentration range; these selectivity profiles are provided in Figures 7.1 and 7.2. Additionally, the average selectivity coefficients were calculated, while a complete set of these K values may be found in the Supplementary Information, Tables S132–137.

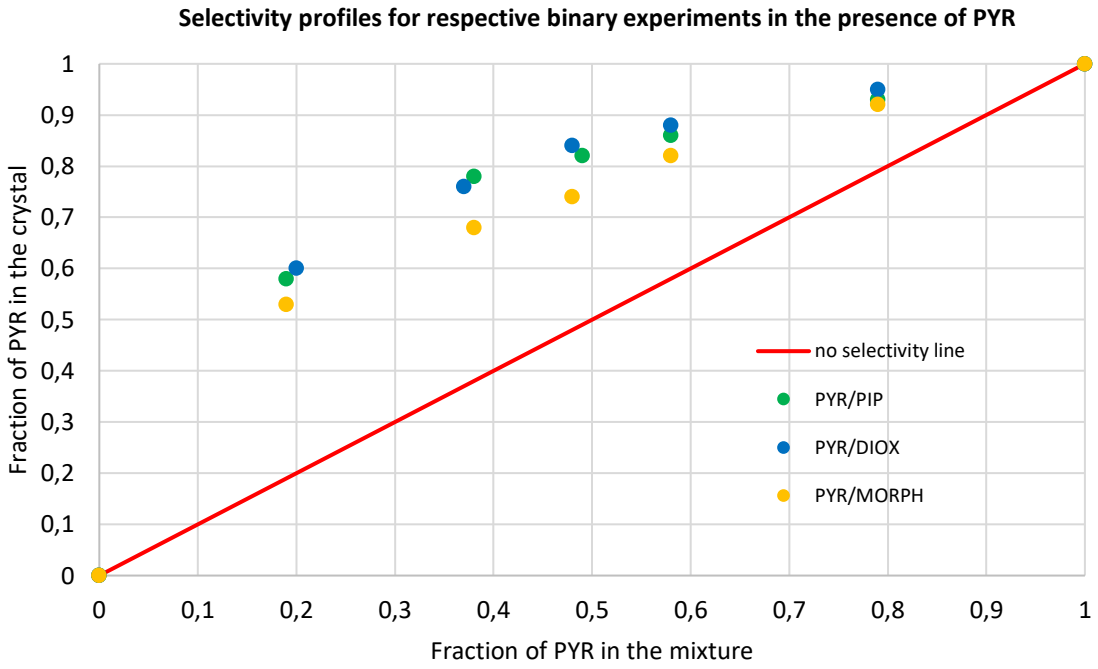

Figure 7.1. Overlaid selectivity profiles of $\mathbf{H_1}$ with binary combinations where PYR is present.

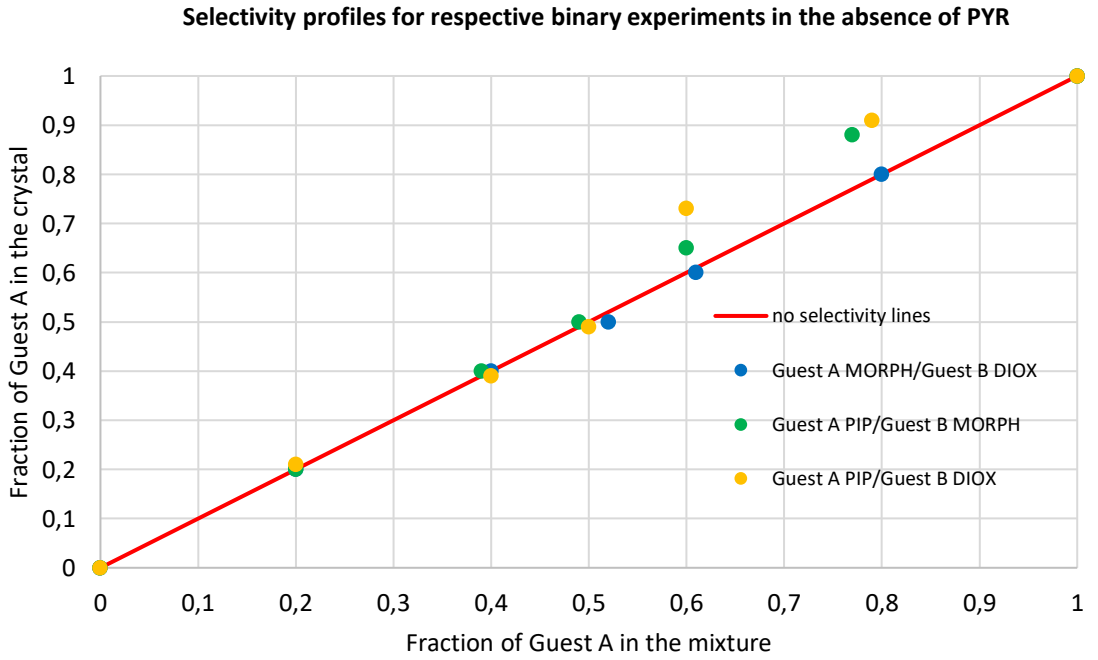

Figure 7.2. Overlaid selectivity profiles of $\mathbf{H_1}$ with binary combinations where PYR is absent.

By considering the results of the previous equimolar competition experiments, it is not surprising that $\mathbf{H_1}$ is constantly selective for PYR whenever it is present over the entire concentration range assessed, irrespective of the other guest types and even at low concentrations of PYR [PYR/DIOX (blue profile, K = 5.5), PYR/PIP (green profile, 4.9) and

PYR/MORPH (yellow profile, 3.5), Figure 7.1]. Furthermore, as alluded to from those same results, **H_1** does not discriminate between MORPH and DIOX at any stage: the percentage of these guests in the crystal is virtually identical to that in the liquid mixture from which the crystals formed (Figure 7.2, blue profile, K = 1). The selectivity profiles for the binary experiments using PIP/MORPH (green profile, K = 1.3) and PIP/DIOX (yellow profile, K = 1.5) illustrate that the host is unselective at high concentrations of MORPH and DIOX respectively while, in both cases at high concentrations of PIP (> 50%), this guest is the preferred one, but not overwhelmingly so.

In order to explain the host selectivity behaviour, SCXRD analyses were carried out on the four inclusion compounds.

7.1.5 SCXRD

Table 7.4 summarizes the relevant crystallographic data obtained for the four complexes. Each crystallizes in the monoclinic crystal system and $P2_1/n$ space group. Upon close analysis of these data, it is apparent that the host packing in **H_1**·PYR, **H_1**·MORPH and **H_1**·DIOX are isostructural, while this is not the case in the PIP complex, which has unique unit cell dimensions. Figure 7.3 displays the unit cells for each complex, where the isostructural host packing in **H_1**·PYR, **H_1**·MORPH and **H_1**·DIOX is clearly evident and different from **H_1**·PIP.

Table 7.4. Crystallographic data for **H₁**·PYR, **H₁**·MORPH, **H₁**·PIP and **H₁**·DIOX.

	H₁·PYR	**H₁**·MORPH	**H₁**·PIP	**H₁**·DIOX
Chemical formula	$C_{40}H_{32}N_2S_2$ $\cdot C_5H_5N$	$C_{40}H_{32}N_2S_2$ $\cdot C_4H_8NO$	$C_{40}H_{32}N_2S_2$ $\cdot C_5H_{11}N$	$C_{40}H_{32}N_2S_2$ $\cdot C_4H_8O_2$
Formula weight	683.90	690.91	689.94	692.90
Crystal system	Monoclinic	Monoclinic	Monoclinic	Monoclinic
Space group	$P2_1/n$	$P2_1/n$	$P2_1/n$	$P2_1/n$
μ (Mo Kα)/mm^{-1}	0.195	0.194	0.187	0.195
a/Å	10.1347(3)	10.2905(7)	13.9591(11)	10.3115(7)
b/Å	13.3006(3)	13.3919(9)	13.7868(10)	13.3115(7)
c/Å	25.3821(7)	25.2637(17)	19.7327(15)	25.2886(17)
alpha/°	90	90	90	90
beta/°	91.964(2)	92.547(3)	109.750(3)	91.892(3)
gamma/°	90	90	90	90
V/Å^3	3419.44(2)	3478.1(4)	3574.2(5)	3481.0(4)
Z	4	4	4	4
F(000)	1440	1460	1464	1464
Temp./K	200	200	200	200
Restraints	0	12	0	6
Nref	8508	8662	8852	8660
Npar	459	454	463	429
R	0.0343	0.0440	0.0348	0.0782
wR2	0.0970	0.1221	0.0918	0.2361
S	1.06	1.03	1.03	1.03
θ min–max/°	1.6, 28.3	1.6, 28.3	1.8, 28.3	1.6, 28.4
Tot. data	74142	130407	82206	127974
Unique data	8508	8662	8852	8660
Observed data [I > 2.0 sigma(I)]	6832	7392	7194	7645
R_{int}	0.035	0.021	0.021	0.020
Dffrn measured fraction θ full	1.000	1.000	1.000	1.000
Min. resd. dens. (e/Å^3)	–0.25	–0.40	–0.30	–1.20
Max. resd. dens. (e/Å^3)	0.31	0.81	0.34	2.29

Of the four inclusion compounds, only the guests in **H₁**·PYR and **H₁**·PIP showed no disorder. For the complex containing MORPH, not all of the guest disorder could be modelled while the DIOX molecule, on the other hand, is disordered around its centroid and, consequently, there exists too much overlap of the disordered components to model this disorder. As a result, the wR2 values for both of these inclusion compounds are rather high (Table 7.4). As a result, it was not possible to assess and compare H···G interactions confidently in the **H₁**·MORPH and **H₁**·DIOX complexes relative to the other two (where no disorder existed).

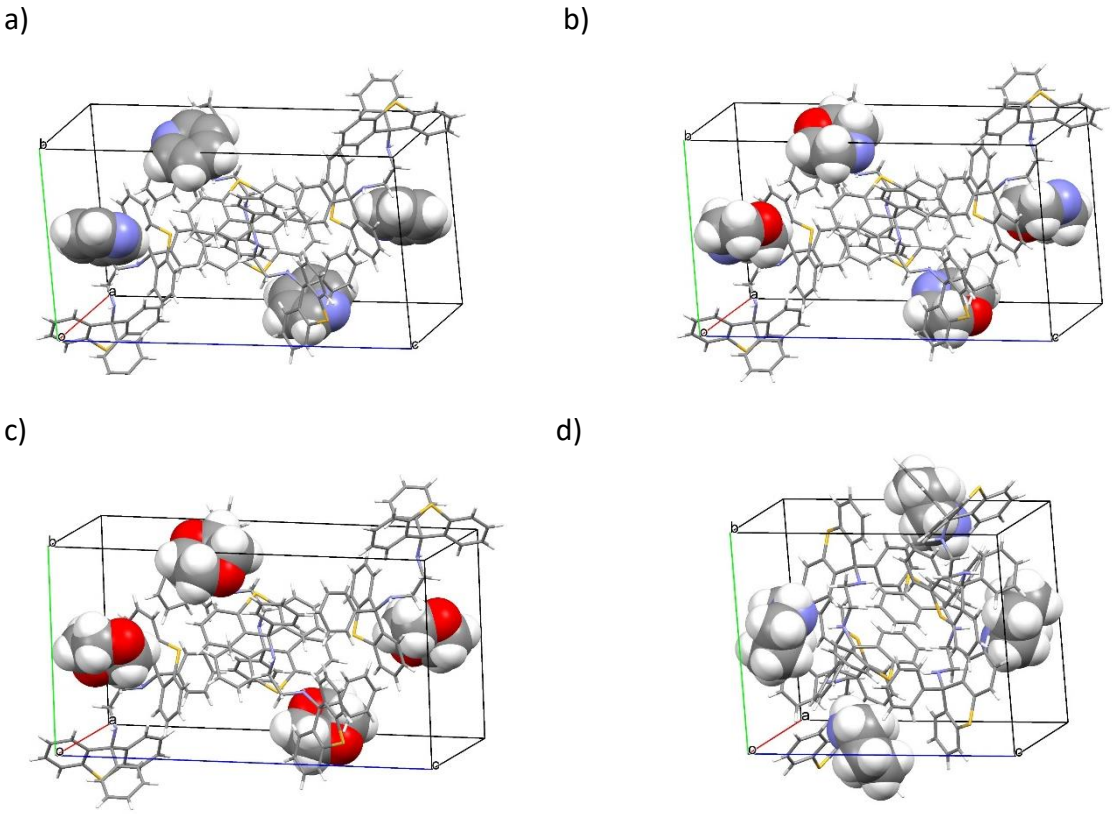

Figure 7.3. Unit cells for complexes a) **H$_1$**·PYR, b) **H$_1$**·MORPH, c) **H$_1$**·DIOX and d) **H$_1$**·PIP.

Guests were removed from the packing calculation to display the voids, as shown in Figure 7.4. In all four, guests are accommodated within discrete cavities; while two guests occupy each cavity in the **H$_1$**·PYR, **H$_1$**·MORPH and **H$_1$**·DIOX crystals, only one guest is found in each void in the **H$_1$**·PIP inclusion compound.

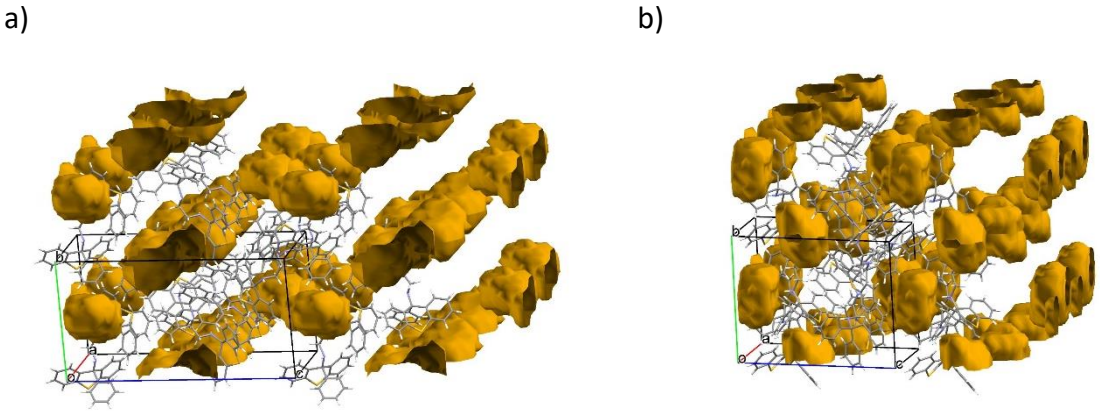

Figure 7.4. Voids (dark yellow) present in the **H$_1$**·PYR (as a representative example for the three isostructural inclusion compounds) and **H$_1$**·PIP inclusion compounds after the guests were removed from the packing calculation.

Table 7.5 is a summary of the significant H···G interactions experienced by PYR and PIP in the **H_1** crystals.

Table 7.5. Significant H···G interactions in **H_1**·PYR and **H_1**·PIP.[a,b]

Non-covalent interaction	**H_1**·PYR	**H_1**·PIP	Symmetry operation
π···π	4.782(1)–5.975(1) Å [9]		
H-bonding (H···A, D–H···A) $N_{(H)}$–$H_{(H)}$···$N_{(G)}$–$C_{(G)}$		2.45 Å, 157° (<<)	x, y, z

[a]Values in square brackets indicate the number of H···G π···π interactions.
[b]**H_1**·MORPH and **H_1**·DIOX displayed disorder that could not be adequately modelled; consequently, H···G interactions could not be trusted.

The only H···G contacts experienced by the PYR guests are π···π stacking in nature and are very weak, ranging between 4.782(1) and 5.975(1) Å (Table 7.4). The host affinity for PYR, if this is due to intermolecular interactions may, therefore, be as a result of these stacking interactions, which are obviously not a possibility for the saturated heterocyclics, given their nature. The only noteworthy contact experienced by PIP is a classical $N_{(H)}$–$H_{(H)}$···$N_{(G)}$–$C_{(G)}$ hydrogen bond, measuring 2.45 Å (157°). It is tentatively proposed that MORPH and DIOX, due to the extent of their disorder, are not involved in any hydrogen bonding or any other significant interactions with the host since these would serve to anchor these species in their respective positions, affording less disorder. As observed earlier in the DIOX/MORPH binary competition experiment, the host showed absolutely no selectivity for either of these guests, irrespective of their concentrations (Figure 7.2, blue profile). Perhaps this ambivalence of **H_1** across the entire MORPH/DIOX concentration range is indicative of near-absent H···G stabilizing interactions, and that these guests are retained in the host crystal by other, more significant, factors. (All host···host interactions are provided in the Supplementary Information, Table S138).

7.1.6 Hirshfeld surface analyses

Hirshfeld surface analyses of the **H$_1$**·PYR and **H$_1$**·PIP complexes were considered, and the 2D fingerprint plots which were derived from the 3D surfaces are provided in the Supplementary Information, Figure S139. (Due to the guests of **H$_1$**·MORPH and **H$_1$**·DIOX showing significant disorder, H···G interactions could, consequently, not be analysed here with confidence either.) From the 2D fingerprint plots, the relative areas of the significant interactions were obtained and are summarized in Figure 7.5.

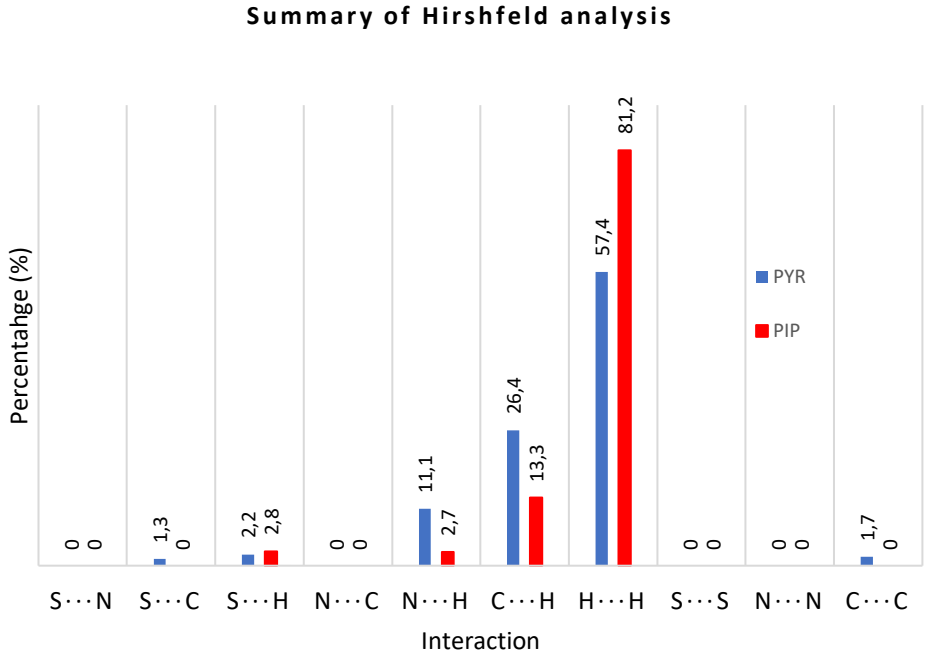

Figure 7.5. H···G interaction types and quantities after Hirshfeld surface analyses of the **H$_1$**·PYR and **H$_1$**·PIP complexes.

It is expected that **H$_1$**·PIP would experience a larger percentage of H···H interactions, being a saturated compound, compared with **H$_1$**·PYR, and this is indeed the case here (81.2 versus 57.4%). Surprisingly, despite **H$_1$**·PIP experiencing a classical hydrogen bond with the host, **H$_1$**·PYR has significantly more N···H/H···N interactions between the host and guest (11.1 versus 2.7%). Furthermore, **H$_1$**·PYR experiences an increased number of H···C/C···H H···G interactions (26.4 versus 13.3%), and these latter observations may explain the enhanced selectivity of **H$_1$** for PYR.

7.1.7 Thermal analyses (DSC and TG)

Thermal analyses were carried out on the four inclusion compounds to gain an understanding of the thermal events that occur as each sample is heated at 10 °C·min^{-1}. The overlaid DSC, TG and DTG traces are given in Figures 7.6–7.8, from which the relevant thermal data were summarized (Table 7.6).

Table 7.6. Thermal properties of the four complexes formed with **H_1**.

Guest	T_{on} /°C	T_p /°C	Mass loss expected/%	Actual mass loss measured/%
DIOX	70.8	113.8, 120.3	12.8	12.6
MORPH	[a]	45.9, 124.6	12.6	[b]
PIP	83.3	105.8, 110.6	12.4	12.8
PYR	91.3	137.1, 142.3	11.7	12.5

[a]The onset temperature for the guest release process could not be stipulated since some of the guest escapes from the crystal prior to the thermal experiment.
[b]Guest release initiated even prior to this analysis, and hence actual mass loss could not be measured.

a)

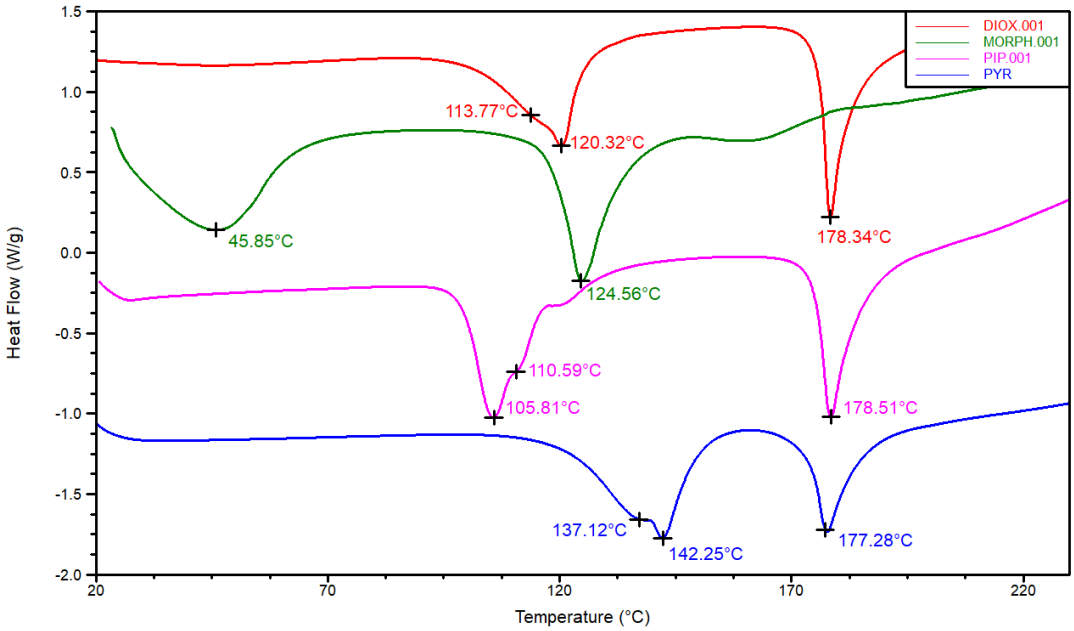

b)

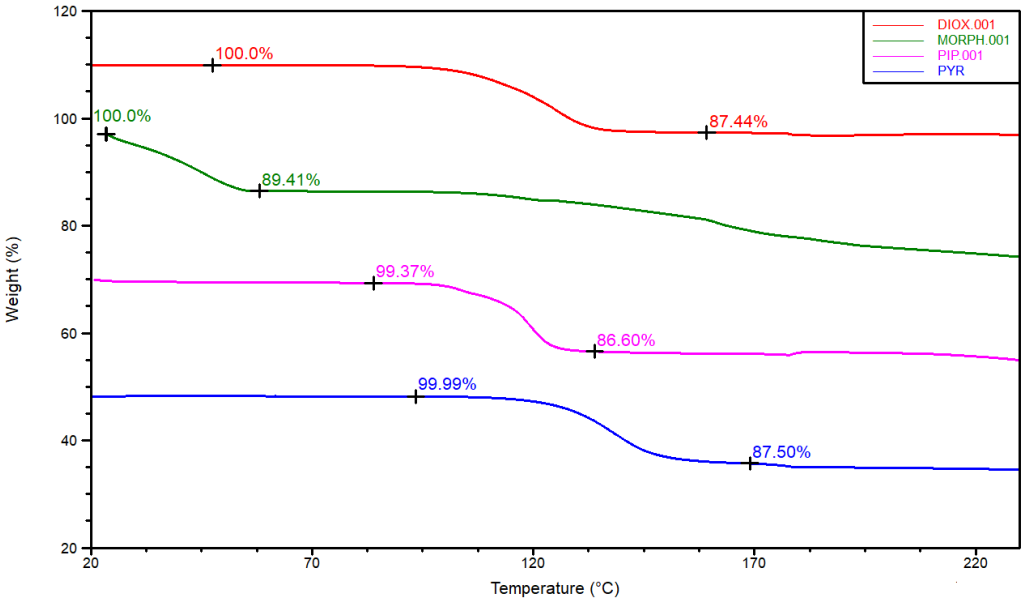

c)

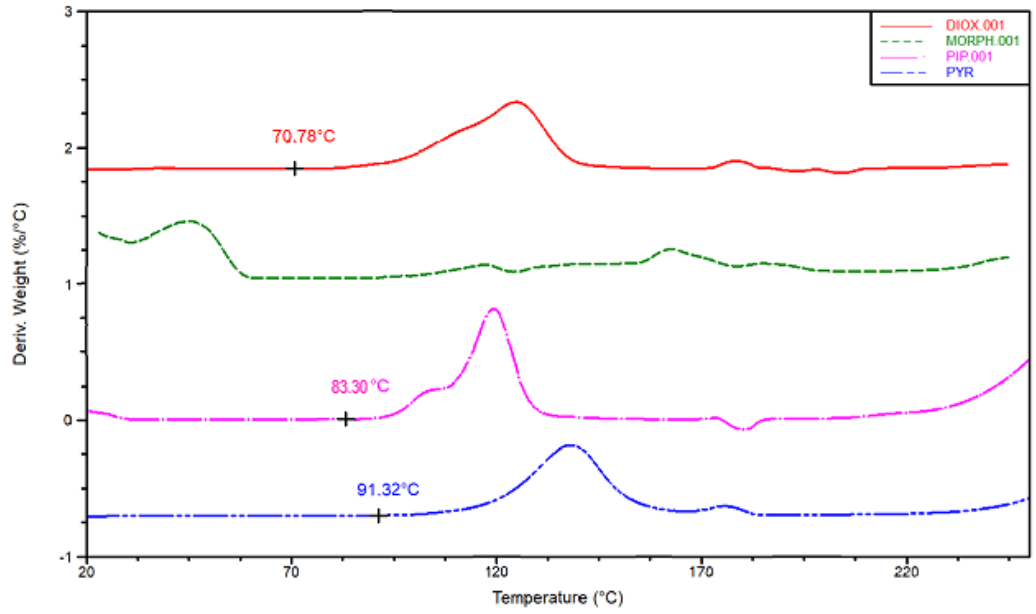

Figure 7.6. Overlaid a) DSC, b) TG and c) DTG traces for the **H$_1$**·PYR (blue), **H$_1$**·MORPH (green), **H$_1$**·DIOX (red) and **H$_1$**·PIP (fuchsia) complexes.

The traces for the PYR-, PIP- and DIOX- containing inclusion compounds are largely as expected: the first thermal event is that of the release of the guest and is represented by more than one overlapping endotherm (Figure 7.6a). Naturally, associated with each of these

guest release processes is a mass loss (Figure 7.6b) which agrees essentially with that which one would expect theoretically (Table 7.6). The final endotherm represents the melting of the host species (the endotherm peaks at 177.3–178.5 °C for the three inclusion compounds under discussion). The thermal events experienced by **H_1**·MORPH, however, is more complicated. This guest escapes from the host cavities in a minimum of two distinct steps (T_p 45.9, 124.6 °C), but guest loss was initiated prior to this experiment, and the complex displays instability as observed by the release of MORPH right from the outset of this experiment, in accordance with the low affinity of **H_1** for this guest. The mass loss measurement, therefore, could not be carried out here, owing to this instability.

Also notable from these data is that the **H_1**·PYR inclusion compound displays the highest T_{on} (91.3 °C) and T_p (137.1 and 142.3 °C) values of the four complexes, suggesting that this complex possesses an increased thermal stability relative to the others; this observation corresponds with the enhanced selectivity of **H_1** for PYR. [DSC, TG and DTG traces for each individual inclusion compound may be found in the Supplementary Information (Figure S140).]

7.1.8 Conclusions

In this work, the affinity of host compound **H_1** was assessed in the presence of PYR, MORPH, PIP and DIOX, and each of these heterocyclic solvents was individually enclathrated (H:G 1:1). Experiments employing various equimolar binary, ternary and quaternary mixtures of these guests revealed that the host is overt in its selectivity for PYR, and significantly ambivalent towards the three saturated heterocyclic compounds (whether PYR was present or not). Guest ratios were also varied from 0 to 100 mol% in binary competition experiments and these affirmed the significant selectivity of the host towards the aromatic guest. SCXRD experiments were conducted on all of the inclusion compounds and it was suggested that, owing to the aromatic moieties present in both the host and guest structures, H···G π···π stacking interactions, although extremely weak [4.782(1)−5.975(1) Å], possibly play a significant role in the selectivity displayed by this host for PYR. Naturally, these contact types are not possible in complexes containing the saturated heterocyclics. H···G interactions in two of the inclusion compounds, those with MORPH and DIOX, were not considered here due to the significant disorder displayed by the guest molecules which could not be modelled with

confidence. However, owing to the amount of disorder, it was tentatively proposed that both of these guests possibly do not experience significant H···G interactions in the crystal (which would have anchored these guests in their cavities). Thermal analyses confirmed this proposal for the **H$_1$**·MORPH inclusion compound: some of the guest is released prior to the thermal experiment, and therefore this complex displays much instability. On the other hand, PYR experiences higher T_p and T_{on} values compared to the guests in the other complexes, alluding to an increased thermal stability, in accordance with the host selectivity order.

7.1.9 Supporting information

Relevant NMR data, the associated % e.s.d.s and thermal traces for the inclusion compounds may be found in the Supplementary Information. The crystal structures were deposited at the Cambridge Crystallographic Data Centre, and CCDC 1549682 (**H$_1$**·PYR), 1551195 (**H$_1$**·MORPH), 1551196 (**H$_1$**·PIP) and 1551197 (**H$_1$**·DIOX) contain the supplementary crystallographic data for this section.

7.2 Inclusion compounds with **H$_2$**

7.2.1 Introduction

For comparative purposes with **H$_1$**, the host capabilities of **H$_2$** were evaluated in the presence of PYR, MORPH, PIP and DIOX, and the findings are reported here.

7.2.2 Individual inclusions

When **H$_2$** was recrystallized from the four heterocyclic organic solvents in order to determine whether complexes would form, ^{1}H-NMR analysis revealed that, once more, each of these compounds was enclathrated. With the exception of **H$_2$**·2(PYR) (H:G 1:2), all of the complexes crystallized with a 1:1 H:G ratio (Table 7.7). (The ^{1}H-NMR spectra of the respective complexes may be found in the Supplementary Information, Figures S141–144.)

Table 7.7. H:G ratios of inclusion compounds formed by **H₂**.[a]

Guest (G)	H:G
PYR	1:2
MORPH	1:1
PIP	1:1
DIOX	1:1

[a]Determined using ^{1}H-NMR spectroscopy with $CDCl_3$ as solvent.

Since each of the four solvents was included by **H₂**, the selectivity of the host was investigated by recrystallizing the compound from equimolar binary, ternary and quaternary mixtures of these guests, as was the case for **H₁**.

7.2.3 Equimolar competition experiments

Once again, ^{1}H-NMR spectroscopy was utilized to determine the H:G and G:G ratios from these experiments (Supplementary Information, Figure S145). Table 7.8 is a summary of the so-obtained results, together with the % e.s.d.s. (The duplicate data are provided in the Supplementary Information, Table S146).

Table 7.8. Results of competitions using **H₂** and various equimolar mixtures of the heterocyclic guests.[a,b,c]

PYR	MORPH	PIP	DIOX	Average guest ratios	Overall H:G ratio	% e.s.d.s
x			x	10.1:89.9	1:1	(0.7):(0.7)
x		x		[c]	-	-
x	x			14.7:85.3	1:1	(1.0):(1.0)
		x	x	4.7:95.3	1:1	(0.4):(0.4)
	x		x	29.8:70.2	1:1	(1.0):(1.0)
	x	x		94.2:5.8	1:1	(2.0):(2.0)
x	x	x		8.3:84.2:7.5	1:1	(0.4):(0.3):(0.1)
x		x	x	8.0:3.7:88.3	1:1	(0.4):(0.7):(1.1)
x	x		x	11.1:22.5:66.4	1:1	(0.4):(0.6):(0.2)
	x	x	x	22.6:5.0:72.4	1:1	(0.9):(0.4):(0.5)
x	x	x	x	8.2:20.0:3.8:68.0	1:1	(0.1):(0.2):(0.6):(0.9)

[a]G:G and overall H:G ratios were determined using ^{1}H-NMR spectroscopy with $CDCl_3$ as solvent.
[b]Experiments were conducted in duplicate for confirmation purposes; % e.s.d.s are provided in parentheses.
[c]Did not crystallize.

It is clear from Table 7.8 that **H_2** behaves entirely differently in the presence of the various combinations of equimolar guest solvents relative to **H_1**. When recrystallized from binary guest mixtures involving DIOX, **H_2** displayed high selectivity for this guest compound (89.9%, 95.3% and 70.2% when the other guest solvent was PYR, PIP and MORPH, respectively). This enhanced selectivity for DIOX was also evident in the ternary experiments where this guest was present, resulting in mixed complexes that contained 8.0%:3.7%:88.3% (PYR/PIP/DIOX), 11.1%:22.5%:66.4% (PYR/MORPH/DIOX) and 22.6%:5.0%:72.4% (MORPH/PIP/DIOX) of the respective guests. Furthermore, an analysis of the binary experiments where PYR was present revealed that inclusion of this guest was distinctly disfavoured by **H_2** (PYR/DIOX and PYR/MORPH resulted in crystals with only 10.1% and 14.7% PYR, respectively; notably, crystallization was not successful in the PYR/PIP experiment). These results are in direct contrast to similar experiments involving **H_1**. Also evident is that **H_2** is not ambiguous towards the other guests present in the solution, while **H_1** significantly preferred PYR and was quite ambivalent in its selection of the remaining guests. This was evident in the MORPH/PIP/DIOX ternary experiment, where the host displayed an enhanced preference for DIOX (72.4%), followed by a lesser preference for MORPH (22.6%) and even less so for PIP (5.0%). From the quaternary experiment, it is apparent that the host selectivity is in the order DIOX (68.0%) > MORPH (20.0%) > PYR (8.2%) > PIP (3.8%).

Subsequently, binary competition experiments in which varying guest molar ratios were employed were conducted and the host behaviour observed in these conditions.

7.2.4 Ratio-dependent competition experiments

When the host compound was dissolved in a mixture of known amounts of any two of the four solvents and crystallization allowed to occur, the mother liquor and the resulting crystals were analysed by means of ^{1}H-NMR spectroscopy. These data were used to construct the selectivity profiles provided in Figures 7.7 and 7.8. The average selectivity coefficients were calculated, and the complete data sets of these values are provided in the Supplementary Information, Tables S147–152.

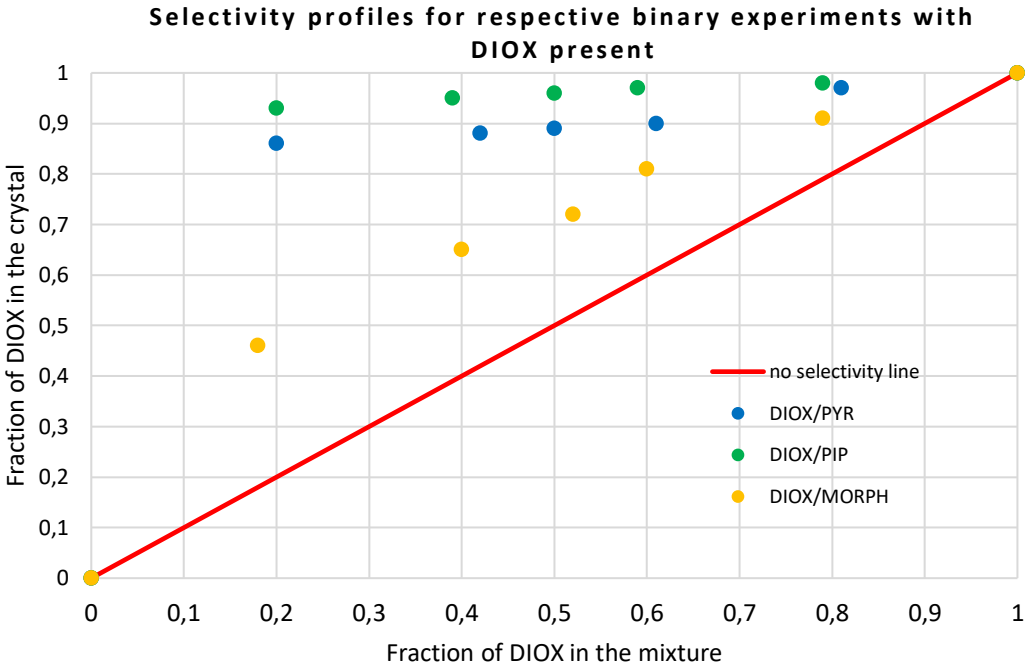

Figure 7.7. Overlaid selectivity profiles of H_2 with binary combinations where DIOX was present.

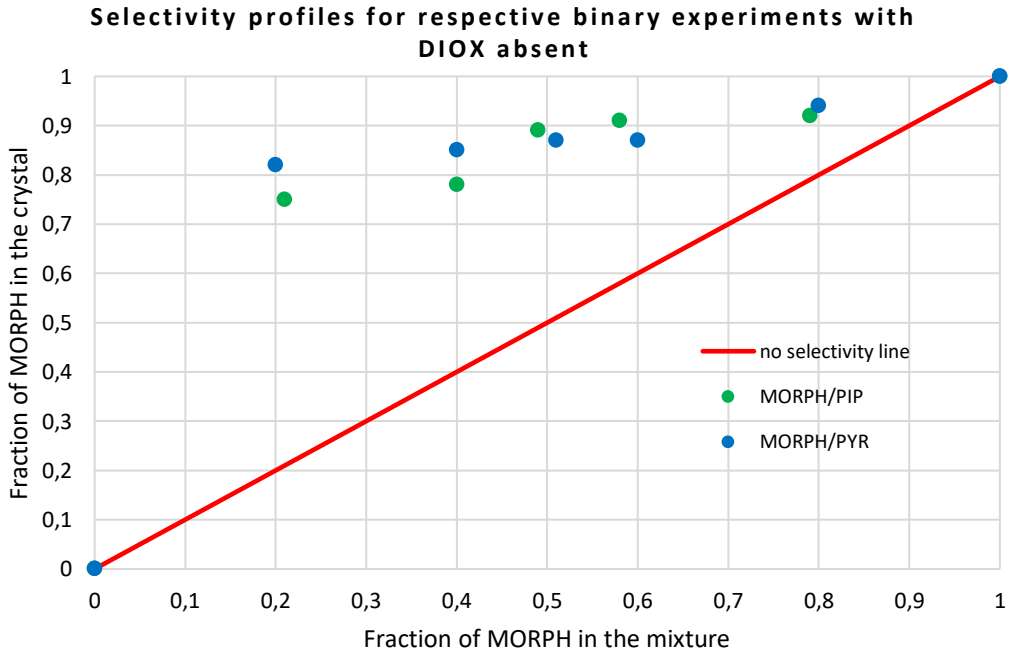

Figure 7.8. Overlaid selectivity profiles of H_2 with binary combinations where DIOX was absent.

Here, H_2 displays a significant preference for DIOX whenever it is present: in the DIOX/PYR and DIOX/PIP experiments [Figure 7.7, K = 11.2 (blue profile) and K = 28.5 (green profile), respectively], the amount of DIOX in the complexes was always much greater than that present in the solution from which the complexes had formed. Furthermore, in the

DIOX/MORPH experiment, DIOX was also consistently favoured, but the deviation from the no selectivity line was much reduced (K = 3.2). In the absence of the preferred DIOX guest, only binary guest/guest combinations that involved MORPH crystallized out, and this was in accordance with observations from the equimolar experiments (Table 7.8). MORPH was always preferred in these experiments (Figure 7.8, K = 8.3 and 7.1 for MORPH/PYR and MORPH/PIP, respectively). Also evident from these figures and computed K values is the enhanced selectivity of **H_2** compared with **H_1**.

The divergent behaviour of the two host compounds when recrystallized from these guest mixtures was unexpected, prompting a SCXRD investigation of the complexes successfully formed by **H_2** for comparative purposes with those of **H_1**.

7.2.5 SCXRD

Table 7.9 summarizes the relevant crystallographic data for the four inclusion compounds **H_2**·2(PYR), **H_2**·MORPH, **H_2**·PIP and **H_2**·DIOX. The host compound consistently crystallizes in the triclinic crystal system and *P*-1 space group, but isostructural host packing is not evident in any of these. In the **H_2**·2(PYR), **H_2**·MORPH and **H_2**·DIOX experiment, the guest molecules displayed positional disorder (which was modelled over two positions), while during the resolution of the **H_2**·PIP crystal structure, it was observed that one of the host nitrogen hydrogens is disordered over two positions. The unit cells of the respective complexes are depicted in Figure 7.9.

Table 7.9. Crystallographic data for **H₂**·2(PYR), **H₂**·MORPH, **H₂**·PIP and **H₂**·DIOX.

	H₂·2(PYR)	**H₂**·MORPH	**H₂**·PIP	**H₂**·DIOX
Chemical formula	$C_{40}H_{32}N_2O_2$ ·2(C_5H_5N)	$C_{40}H_{32}N_2O_2$ ·C_4H_9NO	$C_{40}H_{32}N_2O_2$ ·$C_5H_{11}N$	$C_{40}H_{32}N_2O_2$ ·$C_4H_8O_2$
Formula weight	730.88	659.80	657.82	660.78
Crystal system	Triclinic	Triclinic	Triclinic	Triclinic
Space group	*P*-1	*P*-1	*P*-1	*P*-1
μ (Mo Kα)/mm^{-1}	0.078	0.080	0.076	0.082
a/Å	9.3906(4)	9.5795(8)	8.5909(3)	8.2083(4)
b/Å	13.9667(7)	16.4528(12)	9.6596(3)	12.7907(6)
c/Å	15.8401(8)	22.9013(16)	22.6958(7)	17.7256(8)
alpha/°	112.772(2)	75.579(2)	88.176(2)	69.522(2)
beta/°	92.849(2)	81.758(2)	88.027(2)	87.087(2)
gamma/°	93.679(2)	88.166(2)	68.416(2)	79.972(2)
V/$Å^3$	1905.05(16)	3459(5)	1749.93(10)	1716.71(14)
Z	2	4	2	2
F(000)	772	1400	700	700
Temp./K	200	200	200	200
Restraints	0	15	6	0
Nref	8482	17227	8704	8510
Npar	513	925	462	459
R	0.0397	0.0577	0.0536	0.0452
wR2	0.1052	0.1631	0.1531	0.1216
S	1.02	1.02	1.03	1.03
θ min–max/°	1.7, 28.4	0.9, 28.4	0.9, 28.3	1.2, 28.3
Tot. data	68864	108771	47758	51503
Unique data	9492	17227	8704	8510
Observed data [I > 2.0 sigma(I)]	7634	11185	6495	6464
R_{int}	0.021	0.034	0.027	0.023
Dffrn measured fraction θ full	0.998	1.000	1.000	0.998
Min. resd. dens. (e/$Å^3$)	–0.25	–0.66	–0.39	–0.27
Max. resd. dens. (e/$Å^3$)	0.33	0.81	0.44	0.47

a)

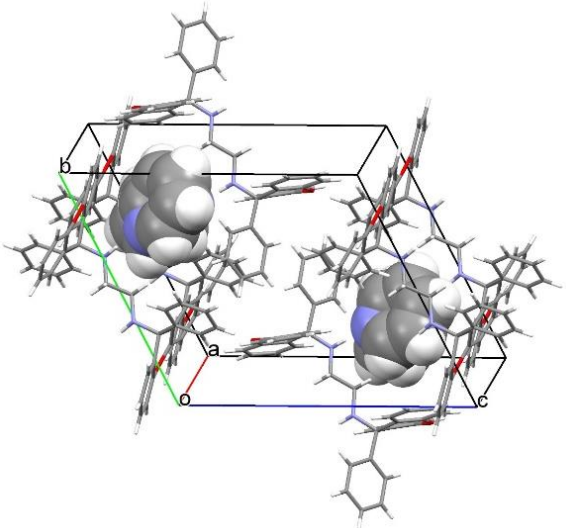

b)

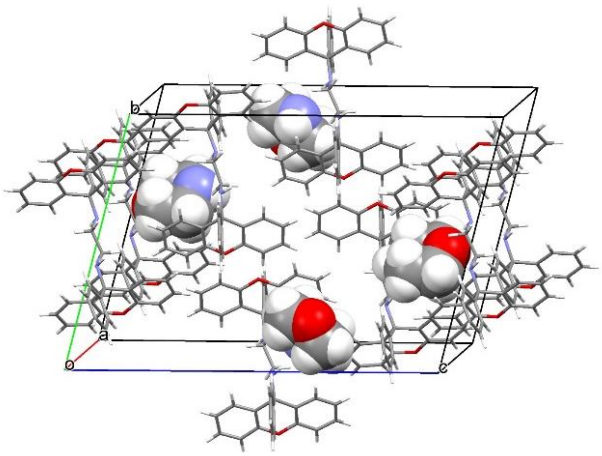

c) d)

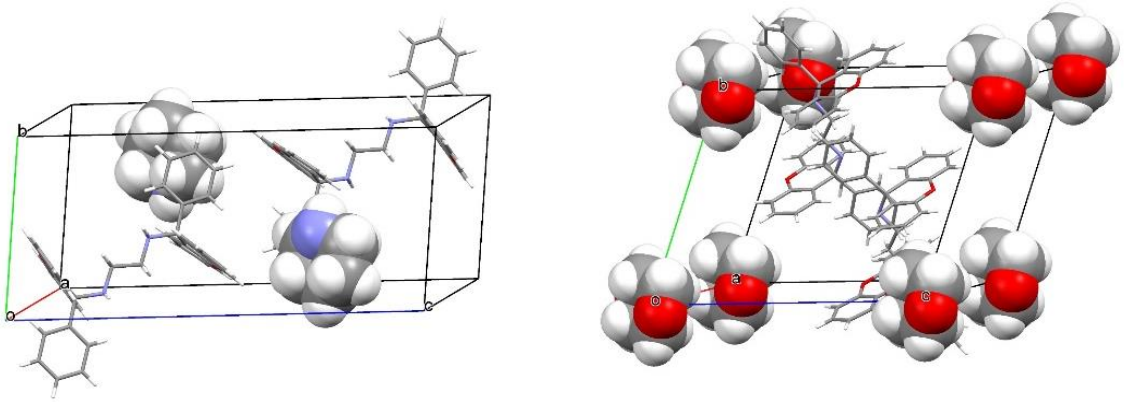

Figure 7.9. Unit cells for complexes a) **H₂**·2(PYR), b) **H₂**·MORPH, c) **H₂**·DIOX and d) **H₂**·PIP.

Additionally, the mode of guest accommodation was investigated by removing these molecules from the packing calculation and displaying the resultant voids (Figure 7.10). All the guest compounds in these complexes experience discrete cavity occupation apart from PYR, which is accommodated in multidirectional, infinite, and open channels.

a) b)

c) d)

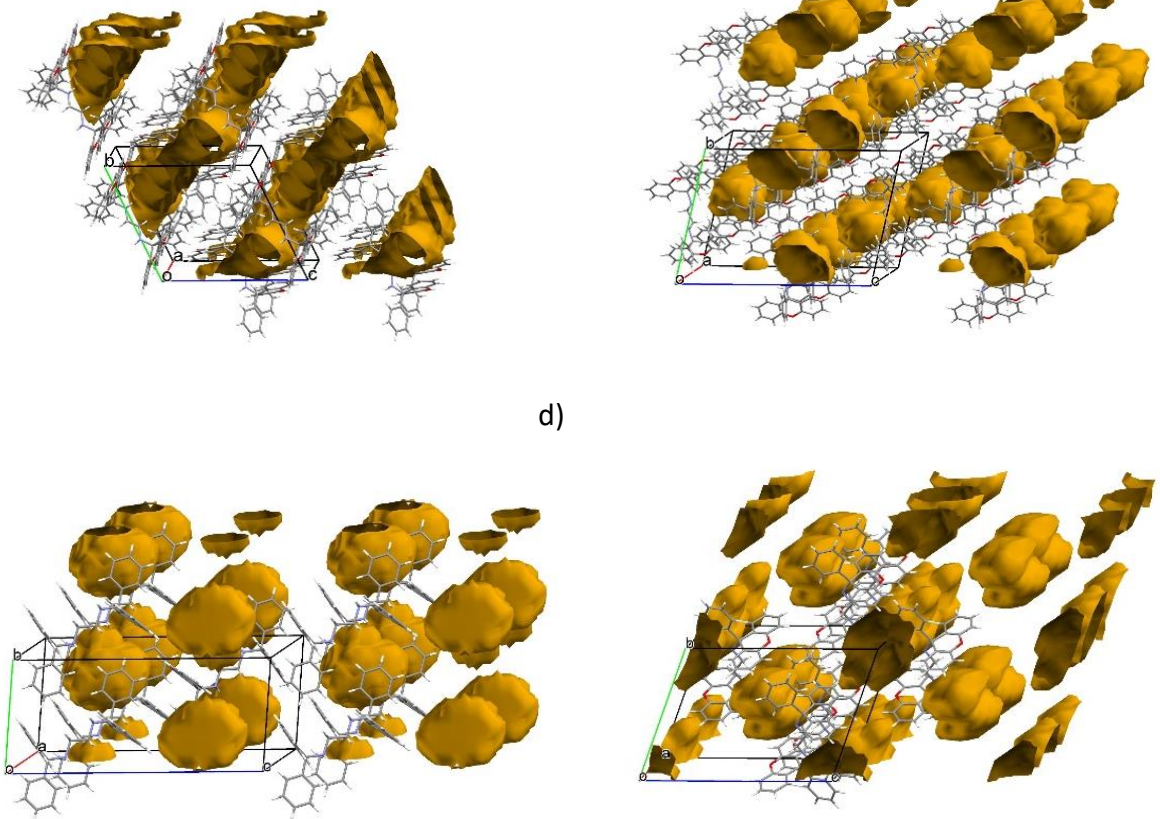

Figure 7.10. Calculated voids for complexes a) **H₂**·2(PYR), b) **H₂**·MORPH, **H₂**·DIOX and **H₂**·PIP after guest removal.

Table 7.10 contains a summary of the significant H···G interactions present in the complexes with **H_2**. As expected, **H_2**·2(PYR) was the only inclusion compound that experienced very weak H···G π···π interactions [G1 4.947(1)–5.987(1) Å and G2 4.402(1)–5.512(1) Å]. Surprisingly, DIOX was not involved in a $C_{(G)}$–$H_{(G)}$···$\pi_{(H)}$ contact, whilst the other three guests each experienced one of these interaction types, with MORPH having the shortest one (2.65 Å, 146°). Additionally, classical hydrogen bonding was present in each of these complexes. Both disordered components of PYR have $N_{(H)}$–$H_{(H)}$···$N_{(G)}$ H-bonding [2.38 Å (167°) and 2.36 Å (173°)], while component G2 of MORPH experienced two of these H-bonds (2.50–2.51 Å, 159–168°) and one $N_{(H)}$–$H_{(H)}$···$O_{(G)}$ interaction (2.50 Å, 170°). G1 was held in the host crystal by two $N_{(H)}$–$H_{(H)}$···$O_{(G)}$ and two $C_{(H)}$–$H_{(H)}$···$O_{(G)}$ contacts (2.35–2.69 Å, 129–170°). PIP, on the other hand, was only involved in one $N_{(H)}$–$H_{(H)}$···$N_{(G)}$ H-bond (2.49 Å, 166°). Lastly, each disordered component of DIOX experienced a single classical $N_{(H)}$–$H_{(H)}$···$O_{(G)}$ bond [G1 2.40 Å (171°) and G2 2.28 Å (174°)]. The G2 DIOX component was additionally involved in two non-classical $C_{(H)}$–$H_{(H)}$···$O_{(G)}$ interactions [2.55, 2.61 Å (142, 100°)]. The **H_2**·2(PYR), **H_2**·PIP and **H_2**·DIOX complexes each also experienced one other H···G short contact [2.87 Å (139°), 2.18 Å (169°) and 2.31 Å (169°), respectively], but MORPH two of these [G1 2.18, 2.30 Å (111, 141°)]. Overall, these data do not explain the extremely high selectivity of **H_2** for DIOX.

It should be noted that **H_2** experiences a significantly larger number of interactions with each guest compared with **H_1**.

Table 7.10. H···G interactions present in complexes **H₂**·2(PYR), **H₂**·MORPH, **H₂**·PIP and **H₂**·DIOX.[a,b,c]

Non-covalent interaction	**H₂**·2(PYR)	**H₂**·MORPH	**H₂**·PIP	**H₂**·DIOX	Symmetry
π···π					
H···G G1	4.947(1)–5.987(1) Å [9]				
H···G G2	4.402(1)–5.512(1) Å [7]				
C–H···π (H···Cg, C–H···Cg)					
$C_{(G2)}$–$H_{(G2)}$···$Cg_{(H)}$	2.70 Å, 124°				–x, 1–y, –z
$C_{(G1)}$–$H_{(G1)}$···$Cg_{(H)}$		2.65 Å, 146°			x, y, z
$C_{(G)}$–$H_{(G)}$···$Cg_{(H)}$			2.84 Å, 149°		x, 1+y, z
H-bonding (H···A, D–H···A)	Classical	Non-classical and classical	Classical	Non-classical and classical	
$N_{(H)}$–$H_{(H)}$···$N_{(G2)}$–$C_{(G2)}$	2.38 Å, 167° (<)				–x, 1–y, –z
$N_{(H)}$–$H_{(H)}$···$N_{(G1)}$–$C_{(G1)}$	2.36 Å, 173° (<)				x, y, z
$N_{(H)}$–$H_{(H)}$···$O_{(G1)}$–$C_{(G1)}$		2.35 Å, 167˚ (<<)			x, y, z
$N_{(H)}$–$H_{(H)}$···$N_{(G2)}$–$C_{(G2)}$		2.51 Å, 159˚ (<<)			1–x, –y,1–z
$N_{(H)}$–$H_{(H)}$···$O_{(G1)}$–$C_{(G1)}$		2.50 Å, 170˚ (<<)			–x, 1–y, 1–z
$N_{(H)}$–$H_{(H)}$···$N_{(G2)}$–$C_{(G2)}$		2.50 Å, 168˚ (<<)			x, y, z
$N_{(H)}$–$H_{(H)}$··$O_{(G2)}$–$C_{(G2)}$		2.50 Å, 170˚ (<<)			x, y, z
$C_{(H)}$–$H_{(H)}$···$O_{(G1)}$ –$C_{(G1)}$		2.58 Å, 150˚ (<)			–x, 1–y, 1–z
$C_{(H)}$–$H_{(H)}$···$O_{(G1)}$–$C_{(G1)}$		2.69 Å, 129˚ (<)			1–x, 1–y, –z
$N_{(H)}$–$H_{(H)}$···$N_{(G)}$–$C_{(G)}$			2.49 Å, 166˚ (<<)		–1+x, y, z
$N_{(H)}$–$H_{(H)}$···$O_{(G2)}$–$C_{(G2)}$				2.28 Å, 174˚ (<<)	x, y, z
$N_{(H)}$–$H_{(H)}$···$O_{(G1)}$–$C_{(G1)}$				2.40 Å, 171˚ (<<)	x, y, z
$C_{(H)}$–$H_{(H)}$···$O_{(G2)}$–$C_{(G2)}$				2.55 Å, 142˚ (<)	x, y, z
$C_{(H)}$–$H_{(H)}$···$O_{(G2)}$–$C_{(G2)}$				2.61 Å, 100˚ (<)	1–x, –y, 2–z
Other short contacts (X···Z, X–Y···Z)					
$C_{(H)}$–$H_{(H)}$···$C_{(G2)}$–$C_{(G2)}$	2.87 Å, 139° (<)				1+x, –1+y, z
$C_{(H)}$–$H_{(H)}$ ···$H_{(G1)}$–$C_{(G1)}$		2.18 Å, 111˚(<)			x, y, z
$C_{(H)}$–$H_{(H)}$ ···$H_{(G1)}$–$N_{(G1)}$		2.30 Å, 141˚(<)			2–x, 1–y, 1–z
$C_{(H)}$–$H_{(H)}$···$H_{(G)}$–$N_{(G)}$			2.18 Å, 169° (<)		x, y, z
$C_{(H)}$–$H_{(H)}$···$H_{(G1)}$–$C_{(G1)}$				2.31 Å, 169° (<)	x, y, z

[a]A summary of the H···H interactions can be found in the Supplementary Information (Table S152).
[b]Guest 1 (G1) and guest 2 (G2) represent the disordered guest components in the host crystal.
[c]Distances denoted by < are contacts that measure less than the sum of the van der Waals radii of the atoms involved.

7.2.6 Hirshfeld surface analyses

The multiple intermolecular H···G interactions that are present in these complexes were visualized and quantified by carrying out Hirshfeld surface analyses on each guest. The 2D fingerprint plots are provided in the Supplementary Information (Figure S153), while a summary of the percentage of each interaction type is displayed graphically in Figures 7.11 and 7.12.

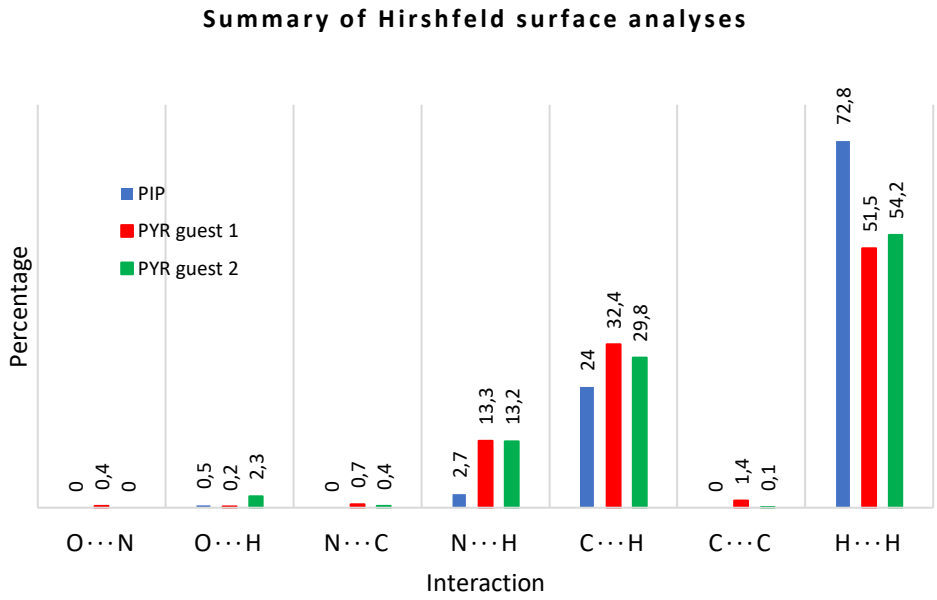

Figure 7.11. Quantitative interactions after Hirshfeld surface analyses of H_2 with PIP and PYR.

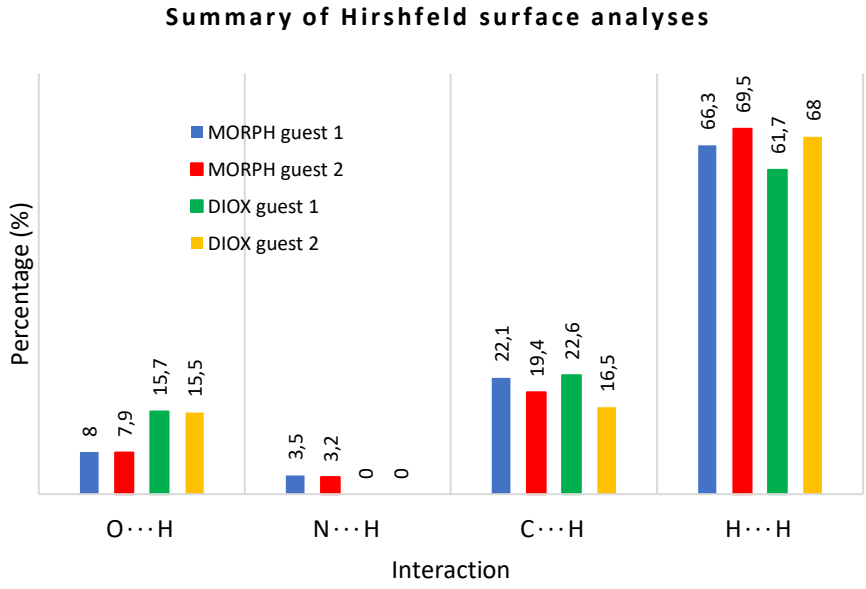

Figure 7.12. Quantitative interactions after Hirshfeld surface analyses of H_2 with MORPH and DIOX.

As expected, the saturated guests (PIP, MORPH and DIOX) experienced a greater percentage of H···H interactions compared with PYR. The only significant finding here was that DIOX, the preferred guest, experienced the largest percentage of O···H interactions (15.5 and 15.7% for the two components), but this is possibly as a result of the two oxygen atoms present in the guest.

7.2.7 Thermal analyses (DSC and TG)

As is the norm, thermal analyses were carried out on each of the four complexes with **H_2**. Figure 7.13a–c is the overlaid DSC, TG and DTG traces, respectively, so-obtained. Table 7.11 summarizes the relevant thermal data from these traces, and the high selectivity of **H_2** for DIOX is clearly evident here. This guest compound forms a significantly more stable complex with the host compound as is observed by the increased onset temperature at which it is released (T_{on} 79.7 °C, Table 7.11) relative to the other guest solvents (PYR and PIP were released at much lower temperatures, T_{on} 34.6 and 25.2 °C, respectively). Furthermore, **H_2**·MORPH experienced mass loss from the outset of the experiment and this complex therefore possesses low thermal stability and an accurate onset temperature could not be reported. (Notably, the case was similar for the **H_1**·MORPH complex.)

In all cases, the guest solvent was released in a stepwise manner, and T_p values for the highly preferred guest compound (DIOX) are expectedly higher than those for the guest solvents less preferred, further alluding to the stability of **H_2**·DIOX. (Figure 7.13a, 118.9 and 169.0 °C).

For the **H_2**·2(PYR) complex, there is a discrepancy between the expected mass loss (21.7%) and the measured mass loss (18.1%): this observation cannot be explained at this time. Furthermore, the mass loss experienced by **H_2**·PIP is greater than expected (18.0% versus 12.9%) possibly owing to the presence of water (mass loss is observed at approximately 100 °C). Due to the instability of the **H_2**·MORPH complex, accurate mass loss measurements could not be made in this case, but results from the **H_2**·DIOX experiment were as expected (mass loss calculated, 13.3%, measured 12.9%).

a)

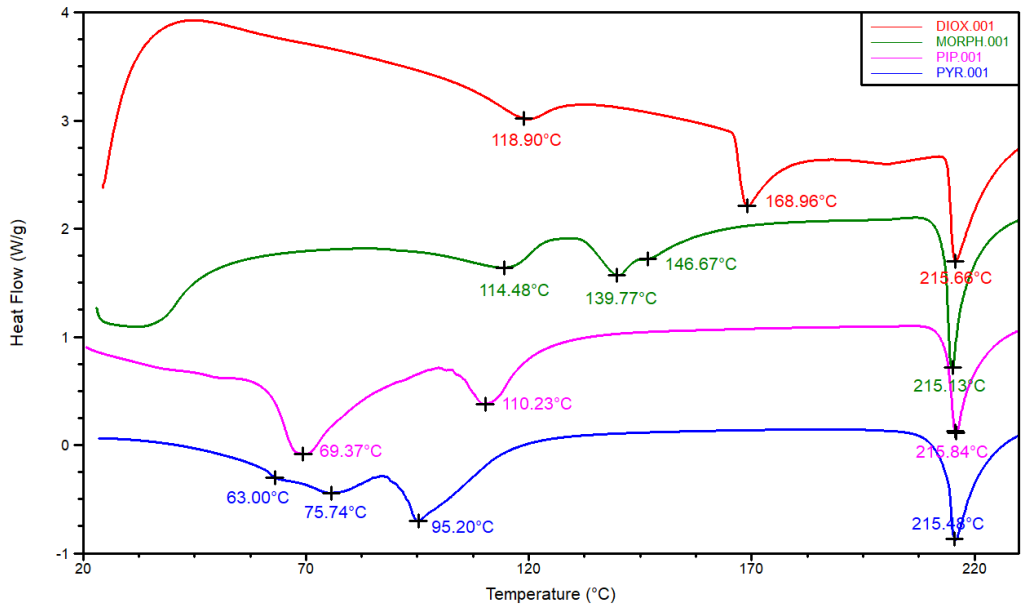
DIOX.001
MORPH.001
PIP.001
PYR.001
118.90°C
168.96°C
114.48°C
139.77°C
146.67°C
215.66°C
215.13°C
110.23°C
69.37°C
215.84°C
63.00°C
75.74°C
95.20°C
215.48°C
Heat Flow (W/g)
Temperature (°C)

b)

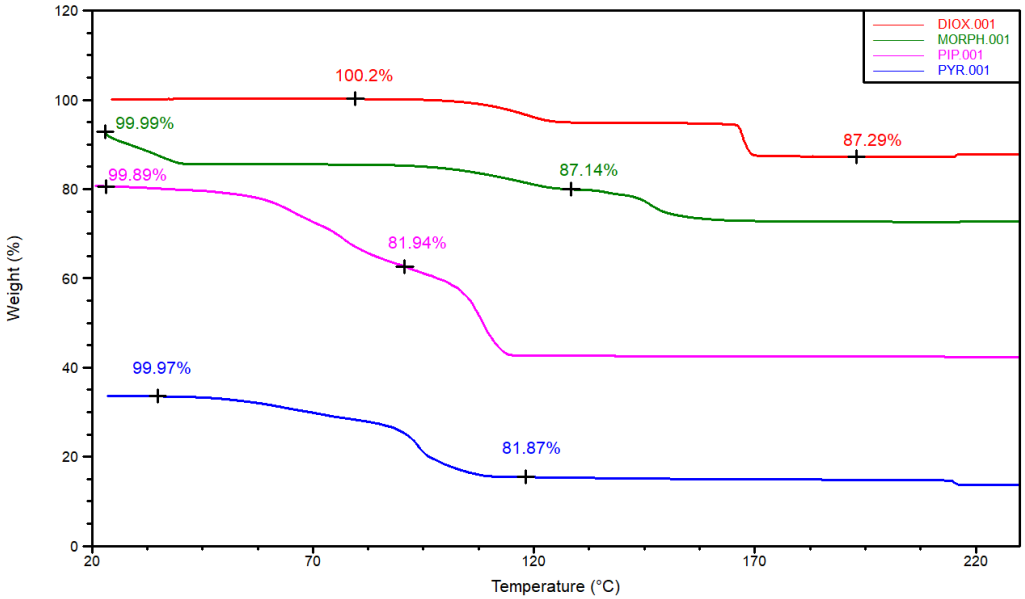
DIOX.001
MORPH.001
PIP.001
PYR.001
100.2%
99.99%
87.29%
87.14%
99.89%
81.94%
99.97%
81.87%
Weight (%)
Temperature (°C)

c)

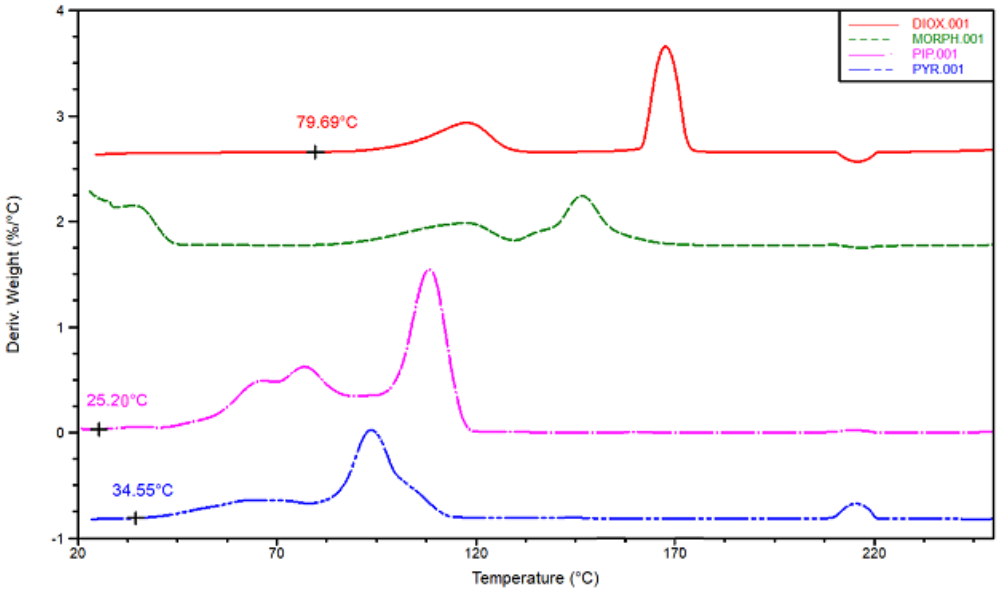

Figure 7.13. Overlaid traces for a) DSC and b) TG and c) DTG traces for the **H₂**·2(PYR) (blue), **H₂**·MORPH (green), **H₂**·DIOX (red) and **H₂**·PIP (fuchsia) complexes.

Table 7.11. Thermal data for complexes **H₂**·2(PYR), **H₂**·MORPH, **H₂**·PIP and **H₂**·DIOX.

Guest (G)	T_{on} /°C	T_p /°C	Mass loss expected /%	Actual mass loss /%
PYR	34.6	63.0,75.7, 95.2	21.7	18.1
MORPH	[a]	114.5, 139.7, 146.7	13.2	[a]
PIP	25.2	69.4, 110.2	12.9	18.0[b]
DIOX	79.7	118.9, 169.0	13.3	12.9

[a]Could not be accurately determined since the complex experienced mass loss from the outset of the experiment.
[b]The mass loss was greater than expected which may be due to the presence of water.

7.2.8 Conclusions

H₂ was recrystallized from DIOX, MORPH, PIP and PYR independently, and successfully included each one consistently with a 1:1 H:G ratio, except for PYR (1:2). Recrystallization of this host from various equimolar mixtures revealed the host to display preference in favour of DIOX in all cases where this guest was present. Overall, the selectivity order was found to be DIOX > MORPH > PYR > PIP. Binary G:G ratios were also varied, but the host remained consistently selective for DIOX, even at low concentrations of this guest. When these experiments were carried out between PIP and PYR (the least preferred guests), the inclusion compound did not crystallize out. SCXRD experiments revealed that the four inclusion

compounds of **H_2** crystallized in the triclinic *P*-1 crystal system but the host packing was not isostructural. Furthermore, the PYR, MORPH and DIOX molecules were disordered but this was satisfactorily modelled over two positions. Analysis of the H···G interactions obtained from SCXRD experiments could not be used to explain the observed host selectivity order. Finally, thermal analyses revealed the preferred guest complex (containing DIOX) to have an enhanced thermal stability relative to the other inclusion complexes based on T_{on} and T_p values.

7.2.9 Supporting information

Related NMR spectra, duplicate data, associated % e.s.d.s and thermal traces for the four inclusion compounds are provided in the Supplementary Information. The crystal structures were deposited at the Cambridge Crystallographic Data Centre, and CCDC 1587302 [**H_2**·2(PYR)], 1587304 (**H_2**·MORPH), 1587305 (**H_2**·PIP) and 1587303 (**H_2**·DIOX) contain the supplementary crystallographic data for this section.

7.3 Molecular modelling

7.3.1 Introduction

Previous chapters report on the host behaviour of **H_1** and **H_2** when exposed to isomeric guests. It was established that, in the presence of guests related in this way, **H_2** displayed enhanced selectivities compared with **H_1**, but the selectivity order for both hosts concurred. However, in this current chapter where the guests are not isomers, the two hosts displayed completely opposing selectivity behaviour. This prompted an in-depth study of the crystal structures of the two apohosts, together with a computational analysis of the geometries of both hosts alone and in the presence of guest species.

Pyramidal nitrogen atoms are usually easily displaced (labile) due to their low inversion barriers, and this inversion can lead to amino stereocentres. However, inversion may be restricted in certain circumstances,[268] leading to arrested inversion. With one exception, the configurations of the N atoms in the crystal structures of **H_1** and **H_2** (in the absence and presence of guests) were found to be well-defined which is indicative of arrested inversion of the amino centres, because the amino hydrogens could be located with confidence in

difference electron density maps. Only one case involved a disordered host amino hydrogen atom (as a result of the inversion of the N atom in the ethylenediamine linker), but the site occupancies of the two components could be refined and resulted in two disordered positions.

Based on the relative configurations of pairs of amino stereocentres in a molecule, *syn* or *anti* diastereomers may arise. This leads to energy differences for the respective conformations, which was the case for **H_1** and **H_2**. The amino stereocentres of the hosts were defined in terms of the Cahn-Ingold-Prelog sequence rule. The configuration of each stereocentre was designated as *R*/*S*, with *syn* describing groups that exist on the same face (*R,R* or *S,S*) and *anti* those on opposite faces (*R,S*) of the molecule. The priority of these moieties in the host structures was assigned in the order tricyclic unit > ethylenediamine chain > hydrogen atom > lone pair (for the N atom in the ethylenediamine unit). The arrangement of the moieties around the stereocentres was investigated in both the apohost as well as the hosts in their respective complexes.

This study has required a detailed comparison of the host compounds in their various crystal structures, as well as a computational investigation at the molecular mechanics and DFT levels in which their conformational distributions and associated energies were determined. The DFT methodology included application of the semi-empirical range-separated hybrid *ω*B97X-D and *ω*B97X-V density functionals that capture both short and long range exchange and correlation interactions. A rigorous assessment[269] against fifteen existing density functionals with respect to main group thermochemistry and non-covalent interactions revealed that *ω*B97X-V was the best functional tested for non-bonded interactions by a significant margin, and which also offers very good performance for thermochemistry.

7.3.2 Structures of compounds **H_1** and **H_2** in their apohost crystal structures

In the absence of guest compounds, hosts **H_1** and **H_2** have common features in their crystal structures, but there are nevertheless some key differences. Table 7.12 summarizes the relevant crystallographic data for the two apohost compounds. Both crystallize in the triclinic (*P*-1) crystal system and appear isostructural owing to their very similar unit cell dimensions. These data were deposited at the Cambridge Crystallographic Data Centre [CCDC reference numbers 1540116 (**H_1**) and 1587301 (**H_2**)].

Table 7.12. SCXRD data for apohosts **H_1** and **H_2**.

	H_1	**H_2**
Chemical formula	$C_{40}H_{32}N_2S_2$	$C_{40}H_{32}N_2O_2$
Formula weight	604.79	572.67
Crystal system	Triclinic	Triclinic
Space group	*P*-1	*P*-1
μ (Mo Kα)/mm^{-1}	0.205	0.077
a/Å	9.0912(5)	9.0854(4)
b/Å	12.3688(7)	12.2325(5)
c/Å	14.9416(8)	14.9806(6)
alpha/°	77.362(2)	76.534(2)
beta/°	82.375(2)	79.787((2)
gamma/°	70.793(2)	69.738(2)
V/$Å^3$	1544.81(15)	1510.39(11)
Z	2	2
F(000)	636	604
Temp./K	200	200
Restraints	0	0
Nref	7386	7504
Npar	405	405
R	0.0391	0.0442
wR2	0.1043	0.1064
S	1.03	1.03
θ min−max/°	1.8, 27.9	1.8, 28.4
Tot. data	39535	39884
Unique data	7386	7504
Observed data [I > 2.0 sigma(I)]	6497	5175
R_{int}	0.017	0.032
Dffrn measured fraction θ full	0.999	0.999
Min. resd. dens. (e/$Å^3$)	−0.78	−0.19
Max. resd. dens. (e/$Å^3$)	0.50	0.24

In order to confirm the isostructural nature of the crystal packing in these two compounds, the host molecules were overlaid using Mercury, and the result is shown in Figure 7.14a, together with a stereoview of the two overlaid host structures (Figure 7.14b). Furthermore, PXRD traces were computed for the two solids (Figure 7.15).

a) b)

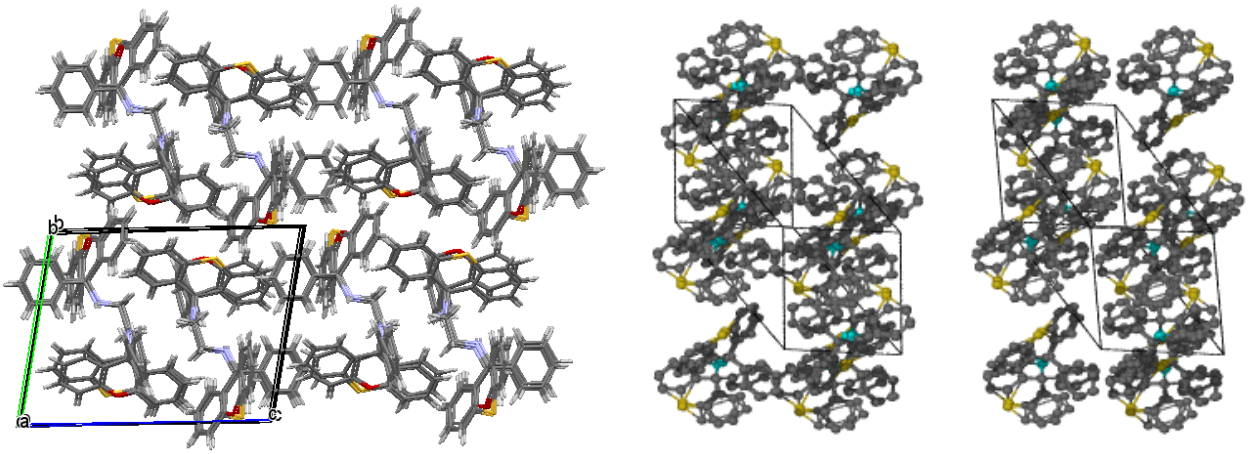

Figure 7.14. Overlaid a) extended crystal structures (O–red, S–yellow) and b) stereoviews for **H_1** and **H_2** (O and S–yellow).

a)

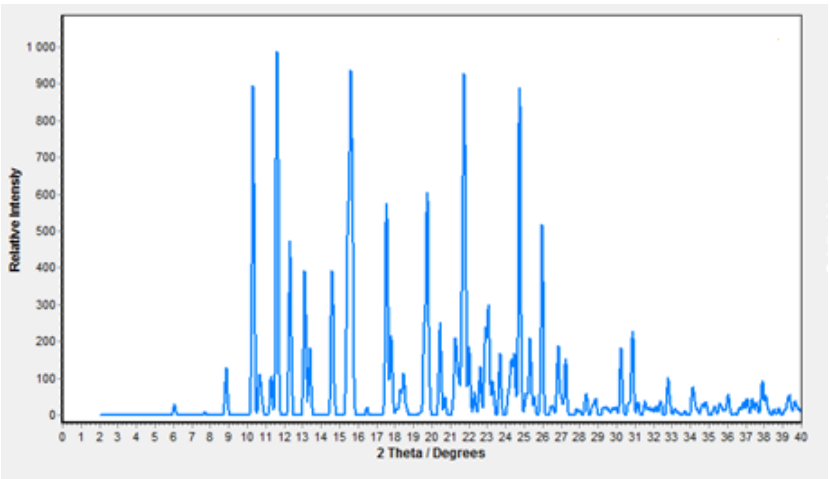

b)

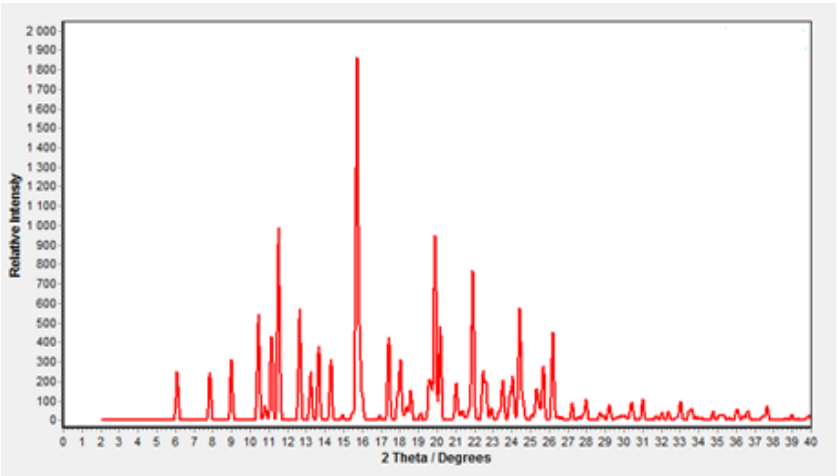

Figure 7.15. Computed PXRD patterns for a) **H_1** and b) **H_2**.

From Figure 7.14a and b, the host atoms appear to occupy similar positions when crystallized. However, the diffraction traces appear to be different (Figure 7.15).

PXRD traces of specific compounds are characterized by the angular position (2θ values) and intensity of the peaks. The angular position is determined by the six unit cell dimensions of the molecule, which means that every atom in the crystal contributes to the profile of the traces based on its positional coordinates (x, y, z). Moreover, the intensity of the peaks relies on the location of the atoms in space as well as its X-ray scattering power. For **H_1** and **H_2**, the unit cell parameters are practically the same (with differences ranging from < 0.1% to 3.2%) and the 2θ values correspond reasonably regarding the position of the peaks. However, the relative intensities of these peaks are in very poor correlation, which is expected since the S atoms in **H_1** are replaced by O atoms in **H_2**, and sulfur has a scattering power approximately twice that of oxygen at low angles.

The replacement of S atoms by O atoms also results in geometrical changes in the molecule. The S–C bond lengths are significantly greater than O–C (due to the different atomic radii of S and O), resulting in the S and O atoms having dissimilar coordinates. This induces distortion of the tricyclic system within **H_1** and this contributes to the different peak intensities in the traces in Figure 7.15. Additionally, there exists slight deviations (a few degrees) of the aromatic moieties of the hosts, which also contributes to the coordination differences of the corresponding S and O atoms. To illustrate the effect of the atom replacement, the S and O atoms were removed from the calculations and this resulted in the PXRD traces in Figure 7.16.

a)

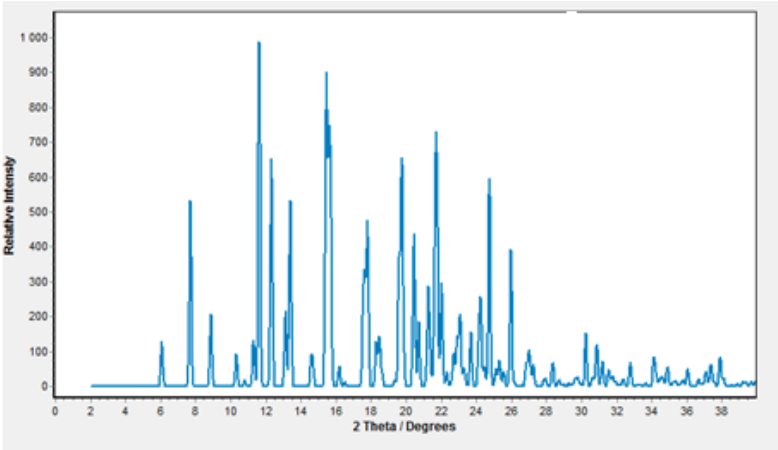

b)

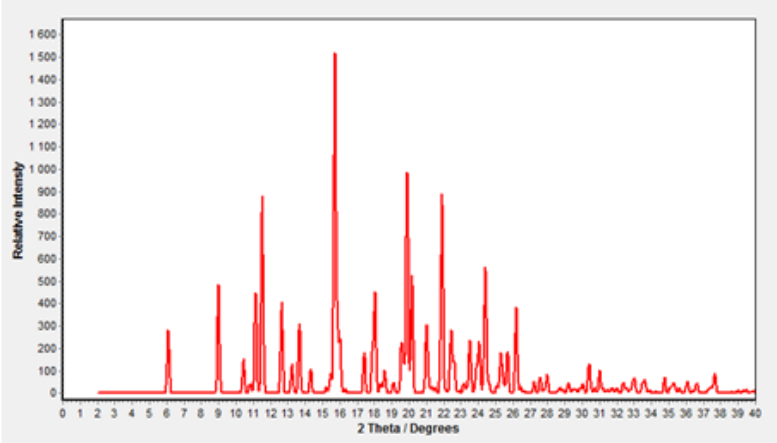

Figure 7.16. Computed PXRD patterns for modified a) **H_1** and b) **H_2** after omitting atoms O and S from the computation.

The powder patterns now appear to be more similar, but significant intensity differences are still evident. This is attributed to the different coordinates of the C and N atoms of the ethylenediamine chain as a direct result of the geometrical changes caused by replacing the S with the O atoms. Therefore, **H_1** and **H_2** can be loosely/quantitatively identified as isostructural compounds.

Selected structural parameters and relative ωB97X-V/6-311+G(2DF,2P) single point energies were calculated on ωB97X-D/6-31G* optimized geometries for the apohosts **H_1** and **H_2** and in their various crystal structures. These data are provided in the Supplementary Information, Table S155.

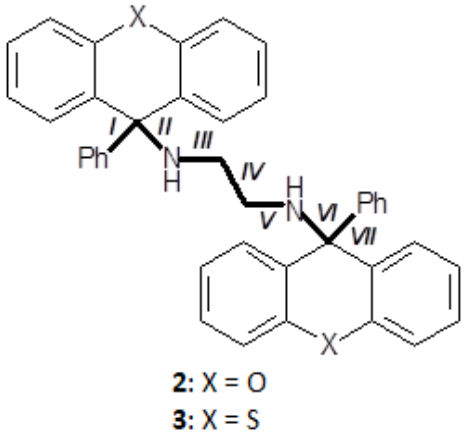

Scheme 7.2. Labels assigned to bonds and angles.

Many geometric similarities were found in the $\mathbf{H_1}$ and $\mathbf{H_2}$ host molecules. Both apohosts crystallize as *anti* diastereomers and the Ph–C–N(*R*)–C–C–N(*S*)–C–Ph chains are found to adopt similar conformations. From the *R* amino stereocentre's end, the torsion angles *II* – *VI* (Scheme 7.2) crystallize with the following stereochemical arrangements: *-ap*, *-ap*, *sc*, *ap* and *ap*, respectively (where *ap* is antiperiplanar and *sc* is synclinal).[270] When overlaid (Figure 7.17), the two hosts align almost perfectly and Figure 7.18 is the unit cells which shows in both cases how one molecule is rotated with respect to the other along its alignment axis. As a result, one xanthenyl unit positions itself in the fold of the neighbouring host's xanthenyl system (which also accommodates this interaction by folding of the xanthenyl system).

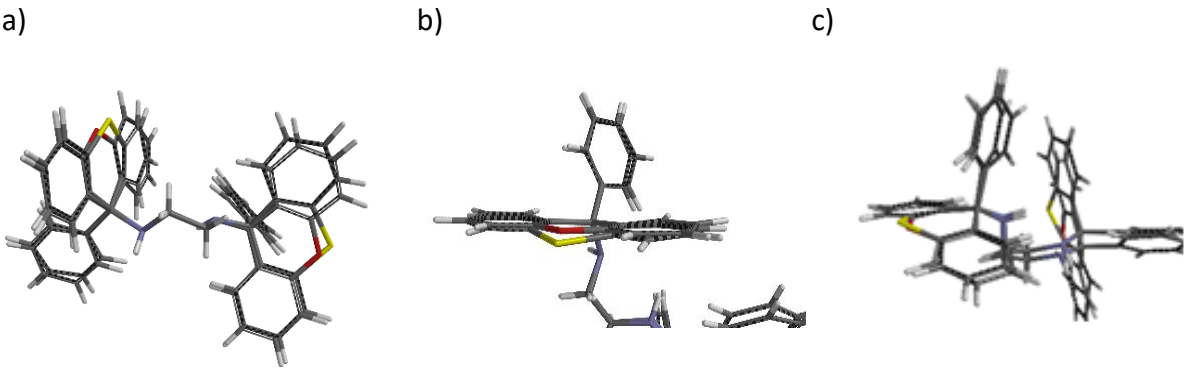

Figure 7.17. Views of overlaid crystal structures of a) apohost $\mathbf{H_1}$ and $\mathbf{H_2}$, with b) and c) as alternative views of the correspondence between the respective tricyclic termini.

a) b)

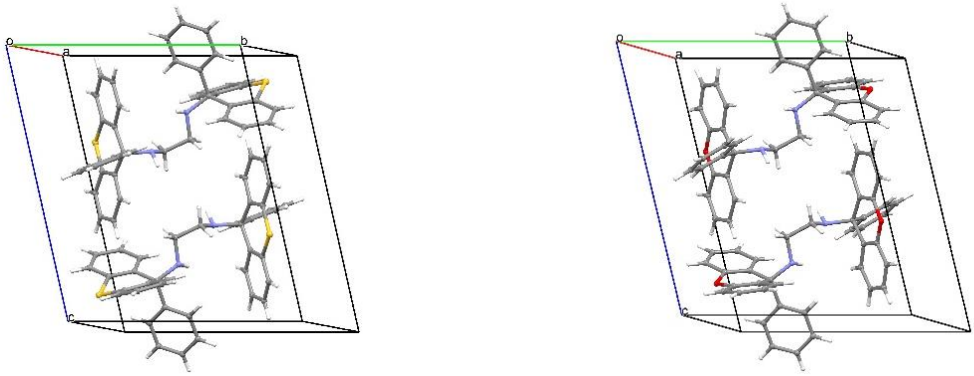

Figure 7.18. Unit cells of a) $\mathbf{H_1}$ and b) $\mathbf{H_2}$.

However, subtle structural differences are observed between apohosts $\mathbf{H_1}$ and $\mathbf{H_2}$. The S–C bonds are ~0.4 Å longer than the O–C bonds, and this affects the geometry of the tricyclic ring. Additionally, the C–Ŝ–C bond angles deviate from planarity by 15−16° more than C–Ô–C and this results in the distortion of the reasonably regular hexagonal geometry of the central ring of the xanthene moiety. This, in turn, causes the characteristic buckling about the central ring in the thioxanthene system and results in a boat-like structure.

For both $\mathbf{H_1}$ and $\mathbf{H_2}$, the tricyclic units attached to the respective *R* amino stereocentres are more planar (folded by 10° and 3°, respectively) while greater buckling is observed in the units adjacent to the *S* stereocentres (33° and 19°, respectively). [The angle is defined as the angular deviation from planarity for the two planes involving the central ring of the xanthone and thioxanthone system]. In the thioxanthone derivative, the phenyl groups adopt pseudo axial orientations where they are slanted perpendicularly with respect to the plane of the tricyclic system, while the amino groups are pseudo equatorial and nearly eclipsing the *peri* C–H bonds. The ring plane of the pseudo axial phenyl group is twisted further from alignment with the C(9)–N bond than at the other terminus of the molecule or as observed in $\mathbf{H_2}$. Notably, in the less folded second thioxanthenyl unit of apohost $\mathbf{H_1}$, the amino group is inclined pseudo axially and the phenyl pseudo equatorially.

7.3.3. Structures of compounds **H₁** and **H₂** in their host-guest complexes

Many differences were observed in the conformations of the complexes of **H₁** and **H₂** and these have been summarized in Table S155 in the Supplementary Information.

Host **H₂** maintains the *anti* configuration in its complexes and, with two exceptions, crystallizes with all antiperiplanar arrangements for the torsion angles of its ethylenediamine linker, with planar or only weakly bent xanthenyl units. The exceptions occur in the PYR and PIP complexes with **H₂**. In the former case, two conformations of the host molecule are observed in the unit cell. The first conformer is significantly more bent in its xanthenyl units, where the C(9) amino groups are pseudo equatorially orientated. In the second, torsion angles *II* and *VI* are synclinal and both xanthenyl systems significantly bent with their amino groups now in pseudo axial situations. The latter conformer has the higher calculated energy. Since in the PIP complex, the hydrogen atom of one of the amino groups was found to be disordered over two positions with 69%:31% *syn*:*anti* weightings, both configurations were considered for the host molecule. The *anti* configuration conformer of the PIP complex has a significantly higher energy than its *syn* analogue, which was attributed to a closer contact between the disordered amino hydrogen atom and an *ortho* hydrogen on the adjoining C(9) phenyl group in the former (1.98 Å) compared to a larger separation for the latter (2.49 Å).

Host **H₁** adopts the *syn* configuration in the four complexes investigated, three of whose amino configurations are *R*,*R* and the fourth, *S*,*S*. The conformations adopted by **H₁** in the complexes are otherwise very similar. For all the complexes with **H₁**, both thioxanthenyl units are strongly folded in the complexes and the planes of both C(9) phenyl groups twisted out of alignment with the C(9)–N bonds. Interestingly, this contrasted with the configuration of the apohost which crystallizes as *anti*.

There are significant differences in the relative energies of **H₁** and **H₂** in their various complexes when compared at the MMFF94, B3LYP/6-31G* and ωB97X-V/6-311+G(2df,2p) levels, the latter being single point energies based on ωB97D-V/6-31G* geometries. The ranges of conformational energies obtained at the DFT levels are found to be significantly larger for host **H₂** compared to **H₁**.

7.3.4 Conformational features of components of **H_1** and **H_2**

The conformational analyses involved molecular mechanics calculations (with refinement at the DFT level) of the xanthene and thioxanthene building blocks, together with the systematic determination of the effect of introducing the other moieties (phenyl and amino) to the C(9) atom. Selected geometrical features for the optimized structures of the xanthene and thioxanthene series are highlighted in Table S156 and Figure S157 in the Supplementary Information, but the key differences are discussed here.

Calculations show xanthene to be planar with its central ring adopting an irregular hexagon shape. This central ring is narrowed at the C–O–C apex as a result of shorter C–O bonds compared with C–CH_2. The C–S bonds of thioxanthene are longer than the C–CH_2 bonds, resulting in a hexagon that is widened at the C–S–C apex. Furthermore, the C–$\hat{S}$–C bond angles are 20° more acute than C–$\hat{O}$–C, and result in a central ring that is more bent along the S---CH_2 axis and adopts a boat shape. This conformation resulted in one of the methylene hydrogens rotating towards the centre of the ring in a pseudo axial orientation while the other is pseudo equatorial and nearly eclipsing the *peri* C–H bonds. Greater congestion around the outer face of the C(9) atom is also observed in thioxanthene compared to xanthene, with the separation between the *peri* hydrogen atoms in thioxanthene being almost 0.7 Å smaller than in xanthene.

Introduction of a 9-phenyl group to C(9) results in some bending of the xanthenyl framework and displacement of the phenyl bond towards the pseudo axial location, giving a O···C(9)–Ph angle of 115°. Similar effects occur with the addition of 9-amino and 9-methylamino groups although the amino group is even closer to a true pseudo axial position. In contrast, when both 9-phenyl and 9-amino or 9-methylamino groups are considered in the calculations, comparatively little distortion of the planar xanthenyl moiety is observed in the lowest energy conformers. However, in both instances, second higher energy conformers are detected where the xanthenyl systems are slightly more bent and with the amino substituents conforming to a more pseudo axial position.

For thioxanthene, addition of a 9-phenyl substituent substantially reduces the ring bending angle, resulting in a more distinctly pseudo axial orientation of the substituent [the S···C(9)–

Ph angle being more acute than the oxygen analogue, 107°]. After consideration of a 9-amino group, it was found to marginally prefer the pseudo equatorial orientation rather than pseudo axial, but the energy difference between the conformers was calculated to be only 0.03 kJ·mol^{-1}. The energy difference between the lowest adjacent conformers after the addition of 9-methylamino is 4.39 kJ·mol^{-1} and the substituent adopts the pseudo axial orientation. For the higher energy conformer, the substituent is pseudo equatorial. In contrast to the xanthenyl system, there are striking differences between 9-amino-9-phenylthioxanthene and its 9-methylamino-9-phenyl analogue. In the former case, the two lowest energy conformers both contain strongly bent thioxanthenyl moieties with the amino group orientated pseudo equatorially in the lower energy conformer and pseudo axially in the other. In the 9-methylamino-9-phenyl derivative, the lowest energy conformer contains a pseudo axial amino group. Then follow two conformers of equal energy, the first of which is similar to the lowest energy conformer except that the amino group is now pseudo equatorial. In the second, the thioxanthenyl system is substantially flattened and the amino group is only marginally pseudo axial.

7.3.5 Conformations of compound **H$_2$**

Calculations for **H$_2$** were carried out up to a relative energy limit of 100 kJ·mol^{-1}. A large set of enantiomers and other symmetrically related isomeric conformers were determined, and these data were simplified by excluding conformers with similar energies. For the sake of brevity, the relative energies, configurations of the N atoms (ethylenediamine chain), torsion angles in the ethylenediamine linker, the degree of bending in the xanthenyl moieties, and the orientations of the 9-amino and 9-phenyl groups are summarized in Table S158 in the Supplementary Information. The key characteristics are discussed here.

The set of lowest energy conformers ranged between E_{rel} 0–7.75 kJ·mol^{-1}. The two lowest energy conformers are characterized by ethylenediamine chains where the torsion angles are antiperiplanar, except for the synclinal central bond (*IV)*, while one of the adjoining bonds (*III* or *V*) is anticlinal. The two subsequent higher energy conformers have all bonds antiperiplanar except for the *IV* bond. Lastly, conformers displaying all antiperiplanar torsion angles have calculated energies that ranged between 9.11 and 11.48 kJ·mol^{-1}. In all the above-mentioned conformers, the xanthenyl units are near planar.

The highest energy conformers have synclinal *II* and *VI* bonds, together with significantly bent xanthenyl moieties and, consequently, have pseudo axial 9-amino and pseudo equatorial 9-phenyl groups. Conformers with synperiplanar *IV* bonds were calculated, with the first occurring at E_{rel} 25.06 kJ·mol^{-1}.

The structural features of **H_2** in the respective complexes were also considered for comparison (Supplementary Information, Table S158 and Figure S159). All these conformers have relatively high energies. When the geometries of the host crystal structures were optimized without constraints at the molecular mechanics level, the apohost relaxed to the lowest energy conformer that was calculated in the conformational search; six others settled into the all periplanar conformer, and another reorganized similarly except with a slightly higher energy (all have generally planar xanthenyl moieties). In the case of the PYR complex, the host structure settled into a significantly higher energy conformer (E_{rel} 42.97 kJ·mol^{-1}) with bonds *II* and *VI* remaining synclinal and the xanthenyl rings bent. The *anti* configuration of the PIP complex was now found to be about 2.4 kJ·mol^{-1} lower in energy than its *syn* analogue.

The molecular mechanics structures were then refined at the DFT level (these data are provided in the Supplementary Information, Table S160), resulting in a more varied array of torsion angles in the ethylenediamine linkage and a greater tendency for bending in the xanthenyl units among the lower energy conformers. The lowest energy conformer contains a synclinal central bond (*IV)* while the remainder of its bonds are antiperiplanar, and both xanthenyl ring systems are only marginally bent. These are followed by conformers containing up to three synclinal or anticlinal bonds as well as combinations of these orientations. In most cases, one or both xanthenyl units are significantly bent. The orientations of the C(9) amino and phenyl groups as a function of the extent of folding in the xanthenyl ring systems are displayed graphically in Figure 7.19. It is apparent that where the xanthenyl systems are bent, the preferred orientations of the C(9) amino and phenyl substituents are respectively pseudo axial and pseudo equatorial, although there are several exceptions. Interestingly, pseudo equatorial amino groups were never found to occur simultaneously on both xanthenyl groups.

a)

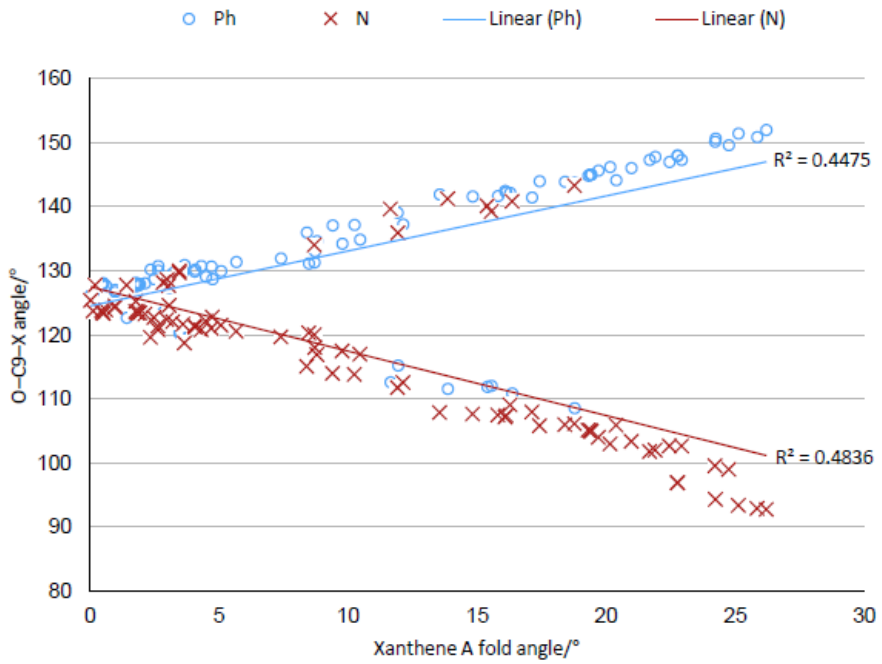

b)

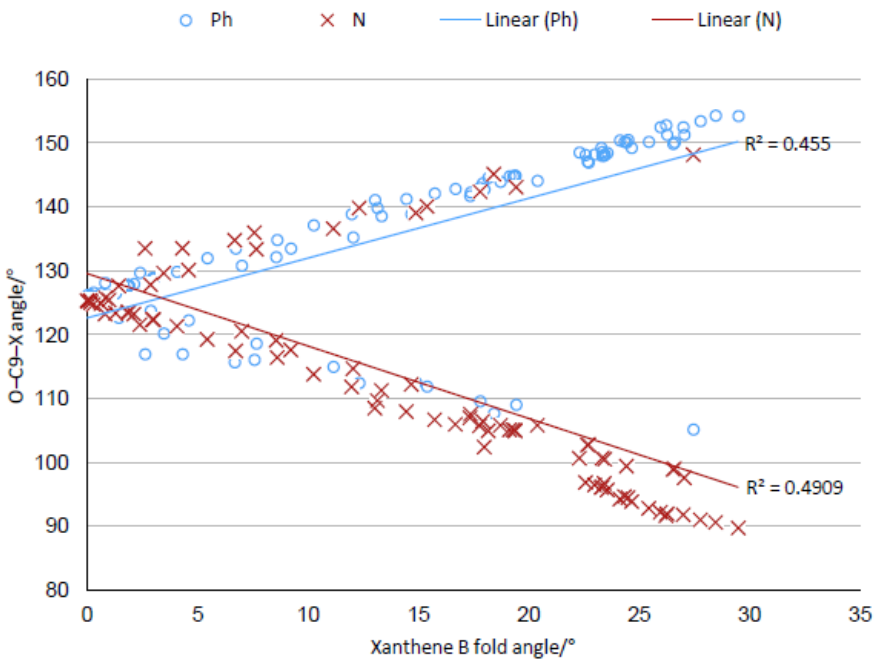

Figure 7.19. Host **H_2** angular orientations of the C(9) substituents with respect to the O···C(9) axis for a) xanthene A and b) xanthene B (where xanthene A and B represents the two xanthenyl units of the host molecule).

The first conformer displaying an all antiperiplanar array of torsion angles has an energy of E_{rel} 19.99 kJ·mol^{-1} and planar xanthenyl rings.

The relative energies of the various conformers were compared against those of the *syn* and *anti* configurations (Figure 7.20). Since the average energy of the *anti* conformers are about 4 kJ·mol^{-1} lower in energy than the *syn* diastereomers, evidently the energy distributions of the conformers are not strongly influenced by the relative configurations of the amino centres.

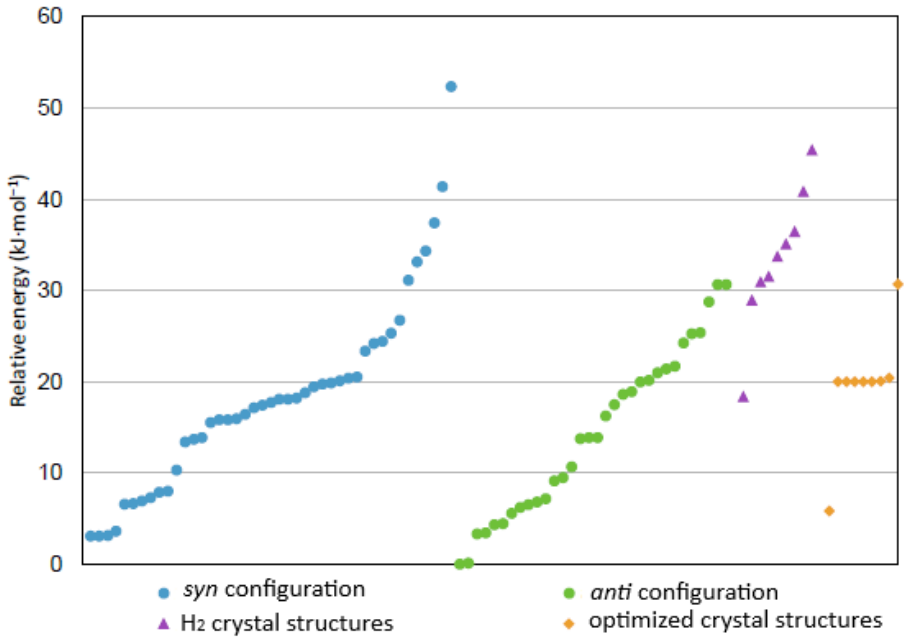

Figure 7.20. Host **H₂** conformer energy distributions as a function of N-atom relative configurations.

Figure 7.20 also shows that in the DFT calculations the host **H₂** crystal structures rank as relatively high energy conformers, relaxing to lower energy arrangements when allowed to optimize without constraint. In the latter case, all antiperiplanar torsion angles are again preferred, except for the lowest energy conformer, E_{rel} 5.80 kJ·mol^{-1}, where the torsion angles of bonds *IV* and *V* are synclinal and anticlinal respectively, as well as in the PYR complex, where bonds *II* and *VI* are synclinal. The xanthenyl systems are essentially planar in the optimized crystal structures, except for one of the conformations of the PYR complex where there is marked bending of both xanthenyl units. The *anti* configuration of the PIP complex was calculated to be only marginally lower in energy than its *syn* analogue. It is interesting that exclusively the *anti* diastereomer of host **H₂** was consistently selected during crystallization with the other guest compounds.

7.3.6 Conformations of compound **H$_1$**

Conformational analysis of host **H$_1$** results in broadly similar trends to those found for **H$_2$** at both the molecular mechanics and DFT levels (these data are provided in the Supplementary Information, Tables S161 and S162). The various conformers of the crystal structures of **H$_1$** are also included in the Supplementary Information for comparison and are illustrated in Figure S163.

The molecular mechanics conformers in the lowest calculated energy range (E_{rel} 0−8.86 kJ·mol^{-1}) has antiperiplanar bonds in the ethylenediamine chains, except for the central bond *IV* (synclinal). The subsequent higher energy structures have similar chain conformations, but one of the adjacent bonds (*III* or *V*) is in an anticlinal arrangement. One conformer (E_{rel} 9.58 kJ·mol^{-1}) possessed all antiperiplanar torsion angles. In all cases the thioxanthenyl ring moieties are only slightly bent (<7°). The optimized structures of host **H$_1$** also fall into this set. The higher energy conformers displayed synclinal bonds and bending of the thioxanthenyl moieties. The various complexes of **H$_1$** rank as relatively high energy arrangements in the calculated range.

At the DFT level the lower energy conformers (E_{rel} 0−7.5 kJ·mol^{-1}) are characterized by synclinal *IV* bonds, while the rest have a combination of synclinal and anticlinal bonds. In most cases, the thioxanthenyl moiety is buckled but some conformers had one unit that is planar. The higher energy structures have an increasing number of antiperiplanar bonds and both thioxanthenyl units are planar. Two conformers with only antiperiplanar arrangements were calculated (E_{rel} 26.7 and 29.0 kJ·mol^{-1}) and contained somewhat planar tricyclic rings.

In the folded thioxanthenyl ring systems, the preferred orientations of the C(9) amino and phenyl substituents are also pseudo axial and pseudo equatorial, respectively, although a larger number of reversals are evident, especially where the ring units are strongly buckled. This relationship between the orientations and buckling is illustrated in Figure 7.21.

a)

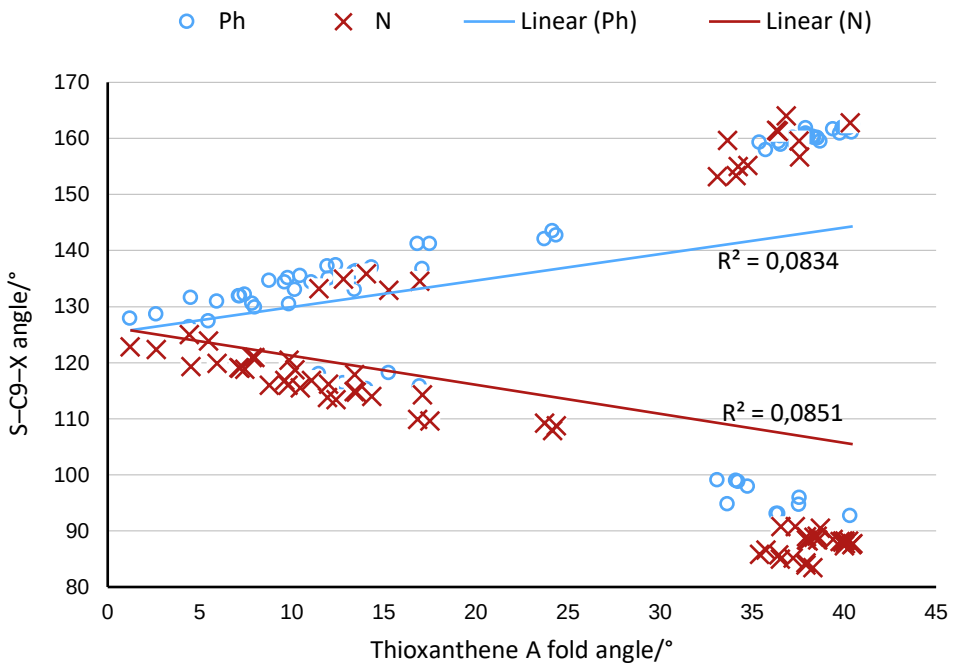

b)

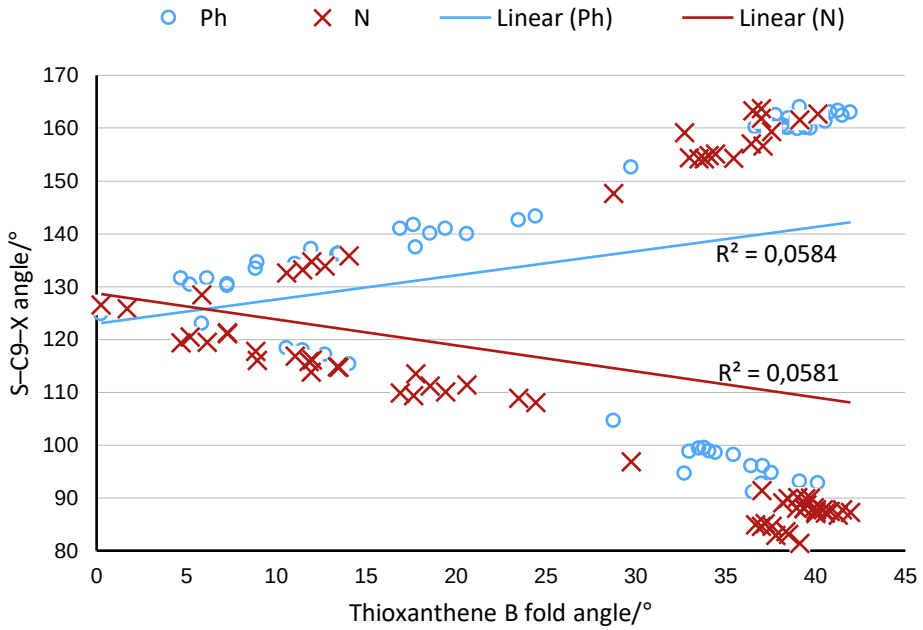

Figure 7.21. Host $\mathbf{H_1}$ angular orientations of the C(9) substituents with respect to the S···C(9) axis for a) thioxanthone A and b) thioxanthone B (where thioxanthene A and B represents the two thioxanthenyl units of the host molecule).

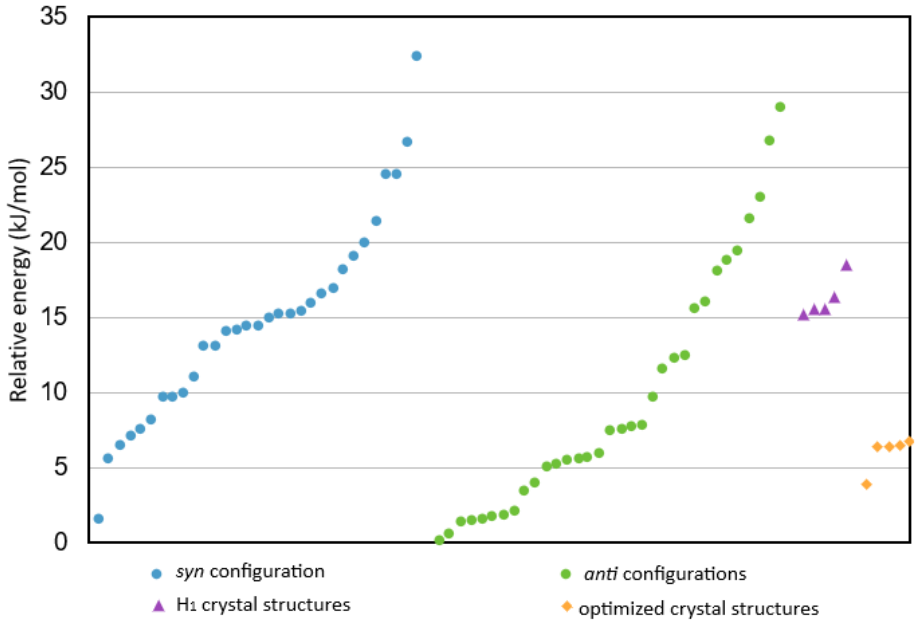

Figure 7.22. Host **H₁** conformer energy distributions as a function of N-atom relative configurations.

The relative energies of the various conformers grouped according to the relative configurations of their amino centers are displayed in Figure 7.22. Similar to the xanthenyl analogue **H₂**, the average energy of the *anti* configurations of host **H₁** are significantly lower (by more than 5 kJ·mol^{-1}) than the *syn* set, suggesting that the *anti* configuration might be preferred when the host compound crystallizes. This proves to be the case when compound **H₁** was recrystallized in the absence of guest compounds. However, in all cases where H···G complexation occurred, the *syn* configuration is preferred. This contrasts with host **H₂** (when complexed) where the favoured configuration is *anti* and may be the reason for the host displaying contrasting selectivity behavior in the presence of these heterocyclics.

The factors that determine the stability order of the computed conformers for **H₂** and **H₁** are not explicit. However, it appears from Tables S160 and S162 (Supplementary Information) that staggered arrangements for the bonds *II*–*VI* are unfavourable and that a measure of coiling in the ethylenediamine linkage is favoured. Moreover, Figures 7.23 and 7.24 reveal a rough correlation in each case between relative energies of the conformers and the separation between their xanthenyl or thioxanthenyl termini. The preference for conformers where the separations are smaller suggests that dispersive interactions between the aromatic termini could be a stabilizing effect in the gas phase.

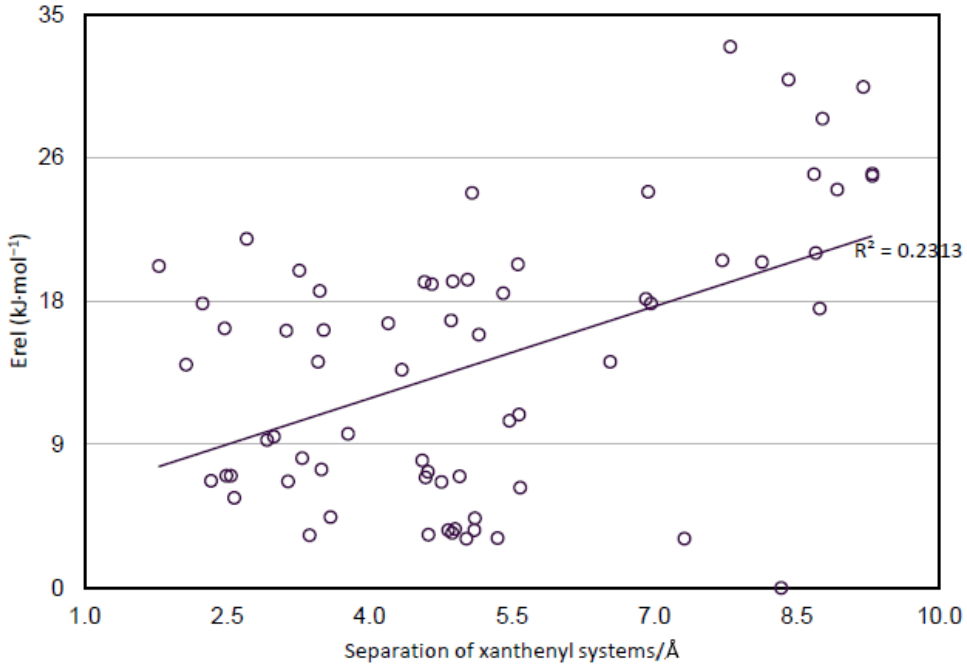

Figure 7.23. Effect of separation distance between the xanthenyl systems in host compound **H_2**.

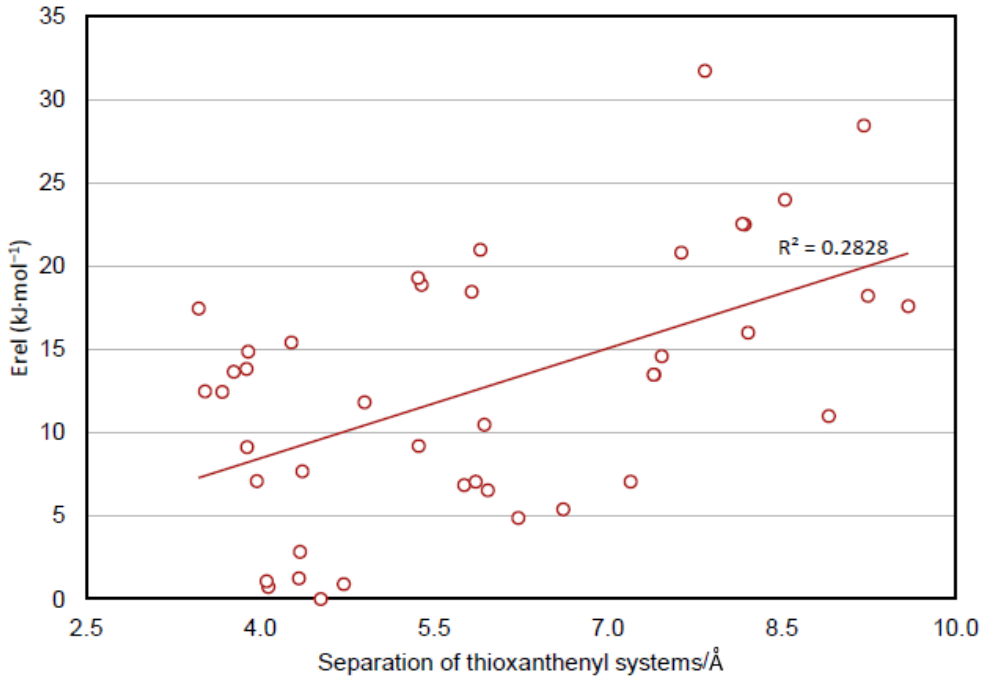

Figure 7.24. Effect of separation distance between the thioxanthenyl systems in host compound **H_1**.

7.3.7 Selectivity effects

When two chemical species interact, there is an energy change associated and this interaction which may be quantified by the Klopman-Salem equation.[271-274] It comprises three terms, the first accounting for closed-shell repulsion of the occupied molecular orbitals of the reactants, the second Coulombic attraction or repulsion, and the third bonding interactions between the occupied and unoccupied molecular orbitals of the reactants. The first and third terms are likely to be of secondary importance in H···G complexation as the contacts between host and guest molecules are usually too far apart for significant orbital interactions to possibly occur. Instead, Coulombic effects as a result of van der Waals attractions and hydrogen bonding are expected to be a determining factor. The differing selectivities displayed by hosts **H_1** and **H_2** upon recrystallization from the heterocyclic mixtures most likely arise from subtle differences in the interstitial space and electrostatic environment associated with each host compound during crystallization.

Two key conformational differences were identified in the structures of **H_1** and **H_2**. The first was the geometrical differences between the xanthene and thioxanthene systems, arising chiefly from longer S–C bonds and more acute C–Ŝ–C bond angles compared to their oxygen analogues that result in folding in the thioxanthene system and a boat-like structure for its central ring. Consideration of the crystal structures in Tables S160 and S162 (Supplementary Information) show that in host **H_2** the xanthenyl units are mostly planar, while for host **H_1** there is significant buckling of the thioxanthenyl units. Consequently, as crystallization occurs, the accessible volumes in the interstitial voids in which the guest molecules reside are likely to be different for the two host compounds, hence influencing their H···G selectivities in these conditions.

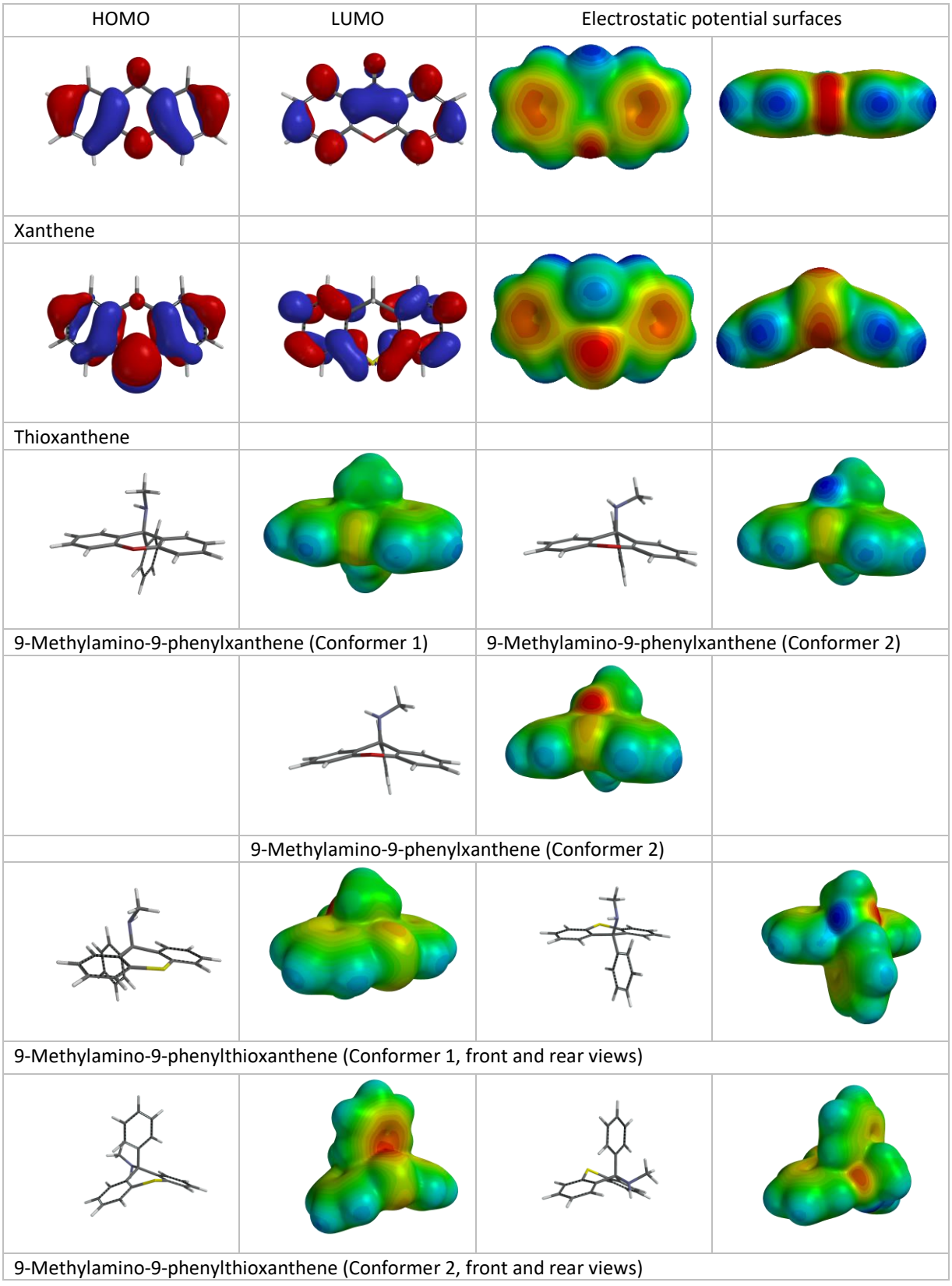

Figure 7.25. HOMO and LUMO features and electrostatic potential surfaces.

Graphical representations of the computed HOMOs and LUMOs for xanthene and thioxanthene are shown in Figure 7.25. The HOMOs have similar distributions of contributing atomic orbitals, but it is notable how much larger the coefficient for the sulfur atom is compared to oxygen. Together with the effect of folding in the thioxanthenyl system, substantively different electron distributions result in the two molecules. The overall effect is evident in the respective computed electrostatic potential surfaces. These surfaces are furthermore sensitive to the nature and orientation of the C(9) substituents, as illustrated for 9-amino-9-phenylthioxanthene and 9-methylamino-9-phenylthioxanthene (Figure 7.25).

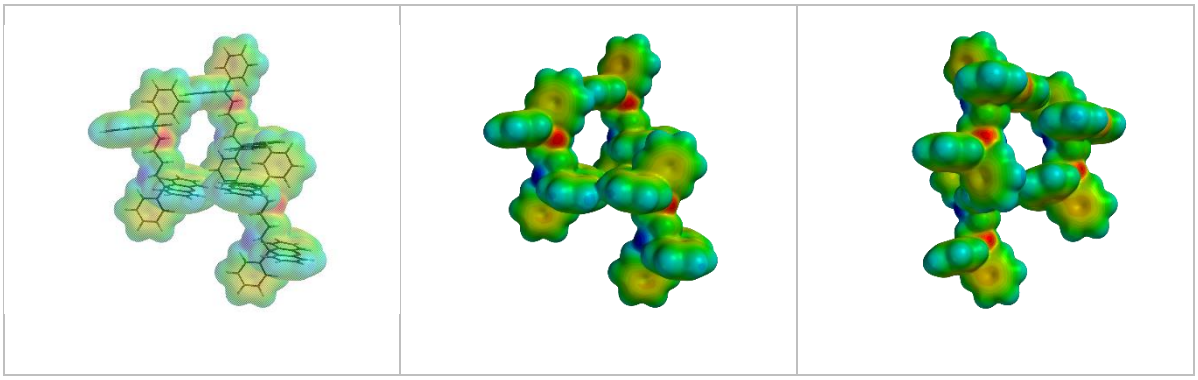

Figure 7.26. Electrostatic potential surface for the crystal structure lattice of **H_2**·(MORPH) after removal of MORPH.

Figure 7.26 displays the electrostatic potential surface associated with the host compound **H_2** where an interstitial void was exposed through deletion of the guest molecule from a unit cell of its crystal structure involving MORPH. Numerous sites of varied electrostatic potential are apparent on the surface whose cumulative effect would be to favour the inclusion of guest molecules with certain polarity characteristics in the voids, while disfavouring others. The presence of nitrogen atoms in the ethylenediamine linkers as well as the aromatic rings containing conjugated O and S atoms will give rise to local dipoles, while the conjugated aromatic systems can furthermore be expected to facilitate dipole/induced-dipole interactions between host and guest molecules.

7.3.8 Conclusions

The selectivity observations were investigated in detail through X-ray diffraction and computational analyses. The relatively high energy rankings of the conformers of both hosts **H_1** and **H_2** in the crystal structures of their H···G complexes, as compared against the array of conformers obtained computationally, suggests that the conformations selected are largely dictated by the thermodynamics of the crystallization process which could be subtly influenced by the nature of the available potential guest compounds.

An examination of the effect of the proximities of the xanthenyl or thioxanthenyl termini on the relative energies of the conformers of **H_1** and **H_2**, respectively, show that extended arrangements of the molecules are disfavoured. This suggests that dispersive interactions between the aromatic termini could be a stabilizing effect in the gas phase. Exploration of the electrostatic potential surfaces associated with host compounds **H_1** and **H_2** attribute their differing guest inclusion selectivities to subtle variations in the electrostatic environment that develops in each case during crystallization, thereby influencing their van der Waals force and hydrogen bonding abilities towards potential guest compounds and ultimately resulting in the observed opposing host behaviour.

Presumably it is speculated that the H···G selectivity effects observed for host compounds **H_1** and **H_2** arise from the interplay of their differing geometrical and electronic characteristics.

7.4 Host/host competition experiments

As an interesting alternative to the standard guest/guest competition experiments, the two host compounds were made to compete instead by dissolving equimolar amounts of **H_1** and **H_2** (0.05 mmol each) in each of the four guest solvents (10 mmol). The vials were treated in the same manner as in the single solvent experiments, and complexes analysed by means of ^{1}H-NMR spectroscopy. Table 7.13 summarizes the results obtained.

Table 7.13. H_1:H_2 ratios of complexes obtained when the two host compounds were made to compete.

Guest compound	**H_1:H_2** ratio	Overall H:G ratio
PYR	100.0:0.0	1:1
MORPH	23.1:76.9	1:1
PIP	~100.0:100.0[a]	1:1
DIOX	31.9:68.1	1:1

[a]This result is a plausible estimate due to overlapping of the host and guest (broad NH groups) resonances which made accurate integration of the ^{1}H-NMR spectrum not as facile; the addition of D_2O did not solve this problem owing to the partial miscibility of piperidine in water.

Using PYR as the solvent, which was significantly preferred by **H_1** but not **H_2** in competition experiments, afforded a 1:1 H:G complex in which only host **H_1** was present. On the other hand, the use of DIOX, a guest compound for which **H_2** showed enhanced selectivity, yielded crystals that contained more of **H_2** (68.1%) than **H_1** (the overall H:G ratio remained 1:1). From these experiments, it is clear that complexes that formed under these conditions comprised an increased amount of host **H_2** when the guest compound employed was favoured by **H_2** (DIOX) and, similarly, an enhanced amount of **H_1** when the guest compound present was preferred by **H_1** (PYR). The MORPH experiment is not as readily explained, but ambivalence of both host compounds for PIP resulted in a complex containing approximately equal amounts of each host compound.

8. HETEROCYCLIC FIVE-MEMBERED RING COMPOUNDS

8.1. Inclusion compounds with $\mathbf{H_1}$

8.1.1 Introduction

Many drug actives contain five-membered ring heterocyclic motifs,[275-277] and therefore an investigation of the host ability of $\mathbf{H_1}$ in the presence of six common five-membered ring heterocyclics, namely the saturated compounds pyrrolidine, tetrahydrofuran (THF) and tetrahydrothiopene (THT), and their aromatic counterparts pyrrole, furan and thiophene (Scheme 8.1) was undertaken.

There exist many methods to produce THF but the most widely used industrial process involves the acid-catalyzed dehydration of 1,4-butanediol.[278] Other methods include the oxidation of *n*-butane to crude maleic anhydride followed by catalytic hydrogenation,[279] the catalytic hydrogenation of furan,[280] or catalytic conversion of certain sugars.[281] In the presence of strong acids, THF forms a linear polymer called poly(tetramethylene ether)glycol (PTMEG) which is primarily used to synthesize elastomeric polyurethane fibres like those in Spandex.[282] Other applications of THF include the liquefication and delignification of plant biomass for the production of renewable chemicals and sugars as potential precursors to biofuels, in polymer sciences (dissolving polymers in 3D printing), as part of a mobile phase for reverse-phase liquid chromatography, and as a solvent for many chemical reactions (hydroboration, Grignard, etc.).[283]

Industrially, furan is manufactured by the palladium-catalyzed decarbonylation of furfural, or the copper-catalyzed oxidation of 1,3-butadiene. Other methods involve the conversion of carbohydrates from agricultural waste into furan derivatives such as furan-2-aldehyde or furfural, the latter of which is used extensively as a solvent, in the manufacture of plastics, and in the preparation of other furan derivatives.[284]

Tetrahydrothiophene (THT) is prepared by the reaction of THF with hydrogen sulfide via a catalyzed vapour phase reaction.[285] Both unsubstituted and substituted tetrahydrothiophenes occur in nature [e.g. *Eruca sativa Mill.* (salad rocket), *Allium sativum* (garlic), *Allium cepa* (onion), *Allium schoenoprasum* (chives), and *Salacia prinoides*].[286-288] The THT motif is also

present in Albomycin antibiotics and many naturally occurring alkaloids.[289] THT has been used in the biosynthesis of these natural products and as an odourant in LPG and natural gas.[290]

Thiophene is found in deposits of lignite, coal, crude oils, plants and fungi, but the extraction processes from these sources are not feasible.[291] Laboratory procedures for its preparation involve the reaction of 1,4-diketones, diesters, or dicarboxylates with sulfidizing reagents. Industrially, thiophene is produced via continuous vapour phase techniques that use C_4 raw materials and sulfur compounds in the presence of metal oxide catalysts.[292] Thiophenes are widely used as building blocks in many agrochemicals and pharmaceuticals.[290]

Pyrrolidine is synthesized by treatment of 1,4-butanediol with ammonia over an oxide catalyst or by reacting 4-chlorobutan-1-amine with a strong base.[261] This compound and its derivatives are found in numerous natural alkaloids (e.g., nicotine and hygrine), drugs (e.g., procyclidine and bepridil), and forms the basis for the racetam compounds (e.g., piracetam, aniracetam) and certain amino acids (e.g., proline and hydroxyproline). Pyrrolidine is used as a base, a building block in the synthesis of more complex organic compounds and in reactions to activate ketones and aldehydes toward nucleophilic addition by the formation of enamines.[293,294]

Pyrrole is prepared industrially by the treatment of furan with ammonia in the presence of solid acid catalysts or the catalytic dehydrogenation of pyrrolidine. There exist several laboratory syntheses of pyrrole, and these include the Hantzsch, Knorr, Paal–Knorr, Van Leusen, Barton–Zard and Piloty–Robinson pyrrole syntheses, to name a few.[295] Cycloaddition-based and biosynthetic routes for the production of pyrroles also exist. Pyrrole and its derivatives are widely used as intermediates in the synthesis of pharmaceuticals, medicines, agrochemicals, dyes, photographic chemicals, perfumes and other organic compounds.[295,296]

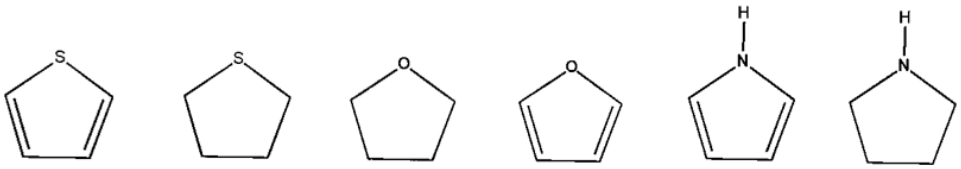

Thiophene	THT	THF	Furan	Pyrrole	Pyrrolidine
84 °C	119 °C	66 °C	31 °C	129 °C	87 °C

Scheme 8.1. Structures of the heterocyclic five-membered ring guest compounds.

8.1.2 Individual inclusions

To establish the inclusion ability of **H_1**, the host compound was recrystallized independently from the six guests and analysed by means of ^{1}H-NMR spectroscopy. Table 8.1 summarizes the results obtained from these experiments, together with the H:G ratios obtained after analyses (by means of ^{1}H-NMR spectroscopy).

Table 8.1. Results of the single solvent experiments and consequential H:G ratios.

Guest	H:G ratio
THF	1:1
Furan	1:1
THT	1:1
Thiophene	1:1
Pyrrolidine	1:1
Pyrrole	1:1

H_1 successfully formed 1:1 H:G complexes with each of these compounds (Table 8.1). (^{1}H-NMR spectra of each complex may be found in the Supplementary Information, Figures S164–169.) Subsequently, equimolar experiments were carried out to determine if the host would display selectivity towards any of these guests.

8.1.3 Equimolar competition experiments

The results of equimolar recrystallization experiments are summarized in Table 8.2. In each case mixed complexes were obtained, and the table provides the G1:G2 ratios that were determined by means of either ^{1}H-NMR spectroscopy or GC-MS, as applicable. The experiments were conducted in duplicate, and an average value and the % e.s.d.s. are provided here (the duplicate values may be obtained from the Supplementary Information, Table S170.)

For the THF/furan and THT/thiophene experiments, guests with corresponding heteroatoms but with ring saturation differing (i.e., aromatic versus saturated), **H_1** displayed enhanced selectivity for the saturated guests in each case (THF and THT, 63.2 and 63.3%, respectively). However, the host was more ambivalent when recrystallized from an equimolar pyrrolidine/pyrrole mixture (49.5:50.5%).

Experiments comprising only saturated guest mixtures resulted in the host compound consistently displaying a preference for the THT guest (THF/THT and THT/pyrrolidine, 70.3 and 78.4% THT, respectively). On the other hand, in the absence of THT, the host favoured THF relative to pyrrolidine (69.5%:30.5%). Interestingly, the same trend was observed for the aromatic guests, where thiophene/furan and thiophene/pyrrole binary mixtures afforded mixed complexes that contained 75.0 and 85.4% thiophene (the S-containing guest), respectively. When furan and pyrrole competed, the oxygen-containing guest was favoured once more, as was the case for the saturated guests (66.3% furan:33.7% pyrrole).

Overall, these equimolar experiments have shown that **H_1** prefers saturated heterocyclic guests relative to their aromatic analogues (but not strikingly so in the pyrrole/pyrrolidine experiment) and, additionally, the host affinity for guests with differing heteroatoms is in the order S > O > N. The host selectivity orders may thus be written as THT > THF > pyrrolidine and thiophene > furan > pyrrole.

Table 8.2. Results of the equimolar binary solvent experiments with **H_1**.[a,b]

THF	furan	THT	thiophene	pyrrolidine	pyrrole	Guest ratios	Overall H:G ratio	% e.s.d.s
x	x					63.2:36.8	1:1	(0.9):(0.9)
		x	x			63.3:36.7	1:1	(0.8):(0.8)
				x	x	49.5:50.5	1:1	(0.5):(0.5)
x		x				29.7:70.3	1:1	(0.9):(0.9)
x				x		69.5:30.5	1:1	(2.3):(2.3)
		x		x		78.4:21.6	1:1	(1.3):(1.3)
	x		x			25.0:75.0	1:1	(1.5):(1.5)
	x				x	66.3:33.7	1:1	(0.1):(0.1)
			x		x	85.4:14.6	1:1	(0.2):(0.2)

[a]G:G ratios were determined using ^{1}H-NMR spectroscopy ($CDCl_3$ as solvent) or GC-MS (dichloromethane as solvent); overall H:G ratios were obtained by means of ^{1}H-NMR spectroscopy.
[b]Experiments were conducted in duplicate for confirmation purposes; % e.s.d.s are provided in parentheses.

8.1.4 Ratio-dependent competition experiments

The binary experiments were further investigated but guest concentrations were varied, and the results are graphically depicted in the form of overlaid selectivity profiles (Figure 8.1a–c). Analyses were carried out using ^{1}H-NMR spectroscopy and GC-MS methods, as before. The average selectivity coefficient was calculated for each profile, and the complete set of these data may be found in the Supplementary Information, Tables S171–179.

a)

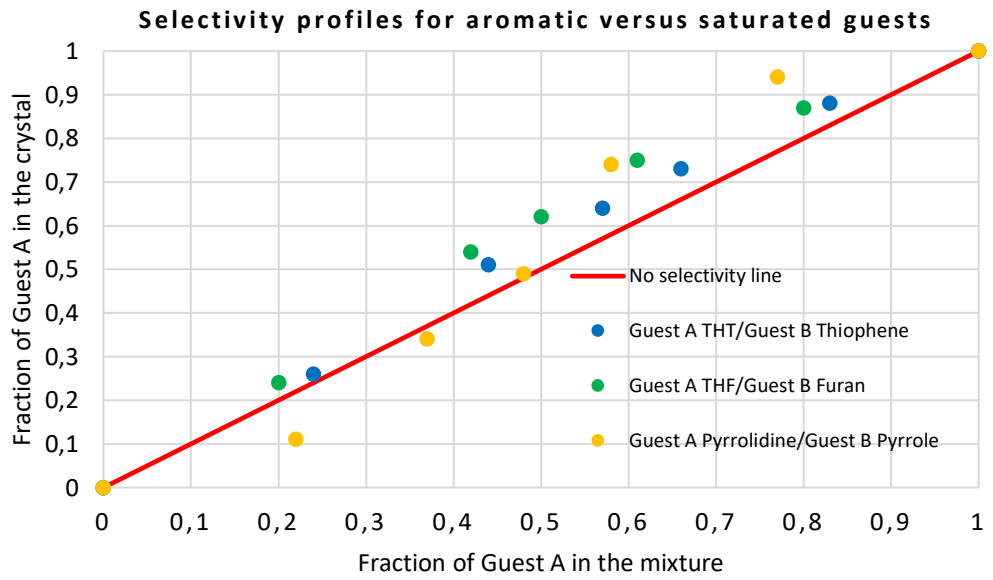

b)

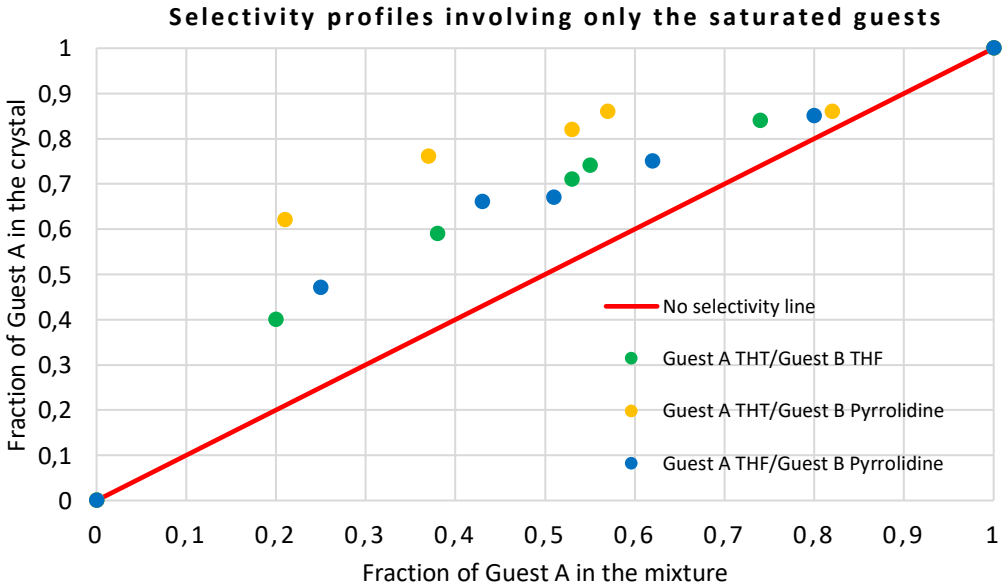

c)

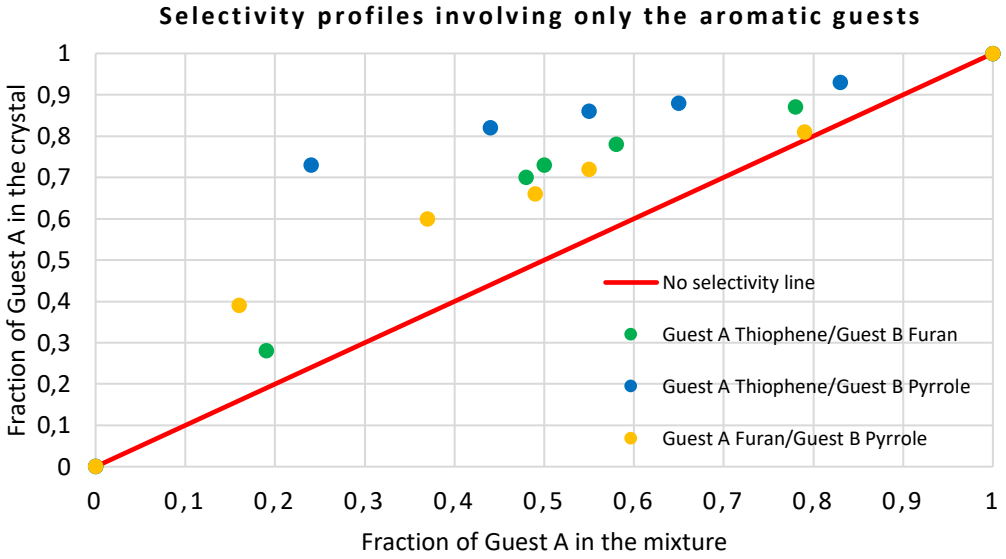

Figure 8.1. Overlaid selectivity profiles for **H_1** when recrystallized from a) saturated and aromatic b) solely saturated and c) solely aromatic binary guest mixtures.

When considering Figure 8.1a for THT/thiophene and THF/furan, the two profiles (blue and green) display the selectivity of the host to be consistently in favour of the saturated counterparts (K = 1.3 and 1.6, respectively). For the pyrrolidine/pyrrole experiment (Figure 8.1a, yellow profile), however, the host selectivity varies depending on the relative G:G concentrations from which it was recrystallized. This ambivalent behaviour is plausibly as a result of the fact that **H_1** does not prefer the N-containing guests, which was also apparent from the results determined in the equimolar experiments. Figure 8.1b shows an overlay of the results obtained when **H_1** was recrystallized from various saturated guest solutions. Average selectivity coefficients were calculated as K = 4.31, 2.27 and 2.09 for the THT/pyrrolidine, THT/THF and THF/pyrrolidine experiments, respectively. These profiles demonstrate that **H_1** is selective for THT whenever it is present and at any concentration, followed by THF. The latter guest is also consistently favoured over pyrrolidine. Figure 8.1c represents the data obtained from binary aromatic guest solutions thiophene/pyrrole, thiophene/furan and furan/pyrrole, with calculated K values of 5.21, 2.27 and 2.23, once again confirming the preference for the S-containing guest. (In all cases in Figure 8.1b and c, the preferred Guest A was favoured over the entire concentration range.) The results from Figure 8.1b and c are in direct accordance with those from the equimolar experiments: the guest heteroatom preference of **H_1** is in the order S > O > N, and therefore the host selectivity is in the order THT > THF > pyrrolidine and thiophene > furan > pyrrole, as observed in the equimolar experiments.

8.1.5 SCXRD

SCXRD analyses were carried out on the **H$_1$**·THF, **H$_1$**·THT, **H$_1$**·pyrrolidine, **H$_1$**·furan, **H$_1$**·thiophene and **H$_1$**·pyrrole complexes, and Tables 8.3 and 8.4 contain a summary of the relevant crystallographic data and refinement parameters for each. All of the complexes, with the exception of **H$_1$**·pyrrolidine, demonstrate isostructural host packing, crystallizing in the monoclinic crystal system and $P2_1/n$ space group. The **H$_1$**·pyrrolidine complex shares the same crystal system and space group, but the unit cell dimensions are very different. Figure 8.2 depicts the unit cells for these complexes (**H$_1$**·THF is representative here for the isostructural complexes). (The complete set of figures of all unit cells are provided in the Supplementary Information, Figures S180 and S181.)

Table 8.3. Crystallographic data for complexes of **H$_1$** with saturated guests THF, THT and pyrrolidine.

	H$_1$·THF	**H$_1$**·THT	**H$_1$**·pyrrolidine
Chemical formula	$C_{40}H_{32}N_2S_2{\cdot}C_4H_8O$	$C_{40}H_{32}N_2S_2{\cdot}C_4H_8S$	$C_{40}H_{32}N_2S_2{\cdot}C_4H_9N$
Formula weight	676.90	692.96	675.92
Crystal system	Monoclinic	Monoclinic	Monoclinic
Space group	$P2_1/n$	$P2_1/n$	$P2_1/n$
μ (Mo Kα)/mm^{-1}	0.193	0.250	0.191
a/Å	10.2641(14)	10.2480(8)	13.8769(8)
b/Å	13.4071(18)	13.4291(10)	13.6064(7)
c/Å	25.060(3)	25.2183(19)	19.5494(3)
alpha/°	90	90	90
beta/°	92.326(6)	93.048(3)	109.984(3)
gamma/°	90	90	90
V/Å^3	3445.7(8)	3465.7(5)	3469.0(3)
Z	4	4	4
F(000)	1432	1464	1432
Temp./K	200	200	200
Restraints	0	0	6
Nref	8570	8641	8635
Npar	448	484	469
R	0.0386	0.0360	0.0374
wR2	0.1050	0.0990	0.0998
S	1.05	1.04	1.03
θ min−max/°	1.6, 28.3	1.6, 28.3	1.6, 28.3
Tot. data	126118	112840	79945
Unique data	8570	8641	8635
Observed data [I > 2.0 sigma(I)]	7383	7418	6908
R_{int}	0.022	0.019	0.026
Dffrn measured fraction θ full	1.000	1.000	1.000
Min. resd. dens. (e/Å^3)	−0.27	−0.37	−0.28
Max. resd. dens. (e/Å^3)	0.41	0.38	0.33

Table 8.4. Crystallographic data for complexes of **H$_1$** with the aromatic guests furan, thiophene and pyrrole.

	H$_1$·furan	**H$_1$**·thiophene	**H$_1$**·pyrrole
Chemical formula	$C_{40}H_{32}N_2S_2{\cdot}C_4H_4O$	$C_{40}H_{32}N_2S_2{\cdot}C_4H_4S$	$C_{40}H_{32}N_2S_2{\cdot}C_4H_5N$
Formula weight	672.87	688.93	671.89
Crystal system	Monoclinic	Monoclinic	Monoclinic
Space group	$P2_1/n$	$P2_1/n$	$P2_1/n$
μ (Mo Kα)/mm^{-1}	0.196	0.254	0.196
a/Å	10.0680(7)	10.0499(7)	9.9938(5)
b/Å	13.3209(10)	13.339(1)	13.3208(8)
c/Å	25.2560(18)	25.4586(19)	25.4169(15)
alpha/°	90	90	90
beta/°	92.502(3)	92.980(3)	92.988(3)
gamma/°	90	90	90
V/Å^3	3388.0(4)	3408.3(4)	3379.0(3)
Z	4	4	4
F(000)	1416	1448	1416
Temp./K	200	200	200
Restraints	21	0	0
Nref	8444	8472	8434
Npar	448	433	451
R	0.0396	0.0548	0.0370
wR2	0.1097	0.1659	0.1028
S	1.03	1.04	1.04
θ min−max/°	1.6, 28.4	1.6, 28.3	1.7, 28.4
Tot. data	64232	128763	98563
Unique data	8444	8472	8434
Observed data [I > 2.0 sigma(I)]	6789	7469	7019
R_{int}	0.031	0.017	0.025
Dffrn measured fraction θ full	1.000	1.000	1.000
Min. resd. dens. (e/Å^3)	−0.47	−1.12	−0.31
Max. resd. dens. (e/Å^3)	0.50	1.86	0.34

a) b)

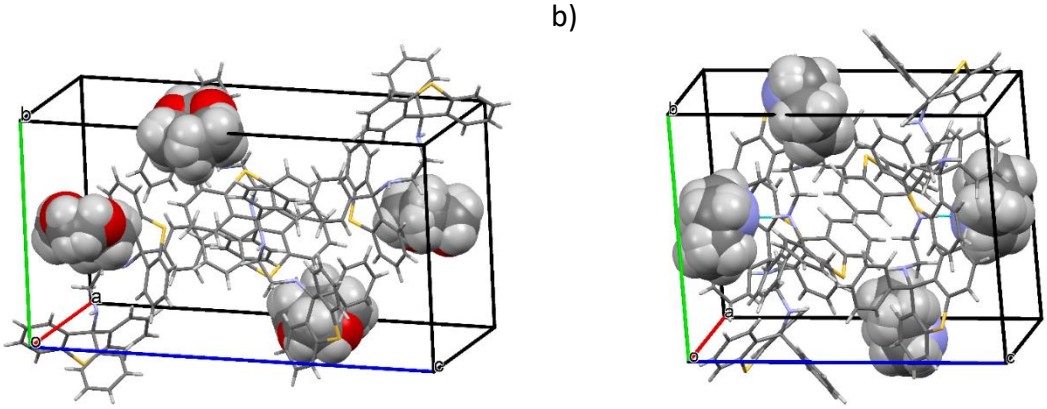

Figure 8.2. Unit cells for a) **H$_1$**·THF (representing isostructural complexes) and b) **H$_1$**·pyrrolidine (blue lines depict intermolecular $N_{(H)}$–$H_{(H)}$···$N_{(G)}$ classical hydrogen bonding interactions); guests are in space-filling mode and hosts in stick representation.

All guests displayed disorder that was modelled over two positions, and this may be observed in the stereoviews provided in Figure 8.3. (Once again, **H$_1$**·THF was selected as a representative example of the isostructural complexes).

a) b)

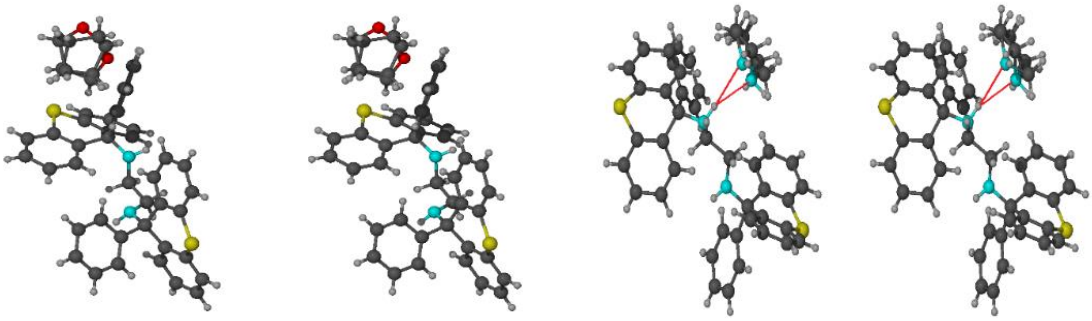

Figure 8.3. Stereoviews of a) **H$_1$**·THF (as representative example of the isostructural complexes) and b) **H$_1$**·pyrrolidine [red lines depict intermolecular $N_{(H)}$–$H_{(H)}$···$N_{(G)}$ classical hydrogen bonding interactions in both disordered guest components].

Subsequently, the guests were removed from the packing calculations and the resulting voids were calculated and are depicted in Figure 8.4.

a) b)

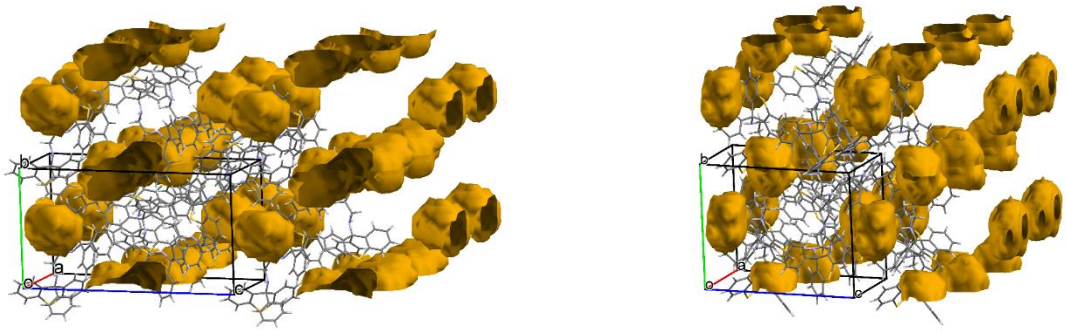

Figure 8.4. Calculated voids (dark yellow) for a) **H$_1$**·THF (representative) and b) **H$_1$**·pyrrolidine after removal of the guests from the packing calculation.

Upon close analysis of these voids, it was determined that the guests in the isostructural complexes all occupy discrete cavities, with two guests located in each of these (Figure 8.4a), while single guest-cavity occupation was observed in the **H$_1$**·pyrrolidine complex (Figure 8.4b). (The complete set of figures of the calculated voids may be seen in the Supplementary Information, Figures S182 and S183.)

Additionally, the more significant H···G and G···G interactions were investigated and are summarized in Table 8.5 (a more detailed table of the H···G, H···H and G···G interactions is provided in the Supplementary Information, Tables S184 and S185).

Table 8.5. H···G and G···G interactions present in complexes of **H_1** with THF, THT, pyrrolidine, furan, thiophene and pyrrole.[a,b]

Non-covalent interaction	**H_1**·THF	**H_1**·THT	**H_1**·pyrrolidine	**H_1**·furan	**H_1**·thiophene	**H_1**·pyrrole
CH···π (H···Cg, C–H···Cg)						
$C_{(G1)}$–$H_{(G1)}$···$Cg_{(H)}$	2.99 Å, 129°		2.90 Å, 141°			
$C_{(G2)}$–$H_{(G2)}$···$Cg_{(H)}$	2.90 Å, 163°		2.83 Å, 151°			
H-bonding (H···A, D–H···A)						
$N_{(H)}$–$H_{(H)}$···$N_{(G1)}$			2.42 Å, 167° (<<)			
$N_{(H)}$–$H_{(H)}$···$N_{(G2)}$			2.33 Å, 158° (<<)			
Other short contacts (X···Z, X–Y···Z)						
$C_{(G1)}$–$H_{(G1)}$···$S_{(H)}$–$C_{(H)}$	2.93 Å, 145° (<)	2.92 Å, 138° (<)				
$C_{(G1)}$–$H_{(G1)}$···$C_{(H)}$–$S_{(H)}$	2.87 Å, 135° (<)					
$C_{(G2)}$–$H_{(G2)}$···$H_{(G2)}$–$C_{(G)}$		2.27 Å, 108° (<)				
$C_{(G2)}$–$H_{(G2)}$···$C_{(H)}$–$C_{(H)}$		2.68 Å, 157° (<<)				
$C_{(G2)}$–$H_{(G2)}$···$H_{(H)}$–$C_{(H)}$		2.88 Å, 152° (<)		2.36 Å, 122° (<)		
$C_{(G2)}$–$H_{(G2)}$···$S_{(H)}$–$C_{(H)}$			2.94 Å, 121° (<)			

[a]Guest 1 and Guest 2 (G1 and G2) represent the two disordered guest components in the host crystal.
[b]Distances denoted by < are contacts that measure less than the sum of the van der Waals radii of the atoms involved, while those denoted by << is this sum minus 0.2 Å.

Immediately evident from this table is that the saturated guests (THF, THT and pyrrolidine) experience a remarkably greater number and variety of interactions compared to their aromatic counterparts. Surprisingly, none of the aromatic guests experience significant H···G π···π stacking interactions, and only one significant contact could be identified, namely a $C_{(G2)}$–$H_{(G2)}$···$H_{(H)}$–$C_{(H)}$ interaction (2.36 Å, 122°), and this only in the complex with furan. It is plausible that the lack of significant H···G interactions in the aromatic complexes and the substantial number in the saturated analogues explains the clear preference of **H_1** for the saturated heterocyclics. Furthermore, due to the proximity of pairs of guests that are accommodated in each cavity, additional stabilizing G···G interactions were also identified in the preferred THT-containing complex. Counterintuitively, both disordered pyrrolidine molecules (the least preferred guest from the saturated range) behave as acceptors in classical hydrogen bonding with an N–H moiety of the host (2.42 Å, 167° and 2.33 Å, 158°, Figures 8.2b and 8.3b) and is the only guest to do so. One disordered component of THT is involved in a short contact of the $C_{(G2)}$–$H_{(G2)}$···$C_{(H)}$–$C_{(H)}$ type, where this interaction measures significantly less than the sum of the van der Waals radii of the atoms involved (2.68 Å, 157°). Considering

the other short contacts, THT experiences the greatest number in accordance with the enhanced preference of **H_1** for this guest. Each of the THF and pyrrolidine molecules (both disordered components), furthermore, experience $C_{(G)}–H_{(G)}\cdots\pi_{(H)}$ interactions, while this interaction type is absent in complexes comprising THT as well as the aromatic guests. To accurately quantify the types of significant interactions, Hirshfeld surface analyses were carried out on all of these complexes.

8.1.6 Hirshfeld surface analyses

The surfaces were calculated around the guest molecules, and 2D fingerprint plots (Supplementary Information, Figure S186) were derived from the 3D surfaces. (A graphical summary of the overall H···G/G···H interactions present in complexes of **H_1** with saturated and aromatic guests may be found in the Supplementary Information, Figure S187). From these plots, we successively identified and highlighted, quantitatively, all the guest heteroatom···host interactions, and these are provided in Figure 8.5a–l for both disordered components. Figure 8.6a and b is a graphical summary of these interactions for the saturated and aromatic guest series', respectively.

a)

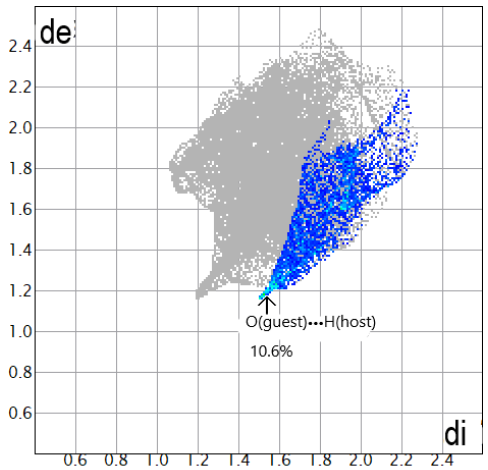

b)

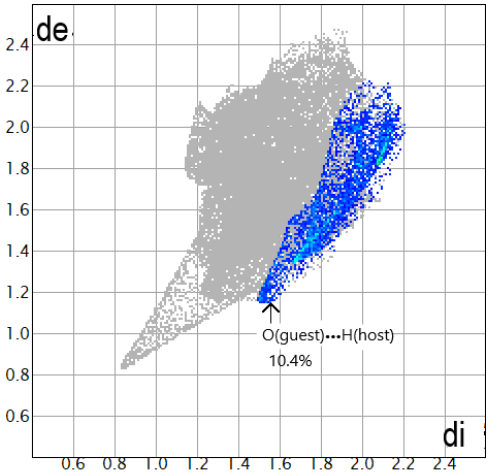

c)

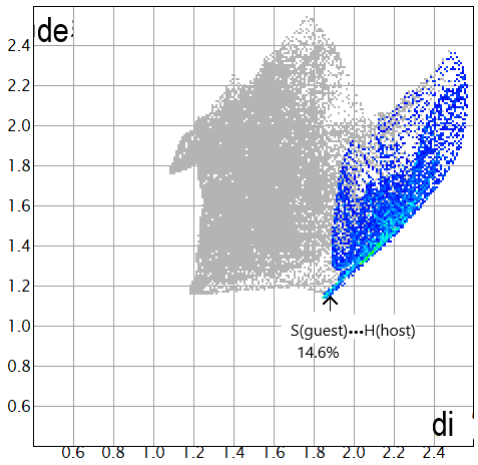
de
di
S(guest)···H(host)
14.6%

d)

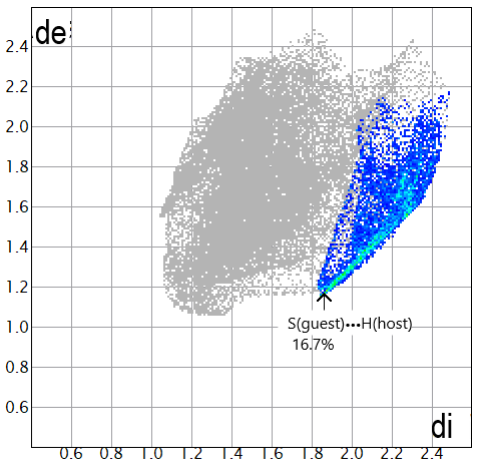
de
di
S(guest)···H(host)
16.7%

e)

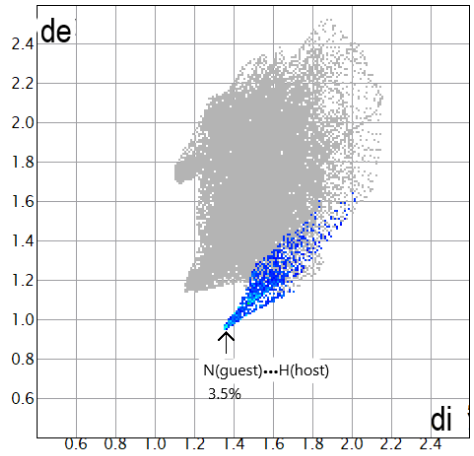
de
di
N(guest)···H(host)
3.5%

f)

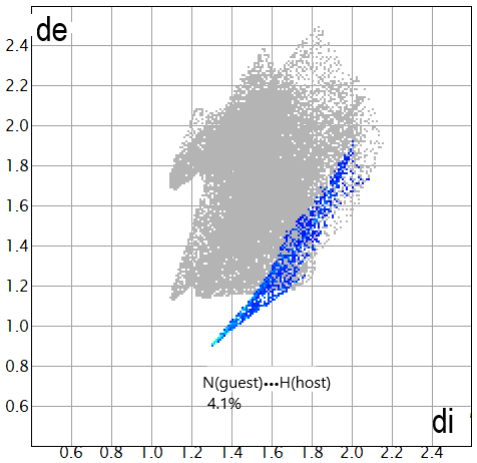
de
di
N(guest)···H(host)
4.1%

g)

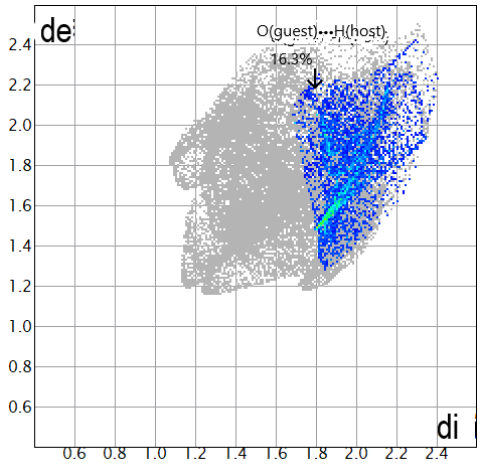
de
di
O(guest)···H(host)
16.3%

h)

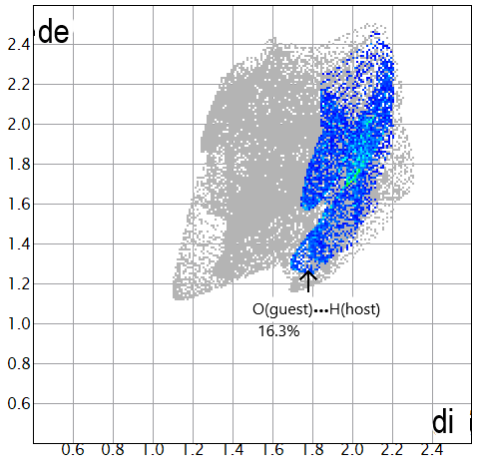
de
di
O(guest)···H(host)
16.3%

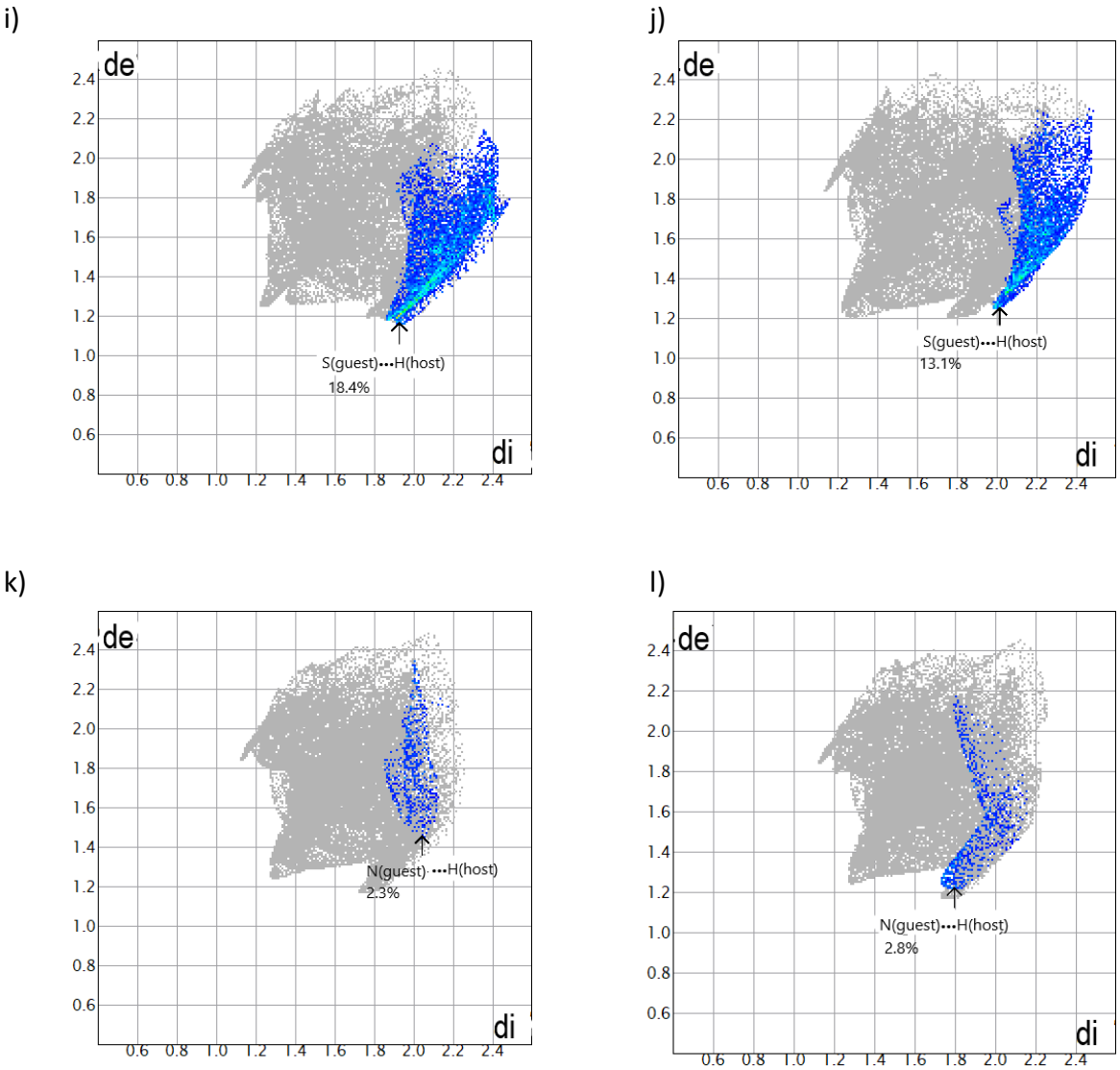

Figure 8.5. The 2D fingerprint plots for a) THF (major component), b) THF (minor component), c) THT (major component), d) THT (minor component), e) pyrrolidine (major component), f) pyrrolidine (minor component), g) furan (major component), h) furan (minor component), i) thiophene (major component), j) thiophene (minor component), k) pyrrole (major component) and l) pyrrole (minor component) that display heteroatom···host interactions.

a)

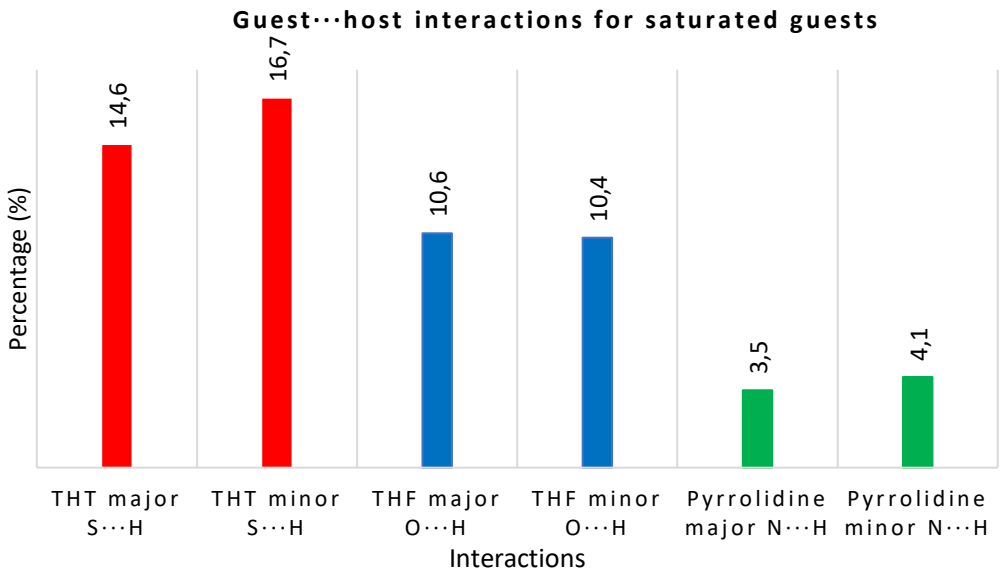

b)

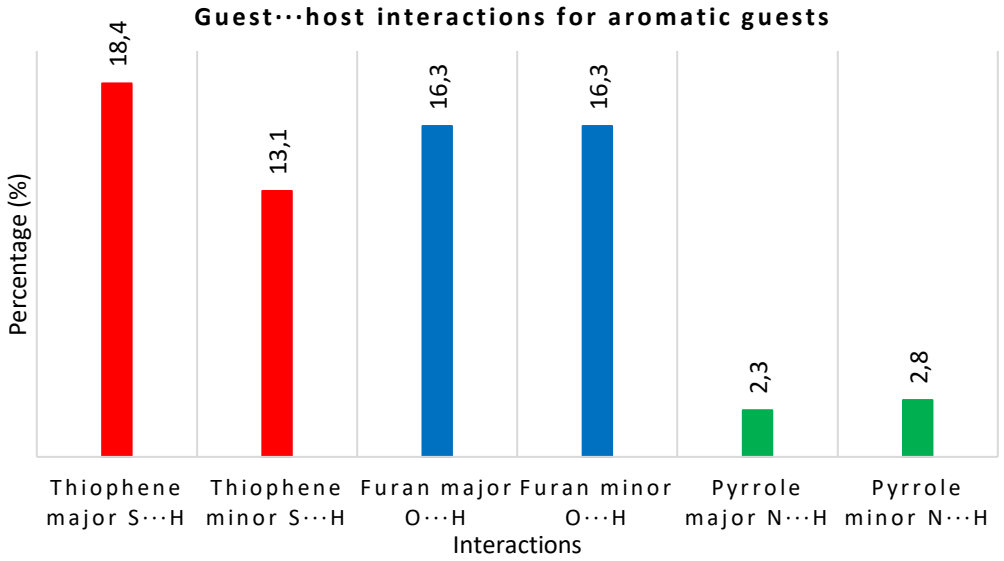

Figure 8.6. A graphical display emphasizing, quantitatively, the guest heteroatom···host interactions present in complexes of **H_1** with a) saturated guests and b) aromatic guests.

Both Figures 8.5 and 8.6 show that the S-containing guests (THT and thiophene) experience, overall, a significantly larger number of guest heteroatom···host interactions (14.6/16.7 and 18.4/13.1%, respectively), followed by guests containing oxygen (THF 10.6/10.4 and furan 16.3/16.3%) for the major/minor disordered guests for both saturated and aromatic guests.

Guests containing nitrogen atoms were involved in the lower number of these interaction types (pyrrolidine 3.5/4.1 and pyrrole 2.3/2.8%). Satisfyingly, these observations correlate directly with the selectivity order, S > O > N, noted for **H_1** and therefore explain the results of the competition experiments.

8.1.7 Thermal analyses (DSC and TG)

In order to assess the thermal stability of the complexes, each was heated from room temperature to approximately 250 °C to produce the resultant overlaid thermograms in Figure 8.6a–f [DSC (green) TG (blue) and DTG (red)]. The relevant thermal data are summarized in Table 8.6

a)

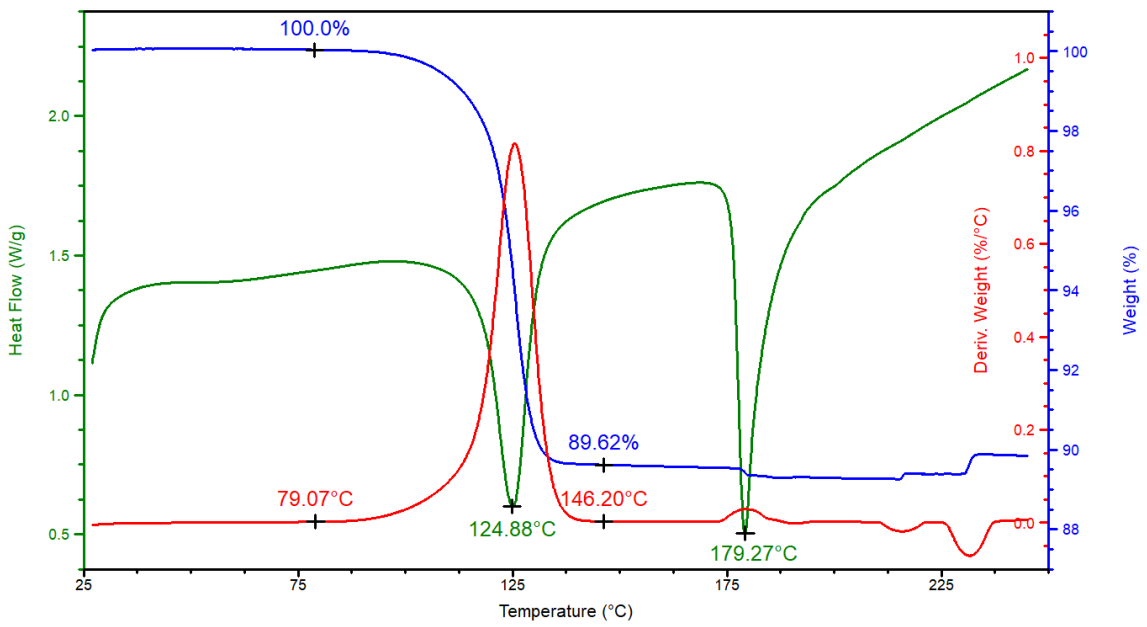

b)

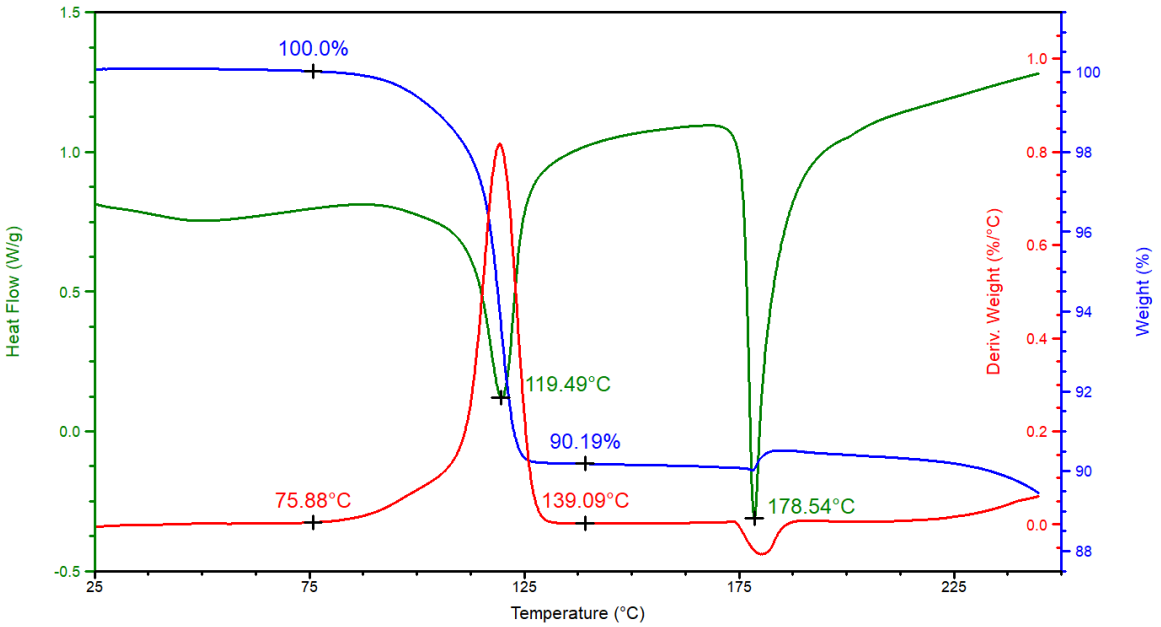
100.0%
119.49°C
90.19%
75.88°C
139.09°C
178.54°C
Heat Flow (W/g)
Deriv. Weight (%/°C)
Weight (%)
Temperature (°C)

c)

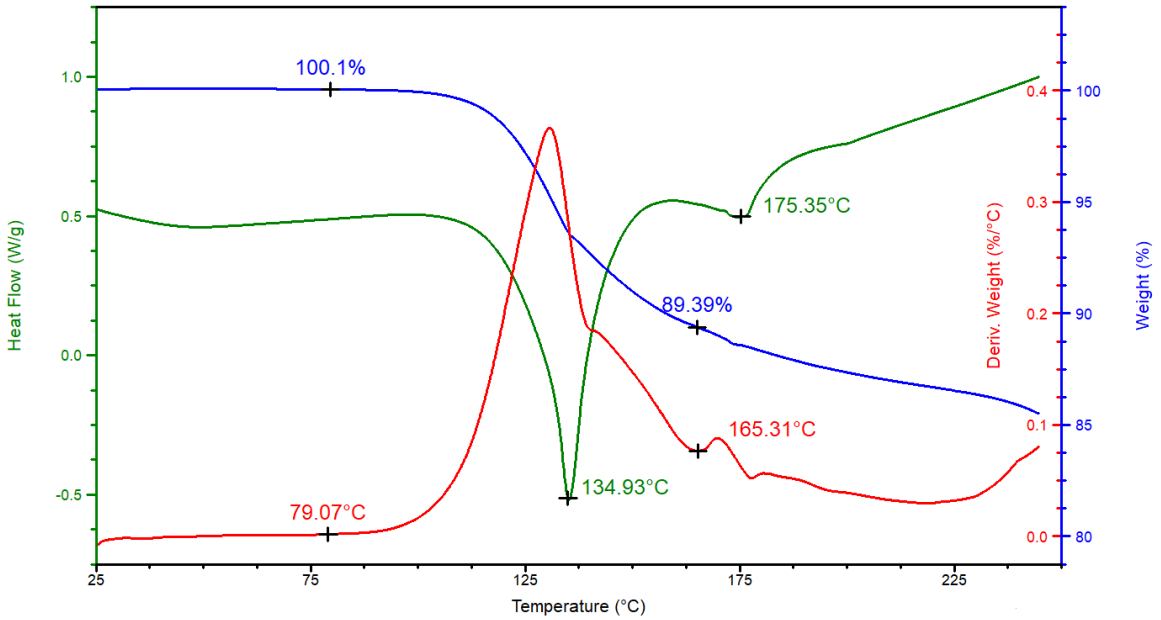
100.1%
175.35°C
89.39%
165.31°C
134.93°C
79.07°C
Heat Flow (W/g)
Deriv. Weight (%/°C)
Weight (%)
Temperature (°C)

d)

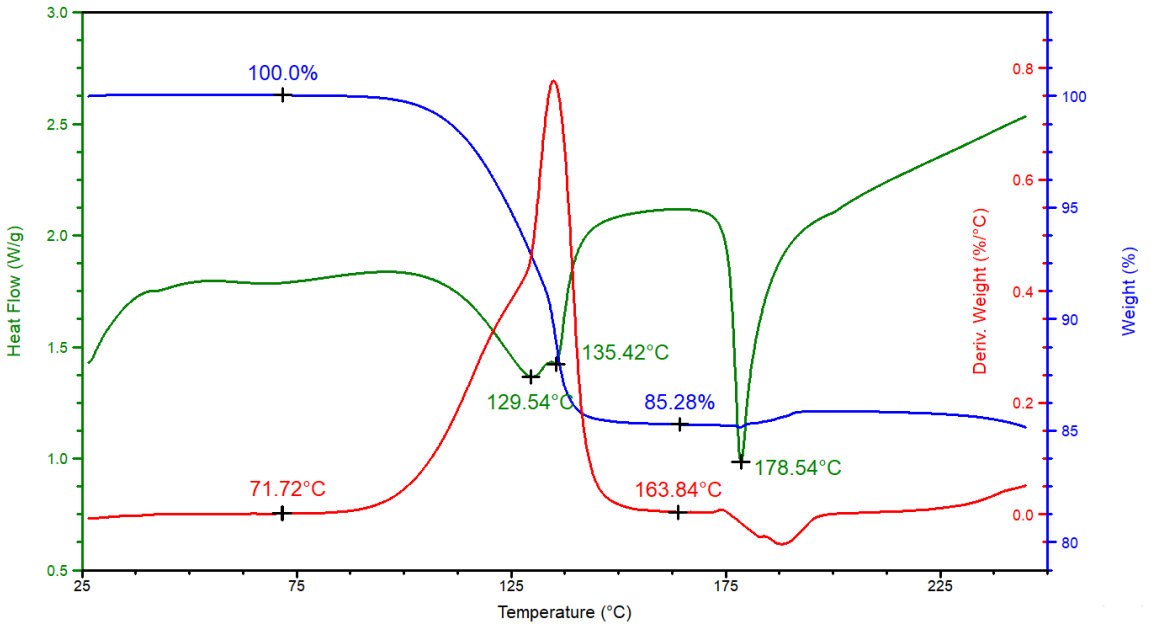
100.0%
135.42°C
129.54°C
85.28%
178.54°C
71.72°C
163.84°C
Heat Flow (W/g)
Deriv. Weight (%/°C)
Weight (%)
Temperature (°C)

e)

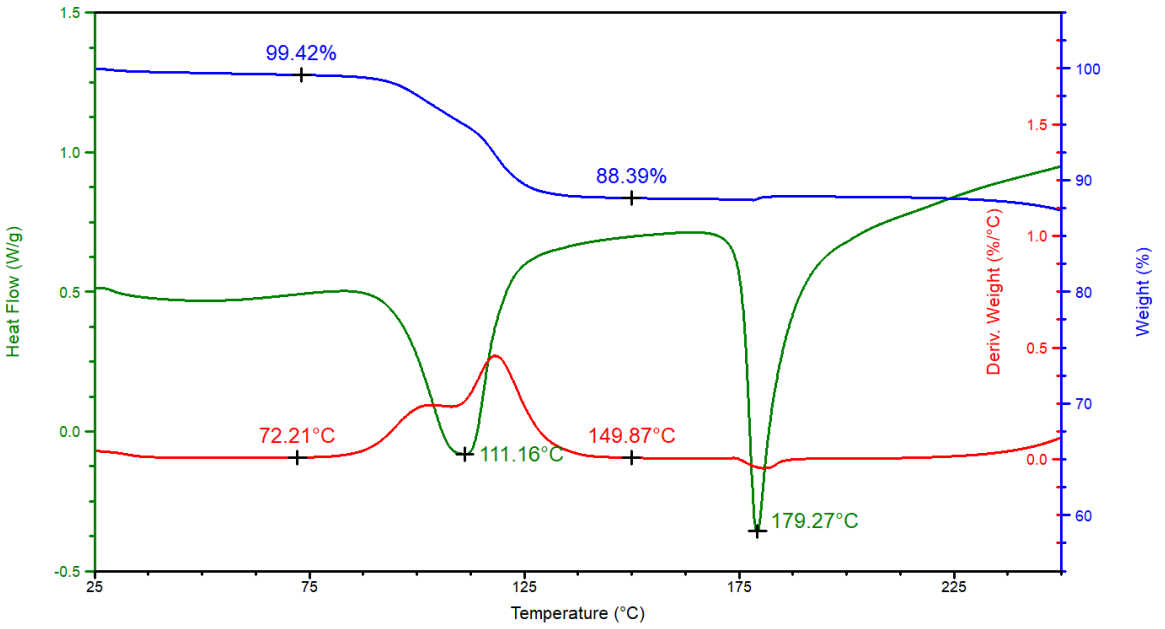
99.42%
88.39%
72.21°C
111.16°C
149.87°C
179.27°C
Heat Flow (W/g)
Deriv. Weight (%/°C)
Weight (%)
Temperature (°C)

f)

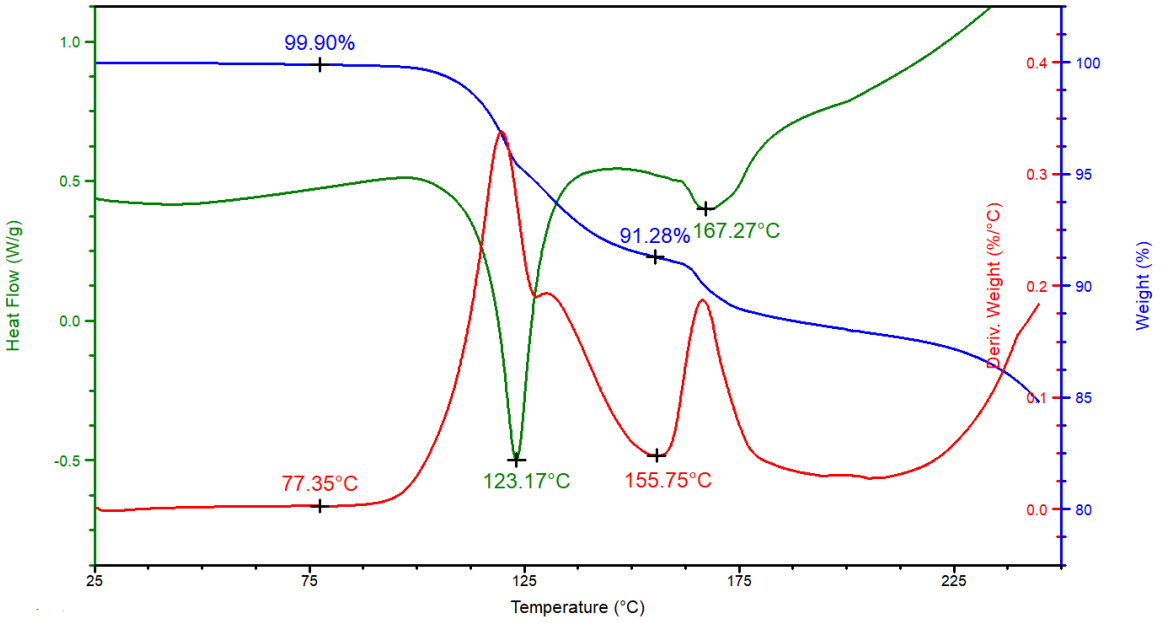

Figure 8.6. Thermograms for a) **H₁**·THF, b) **H₁**·furan, c) **H₁**·THT, d) **H₁**·thiophene, e) **H₁**·pyrrolidine and f) **H₁**·pyrrole [DSC (green), TG (blue) and DTG (red)].

Table 8.6. Temperatures of the thermal events that occur when heating each of the six complexes of **H₁**.

Guest (G)	T_{on} /°C	T_p /°C	Theoretical mass loss /%	Observed mass loss measured /%
THF	79.1	124.9	10.7	10.4
Furan	75.9	119.5	10.1	9.8
THT	79.1	134.9	12.7	10.7
Thiophene	71.7	129.5, 135.4	12.2	14.7
Pyrrolidine	72.2	111.2	10.5	11.0
Pyrrole	77.4	123.2	10.9	8.6

For all the complexes, the expected and observed mass losses are in reasonable agreement (Table 8.6). The relative thermal stabilities of these complexes were assessed by analysing and comparing the T_{on} and T_p values. Considering the saturated guest series, the more preferred THT and THF guests were released from the host crystal at the same temperature (79.1 °C) while the least preferred of these experienced a lower T_{on} value (pyrrolidine, 72.2 °C), in accordance, somewhat, with the host selectivity order. The T_{on} values for the aromatic guest series, unfortunately, did not adhere to the expected trend and the reasons for this observation could not be identified at this time. However, saturated guests THT and THF

exhibited increased thermal stabilities relative to their aromatic equivalents (THF/furan 79.1/75.9 and THT/thiophene 79.1/71.7 °C), while the results obtained for pyrrolidine/pyrrole (72.2/77.4 °C) are not as readily explained. After consideration of the T_p values, it was determined that preferred guests THT (134.9 °C) and thiophene (129.5 and 135.4 °C) possess the highest of these compared to their N- and O- containing analogues, which allude to higher thermal stabilities of these complexes.

8.1.8 Conclusions

H_1 was investigated for its host ability in the presence of five-membered heterocyclic guests and successfully clathrated the six heterocyclics, thiophene, THT, furan, THF, pyrrole and pyrrolidine, each with a 1:1 H:G ratio. Competition experiments were carried out which revealed that the host compound preferred the saturated heterocycles relative to the aromatic analogues (except for the pyrrolidine/pyrrole experiment in which the selectivity depended on the guest concentration). Independently, for the aromatic and saturated guest series', the host selectivity for the three different heteroatom-containing guests was in the order S > O > N. The selectivities were explained by considering SCXRD experiments: the saturated guests experienced a larger number and type of interactions with the host compared with the aromatic guests. Considering the saturated guests, THT experienced the greatest number and strongest interactions. Furthermore, Hirshfeld surface analyses explained the selectivity order of the host for the various heteroatomic guests, S > O > N, since the number of guest heteroatom···host interactions decreased in the same order. Thermal analyses also provided some insight in this regard, where complexes containing the preferred guests displayed higher thermal stabilities than the other competing guests, based on T_{on} and T_p values.

8.1.9 Supporting information

Relevant NMR and GC-MS data, the associated % e.s.d.s and crystallographic data for these inclusion compounds may be found in the Supplementary Information. The crystal structures were deposited at the Cambridge Crystallographic Data Centre, and CCDC 1867112 (**H_1**·THF), 1867113 (**H_1**·furan), 1867111 (**H_1**·THT), 1867110 (**H_1**·thiophene), 1867115 (**H_1**·pyrrolidine) and 1867114 (**H_1**·pyrrole) contain the supplementary crystallographic data for this section.

8.2 Inclusion compounds with $\mathbf{H_2}$

Surprisingly, no crystallization occurred when $\mathbf{H_2}$ was introduced to any of the five-membered ring heterocyclics. From previous sections, it was shown that $\mathbf{H_2}$ is much more selective than $\mathbf{H_1}$. At this stage, the reason for this behaviour cannot be explained with confidence, but it is presumed that $\mathbf{H_2}$ is unable to crystallize with an energetically feasible crystal packing to efficiently accommodate these guests.

9. ALKYL-SUBSTITUTED BENZENE COMPOUNDS

9.1. Inclusion compounds with **H_1**

9.1.1 Introduction

Toluene (TOL), ethylbenzene (EB) and cumene (CU) represent a series of aromatic molecules with increasing molecular weight and varying molecular shapes in their side-chain regions (Scheme 9.1). Barton *et al*. investigated the selectivity behaviour of host compounds TETROL and DMT when recrystallized from this guest series.[155,297] The study compared the behaviour of the two hosts to establish whether molecular shape influences the selectivity of the host. Therefore, in this present work, the host ability of **H_1** was also investigated in the presence of these alkyl aromatic guests, and the results are reported here. Note that, once more, these guests are non-isomeric but are structurally related.

TOL is isolated from crude oil and is a byproduct in the production of gasoline and high purity fuel from coal.[298] The final separation and purification of this compound is carried out by distillation or solvent extraction processes. However, TOL may also be produced inexpensively in the laboratory by a variety of methods, such as the reaction of benzene with methyl chloride in the presence of a Lewis acid.[244] TOL is mainly used as a precursor to produce benzene, a mixture of benzene and xylenes, or benzaldehyde and benzoic acid. It is a common solvent for paints, paint thinners, silicone sealants, chemical reactants, rubber, printing ink, adhesives, polishes, leather tanners, and disinfectants. It is also a precursor for toluene diisocyanate (used in the manufacture of foam), trinitrotoluene (the explosive, TNT), and several synthetic drugs.[244]

As mentioned in Chapter 3, EB occurs naturally in coal tar and petroleum. The main application is its use as an intermediate in the production of polystyrene, but it is often found in other manufactured products including pesticides, cellulose acetate, synthetic rubber, paints, and inks.[299] Currently, EB is produced on a large scale by combining benzene and ethylene in an acid-catalyzed chemical reaction. Additionally, small amounts are recovered from the mix of xylenes by an extension of the distillation process of these compounds.[300]

CU is a constituent of crude oil and refined fuels and is commercially produced by the Friedel-Crafts alkylation of benzene. The pure compound is usually then converted to cumene hydroperoxide, which is an intermediate in the synthesis of other industrially important chemicals, primarily phenol and acetone.[301]

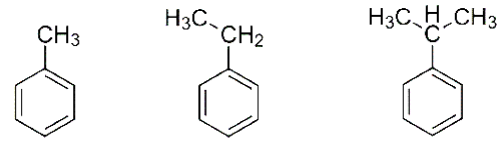

Toluene 111 °C | Ethylbenzene 136 °C | Cumene 152 °C

Scheme 9.1. Molecular structures of the potential guest compounds.

9.1.2 Individual inclusions

Host compound **H_1** was recrystallized from each of the organic solvents in the series, and Table 9.1 summarizes the results obtained after analysis of the so-formed crystals by ^{1}H-NMR spectroscopy. (The ^{1}H-NMR spectrum for the novel complex, **H_1**·TOL, is provided in the Supplementary Information, Figure S188.) **H_1** included the smaller guest molecules, TOL and EB, while the larger guest, CU, was not clathrated in this way. The H:G ratio was 1:1 for both of the successfully formed complexes.

Table 9.1. Results of the single solvent experiments and consequential H:G ratios.[a]

Guest (G)	H:G
TOL	1:1
EB	1:1
CU	[b]

[a]Determined using ^{1}H-NMR spectroscopy using $CDCl_3$ as solvent.
[b]Resultant crystals contained no guest.

Subsequently, the host selectivity was assessed by recrystallizing **H_1** from mixtures of these guests.

9.1.3 Equimolar competition experiments

The host was recrystallized from equimolar binary and ternary mixtures of the three alkyl aromatics which afforded mixed crystalline complexes. These were analysed by means of GC-FID in order to determine the G:G ratios. (^{1}H-NMR spectroscopy was not a suitable analytical technique here owing to G/G resonance signal overlap on the relevant spectra.) These experiments were conducted in duplicate, and the averaged guest ratios are provided in Table 9.2, with the % e.s.d.s in parentheses. (The complete set of data may be found in the Supplementary Information, Table S189.) The preferred guest is indicated in red, and the overall H:G ratios (determined by means of ^{1}H-NMR spectroscopy) are also provided.

Table 9.2. Results for **H$_1$** when presented with equimolar mixed alkyl aromatics.[a,b]

TOL	EB	CU	Average guest ratios	Overall H:G ratio	% e.s.d.s
x	x		91.8:8.2	1:1	(0.3):(0.3)
x		x	96.4:3.6	1:1	(0.3):(0.3)
	x	x	62.9:37.1	1:1	(0.8):(0.8)
x	x	x	89.9:8.2:1.9	1:1	(0.7):(0.5):(0.2)

[a]The mol% of the preferred guest in the mixed complexes is in red for ease of examination.
[b]The overall H:G ratio was determined by means of ^{1}H-NMR spectroscopy, and G:G ratios using GC-FID.

The resulting mixed complexes displayed an overall H:G ratio of 1:1 (Table 9.2). **H$_1$** was revealed to possess a significant preference for TOL (the smaller of the three guests) in all the experiments that contained this guest (TOL/EB, TOL/CU and TOL/EB/CU afforded mixed complexes with 91.8, 96.4 and 89.9% TOL present, respectively). In the absence of TOL, EB was favoured but to a much lesser extent (EB/CU, 62.9%). The host selectivity thus decreases in the order TOL > EB > CU which corresponds, interestingly, with guest size increase. We subsequently considered experiments where the guest molar ratios were varied in order to ascertain whether the host selectivity was guest concentration dependent.

9.1.4 Ratio-dependent competition experiments

Binary mixtures of varying concentrations were prepared, and **H$_1$** was recrystallized from each of these. After crystallization occurred, GC-FID was employed in order to determine the G:G ratios in both the complex and the solution, and these data afforded the selectivity profiles in

Figure 9.1. The average K value was calculated for each profile, while a complete set of the individual K values are provided in the Supplementary Information, Tables S190–192.

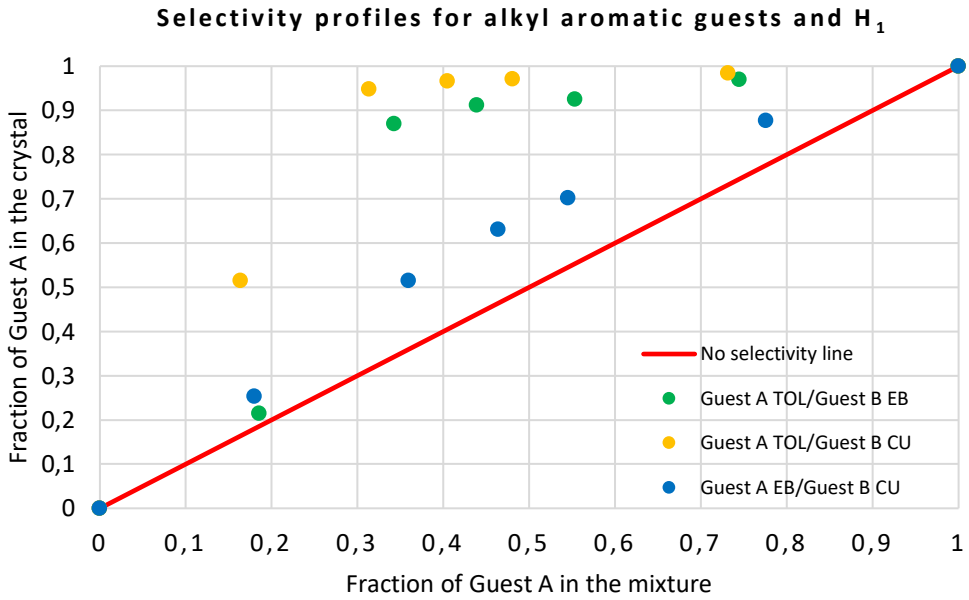

Figure 9.1. Selectivity profiles for **H₁** when recrystallized from binary solutions containing varying concentrations of the alkyl aromatic guests.

H₁ displayed enhanced selectivity towards TOL (Figure 9.1) when recrystallized from binary mixtures containing this guest, even if the solution contained low concentrations of TOL. This is clear in both the TOL/EB (green) and TOL/CU (yellow) profiles, and K values were calculated to be 9.7 and 29.5, respectively. In the absence of TOL [the EB/CU experiment (blue profile)], the host selectivity was much reduced, and only a slight preference for EB was observed (K = 1.9). Based on these results, the host selectivity order was once again found to be in the order TOL > EB > CU. In order to rationalize these findings, SCXRD experiments were carried out on the successfully formed complexes.

9.1.5 SCXRD

Table 9.3 lists crystallographic data and refinement parameters for the **H₁**·TOL complex, while Figure 9.2a and b depicts the unit cell and calculated voids after guest removal from the packing calculation, respectively. (Note that these data and figures for **H₁**·EB were provided in Chapter 3.)

Table 9.3. Crystallographic data for complexes of **H_1** with TOL.

	H_1·TOL
Chemical formula	$C_{40}H_{32}N_2S_2 \cdot C_7H_8$
Formula weight	696.93
Crystal system	Monoclinic
Space group	$P2_1/n$
μ (Mo Kα)/mm^{-1}	0.187
a/Å	10.4791(5)
b/Å	13.3723(7)
c/Å	25.4054(1)
alpha/°	90
beta/°	91.115(2)
gamma/°	90
V/$Å^3$	3567.8(3)
Z	4
F(000)	1472
Temp./K	200
Restraints	0
Nref	8904
Npar	469
R	0.0379
wR2	0.1003
S	1.03
θ min–max/°	1.7, 28.4
Tot. data	76887
Unique data	8904
Observed data [I > 2.0 sigma(I)]	7079
R_{int}	0.031
Dffrn measured fraction θ full	1.000
Min. resd. dens. (e/$Å^3$)	–0.23
Max. resd. dens. (e/$Å^3$)	0.32

a) b)

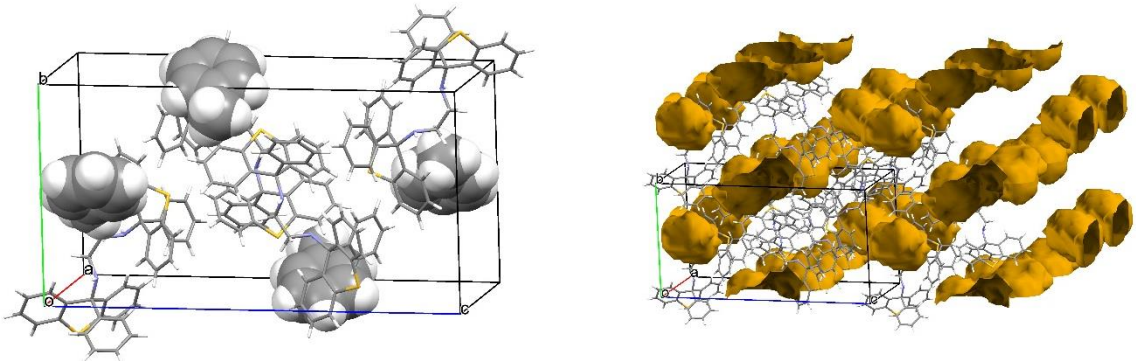

Figure 9.2. a) Unit cell and b) calculated voids (dark yellow) for **H_1**·TOL.

The **H$_1$**·TOL inclusion compound crystallizes in the monoclinic crystal system and $P2_1/n$ space group (Table 9.3) and does not experience an isostructural host packing with the EB-containing complex (Figure 9.3), [see Table 3.4 (triclinic, *P*-1)]. Additionally, the guests in **H$_1$**·TOL are accommodated in discrete cavities (Figure 9.2b). Interestingly, the host molecule conformations were found to be similar in the two complexes (with TOL and EB) in that the tricyclic fused ring system of **H$_1$** adopted a buckled geometry that deviated from linearity by between 29.1 and 30.5° (Figure 9.4 displays the geometry of **H$_1$** in the **H$_1$**·TOL and **H$_1$**·EB complexes). Also notable is the geometry in the ethylenediamine linker where the nitrogen atoms in **H$_1$** assume a synclinal (gauche) conformation in both complexes.

a) b)

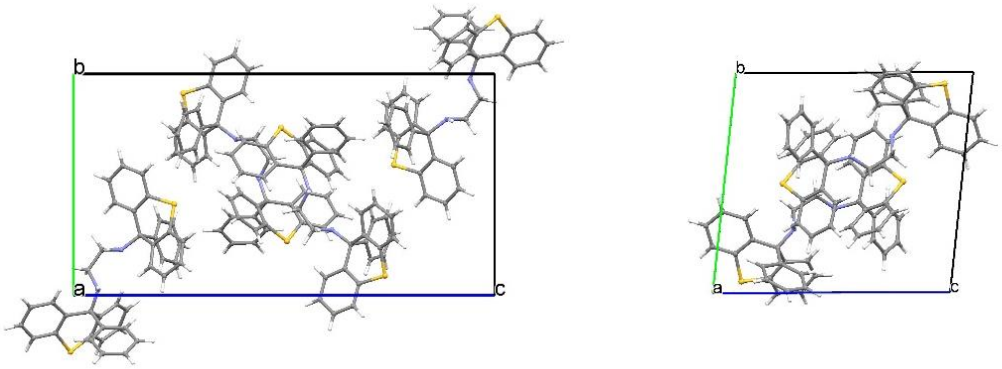

Figure 9.3. Host packing in complexes a) **H$_1$**·TOL and b) **H$_1$**·EB; guests were removed for clarity.

a) b)

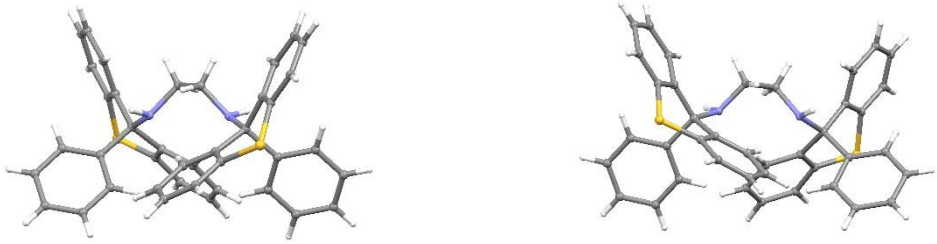

Figure 9.4. Host geometry in complexes a) **H$_1$**·TOL and b) **H$_1$**·EB.

Table 9.4 contains a summary of the significant H···G interactions, while a detailed table showing all interactions may be found in the Supplementary Information (Table S193).

Table 9.4. H···G interactions present in complexes of **H$_1$**.[a,b,c]

Non-covalent interaction	**H$_1$**·TOL	Symmetry
π···π	5.045(1)–5.919(1) Å [8]	
C–H···π (H···Cg, C–H···Cg) $C_{(G)}$–$H_{(G)}$···$Cg_{(H)}$	 2.66 Å, 162°	 3/2–x, –1/2+y, 1/2–z
Other short contacts (X···Z, X–Y···Z) $C_{(H)}$–$H_{(H)}$···$H_{(G)}$–$C_{(G)}$ $C_{(H)}$–$H_{(H)}$···$H_{(G)}$–$C_{(G)}$	 2.35 Å, 138° (<) 2.37 Å, 129° (<)	 3/2–x, 1/2+y, 1/2–z x, y, z

[a]A detailed table of H···H and H···G interactions can be found in the Supplementary Information (Table S193).
[b]Values in square brackets indicate the number of H···G π···π interactions.
[c]Distances denoted by < are contacts that measure less than the sum of the van der Waals radii of the atoms involved.

The high selectivity of **H$_1$** for TOL compared with EB may be rationalized by the fact that TOL experiences two short contacts [2.35 Å (138°) and 2.37 Å (129°)] and one C–H···π interaction [2.66 Å (162°)] (Table 9.4), while EB was held within the crystal by means of only one C–H···π contact [2.99 Å (155°) and 2.88 Å (163°) for the two disordered components] (see Table 3.5).

9.1.6 Hirshfeld surface analyses

Hirshfeld surface analyses were carried out on the successfully formed complexes, but the results obtained could not be used to explain the high selectivity of **H$_1$** for TOL since, quantitatively, the interactions experienced by both guests are comparable in both **H$_1$**·TOL and **H$_1$**·EB, as depicted in Figure 9.5.

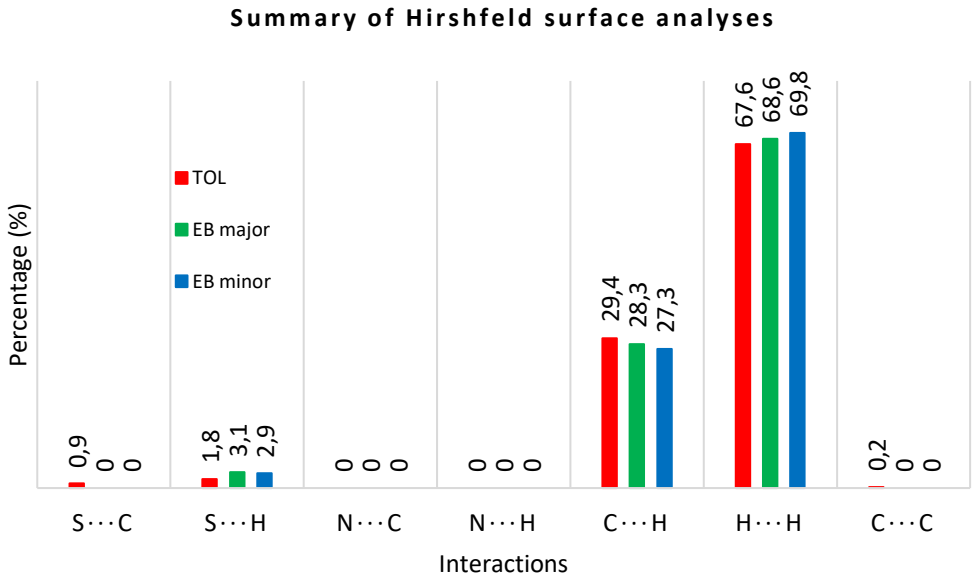

Figure 9.5. Graphical summary of Hirshfeld surface analyses.

9.1.7 Thermal analyses (DSC and TG)

Figure 9.6 illustrates the overlaid DSC (green), TG (blue) and DTG (red) traces that were obtained upon thermal analysis of the TOL-containing complex. The guest in this complex is released, largely, in one step which is followed by an endotherm representing the host melt. Table 9.5 summarizes the relevant thermal data obtained from these traces.

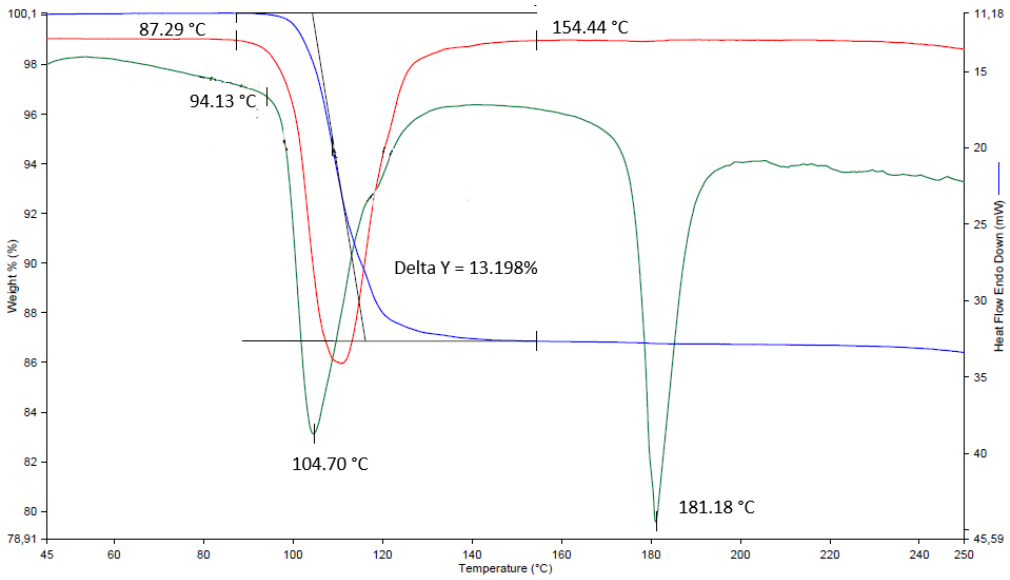

Figure 9.6. Overlaid thermal traces (DSC, TG and DTG) for **H₁**·TOL.

Table 9.5. Thermal properties of complexes formed with **H₁**.

Complex	T_{on} /°C	T_p /°C	Mass loss expected /%	Mass loss observed /%
H₁·TOL	87.3	104.7	13.2	13.2

The observed mass loss for the complex is in direct agreement with that expected (13.2%, Table 9.5). The T_{on} values also correlate very closely with selectivity considerations made from previous experiments: the onset temperature of guest release by **H₁** for TOL (87.3 °C) is significantly increased compared with that for EB (49.7 °C, see Table 3.6), alluding to TOL being held more tightly in the host crystal relative to EB, and hence the enhanced preference of **H₁** for this guest. T_p values also correlate with this order [TOL (104.7 °C) > EB (81.3 °C)].

9.1.8 Conclusions

The host compound **H_1** included the smaller guests TOL and EB but not the larger CU compound. Competition experiments highlighted these host behaviour differences further: the host selectivity was found to be in the order TOL > EB > CU. Observations made from SCXRD analyses carried out on these complexes correlated with the selectivity order: the enhanced preference of **H_1** for TOL was rationalized by the fact that the host was involved in stronger and a greater number of interactions with TOL relative to EB. Thermal analyses were also considered for the single solvent inclusion compounds and, once more, results were in accordance with the host selectivity orders: the preferred guest for **H_1**, TOL, displayed a higher relative thermal stability, based on the T_{on} and T_p values, compared with EB.

9.1.9 Supporting information

All spectra and detailed tables that are relevant to this section are provided in the Supplementary Information. The crystal structure was deposited at the Cambridge Crystallographic Data Centre, and CCDC number 1905942 (**H_1**·TOL) contains the supplementary crystallographic data.

9.2. Inclusion compounds with **H_2**

9.2.1 Introduction

For comparative purposes, the host ability of **H_2** was evaluated with the same guest series to investigate how small variances in the host structure would affect the host behaviour in the presence of these alkyl aromatic guests.

9.2.2 Individual inclusions

Surprisingly, in direct contrast to the inclusion abilities displayed by **H_1**, **H_2** formed complexes with the larger guest, CU (H:G ratio 1:1), but not with the smaller TOL and EB compounds (Table 9.6). (The ^{1}H-NMR spectrum for the CU-containing complex may be found in the Supplementary Information, Figure S194.)

Table 9.6. Results of the single solvent experiments and consequential H:G ratios.[a]

Guest (G)	H:G
TOL	[b]
EB	[b]
CU	1:1

[a]Determined using ^{1}H-NMR spectroscopy using $CDCl_3$ as solvent.
[b]Resultant crystals contained no guest.

These opposing results required the selectivity of the host to be assessed by recrystallizing **H_2** from mixtures of these guests.

9.2.3 Equimolar competition experiments

After recrystallizing **H_2** from equimolar binary and ternary mixtures of these guests, the resultant mixed complexes were analysed by means of GC-FID in order to determine the G:G ratios. These experiments were, once more, carried out in duplicate and the averaged guest ratios are provided in Table 9.7, together with the % e.s.d.s (in parentheses) and overall H:G ratios. Preferred guests are indicated in red. (The duplicate data for these experiments may be found in the Supplementary Information, Table S195.)

Table 9.7. Results for **H_2** when presented with equimolar mixed alkyl aromatics.[a,b]

TOL	EB	CU	Average guest ratios	Overall H:G ratio	% e.s.d.s
x	x		[c]	-	-
x		x	[c]	-	-
	x	x	48.6:51.4	1.0:0.5	(1.5):(1.5)
x	x	x	[c]	-	-

[a]The mol% of the preferred guest in the mixed complexes is in red for ease of examination.
[b]The overall H:G ratio was determined by means of ^{1}H-NMR spectroscopy, and G:G ratios using GC-FID.
[c]Resultant crystals contained no guest.

H_2 only formed a complex from the equimolar EB/CU mixture, and the host selectivity was rather ambivalent here, with only a slight preference (51.4%) for the larger guest (CU). Consequently, experiments where the guest molar ratios were varied were considered. This would assess the host behaviour over a concentration range and convey additional information, if any, on the host selectivity.

9.2.4 Ratio-dependent competition experiments

When the molar ratios of the guests in binary mixtures were varied and the host recrystallized from these, the resulting crystals were once again analysed by employing GC-FID to determine the amount of each guest in both the complex and the solution from which the complex emanated. These data were employed to construct the selectivity profile in Figure 9.7. (Note that the profiles for mixtures of TOL/CU and TOL/EB could not be constructed here since the formed crystals were found to be only the apohost **H₂**.)

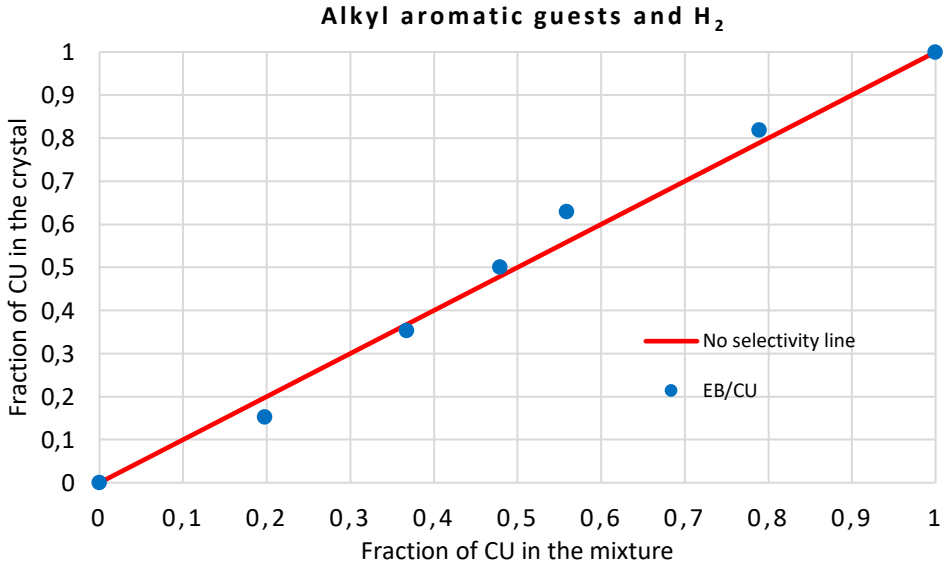

Figure 9.7. Selectivity profile for **H₂** when recrystallized from binary solutions containing varying concentrations of the EB and CU guests.

H₂ exhibited poor selectivity when recrystallized from EB/CU mixtures (Figure 9.7), and data points deviated only very slightly from the straight line that represents no selectivity. (K values for each data point are provided in the Supplementary Information, Table S196, and range between 1.1 and 1.4.)

9.2.5 SCXRD

The guest in **H₂**·CU displays positional disorder, which was modelled satisfactorily, and Table 9.8 lists crystallographic data and refinement parameters. The complex crystallized in a triclinic *P*-1 crystal system and no host packing isostructurality was evident with any of the complexes of **H₁** (considering complexes with both EB and TOL). The unit cell of the complex

is depicted in Figure 9.8a, and Figure 9.8b displays the calculated voids after guest removal: guests are accommodated in constricted channels.

Table 9.8. Crystallographic data for complexes of **H_2** with CU.

	H_2·CU
Chemical formula	$C_{40}H_{32}N_2O_2 \cdot C_9H_{12}$
Formula weight	692.84
Crystal system	Triclinic
Space group	*P*-1
μ (Mo Kα)/mm^{-1}	0.074
a/Å	9.1545(5)
b/Å	14.6714(7)
c/Å	15.1254(8)
alpha/°	109.272(2)
beta/°	92.888(2)
gamma/°	97.644(2)
V/Å^3	1890.9(2)
Z	2
F(000)	736
Temp./K	200
Restraints	20
Nref	9360
Npar	452
R	0.0667
wR2	0.2038
S	1.04
θ min−max/°	2.3, 28.4
Tot. data	53340
Unique data	9360
Observed data [I > 2.0 sigma(I)]	7030
R_{int}	0.022
Dffrn measured fraction θ full	0.999
Min. resd. dens. (e/Å^3)	–0.68
Max. resd. dens. (e/Å^3)	0.84

a) b)

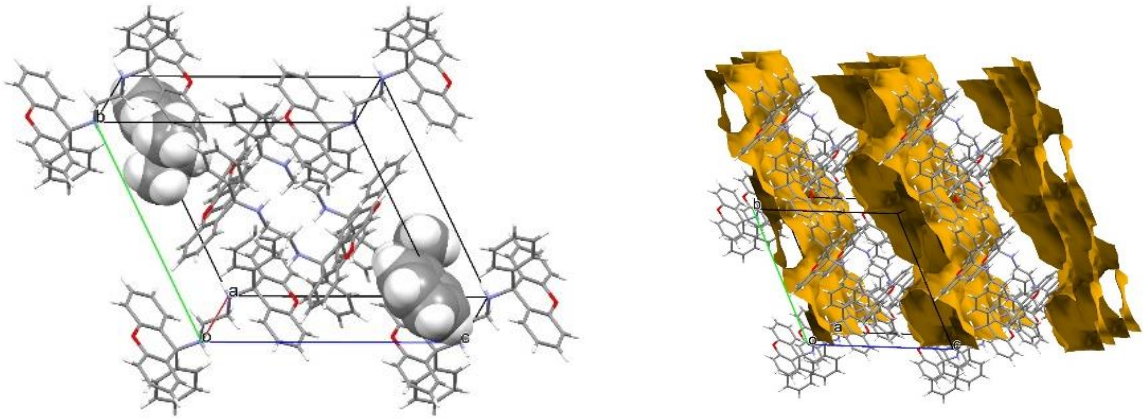

Figure 9.8. a) Unit cell and b) calculated voids (dark yellow) for **H_2**·CU.

When considering the host geometry and packing, the tricyclic fused ring system is near-planar (the deviation from linearity measures only 2.1°), and this is evident in Figure 9.9a. Also notable is the geometry difference in the ethylenediamine linker where the nitrogen atoms in **H_1** assume a synclinal (gauche) conformation, while in **H_2** these are antiperiplanar with respect to one another. **H_2** displays a very ordered host–host packing (Figure 9.9b) that is facilitated by the more planar O-containing ring and more linear linker. For **H_1**, on the other hand, the buckled S-containing ring and gauche N/N linker results in less ordered packing. This observation may be the reason for the contrasting behaviour of the two host compounds in the presence of these guests.

a) b)

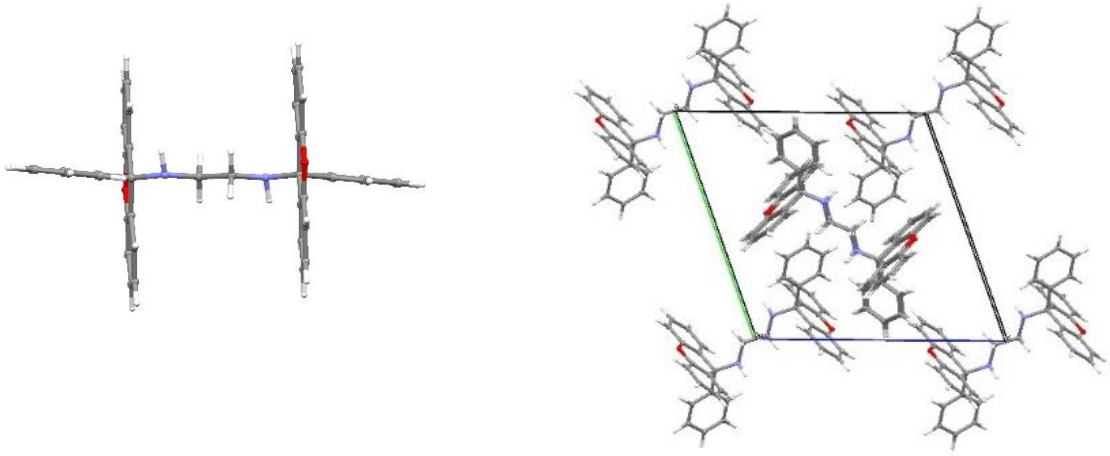

Figure 9.9. Host a) geometry and b) packing in **H_2**·CU; guests were removed for ease of examination.

Since CU was the only successfully included guest, the results of the SCXRD experiments could not be compared with any other data for this host. Table 9.9 contains a summary of the significant H···G interactions, while a detailed table showing all interactions (H···G and H···H) may be found in the Supplementary Information (Table S197).

Table 9.9. H···G interactions present in complexes of **H_2**.[a,b,c,d]

Non-covalent interaction	**H_2**·CU	Symmetry
π···π	4.529(3)–5.967(2) Å [G1 8] [G2 7]	
C–H···π (H···Cg, C–H···Cg) $C_{(H1)}$–$H_{(H1)}$···$Cg_{(G1)}$	 3.00 Å, 117°	 x, y, z
Other short contacts (X···Z, X–Y···Z) $C_{(H1)}$–$C_{(H1)}$···$C_{(G1)}$–$C_{(G1)}$ $C_{(G1)}$–$H_{(G1)}$···$C_{(H2)}$–$O_{(H2)}$ $C_{(G2)}$–$H_{(G2)}$···$C_{(H1)}$–$O_{(H2)}$ $C_{(G1)}$–$C_{(G1)}$···$H_{(H1)}$–$C_{(H2)}$	 3.33 Å, 112° (<) 2.83 Å, 169° (<) 2.72 Å, 150° (<) 2.88 Å, 131° (<)	 x, y, z x, –1+y, z x, –1+y, z –x, –y, –z

[a]A detailed table of H···H and H···G interactions may be found in the Supplementary Information (Table S197).
[b]Values in square brackets indicate the number of H···G π···π interactions.
[c]Guest 1 (G1), Guest 2 (G2), Host 1 (H1) and Host 2 (H2) represent the disordered components in the crystal.
[d]Distances denoted by < are contacts that measure less than the sum of the van der Waals radii of the atoms involved.

CU is clathrated in the host crystal by means of a number of very weak π···π [4.529(3)–5.967(2) Å (G1 8 H···G and G2 7 H···G)], one C–H···π (3.00 Å, 117°) and multiple other short interactions (2.72–3.33 Å, 112–169°).

9.2.6 Hirshfeld surface analyses

Due to the extent of the disorder in the **H_2**·CU complex, Hirshfeld surface analysis could not be carried out on this complex.

9.2.7 Thermal analyses (DSC and TG)

In Figure 9.10, the DSC (green), TG (blue) and DTG (red) traces are overlaid after a thermal experiment on the **H_2**·CU complex. The guest release process is somewhat convoluted, and the relevant thermal data obtained from these traces are summarized in Table 9.10. The observed mass loss is in reasonable agreement with that expected (14.9 and 16.2%, respectively) and, once again, these thermal data could not be compared to other samples, since CU was the only guest to be included from this series by **H_2**. Initial guest release occurs at 40.6 °C, and the process appears to take place over two steps (T_p values of 63.4 and 89.6 °C). This is then followed by an endotherm that represents the host melt, which has a peak temperature of 215.6 °C.

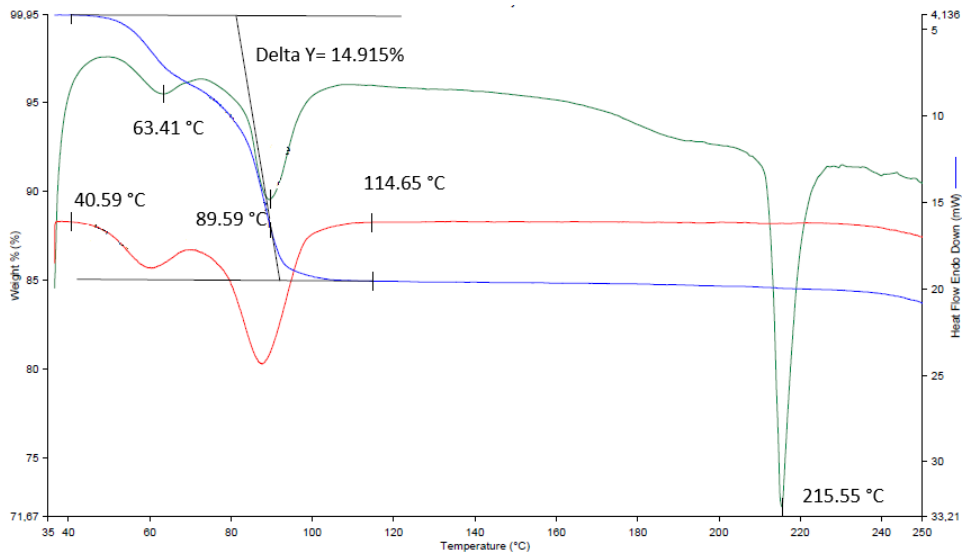

Figure 9.10. Overlaid thermal traces (DSC, TG and DTG) for **H₂**·CU.

Table 9.10. Thermal properties of complexes formed with **H₂**.

Complex	T_{on} /°C	T_p /°C	Mass loss expected /%	Mass loss observed /%
H₂·CU	40.6	63.4, 89.6	16.2	14.9

9.2.8 Conclusions

The two host compounds displayed opposing inclusion abilities, with **H₁** clathrating the smaller guests (TOL and EB, but not CU) and **H₂** the larger guest (CU, but not TOL nor EB). Competition experiments further highlighted these host behaviour differences: the host selectivity was found to be in the order TOL > EB > CU for **H₁**, but CU ≥ EB for **H₂**. SCXRD analyses were carried out on the **H₂**·CU complex, but data could not be compared to any further structures of **H₂** since CU was the only guest from this series to be included by the host. It was suggested that the opposing host behaviours may be as a result of the difference in the geometries of both the tricyclic fused ring systems and the ethylenediamine linkers in the two host compounds. Thermal analyses were also considered for the single solvent inclusion compound.

Interestingly, **H₁** and **H₂** once again, displayed opposing host behaviour when presented with non-isomeric guests and this could be attributed to the geometry and resultant packing of the respective host compounds, which certainly affect the H···G interactions in the complexes.

9.2.9 Supporting information

All spectra and detailed tables that are relevant to this section are provided in the Supplementary Information. The crystal structure was deposited at the Cambridge Crystallographic Data Centre, and CCDC number 1905945 (**H_2**·CU) contains the supplementary crystallographic data.

10. ANILINE AND *N*-ALKYL-SUBSTITUTED DERIVATIVES

10.1. Inclusion compounds with $\mathbf{H_1}$

10.1.1 Introduction

After identifying the opposing host behaviour of $\mathbf{H_1}$ and $\mathbf{H_2}$ in the previous chapter, it was deemed of interest to carry out the same experiments in the presence of the aniline guest series , namely aniline (ANL), *N*-methylaniline (NMA) and *N*,*N*-dimethylaniline (NNDMA) (Scheme 10.1). Barton *et al*.[155,297] reported that the guest pairs TOL/ANL, EB/NMA and CU/NNDMA have certain common structural features but that there are also significant electronic differences. In the present work, the host behaviour of $\mathbf{H_1}$ and $\mathbf{H_2}$ will be investigated in the presence of this non-isomeric guest series (ANL, NMA and NNDMA).

ANL is commercially synthesized by the nitration of benzene to yield nitrobenzene, which is then hydrogenated in the presence of metal catalysts.[302] Alternatively, ANL is prepared from ammonia and phenol.[303] The largest application of ANL is for the manufacture of precursors for the production of polyurethane and other industrial chemicals such as rubber processing compounds, herbicides, pharmaceuticals, and dyes and pigments.[303]

NMA is synthesized via the methylation reaction of ANL and is used as an antiknocking agent (for petroleum refinement), and also as an intermediate for dyes and agrochemicals, amongst others.[304]

NNDMA is prepared by reacting ANL with iodomethane or methanol in the presence of an acid catalyst, or by employing dimethyl ether in the methylation reaction.[305,306] NNDMA is a key precursor to commercially important dyes such as malachite green and crystal violet,[307] serves as a promoter in the curing of polymer resins, and is also used as a precursor to other important organic compounds.[304]

The separation of these three compounds is of industrial importance since it is carried out through fractional distillation, and the process is challenging due to their similar boiling points (184.2, 196.2 and 194.2 °C, for ANL, NMA and NNDMA, respectively). Alternative methods have been considered to obtain these compounds in their pure form, such as selective *N*-

alkylation through better reaction control, [308,309] but improved alternative separation techniques remain appealing. In the present work, the affinity and possible selectivity of **H_1** and **H_2** in the presence of these guests is investigated for possible future application in their separation.

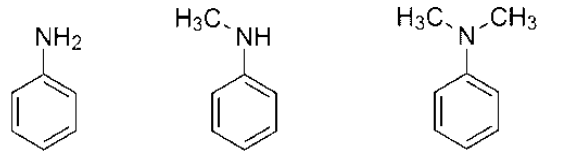

Aniline 184 °C | *N*-Methylaniline 196 °C | *N*,*N*-Dimethylaniline 194 °C

Scheme 10.1. Molecular structures of the guests in the aniline series.

10.1.2 Individual inclusions

The affinity of **H_1** for the anilines was assessed by recrystallizing the host independently from each of the three organic solvents. Table 10.1 summarizes the results obtained after analysis of the so-formed crystals by means of ^{1}H-NMR spectroscopy. Interestingly, **H_1** exhibited similar inclusion trends in the presence of the aniline series compared to the alkyl aromatic series (Chapter 9), and the host included only the smaller guest molecules, ANL and NMA, while the larger guest, NNDMA, was not clathrated in this manner. (**H_1** included TOL and EB from the alkyl aromatic series, and not CU). (The ^{1}H-NMR spectra for the complexes are provided in the Supplementary Information, Figures S198−199.)

Table 10.1. Results of the single solvent experiments and consequential H:G ratios.[a]

Guest (G)	H:G
ANL	1:1
NMA	1:1
NNDMA	[b]

[a]Determined using ^{1}H-NMR spectroscopy with $CDCl_3$ as solvent.
[b]Resultant crystals contained no guest.

Following these results, the selectivity of the host was investigated by recrystallization experiments involving mixtures of these aniline guests.

10.1.3 Equimolar competition experiments

After the host was recrystallized from equimolar binary and ternary mixtures of the anilines, the resultant crystals were analysed by means of GC-FID in order to determine the G:G ratios (^{1}H-NMR spectroscopy was, once again, not a suitable analytical method due to the overlap of important resonance signals). These experiments were conducted in duplicate and the averaged guest ratios are provided in Table 10.2. (The duplicate data may be found in the Supplementary Information, Table S200.) The overall H:G ratios were determined by means of ^{1}H-NMR spectroscopy, and these are also provided in the table, together with the % e.s.d.s in parentheses.

Table 10.2. Results of recrystallization experiments of **H$_1$** from equimolar mixed anilines.[a,b]

ANL	NMA	NNDMA	Average guest ratios	Overall H:G ratio	% e.s.d.s
x	x		89.1:10.9	1:1	(0.9):(0.9)
x		x	92.2:7.8	1:1	(1.5):(1.5)
	x	x	[c]	-	-
x	x	x	89.2:5.8:5.0	1:1	(0.3):(0.1):(0.2)

[a]The mol% of the preferred guest in the mixed complexes is in red for ease of examination.
[b]The overall H:G ratio was determined by means of ^{1}H-NMR spectroscopy, and G:G ratios using GC-FID.
[c]Resultant crystals contained no guest.

Once more, similar trends were observed for experiments with the anilines as with the alkyl aromatic series (Chapter 9). **H$_1$** displayed an enhanced selectivity for the smaller ANL guest in the ANL/NMA (89.1%), ANL/NNDMA (92.2%) and ANL/NMA/NNDMA (89.2%) experiments while, in the absence of ANL (the NMA/NNDMA experiment), a complex was not formed and the isolated solid was the pure apohost compound (Table 10.2). The host selectivity thus decreased as guest size increased (ANL > NMA > NNDMA), as was the case for the alkyl aromatics (TOL > EB > CU, see Table 9.2).

The host selectivity was further investigated by varying the molar ratios of guests in binary mixtures to provide information on whether the host selectivity is guest concentration dependent.

10.1.4 Ratio-dependent competition experiments

Binary mixtures with varying concentrations of the aniline guests were prepared and **H$_1$** was recrystallized from each of these. Thereafter, GC-FID was employed in order to determine the G:G ratios in both the complex and the solution. These data were utilized to construct the selectivity profiles in Figure 10.1, and the average selectivity coefficient was calculated for each profile. (The complete set of K values are provided in the Supplementary Information, Tables S201–202). Note that the profile for the NMA/NNDMA experiment could not be constructed here owing to the fact that crystals that formed from the various G/G solutions contained no guest species.

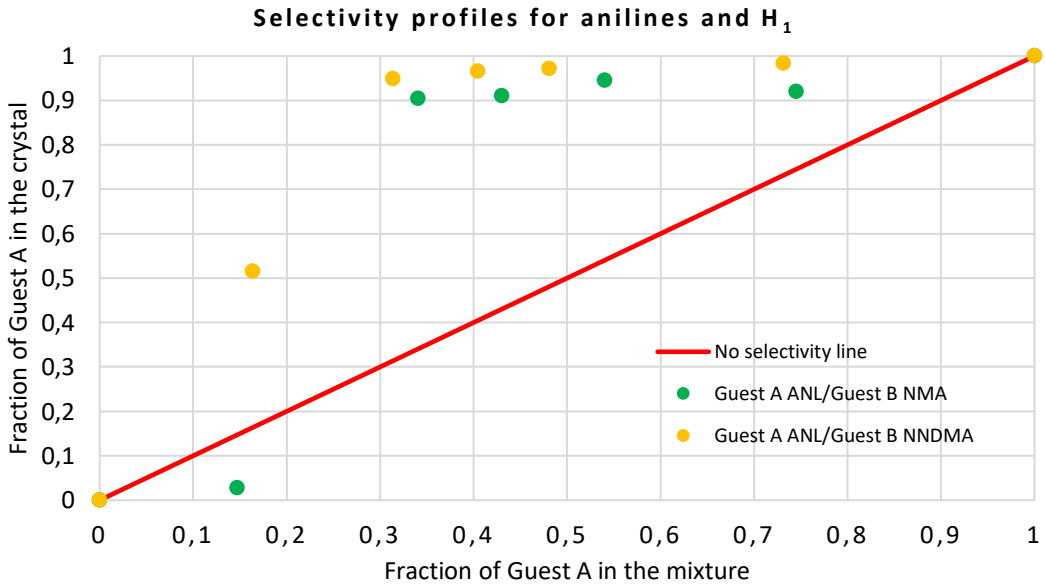

Figure 10.1. Selectivity profiles of **H$_1$** when recrystallized from binary solutions containing varying concentrations of the aniline guests.

Similar to the results for the alkyl aromatic series where TOL was preferred (Chapter 9), the selectivity of **H$_1$** for ANL in the presence of NMA (green profile) and NNDMA (yellow profile) was significant and, in the latter investigation, the average K value was determined to be 8.7. An exception was noted in the ANL/NMA experiments where, at low concentrations of ANL (< 15%), NMA was preferred, but at higher concentrations of ANL, the selectivity changed significantly in favour of ANL, with the highest K value calculated to be 12.0 (at ~34% ANL/66% NNDMA of these guests).

In order to elucidate the reasons for the enhanced selectivity of **H_1** for ANL, the various H···G interactions that are involved in these complexes were considered by means of SCXRD.

10.1.5 SCXRD

These experiments were carried out on both **H_1**·ANL and **H_1**·NMA. Guests in the former complex display positional disorder and, as a result, the hydrogen (of the nitrogen) positions could not be determined. Table 10.3 lists the crystallographic data and refinement parameters for these inclusion compounds.

Table 10.3. Crystallographic data for complexes of **H_1** with ANL and NMA.

	H_1·ANL	**H_1**·NMA
Chemical formula	$C_{40}H_{32}N_2S_2 \cdot C_6H_7N$	$C_{40}H_{32}N_2S_2 \cdot C_7H_9N$
Formula weight	695.90	711.95
Crystal system	Monoclinic	Triclinic
Space group	$P2_1/n$	P-1
μ (Mo Kα)/mm^{-1}	0.190	0.184
a/Å	10.3099(3)	10.5138(7)
b/Å	13.3066(4)	13.5904(9)
c/Å	25.6537(8)	13.7298(9)
alpha/°	90	84.174(3)
beta/°	91.686(1)	86.227(2)
gamma/°	90	70.040 (3)
V/Å^3	3517.90(18)	1833.4(2)
Z	4	2
F(000)	1464	752
Temp./K	200	200
Restraints	15	0
Nref	8699	9100
Npar	448	482
R	0.0444	0.0364
wR2	0.1160	0.0972
S	1.02	1.02
θ min–max/°	1.6, 28.3	2.1, 28.3
Tot. data	49190	53745
Unique data	8699	9100
Observed data [I > 2.0 sigma(I)]	6688	7547
R_{int}	0.029	0.020
Dffrn measured fraction θ full	1.000	1.000
Min. resd. dens. (e/Å^3)	–0.32	–0.32
Max. resd. dens. (e/Å^3)	0.45	0.32

H₁·ANL crystallizes in the monoclinic crystal system and $P2_1/n$ space group while the less favoured guest, NMA, preferred a different host packing (triclinic, *P*-1). (Note that the complexes with the preferred guests for the respective aniline and alkyl aromatic guest series', **H₁**·ANL and **H₁**·TOL, share isostructural host packing.) The unit cells of the two aniline complexes are depicted in Figure 10.2.

a) b)

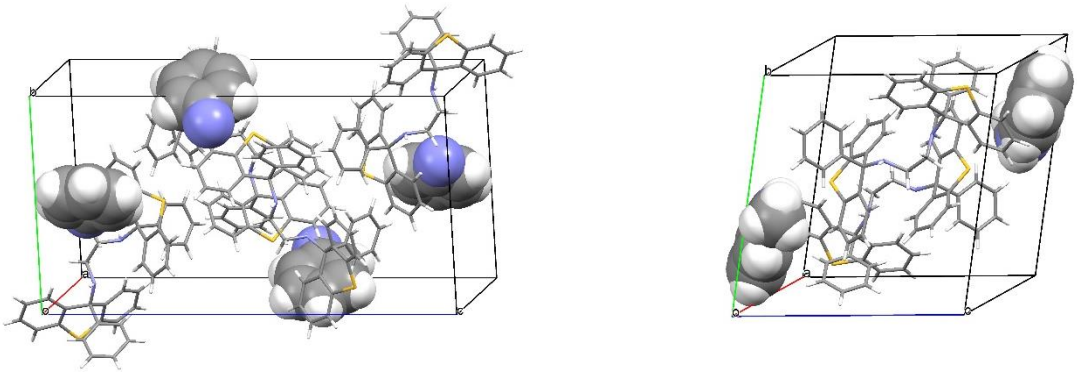

Figure 10.2. Unit cells for a) **H₁**·ANL and b) **H₁**·NMA; guests are in spacefill and hosts in stick representation.

In both complexes, the host adopted similar geometries (Figure 10.3), where the buckled nature of the central ring of the thioxanthenyl moiety is evident. The deviation from planarity of these units was calculated to range between 28.4 and 31.6°. The ethylenediamine linker adopted a synclinal (gauche) arrangement with respect to the two N atoms. These features were also observed for the complexes of **H₁** in the presence of the alkyl aromatic guests.

a) b)

Figure 10.3. Host geometry in complexes a) **H₁**·ANL and b) **H₁**·NMA.

The nature of the host packing is depicted in Figure 10.4a and b for both complexes after guest removal. Once more, the host–host packing appears less tightly packed compared with that in complexes with **H₂**.

a) b)

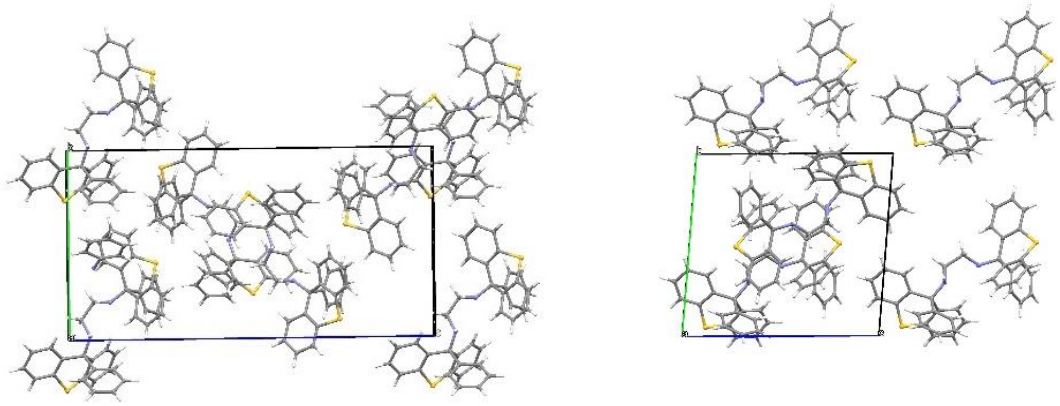

Figure 10.4. Host packing in complexes a) **H$_1$**·ANL and b) **H$_1$**·NMA; guests were removed for ease of examination.

Subsequently, the guests were removed from the packing calculation, and the resultant voids (Figure 10.5) showed that the guests in **H$_1$**·ANL are accommodated in discrete cavities, while the less favoured guest (NMA) occupies constricted channels in the host crystal.

a) b)

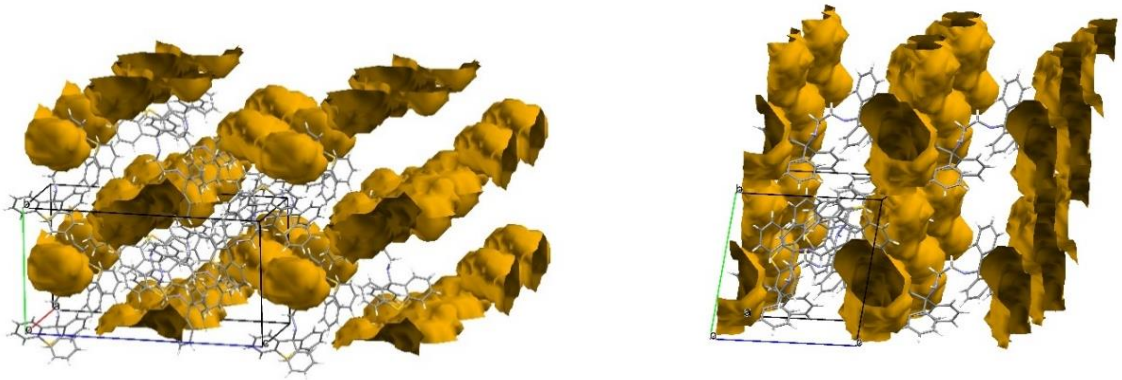

Figure 10.5. Calculated voids (dark yellow) for a) **H$_1$**·ANL and b) **H$_1$**·NMA.

The more significant H···G and G···G interactions were then considered, and Table 10.4 contains a summary of these, while a detailed table showing all interactions (H···G, H···H and G···G) may be found in the Supplementary Information (Table S203).

Table 10.4. H···G and G···G interactions present in complexes of **H_1**.[a,b,c,d]

Non-covalent interaction	**H_1**·ANL	**H_1**·NMA·0.406(H_2O)	Symmetry
π···π	4.717(4)–5.935(3) Å [G1 7] [G2 8]	4.935(1)–5.893(1) Å [7]	
C–H···π (H···Cg, C–H···Cg)			
$C_{(G)}$–$H_{(G)}$···$Cg_{(H)}$		2.93 Å, 140°	–x, 1–y, 1–z
X–Y···π (H···Cg, C–H···Cg)			
$C_{(G1)}$–$N_{(G1)}$···$Cg_{(H)}$	3.52(1) Å, 109°		2–x, 1–y,1–z
Other short contacts (X···Z, X–Y···Z)			
$C_{(H)}$–$H_{(H)}$···$H_{(G)}$–$C_{(G)}$		2.37 Å, 143° (<)	x, 1+y, 1+z
$C_{(H)}$–$H_{(H)}$···$H_{(G1)}$–$C_{(G1)}$	2.34 Å, 134° (<)		–1/2+x, 1/2–y, –1/2+z
$C_{(H)}$–$H_{(H)}$···$H_{(G2)}$–$C_{(G2)}$	2.30 Å, 149° (<)		–1/2+x, 1/2–y, –1/2+z
$C_{(G2)}$–$N_{(G2)}$···$N_{(G2)}$–$C_{(G2)}$	2.38 Å, 126° (<<)		2–x, –y, 1–z
$C_{(G2)}$–$H_{(G2)}$···$H_{(H)}$–$C_{(H)}$	2.35 Å, 138° (<)		1–x, 1–y, 1–z
$C_{(G2)}$–$N_{(G2)}$···$C_{(H)}$–$C_{(H)}$	3.24 Å, 106° (<)		x, 1+y, z

[a]A detailed table of H···H, G···G and H···G interactions may be found in the Supplementary Information (Table S203).
[b]Values in square brackets indicate the number of H···G π···π interactions.
[c]Guest 1 (G1) and Guest 2 (G2) represent the two disordered guest components in the host crystal.
[d]Distances denoted by < are contacts that measure less than the sum of the van der Waals radii of the atoms involved while those denoted by << are this sum minus 0.2 Å.

The guest in the **H_1**·ANL complex (containing the preferred guest) experiences stronger (shorter) and a greater number of interactions with the host compared with NMA. These include one $C_{(G)}$–$N_{(G)}$···$Cg_{(H)}$ [3.52 Å (109°)] and four other H···G short contacts ranging between 2.30 and 3.24 Å (106–149°) (Table 10.4). One G···G interaction measured significantly less (<<) than the van der Waals radii of the atoms [$C_{(G2)}$–$N_{(G2)}$···$N_{(G2)}$–$C_{(G2)}$, 2.38 Å (126°)]. NMA, on the other hand, was enclathrated by means of one $C_{(G)}$–$H_{(G)}$···$Cg_{(H)}$ [2.93 Å (140°)] and only one other short interaction [$C_{(H)}$–$H_{(H)}$···$H_{(G)}$–$C_{(G)}$] measuring 2.37 Å with an angle of 143°. These findings explain the enhanced preference of **H_1** for ANL relative to NMA.

10.1.6 Hirshfeld surface analyses

The Hirshfeld surfaces were calculated around the guest molecules in the two complexes and the resultant 2D fingerprint plots that were generated from these experiments are provided in the Supplementary Information (Figure S204). The data were then summarized as depicted in Figure 10.6. (Note that the surfaces for the disordered components of ANL were generated independently.)

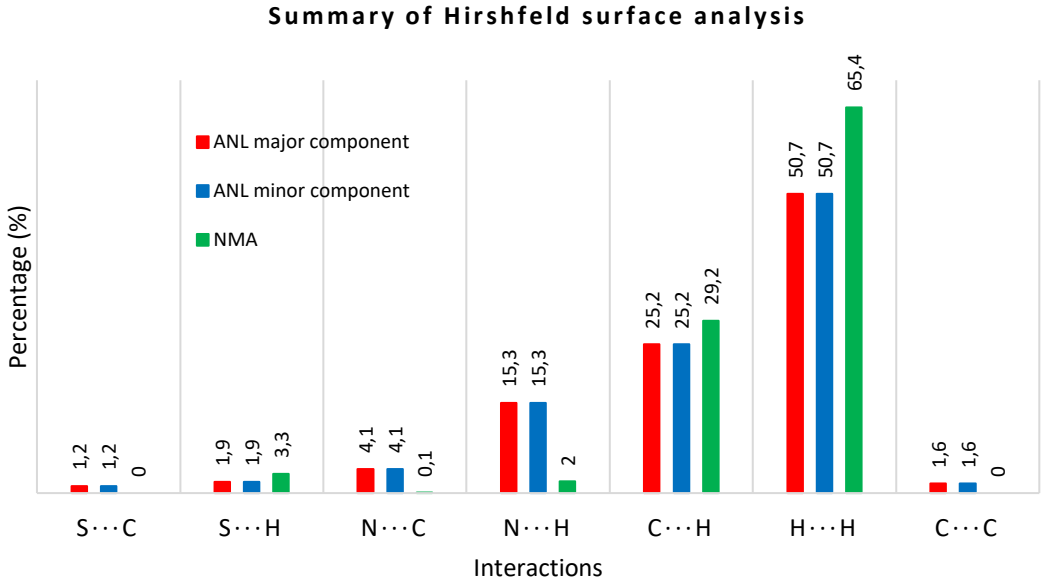

Figure 10.6. Interaction types and quantities after Hirshfeld surface analyses of the **H$_1$**·ANL and **H$_1$**·NMA complexes.

These analyses do not contribute to an understanding of the reasons for the high selectivity of **H$_1$** towards ANL. However, it was noted that ANL was involved in a significantly larger number of N···H interactions, but these were not of sufficient strength to be significant (and so are absent from Table 10.4); NMA, on the other hand, experienced a larger number of H···H interactions.

10.1.7 Thermal analyses (DSC and TG)

The thermal stability of each complex was assessed by heating these solids in a controlled temperature sequence. The data was then utilized to construct the overlaid DSC (green), TG (blue) and DTG (red) traces that are depicted in Figure 10.7. The guest in **H$_1$**·ANL is released primarily in one step, while this process is somewhat more convoluted for **H$_1$**·NMA. Table 10.5 summarizes the relevant thermal data obtained from these traces.

a)

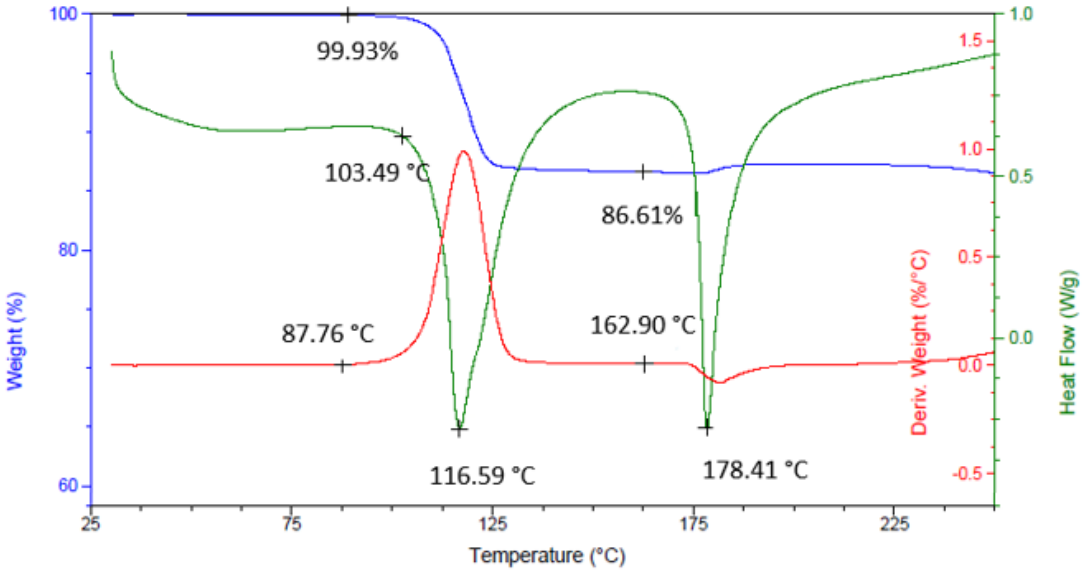

b)

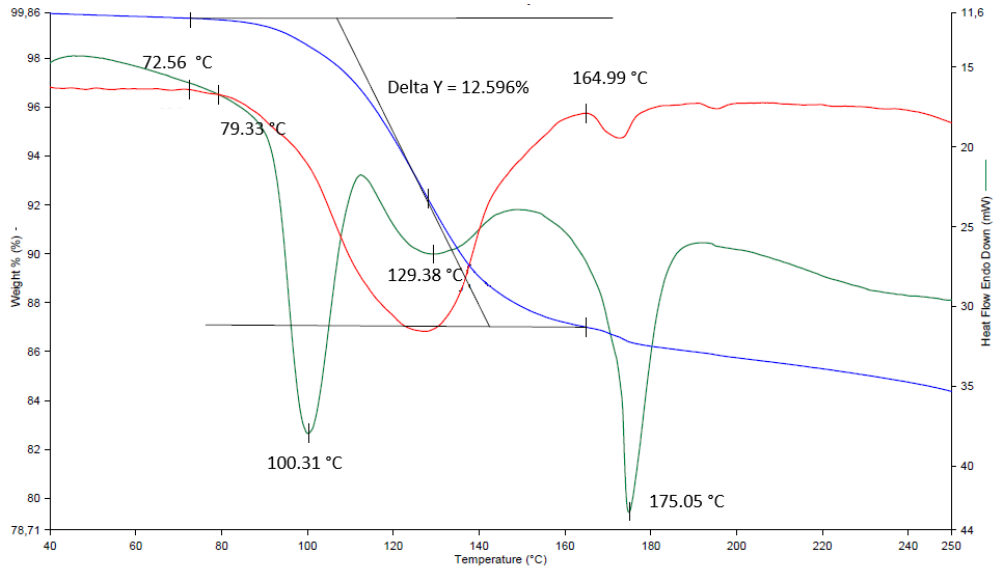

Figure 10.7. Overlaid thermal traces (DSC, TG and DTG) for a) **H₁**·ANL and b) **H₁**·NMA.

Table 10.5. Thermal properties of complexes formed with **H₁**.

Complex	T_{on} /°C	T_p /°C	Mass loss expected /%	Mass loss observed /%
H₁·ANL	87.8	116.6	15.2	13.3
H₁·NMA	72.6	100.3, 129.4	15.1	12.6

The observed mass losses in both complexes are lower than expected, and the reasons for this is not clear currently. However, the T_{on} values correlate very closely with observations made from previous experiments: the preferred ANL guest was released from the complex at a much higher temperature compared to NMA (87.8 versus 72.6 °C, respectively), and the initial T_p values also agree [ANL (116.6) > NMA (100.3°C)]. (**H₁**·TOL also showed an enhanced thermal stability relative to EB, Table 9.5 and 3.6.)

10.1.8 Conclusions

H₁ included the smaller guests ANL and NMA, but not NNDMA. The equimolar competition experiments established the host selectivity to be in the order ANL > NMA > NNDMA. Results from SCXRD analyses were carried out on the novel complexes and the results were correlated to the host's behaviour. The preference of this host for ANL was as a result of stronger and a greater number of interactions with this guest: one $C_{(G)}$–$N_{(G)}$···$Cg_{(H)}$ [3.52 Å (109°)] and four other H···G short contacts ranging between 2.30 and 3.24 Å (106–149°) were identified, while NMA was enclathrated by means of one $C_{(G)}$–$H_{(G)}$···$Cg_{(H)}$ [2.93 Å (140°)] and only one other short interaction [$C_{(H)}$–$H_{(H)}$···$H_{(G)}$–$C_{(G)}$, 2.37 Å (143°)]. Thermal analyses showed the complex with the preferred guest ANL to possess an increased relative thermal stability, based on the T_{on} and T_p values, compared to **H₁**·NMA. Similarities in the geometry and packing of **H₁** in complexes containing preferred TOL (from the alkyl aromatics) and ANL (from the present guest series) were observed and were responsible for possibly the comparable host behaviour noted in the presence of these two guest series. These similarities include a buckled S-containing central ring, a synclinal (gauche) arrangement of the nitrogen atoms in the ethylenediamine linker, and a consequential less ordered host packing. Additionally, these results have shown that host-guest chemistry may be considered as a viable alternative for the separation of such anilines.

10.1.9 Supporting information

All relevant traces, detailed tables and associated data for this section are provided in the Supplementary Information. The crystal structures were deposited at the Cambridge Crystallographic Data Centre, and CCDC 1905943 (**H₁**·ANL) and 1905944 (**H₁**·NMA) contain the crystallographic data for this section.

10.2. Inclusion compounds with **H_2**

10.2.1 Introduction

Thus far the host behaviour of **H_1** has been assessed in the presence of two analogous guest series', namely the alkyl aromatics and the anilines. The host ability of **H_2** was also evaluated when presented with the guests from the former series and, hence, for the sake of completeness, **H_2** was also exposed to the aniline guests by utilizing similar experiments. This investigation shall highlight any variances in the host ability as a direct consequence of the minor structural modifications within each of **H_1** and **H_2** in the presence of these non-isomeric guests, and may then also be used to determine whether these hosts display opposing behaviours here, as they did in Chapters 7 and 8 (which also involved structurally related non-isomeric guests).

10.2.2 Individual inclusions

Interestingly, the independent recrystallization experiments with **H_2** yielded complexes with NMA and the larger NNDMA guest compounds, but not with the smaller ANL, which is in direct contrast to the behaviour of **H_1** (which included ANL and also NMA). (This size exclusion trend was also observed for these hosts in the presence of the alkyl aromatics.) The H:G ratios were consistently 1:1 for the successfully formed complexes, and the ^{1}H-NMR spectra for **H_2**·NMA and **H_2**·NNDMA are provided in the Supplementary Information, Figures S205 and S206.

Table 10.6. Results of the single solvent experiments and consequential H:G ratios.[a]

Guest (G)	H:G
ANL	[b]
NMA	1:1
NNDMA	1:1

[a]All ^{1}H-NMR spectra of successfully formed complexes are provided in the Supplementary Information (Figures S205 and S206).
[b]Resultant crystals contained no guest.

The selectivity of **H_2** was subsequently assessed by recrystallizing the host from equimolar mixtures of the aniline guests.

10.2.3 Equimolar competition experiments

Equimolar binary and ternary mixtures of the guests were prepared and **H_2** was recrystallized from each of these, and the resultant solids analysed by means of GC-FID. These experiments were carried out in duplicate, and the averaged guest ratios are provided in Table 10.7, together with the % e.s.d.s and the overall H:G ratios (determined by means of ^{1}H-NMR spectroscopy). [The duplicate data may be found in the Supplementary Information (Table S207).]

Table 10.7. Results for **H_2** when presented with equimolar mixed anilines.[a,b]

ANL	NMA	NNDMA	Average guest ratios	Overall H:G ratio	% e.s.d.s
x	x		22.9:77.1	1:1	(1.2):(1.2)
x		x	1.3:98.7	1:1	(0.0):(0.0)
	x	x	6.7:93.3	1:1	(0.9):(0.9)
x	x	x	3.7:6.1:90.2	1:1	(1.7):(0.1):(1.8)

[a]The mol% of the preferred guest in the mixed complexes is in red for ease of examination.
[b]The overall H:G ratio was determined by means of ^{1}H-NMR spectroscopy, and G:G ratios using GC-FID.

The contrasting host behaviour displayed by **H_2** and **H_1** remain evident from these results. The larger of the three guests, NNDMA, was always distinctly favoured by **H_2** when present: the ANL/NNDMA, NMA/NNDMA and ANL/NMA/NNDMA experiments afforded mixed complexes containing 98.7, 93.3 and 90.2% NNDMA. When NNDMA was not present, as in the ANL/NMA experiment, NMA was preferred but to a lesser extent (77.1%). Here the host selectivity decreases as guest size decreases, NNDMA > NMA > ANL, and this observation is in direct contrast with results for **H_1** (ANL > NMA > NNDMA).

This selectivity was then further affirmed by exposing the host to binary mixtures where G/G concentrations were varied.

10.2.4 Ratio-dependent competition experiments

Binary mixtures of the aniline guests with ratios approximating 80:20, 60:40, 50:50, 40:60 and 20:80 were prepared, and **H₂** was recrystallized from each of these. The solids, and solutions from which they formed, were analysed using GC-FID in order to determine the G:G ratios and to afford the selectivity profiles as depicted in Figure 10.7.

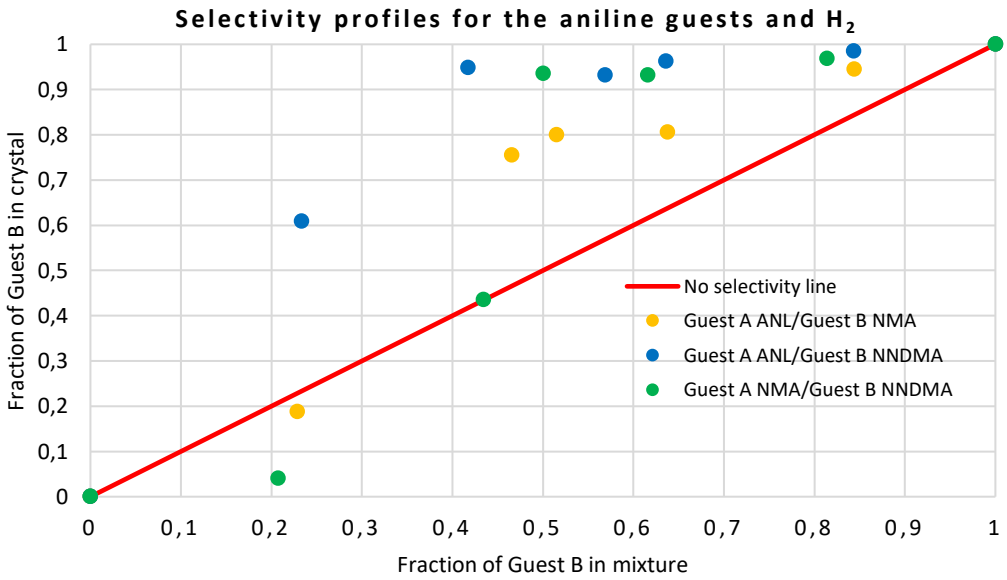

Figure 10.7. Selectivity profiles for **H₂** when recrystallized from binary solutions containing varying concentrations of the aniline guests.

These experiments revealed that **H₂** possesses an enhanced selectivity for the *N*-alkylated anilines relative to ANL. For the ANL/NNDMA experiment (Figure 10.7, blue profile), an average K value of 13.8 was calculated in favour of NNDMA. Ambivalent host selectivity was noted in the NMA/NNDMA and ANL/NMA experiments (Figure 10.7, green and yellow profiles, respectively), and here the selectivity was dependent on guest concentration. In the case of the ANL/NMA experiment, ANL was preferred at low concentrations of NMA, but at higher concentrations of this guest, the selectivity changed and NMA was the preferred one. The NMA/NNDMA experiment revealed that NMA was preferentially selected until the mixture contained ~43% NNDMA, whereafter NNDMA was the favoured guest (the mixture that afforded the highest K value comprised 50% NMA and 50% NNDMA, and K = 14.4). The overall selectivity order (based on K values) may thus be written as NNDMA > NMA > ANL. This selectivity required rationalization and SCXRD analysis was selected as the technique which could provide such information.

10.2.5 SCXRD

SCXRD experiments were conducted on the complexes containing NMA and NNDMA. **H_2**·NMA crystallized with trace amounts of water in duplicate experiments. Both NNDMA and NMA displayed disorder, but this was modelled effectively. Table 10.8 lists the crystallographic data and refinement parameters for both complexes, and despite each of these crystallizing in the triclinic (*P*-1) crystal system, no isostructurality was evident owing to the cell parameter variances. The unit cells of the two complexes are provided in Figure 10.8. (Note that for the **H_2**·NNDMA, both disordered components are shown, due to the nature of the disorder.)

Table 10.8. Crystallographic data for complexes of **H_2** with NMA and NNDMA.

	H_2·NMA	**H_2**·NNDMA
Chemical formula	$C_{40}H_{32}N_2O_2$·C_7H_9N·0.416(O)	$C_{40}H_{32}N_2O_2$ ·$C_8H_{11}N$
Formula weight	686.32	693.85
Crystal system	Triclinic	Triclinic
Space group	*P*-1	*P*-1
μ (Mo Kα)/mm^{-1}	0.078	0.076
a/Å	8.9265(4)	8.7675(5)
b/Å	9.1183(4)	8.7903(7)
c/Å	12.5759(5)	13.7121(1)
alpha/°	92.594(2)	72.461(4)
beta/°	107.264(2)	76.622(4)
gamma/°	111.066(2)	67.418(4)
V/$Å^3$	898.81(7)	922.33(1)
Z	1	1
F(000)	363	368
Temp./K	200	200
Restraints	1	0
Nref	4488	4016
Npar	257	269
R	0.0404	0.0829
wR2	0.1140	0.2680
S	1.03	1.05
θ min−max/°	1.7, 28.4	1.6, 27.3
Tot. data	41057	4016
Unique data	4488	4016
Observed data [I > 2.0 sigma(I)]	3979	3067
R_{int}	0.018	0.000
Dffrn measured fraction θ full	1.000	0.991
Min. resd. dens. (e/$Å^3$)	–0.21	–0.41
Max. resd. dens. (e/$Å^3$)	0.33	0.73

a) b)

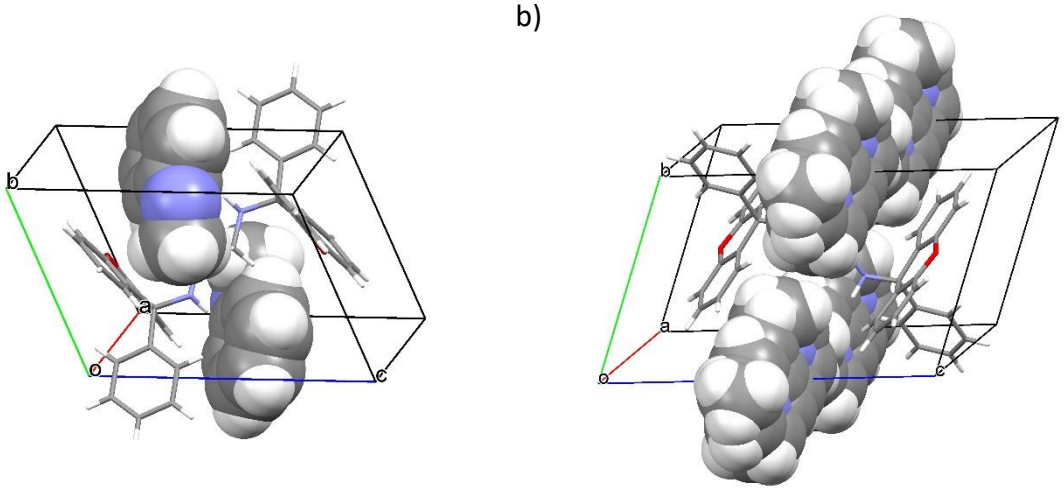

Figure 10.8. Unit cells for a) **H₂**·NMA (with only one of the disordered components displayed) and b) **H₂**·NNDMA (where both disordered components are shown); guests are in spacefill and hosts in stick representation.

Following this, the host geometry was considered, and it was found that in these complexes, the tricyclic fused ring system is near-planar (the deviation from planarity measuring only 9.6° and 6.7°, respectively), and this is evident in Figure 10.9. Also notable is the geometry of the ethylenediamine linker where the host N atoms assume an antiperiplanar conformation (while in **H₁** these were found to be synclinal with respect to one another).

a) b)

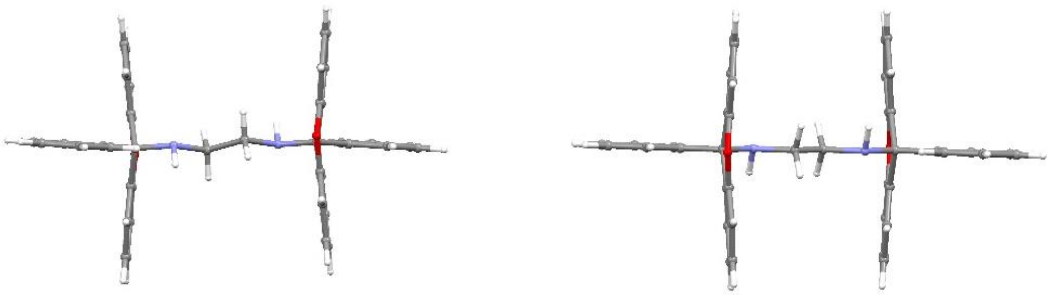

Figure 10.9. Host geometry in complexes a) **H₂**·NMA and b) **H₂**·NNDMA; guests were removed for ease of examination.

Once more, these geometry variances may explain the different host packing evident in these complexes, where this is considerably more ordered for **H₂** compared with **H₁** owing to the more planar O-containing ring and more linear ethylenediamine linker (Figure 10.10). (In **H₁**, the buckled S-containing ring and synclinal N/N linker resulted in a less ordered host–host packing.) This observation must again be responsible for the differences in the behaviour of **H₁** and **H₂** when in the presence of these aniline guests.

a) b)

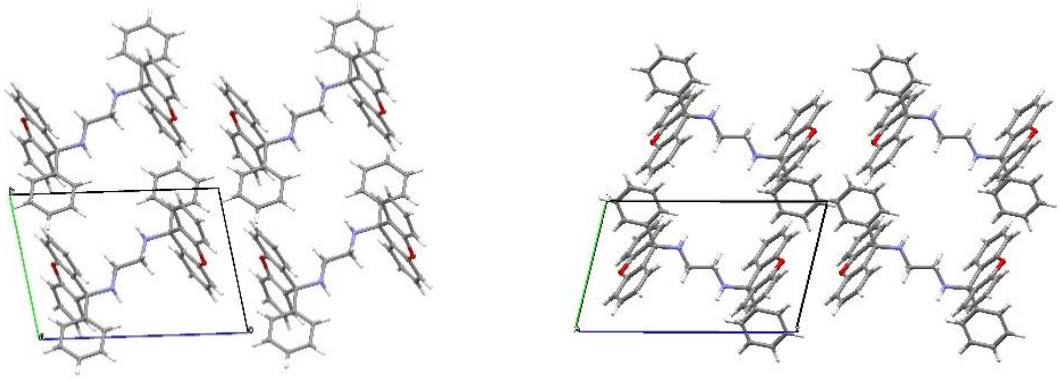

Figure 10.10. Host packing in complexes a) **H₂**·NMA and b) **H₂**·NNDMA.

Additionally, voids that remained after guest removal (from the packing calculation) showed that both NMA and NNDMA are accommodated in channels (Figure 10.11).

a) b)

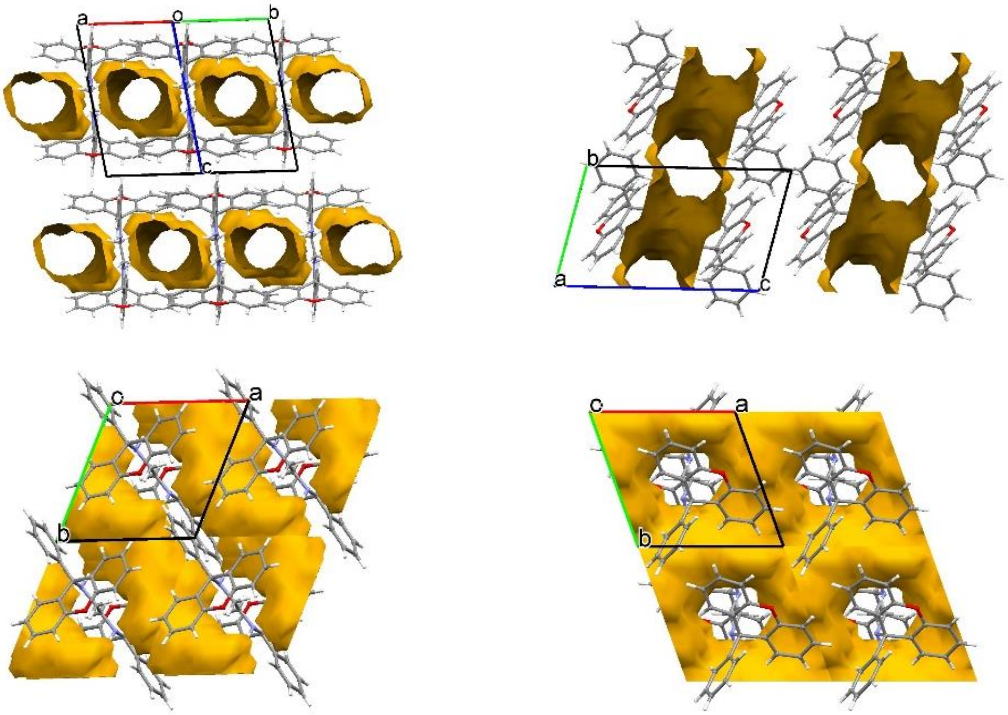

Figure 10.11. Calculated voids (dark yellow) for a) **H₂**·NMA and b) **H₂**·NNDMA.

Furthermore, the H···G interactions were analysed in order to rationalize the enhanced selectivity of **H₂** for NNDMA. Table 10.9 contains a summary of the significant H···G interactions, while a detailed table showing all interactions (H···G and H···H) may be found in the Supplementary Information (Table S211).

Table 10.9. H···G interactions present in complexes of **H_2** with NMA and NNDMA.[a,b,c]

Non-covalent interaction	**H_2**·NMA	**H_2**·NNDMA	Symmetry
π···π	4.735(1)–5.930(1) Å [6]	4.977(3)–5.839(3) Å [8]	
C–H···π (H···Cg, C–H···Cg)			
$C_{(G)}$–$H_{(G)}$···$Cg_{(H)}$	2.89 Å, 139°		x, y, z
$C_{(H)}$–$H_{(H)}$···$Cg_{(G)}$		2.95 Å, 141°	1–x, 1–y,1–z
$C_{(H)}$–$H_{(H)}$···$Cg_{(G)}$	2.95 Å, 127°		x, 1+y, z
Other short contacts (X···Z, X–Y···Z)			
$C_{(H)}$–$H_{(H)}$···$H_{(G)}$–$C_{(G)}$	2.32 Å, 132° (<)		2–x, 1–y, 1–z
$N_{(H)}$–$H_{(H)}$···$H_{(G)}$–$C_{(G)}$		2.26 Å, 168° (<)	–1+x, 1+y, z
$N_{(G)}$–$C_{(G)}$···$H_{(H)}$–$C_{(H)}$		2.75 Å, 146° (<)	1–x, 1–y, 1–z

[a]A detailed table of H···H and H···G interactions may be found in the Supplementary Information (Table S211).
[b]Values in square brackets indicate the number of H···G π···π interactions.
[c]Distances denoted by < are contacts that measure less than the sum of the van der Waals radii of the atoms involved.

Both NMA and NNDMA are involved in C–H···π contacts with the host compound that ranges between 2.89 and 2.95 Å (127–141°), and both also experience a comparable number of very weak π···π interactions with the host [Table 10.9, 4.735(1)–5.930(1) Å]. Furthermore, the preferred guest experiences two additional stabilizing interactions that measure 2.26 Å [$N_{(H)}$–$H_{(H)}$···$H_{(G)}$–$C_{(G)}$] and 2.75 Å [$N_{(G)}$–$C_{(G)}$···$H_{(H)}$–$C_{(H)}$] (168° and 146°, respectively) compared with only one in the complex with the less favoured NMA guest [$C_{(H)}$–$H_{(H)}$···$H_{(G)}$–$C_{(G)}$, 2.32 Å, 132°) which may explain the preference order for this host compound.

10.2.6 Hirshfeld surface analyses

Due to the disorder of the guests in these complexes, Hirshfeld surface analysis could not be carried out.

10.2.7 Thermal analyses (DSC and TG)

After heating the aniline complexes from room temperature to approximately 250 °C, the thermal traces (TG, DSC and DTG) displayed in Figure 10.12 were obtained, and Table 10.10 summarizes the relevant thermal data obtained from these traces.

a)

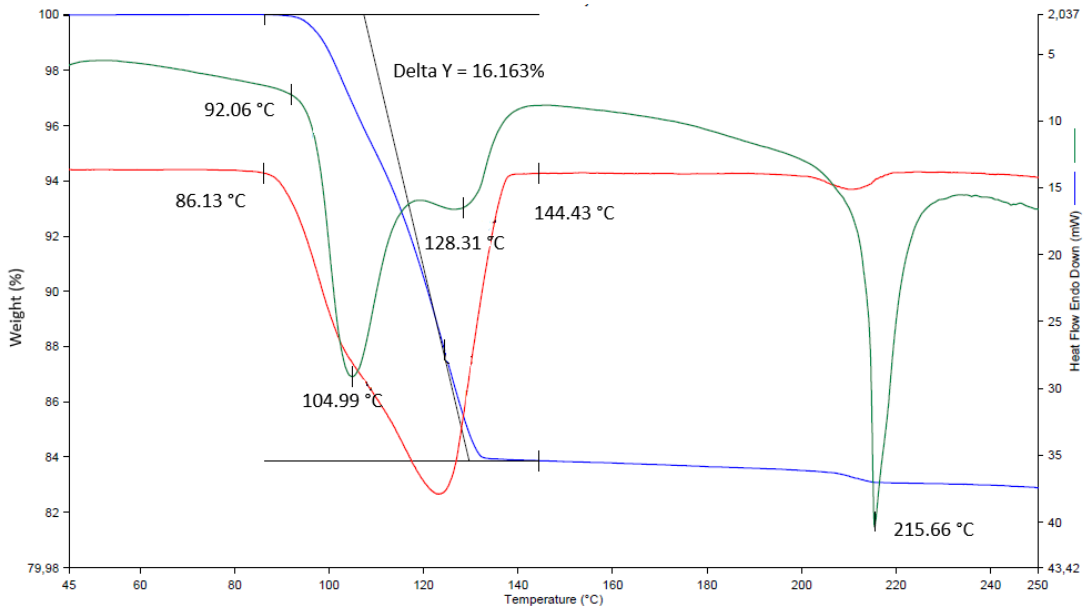

b)

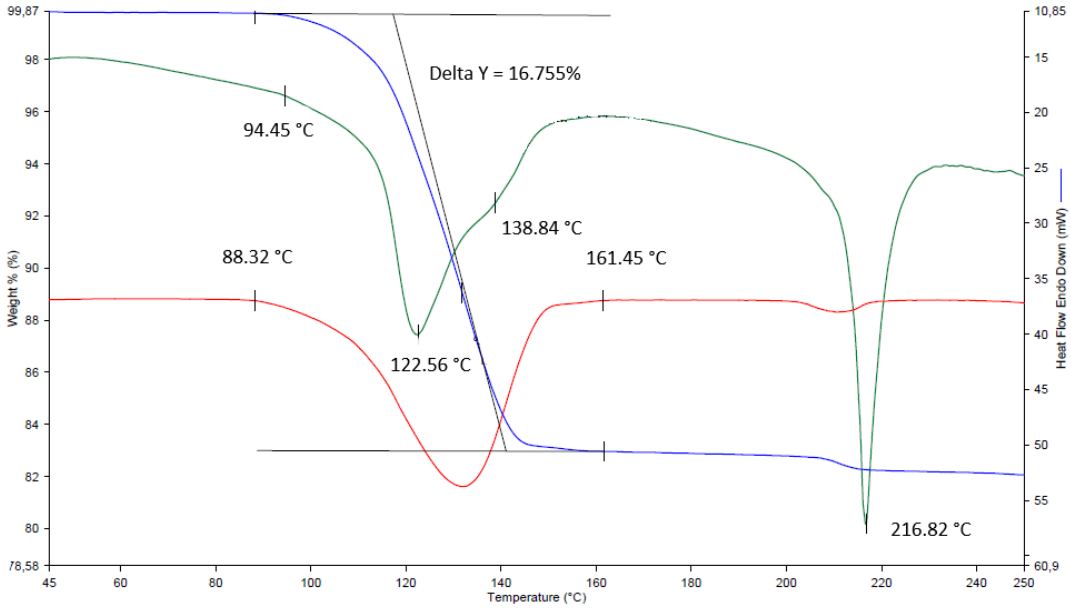

Figure 10.12. Overlaid thermal traces [DSC (green), TG (blue) and DTG(red)] for a) **H₂**·NMA·0.406(H_2O) and b) **H₂**·NNDMA.

Table 10.10. Thermal properties of complexes formed with **H₂**.

Complex	T_{on} /°C	T_p /°C	Mass loss expected /%	Mass loss observed /%
H₂·NMA·0.406(H_2O)	86.1	105.0, 128.3	16.6	16.2
H₂·NNDMA	88.3	122.6, 138.8	17.5	16.8

The T_{on} value for **H_2**·NNDMA was 88.3 °C, while that for NMA was somewhat lower at 86.1 °C, in accordance with the host selectivity order. The initial T_p values also correlated with this order: **H_2**·NNDMA (122.6°C) > **H_2**·NMA (105.0°C) was observed for the initial guest release endotherms. Therefore, the complex with the preferred guest (NNDMA) possesses a higher thermal stability compared with the **H_2**·NMA complex and this, once more, explains the preferential behaviour of the host.

10.2.8 Conclusions

Once again, **H_2** displayed opposing inclusion abilities compared with **H_1**, clathrating the larger guests NMA and NNDMA but not ANL. The host selectivity was found to be in the order NNDMA > NMA > ANL, which mimicked the size-dependent inclusion behaviour of **H_2** in the presence of the alkyl aromatic guests (CU > EB > TOL). Single crystal X-ray diffraction analyses were carried out on the novel complexes and observations correlated with the selectivity order: the enhanced preference of **H_2** for NNDMA was rationalized by the fact that this host was involved in stronger and a greater number of interactions relative to the other guest (NMA). Thermal analyses also provided results that were in accordance with the **H_2** selectivity order: the preferred guest NNDMA (88.3 and 122.6 °C) displayed an increased relative thermal stability compared with NMA (86.1 and 105.0 °C), based on the T_{on} and initial T_p values, respectively. Once again, these hosts, when presented with non-isomeric guests, exhibited opposing host behaviour. It was suggested that this may be as a result of the difference in the geometries of both the tricyclic fused ring systems and the ethylenediamine linkers in these compounds.

In summary, **H_1** and **H_2** possess contrasting selectivities for guest solvents from the two series, with the former host preferring the smaller guest species, and the latter the larger of these present in the mixtures. The overall host selectivity orders thus appear to be guest-size dependent here and must be as a direct result of substitution of the sulfur atom (in the central ring of the thioxanthenyl moiety) for an oxygen atom.

The analyses and rationalization of this behaviour has thus led to an improved understanding of the structure-property relationships of these systems in the presence of such structurally

related non-isomeric guests. Also, due to the high selectivity displayed by both **H_1** and **H_2**, these hosts may be considered as an alternative in separation of the anilines.

10.2.9 Supporting information

All relevant graphs, tables and associated data for this section are provided in the Supplementary Information. The crystal structures were deposited at the Cambridge Crystallographic Data Centre, and CCDC 1905946 (**H_2**·NMA) and 1905947 (**H_2**·NNDMA) contain the supplementary crystallographic data for this section.

11. DIHALOALKANE DERIVATIVES

11.1 Inclusion compounds with $\mathbf{H_1}$

11.1.1 Introduction

Haloalkanes are organic compounds that contain one or more elements from the halogen family, namely chlorine, bromine, fluorine and iodine. These compounds are often used in reactions as both reagents and solvents.[141]

Many host compounds, such as tetrakis(4-bromophenyl)ethylene,[140] 3-amino-2-carbamimidoylacrylamides,[310] and *N*,*N*'-bis(5-phenyl-5-dibenzo[*a,d*]cycloheptenyl)ethylenediamine and its 10,11-dihydro analogue,[311] have been investigated for their inclusion ability in the presence of bromo-, chloro- and iodo- methanes. Experiments involving these compounds provided information on the structures and kinetics of the enclathration process through crystal structure and thermal analyses of the resultant inclusion compounds.

In this work, the primary focus is to gain an understanding of the reasons for any discriminatory behaviour displayed by $\mathbf{H_1}$ and $\mathbf{H_2}$ in the presence of mixtures of related halogen-containing guests, more specifically the three dihalomethanes, dichloromethane (DCM), dibromomethane (DBM) and diiodomethane (DIM) (Scheme 11.1), and also to assess whether enclathration would be successful when using alternative alkyl halides.

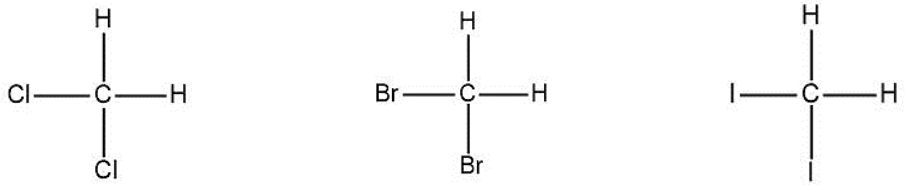

DCM 40 °C | DBM 97 °C | DIM 181 °C

Scheme 11.1. Molecular structures of the dihalomethane compounds.

11.1.2 Individual inclusions

Table 11.1 is a summary of the potential alkyl halide guests investigated in the recrystallization experiments using **H_1**, as well as the H:G ratios of complexes successfully formed determined through ^{1}H-NMR spectroscopy. (These spectra are provided in the Supplementary Information, Figures S212–214). In addition to the three dihaloalkanes, five other alkyl halides with varying molecular sizes and numbers of halide atoms were also employed in this investigation.

Table 11.1. Results of the single solvent experiments and consequential H:G ratios.[a]

Guest (G)	H:G
CH_2Cl_2 [DCM]	1:1
CH_2Br_2 [DBM]	1:1
CH_2I_2 [DIM]	1:1
$CHCl_3$	1:1
$CHBr_3$	[b]
CHI_3	[b]
CH_3I	1:1
CH_2BrCl	1:1

[a]Determined by means of ^{1}H-NMR spectroscopy using $CDCl_3$ as solvent.
[b]No inclusion occurred.

It is clear from Table 11.1 that **H_1** has an affinity for the haloalkanes. The preferred H:G ratio is consistently 1:1, and whether the guest is included or not appears to depend on its relative size: all guest molecules bearing one or two halogen atoms form complexes with **H_1**, namely DCM, DBM, DIM, bromochloromethane and idodomethane, whilst only the smallest of the three haloforms used, chloroform, was successfully clathrated. Bromoform and iodoform, having three large halogen atoms bonded to the central carbon atom, were not included by this host.

The selectivity of **H_1** was then assessed by recrystallizing the host from various equimolar mixtures of only the dihaloalkane guests.

11.1.3 Equimolar competition experiments

After recrystallizing **H_1** from the equimolar binary and ternary mixtures of these dihalomethanes, analysis of the resultant crystals by means of ^{1}H-NMR spectroscopy was feasible since the important resonance signals of these guests do not overlap with each other (Table 11.2) nor with the host. (As evidence, an ^{1}H-NMR spectrum of a mixed complex with all three guests may be found in the Supplementary Information, Figure S218.)

Table 11.2. ^{1}H-NMR resonance data for pure DCM, DBM and DIM.

DCM		DBM		DIM	
Assignment	**δ(ppm)**	**Assignment**	**δ(ppm)**	**Assignment**	**δ(ppm)**
CH	5.32	CH	4.95	CH	3.88

Table 11.3 summarizes the average G:G and overall H:G ratios, as well as the % e.s.d.s, obtained from these experiments. [The experiments were carried out in triplicate and the complete data set may be found in the Supplementary Information (Table S219).]

Table 11.3. Results for **H_1** when presented with equimolar mixed dihaloalkanes.[a,b]

DBM	DIM	DCM	Average guest ratios	Overall H:G ratio	% e.s.d.s
x	x		64.1:35.9	1:1	(2.2):(2.2)
x		x	77.7:22.3	1:1	(1.0):(1.0)
	x	x	64.8:35.2	1:1	(0.4):(0.4)
x	x	x	46.2:37.5:16.3	1:1	(1.4):(0.6):(1.8)

[a]The mol% of the preferred guest in the mixed complexes is displayed in red.
[b]The overall H:G and G:G ratios were determined by means of ^{1}H-NMR spectroscopy.

The overall H:G ratio remains 1:1 for all of the mixed complexes, the same as the preferred ratio in the single solvent experiments (Table 11.1). Furthermore, **H_1** shows discriminatory behaviour under these competition experiment conditions. Whether in the presence of equimolar binary (DBM/DCM, DBM/DIM) or ternary (DCM/DBM/DIM) solutions, this host is selective for the dibromo derivative (77.7 and 64.1% in the binary experiments, respectively, and 46.3% in the ternary experiment). When DBM is absent (DIM/DCM), the host discriminates against DCM in favour of DIM (64.8%:35.2%). The selectivity of this host compound in the presence of these guests is thus in the order DBM > DIM > DCM.

The preferential behaviour of **H_1** was subsequently assessed when guest concentrations were varied.

11.1.4 Ratio-dependent competition experiments

Binary competition experiments were prepared as before but, in each case, the relative ratios of the two guests in the competition were varied. The resulting crystals and mother liquors were once again analysed using ^{1}H-NMR spectroscopy to obtain values for the mole fractions of the guests in both phases. These data were used to construct the profiles in Figure 11.1. Additionally, the average selectivity coefficients were calculated for these profiles and the complete set of values are provided in the Supplementary Information (Tables S220–222).

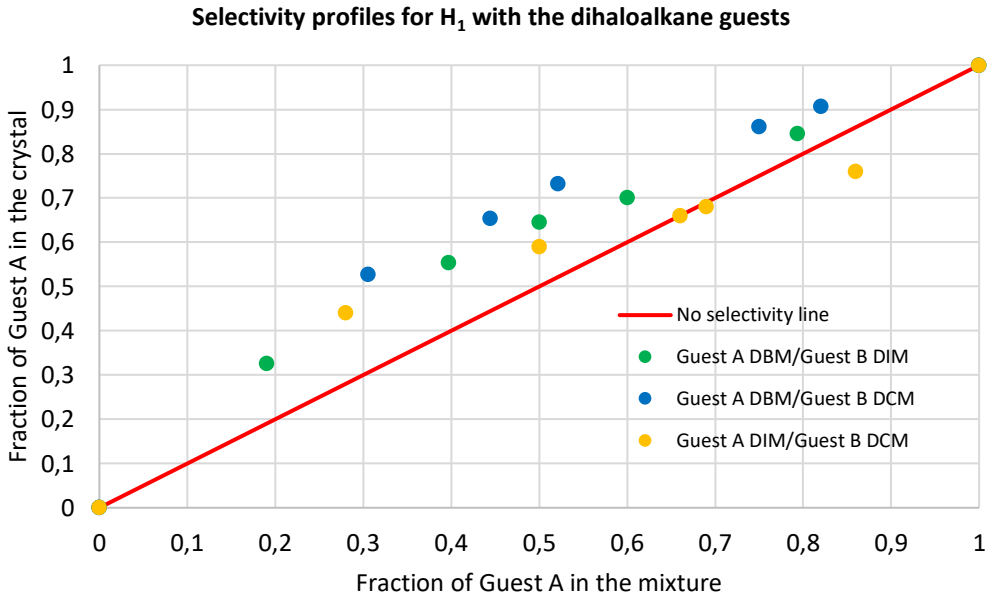

Figure 11.1. Selectivity profiles for **H₁** after recrystallization from binary solutions containing varying concentrations of the dihaloalkane guests.

From Figure 11.1 (the green and blue profiles), **H₁** is selective for DBM over the entire concentration range, even at low concentrations of this guest (K = 1.7 and 2.3, respectively). However, and surprisingly, in the absence of DBM (yellow profile), the host initially shows selectivity for DIM, even at low concentrations, while from a ~66%:34% DIM:DCM mixture, the host extracts precisely 66% of DIM, and it is at this point that K = 1. Beyond this point, the selectivity is for DCM and the profile curves below the no selectivity line. The highest recorded K value for this profile was from a ~28% DIM/72% DCM mixture where K = 2.0 in favour of DIM. This last result is counterintuitive since the host appears to be selective for the guest that is present in low concentrations. The experiment was therefore repeated but the findings did not change, and at this time this peculiar observation cannot be explained.

11.1.5 SCXRD

SCXRD experiments were subsequently carried out to determine which intermolecular forces were responsible for retaining the guest in the host crystal and which factor(s) might explain the selectivity order of this host compound. Table 11.4 contains the crystal structure data from these analyses for inclusion compounds **H$_1$**·DCM, **H$_1$**·DBM and **H$_1$**·DIM. The guests in all three complexes displayed disorder but this was acceptably modelled over two positions.

Table 11.4. Crystallographic data for complexes of **H$_1$** with DCM, DBM and DIM.

	H$_1$·DCM	**H$_1$**·DBM	**H$_1$**·DIM
Chemical formula	$C_{40}H_{32}N_2S_2{\cdot}CH_2Cl_2$	$C_{40}H_{32}N_2S_2{\cdot}CH_2Br_2$	$C_{40}H_{32}N_2S_2{\cdot}CH_2I_2$
Formula weight	689.72	778.62	872.62
Crystal system	Monoclinic	Monoclinic	Monoclinic
Space group	$P2_1/n$	$P2_1/n$	$P2_1/n$
μ (Mo Kα)/mm^{-1}	0.349	2.539	1.939
a/Å	10.1138(8)	10.2014(5)	10.5803(7)
b/Å	13.3589(10)	13.3548(6)	13.3472(8)
c/Å	25.0909(17)	25.0025(16)	24.9308(17)
alpha/°	90	90	90
beta/°	92.771(3)	92.864(3)	92.337(3)
gamma/°	90	90	90
V/Å^3	3386.1(4)	3402.0(3)	3517.7(4)
Z	4	4	4
F(000)	1440	1584	1728
Temp./K	200	200	200
Restraints	6	7	8
Nref	8332	8458	8736
Npar	448	460	454
R	0.0503	0.0470	0.0642
wR2	0.1462	0.1358	0.1979
S	1.01	1.02	1.03
θ min–max/°	1.6, 28.4	2.1, 28.3	1.6, 28.3
Tot. data	47384	47750	49817
Unique data	8332	8458	8736
Observed data [I > 2.0 sigma(I)]	6934	6471	6779
R_{int}	0.025	0.022	0.021
Dffrn measured fraction θ full	1.000	0.999	1.000
Min. resd. dens. (e/Å^3)	−1.18	−1.01	−2.13
Max. resd. dens. (e/Å^3)	0.88	1.29	4.77

All three complexes crystallize in the monoclinic crystal system and $P2_1/n$ space group and display isostructural host packing. This is clear from the three unit cells displayed in Figure 11.2.

a)

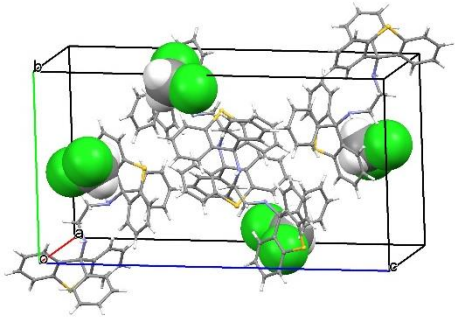

b)

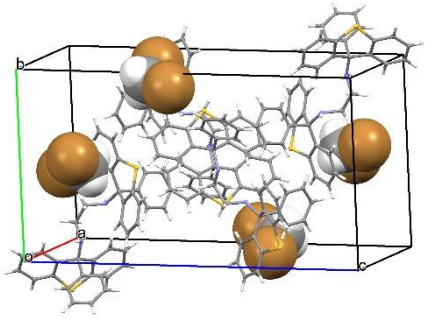

c)

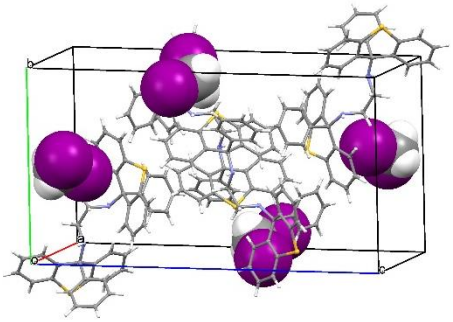

Figure 11.2. Unit cells for a) **H₁**·DCM, b) **H₁**·DBM and c) **H₁**·DIM; host molecules are shown in ball-and-stick representation and guests in space-fill form.

The voids were calculated, and it was observed that guests occupy discrete cavities in the crystals of these complexes, with two guests accommodated in each (Figure 11.3). (Only the voids in **H₁**·DCM are provided here as representative of the other two complexes due to the isostructurality.)

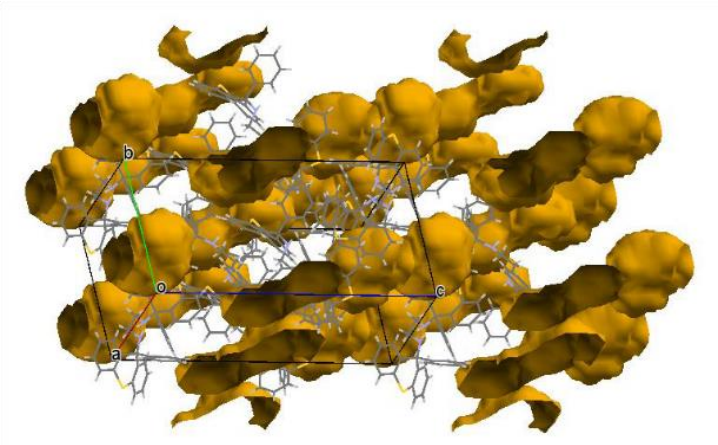

Figure 11.3. Calculated voids of **H₁**·DCM as a representative example.

As expected, the host geometry was found to be very similar in the three complexes, with the central ring of the thioxanthenyl units buckled; the deviation from planarity was calculated to range between 27.3 and 29.4° with the N atoms of the linker in an synclinal (gauche) arrangement (Figure 11.4).

a) b) c)

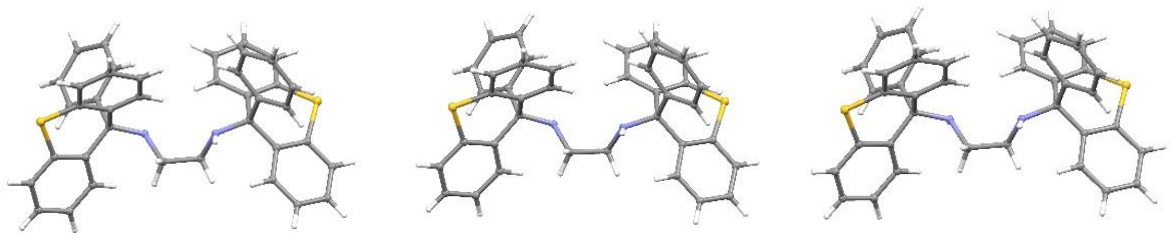

Figure 11.4. Host geometry in complexes a) **H$_1$**·DCM, b) **H$_1$**·DBM and c) **H$_1$**·DIM.

The SCXRD data were analysed closely and, more specifically, the appropriate H···G and G···G intermolecular contacts were considered. These interactions are summarized in Table 11.5. (A table of the H···H interactions may be found in the Supplementary Information, Table S223.)

Table 11.5. H···G and G···G interactions present in complexes of **H$_1$**.[a,b]

Non-covalent interaction	**H$_1$**·DCM	**H$_1$**·DBM	**H$_1$**·DIM	Symmetry
Short contacts (X···Z, X–Y···Z)				
$C_{(G1)}$–$H_{(G1)}$···$C_{(H)}$–$C_{(H)}$	2.79 Å, 152° (<)			2–x, 1–y, 1–z
$C_{(G2)}$–$H_{(G2)}$···$S_{(H)}$–$C_{(H)}$	2.82 Å, 140° (<)			x, y, z
$C_{(G1)}$–$H_{(G1)}$···$C_{(H)}$–$C_{(H)}$		2.87 Å, 148° (<)		1+x, y, z
$C_{(G2)}$–$H_{(G2)}$···$S_{(H)}$–$C_{(H)}$		2.78 Å, 142° (<<)		1–x, 1–y, 1–z
$C_{(G2)}$–$Br_{(G2)}$···$C_{(H)}$–$S_{(H)}$		3.40 Å, 159° (<)		1+x, y, z
$C_{(H)}$–$H_{(H)}$···$I_{(G2)}$–$C_{(G2)}$			3.14 Å, 116° (<)	1/2+x, 1/2–y, 1/2+z
$C_{(H)}$–$H_{(H)}$···$I_{(G1)}$–$C_{(G1)}$			3.17 Å, 145° (<)	1/2–x, –1/2+y, 1/2–z
$C_{(G1)}$–$H_{(G1)}$···$S_{(H)}$–$C_{(H)}$			2.83 Å, 145° (<)	1/2+x, 1/2–y, 1/2+z
$C_{(G2)}$–$I_{(G2)}$···$I_{(G2)}$–$C_{(G2)}$			3.79 Å, 128° (<)	1–x, 1–y, –z

[a]Guest 1 and Guest 2 (G1 and G2) represent the two disordered guest components in the host crystal.
[b]Distances denoted by < are contacts that measure less than the sum of the van der Waals radii of the atoms involved, while those denoted by << is this sum minus 0.2 Å.

Since the guest molecules lack aromatic groups, very weak π···π stacking interactions are only observed between host species (Table S223). Furthermore, these guests are devoid of any conventional hydrogen bond donating and accepting capability, and so no hydrogen bonding

of this type is observed between host and guest. Also noticeable is that there are no significant $C_{(G)}–H_{(G)}\cdots\pi_{(H)}$ interactions present at all in any of these complexes. Only two short contacts were identified in the DCM inclusion compound, three in that containing DBM, and three also in **H₁**·DIM. The host preference order (DBM > DIM > DCM) may be rationalized by considering these numbers of contacts, where the DBM and DIM inclusion compounds experience more of these compared with that having DCM in the host crystals. Furthermore, each guest experiences one $C_{(G)}–H_{(G)}\cdots S_{(H)}–C_{(H)}$ interaction, and the strongest of these is between the host and DBM (2.78 Å, 142°), in accordance with the enhanced preference of **H₁** for this guest.

Due to the isostructural host packing in these complexes, the DCM molecule, since it has the smallest volume of the three guests, quite plausibly experiences more spacious accommodation compared with the DBM and DIM molecules, while this latter guest (possessing the largest molecular volume of the three) is likely to be the most closely confined in the void. The DIM molecules even experience a G···G interaction since the lack of space enables two of these guests to be in close proximity, thus allowing such an interaction to occur [$C_{(G2)}–I_{(G2)}\cdots I_{(G2)}–C_{(G2)}$, 3.79 Å (128°)]. It is plausible that during the crystallization process, the void volume accommodating DBM is more ideal than that for DIM (most closely confined) and DCM (least closely confined), and perhaps this is an additional reason for the observed host selectivity order.

11.1.6 Hirshfeld surface analyses

Hirshfeld surface analyses were carried by generating 3D surfaces around the guest species in each of these complexes. (The resultant 2D fingerprint plots are provided in the Supplementary Information, Figure S224.) Since all three guest types were disordered over two positions, these surfaces were generated separately around each of the disordered components. From the 2D fingerprint plots, the relative quantities of the more notable interactions were obtained and are summarized in Figure 11.5.

a)

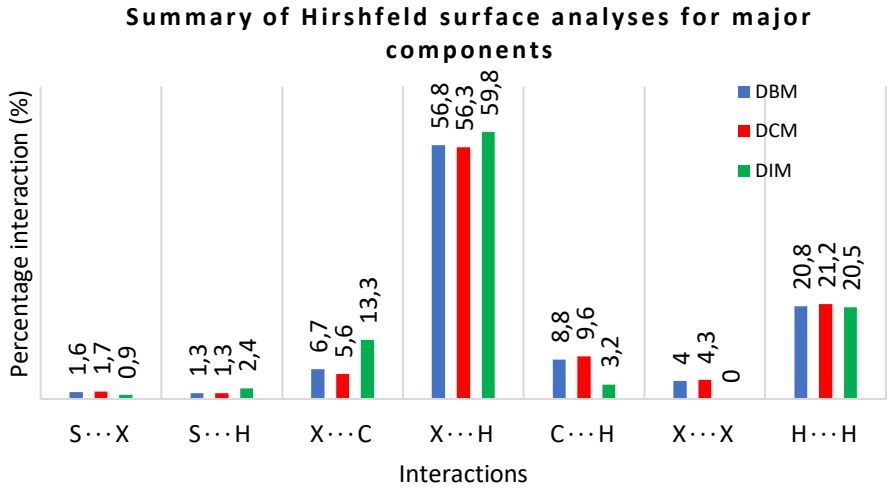

b)

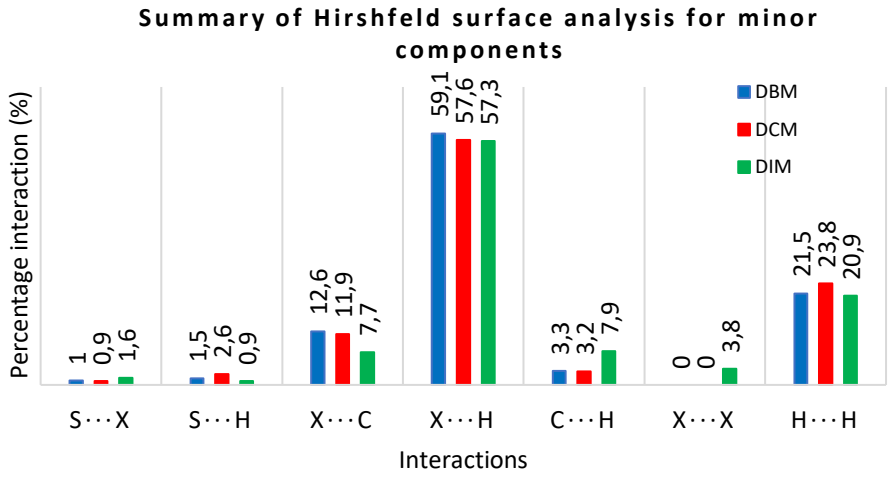

Figure 11.5. Quantitative interactions after Hirshfeld surface analyses, where X represents the halogen atoms for a) major and b) minor disordered components.

Significant amounts of the G···H/H···G hydrogen···hydrogen interactions are observed since these atoms are found on the periphery of each molecule and are therefore expected to interact more often. This was also the case for the X···H interactions (where X represents a halogen atom), and it is clear from Figure 11.5 that DBM experiences a slightly higher number of X···H/H···X interactions (56.8% and 59.1%, for the respective disordered components). However, these differences are not marked.

11.1.7 Thermal analyses (DSC and TG)

Thermal experiments were carried out by heating each of the three complexes and observing the thermal events that resulted. The so-obtained TG (blue), DSC (green) and DTG (red) traces

are provided in Figure 11.6. For both **H$_1$**·DCM and **H$_1$**·DBM (Figure 11.6a and b), the guest release process is rather uneventful: guest release initiates prior to the host melt and two endotherms are thus observed on each DSC trace. However, DIM is released largely in two steps, and the last of these endotherms overlaps with the host melt (Figure 11.6c). The relevant thermal data are summarized in Table 11.6.

a)

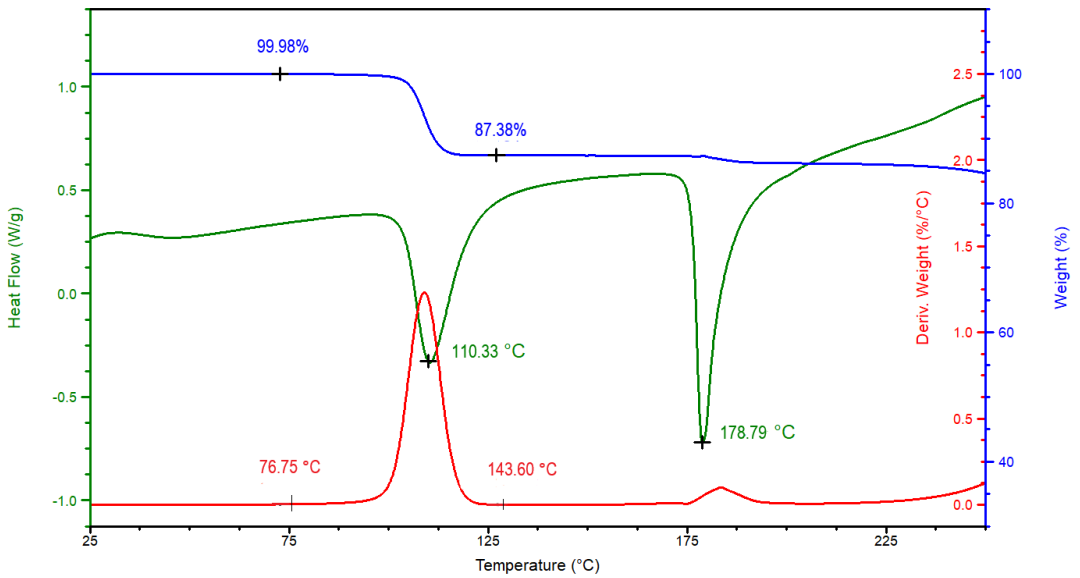

b)

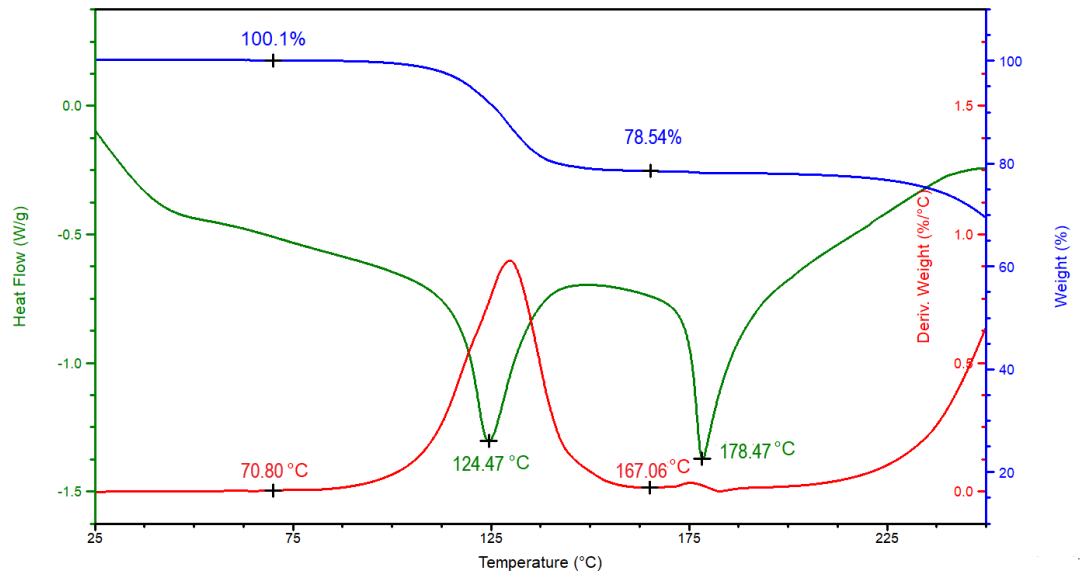

c)

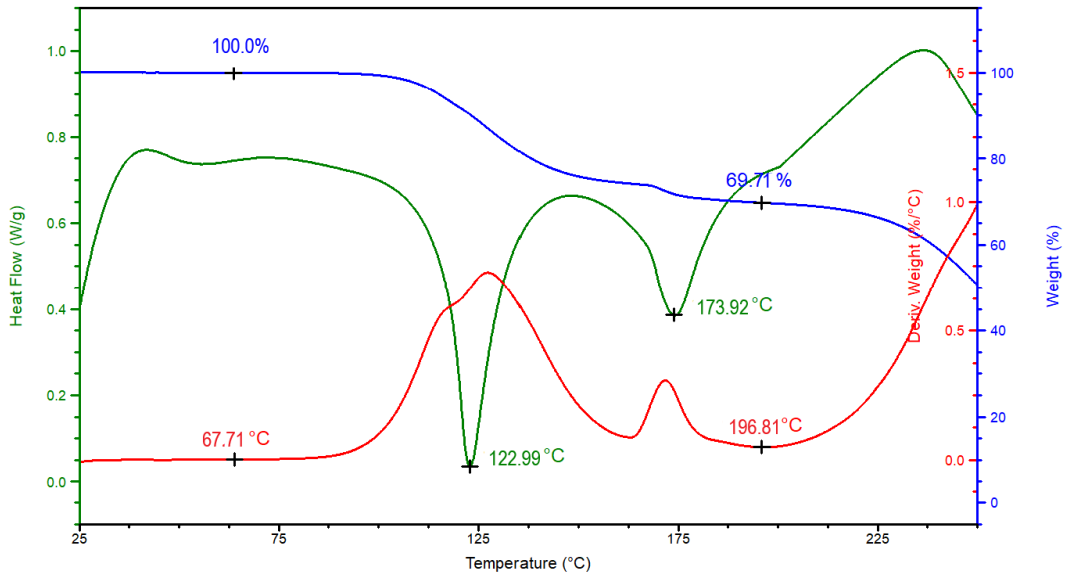

Figure 11.6. Overlaid thermal traces (DSC, TG and DTG) for a) $\mathbf{H_1}$·DCM, b) $\mathbf{H_1}$·DBM and c) $\mathbf{H_1}$·DIM.

The expected mass loss upon complete guest removal through heating is in close agreement with that theoretically expected for all three complexes (Table 11.6). Furthermore, the T_{on} values decrease as the size of the dihalide increases (76.8, 70.8 and 67.7 °C for complexes with DCM, DBM and DIM, respectively) and, in this case, these data contradict the host preference order from competition experiments. Interestingly, however, the T_p values do correlate with this order [DBM (124.5 °C) > DIM (123.0 °C) > DCM (110.3 °C)].

Table 11.6. Thermal properties of complexes formed with $\mathbf{H_1}$.

Guest (G)	T_{on} /°C	T_p /°C	Mass loss expected /%	Actual mass loss measured /%
DCM	76.8	110.3	12.3	12.6
DBM	70.8	124.5	22.3	21.6
DIM	67.7	123.0	30.7	30.3

11.1.8 Conclusions

$\mathbf{H_1}$ was found to be highly effective for the enclathration of alkyl halides, including six of the eight potential guests investigated with a preferred H:G ratio of 1:1.

Competition experiments using equimolar binary and ternary mixtures of DCM, DBM and DIM showed that the host has a significant preference for the dibromo guest, and the selectivity of

H_1 was ascertained to be in the order DBM > DIM > DCM. Further selectivity experiments in which two guests were mixed in varying molar ratios showed that whenever DBM was present, the host selectivity was towards this guest over the entire concentration range investigated, even at low concentrations of DBM in the mixture (DBM/DCM and DBM/DIM). Extraordinarily, in the DIM/DCM experiment, the host displayed increased selectivity for DIM at low concentrations of this guest in the solution, while DCM was favoured when it too was only present in low concentrations. This finding was contrary to intuition and this behaviour could not be rationalized at this time.

Data from SCXRD experiments provided explanations for the observed selectivity order: the DBM and DIM guests both experience a larger number of contacts with **H_1** than DCM. Furthermore, each of the three guests experiences a $C_{(G)}–H_{(G)}\cdots S_{(H)}–C_{(H)}$ interaction with the host, and the most preferred guest, DBM, experiences the strongest of these. Void calculations revealed that all three guests are accommodated in similar discrete cavities (due to the isostructural host packing), with each cavity enclosing two guest molecules. It is plausible that, owing to the isostructurality present in these complexes, the voids created by **H_1** during crystallization are of an optimal size for the accommodation of DBM and possibly less so for DCM and DIM, which may explain the host selectivity order. The fact that the iodoform and bromoform were not included by **H_1** may be as a result of their enhanced sizes: perhaps these molecules could not be accommodated owing to the close proximity of host and guest atoms as a result of the large guest molecular volumes.

Thermal experiments revealed that the relative stabilities of the inclusion compounds, based on T_p data, increases in the order DCM < DIM < DBM, which is in accordance with the observed selectivity of this host, while T_{on} values, inexplicably, contradict this order.

11.1.9 Supporting information

Relevant NMR spectra, additional data and traces for the inclusion compounds may be found in the Supplementary Information. The crystal structures were deposited at the Cambridge Crystallographic Data Centre, and CCDC 1533422 (**H_1**·DCM), 1533423 (**H_1**·DBM) and 1533424 (**H_1**·DIM) contain the supplementary crystallographic data for this section.

11.2 Inclusion compounds with **H_2**

11.2.1 Introduction

H_2 was consequently exposed to these halogen-containing guests to assess its possible discriminatory behaviour in equivalent experiments, and to compare these data with those for **H_1**.

11.2.2 Individual inclusions

The host was dissolved in each of the respective potential guest solvents and the so-formed crystals analysed by means of ^{1}H-NMR spectroscopy to determine whether inclusion had occurred and, if so, the H:G ratio. (Note that the focus here was only on the dihalomethanes). Table 11.7 is a summary of these results. (The ^{1}H-NMR spectra of these complexes may be found in the Supplementary Information, Figures S225–227.)

Table 11.7. Results of the single solvent experiments and consequential H:G ratios.[a]

Guest (G)	H:G
DCM	1:2
DBM	1:2
DIM	1:1

[a]Determined using ^{1}H-NMR spectroscopy with $CDCl_3$ as solvent.

H_2 successfully formed inclusion compounds with all three dihaloalkanes, with complexes containing DCM and DBM preferring 1:2 H:G ratios, while DIM was enclathrated with a 1:1 ratio. (Experiments with **H_1** showed the host to prefer the 1:1 H:G ratio consistently with the three guests.) Competition experiments were subsequently conducted in order to determine the effect of the presence of multiple guests on the inclusion behaviour of the host.

11.2.3 Equimolar competition experiments

These competition experiments were carried out by dissolving **H_2** in equimolar binary and ternary combinations of the guests. The resultant mixed inclusion compounds were analysed in the same manner as in the single solvent inclusions. The experiments were carried out in duplicate, and the complete data set is provided in the Supplementary Information (Table

S228). Table 11.8 is a summary of the averaged results from these experiments, and displays the relative ratios of the guests present, and also the overall H:G ratios (as usual, % e.s.d.s are in parentheses).

Table 11.8. Results for **H₂** when presented with equimolar mixed dihaloalkanes.[a,b]

DCM	DBM	DIM	Average guest ratios	Overall H:G ratio	% e.s.d.s
x	x		38.5:61.5	1:2	(2.0):(2.0)
x		x	77.8:22.2	1:1	(0.3):(0.3)
	x	x	84.2:15.8	1:1	(0.1):(0.1)
x	x	x	35.7:51.7:12.6	1:1	(3.9):(2.6):(1.3)

[a]Ratios determined using ^{1}H-NMR spectroscopy with $CDCl_3$ as solvent.
[b]Experiments were conducted in duplicate.

The overall H:G ratios (Table 11.8) are in agreement with data from Table 11.7: employing DCM or DBM in the single solvent studies afforded complexes with 1:2 H:G ratios and, when these two guests were mixed, the overall H:G remained 1:2. However, when either of these guests was mixed with DIM, the H:G ratio reverted to 1:1 (Table 11.7, the preferred ratio for **H₂**·DIM).

As was the case for **H₁**, **H₂** also preferred DBM in these competitions. In the DCM/DBM and DBM/DIM experiments, the resultant cocrystals contained 61.5 and 84.2% of this guest, respectively. In the experiment involving DCM and DIM, the former guest was the preferred one (77.8%). An equimolar ternary experiment provided a host selectivity order of DBM (51.7%) > DCM (35.7%) > DIM (12.6%) [which differs somewhat from the results obtained with **H₁**, DBM (46.2%) > DIM (37.5%) > DCM (16.3%)]. Following these experiments, the host behaviour in the presence of binary guests where guest concentrations were varied was investigated.

11.2.4 Ratio-dependent competition experiments

After recrystallizing **H₂** from the different G/G mixtures, the relative guest ratios in the resultant mixed complexes and mother liquors were determined by utilizing ^{1}H-NMR spectroscopy. These data are graphically summarized as the selectivity profiles in Figure 11.7. The average selectivity coefficients were, once more, calculated for each profile, while a complete set of K values may be found in the Supplementary information (Tables S229–231).

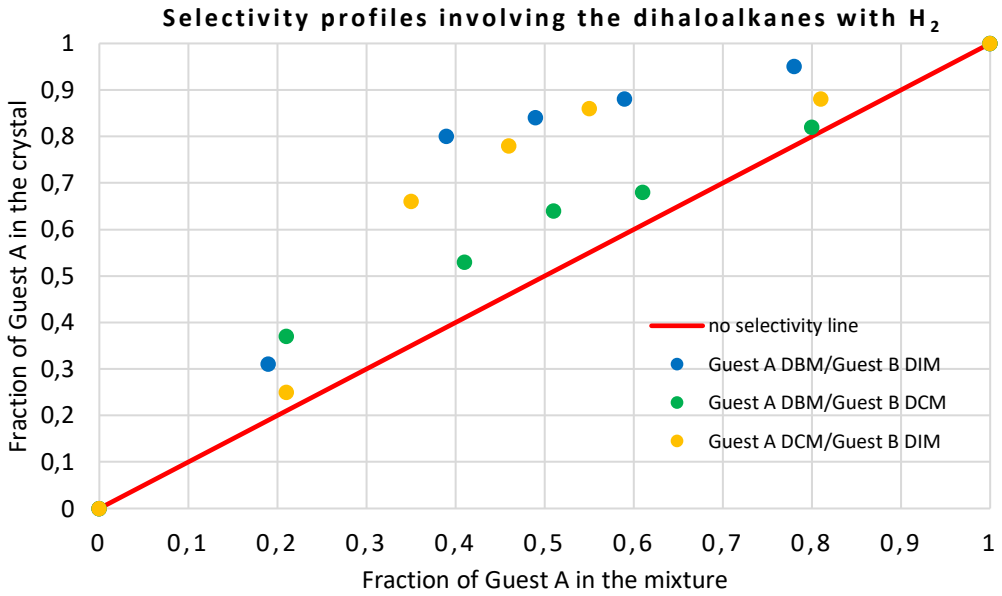

Figure 11.7. Overlaid selectivity profiles for G/G combinations of the dihaloalkane guests.

Figure 11.7 (the blue and green profiles) clearly shows that **H_2** is selective for DBM over the entire range assessed, even when the relative amount of this guest in the solution was low, when competing with DIM and DCM, respectively. Furthermore, a significant deviation of the experimental data points from the hypothetical line of no selectivity is noted for the blue profile (K = 4.8) compared with the green profile (K = 1.6), where data points lie closer to this linear plot. These observations confirm the host preference of DCM over DIM, and this was confirmed by the experiment employing DCM/DIM mixtures, where K = 3.1 in favour of DCM (Figure 11.7, yellow profile).

To understand the observed host selectivity, any suitable crystals of each complex were analysed by means of SCXRD.

11.2.5 SCXRD

Unfortunately, the crystal structure of the inclusion compound **H_2**·DIM could not be determined due to poor crystal quality. However, structures were successfully obtained for **H_2**·2(DCM) and **H_2**·2(DBM). Both DCM and DBM displayed positional disorder which was adequately modelled. The relevant crystallographic data for these experiments are summarized in Table 11.9.

Table 11.9. Crystallographic data for complexes of **H₂** with DCM and DBM.

	H₂·2(DCM)	**H₂**·2(DBM)
Chemical formula	$C_{40}H_{32}N_2O_2{\cdot}2(CH_2Cl_2)$	$C_{40}H_{32}N_2O_2{\cdot}2(CH_2Br_2)$
Formula weight	742.53	920.33
Crystal system	Triclinic	Triclinic
Space group	*P*-1	*P*-1
μ (Mo Kα)/mm^{-1}	0.366	0.415
a/Å	8.8213(4)	8.8555(4)
b/Å	8.8657(4)	8.8981(4)
c/Å	13.5055(6)	13.5996(6)
alpha/°	73.237(2)	72.633(2)
beta/°	72.035(2)	72.998(2)
gamma/°	66.861(2)	66.578(2)
V/Å^3	906.87(7)	919.83(7)
Z	1	1
F(000)	386	458
Temp./K	200	200
Restraints	6	6
Nref	4501	4561
Npar	251	251
R	0.0467	0.0387
wR2	0.1369	0.1013
S	1.03	1.04
θ min–max/°	1.6, 28.3	1.6, 28.4
Tot. data	24198	28553
Unique data	4501	4561
Observed data [I > 2.0 sigma(I)]	3477	3360
R_{int}	0.023	0.028
Dffrn measured fraction θ full	0.999	1.000
Min. resd. dens. (e/Å^3)	–0.38	–0.60
Max. resd. dens. (e/Å^3)	0.34	0.37

Once more, the inclusion compounds display isostructural host packing, crystallizing in the triclinic (*P*-1) crystal system. Figure 11.8 shows the unit cells of the two complexes, where the host is represented by ball-and-stick and the guests with space-fill representation.

a) b)

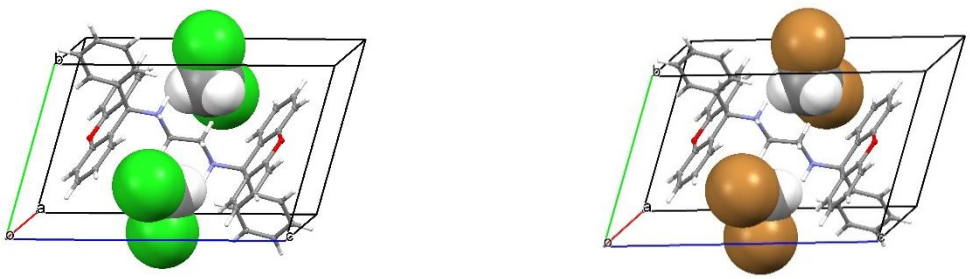

Figure 11.8. Unit cells for a) **H₂**·2(DCM) and b) **H₂**·2(DBM).

The host geometry was found to be near-identical in the two complexes (Figure 11.9). As previously noted for inclusion compounds of **H_2**, the xanthenyl unit is planar with the deviation from planarity calculated, in this case, to be only 1.0° for both complexes. The ethylenediamine linker assumed a more linear arrangement, with the N atoms adopting an antiperiplanar geometry.

a) b)

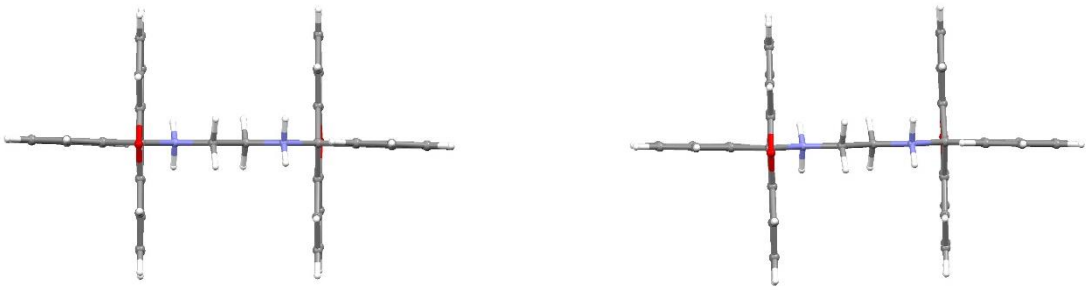

Figure 11.9. The host geometry in a) **H_2**·2(DCM) and b) **H_2**·2(DBM).

As a result of this geometry, the host packs in a very ordered manner, which may be viewed in Figure 11.10, and guests therefore reside in well-defined and distinct spaces.

a) b)

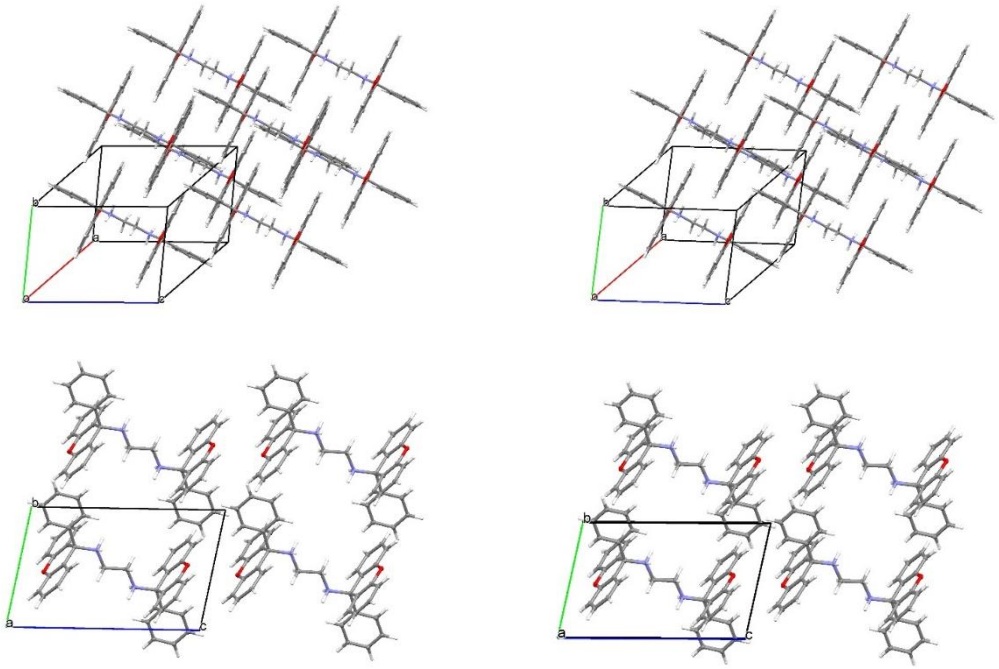

Figure 11.10. The host packing in a) **H_2**·2(DCM) and b) **H_2**·2(DBM), with views from two different angles.

The nature of the guest accommodation is shown in Figure 11.11, and these voids were calculated after the guests were removed from the packing calculations. Since the host packing in **H₂**·2(DCM) and **H₂**·2(DBM) is isostructural, only the voids for the DCM is depicted as a representative example. In both complexes of **H₂**, the guest is accommodated in infinite multidirectional channels. Interestingly, **H₁** enclathrated its guests as pairs in discrete cavities.

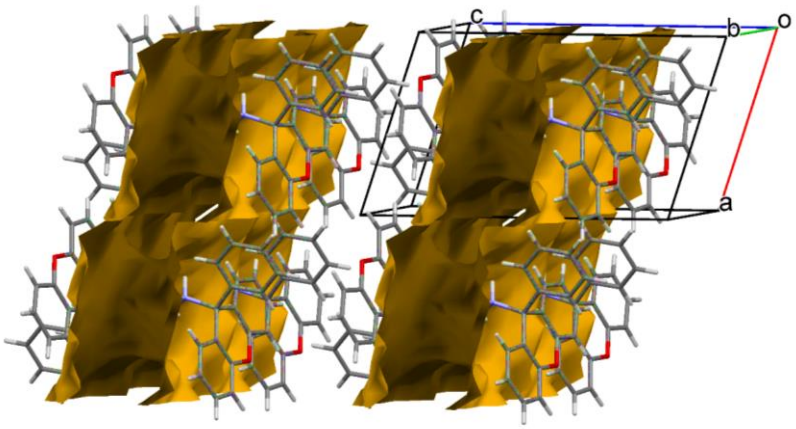

Figure 11.11. Calculated voids for the **H₂**·2(DCM) complex.

Since SCXRD data could not be obtained for the **H₂**·DIM complex, an experimental PXRD pattern was aquired in order to determine whether the host packing was the same here as in the other two complexes (where the patterns were generated using the Mercury software). No similarities were evident and so the host packing in the complex containing DIM differed from that in **H₂**·2(DCM) and **H₂**·2(DBM). (This was not the case in the complexes with **H₁**, where all three displayed isostructural host packing.) [The generated (for DCM and DBM complexes) and experimental (DIM) powder patterns are provided in the Supplementary Information, Figure S232.]

From further investigation of the SCXRD data, the significant H···G interactions were obtained and are summarized in Table 11.10. (A table of H···H interactions may be found in the Supplementary Information, Table S233.)

Table 11.10. H···G interactions present in complexes of **H_2**.[a,b]

Non-covalent interaction	**H_2**·2(DCM)	**H_2**·2(DBM)	Symmetry operator
Short contacts (X···Z, X–Y···Z)			
$C_{(H)}$–$C_{(H)}$···$H_{(G2)}$–$C_{(G2)}$	2.77 Å, 113° (<)		x, y, z
$C_{(H)}$–$C_{(H)}$···$H_{(G1)}$–$C_{(G1)}$	2.77 Å, 107° (<)		1−x, 1−y, 1−z
$N_{(H)}$–$H_{(H)}$···$Cl_{(G2)}$–$C_{(G2)}$	2.82 Å, 156° (<)		1+x, y, z
$C_{(G2)}$–$H_{(G2)}$···$H_{(H)}$–$C_{(H)}$	2.80 Å, 145° (<)		1−x, 1−y, 1−z
$C_{(H)}$–$C_{(H)}$···$H_{(G2)}$–$C_{(G2)}$		2.70 Å, 116° (<<)	x, y, z
$N_{(H)}$–$H_{(H)}$···$Br_{(G2)}$–$C_{(G2)}$		2.90 Å, 154° (<)	1−x, y, z
$C_{(H)}$–$H_{(H)}$···$Br_{(G2)}$–$C_{(G2)}$		2.91 Å, 145° (<)	−x, 1−y, 1−z
$C_{(G2)}$–$H_{(G2)}$···$C_{(H)}$–$C_{(H)}$		2.83 Å, 143° (<)	1−x, 1−y, 1−z
$C_{(G1)}$–$Br_{(G1)}$··$H_{(H)}$–$N_{(H)}$		2.87 Å, 137° (<)	−1+x, y, z
$C_{(G1)}$–$Br_{(G1)}$···$H_{(H)}$–$C_{(H)}$		2.91 Å, 160° (<)	x, −1+y, z

[a]Guest 1 and Guest 2 (G1 and G2) represent the two disordered guest components in the host crystal.
[b]Distances denoted by < are contacts that measure less than the sum of the van der Waals radii of the atoms involved, while those denoted by << is this sum minus 0.2 Å.

The two inclusion compounds experience no H···G π···π (expectedly) nor CH···π interactions (Table 11.10). The chlorine atom in DCM is involved in one stabilizing interaction with the host compound [$N_{(H)}$–$H_{(H)}$···$Cl_{(G2)}$–$C_{(G2)}$, 2.82 Å (156°)], while bromine in DBM is involved in four contacts ranging between 2.87–2.91 Å (137–160°), with each disordered component experiencing two of these, and this observation correlates with the high selectivity of **H_2** for DBM. DCM is held in the crystal by an additional three short contacts [2.77–2.80 Å (107–145°)], whereas DBM experiences a further two of these, but with one of these being particularly stabilizing [$C_{(H)}$–$C_{(H)}$···$H_{(G2)}$–$C_{(G2)}$, 2.70 Å (116°)]. The data for **H_1** also showed that the preferred DBM guest experienced a more significant number of H···G interactions compared with the other two guests, and that the DIM complex displayed a stabilizing G···G interaction due to the increased size of the molecule. However, since a crystal structure could not be obtained for **H_2**·DIM, it was not possible to make comparisons with **H_1**·DIM.

11.2.6 Hirshfeld surface analyses

Hirshfeld surface analyses were carried out on both the **H_2**·2(DCM) and **H_2**·2(DBM) complexes. The resulting 2D fingerprint plots are provided in the Supplementary Information (Figure S234). (All surfaces in this instance were generated around the guest molecules and since the guests in both **H_2**·2(DCM) and **H_2**·2(DBM) showed disorder, these surfaces were mapped for both major and minor components). Figure 11.12 illustrates the percentage of intermolecular interactions (G···H/H···G) present in these complexes.

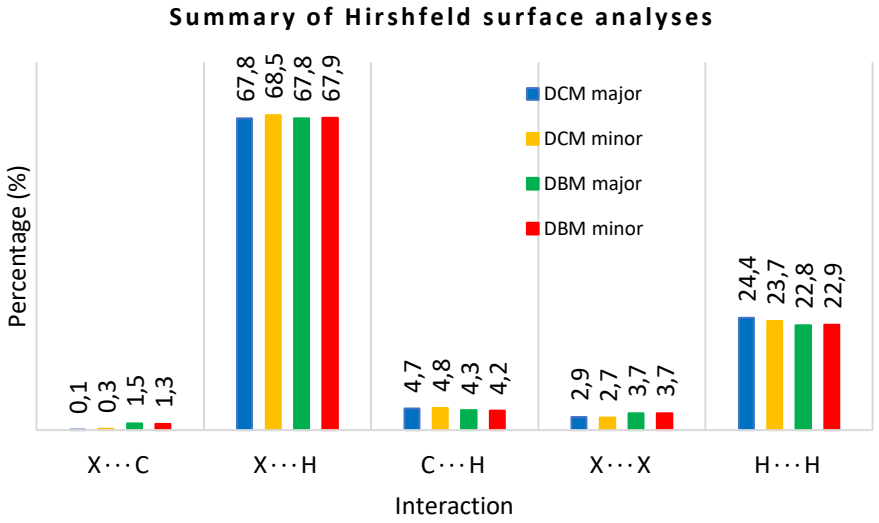

Figure 11.12. Quantitative interactions after Hirshfeld surface analyses.

Unfortunately, this analysis of the H···G interactions does not provide any information regarding the reasons for the selectivity order of the host since the quantities of specific interactions types are all comparable.

11.2.7 Thermal analyses (DSC and TG)

Thermal analyses were carried out on each of the three complexes with **H_2**, and the resultant overlaid TG (blue), DSC (green) and DTG (red) traces are provided in Figure 11.13. The relevant thermal data are summarized in Table 11.11.

a)

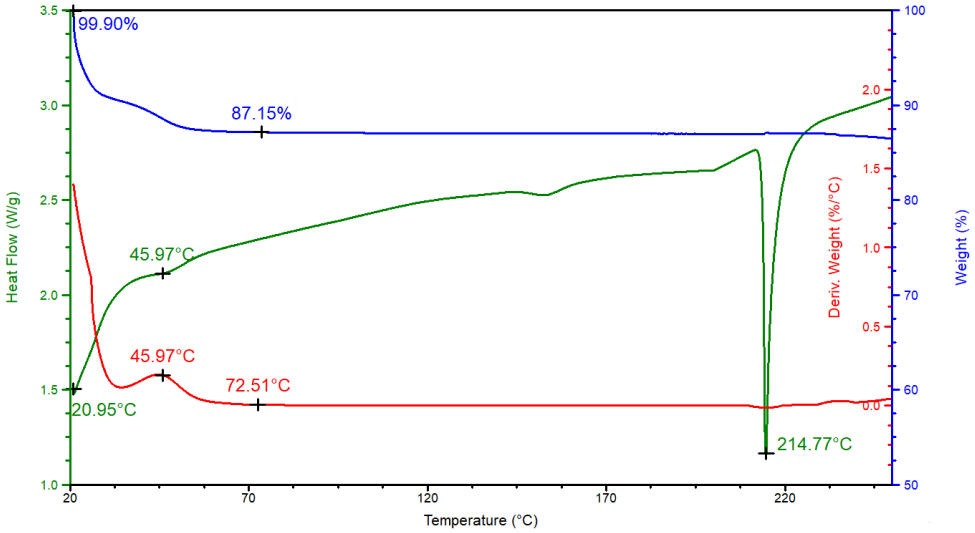

b)

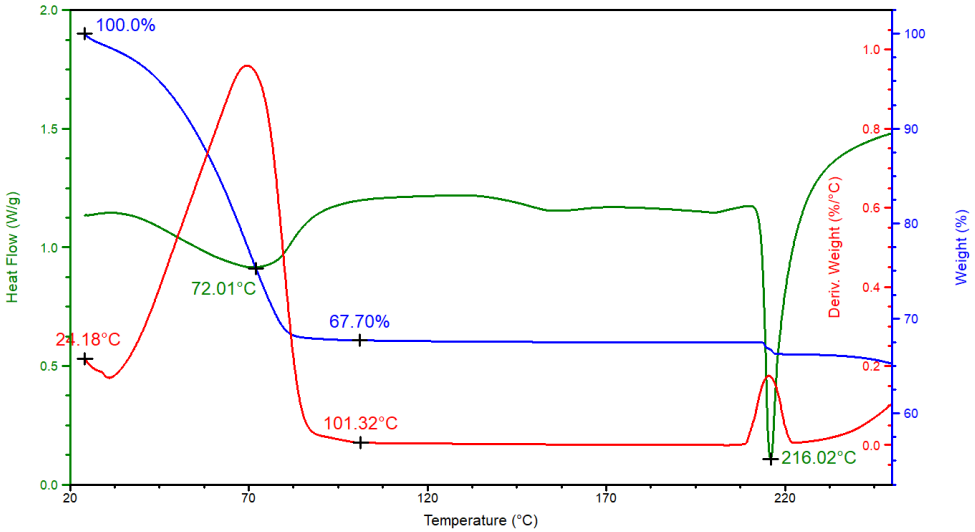

c)

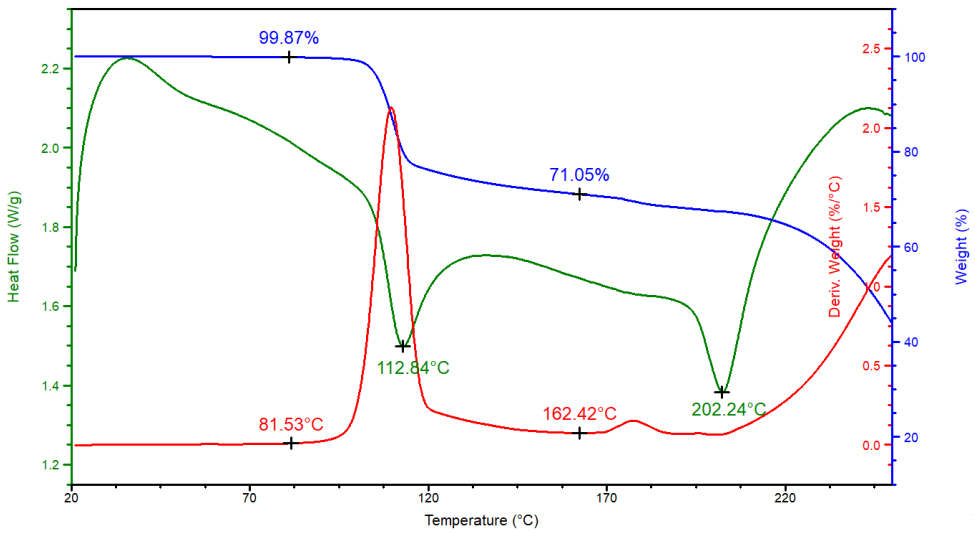

Figure 11.13. Overlaid thermal traces (DSC, TG and DTG) for a) **H₂**·2(DCM), b) **H₂**·2(DBM) and c) **H₂**·DIM.

Table 11.11. Thermal data for complexes formed with **H_2**.

Guest (G)	T_{on} /°C	T_p /°C	Mass loss expected /%	Actual mass loss measured /%
DCM	[a]	46.0	22.9	12.8[b]
DBM	[a]	72.0	37.8	32.3[b]
DIM	81.5	112.8	32.6	28.8

[a]These could not be accurately determined since mass loss occurred from the outset of the experiments.
[b]The inclusion compounds with DCM and DBM were unstable at room temperature; therefore, the observed mass loss is significantly lower than that expected.

Figure 11.13a and b shows that the DBM and DCM complexes are unstable at room temperature. These experience mass loss from the outset of these analyses, as observed in the two respective TG traces, and so mass loss measurements differ significantly from those expected. However, the DIM complex is notably more stable than the previous two, and the expected (32.6%) and experimental (28.8%) mass losses are in better agreement. In this complex, the host releases the guest at an increased temperature of 81.5 °C. These data do not correlate with the selectivity order observed for **H_2**, which was also the case for **H_1**. However, a previous report has associated higher relative thermal stabilities with discrete cavity occupation by the guest, while lower stabilities accompany complexes where the guests reside in channels.[312] The DBM and DCM guest in complexes with **H_2** occupy channels, as observed earlier (Figure 11.11), and this observation therefore agrees with that report here, since these two guests form thermally unstable complexes with **H_2**.

11.2.8 Conclusions

H_2 displayed an affinity for the dihalomethanes (DCM, DBM and DIM), and the host included DCM and DBM with a 1:2 ratio, and DIM with a ratio of 1:1. Equimolar and non-equimolar G/G experiments showed that the host preferred the bromo derivative. The selectivity was established to be in the order DBM > DCM > DIM. SCXRD showed the most favoured guest, DBM, to experience a larger number of H···G interactions. **H_2**, furthermore, accommodated its guests in channels, while **H_1** formed discrete cavities which held two guest molecules per void. This observation again highlights the significant changes in crystal packing between the two host compounds. Thermal analyses were used to determine the relative thermal stabilities of the three inclusion compounds, but these data could not be related back to host selectivity observations, as was also the case for **H_1**.

11.2.9 Supporting information

The relevant NMR spectra, additional data and traces for the two inclusion compounds may be found in the Supplementary Information. The crystal structures were deposited at the Cambridge Crystallographic Data Centre, and CCDC 1824152 **H_2**·2(DCM), and 1824153 **H_2**·2(DBM) contain the supplementary crystallographic data for this section.

11.3 Vapour inclusion of the dihaloalkane guests

Crystalline hosts **H_1** and **H_2** were subjected to each dihaloalkane (DCM, DBM and DIM) in their vapour phases. This was achieved by suspending the solid host material inside a vial above the liquid guest (see §2.7.3) The resultant solids were monitored intermittently over several days (1–31 days) by ^{1}H-NMR spectroscopy to determine whether these hosts have the ability to enclathrate these guests from the gas phase. Comparable experiments were also conducted but where **H_1** and **H_2** were suspended above an equimolar ternary (DCM/DBM/DIM) solvent mixture.

H_2 did not include any of the three guests in this manner over the allocated time period (1–31 days). Additionally, this host also displayed no inclusion ability in the presence of the mixture of gaseous guests. Surprisingly, and in direct contrast, **H_1** possessed the ability to absorb guests from the gaseous phase, and Figure 11.14 illustrates the results obtained when this host was subjected to these gaseous guests. The y-axis indicates the percentage of guest inclusion that was calculated using the integration of applicable resonances from the ^{1}H-NMR spectra, and the x-axis displays the amount of time that the host was subjected to these gases.

a)

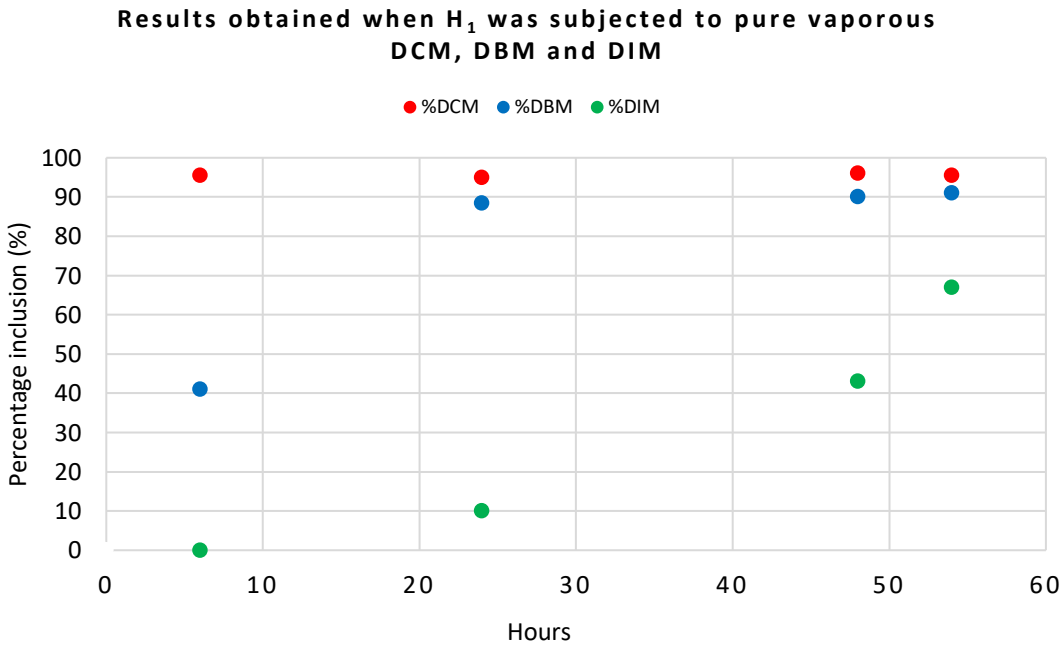

b)

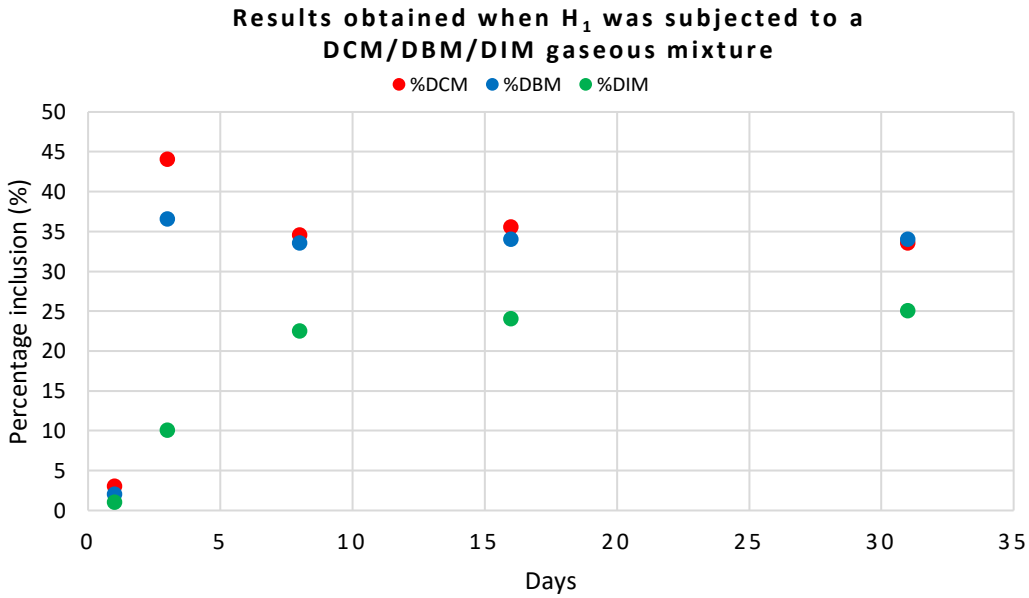

Figure 11.14. Graphical representation of the inclusion behaviour of **H_1** when in the presence of a) pure gaseous guests, and b) a gaseous guest mixture.

From Figure 11.14a, it is clear that DCM was included with a H:G ratio of almost 1:1 after only 6 h, and this ratio remained relatively consistent until 54 h had lapsed. The DBM uptake was much slower, however, with approximately a 1:1 ratio being observed at only ~24 h, while only 67% of DIM had been absorbed after 54 h. These results are in accordance with the volatility of the three guests as DCM is the most volatile, followed by DBM and DIM.

In the mixed guest experiment (Figure 11.14b), **H_1** initially selected for the guests in the order DCM > DBM > DIM, according to guest volatility once more. After three days, however, a guest exchange was observed to occur and, while the DBM percentage remained relatively constant (since the three-day analysis), DCM was exchanged for DIM molecules (the percentage of DCM in the crystals decreased from 45 to 35% while that of DIM increased from 10 to 23%). This observation correlated with the recrystallization experiments (DBM > DIM > DCM), where **H_1** showed increased selectivity for DIM relative to DCM. The overall H:G ratio remained 1:1 throughout the entire experiment.

The fact that **H_2** did not include any guest from the gas phase was interesting. Throughout this work, **H_1** was generally less selective than **H_2** for the preferred guest, DBM (see Tables 11.3 and 11.8), and guests taken up by **H_1** experienced fewer H···G interactions compared with **H_2**. Therefore, it is plausible that guests are readily enclathrated from the gas phase by the less-discerning **H_1** compared with **H_2**, which did not absorb guest from the gas phase. Furthermore, it was observed (from thermal analyses) that **H_1** recrystallized from all three dihaloalkanes to form stable inclusion complexes with a H:G ratio of 1:1. Contrastingly, **H_2** only formed one stable complex, that with DIM. It is thus conceivable that **H_1** successfully included these guests from the vapour phase since the resulting complexes were stable, while **H_2** did not, owing to the instability of complexes **H_2**·2(DCM) and **H_2**·2(DBM).

In conclusion, the experiment of **H_1** with a mixture of vaporous guests was initially affected by volatility and, after a period of time, the selectivity of the host became more prominent, and guest exchange was observed to occur, with the more preferred guest (DIM) being absorbed in favour of the less favoured one (DCM). This process was possibly facilitated by the fact that the host packing in all the complexes was isostructural. Host **H_2**, on the other hand, did not form stable complexes with the preferred guests DBM and DCM (in the liquid phase), which was possibly the reason for its reluctance to absorb these guests from the vaporous phase. DIM, though forming a stable complex with **H_2** from solution, was not a preferred guest (DBM > DCM > DIM) and this may explain, once more, why **H_2** did not form a complex with this guest from the vaporous phase.

12. MISCELLANEOUS AND FUTURE WORK

12.1 Miscellaneous

In addition to the guest compounds that were successfully enclathrated by **H_1** and **H_2** (discussed in Chapters 3–11), the inclusion ability of these hosts was assessed with a variety of other aromatic, heterocyclic and aliphatic compounds. Table 12.1 summarizes the results obtained, together with the H:G ratios as determined by means of ^{1}H-NMR spectroscopy. (The spectra for these complexes are provided in the Supplementary Information, Figures S235–252.)

Table 12.1. Additional miscellaneous inclusions of **H_1** and **H_2**.

Guest	H:G ratio of **H_1** complexes	H:G ratio of **H_2** complexes
1,2-Dimethoxyethane	1:1[a]	1:1[a]
3-Picolylamine	1:1[a]	[c]
4-Methylmorpholine	1:1[a]	[c]
Acetone	1:1[a]	1:1.5[a]
Anethole	1:1	[c]
Benzene	1:1[a]	1:1
Bromochloromethane	1:1[a]	1:2[a]
Butanone	1:1	[c]
Chlorobenzene	1:1[a]	[c]
Chlorocyclohexane	1:1	[c]
Cyclohexane	1:1	[c]
Cyclohexene	1:1[a]	[c]
Dimethylformamide	1:1	[c]
Ethyl acetate	[b]	1:1
Nitromethane	[b]	1:2
Tetrahydropyran	1:1[a]	[c]

[a]SCXRD analysis was carried out on this complex, but is not provided here owing to relevance.
[b]Inclusion of this guest did not occur.
[c]Inclusion ability was not assessed.

H_1 successfully included a variety of guests that were, to some extent, related to the guests in Chapters 3–11. These include 3-picolylamine (Chapter 10), 4-methylmorpholine and tetrahydropyran (Chapter 7), and bromochloromethane, chlorobenzene and chlorocyclohexane (Chapter 11). In addition to these, **H_1** also enclathrated many other aliphatic compounds (1,2-dimethoxyethane, acetone, butanone and dimethylformamide). Despite the wide-ranging inclusion ability of **H_1**, there was found to be many solvents that this host did not include or guest solvents in which the host was insoluble. (These compounds are provided in the Supplementary Information, Table S253.)

Interestingly, the different host behaviours of **H_1** and **H_2** are, once again, apparent here, where **H_2** included guests that **H_1** did not (Table 12.1, nitromethane and ethyl acetate). It is therefore clear that the investigation of these two host compounds has not been exhausted in the present work, and much future work remains.

12.2 Future work

12.2.1 Additional selectivity studies with **H_1** and **H_2**

Based on the miscellaneous compounds that were included by **H_1** and **H_2**, additional selectivity investigations may be carried out to further assess the host behaviour of these compounds in the presence of alternative guest series'.

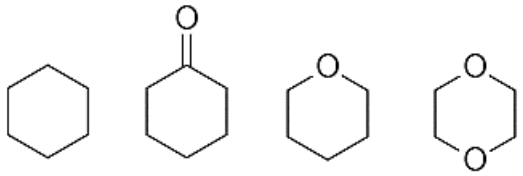

Scheme 12.1. Guest series involving cyclohexane, cyclohexanone, tetrahydro-2H-pyran and 1,4-dioxane.

A study comprising cyclohexane, cyclohexanone, tetrahydro-2H-pyran and 1,4-dioxane (Scheme 12.1) may provide information on how the presence, position and number of oxygen atoms would affect the preference and selectivity of the host.

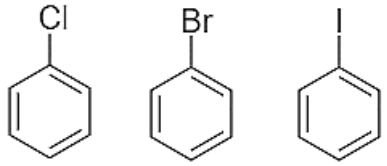

Scheme 12.2. Guest series involving chlorobenzene, bromobenzene and iodobenzene.

Similar to the dihaloalkane guest series, employing chloro-, bromo- and iodo- benzene (Scheme 12.2) may provide information on the preference of the host for these halogenated compounds but, in this case, more interactions are possible between the host and guest, owing to the aromaticity now present in the guest species (π···π and C–H···π).

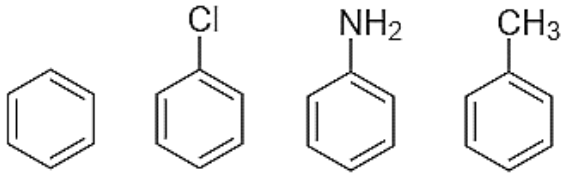

Scheme 12.3. Guest series involving benzene, chlorobenzene, aniline and toluene.

The host selectivity was independently analysed with aromatic, alkyl aromatic, amines and halogenated compounds. Combining these guest series by utilizing benzene, chlorobenzene, aniline and toluene (that is, varying one functional group on the benzene moiety, Scheme 12.3) may make it possible to determine which functional groups are favoured, based on the selectivity displayed in competition experiments.

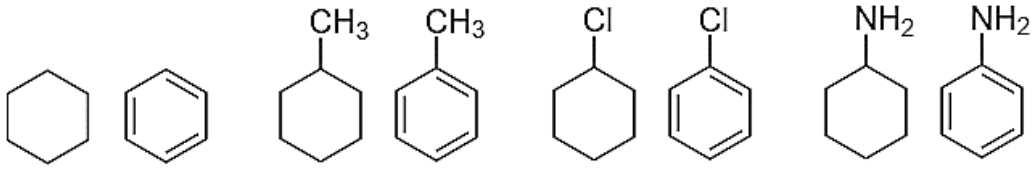

Scheme 12.4. Guest series involving cyclohexane, benzene, methylcyclohexane, toluene, chlorocyclohexane, chlorobenzene, cyclohexamine and aniline.

The preference of the hosts for aromatic and saturated compounds was assessed in Chapter 8 and involved five-membered heterocyclic rings. This preference (aromatic vs saturated) may also be investigated with a series of six-membered rings (Scheme 12.4). Guests would include cyclohexane vs benzene, methylcyclohexane vs toluene, chlorocyclohexane vs chlorobenzene and cyclohexamine vs aniline.

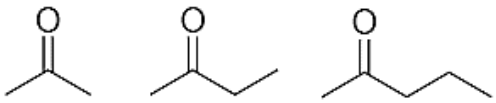

Scheme 12.5. Guest series involving acetone, 2-butanone and 2-pentanone.

Since **H_1** has the ability to include acetone and 2-butanone, the competition of acetone, 2-butanone and 2-pentanone (Scheme 12.5) may provide information on the preference of the host as chain length increases.

12.2.2. Derivatization of **H_1** and **H_2**

An improvement in the selectivity displayed by the title host compounds remains, however, attractive, and this might be achieved by derivatization of these compounds. The synthetic route to **H_1** and **H_2** allows for modifications to the phenyl moieties, the linker unit, as well as the central ring of the fused ring system (Scheme 12.6). The synthetic route to these host compounds may be modified by employing alternative starting reagents than xanthone or thioxanthone (Scheme 12.6, where X is varied). Other derivatives may be synthesized by utilizing alternative Grignard reagents (where Y is varied) rather than bromobenzene. Finally, novel hosts may be synthesized by replacing the ethylenediamine linker with an alternative (A–A linker, Scheme 12.6). Such derivatives have successfully been synthesized and these do display inclusion ability. Recently, derivatives were prepared by substitution of the ethylenediamine linker with cyclohexane-1,4-diamine,[313] and the phenyl moiety with cyclohexane.[314]

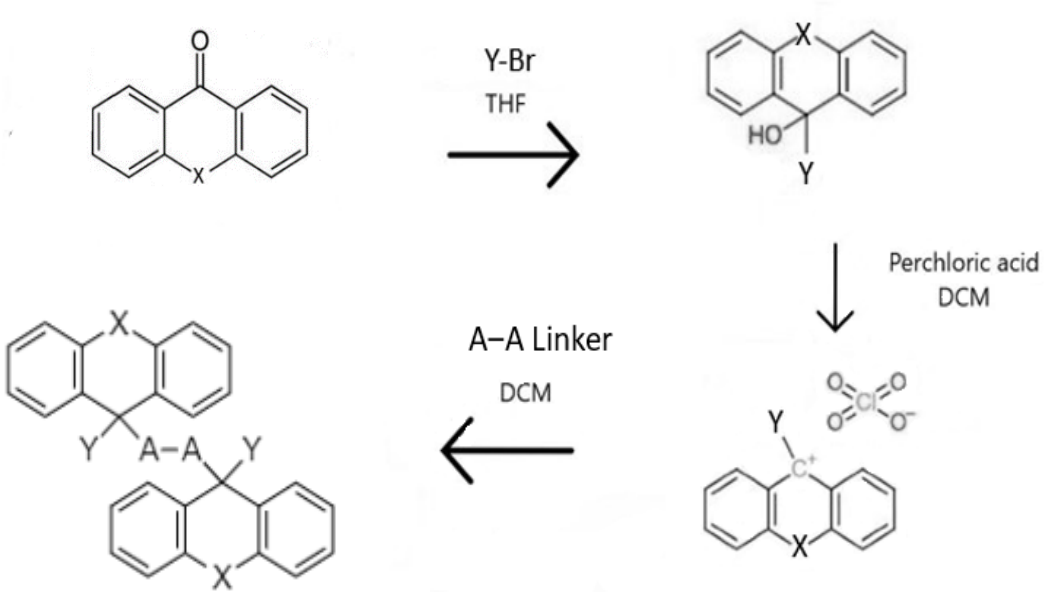

Scheme 12.6. Possible derivatives of **H_1** and **H_2**.

OVERALL CONCLUSION

The host compounds **H_1** and **H_2** were readily synthesized through a Grignard addition reaction, using phenylmagnesium bromide, on thioxanthone and xanthone, respectively. The resultant alcohols were reacted with perchloric acid to afford the corresponding perchlorate salts and, finally, two of these molecules were linked by utilizing ethylenediamine as a reagent.

H_1 displayed excellent inclusion ability when exposed to xylenes and ethylbenzene, methylanisoles and anisole, methylpyridines and pyridine, and methylcyclohexanones and cyclohexanone. This host compound also included heterocyclic five- and six- membered ring compounds, alkyl-substituted benzenes, anilines and dihaloalkanes. A 1:1 H:G ratio was consistently preferred in all cases. **H_2** also included most of the same guests, but not the methylcyclohexanones and cyclohexanone, nor the heterocyclic five-membered ring guest species. Additionally, varying H:G ratios were observed for complexes formed with **H_2**.

Both enhanced and contrasting host behaviours were observed when each of **H_1** and **H_2** was employed in a range of competition experiments in the presence of isomeric guest species (Chapters 3–6), on the one hand, and non-isomeric guest species (Chapters 7–11) on the other.

Whether these host compounds possessed the ability to selectively include guests from a mixture was also considered in order to determine if they would be suitable in the design of alternative separation strategies in order to replace existing expensive, inefficient and time-consuming methods for the purification of such guest mixtures.

The results obtained from this work may be summarized as follows:

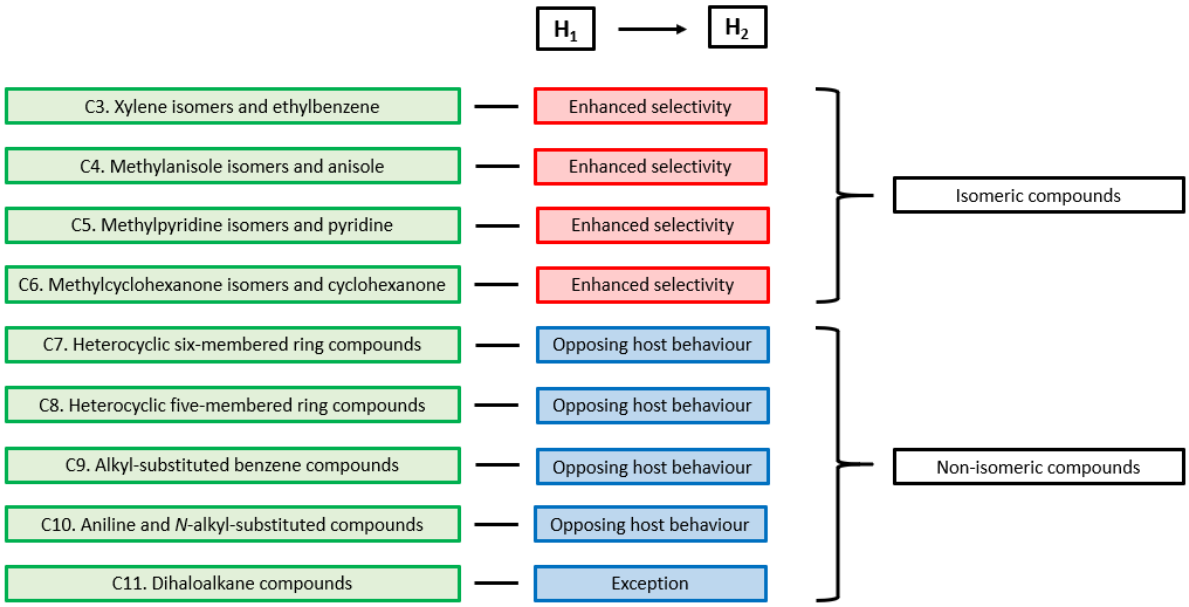

When **H₁** and **H₂** were exposed to isomeric mixtures, **H₂** exhibited an enhanced selectivity for the preferred guests compared with **H₁** (in each series, the selectivity *order* was found to be similar for both hosts). However, contrastingly, in the presence of non-isomeric compounds, the hosts displayed distinctly opposing behaviours (with the exception of the dihaloalkane compounds). **H₁** and **H₂** also demonstrated very high selectivities for *p*-xylene, aniline and *N*,*N*-dimethylaniline from the C_8H_{10} and aniline guest series, respectively, where the selectivity was ~90% or higher for these preferred guests. These observations may be exploited for industrial application to replace existing cumbersome separation processes.

SCXRD analyses of the complexes showed that, in most cases, the inclusion of these guests was greatly influenced by the H···G interactions, which included π···π stacking, C–H···π, hydrogen bonding and various other short contacts. Guest compounds were found to be accommodated in either cavities or channels, and this depended on the nature of the guests present. The host molecule conformations of **H₁** and **H₂** were analysed in their respective complexes, and it was found that the tricyclic fused ring system of **H₁** usually adopted a buckled geometry and the N atoms of the linker a synclinal arrangement. However, in the complexes with **H₂**, the tricyclic fused ring system was consistently near-planar and the N atoms normally in an antiperiplanar conformation. These variances in host geometry may explain the different host packing in the complexes, where this was more ordered in inclusion compounds with **H₂**, facilitated by the more planar O-containing ring and linear linker. For **H₁**, on the other hand, the buckled S-containing ring and gauche-orientated N atoms resulted in

a less ordered packing. These packing differences, in turn, may explain why **H_1** and **H_2** displayed different host behaviours, either enhanced selectivities (as in the presence of the isomeric guest series') or contrasting (as in the presence of the non-isomeric guest series').

Hirshfeld surface analyses were conducted on many of the H···G complexes to determine if there was any quantitative interaction type between host and guest that contributed to an understanding of the observed selectivity orders displayed by the host. This form of analysis did not, generally, yield any further information with regards to the reasons for these selectivities, and was most useful only in one instance, that is, when understanding the host selectivity order displayed by **H_1** in the presence of the five-membered heterocyclic guest species.

Thermal analyses were additionally performed on all suitable H···G complexes in this investigation. The terms T_{on} and T_p correlated with the selectivity order displayed by these host compounds in most cases, but not all.

In conclusion, the host behaviour of compounds may be profoundly affected by small changes in host structure, as was observed for **H_1** and **H_2**, where the only difference was in the B rings of the tricyclic fused ring system (**H_1** possessed a sulfur atom here while this was substituted for oxygen in **H_2**). Furthermore, this work has demonstrated that host-guest chemistry has a promising future in separation science applications owing to the excellent selectivities displayed by these hosts when presented with guest mixtures.

REFERENCES

(1) Lehn, J.-M.; Sanders, J. *Angew. Chem. Eng. Ed.* **1995**, *34*, 2429.

(2) Atwood, J. L.; Suslick, K. S.; Lehn, J.-M.; Comprehensive Supramolecular Chemistry 4: Supramolecular reactivity and transport : bioinorganic systems, Elsevier, 1996, *5*.

(3) Atwood, J. L.; Steed, J. W. Encyclopedia of supramolecular chemistry, Marcel Dekker Inc., New York, 2004, *1*.

(4) Nagendrappa, G. *Resonance,* **2011**, *16*, 606.

(5) Patel, L. D. MSc Thesis, Cape Peninsula University of Technology, Cape Town, 2014.

(6) Weber, E., Encyclopedia of Supramolecular Chemistry, Marcel Dekker Inc., New York, 2004.

(7) Steed, J. W.; Turner, D. R.; Wallace, K.; Core Concepts in Supramolecular Chemistry and Nanochemistry, John Wiley & Sons, 2007.

(8) Desiraju, G. R. *J. Am. Chem. Soc.* **2013**, *135*, 9952.

(9) Matsumoto, K.; Hayashi, N.; Heterocyclic Supramolecules II, Springer, 2009; *18*.

(10) Barton, B. PhD Thesis, University of Port Elizabeth, Port Elizabeth, 1997.

(11) Weber, E.; Josel, H.-P. *J. Incl. Phenom.* **1983**, *1*, 79.

(12) Schmidt, G. *Pure Appl. Chem.* **1971**, *27*, 647.

(13) Desiraju, G. R.; Parshall, G. W.; Crystal engineering: the design of organic solids, Elsevier, Amsterdam, 1989, *54*.

(14) Dianin, A. *J. Russ. Phys. Chem. Soc.* **1914**, *46*, 1310.

(15) Flippen, J.; Karle, J.; Karle, I. L. *J. Am. Chem. Soc.* **1970**, *92*, 3749.

(16) Nassimbeni, L. R.; Niven, M. L.; Taylor, M. W. *Inorg. Chim. Acta.* **1987**, *132*, 67.

(17) Harris, K. D. *Supramol. Chem.* **2007**, *19*, 47.

(18) Hollingsworth, M. D. *Science,* **2002**, *295*, 2410.

(19) Peraka, K. S.; Lusi, M.; Bajpai, A.; Zaworotko, M. J. *Cryst. Growth Des.* **2017**, *17*, 959.

(20) Jeffrey, G. A.; An introduction to hydrogen bonding, Oxford university press, New York, 1997, *12*.

(21) Aakeröy, C. B.; Seddon, K. R. *Chem. Soc. Rev.* **1993**, *22*, 397.

(22) Russell, V. A.; Etter, M. C.; Ward, M. D. *J. Am. Chem. Soc.* **1994**, 116, 1941.

(23) Moulton, B.; Zaworotko, M. J. *Chem. Rev.* **2001**, *101*, 1629.

(24) Metrangolo, P.; Neukirch, H.; Pilati, T.; Resnati, G. *Acc. Chem. Res.* **2005**, *38*, 386.

(25) Russell, V. A.; Evans, C. C.; Li, W.; Ward, M. D. *Science,* **1997**, *276*, 575.

(26) Shan, N.; Bond, A. D.; Jones, W. *Tetrahedron Lett.* **2002**, *43*, 3101.

(27) Holman, K. T.; Ward, M. D. *Angew. Chem.* **2000**, *112*, 1719.

(28) Hunter, C. A.; Sanders, J. K. *J. Am. Chem. Soc.* **1990**, *112*, 5525.

(29) Desiraju, G. R. *Acc. Chem. Res.* **1996**, *29*, 441.

(30) Nishio, M. *CrystEngComm,* **2004**, *6*, 1757.

(31) Novoa, J. J.; Mota, F. *Chem. Phys. Lett.* **2000**, *318*, 345.

(32) Lehn, J. M. *Angew. Chem. Int. Ed.* **1990**, *29*, 1304.

(33) Lehn, J. M. *Angew. Chem. Int. Ed. Eng.* **1988**, *27*, 89.

(34) Desiraju, G. R. *Angew. Chem. Int. Ed. Eng.* **1995**, *34*, 2311.

(35) Nangia, A.; Desiraju, G. R. *Acta Crystallogr. A.* **1998**, *54*, 934.

(36) Shattock, T. R.; Arora, K. K.; Vishweshwar, P.; Zaworotko, M. J. *Cryst.Growth Des.* **2008**, *8*, 4533.

(37) Almarsson, Ö.; Zaworotko, M. J. *Chem. Comm.* **2004**, 1889.

(38) Maly, K. E.; Maris, T.; Gagnon, E.; Wuest, J. D. *Cryst. Growth Des.* **2006**, *6*, 461.

(39) Aitipamula, S.; Banerjee, R.; Bansal, A. K.; Biradha, K.; Cheney, M. L.; Choudhury, A. R.; Desiraju, G. R.; Dikundwar, A. G.; Dubey, R.; Duggirala, N. *Cryst. Growth Des.* **2012**, *12*, 2147.

(40) Aakeröy, C. B.; Beatty, A. M.; Helfrich, B. A. *Angew. Chem. Int. Ed.* **2001**, *40*, 3240.

(41) Tothadi, S.; Mukherjee, A.; Desiraju, G. R. *Chem. Comm.* **2011**, *47*, 12080.

(42) Bajpai, A.; Scott, H. S.; Pham, T.; Chen, K.-J.; Space, B.; Lusi, M.; Perry, M. L.; Zaworotko, M. J. *IUCrJ,* **2016**, *3*, 430.

(43) Barth, J. V.; Costantini, G.; Kern, K., Engineering atomic and molecular nanostructures at surfaces, In Nanoscience And Technology: A Collection of Reviews from Nature Journals, 2010, *67*.

(44) Palma, C. A.; Bonini, M.; Breiner, T.; Samorì, P. *Adv. Mater.* **2009**, *21*, 1383.

(45) Xiao, W.; Hu, C.; Ward, M. D. *J. Am. Chem. Soc.* **2014**, *136*, 14200.

(46) Bajpai, A.; Venugopalan, P.; Moorthy, J. N. *CrystEngComm,* **2014**, *16*, 4853.

(47) Carletta, A.; Meinguet, C. l.; Wouters, J.; Tilborg, A. l. *Cryst. Growth Des.* **2015**, *15*, 2461.

(48) Braga, D.; Grepioni, F.; Maini, L.; Polito, M.; Crystal polymorphism and multiple crystal forms, Springer, Berlin, Heidelberg, 2009, *87*.

(49) Neumann, M. A.; Leusen, F. J.; Kendrick, J. *Angewandte Chemie* **2008**, *120*, 2461.

(50) Price, S. L. *Acc. Chem. Res.* **2008**, *42*, 117.

(51) Steed, J. W.; Atwood, J. L.; Gale, P. A.; Definition and emergence of supramolecular chemistry, Wiley Online Library, 2012.

(52) Pérez, E. M.; Martín, N. *Chem. Soc. Rev.* **2015**, *44*, 6425.

(53) Csöregh, I.; Czugler, M.; Weber, E. *J. Phys. Org. Chem.* **1993**, *6*, 171.

(54) Weber, E.; Dörpinghaus, N.; Csöregh, I. *J. Chem. Soc. Perkin Trans. 2,* **1990**, 2167.

(55) Csöregh, I.; Weber, E.; Nassimbeni, L. R.; Gallardo, O.; Dörpinghaus, N.; Ertan, A.; Bourne, S. A. *J. Chem. Soc. Perkin Trans. 2,* **1993**, 1775.

(56) Weber, E.; Skobridis, K.; Wierig, A.; Nassimbeni, L. R.; Johnson, L. *J. Chem. Soc. Perkin Trans. 2,* **1992**, 2123.

(57) Pohl, P. L. MSc Thesis, Nelson Mandela Metropolitan University, Port Elizabeth, 2015.

(58) Toda, F.; Tanaka, K. *Tetrahedron Lett.* **1988**, *29*, 551.

(59) Elwahy, A. H. *Tetrahedron Lett.* **2001**, *42*, 5123.

(60) Biradha, K.; Santra, R. *Chem. Soc. Rev.* **2013**, *42*, 950.

(61) Tozawa, T.; Jones, J. T.; Swamy, S. I.; Jiang, S.; Adams, D. J.; Shakespeare, S.; Clowes, R.; Bradshaw, D.; Hasell, T.; Chong, S. Y. *Nature materials,* **2009**, *8*, 973.

(62) Man, Y. M.; Mak, T. C.; Wong, H. N. *J. Org. Chem.* **1990**, *55*, 3214.

(63) Weber, E.; Hecker, M.; Csoeregh, I.; Czugler, M. *J. Am. Chem. Soc.* **1989**, *111*, 7866.

(64) Barton, B.; Hosten, E. C.; Jooste, D. V. *Tetrahedron,* **2017**, *73*, 2662.

(65) Hapiot, F.; Tilloy, S.; Monflier, E. *Chem. Rev.* **2006**, *106*, 767.

(66) Harata, K. *Chem. Rev.* **1998**, *98*, 1803.

(67) Del Valle, E. M. *Process biochemistry,* **2004**, *39*, 1033.

(68) Hu, Q. D.; Tang, G. P.; Chu, P. K. *Acc. Chem. Res.* **2014**, *47*, 2017.

(69) Fonari, M.; Simonov, Y. A.; Kravtsov, V. C.; Lipkowski, J.; Ganin, E.; Yavolovskii, A. *J. Mol. Struct.* **2003**, *647*, 129.

(70) Kuhn, R.; Erni, F.; Bereuter, T.; Haeusler, J. *Analyt. Chem.* **1992**, *64*, 2815.

(71) Lehn, J. M. *Pure Appl. Chem.* **1979**, *51*, 979.

(72) Skelton, A.; Agrawal, N.; Fried, J. *RSC Adv.* **2015**, *5*, 55033.

(73) Lindoy, L. F.; Park, K. M.; Sung Lee, S.; Cryptands and Spherands, Wiley Online Library, 2012.

(74) Landini, D.; Maia, A.; Montanari, F.; Tundo, P. *J. Am. Chem. Soc.* **1979**, *101*, 2526.

(75) Cram, D. J.; Kaneda, T.; Helgeson, R. C.; Brown, S. B.; Knobler, C. B.; Maverick, E.; Trueblood, K. N. *J. Am. Chem. Soc.* **1985**, *107*, 3645.

(76) Cacciapaglia, R.; Di Stefano, S.; Mandolini, L.; Salvio, R. *Supramol. Chem.* **2013**, *25*, 537.

(77) Rebilly, J. N.; Reinaud, O. *Supramol. Chem.* **2014**, *26*, 454.

(78) Gavin, J. A.; Garcia, M. E.; Benesi, A. J.; Mallouk, T. E. *J. Org. Chem.* **1998**, *63*, 7663.

(79) Clausen, H. F.; Iversen, B. B.; Christensen, M.; Spackman, M. iNANO annual meeting, 2009.

(80) Lee, J. W.; Choi, K. J.; Lee, Y.; Yoon, J. H. *Chem. Phys. Lett.* **2012**, *528*, 34.

(81) Lee, J. W.; Kang, S. P.; Yoon, J. H. *J. Phys. Chem. C,* **2014**, *118*, 6059.

(82) Han, K. W.; Lee, Y. J.; Jang, J. S.; Jeon, T. I.; Park, J.; Kawamura, T.; Yamamoto, Y.; Sugahara, T.; Vogt, T.; Lee, J. W. *Chem. Phys. Lett.* **2012**, *546*, 120.

(83) Seebach, D.; Beck, A. K.; Heckel, A. *Angew. Chem. Int. Ed.* **2001**, *40*, 92.

(84) Toda, F.; Tanaka, K.; Ootani, M.; Hayashi, A.; Miyahara, I.; Hirotsu, K. *J. Chem. Soc., Chem. Comm.* **1993**, 1413.

(85) Zhu, J.; Qin, Y.; He, Z.; Fu, F. M.; Zhou, Z. Y.; Deng, J. G.; Jiang, Y. Z.; Chau, T. Y. *Tetrahedron: Asymmetry,* **1997**, *8*, 2505.

(86) Nishikawa, K.; Tsukada, H.; Abe, S.; Kishimoto, M.; Yasuoka, N. *Chirality,* **1999**, *11*, 166.

(87) Toda, F.; Tanaka, K.; Okada, T. *J. Chem. Soc., Chem. Comm.* **1995**, 639.

(88) Novák, T.; Schindler, J.; Ujj, V.; Czugler, M.; Fogassy, E.; Keglevich, G. *Tetrahedron: Asymmetry,* **2006**, *17*, 2599.

(89) Novák, T.; Ujj, V.; Schindler, J.; Czugler, M.; Kubinyi, M.; Mayer, Z. A.; Fogassy, E.; Keglevich, G. *Tetrahedron: Asymmetry,* **2007**, *18*, 2965.

(90) Dem Bussche-Hünnefeld, V.; Beck, A. K.; Lengweiler, U.; Seebach, D. *Helv. Chim. Acta,* **1992**, *75*, 438.

(91) Shan, Z.; Hu, X.; Zhou, Y.; Peng, X.; Li, Z. *Helv. Chim. Acta,* **2010**, *93*, 497.

(92) Ujaque, G.; Lee, P. S.; Houk, K.; Hentemann, M. F.; Danishefsky, S. J. Chem. *Eur. J.* **2002**, *8*, 3423.

(93) Barton, B.; Caira, M. R.; Hosten, E. C.; McCleland, C. W. *Tetrahedron,* **2013**, *69*, 8713.

(94) Barton, B.; Caira, M.; Hosten, E.; McCleland, C.; Weitz, S. *Chem. Commun.* **2014**, *50*, 13353.

(95) Barton, B.; Hosten, E. C.; Pohl, P. L. *Tetrahedron,* **2016**, *72*, 8099.

(96) Toda, F.; Tanaka, K.; Stein, Z.; Goldberg, I. *J. Chem. Soc., Perkin Trans. 2,* **1993**, 2359.

(97) Barton, B.; Pohl, P. L.; Hosten, E. C. *J. Incl. Phenom. Macrocycl. Chem.* **2018**, *92*, 357.

(98) Barton, B.; Hosten, E. C.; Pohl, P. L. *J. Incl. Phenom. Macrocycl. Chem.* **2018**, *92*, 329.

(99) Ng, K. K. D.; Hart, H. *Tetrahedron,* **1995**, *51*, 7883.

(100) Toda, F.; Akagi, K. *Tetrahedron Lett.* **1968**, *9*, 3695.

(101) Katzsch, F.; Weber, E. *CrystEngComm,* **2015**, *17*, 2737.

(102) Batten, S. R.; Champness, N. R.; Chen, X. M.; Garcia-Martinez, J.; Kitagawa, S.; Öhrström, L.; O'Keeffe, M.; Suh, M. P.; Reedijk, J. *Pure Appl. Chem.* **2013**, *85*, 1715.

(103) Li, H.; Eddaoudi, M.; O'Keeffe, M.; Yaghi, O. M. *Nature,* **1999**, *402*, 276.

(104) Lee, J.; Farha, O. K.; Roberts, J.; Scheidt, K. A.; Nguyen, S. T.; Hupp, J. T. *Chem. Soc. Rev.* **2009**, *38*, 1450.

(105) Rodenas, T.; Luz, I.; Prieto, G.; Seoane, B.; Miro, H.; Corma, A.; Kapteijn, F.; i Xamena, F. X. L.; Gascon, J. *Nat. Mater.* **2015**, *14*, 48.

(106) Rosi, N. L.; Eckert, J.; Eddaoudi, M.; Vodak, D. T.; Kim, J.; O'keeffe, M.; Yaghi, O. M. *Science,* **2003**, *300*, 1127.

(107) Venna, S. R.; Carreon, M. A. *Chem. Eng. Sci.* **2015**, *124*, 3.

(108) Yu, F.; Li, D.-D.; Cheng, L.; Yin, Z.; Zeng, M.-H.; Kurmoo, M. *Inorg. Chem.* **2015**, *54*, 1655.

(109) Xia, B. Y.; Yan, Y.; Li, N.; Wu, H. B.; Lou, X. W. D.; Wang, X. *Nat. Energy,* **2016**, *1*, 15006.

(110) Huang, Y.-B.; Liang, J.; Wang, X.-S.; Cao, R. *Chem. Soc. Rev.* **2017**, *46*, 126.

(111) Kreno, L. E.; Leong, K.; Farha, O. K.; Allendorf, M.; Van Duyne, R. P.; Hupp, J. T. *Chem. Rev.* **2011**, *112*, 1105.

(112) Horcajada, P.; Chalati, T.; Serre, C.; Gillet, B.; Sebrie, C.; Baati, T.; Eubank, J. F.; Heurtaux, D.; Clayette, P.; Kreuz, C. *Nat. Mater.* **2010**, *9*, 172.

(113) Liang, Z.; Yang, Z.; Yuan, H.; Wang, C.; Qi, J.; Liu, K.; Cao, R.; Zheng, H. *Dalton Trans.* **2018**, *47*, 10223.

(114) Rosi, N. L.; Kim, J.; Eddaoudi, M.; Chen, B.; O'Keeffe, M.; Yaghi, O. M. *J. Am. Chem. Soc.* **2005**, *127*, 1504.

(115) Gellman, S. H.; Introduction: molecular recognition, ACS Publications, 1997.

(116) Ariga, K.; Hill, J. P.; Lee, M. V.; Vinu, A.; Charvet, R.; Acharya, S. *Sci. Technol. Adv. Mater.* **2008**, *9*, 14109.

(117) Abrikosov, A. A.; Gorkov, L. P.; Dzyaloshinski, I. E.; Methods of quantum field theory in statistical physics, Courier Corporation, 2012.

(118) Sethi, M.; Satake, M.; Chemical bonding, Discovery Publishing House, New Delhi, India, 2010.

(119) Leite, F. L.; Bueno, C. C.; Da Róz, A. L.; Ziemath, E. C.; Oliveira, O. N. *Int. J. Mol. Sci.* **2012**, *13*, 12773.

(120) LeFèvre, R. J. W.; Dipole Moments—Their Measurement and Application in Chemistry, Methuen & Co. ltd., London, 1948, *2*.

(121) Roberts, J.; Orr, W. *J. Chem. Soc. Faraday Trans.* **1938**, *34*, 1346.

(122) Parsegian, V. A.; Van der Waals Forces: A Handbook for Biologists, Chemists, Engineers, and Physicists, Cambridge University Press, Cambridge, UK, 2005.

(123) Steiner, T. *Angew. Chem. Int. Ed.* **2002**, *41*, 48.

(124) Caira, M. R.; Nassimbeni, L. R.; Wildervanck, A. F. *J. Chem. Soc., Perkin Trans. 2,* **1995**, 2213.

(125) Desiraju, G. R.; Steiner, T.; The Weak Hydrogen Bond.Structural Chemistry and Biology; International Union of Crystallography, Oxford Science Publications, Oxford, 2001, *9*.

(126) Legon, A.; Millen, D. *Chem. Soc. Rev.* **1987**, *16*, 467.

(127) Martinez, C. R.; Iverson, B. L. *Chem. Sci.* **2012**, *3*, 2191.

(128) Sinnokrot, M. O.; Valeev, E. F.; Sherrill, C. D. *J. Am. Chem. Soc.* **2002**, *124*, 10887.

(129) Barton, B.; de Jager, L.; Hosten, E. C. *Supramol. Chem.* **2017**, 61.

(130) Ben-Naim, A. Hydrophobic Interactions, Springer Science & Business Media, 2012.

(131) Meyer, E. E.; Rosenberg, K. J.; Israelachvili, J. *Proc. Natl. Acad. Sci.* **2006**, *103*, 15739.

(132) Seddon, K. R.; Zaworotko, M.; Crystal Engineering The Design and Application of Functional Solids, Springer Science & Business Media, 1999.

(133) Guiseppone, N.; Lehn, J.M.; *J. Am. Chem. Soc*., **2004**, *126*, 11448.

(134) Weber, E.; Skobridis, K.; Wierig, A.; Goldberg, I. *J. Incl. Phenom. Macrocycl. Chem.* **1997**, *28*, 163.

(135) Toda, F. *Synlett,* **1993**, *1993*, 303.

(136) Caira, M. R.; Nassimbeni, L. R.; Niven, M. L.; Schubert, W. D.; Weber, E.; Dörpinghaus, N. *J. Chem. Soc., Perkin Trans. 2,* **1990**, 2129.

(137) Reinbold, J.; Buhlmann, K.; Cammann, K.; Wierig, A.; Wimmer, C.; Weber, E. *Sens. Actuators B: Chem.* **1994**, *18*, 77.

(138) Buhlmann, K.; Reinbold, J.; Cammann, K.; Skobridis, K.; Wierig, A.; Weber, E. *Fresenius J. Anal. Chem.* **1994**, *348*, 549.

(139) Gabdulkhaev, M. N.; Gatiatulin, A. K.; Ziganshin, M. A.; Gorbatchuk, V. V. *J. Therm. Anal. Calorim.* **2016**, *126*, 627.

(140) Amombo Noa, F. M.; Bourne, S. A.; Nassimbeni, L. R. *Cryst. Growth Des.* **2015**, *15*, 3271.

(141) Amombo Noa, F. M.; Bourne, S. A.; Su, H.; Nassimbeni, L. R. *Cryst. Growth Des.* **2016**, *16*, 1636.

(142) Dickert, F. L.; Haunschild, A. *Adv. Mater.* **1993**, *5*, 887.

(143) Atwood, J. L.; Barbour, L. J.; Jerga, A. *Science,* **2002**, *296*, 2367.

(144) Tsukushi, I.; Yamamuro, O.; Suga, H. *Thermochim. Acta,* **1992**, *200*, 71.

(145) Rothenberg, G.; Downie, A. P.; Raston, C. L.; Scott, J. L. *J. Am. Chem. Soc.* **2001**, *123*, 8701.

(146) Braun, T.; Buvári-Barcza, Á.; Barcza, L.; Konkoly-Thege, I.; Fodor, M.; Migali, B. *Solid State Ionics,* **1994**, *74*, 47.

(147) Gao, Y. A.; Li, Z. H.; Du, J. M.; Han, B. X.; Li, G. Z.; Hou, W. G.; Shen, D.; Zheng, L. Q.; Zhang, G. Y. *Eur. J. Chem. A,* **2005**, *11*, 5875.

(148) Chernov, A. *Contemp. Phys.* **1989**, *30*, 251.

(149) Karathanos, V. T.; Mourtzinos, I.; Yannakopoulou, K.; Andrikopoulos, N. K. *Food Chem.* **2007**, *101*, 652.

(150) Hollingsworth, M.; Brown, M.; Hillier, A.; Santarsiero, B.; Chaney, J. *Science,* **1996**, *273*, 1355.

(151) Vekilov, P. G. *Nanoscale,* **2010**, *2*, 2346.

(152) Davey, R. J.; Schroeder, S. L.; ter Horst, J. H. *Angew. Chem. Int. Ed.* **2013**, *52*, 2166.

(153) Bouanga Boudiombo, J. S.; Su, H.; Bourne, S. A.; Weber, E.; Nassimbeni, L. R. *Cryst. Growth Des.* **2018**, *18*, 2620.

(154) Jie, K.; Zhou, Y.; Li, E.; Zhao, R.; Liu, M.; Huang, F. *J. Am. Chem. Soc.* **2018**, *140*, 3190.

(155) Barton, B.; Hosten, E. C.; Pohl, P. L. *Aust. J. Chem.* **2018**, *71*, 133.

(156) Ziganshin, M. A.; Gubina, N. S.; Gerasimov, A. V.; Gorbatchuk, V. V.; Ziganshina, S. A.; Chuklanov, A. P.; Bukharaev, A. A. *Phys. Chem. Chem. Phys.* **2015**, *17*, 20168.

(157) Boudiombo, J. S. B.; Su, H.; Ravenscroft, N.; Bourne, S. A.; Weber, E.; Nassimbeni, L. R. *J. Mol. Struct.* **2018**, 636.

(158) Nassimbeni, L. R.; Marivel, S.; Su, H.; Weber, E. *RSC Adv.* **2013**, *3*, 25758.

(159) Pivovar, A. M.; Holman, K. T.; Ward, M. D. *Chem. Mater.* **2001**, *13*, 3018.

(160) Venkataraman, D.; Gardner, G. B.; Lee, S.; Moore, J. S. *J. Am. Chem. Soc.* **1995**, *117*, 11600.

(161) Phunpee, S.; Ruktanonchai, U. R.; Yoshii, H.; Assabumrungrat, S.; Soottitantawat, A. *Biosci. Biotechnol. Biochem.* **2017**, *81*, 718.

(162) Mandelcorn, L. *Chem. Rev.* **1959**, *59*, 827.

(163) Toda, F.; Mori, K.; Stein, Z.; Goldberg, I. *J. Org. Chem.* **1988**, *53*, 308.

(164) Szejtli, J. *Chem. Rev.* **1998**, *98*, 1743.

(165) Smith, I.; Paper and Thin Layer Chromatography, Elsevier, 2013, *4*.

(166) Toda, F.; Tanaka, K.; Ueda, H. *Tetrahedron Lett.* **1981**, *22*, 4669.

(167) Mal, N. K.; Fujiwara, M.; Tanaka, Y. *Nature,* **2003**, *421*, 350.

(168) Park, C.; Lim, J.; Yun, M.; Kim, C. *Angew. Chem.* **2008**, *120*, 3001.

(169) Park, C.; Oh, K.; Lee, S. C.; Kim, C. *Angew. Chem. Int. Ed.* **2007**, *46*, 1455.

(170) Slichter, C. P.; Principles of Magnetic Resonance, Springer Science & Business Media, 2013, *1*.

(171) Barton, B.; Dorfling, S. L.; Hosten, E. C.; Pohl, P. L. *Tetrahedron,* **2018**, *74*, 2754.

(172) Hirose, K. *J. Incl. Phenom. Macrocycl. Chem.* **2001**, *39*, 193.

(173) Birkholz, M.; Thin Film Analysis by X-Ray Scattering, Wiley Online Library, 2006, *1*.

(174) Levine, H.; Schwinger, J.; On the theory of diffraction by an aperture in an infinite plane screen part I, *Phys. Rev*., **1948**, 958.

(175) McKinnon, J. J.; Jayatilaka, D.; Spackman, M. A. *Chem. Comm.* **2007**, 3814.

(176) Spackman, M. A.; McKinnon, J. J. *CrystEngComm,* **2002**, *4*, 378.

(177) McKinnon, J. J.; Spackman, M. A.; Mitchell, A. S. *Acta Crystallogr. Section B: Struct. Sci.* **2004**, *60*, 627.

(178) Clausen, H. F.; Chevallier, M. S.; Spackman, M. A.; Iversen, B. B. *New J. Chem.* **2010**, *34*, 193.

(179) Gavezzotti, A. *Z. Kristallogr. Cryst. Mater.* **2005**, *220*, 499.

(180) Nassimbeni, L. R. *Acc. Chem. Res.* **2003**, *36*, 631.

(181) Haines, P. J.; Thermal methods of analysis: principles, applications and problems, Springer Science & Business Media, 2012.

(182) Dash, A. K.; Elmquist, W.; Analytical profiles of drug substances and excipients, Founding Florey Academic Press, 2001, *27*.

(183) Pomeranz, Y., Food analysis: theory and practice, Springer Science & Business Media, 2013.

(184) Kayaci, F.; Uyar, T. *Food Chem.* **2012**, *133*, 641.

(185) Harwood, L. M.; Moody, C. J., Experimental organic chemistry: principles and practice, Blackwell Scientific, Oxford, 1989.

(186) Sparkman, O. D.; Penton, Z.; Kitson, F. G.; Gas chromatography and mass spectrometry: a practical guide, Academic Press, 2011.

(187) Dettmer-Wilde, K.; Engewald, W.; Practical Gas Chromatography, Springer, 2016.

(188) Downard, K.; Mass spectrometry: a foundation course, Royal Society of Chemistry, 2007.

(189) Cullity, B.; Elements of X-ray Diffraction, Addison and Wesley Publishing Company Inc, USA, 1978, *32*.

(190) Brown, J.; Davies, S.; Fleet, G.; Pratt, A. *Chem. Br.* **1989**, *25*, 259.

(191) Chhabra, N.; Aseri, M. L.; Padmanabhan, D. *Int. J. Appl. Med. Res.* **2013**, *3*, 16.

(192) Caira, M. R.; Bourne, S. A.; Samsodien, H.; Smith, V. J. *Beilstein J. Org. Chem.* **2015**, *11*, 2616.

(193) Caira, M. R.; Bourne, S. A.; Mzondo, B. *Molecules,* **2017**, *22*, 866.

(194) Danylyuk, O.; Butkiewicz, H.; Coleman, A. W.; Suwinska, K. *J. Mol. Struct.* **2017**, 239.

(195) Ceborska, M. *J. Mol. Struct.* **2018**, *1165*, 62.

(196) Saleh, N. i.; Khaleel, A.; Al-Dmour, H.; al-Hindawi, B.; Yakushenko, E. *J. Therm. Anal. Calorim.* **2013**, *111*, 385.

(197) Ghasabi, M.; Mansoori, B.; Mohammadi, A.; Duijf, P. H.; Shomali, N.; Shirafkan, N.; Mokhtarzadeh, A.; Baradaran, B. *J. Cell. Physiol.* **2019**, *234*, 2152.

(198) Gao, Z.-Z.; Bai, D.; Xiao, Z.-Y.; Zhu, Q.-J.; Xue, S.-F.; Tao, Z.; Xiao, X. *Inorg. Chem. Comm.* **2016**, *71*, 68.

(199) Lusi, M.; Barbour, L. J. *Angew. Chem. Int. Ed.* **2012**, *51*, 3928.

(200) Jorgensen, W. L.; Nguyen, T. B. *Proc. Natl. Acad. Sci.* **1993**, *90*, 1194.

(201) Pyka, I.; Ryvlin, D.; Waldvogel, S. R. *ChemPlusChem,* **2016**, *81*, 926.

(202) Hughes, E.; Jordan, J.; Gullion, T. *J. Phys. Chem. B,* **2001**, *105*, 5887.

(203) Erdemir, S.; Bahadir, M.; Yilmaz, M. *J. Hazard. Mater.* **2009**, *168*, 1170.

(204) Szente, L.; Szejtli, J. *Trends Food Sci. Technol.* **2004**, *15*, 137.

(205) Shahidi, F.; Han, X. Q. *Crit. Rev. Food Sci. Nutr.* **1993**, *33*, 501.

(206) Szejtli, J. *Starch,* **1982**, *34*, 379.

(207) Sousa, L. R.; Sogah, G.; Hoffman, D. H.; Cram, D. J. *J. Am. Chem. Soc.* **1978**, *100*, 4569.

(208) Bai, C. C.; Tian, B. R.; Zhao, T.; Huang, Q.; Wang, Z. Z. *Molecules,* **2017**, *22*, 1475.

(209) Drabowicz, J.; Mikołajczyk, M. *Phosphorus Sulfur Relat. Elem.* **1984**, *21*, 245.

(210) Czarnik, A. W. *J. Org. Chem.* **1984**, *49*, 924.

(211) Shen, H.-M.; Ji, H.-B. *Carbohydr. Res.* **2012**, *354*, 49.

(212) Park, K. K.; Sim, W.-J.; Park, J. W. *J. Incl. Phenom. Macrocycl. Chem.* **1997**, *27*, 41.

(213) Suresh, P.; Pitchumani, K. *Tetrahedron: Asymmetry,* **2008**, *19*, 2037.

(214) Quinn, D.; MacDonald, J. *Carbon,* **1992**, *30*, 1097.

(215) Wang, W.; Bray, C. L.; Adams, D. J.; Cooper, A. I. *J. Am. Chem. Soc.* **2008**, *130*, 11608.

(216) Kumar, R.; Linga, P.; Moudrakovski, I.; Ripmeester, J. A.; Englezos, P. *AIChE J.* **2008**, *54*, 2132.

(217) Lee, H.; Lee, J.-W.; Park, J.; Seo, Y.-T.; Zeng, H.; Moudrakovski, I. L.; Ratcliffe, C. I.; Ripmeester, J. A. *Nature,* **2005**, *434*, 743.

(218) Arjmandi, M.; Chapoy, A.; Tohidi, B. *J. Chem. Eng. Data,* **2007**, *52*, 2153.

(219) Csöregh, I.; Gallardo, O.; Weber, E.; Dörpinghaus, N. *Supramol. Chem.* **1995**, *5*, 159.

(220) Barton, B.; Caira, M. R.; McCleland, C. W.; Taljaard, B. *J. Chem. Soc., Perkin Trans. 2,* **2000**, 865.

(221) Barton, B.; McCleland, C. W.; Taljaard, B. *S. Afr. J. Chem.* **2002**, *55*, 144.

(222) APEX, B., SAINT. Bruker AXS Inc.: Madison, WI, USA, 2007, *391*.

(223) Sheldrick, G. M. *Acta Crystallogr. Section A: Found. Adv.* **2015**, *71*, 3.

(224) Sheldrick, G. M. *Acta Crystallogr. Section C: Struct. Chem.* **2015**, *71*, 3.

(225) Hübschle, C. B.; Sheldrick, G. M.; Dittrich, B. *J. Appl. Crystallogr.* **2011**, *44*, 1281.

(226) Wolff, S.; Grimwood, D.; McKinnon, J.; Turner, M.; Jayatilaka, D.; Spackman, M. University of Western Australia, Perth, Australia*,* 2013.

(227) Barbour, L. J.; X-Seed–A software tool for supramolecular crystallography, Elsevier, 2001.

(228) Plachetka, T.; POV Ray: persistence of vision parallel raytracer, Proc. of Spring Conf. on Computer Graphics*,* Budmerice, Slovakia*,* 1998, *123*.

(229) M O'Boyle, N.; Banck, M.; James, C.A.; Morley, C.; Vandermeersch T.; Hutchison, G.R., *J. Cheminform.* **2013**, *3*, 33.

(230) Macrae, C. F.; Bruno, I. J.; Chisholm, J. A.; Edgington, P. R.; McCabe, P.; Pidcock, E.; Rodriguez-Monge, L.; Taylor, R.; Streek, J. v.; Wood, P. A. *J. Appl. Crystallogr.* **2008**, *41*, 466.

(231) Shao, Y. *Phys. Chem. Chem. Phys.* **2006**, *8*, 3172.

(232) Arpe, H.-J.; Industrielle Organische Chemie, Wiley-VCH, Weinheim, 2007.

(233) Mohameed, H.; Jdayil, B. A.; Takrouri, K. *Chem. Eng. Process.* **2007**, *46*, 25.

(234) Cottier, V.; Bellat, J.-P.; Simonot-Grange, M.-H.; Méthivier, A. *J. Phys. Chem. B,* **1997**, *101*, 4798.

(235) Turaga, U. T.; Ramanathan, R. *JSIR,* **2003**, 963.

(236) Rahimpour, M. R.; Jafari, M.; Iranshahi, D. *Appl. Energy,* **2013**, *109*, 79.

(237) Santos, K.; Neto, A. D.; Moura, M.; Dantas, T. C. *Brazilian J. Petroleum Gas,* **2011**, 5.

(238) Nassimbeni, L. R.; Báthori, N. B.; Patel, L. D.; Su, H.; Weber, E. *Chem.Comm.* **2015**, *51*, 3627.

(239) Mukherjee, S.; Joarder, B.; Desai, A. V.; Manna, B.; Krishna, R.; Ghosh, S. K. *Inorg. Chem.* **2015**, *54*, 4403.

(240) Toda, F.; Tanaka, K.; Wang, Y.; Lee, G.-H. *Chem. Lett.* **1986**, *15*, 109.

(241) Bourne, S. A.; Johnson, L.; Marais, C.; Nassimbeni, L. R.; Weber, E.; Skobridis, K.; Toda, F. *J. Chem. Soc., Perkin Trans. 2,* **1991**, 1707.

(242) Afonso, R. V.; Durão, J.; Mendes, A.; Damas, A. M.; Gales, L. *Angew. Chem. Int. Ed.* **2010**, *49*, 3034.

(243) Uyar, T.; Hunt, M. A.; Gracz, H. S.; Tonelli, A. E. *Cryst. Growth Des.* **2006**, *6*, 1113.

(244) Bohnet, M.; Ullmann's encyclopedia of industrial chemistry, Wiley-VCH, 2003.

(245) Ishii, Y.; Iwahama, T.; Sakaguchi, S.; Nakayama, K.; Nishiyama, Y. *J. Org. Chem.* **1996**, *61*, 4520.

(246) Sladojevich, F.; Michaelides, I. N.; Darses, B.; Ward, J. W.; Dixon, D. J. *Org. Lett.* **2011**, *13*, 5132.

(247) Kedrowski, B. L.; Hoppe, R. W. *J. Org. Chem.* **2008**, *73*, 5177.

(248) Bianco, G. G.; Ferraz, H. M.; Costa, A. M.; Costa-Lotufo, L. V.; Pessoa, C.; de Moraes, M. O.; Schrems, M. G.; Pfaltz, A.; Silva Jr, L. F. *J. Org. Chem.* **2009**, *74*, 2561.

(249) Von, D. W. C.; Tully, W. F.; Separation and recovery of picolines and lutidines from nitrogen base mixtures, Google Patents, U.S. Patent No. 2,924,602. Washington, DC: US, 1960.

(250) Bacsa, J.; Caira, M. R.; Jacobs, A.; Nassimbeni, L. R.; Toda, F. *Cryst. Eng.* **2000**, *3*, 251.

(251) Tiffin, E. J.; Sykes, N. M.; Weber, E.; Ravenscroft, N.; Nassimbeni, L. R. *Cryst. Growth Des.* **2019**, *19*, 3.

(252) Signaigo, F. K.; Cramer, P. L. *J. Am. Chem. Soc.* **1933**, *55*, 3326.

(253) Musser, M. T.; Cyclohexanol and cyclohexanone ,in Ullmann's Encyclopedia of Industrial Chemistry, Wiley-VCH, 2000.

(254) Barton, B.; Caira, M. R.; Hosten, E. C.; McCleland, C. W.; Weitz, S. *J. Org. Chem.* **2015**, *80*, 7184.

(255) Barton, B.; Dorfling, S.-L.; Hosten, E. C. *Cryst. Growth Des.* **2017**, *17*, 6725.

(256) Joule, J. A.; Mills, K.; Heterocyclic chemistry, John Wiley & Sons, 2008.

(257) Shimizu, S.; Watanabe, N.; Kataoka, T.; Shoji, T.; Abe, N.; Morishita, S.; Ichimura, H.; Pyridine and pyridine derivatives, in Ullmann's Encyclopedia of Industrial Chemistry, Wiley-VCH, 2000.

(258) Bain, P. C.; Whitmire, D.; Furness, S.; Govindarajan, B.; Bowen, J. P.; Vlahos, K. Y.; Perry, B. N.; Matter, W.; Fischl, A.; Cook, J., *Blood*, **2007**, 560.

(259) Farnsworth, N. R.; Bingel, A. S.; Cordell, G. A.; Crane, F. A.; Fong, H. H. *J. Pharm. Sci.* **1975**, *64*, 535.

(260) Kane, V. V.; Jones Jr, M. *Org. Synth.* **2003**, *61*, 129.

(261) Eller, K.; Henkes, E.; Rossbacher, R.; Höke, H.; Amines, aliphatic, in Ullmann's Encyclopedia of Industrial Chemistry, Wiley-VCH, 2000.

(262) Weissermel, K.; Arpe, H.-J.; Lindley, C. R.; Hawkins, S. *Industrial Org. Chem.* **2003**, 145.

(263) Smith, J. R. L.; McKeer, L. C.; Taylor, J. M. *Org. Synth.* **1989**, 222.

(264) Noyori, R.; Yokoyama, K.; Hayakawa, Y. *Org. Synth.* **1978**, 56.

(265) McGuire, R. G.; Dimitroglou, D. A. *Biocontrol Sci. Technol.* **1999**, *9*, 53.

(266) Shimizu, A.; Ikeguchi, M.; Sugai, S. *J. Biomol. NMR,* **1994**, *4*, 859.

(267) Sorensen, H. MSc Thesis, North Carolina State University, North Carolina, 2013.

(268) Kaszyński, P.; Kłys, A.; Domagała, S.; Woźniak, K. *Tetrahedron,* **2017**, *73*, 3823.

(269) Mardirossian, N.; Head-Gordon, M. *Phys. Chem. Chem. Phys.* **2014**, *16*, 9904.

(270) McNaught, A. D.; McNaught, A. D.; IUPAC Compendium of Chemical Terminology, Blackwell Science, Oxford, 1997.

(271) Klopman, G. *J. Am. Chem. Soc.* **1968**, *90*, 223.

(272) Salem, L. *J. Am. Chem. Soc.* **1968**, *90*, 543.

(273) Salem, L. *J. Am. Chem. Soc.* **1968**, *90*, 553.

(274) Fleming, I.; Frontier orbitals and organic chemical reactions, Wiley Online Library, 1976.

(275) Tantawy, M. A.; Nafie, M. S.; Elmegeed, G. A.; Ali, I. A. *Bioorg. Chem.* **2017**, *73*, 128.

(276) Khan, M. F.; Alam, M. M.; Verma, G.; Akhtar, W.; Akhter, M.; Shaquiquzzaman, M. *Eur. J. Med. Chem.* **2016**, *120*, 170.

(277) Küçükgüzel, Ş. G.; Şenkardeş, S. *Eur. J. Med. Chem.* **2015**, *97*, 786.

(278) Kirk, R. E.; Othmer, D.; Encyclopedia of Chemical Technology, Kroschwitz JI, Howe-Grant M. John Wiley & Sons: New York, 1992, *4*.

(279) O'Neil, M.; Smith, A.; Heckelman, P.; Budavari, S. *Inc.* **2001**, *767*, 4342.

(280) Starr, D.; Hixon, R. *Org. Synth.* **1943**, 77.

(281) Tong, X.; Ma, Y.; Li, Y. *Appl. Catal. A: General,* **2010**, *385*, 1.

(282) Pruckmayr, G.; Dreyfuss, P.; Dreyfuss, M. *Kirk-Othmer Encycl. Chem. Technol.* **2000**, 394.

(283) Cai, C. M.; Zhang, T.; Kumar, R.; Wyman, C. E. *Green Chem.* **2013**, *15*, 3140.

(284) Hoydonckx, H.; Van Rhijn, W.; Van Rhijn, W.; De Vos, D.; Jacobs, P.; Furfural and derivatives, Wiley-VCH, 2000.

(285) Woodward, R.; Eastman, R. *J. Am. Chem. Soc.* **1946**, *68*, 2229.

(286) Aissani, N.; Urgeghe, P. P.; Oplos, C.; Saba, M.; Tocco, G.; Petretto, G. L.; Eloh, K.; Menkissoglu-Spiroudi, U.; Ntalli, N.; Caboni, P. *J. Agric. Food Chem.* **2015**, *63*, 6120.

(287) Fukaya, M.; Nakamura, S.; Nakagawa, R.; Nakashima, S.; Yamashita, M.; Matsuda, H. *Org. Lett.* **2017**, *20*, 28.

(288) Aoyagi, M.; Kamoi, T.; Kato, M.; Sasako, H.; Tsuge, N.; Imai, S. *J. Agric. Food Chem.,* **2011**, *59*, 10893.

(289) Korotkov, A.; Li, H.; Chapman, C. W.; Xue, H.; MacMillan, J. B.; Eastman, A.; Wu, J. *Angew. Chem. Int. Ed.* **2015**, *54*, 10604.

(290) Swanston, J.; Thiophene, in Ullmann's Encyclopedia of Industrial Chemistry Wiley-VCH, 2000.

(291) Galpern, G.; Thiophenes occurring in petroleum, shale oil, and coals, in Thiophene and its derivatives, Wiley-VCH, 1985, *1*.

(292) Gronowitz, S.; The Chemistry of Heterocyclic Compounds, in Thiophene and its derivatives, Wiley Online Library, 1985, *1*.

(293) Hall Jr, H. *J. Am. Chem. Soc.* **1957**, *79*, 5441.

(294) Woodward, R.; Pachter, I.; Scheinbaum, M. *Organic Syntheses,* **2003**, *54*, 39.

(295) Harreus, A. L.; 2-Pyrrolidone, in Ullmann's Encyclopedia of Industrial Chemistry Wiley-VCH, 2000.

(296) Kaur, M.; Choi, D. H. *Chem. Soc. Rev.* **2015**, *44*, 58.

(297) Barton, B.; de Jager, L.; Dorfling, S.-L.; Hosten, E. C.; McCleland, C. W.; Pohl, P. L. *Tetrahedron,* **2018**, *74*, 4754.

(298) Otobe, Y.; Goto, O.; Miyano, H.; Kawamoto, M.; Aoki, A.; Ogawa, T., SAE Technical Paper, 1989.

(299) Dean, J. A. McGraw-Hill; Lange's handbook of chemistry, McGraw-Hill, Inc., New york; London, 1999.

(300) Molinier, M.; Knob, K. J.; Stanley, D. J.; Vander Pol, T. S.; Cao, C.; Zheng, X.; Leflour, T.; Rault, J.; Claudel, S.; Prevost, I.; Aromatics production process, Google Patents, US Patent Application No. 10/077,220., 2017.

(301) Zou, Y.; Jiang, H.; Liu, Y.; Gao, H.; Xing, W.; Chen, R. *Sep. Purif. Technol.* **2016**, *170*, 49.

(302) Surry, D. S.; Buchwald, S.L. *J. Am. Chem. Soc*. **2007**, 10354.

(303) Kahl, T.; Schröder, K. W.; Lawrence, F.; Marshall, W.; Höke, H.; Jäckh, R.; Aniline, in Ullmann's Encyclopedia of Industrial Chemistry, Wiley-VCH*,* 2000.

(304) Brown, D. S.; Morris, J. J.; Thomas, A. P.; Aniline derivatives, Google Patents, US Patent No. 5,821,246. Washington, DC: US, 1998.

(305) Watts, H.; A dictionary of chemistry and the allied branches of other sciences, Longmans, Green, and Company, 1854, *3.*

(306) Hofmann, A. W. V. *Philos. Trans. R. Soc. Lond.* **1850**, 93.

(307) Gessner, T.; Mayer, U.; Triarylmethane and diarylmethane dyes, in Ullmann's Encyclopedia of Industrial Chemistry, Wiley-VCH, 2000.

(308) Iranpoor, N.; Firouzabadi, H.; Nowrouzi, N.; Khalili, D. *Tetrahedron,* **2009**, *65*, 3893.

(309) Nehate, M.; Bokade, V. V. *Appl. Clay Sci.* **2009**, *44*, 255.

(310) Wang, J.; Liu, J.; Ding, H.; Wang, J.; Lu, P.; Wang, Y. *J. Org. Chem.* **2015**, *80*, 5842.

(311) Barton, B.; Betz, R.; Caira, M. R.; Hosten, E. C.; McCleland, C. W.; Pohl, P. L.; Taljaard, B. *Tetrahedron,* **2016**, *72*, 7536.

(312) Tanaka, K.; Hori, K.; Tsuyuhara, S.; Motoki, S.; Shide, S.; Arakawa, R.; Caira, M. R. *Tetrahedron,* **2013**, *69*, 1120.

(313) Barton, B.; Jooste, D. V.; Hosten, E. C. *J. Incl. Phenom. Macrocycl. Chem.* **2019**, *93*, 333.

(314) Barton, B.; Senekal, U.; Hosten, E. C. *Tetrahedron,* **2019**.

SUPPLEMENTARY INFORMATION

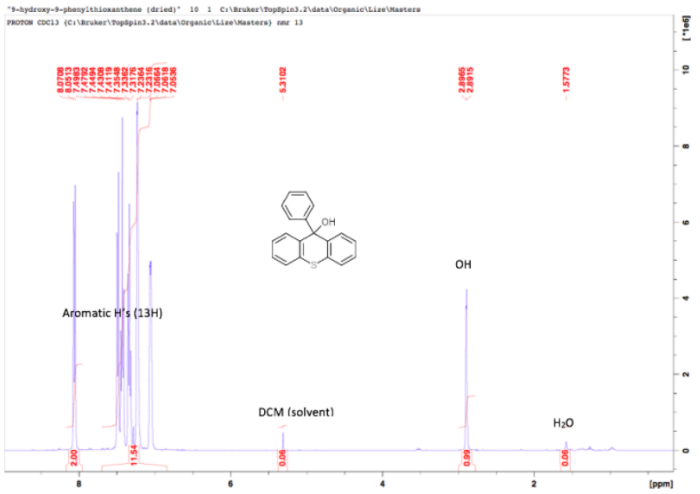

Figure S1. ^{1}H-NMR spectrum for 9-Hydroxy-9-phenylthioxanthene (**23**).

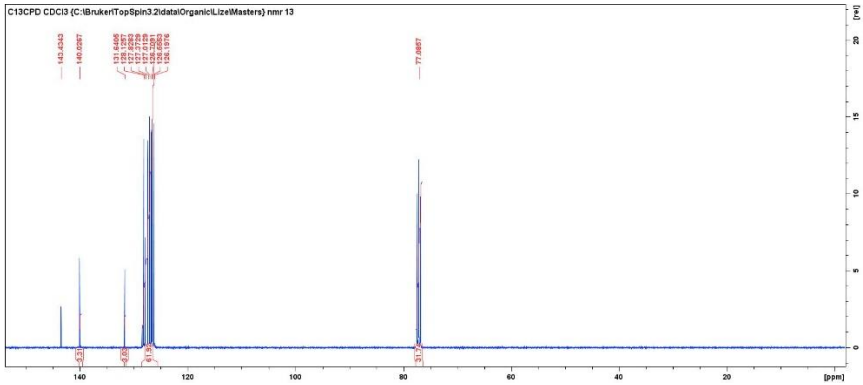

FigureS2. ^{13}C-NMR spectrum for 9-Hydroxy-9-phenylthioxanthene (**23**).

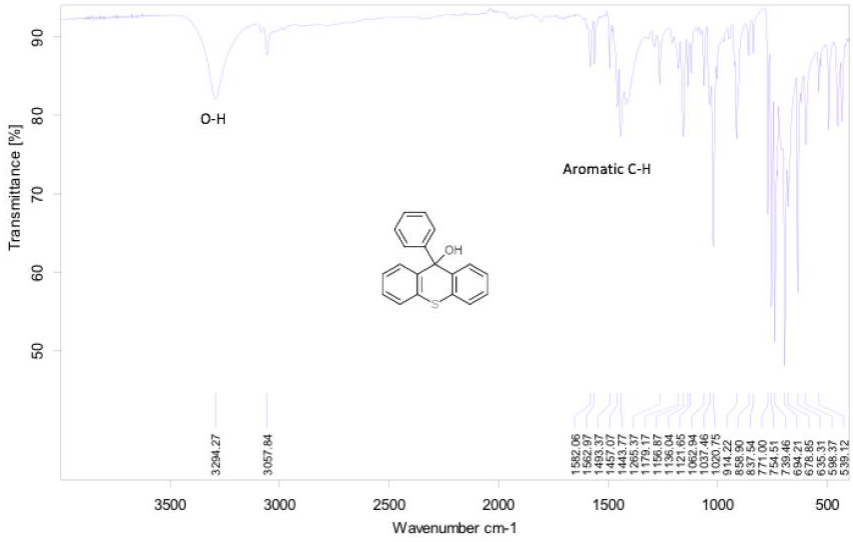

Figure S3. IR spectrum for 9-Hydroxy-9-phenylthioxanthene (**23**).

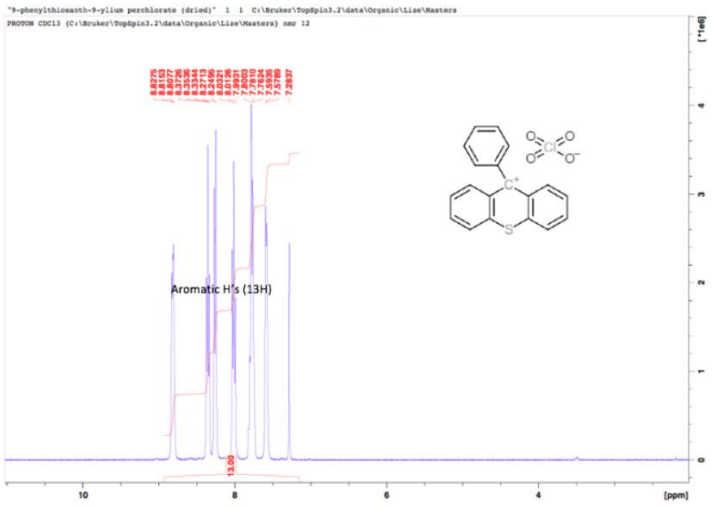

Figure S4. ^{1}H-NMR spectrum for 9-Phenylthioxanth-9-ylium perchlorate (**26**).

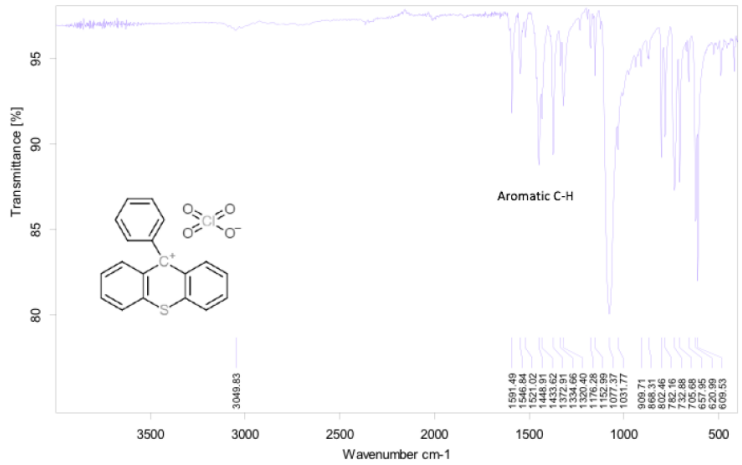

Figure S5. IR spectrum for 9-Phenylthioxanth-9-ylium perchlorate (**26**).

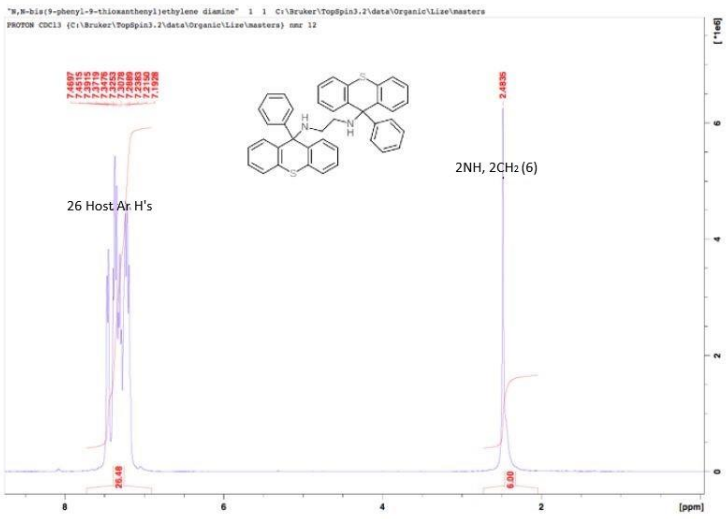

Figure S6. ^{1}H-NMR spectrum for $\mathbf{H_1}$.

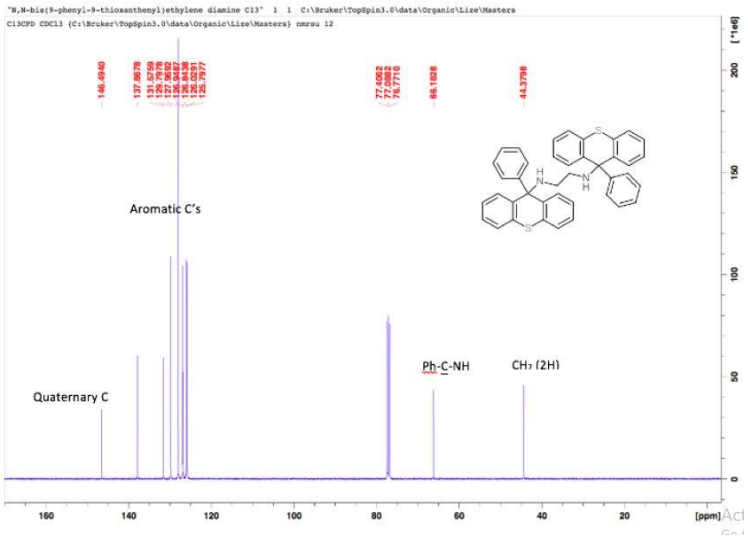

Figure S7. ^{13}C-NMR spectrum for **H_1**.

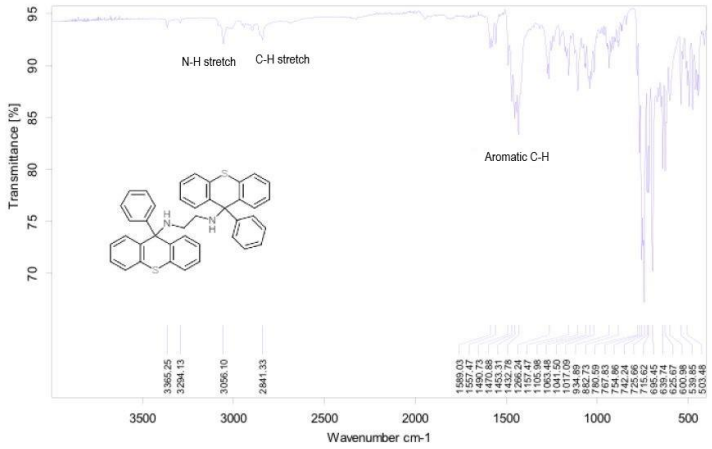

Figure S8. IR spectrum for **H_1**.

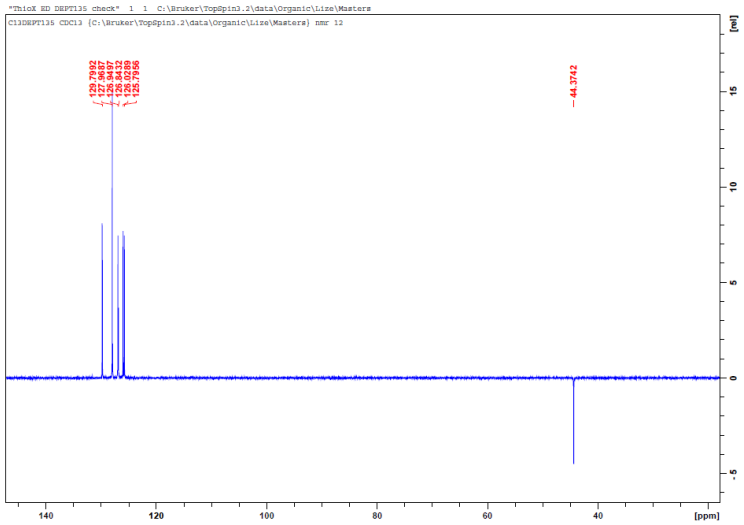

Figure S9. DEPT135 spectrum for **H_1**.

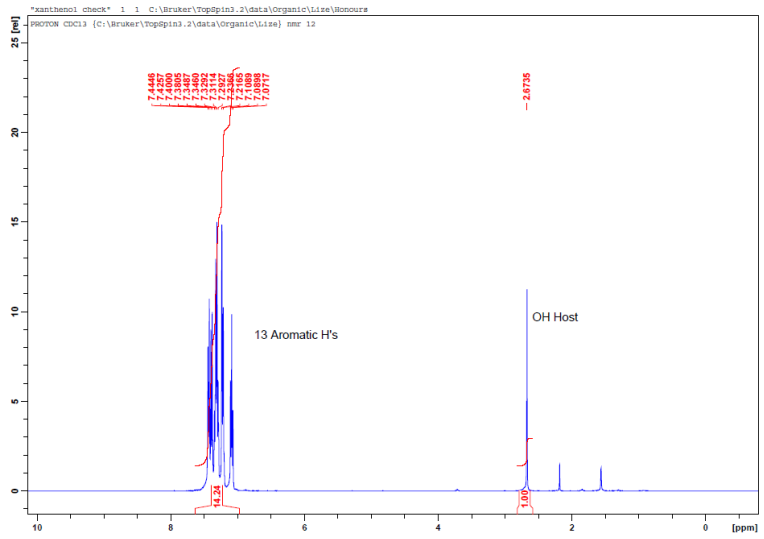

Figure S10. ^{1}H-NMR spectrum for 9-Hydroxy-9-phenylxanthene (**21**).

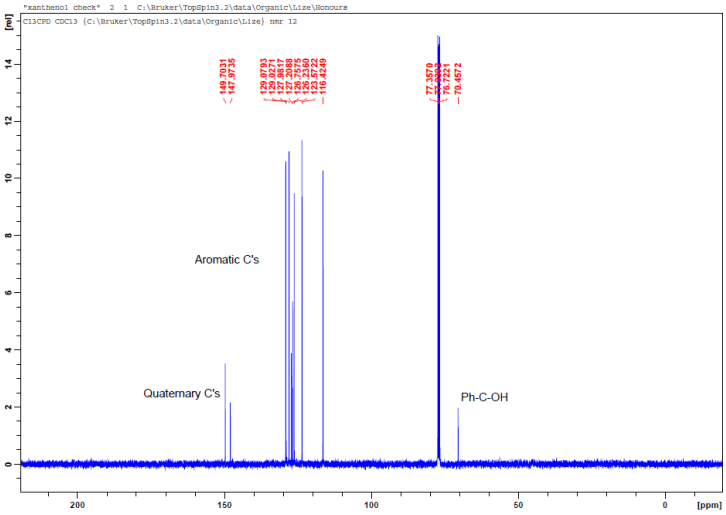

Figure S11. ^{13}C-NMR spectrum for 9-Hydroxy-9-phenylxanthene (**21**).

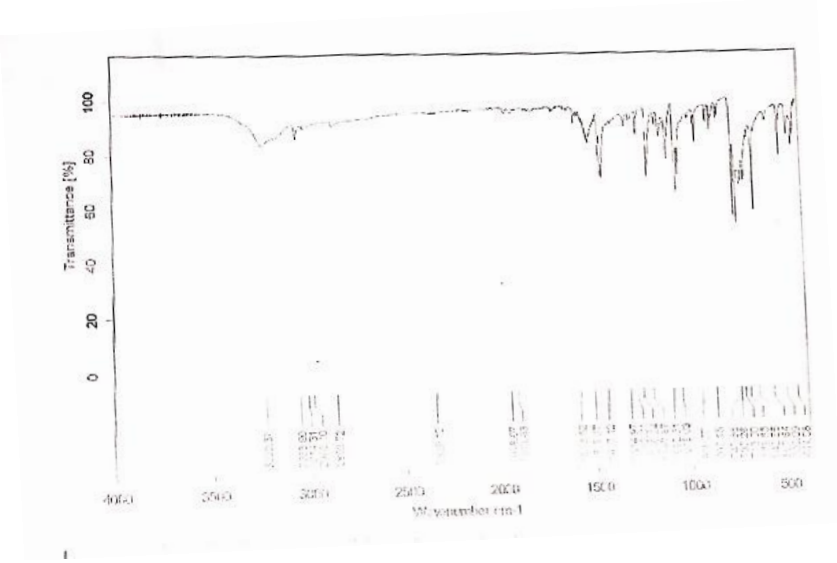

Figure S12. IR spectrum for 9-Hydroxy-9-phenylxanthene (**21**).

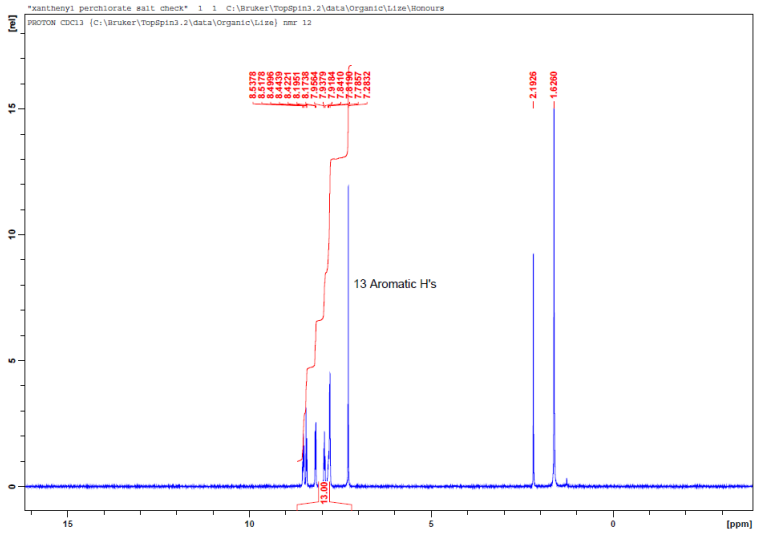

Figure S13. ^{1}H-NMR spectrum for 9-Phenylxanth-9-ylium perchlorate (**27**).

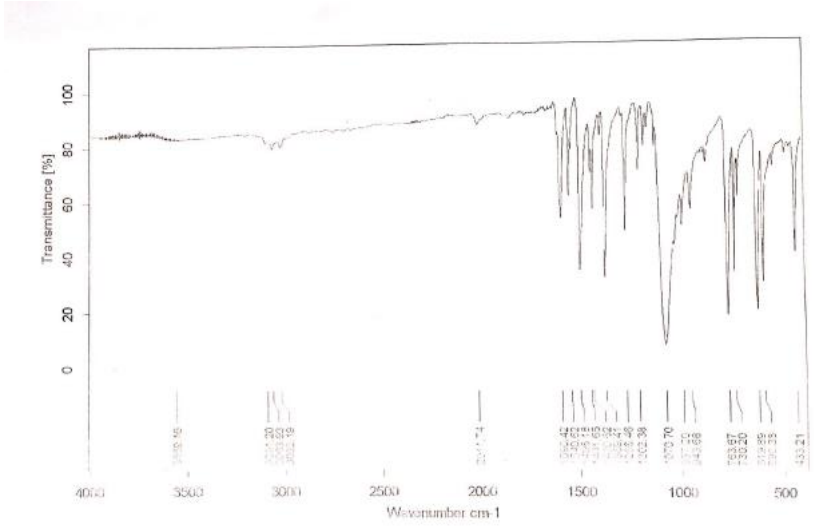

Figure S14. IR spectrum for 9-Phenylxanth-9-ylium perchlorate (**27**).

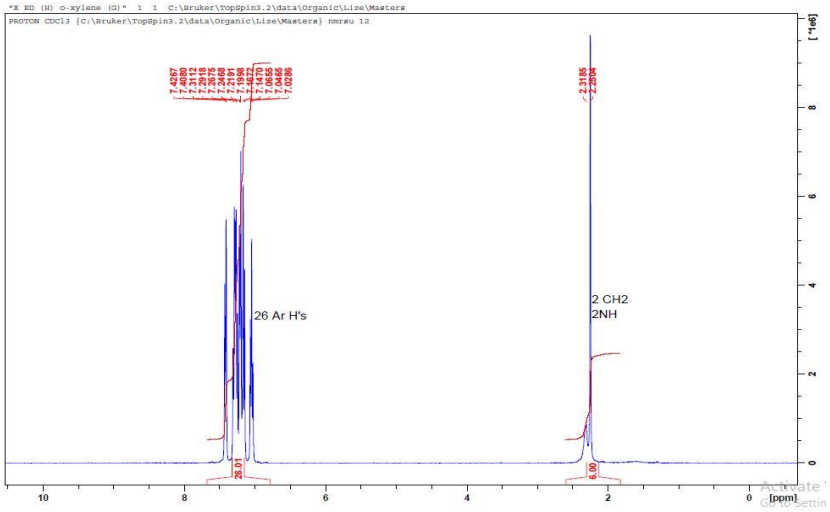

Figure S15. ^{1}H-NMR spectrum for **H_2**.

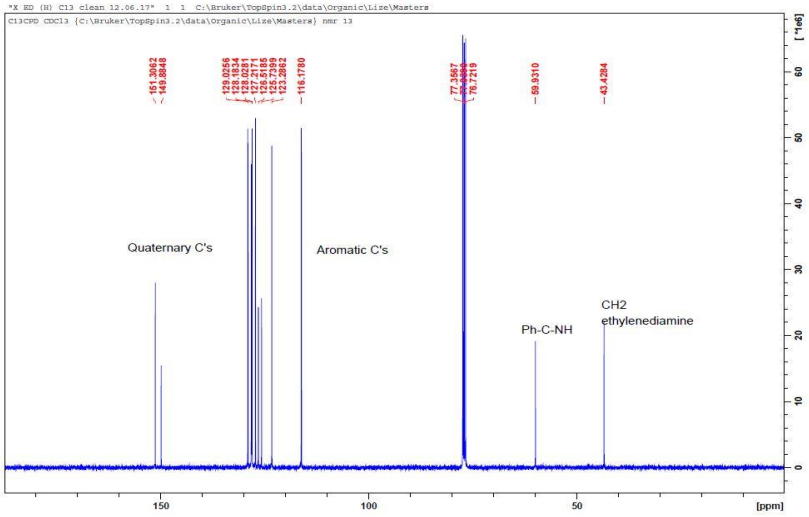

Figure S16. ^{13}C-NMR spectrum for **H_2**.

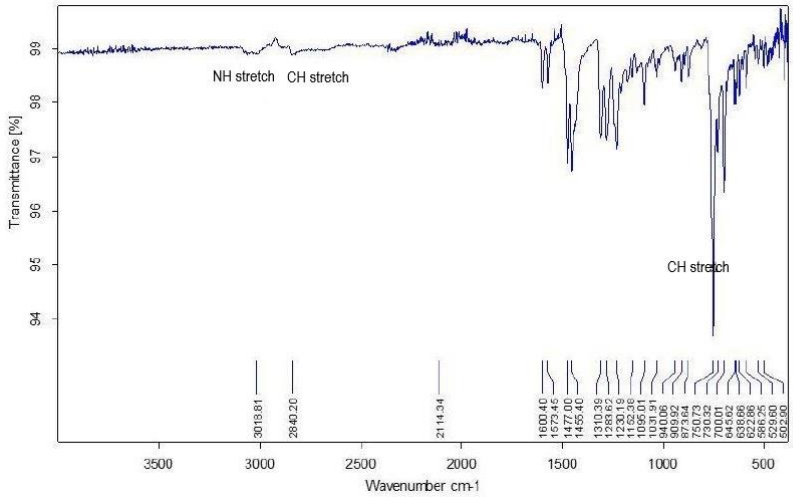

Figure S17. IR spectrum for **H_2**.

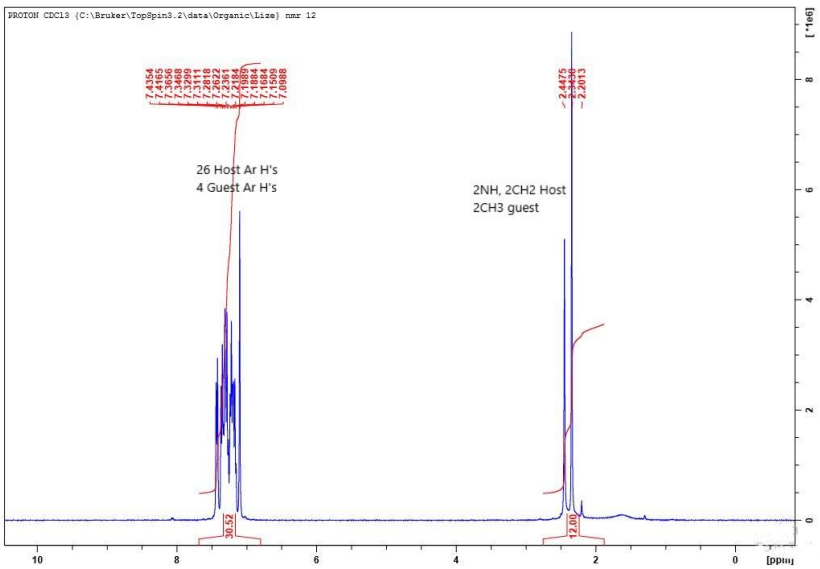

Figure S18. ^{1}H-NMR spectrum for **H_1**·*p*-Xy.

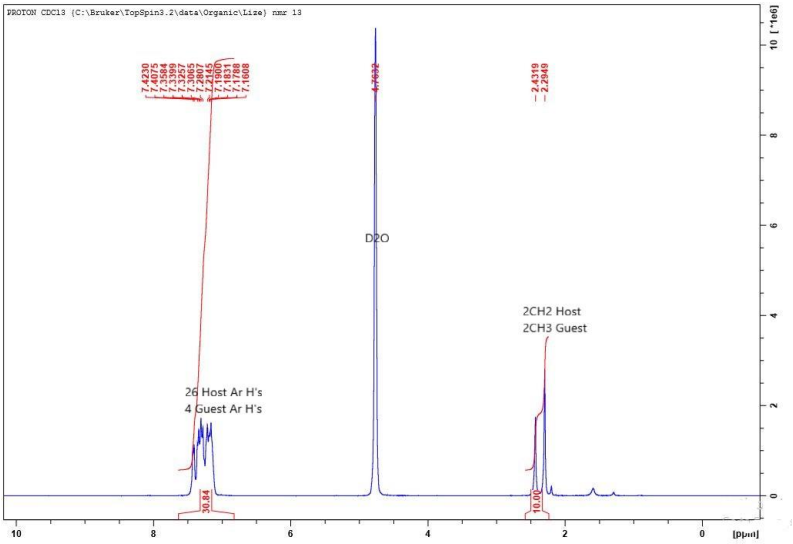

Figure S19. ^{1}H-NMR spectrum for **H$_1$**·*o*-Xy.

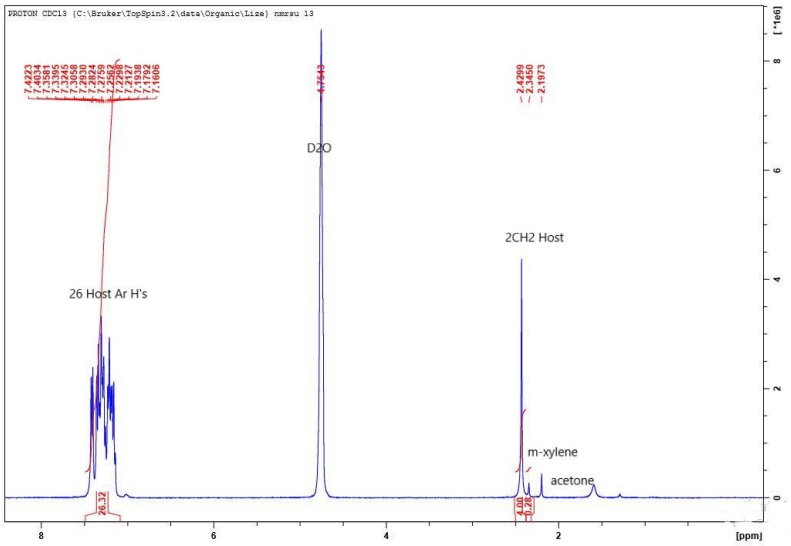

Figure S20. ^{1}H-NMR spectrum for **H$_1$** recrystallized from *m*-Xy.

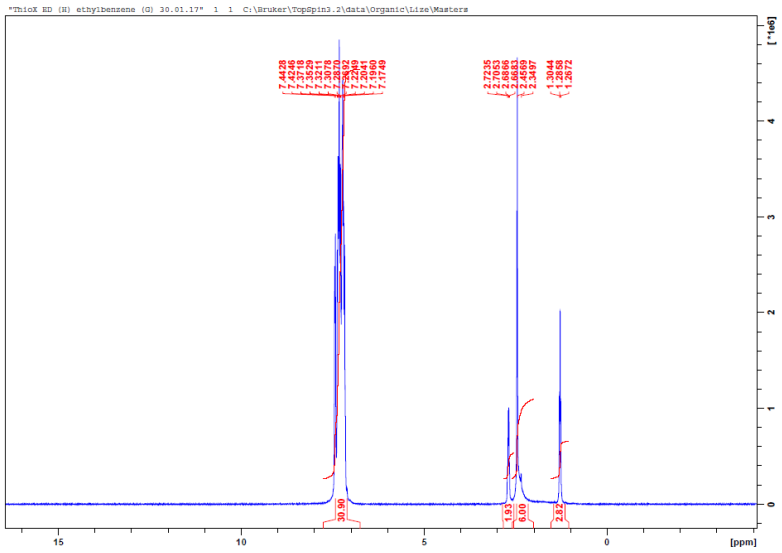

Figure S21. ^{1}H-NMR spectrum for **H$_1$**·EB.

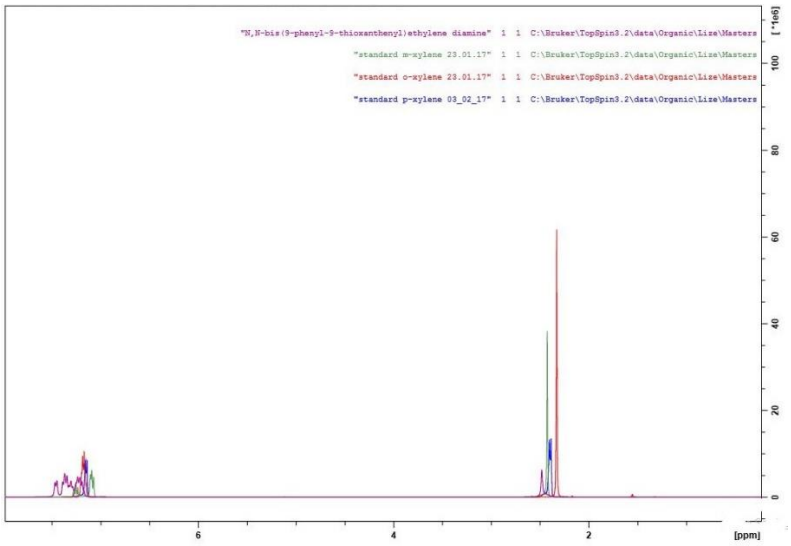

Figure S22. Overlap of xylene isomers and EB guests and **H_1** on ^{1}H-NMR.

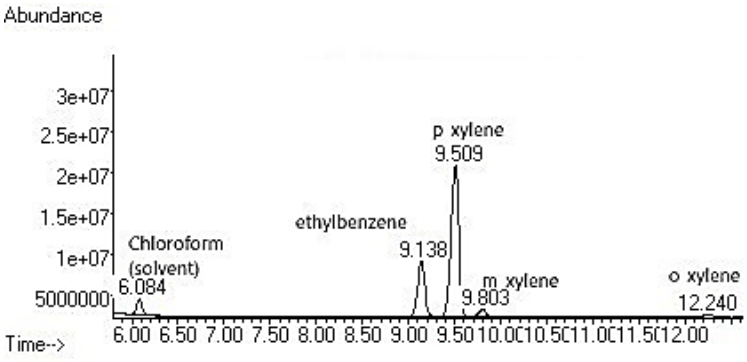

Figure S23. GC-MS chromatograph of a mixture of xylene isomers and EB.

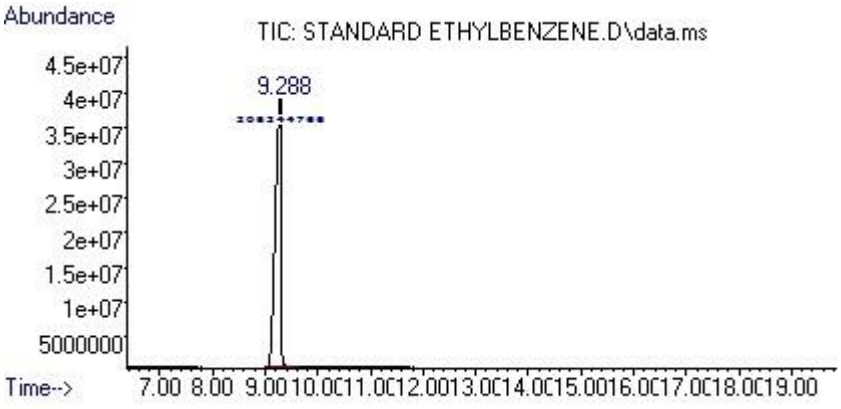

Figure S24. GC-MS chromatograph of a pure standard of EB.

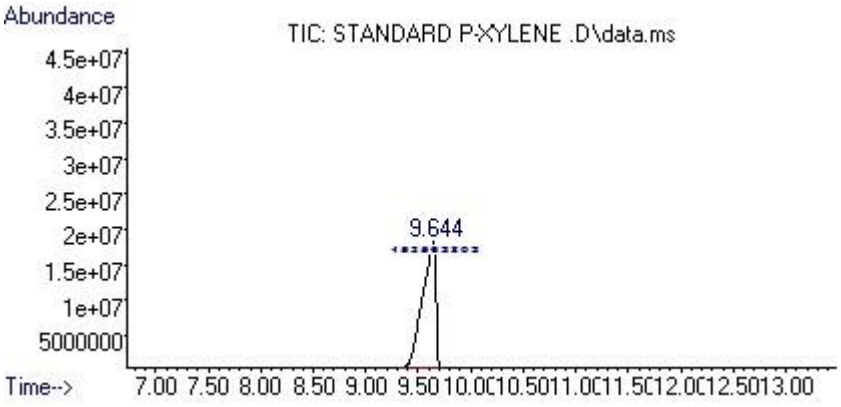

Figure S25. GC-MS chromatograph of a pure standard of *p*-Xy.

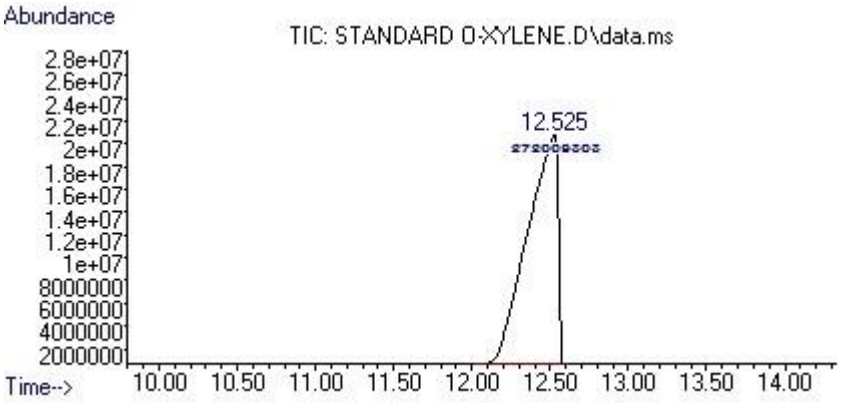

Figure S25. GC-MS chromatograph of a pure standard of *o*-Xy.

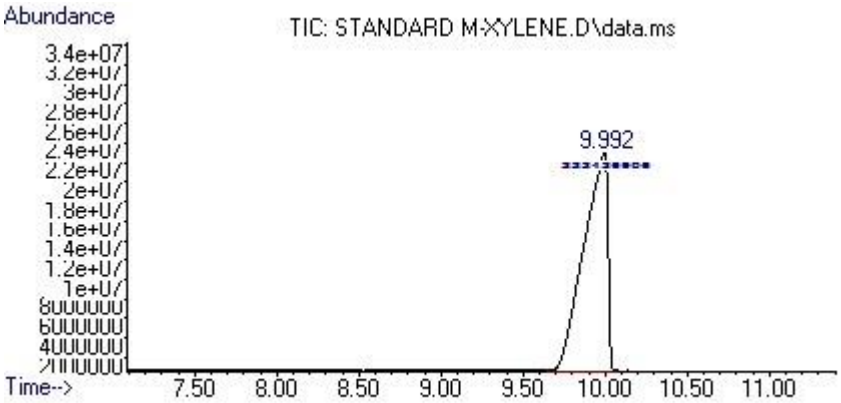

Figure S26. GC-MS chromatograph of a pure standard of *m*-Xy.

Table S27. Triplicate values for equimolar competition experiments of $\mathbf{H_1}$ with *p*-Xy, *m*-Xy, *o*-Xy and EB.

Guests:	Batch 1	Batch 2	Batch 3	Average	% e.s.d.s
p-, *o-* Xy	97.48:2.52	97.11:2.89	98.37:1,63	97.65:2.35	(0.53):(0.53)
p-, *m-* Xy	95.46:4.54	94.98:5.02	96.14:3.86	95.53:4.47	(0.48):(0.48)
m-, *o-* Xy	[a]	[a]	[a]	-	-
p-, *m-*, *o-* Xy	97.02:2.98:0	94.45:4.76:0.79	93.11:6.89:0	94.86: 4.88: 0.26	(1.62):(1.58): (0,37)
p-Xy and EB	74.16:25.84	74.66:25.34	73.84:26.16	74.22:25.78	(0.34):(0.34)
o-Xy and EB	[a]	[a]	[a]	-	-
m-Xy and EB	[a]	[a]	[a]	-	-
p-, *o-* Xy and EB	72.55:2.61:24.84	72.78:2.27:24.94	73.39:2.23:24.37	72.91: 2.37:24.71	(0.35):(0.17): (0,25)
p-, *m-* Xy and EB	70.77:3.80:25.43	70.68:4.53:24.79	70.40:4.25:25.34	70.62:4.19:25.19	(0.16):(0.30): (0.28)
o-, *m-* Xy and EB	[a]	[a]	[a]	-	-
p-, *m-*, *o-* Xy and EB	67.37:4.36:2.84: 25.43	69.44:3.81:2.13: 24.62	68.03:4.18:2.52: 25.27	68.28:4.12:2.50: 25.11	(0.86):(0.22): (0.29):(0,35)

[a]No inclusion occurred.

Table S28. K values for competition experiment of *o*-Xy/*p*-Xy.[a,b]

p-Xy ml	*p*-Xy c	*o*-Xy ml	*o*-Xy c	K-value
1	1	0	0	
0,78	0,9874	0,22	0,0126	22,1029711
0,59	0,9766	0,41	0,0234	29,0023178
0,51	0,9708	0,49	0,0292	31,9427881
0,4	0,9671	0,6	0,0329	44,0927052
0,21	0,21	0,79	0,79	1
0,15	0,15	0,85	0,85	1
0,1	0,1	0,9	0,9	1
0	0	1	1	18,5915403

[a]Abbreviations in the table include ml (mother liquor) and c (crystal).

[b]The average K value is highlighted in yellow.

Table S29. K values for competition experiment of *m*-Xy/*p*-Xy.[a,b]

p-Xy ml	*p*-Xy c	*m*-Xy ml	*m*-Xy c	K-value
1	1	0	0	
0,79	0,9835	0,21	0,0165	15,84464902
0,6	0,968	0,4	0,032	20,16666667
0,5	0,9508	0,5	0,0492	19,32520325
0,4	0,9251	0,6	0,0749	18,52670227
0,13	0,8439	0,87	0,1561	36,17961859
0	0	1	1	22,00856796

[a]Abbreviations in the table include ml (mother liquor) and c (crystal).
[b]The average K value is highlighted in yellow.

Table 30. K values for competition experiment of EB/*p*-Xy[a,b]

p-Xy ml	*p*-Xy c	EB ml	EB c	K-value
1	1	0	0	
0,73	0,9028	0,27	0,0972	3,43531202
0,58	0,802	0,42	0,198	2,93312435
0,5	0,74	0,5	0,26	2,84615385
0,43	0,6928	0,57	0,3072	2,98946221
0,24	0,5175	0,76	0,4825	3,39637306
0	0	1	1	3,1200851

[a]Abbreviations in the table include ml (mother liquor) and c (crystal).
[b]The average K value is highlighted in yellow.

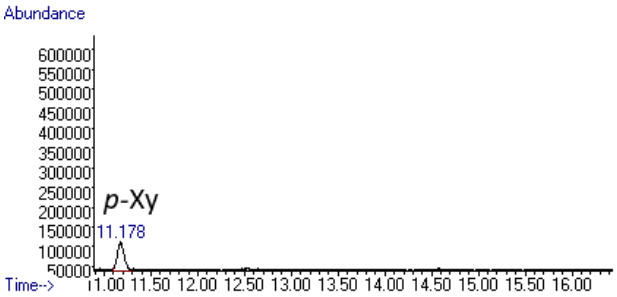

Figure S31. GC trace for the equimolar ternary gas phase experiment (Xy isomers) after 20 days.

Table 32. Summary of the host···host interactions in **H₁**·*o*-Xy, **H₁**·*p*-Xy and **H₁**·EB.[a,b]

Interaction	**H₁**·*o*-Xy	**H₁**·*p*-Xy	**H₁**·EB
π···π	4.43–5.89 Å	4.61–5.60 Å	4.52–5.99 Å
CH···π	2.73–2.92 Å, 135–147˚ [2]	None	2.96 Å, 139˚ [1]
Non-classical H-bonding	2.77–3.49 Å, 102–154˚ [6]	2.76–3.46 Å, 101–153˚ [6]	2.76–3.46 Å, 101–153˚ [6]
Other short contacts	2.84 Å, 112˚ [1] (<)	2.96 Å, 139˚ [1] (<)	2.86 Å, 145˚ [1] (<)

[a]Distances denoted by < are contacts that measure less than the sum of the van der Waals radii of the atoms involved.
[b]Numerous H···H π···π interactions are observed in these complexes, but all are weak.

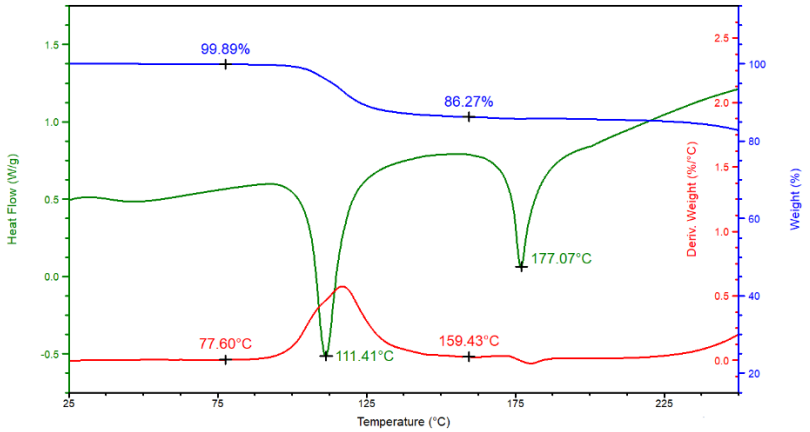

Figure S33. Thermogram of **H₁**·*p*-Xy.

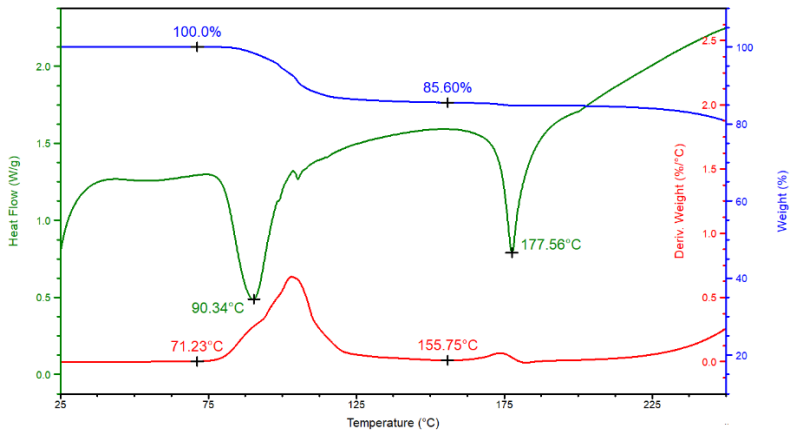

Figure S34. Thermogram of **H₁**·*o*-Xy.

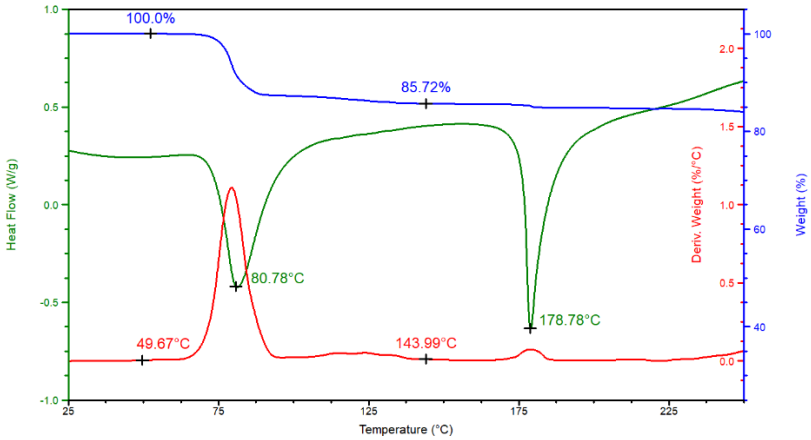

Figure S35. Thermogram of **H₁**·EB.

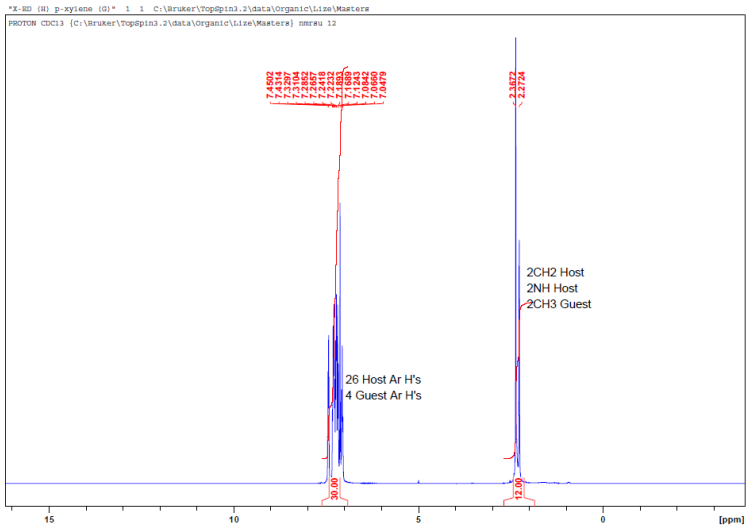

Figure S36. ^{1}H-NMR spectrum for **H₂**·*p*-Xy**.**

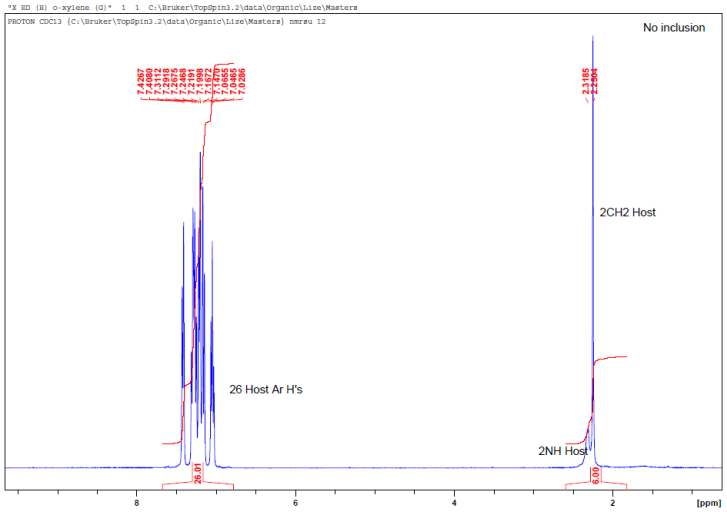

Figure S37. ^{1}H-NMR spectrum for **H₂** recrystallized from *o*-Xy.

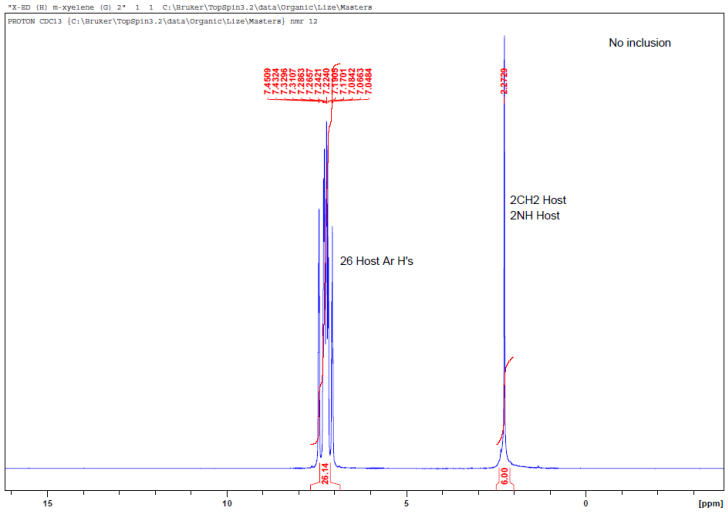

Figure S38. ^{1}H-NMR spectrum for **H₂** recrystallized from *m*-Xy.

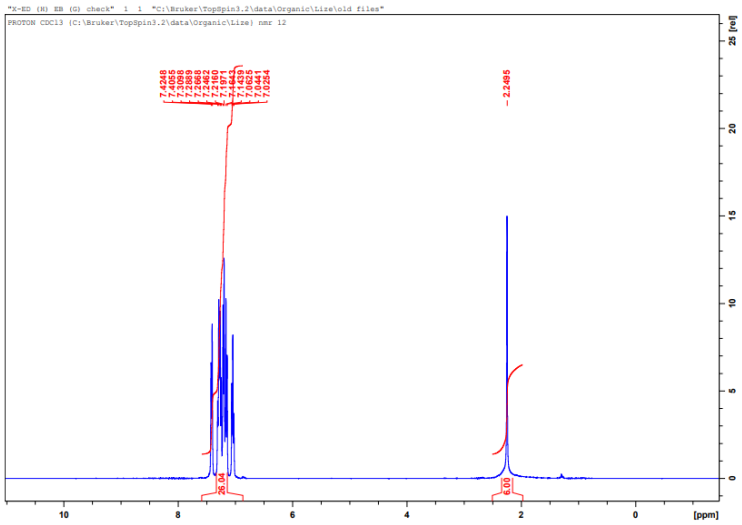

Figure S39. ^{1}H-NMR spectrum for **H₂** recrystallized from EB.

Table S40. Duplicate values for equimolar competition experiments of **H_2** with *p*-Xy, *m*-Xy, *o*-Xy and EB.

Guests:	Batch 1	Batch 2	Average	% e.s.d.s
p-, *o-* Xy	96.66:3.34	96.79:3.21	96.73:3.27	(0.07):(0.07)
p-, *m-* Xy	96.09:3.91	96.39:3.61	96.24:3.76	(0.15):(0.15)
m-, *o-* Xy	[a]	[a]	-	-
p-, *m-*, *o-* Xy	96.85:1.60:1.55	96.12:2.16:1.72	96.49: 1.88: 1.63	(0.37):(0.28):(0.09)
p- Xy and EB	91.94:8.06	92.63:7.37	92.29:7.71	(0.35):(0.35)
o-Xy and EB	[a]	[a]	-	-
m-Xy and EB	[a]	[a]	-	-
p-, *o-* Xy and EB	92.77:1.89:5.35	92.75:2.18:5.08	92.76: 2.04:5.22	(0.01):(0.15):(0.14)
p-, *m-* Xy and EB	90.94:2.85:6.22	92.02:1.97:6.01	91.48:2.41:6.12	(0.54):(0.44):(0.11)
o-, *m-* Xy and EB	[a]	[a]	-	-
p-, *m-*, *o-* Xy and EB	91.42:1.51:1.86: 5.21	92.61:1.04:1.11: 5.25	92.02:1.28:1.49: 5.23	(0.60):(0.24):(0.38):(0.02)

[a]No inclusion occurred.

Table S41. K values for competition experiment of EB/*p*-Xy.[a,b]

p-Xy ml	*p*-Xy c	EB ml	EB c	K-value
1	1	0	0	
0,77864	0,97852	0,22136	0,02148	12,95084
0,58433	0,93157	0,41567	0,06843	9,684104
0,48749	0,9173	0,51251	0,0827	11,66118
0,41517	0,91808	0,58483	0,08192	15,78681
0,21341	0,7761	0,78659	0,2239	12,77607
0,11899	0,68105	0,88101	0,31895	15,80981
0	0	1	1	13,11147

[a]Abbreviations in the table include ml (mother liquor) and c (crystal).
[b]The average K value is highlighted in yellow.

Table S42. K values for competition experiment of *m*-Xy/*p*-Xy.[a,b]

p-Xy ml	*p*-Xy c	*m*-Xy ml	*m*-Xy c	K-value
1	1	0	0	
0,78062	0,98205	0,21938	0,01795	15,3754
0,54883	0,96987	0,45117	0,03013	26,46164
0,48651	0,96268	0,51349	0,03732	27,22579
0,39117	0,94353	0,60883	0,05647	26,00569
0,19979	0,93084	0,80021	0,06916	53,90764
0	0	1	1	29,79523

[a]Abbreviations in the table include ml (mother liquor) and c (crystal).
[b]The average K value is highlighted in yellow.

Table S43. K values for competition experiment of *o*-Xy/*p*-Xy.[a,b]

p-Xy ml	*p*-Xy c	*o*-Xy ml	*o*-Xy c	K-value
1	1	0	0	
0,77862	0,98438	0,22138	0,01562	17,91821
0,58679	0,93641	0,41321	0,06359	10,36968
0,49332	0,96195	0,50668	0,03805	25,96587
0,41526	0,94612	0,58474	0,05388	24,72643
0,21239	0,91576	0,78761	0,08424	40,31257
0,13997	0,93059	0,86003	0,06941	82,37871
0	0	1	1	33,61191

[a]Abbreviations in the table include ml (mother liquor) and c (crystal).
[b]The average K value is highlighted in yellow.

Table S44. Summary of host···host interactions of inclusion compounds.[a,b]

Interaction	**H_2·***p*-Xy
π···π	4.047(1)–5.926(1) Å
CH···π	2.51–2.80 Å, 102–163˚ [3]
Non-classical H-bonding	2.811(2)–3.486(2) Å, 102–165˚[2]
Other short contacts	2.56 Å, 165˚ [1] (<)

[a]Distances denoted by < are contacts that measure less than the sum of the van der Waals radii of the atoms involved.
[b]Numerous H···H π···π interactions are observed in these complexes, but all are weak.

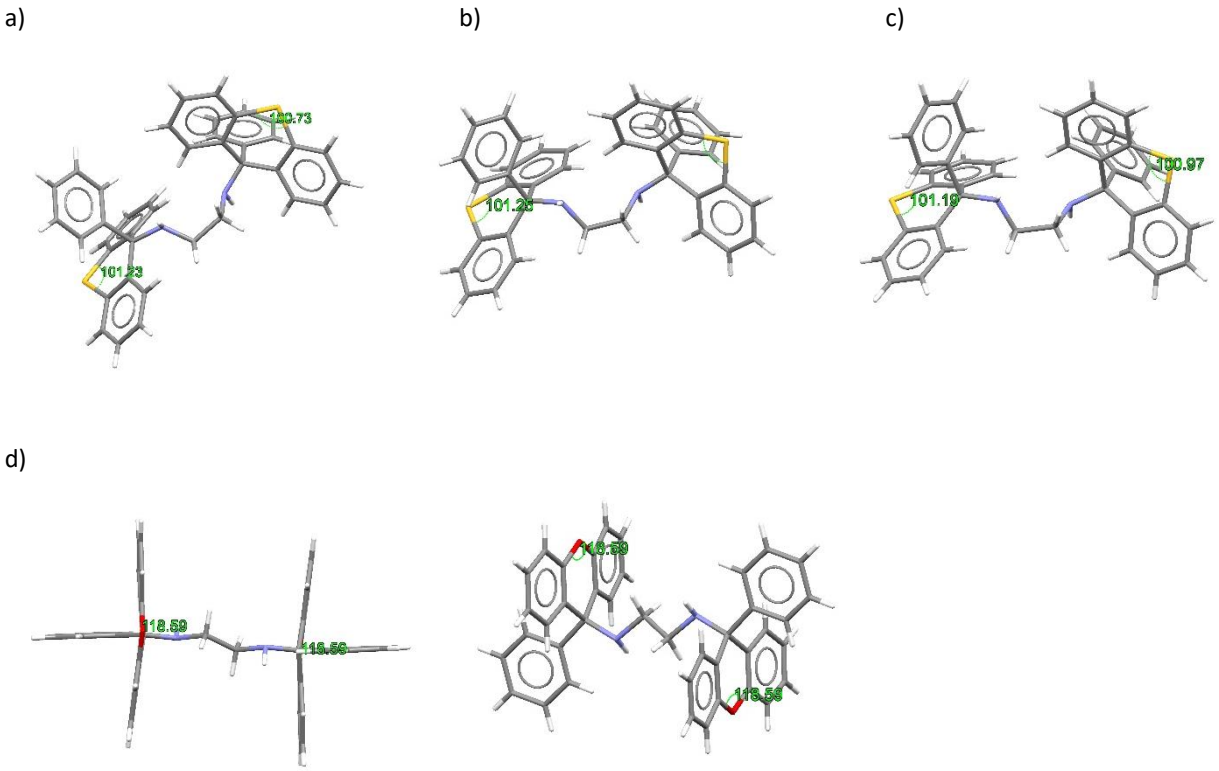

Figure S45. Host geometry within the respective complexes a) **H_1**·*p*-Xy, b) **H_1**·*o*-Xy, c) **H_1**·EB and d) **H_2**·*p*-Xy

a)

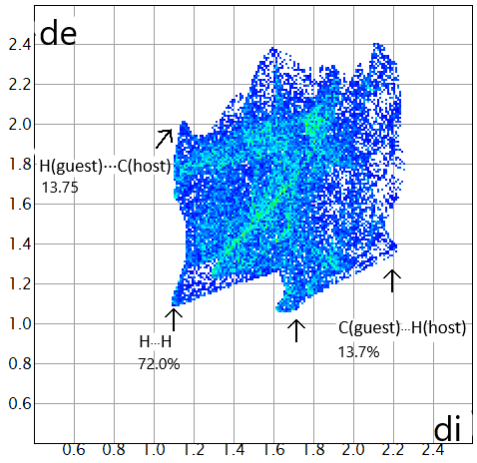

b)

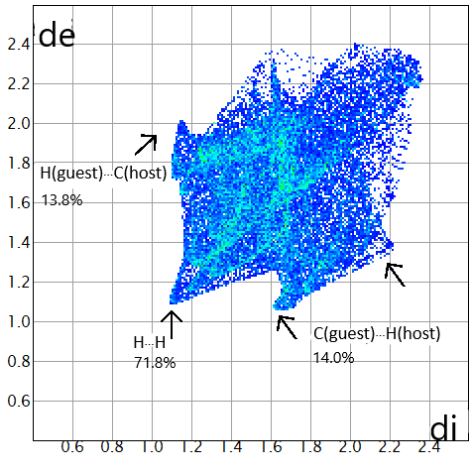

Figure S46. 2D fingerprint plots derived from 3D Hirshfeld surfaces for guests of a) *p*-Xy position 1 and b) *p*-Xy position 2.

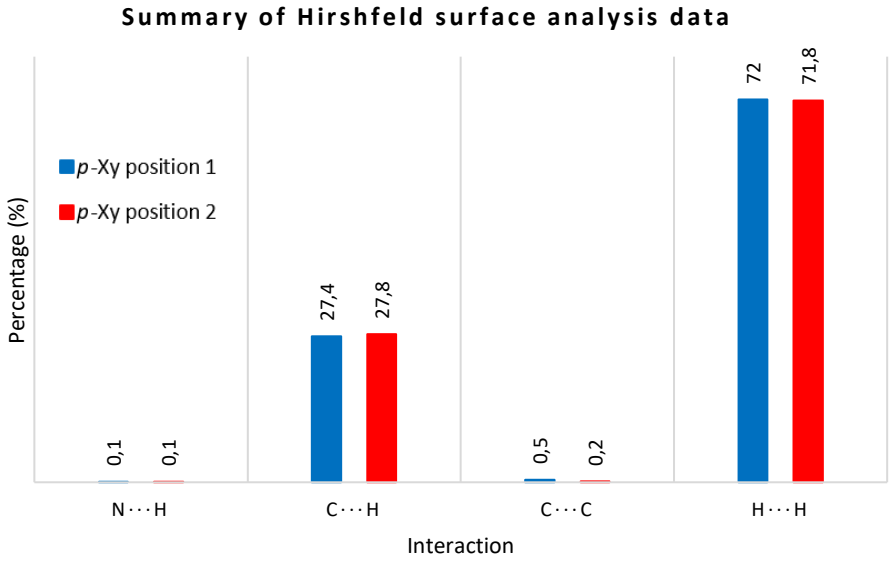

Figure S47. Quantitative data for the various H···G interactions for a) *p*-Xy position 1 and b) *p*-Xy position 2.

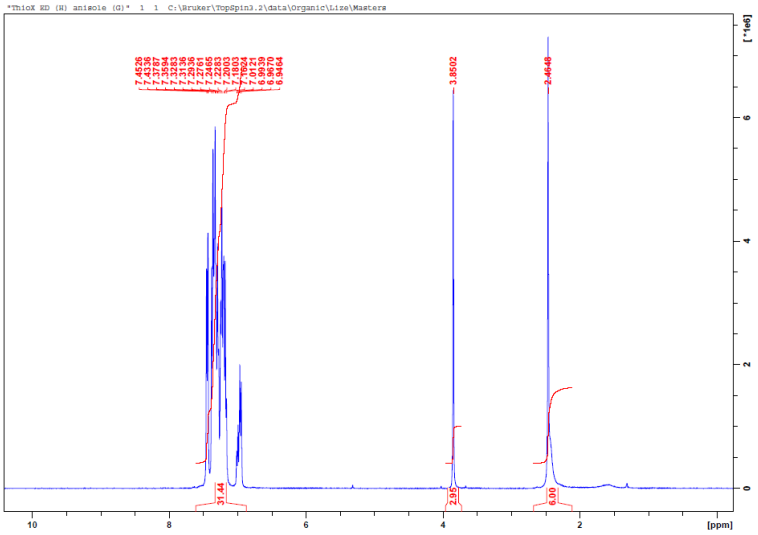

Figure S48. ^{1}H-NMR spectrum for **H$_1$**·ANI.

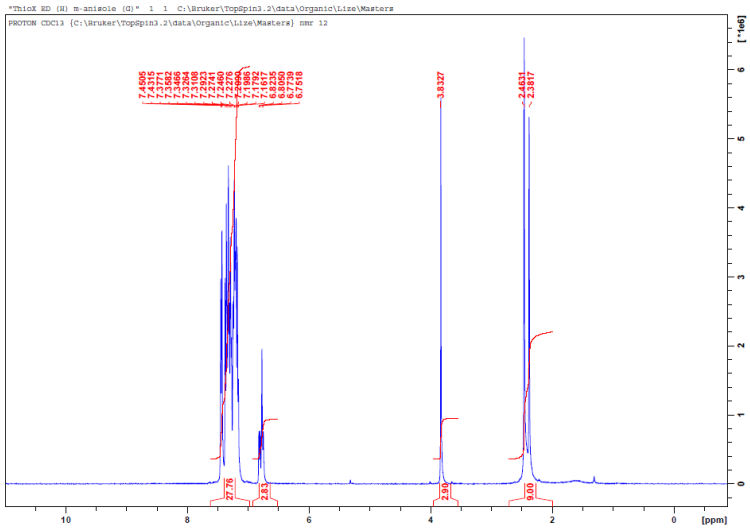

Figure S49. ^{1}H-NMR spectrum for **H$_1$**·3MANI.

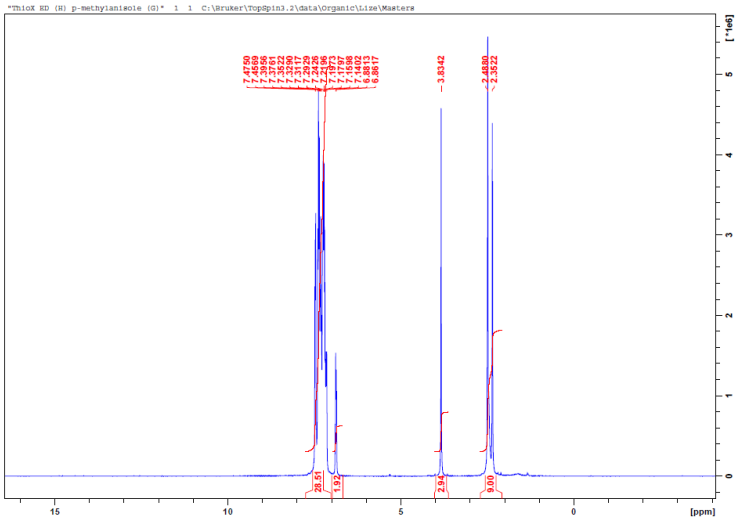

Figure S50. ^{1}H-NMR spectrum for **H$_1$**·4MANI.

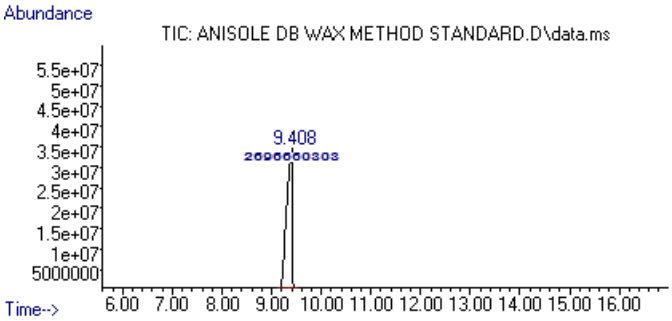

Figure S51. GC-MS chromatograph of a pure standard of ANI.

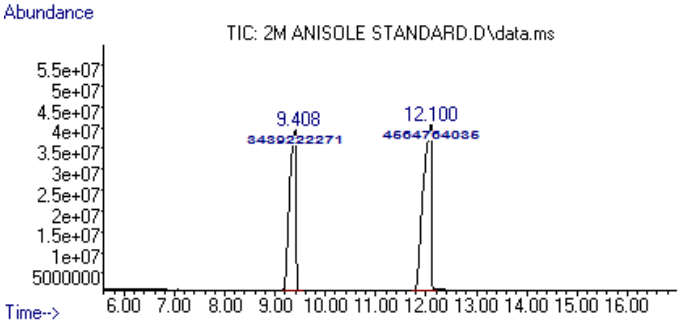

Figure S52. GC-MS chromatograph of a pure standard of ANI and 2MANI.

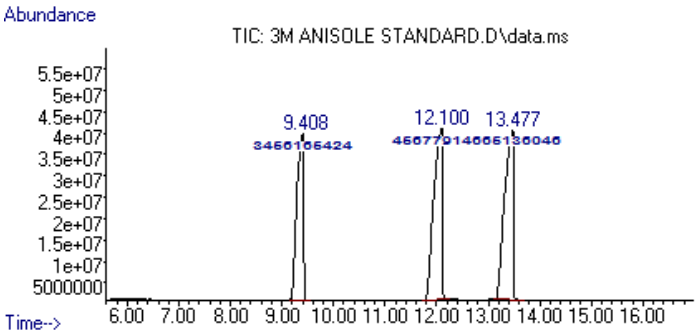

Figure S53. GC-MS chromatograph of a pure standard of ANI, 2MANI and 3MANI.

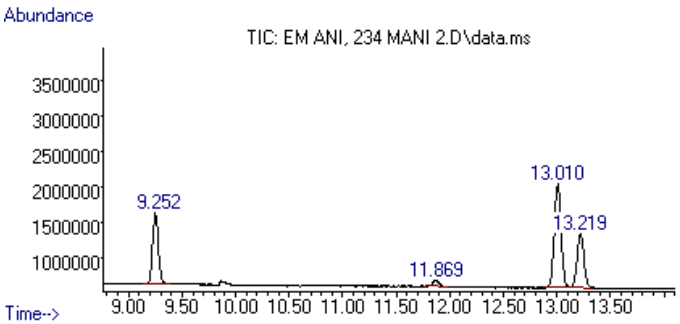

Figure S54. GC-MS chromatograph of a pure standard of ANI, 2MANI, 3MANI and 4MANI.

Table S55. Duplicate values for equimolar competition experiments of **H_1** with ANI, 2MANI, 3MANI and 4MANI.

Guests:	Batch 1	Batch 2	Average	% e.s.d.s
ANI, 2MANI	98.29:1.71	94.09:5.91	96.19:3.54	(2.10):(2.10)
ANI, 3MANI	54.40: 45.60	57.88:42.12	56.14:43.86	(1.74):(1.74)
ANI, 4MANI	35.59:64.42	36.04:63.97	35.82:64.20	(0.23):(0.23)
2-, 3- MANI	11.58:88.42	14.91:85.09	13.25:86.76	(1.67):(1.67)
3-, 4- MANI	40.14:59.86	40.56:59.44	40.35:59.65	(0.21):(0.21)
2-, 4- MANI	3.75:96.25	4.18:95.82	3.79:96.04	(0.22):(0.22)
ANI, 2-, 3- MANI	35.10:8.12:56.78	38.56:7.89:53.55	36.83:8.01:55.17	(1.73):(0.12):(1.62)
ANI, 3-, 4- MANI	27.36:32.73:39.91	29.54:29.97:40.49	28.45:31.38:40.20	(1.09):(1.41):(0.29)
ANI, 2-, 4- MANI	36.31:4.51:59.18	35.69:3.03:61.28	36.00:3.77:60.23	(0.31):(0.74):(1.05)
2-, 3-, 4- MANI	4.50:40.89:54.60	3.12:43.39:53.46	3.18:42.14:54.03	(0.69):(1.25):(0.57)
ANI, 2-, 3-, 4- MANI	31.06:2.88:19.59: 46.47	27.02:3.04:24.10: 45.85	29.04:2.96:21.85: 46.16	(2.02):(0.08):(2.26):(0.31)

Table S56. K values for competition experiment of ANI/4MANI.[a,b]

4MANI ml	4MANI c	ANI ml	ANI c	K values
1	1	0	0	
0,826	0,8701	0,174	0,1299	1,41100716
0,6756	0,7517	0,3244	0,2483	1,45364726
0,5759	0,6405	0,4241	0,3595	1,31202295
0,5004	0,4695	0,4996	0,5305	1,131734781
0,2506	0,2117	0,7494	0,7883	1,245196945
0	0	1	1	1,310721822

[a]Abbreviations in the table include ml (mother liquor) and c (crystal).
[b]The average K value is highlighted in yellow.

Table S57. K values for competition experiment of 3MANI/4MANI.[a,b]

4MANI ml	4MANI c	3MANI ml	3MANI c	K-values
1	1	0	0	
0,7808	0,8711	0,2192	0,1289	1,89721191
0,5856	0,7498	0,4144	0,2502	2,12068815
0,5045	0,6114	0,4955	0,3886	1,54527268
0,4096	0,37	0,5904	0,63	0,84654018
0,2112	0,1446	0,7888	0,8554	0,63135269
0	0	1	1	1,40821312

[a]Abbreviations in the table include ml (mother liquor) and c (crystal).
[b]The average K value is highlighted in yellow.

Table S58. K values for competition experiment of ANI/2MANI.[a,b]

ANI ml	ANI c	2MANI ml	2MANI c	K values
1	1	0	0	
0,7334	0,9825	0,2666	0,0175	20,4086252
0,5188	0,9829	0,4812	0,0171	53,3137064
0,4192	0,9409	0,5808	0,0591	22,0577556
0,3084	0,9137	0,6916	0,0863	23,7428826
0,1624	0,2653	0,8376	0,7347	1,86242097
0	0	1	1	24,2770782

[a]Abbreviations in the table include ml (mother liquor) and c (crystal).
[b]The average K value is highlighted in yellow.

Table S59. K values for competition experiment of ANI/3MANI.[a,b]

ANI ml	ANI c	3MANI ml	3MANI c	K values
1	1	0	0	
0,7179	0,888	0,2821	0,112	3,11554534
0,5282	0,8174	0,4718	0,1826	3,99846593
0,433	0,5977	0,567	0,4023	1,94548724
0,3445	0,26	0,6555	0,74	0,66853646
0,1837	0,13	0,8163	0,87	0,66399489
0	0	1	1	2,07840597

[a]Abbreviations in the table include ml (mother liquor) and c (crystal).
[b]The average K value is highlighted in yellow.

Table S60. K values for competition experiment of 2MANI/3MANI.[a,b]

3MANI ml	3MANI c	2MANI ml	2MANI c	K values
1	1	0	0	
0,7638	0,9726	0,2362	0,0274	10,977007
0,5508	0,8509	0,4492	0,1491	4,65421773
0,3771	0,5035	0,6229	0,4965	1,67510494
0,2026	0,2522	0,7974	0,7478	1,32738349
0	0	1	1	4,65842829

[a]Abbreviations in the table include ml (mother liquor) and c (crystal).
[b]The average K value is highlighted in yellow.

Table S61. H···H and H···G interactions for **H_1**·ANI, **H_1**·3MANI and **H_1**·4MANI.

Non-covalent interaction	**H_1**·ANI	**H_1**·3MANI	**H_1**·4MANI	Symmetry
π···π (H···H and H···G)	4.641(1)–5.989(1) Å 4.909(1)–5.986(1) Å [7][a]	4.527(9)–5.9691(9) Å 5.028(1)–5.757(1) Å [7]	4.571(1)–5.998(1) Å 4.964(2)–5.535(2) Å [6 major] 5.220(2)–5.869(2) Å [7 minor]	
CH···π (host-host and host-guest)				
$C_{(H)}$–$H_{(H)}$···$Cg_{(H)}$	2.85 Å, 144°			x, y, 1+z
$C_{(G)}$–$H_{(G)}$···$Cg_{(H)}$		2.78 Å, 170°		1–x, 2-y,1– z
$C_{(G2)}$–$H_{(G2)}$···$Cg_{(H)}$			2.74 Å, 134°	–1+x, y, z
H-bonding (intramolecular)	Non-classical	Non-classical	Non-classical	
$C_{(H)}$–$H_{(H)}$···$N_{(H)}$	2.62(2) Å, 103°	2.910(2) Å, 102°	2.756(2) Å, 103°	x, y, z
$C_{(H)}$–$H_{(H)}$···$N_{(H)}$	3.443(2) Å, 158°		3.456(2) Å, 155°	x, y, z
$C_{(H)}$–$H_{(H)}$···$N_{(H)}$	2.07(2) Å, 102°	2.763(2) Å, 103°	2.914(2) Å, 102°	x, y, z
$C_{(H)}$–$H_{(H)}$···$N_{(H)}$		3.456(2) Å, 153°		x, y, z
$C_{(H)}$–$H_{(H)}$···$N_{(H)}$	3.455(2) Å, 151°	3.422(2) Å, 151°	3.437(2) Å, 148°	x, y, z
$C_{(H)}$–$H_{(H)}$···$N_{(H)}$	2.768(2) Å, 103°	2.772(2) Å, 103°	2.766(2) Å, 103°	x, y, z
$C_{(H)}$–$H_{(H)}$···$N_{(H)}$	2.898(2) Å, 102°	2.921(2) Å, 101°	2.902(2) Å, 101°	x, y, z
$C_{(H)}$–$H_{(H)}$···$O_{(G1)}$			2.55 Å, 132°	x, y, z
$C_{(H)}$–$H_{(H)}$···$O_{(G)}$–$C_{(G)}$	2.70Å, 127°(<)			x, y, 1+z
$N_{(H)}$–$H_{(H)}$···$C_{(H)}$–$C_{(H)}$	2.83Å, 158°(<)			–x, 1–y, 1–z
Other short contacts (H···G/G···G)[b]				
$C_{(H)}$–$H_{(H)}$···$C_{(G)}$–$C_{(G)}$	2.87Å, 141°(<)			1–x, 1–y, 1–z
$C_{(G)}$–$H_{(G)}$···$C_{(H)}$–$C_{(H)}$	2.86Å, 143°(<)			-x, 1-y, 1-z
$C_{(H)}$–$H_{(H)}$···$S_{(H)}$–$C_{(H)}$		2.95 Å, 146° (<)		1–x, 2–y, 1–z
$C_{(H)}$–$H_{(H)}$···$H_{(H)}$–$C_{(H)}$		2.35 Å, 128° (<)		1–x, 1–y, 1–z
$C_{(H)}$–$H_{(H)}$···$H_{(G)}$–$C_{(G)}$		2.36 Å, 143° (<)		1–x, 2–y, 1–z
$C_{(H)}$–$H_{(H)}$···$H_{(G)}$–$C_{(G)}$		2.94 Å, 130° (<)		x, 1+y, z
$C_{(H)}$–$H_{(H)}$···$H_{(G)}$–$C_{(G)}$		2.34 Å, 158° (<)		2–x, 2–y, 1–z
$C_{(H)}$–$H_{(H)}$···$H_{(H)}$-$C_{(H)}$			2.38 Å, 127° (<)	2–x, 1–y, –z
$C_{(H)}$–$H_{(H)}$···$H_{(G2)}$–$C_{(G2)}$			2.28 Å, 139° (<)	2–x, –y, –z
$C_{(H)}$–$H_{(H)}$···$H_{(G2)}$–$C_{(G2)}$			2.26 Å, 136° (<)	1–x, –y, –z
$C_{(H)}$–$H_{(H)}$···$H_{(G2)}$–$C_{(G2)}$			2.27 Å, 157° (<)	1–x, 1–y, 1–z
$C_{(G1)}$–$H_{(G1)}$···$H_{(H)}$–$C_{(H)}$			2.31 Å, 135° (<)	1–x, –y, 1–z

[a]Number of H···G interactions are indicated in parentheses.

[b]Distances denoted by < are contacts that measure less than the sum of the van der Waals radii of the atoms involved.

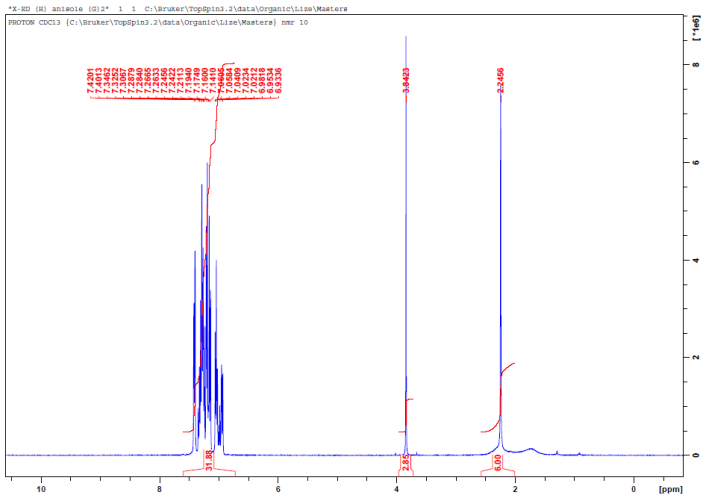

Figure S62. ^{1}H-NMR spectrum for **H_2**·ANI.

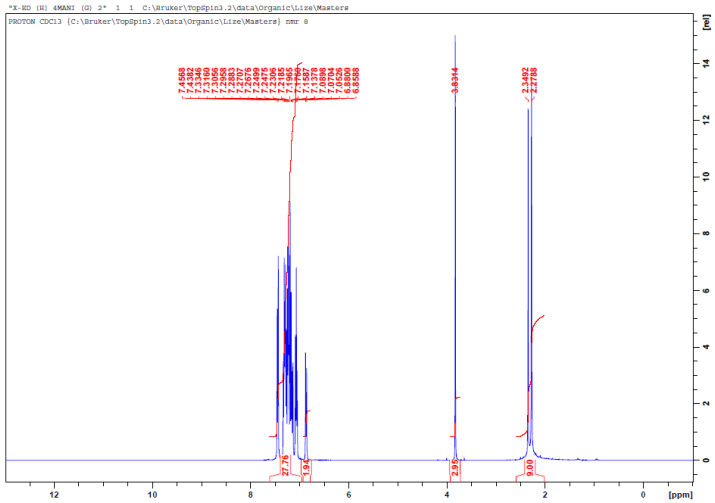

Figure S63. ^{1}H-NMR spectrum for **H_2**·4MANI.

Table S64. Duplicate values for equimolar competition experiments of **H_2** with ANI, 2MANI, 3MANI and 4MANI.

Guests:	Batch 1	Batch 2	Average	% e.s.d.s
ANI, 2MANI	97.47:2.54	95.07:4.93	96.27:3.73	(1.20):(1.20)
ANI, 3MANI	91.80:8.20	89.91:10.09	90.86:9.14	(0.95):(0.95)
ANI, 4MANI	14.54:85.46	14.08:85.92	14.31:85.69	(0.23):(0.23)
2-, 3- MANI	[a]	[a]	-	-
3-, 4- MANI	6.55:93.45	6.20:93.80	6.37:93.63	(0.18):(0.18)
2-, 4- MANI	3.88:96.12	3.50:96.50	3.69:96.31	(0.19):(0.19)
ANI, 2-, 3- MANI	[a]	[a]	-	-
ANI, 3-, 4- MANI	11.25:4.77:83.98	9.81:4.17:86.02	10.53:4.47:85.00	(0.72):(0.30):(1.02)
ANI, 2-, 4- MANI	10.11:1.76:88.13	11.73:2.36:85.91	10.92:2.06:87.02	(0.81):(0.30):(1.11)
2-, 3-, 4- MANI	1.25:3.95:94.80	2.17:5.65:92.18	1.71:4.80:93.49	(0.46):(0.85):(1.31)
ANI, 2-, 3-, 4- MANI	11.58:1.15:5.28: 81.99	11.09:1.76:3.89: 83.26	11.34:1.46:4.59: 82.63	(0.25):(0.31):(0.70): (0.64)

[a]Did not crystallize

Table S65. K values for competition experiment of 4MANI/2MANI.[a,b]

4MANI ml	4MANI c	2MANI ml	2MANI c	K values
1	1	0	0	
0,76895	0,97928	0,23105	0,02072	14,2011987
0,59087	0,97345	0,40913	0,02655	25,3874166
0,4831	0,95868	0,5169	0,04132	24,8246337
0,38051	0,95584	0,61949	0,04416	35,2390638
0,2024	0,9226	0,7976	0,0774	46,9728733
0	0	1	1	29,3250372

[a]Abbreviations in the table include ml (mother liquor) and c (crystal).
[b]The average K value is highlighted in yellow.

Table S66. K values for competition experiment of 4MANI/ANI.[a,b]

4MANI ml	4MANI c	ANI ml	ANI c	K values
1	1	0	0	
0,84755	0,95795	0,15245	0,04205	4,09768851
0,7073	0,91351	0,2927	0,08649	4,37085574
0,61392	0,88071	0,38608	0,11929	4,64295433
0,51476	0,82224	0,48524	0,17776	4,3602999
0,28578	0,70284	0,71422	0,29716	5,91107263
0	0	1	1	4,67657422

[a]Abbreviations in the table include ml (mother liquor) and c (crystal).
[b]The average K value is highlighted in yellow.

Table S67. K values for competition experiment of 4MANI/3MANI.[a,b]

4MANI ml	4MANI c	3MANI ml	3MANI c	K values
1	1	0	0	
0,76304	0,96121	0,23696	0,03879	7,69531207
0,53685	0,92921	0,46315	0,07079	11,3242819
0,44262	0,90883	0,55738	0,09117	12,5531017
0,37035	0,90938	0,62965	0,09062	17,061146
0,19305	0,85919	0,80695	0,14081	25,5054233
0	0	1	1	14,827853

[a]Abbreviations in the table include ml (mother liquor) and c (crystal).
[b]The average K value is highlighted in yellow.

Table S68. K values for competition experiment of ANI/2MANI.[a,b]

ANI ml	ANI c	2MANI ml	2MANI c	K values
1	1	0	0	
0,68096	0,96152	0,31904	0,03848	11,7070317
0,45534	0,95186	0,54466	0,04814	23,65139
0,39066	0,9537	0,60934	0,0463	32,1285802
0,24689	0,92862	0,75311	0,07138	39,684088
0	0	1	1	26,7927725

[a]Abbreviations in the table include ml (mother liquor) and c (crystal).
[b]The average K value is highlighted in yellow.

Table S69. K values for competition experiment of ANI/3MANI.[a,b]

ANI ml	ANI c	3MANI ml	3MANI c	K values
1	1	0	0	
0,70624	0,94776	0,29376	0,05224	7,54632587
0,47964	0,95625	0,52036	0,04375	23,7127488
0,38395	0,92949	0,61605	0,07051	21,1512139
0,29716	0,91947	0,70284	0,08053	27,0051121
0,14036	0,64984	0,85964	0,35016	11,3661442
0	0	1	1	18,156309

[a]Abbreviations in the table include ml (mother liquor) and c (crystal).
[b]The average K value is highlighted in yellow.

Table S70. H···H and H···G interactions for **H_2**·ANI and **H_2**·4MANI.

Non-covalent interaction	**H_1**·ANI	**H_1**·4MANI	Symmetry
π···π (H···H and H···G) H···G interactions	4.080(1)–5.920(1) Å 4.725(1)–5.920(1) Å [5]	4.0427(7)–5.756(3) Å [H···H]	
CH···π			
$C_{(H)}$–$H_{(H)}$···$Cg_{(H)}$	2.94 Å, 76°		x, y, z
$C_{(H)}$–$H_{(H)}$···$Cg_{(H)}$	2.57 Å, 97°		x, y, z
$C_{(H)}$–$H_{(H)}$···$Cg_{(H)}$	2.92 Å, 128°		x, 1+y, z
$C_{(H)}$–$H_{(H)}$···$Cg_{(H)}$	2.63 Å, 162°		2–x, 2–y, 2–z
$C_{(H)}$–H_{36}···$Cg_{(H)}$	2.81 Å, 105°		x, y, z
$C_{(H)}$–$H_{(H)}$···$Cg_{(H)}$	2.92 Å, 128°		1–x, 1–y, 1–z
$C_{(G)}$–$H_{(G)}$···$Cg_{(H)}$	2.90 Å, 137°		x, y, z
$C_{(H)}$–$H_{(H)}$···$Cg_{(H)}$		2.61 Å, 99°	x, y, z
$C_{(H)}$–$H_{(H)}$···$Cg_{(H)}$		2.83 Å, 132°	1+x, y, z
$C_{(H)}$–$H_{(H)}$···$Cg_{(H)}$		2.90 Å, 133°	1–x, –y,1–z
$C_{(H)}$–$H_{(H)}$···$Cg_{(H)}$		2.75 Å, 105°	x, y, z
$C_{(H)}$–$H_{(H)}$···$Cg_{(H)}$		2.69 Å, 155°	1–x, –y, –z
$C_{(G)}$–$H_{(G)}$···$Cg_{(H)}$		2.78 Å, 135°	–1+x, –1+y, z
H-bonding (intramolecular)	Non-classical	Non-classical	
$C_{(H)}$–$H_{(H)}$···$N_{(H)}$	2.805(3) Å, 102°		x, y, z
$C_{(H)}$–$H_{(H)}$···$O_{(H)}$–$C_{(H)}$	2.64Å, 164°(<)		1+x, 1+y, z
$N_{(H)}$–$H_{(H)}$···$C_{(G)}$–$C_{(G)}$		2.63 Å, 156° (<<)	1–x, –y, 1–z
$N_{(H)}$–$H_{(H)}$···$C_{(G)}$–$C_{(G)}$		2.37 Å, 160° (<)	1+x, y, z
$C_{(H)}$–$H_{(H)}$···$O_{(H)}$–$C_{(H)}$		2.63 Å, 155° (<)	–1+x, –1+y, z
Short contacts (H/G and G/G)[a,b]			
$C_{(H)}$–$H_{(H)}$···$H_{(G)}$–$C_{(G)}$		2.30 Å, 127° (<)	1+x, 1+y, z

[a]Number of H···G interactions are indicated in square brackets.
[b]Distances denoted by < are contacts that measure less than the sum of the van der Waals radii of the atoms involved.

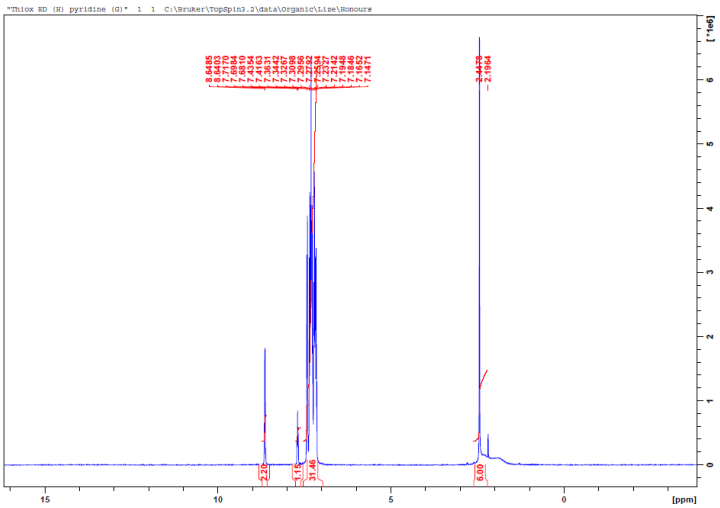

Figure S71. ^{1}H-NMR spectrum for **H$_1$**·PYR**.**

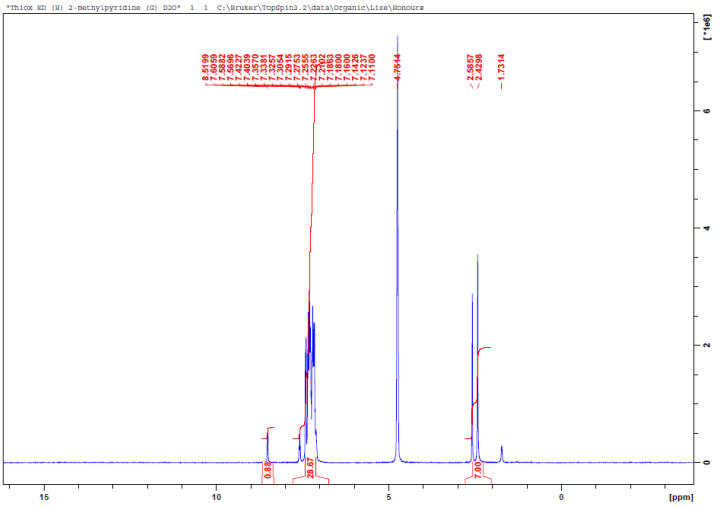

Figure S72. ^{1}H-NMR spectrum for **H$_1$**·2MP**.**

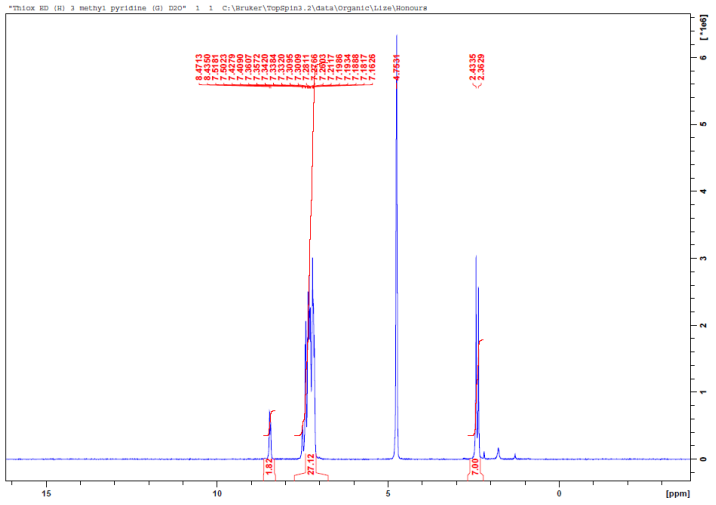

Figure S73. ^{1}H-NMR spectrum for **H$_1$**·3MP**.**

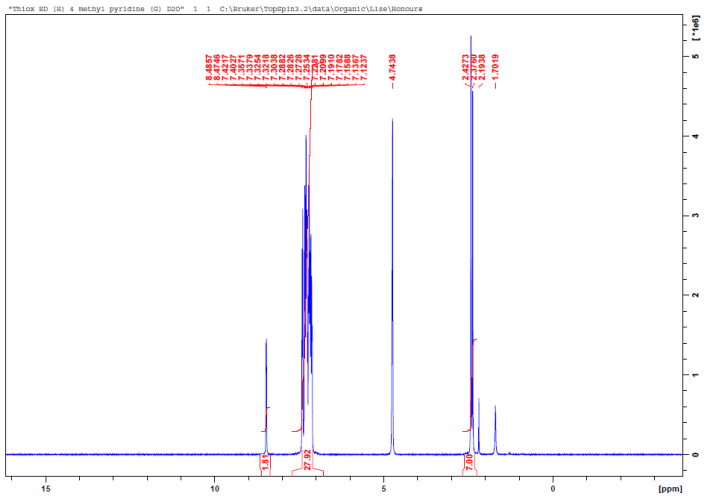

Figure S74. ^{1}H-NMR spectrum for **H$_1$**·4MP**.**

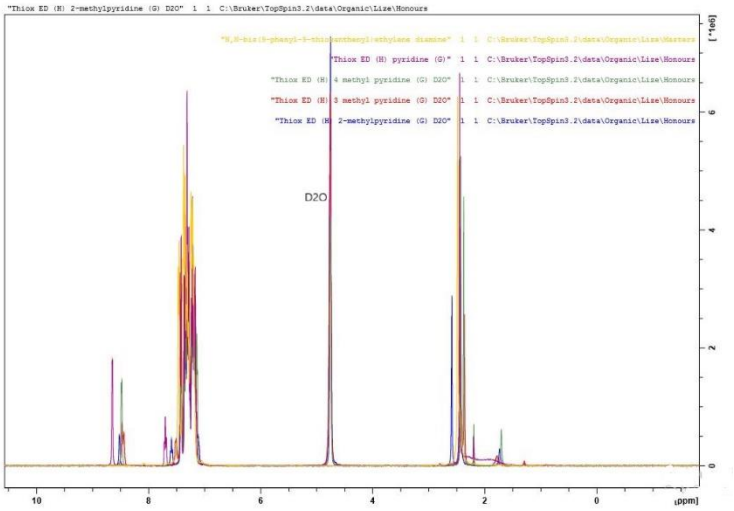

Figure S75. Overlapping spectra of inclusion compounds of **H$_1$** with PYR, 2MP, 3MP and 4MP.

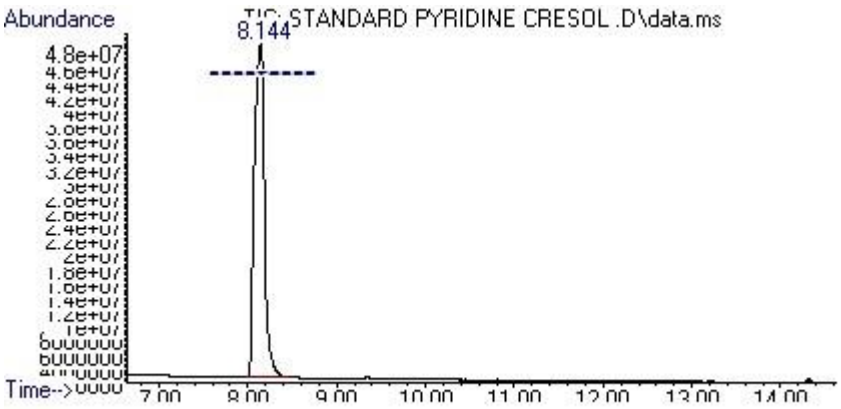

Figure S76. Chromatograph standard of pure PYR.

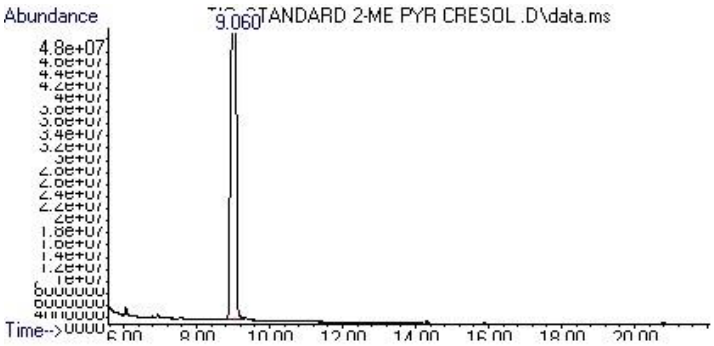

Figure S77. Chromatograph standard of pure 2MP.

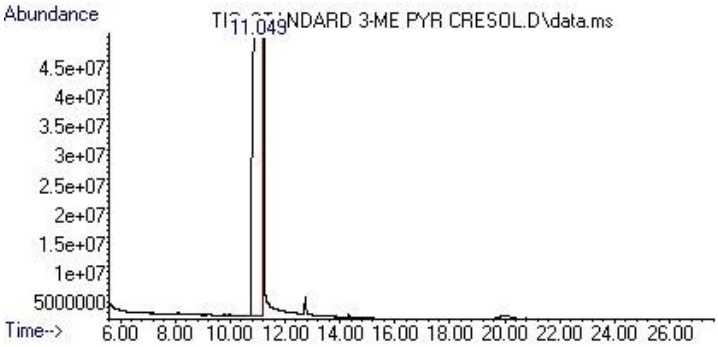

Figure S78. Chromatograph standard of pure 3MP.

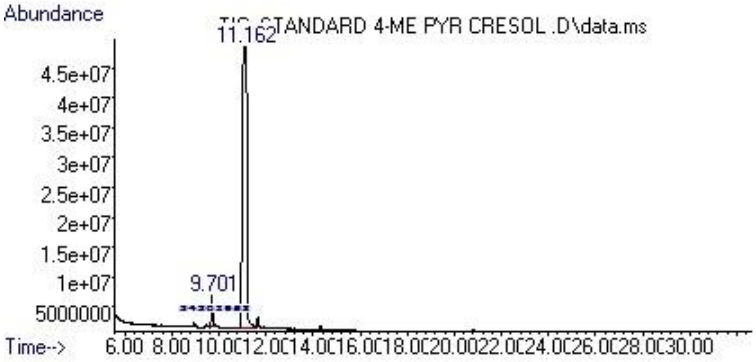

Figure S79. Chromatograph standard of pure 4MP.

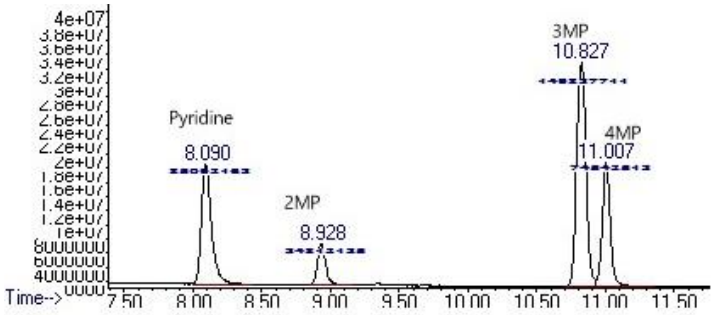

Figure S80. Chromatograph showing separation of pure guests PYR, 2MP, 3MP and 4MP.

Table S81. Triplicate values for equimolar competition experiments of **H_1** with PYR, 2MP, 3MP and 4MP.

Guests:	Batch 1	Batch 2	Batch 3	Average	% e.s.d.s
2- ,3- MP	18.53:81.57	18.07:81.93	16.72:83.28	17.77:82.26	(0.77):(0.77)
2- ,4- MP	24.39:75.61	25.50:74.50	22.73:77.27	24.21:75.79	(1.14):(1.14)
3- ,4- MP	69.17:30.29	70.36:29.64	69.79:30.21	69.11:30.05	(0.49):(0.49)
2-, 3-, 4- MP	8.99:63.81: 27.20	10.21:63.50: 26.29	8.82:63.22: 27.96	9.34: 63.51: 27.15	(0,62):(0,24):(0,68)
2MP and PYR	26.30:73.70	21.23:78.77	21.07:78.93	22.87:77.13	(2.43):(2.43)
3MP and PYR	60.82:39.18	54.48:45.52	60.94:39.06	58.75:41.25	(3.02):(3.02)
4MP and PYR	38.11:61.89	36.57:63.46	38.53:61.47	37.40:62.27	(0.84):(0.84)
2-, 3- MP and PYR	10.50:56.19: 33.31	10.48:53.91: 35.61	11.42:52.46: 36.11	10.8: 54.19:35.01	(0.44):(1.54):(1,22)
2- ,4- MP and PYR	12.14:31.85: 56.01	11.71:29.42: 58.87	13.24:33.13: 53.63	12.36:31.47: 56.17	(0.64):(1.54):(2.14)
3-, 4- MP and PYR	52.63:20.93: 26.44	48.50:21.21: 30.28	50.85:21.53: 27.62	50.66:21.22: 28.11	(1.69):(0,25):(1.61)
2-, 3-, 4- MP and PYR	7.42:44.82: 22.30:25.46	7.13:44.48: 17.69:30.69	6.08:51.56: 19.26:23.10	6.87:46.95: 19.75:26.42	(0.58):(3.26):(1.91):(3.17)

Table S82. K values for competition experiment of 3MP/2MP.[a,b]

3MP ml	3MP c	2MP ml	2MP c	K value
1	100	0	0	#DIV/0!
0,69	93,48	0,31	6,52	6,441451054
0,56	85,66	0,44	14,34	4,693464834
0,49	81,78	0,51	18,22	4,671677233
0,42	78,76	0,58	21,24	5,120706663
0,19	38	0,81	62	2,612903226
0	0	1	100	4,708040602

[a]Abbreviations in the table include ml (mother liquor) and c (crystal).
[b]The average K value is highlighted in yellow.

Table S83. K values for competition experiment of 3MP/4MP.[a,b]

3MP ml	3MP c	4MP ml	4MP c	K value
1	100	0	0	#DIV/0!
0,74	85,42	0,26	14,58	2,058465873
0,59	74,03	0,41	25,97	1,98092323
0,51	69,85	0,49	30,15	2,22589666
0,44	64,67	0,56	35,33	2,329670895
0,27	50,51	0,73	49,49	2,759427643
0	0	1	100	2,27087686

[a]Abbreviations in the table include ml (mother liquor) and c (crystal).
[b]The average K value is highlighted in yellow.

Table S84. K values for competition experiment of PYR/2MP.[a,b]

PYR ml	PYR c	2MP ml	2MP c	K value
1	100	0	0	#DIV/0!
0,68	90,94	0,32	9,06	4,723542397
0,51	85,25	0,49	14,75	5,553007644
0,43	75,33	0,57	24,67	4,047671119
0,37	75,03	0,63	24,97	5,1162909
0,17	58	0,83	42	6,742296919
0	0	1	100	5,236561796

[a]Abbreviations in the table include ml (mother liquor) and c (crystal).
[b]The average K value is highlighted in yellow.

Table S85. K values for competition experiment of 3MP/PYR.[a,b]

3PM ml	3MP c	PYR ml	PYR c	K value
1	100	0	0	#DIV/0!
0,77	84,79	0,23	15,21	1,665146819
0,64	69,63	0,36	30,37	1,289656734
0,56	60,64	0,44	39,36	1,210511034
0,47	56,02	0,53	43,98	1,436368562
0,33	33,77	0,67	66,23	1,035230761
0	0	1	100	1,327382782

[a]Abbreviations in the table include ml (mother liquor) and c (crystal).
[b]The average K value is highlighted in yellow.

Table S86. K values for competition experiment of 4MP/PYR.[a,b]

PYR ml	PYR c	4MP ml	4MP c	K value
1	100	0	0	#DIV/0!
0,7	82,75	0,3	17,25	2,055900621
0,52	69,36	0,48	30,64	2,08957622
0,45	64,24	0,55	35,76	2,195625155
0,42	60,15	0,58	39,85	2,084423732
0,19	36,99	0,81	63,01	2,502685455
0	0	1	100	2,185642237

[a]Abbreviations in the table include ml (mother liquor) and c (crystal).
[b]The average K value is highlighted in yellow.

Table S87. K values for competition experiment of 4MP/2MP.[a,b]

4MP ml	4MP c	2MP ml	2MP c	K value
1	100	0	0	#DIV/0!
0,7494	90,12	0,2506	9,88	3,050223174
0,5803	81,28	0,4197	18,72	3,14025018
0,4901	74,64	0,5099	25,36	3,062123419
0,2769	65,87	0,7231	34,13	5,039956418
0,23	47,17	0,77	52,83	2,989153067
0	0	1	100	3,456341252

[a]Abbreviations in the table include ml (mother liquor) and c (crystal).
[b]The average K value is highlighted in yellow.

Table S88. Summary of H···H interactions of inclusion compounds.[a]

Interaction	**H₁**·PYR	**H₁**·2MP	**H₁**·3MP	**H₁**·4MP
	Range	Range	Range	Range
π···π	4.30–5.98Å	4.31–5.95Å	4.32–5.91Å	4.34–5.95Å
CH···π	2.65–2.78Å, 135–151˚ [3]	2.68–2.99Å, 129–152˚ [3]	2.66–2.81Å, 135–148˚ [3]	2.70–2.95Å, 134–147˚ [2]
Non-classical H-bonding	2.77–3.44Å, 102–152˚ [3]	2.90–3.48Å, 102–152˚ [6]	2.76–3.45Å, 102–150˚ [5]	2.76–3.48Å, 102–153˚ [6]
Other short contacts	2.88Å, 108˚ [3]	2.85–2.88Å, 101–149˚ [3]	None	None

[a]Number of H···H interactions are indicated in square parentheses.

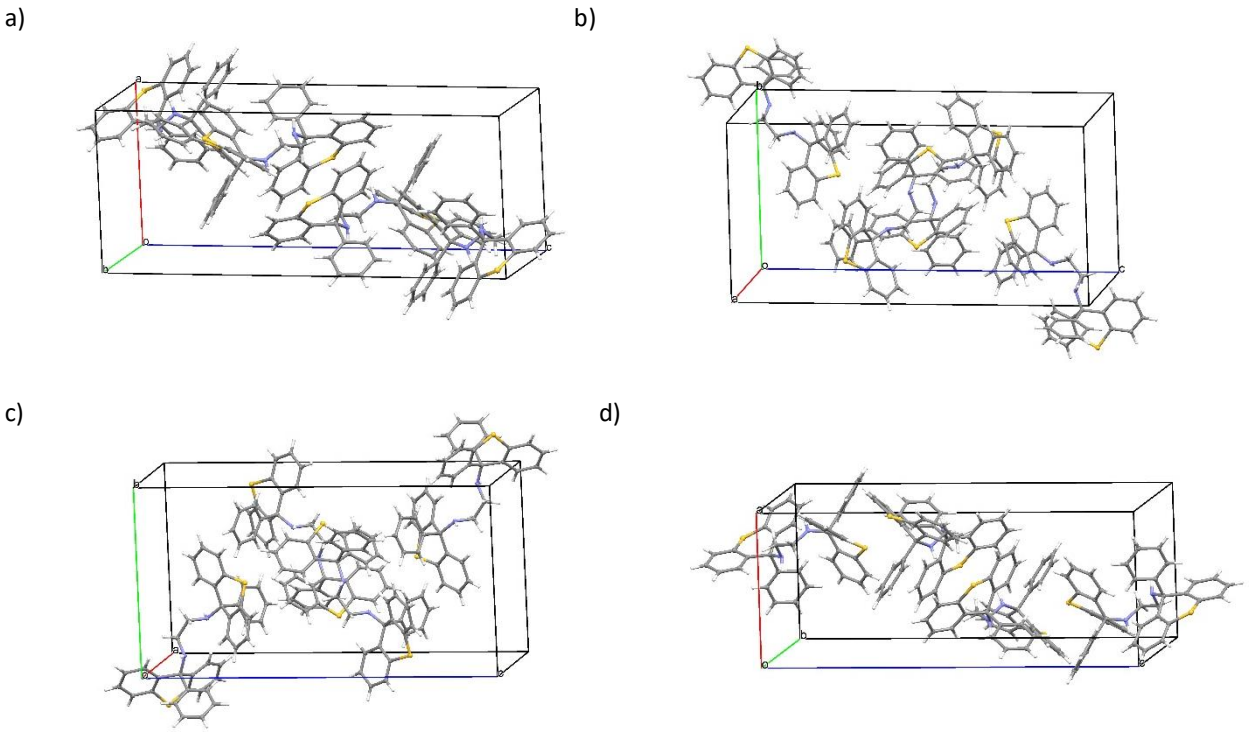

Figure S89. Host packing of **H₁** in complexes with a) PYR, b) 2MP, c) 3MP, and d) 4MP.

a)

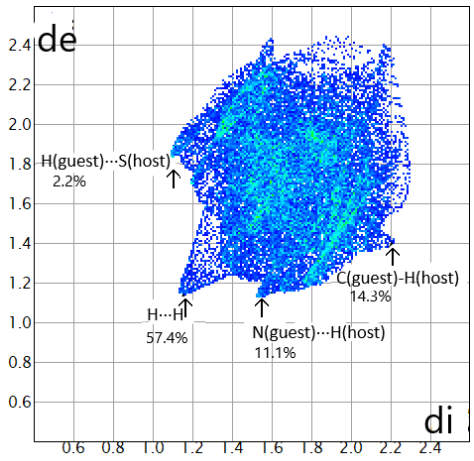

b)

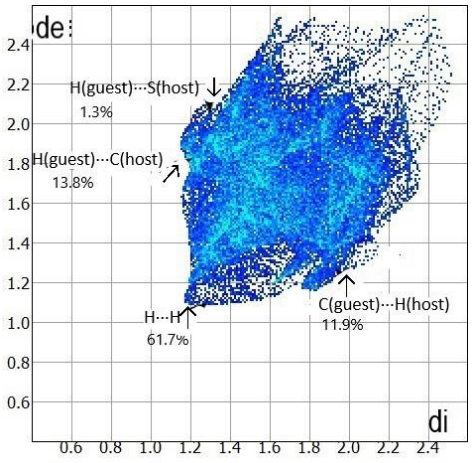

c)

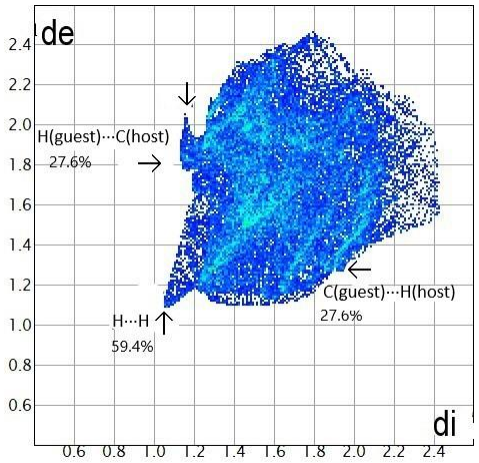

d)

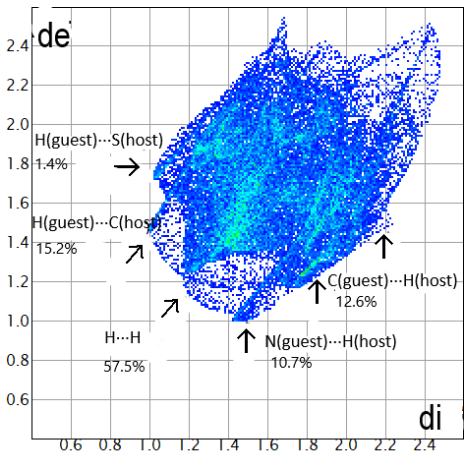

e)

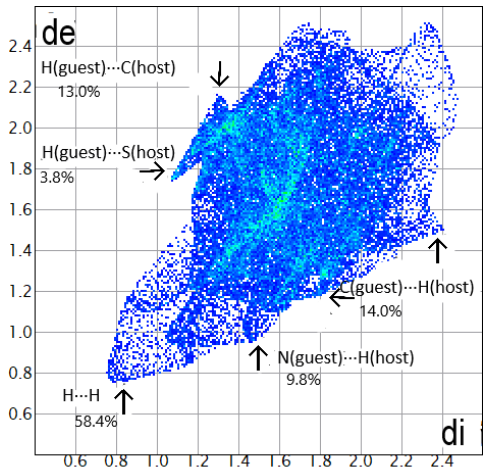

Figure S90. 2D Hirshfeld surfaces of **H_1** in complexes with a) PYR, b) 2MP, c) 3MP, d) 4MP major component, and e) 4MP minor component.

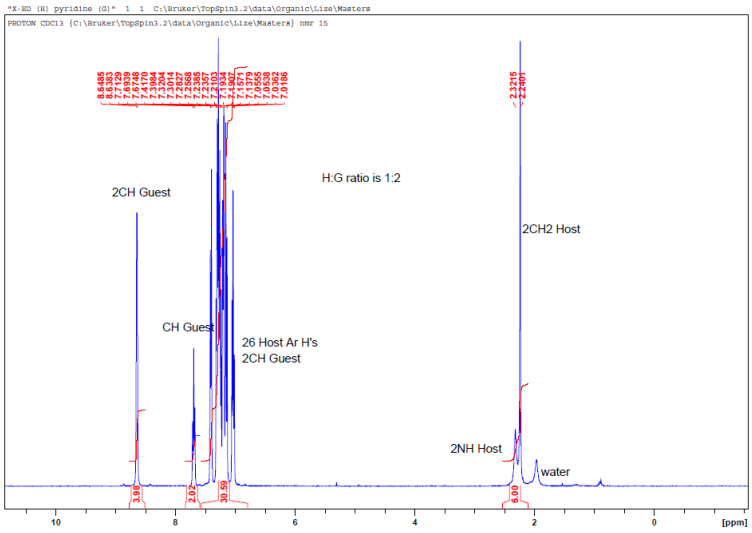

Figure S91. ^{1}H-NMR spectrum for **H_2**·PYR**.**

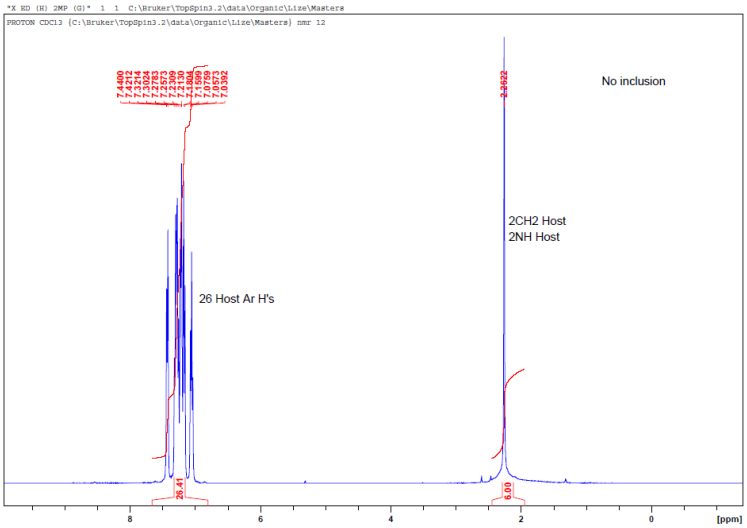

Figure S92. ^{1}H-NMR spectrum for **H_2** after no inclusion of 2MP occured**.**

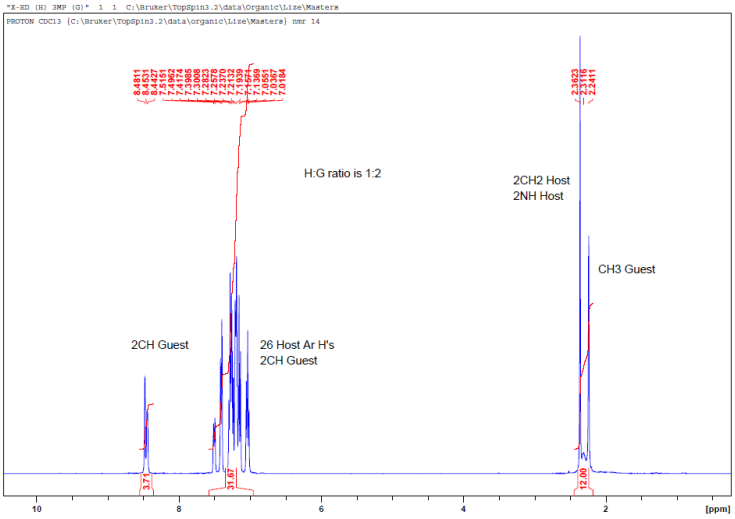

Figure S93. ^{1}H-NMR spectrum for **H_2**·3MP**.**

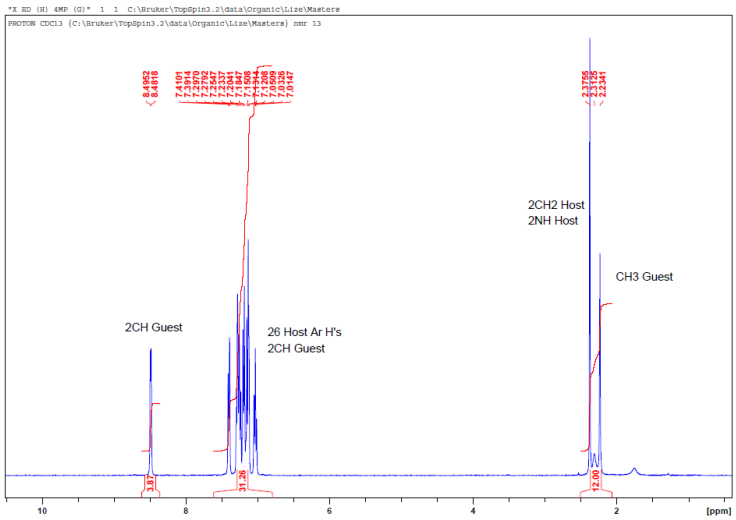

Figure S94. ^{1}H-NMR spectrum for **H_2**·4MP**.**

Table S95. Duplicate values for equimolar competition experiments of **H_2** with PYR, 2MP, 3MP and 4MP.

Guests:	Batch 1	Batch 2	Average	% e.s.d.s
2-, 3- MP	29.67:70.33	29.54:70.46	29.61:70.39	(0.07):(0.07)
2-, 4- MP	*a*	*a*	-	-
3-, 4- MP	8.86:91.14	7.98:02.02	8.42:91.58	(0.44):(0.44)
2-, 3-, 4- MP	20.69:54.79:24.52	20.79:63:59.78:19.43	20.74: 57.29: 21.98	(0.05):(2.50):(2.55)
PYR, 2MP	72.40:27.60	68.71:31.29	70.56:29.45	(1.85):(1.85)
PYR, 3MP	19.29:80.71	20.67:79.33	19.98:80.02	(0.69):(0.69)
PYR, 4MP	37.62: 62.38:	42.55:57.45	40.09: 59.92	(2.47):(2.47)
PYR, 2-, 3- MP	17.61:21.55:60.85	16.96:20.72:62.32	17.15:21.14:61.57	(0.46):(0.42):(0.74)
PYR, 2-, 4- MP	35.98:19.93:44.09	36.55:21.05:42.40	36.27:20.49:43.25	(0.29):(0.56):(0.85)
PYR, 3-, 4- MP	13.84:56.08:30.08	15.70:55.25:29.05	14.77:55.57:29.57	(0.93):(0.42):(0.52)
PYR, 2-, 3-, 4- MP	11.70:19.58:49.22:19.50	12.29:18.87:48.35:20.50	12.00:19.23:48.79: 20.00	(0.30):(0.36):(0.44): (0.50)

[a]Crystals contained only apohost.

Table S96. K values for competition experiment of 2MP/3MP.[a,b]

3MP ml	3MP c	2MP ml	2MP c	K value
1	1	0	0	
0,78006	0,89728	0,21994	0,10272	2,46291367
0,57308	0,75359	0,42692	0,24641	2,27828498
0,49739	0,68754	0,50261	0,31246	2,22350247
0,39473	0,6227	0,60527	0,3773	2,53070239
0,18837	0,49997	0,81163	0,50003	4,30818395
0	0	1	1	2,76071749

[a]Abbreviations in the table include ml (mother liquor) and c (crystal).
[b]The average K value is highlighted in yellow.

Table S97. K values for competition experiment of 3MP/4MP.[a,b]

3MP ml	3MP c	4MP ml	4MP c	K value
1	1	0	0	
0,7166	0,84829	0,2834	0,15171	2,21132808
0,55099	0,77422	0,44901	0,22578	2,79441699
0,45152	0,70793	0,54848	0,29207	2,94433465
0,38673	0,0989	0,61327	0,9011	5,745566305
0,18635	0,05418	0,81365	0,94582	3,998170043
0	0	1	1	3,538763215

[a]Abbreviations in the table include ml (mother liquor) and c (crystal).
[b]The average K value is highlighted in yellow.

Table S98. K values for competition experiment of PYR/2MP.[a,b]

PYR ml	PYR c	2MP ml	2MP c	K value
1	1	0	0	
0,6811	0,96006	0,3189	0,03994	11,2547008
0,43233	0,75	0,56767	0,25	3,93914371
0,3756	0,68	0,6244	0,32	3,53261448
0,28795	0,41163	0,71205	0,58837	1,73001515
0,14252	0,27683	0,85748	0,72317	2,30314318
0	0	1	1	4,55192346

[a]Abbreviations in the table include ml (mother liquor) and c (crystal).
[b]The average K value is highlighted in yellow.

Table S99. K values for competition experiment of PYR/3MP.[a,b]

3MP ml	3MP c	PYR ml	PYR c	K value
1	1	0	0	
0,8352	0,9195	0,1648	0,0805	2,25383737
0,64496	0,80947	0,35504	0,19053	2,33873974
0,61294	0,80466	0,38706	0,19534	2,60124679
0,46204	0,63204	0,53796	0,36796	1,99992801
0,28695	0,0542	0,71305	0,9458	7,022411392
0	0	1	1	3,24323266

[a]Abbreviations in the table include ml (mother liquor) and c (crystal).
[b]The average K value is highlighted in yellow.

Table S100. K values for competition experiment of PYR/4MP.[a,b]

4MP ml	4MP c	PYR ml	PYR c	K value
1	1	0	0	
0,72082	0,9095	0,27918	0,0905	3,89234744
0,6	0,84396	0,4	0,15604	3,60574212
0,44928	0,6238	0,55072	0,3762	2,03254581
0,30664	0,3366	0,69336	0,6634	1,14727788
0,15989	0,19305	0,84011	0,80695	1,25700797
0	0	1	1	2,38698424

[a]Abbreviations in the table include ml (mother liquor) and c (crystal).
[b]The average K value is highlighted in yellow.

a)

b)

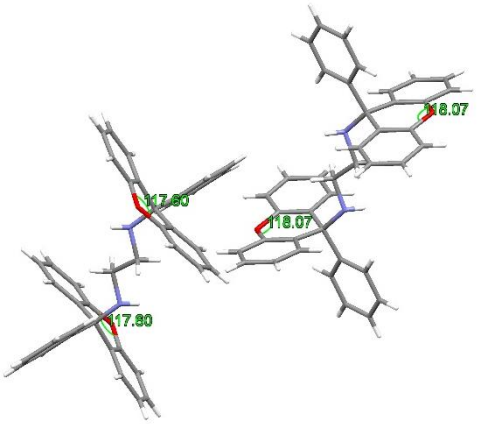

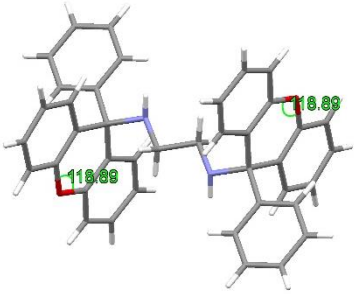

c)

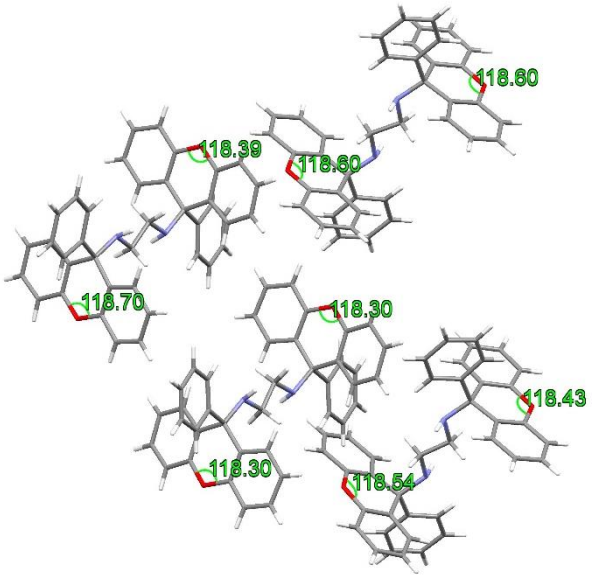

Figure S101. C–Ô–C angles in complexes a) **H_2**·PYR b) **H_2**·4MP and c) **H_2**·3MP, after guest removal.

Table S102. Numbering of hosts and guests for **H_2**·3MP.

HOSTS

a) Host 1 – symmetry generated

Cg1 O_3 – $C_{312, 311, 31, 321, 322}$

Cg2 $C_{311-316}$

Cg3 $C_{322-326}$

Cg4 $C_{331-336}$

$N_3(H_3)$-$C_{32}(H_{32a,32b})$

b) Host 2 – symmetry generated

Cg5 O_4 – $C_{412, 411, 41, 421, 422}$

Cg6 $C_{411-416}$

Cg7 $C_{422-426}$

Cg8 $C_{431-436}$

$N_4(H_4)$-$C_{42}(H_{42a,42b})$

c) Host 3

Cg9 O_{11} – $C_{112, 111, 11, 121, 122}$

Cg10 O_{12} – $C_{142, 141, 14, 151, 152}$

Cg11 $C_{111-116}$

Cg12 $C_{121-126}$

Cg13 $C_{131-136}$

Cg14 $C_{141-146}$

Cg15 $C_{151-156}$

Cg16 $C_{161-166}$

N_{11} - C_{12} – C_{13} – N_{12}

d) Host 4

Cg17 O_{21} – $C_{212, 211, 21, 221, 222}$

Cg18 O_{22} – $C_{242, 241, 24, 251, 252}$

Cg19 $C_{211-216}$

Cg20 $C_{221-226}$

Cg21 $C_{231-236}$

Cg22 $C_{241-246}$

Cg23 $C_{251-256}$

Cg24 $C_{261-266}$

N_{21} – C_{22} – C_{23} – N_{22}

NON-DISORDERED GUESTS

Guest 1: Cg25

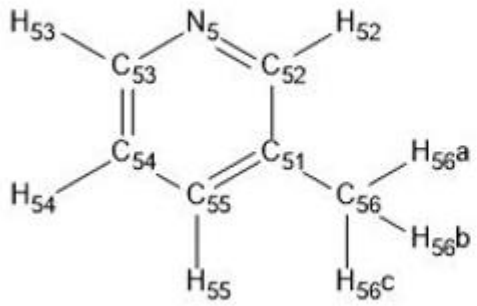

Guest 2: Cg26

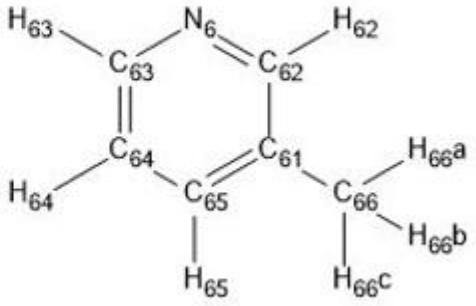

DISORDERED GUESTS

a) Guest 3: Cg27 N_{7A} – $C_{72A, 71A, 75A, 74A, 73A}$

b) Guest 4: Cg28 N_{8A} – $C_{82A, 81A, 85A, 84A, 83A}$

c) Guest 5: Cg29 N_{9A} – $C_{92A, 91A, 95A, 94A, 93A}$

d) Guest 6: Cg30 N_{7B} – $C_{72B, 71B, 75B, 74B, 73B}$

e) Guest 7: Cg31 N_{8B} – $C_{82B, 81B, 85B, 84B, 83B}$

f) Guest 8: Cg32 N_{9B} – $C_{92B, 91B, 95B, 94B, 93B}$

Table S103. H···G and H···H interactions present in complexes **H_2**·PYR and **H_2**·4MP.[a]

Non-covalent interaction	**H_2**·PYR	**H_2**·4MP	Symmetry
π···π (H···H & H···G) H···G major H···G minor	4.043(1) – 5.987(1) Å 4.947(1) – 5.987(1) Å [9] 4.402(1) – 5.512(1) Å [7]	4.005(1) – 5.898(1) Å 4.081(1)- 5.898(1) Å [10]	
C–H···π (H···H & H···G)			
$C_{(G)}$–$H_{(G)}$···$Cg_{(H)}$	2.70 Å, 124°		–x,1–y, –z
$C_{(H)}$–$H_{(H)}$···$Cg_{(H)}$	2.67 Å, 115°		x, y, z
$C_{(H)}$–$H_{(H)}$···$Cg_{(H)}$	2.65 Å, 102°		x, y, z
$C_{(H)}$–$H_{(H)}$···$Cg_{(H)}$	2.86 Å, 154°		1–x, 1–y, 1–z
$C_{(H)}$–$H_{(H)}$···$Cg_{(H)}$		2.96 Å, 81°	x, y, z
$C_{(H)}$–$H_{(H)}$···$Cg_{(H)}$		2.84 Å, 103°	x, y, z
$C_{(H)}$–$H_{(H)}$···$Cg_{(H)}$		2.73 Å, 94°	x, y, z
$C_{(H)}$–$H_{(H)}$···$Cg_{(H)}$		2.75 Å, 113°	x, y, z
$C_{(H)}$–$H_{(H)}$···$Cg_{(H)}$		2.77 Å, 95°	x, y, z
$C_{(H)}$–$H_{(H)}$···$Cg_{(H)}$		2.85 Å, 150°	1+x, y, z
$C_{(H)}$–$H_{(H)}$···$Cg_{(H)}$		2.71 Å, 105°	x, y, z
$C_{(H)}$–$H_{(H)}$···$Cg_{(H)}$		2.95 Å, 107°	x, y, z
$C_{(H)}$–$H_{(H)}$···$Cg_{(H)}$		2.74 Å, 107°	x, y, z
H-bonding	Non-classical & classical	Non-classical & classical	
$N_{(H)}$–$H_{(H)}$···$N_{(G2)}$–$C_{(G2)}$	2.38 Å, 167° (<)		–x, 1–y, –z
$N_{(H)}$–$H_{(H)}$···$N_{(G1)}$–$C_{(G1)}$	2.36 Å, 173° (<)		x, y, z
$C_{(H)}$–$H_{(H)}$···$O_{(H)}$	3.424(2) Å, 155°		–x, –y, –z
$C_{(H)}$–$H_{(H)}$···$N_{(H)}$	2.790(2) Å, 103°		x, y, z
$C_{(H)}$–$H_{(H)}$···$N_{(H)}$	2.784(2) Å, 101°		x, y, z
$N_{(H)}$–$H_{(H)}$···$N_{(G)}$–$C_{(G)}$		2.53 Å, 175.5(13)° (<<)	x, y, z
$C_{(H)}$–$H_{(H)}$···$O_{(H)}$		3.427(2) Å, 163°	1–x, 2–y, 2–z
$C_{(H)}$–$H_{(H)}$···$N_{(H)}$		2.771(1) Å, 103°	x, y, z
Short contacts (H···G and G···G)			
$C_{(H)}$–$C_{(H)}$···$C_{(H)}$–$C_{(H)}$	2.89 Å, 142° (<)		1–x, 1–y, 1–z
$C_{(H)}$–$C_{(H)}$···$O_{(H)}$–$C_{(H)}$	2.54 Å, 155° (<)		–x, –y, –z
$C_{(H)}$–$H_{(H)}$···$C_{(G2)}$–$C_{(G2)}$	2.87 Å, 139° (<)		1+x, –1+y, z
$C_{(H)}$–$H_{(H)}$···$O_{(H)}$–$C_{(H)}$		2.51 Å, 163° (<<)	1–x, 2–y, 2–z
$C_{(H)}$–$H_{(H)}$···$H_{(H)}$–$C_{(H)}$		2.32 Å, 132° (<)	x, 1+y, z

[a]Distances denoted by < are contacts that measure less than the sum of the van der Waals radii of the atoms involved while those denoted by << is this sum minus 0.2 Å.

Table S104. π···π interactions for **H_2**·3MP.[a]

π-systems involved:	Distances:
H···H and H···G	3.868(1)–5.995(1) Å
$Cg_{(G1)}$	4.455(4)–5.908(2) Å [8]
$Cg_{(G2)}$	4.741(2)–5.887(2) Å [8]
$Cg_{(G2)}$	4.063(2)–5.785(2) Å [7]
$Ch_{(G4)}$	4.904(2)–5.887(2) Å [10]
$Cg_{(G5)}$	4.779(2)–5.908(2) Å [9]
$Cg_{(G6)}$	4.389(4)–5.949(4) Å [9]
$Cg_{(G7)}$	5.073(4)–5.874(4) Å [8]
$Cg_{(G8)}$	4.346(4)–5.647(4) Å [6]

[a]Number of interactions are provided in square parentheses.

Table S105. X–H···π interactions for **H_2**·3MP.

Non-covalent interaction	Between	Distance (Å)	Angle(°)	Symmetry
C_{12}–H_{12A}···Cg (9)	H3···H3	2.79	94	x, y, z
C_{13}–H_{13B}···Cg (10)	H3···H3	2.91	92	x, y, z
C_{22}–H_{22A}···Cg (17)	H4···H4	2.57	76	x, y, z
C_{22}–H_{22B}···Cg (17)	H4···H4	2.88	78	x, y, z
C_{23}–H_{23A}···Cg (18)	H4···H4	2.98	80	x, y,z
C_{23}–H_{23B}···Cg (18)	H4···H4	2.73	94	x, y, z
C_{32}–H_{32A}···Cg (1)	H1···H1	2.69	99	x, y, z
C_{42}-H_{42B}···Cg (5)	H2···H2	2.85	100	x, y, z
C_{132}–H_{132}···Cg (9)	H3···H3	2.75	104	x, y, z
C_{144}–H_{144}···Cg (3)	H3···H1	2.89	146	x, y, z
C_{154}–H_{154}···Cg (13)	H3···H3	2.94	153	1–x, 1–y, 2–z
C_{162}–H_{162}···Cg (10)	H3···H3	2.60	105	x, y, z
C_{224}–H_{224}···Cg (4)	H4···H1	2.96	151	1+x, y, z
C_{232}–H_{232}···Cg (17)	H4···H4	2.87	103	x, y, z
C_{235}–H_{235}···Cg (12)	H4···H3	2.66	156	1+x, y, 1+z
C_{244}-H_{244}···Cg (21)	H4···H4	2.80	158	2–x, 2–y, –z
C_{262}–H_{262}···Cg (18)	H4···H4	2.73	105	x, y, z
C_{265}–H_{265}···Cg (7)	H4···H2	2.67	157	x, y, z
C_{315}–H_{315}···Cg (8)	H1···H2	2.96	138	–1+x, y, z
C_{324}–H_{324}···Cg (24)	H1···H4	2.89	150	1–x, 1–y, 1–z
C_{332}–H_{332}···Cg (1)	H1···H1	2.71	105	x, y, z
C_{335}–H_{335}···Cg (14)	H1···H3	2.67	161	1–x, 1–y, 1–z
C_{424}–H_{424}···Cg (20)	H2···H4	2.97	147	–1+x, y, z
C_{432}–H_{432}···Cg (5)	H2···H2	2.56	104	x, y, z
C_{53}–H_{53}···Cg (7)	G1···H2	2.89	144	1–x, 2–y, 1–z
C_{56}–H_{56B}···Cg (25)	G1···G1	2.85	148	2–x, 2–y,1–z
C_{76A}–H_{76A}···Cg (25)	G3···G1	2.88	143	1–x, 2–y, 1–z
C_{75B}–H_{75B}···Cg (25)	G6···G1	2.71	124	1–x, 2–y, 1–z
C_{83A}–H_{83A}···Cg (23)	G4···H4	2.89	139	1–x, 1–y, 1–z
C_{145}–H_{145}···Cg (30)	H3···G6	2.89	114	x, y, z
C_{254}–H_{254}···Cg (26)	H4···G2	2.52	155	2–x, 1–y,1–z
C_{425}–H_{425}···Cg (29)	H2···G5	2.78	142	1–x, 2–y, 1–z
C_{425}–H_{425}···Cg (32)	H2···G8	2.98	150	1–x, 2–y, 1–z
C_{96B}–H_{96F}···Cg (26)	G8···G2	2.54	151	x, y, z

Table S106. Other short interactions for **H_2**·3MP.[a]

Non-covalent interaction	Between	Distance (Å)	Angle(°)	Symmetry
C_{32}–H_{32B}···H_{164}–C_{164}	H3···H1 <	2.38	128	–1+x, y, z
C_{335}–H_{335}···C_{145}–C_{144}	H1···H3 <	2.84	135	1–x, 1–y, 1–z
C_{414}–H_{414}···C_{166}–C_{161}	H2···H3 <	2.88	136	x, y, z
C_{434}–H_{434}···H_{22B}–C_{22}	H2···H4 <	2.37	144	x, y, z
C_{164}–H_{164}···C_{225}–C_{224}	H3···H4 <	2.89	137	2–x, 1–y, 1–z
N_{11}–H_{11}···O_{10} (partial)	H3···water <<	2.88	136	x, y, z
C_{244}–H_{244}···C_{235}–C_{234}	H4···H4 <	2.83	130	2–x, 2–y, –z
C_{214}–H_{214}···O_{10} (partial)	H4···water <	2.58	164	1-x, 2-y, 1-z
C_{233}–H_{233}···H_{113}–C_{113}	H4···H3 <	2.36	166	2–x, 2–y, 1–z
C_{332}–H_{332}···H_{74B}–C_{74B}	H1···G6 <	2.38	145	x, y, z
C_{313}–H_{313}···H_{94B}–C_{94B}	H1···G8 <	2.24	153	–1+x, y, z
C_{314}–H_{314}···N_5–C_{52}	H1···G1 <	2.69	150	–1+x, y, z
N_4–H_4···N_5–C_{52}	H2···G1 <<	2.52	161.7(19)	x, y, z
N_{12}–H_{12}···N_6–C_{62}	H3···G2 <<	2.36	165 (2)	x, y, z
C_{12}–H_{12B}···H_{72A}–C_{72A}	H3···G3 <	2.39	144	x, y, z
C_{254}–H_{254}···C_{63}–N_6	H4···G2 <	2.75	176	2–x, 1–y, 1–z
C_{214}–H_{214}···C_{73A}–N_{7A}	H4···G3 <	2.84	148	1–x, 2–y, 1–z
C_{56}–H_{56A}···O_{21}–C_{212}	G1···H4 <	2.70	156	x, y, z
C_{73A}–H_{73A}···H_{66B}–C_{66}	G3···G2 <	2.36	143	–1+x, y, z
C_{74A}–H_{74A}···O_3–C_{312}	G3···H1 <<	2.52	169	x, y, z
C_{83A}–H_{83A}···C_{254}–C_{253}	G4···H4 <	2.77	152	1–x, 1–y, 1-z
C_{93A}–H_{93A}···C_{212}–O_{21}	G5···H4 <	2.82	165	2–x, 2–y, 1–z
C_{96A}–H_{96A}···H_{12B}–C_{12}	G5···H3 <	2.25	159	x, y, z
C_{72B}–N_{7B}···O_{10} (partial)	G6···water <<	2.639	109.9(6)	x, y, z
C_{76B}–H_{76F}···H_{96C}–C_{96A}	G6···G5 <<	1.88	153	x, y, z
C_{84B}–H_{84B}···H_{86A}–C_{86A}	G7···G4 <<	0.37	148	x, y, z
C_{86B}–H_{86F}···H_{66B}–C_{66}	G7···G2 <<	2.17	161	–1+x, y, z

[a]Distances denoted by < are contacts that measure less than the sum of the van der Waals radii of the atoms involved while those denoted by << is this sum minus 0.2 Å.

Table S107. Hydrogen bond interactions for **H_2**·3MP.[a]

Non-covalent interaction	C/NC	inter/ intra	Between	Distance (Å) D···A	Angle(°)	Symmetry
N_{11}–H_{11}···O_{10}	C	inter	H3···water	3.097(11)	158(2)	x, y, z
N_4–H_4···N_5	C	inter	H2···G1	3.376(3)	161.7(19)	x, y, z
N_{12}–H_{12}···N_6	C	inter	H3···G2	3.224(3)	165(2)	x, y, z
C_{136}–H_{136}···N_{11}	NC	intra	H3···H3	2.757(3)	103	x, y, z
C_{166}–H_{166}···N_{12}	NC	intra	H3···H3	2.781(3)	102	x, y, z
C_{214}–H_{214}···O_{10}	NC	inter	H4···water	3.509(11)	164	1–x, 2–y, 1–z
C_{236}–H_{236}···N_{21}	NC	intra	H4···H4	2.776(3)	103	x, y, z
C_{266}–H_{266}···N_{22}	NC	intra	H4···H4	2.786(3)	103	x, y, z
C_{336}–H_{336}···N_3	NC	intra	H1···H1	2.765(3)	103	x, y, z
C_{436}–H_{436}···N_4	NC	intra	H2···H2	2.792(3)	101	x, y, z
C_{74A}–H_{74A}···O_3	NC	inter	G3···H1	3.459(4)	169	x, y, z

[a]C/NC indicating classical or non-classical hydrogen bonds; and inter/intra indicating whether bonds are inter- or intra-molecular.

a) b) c)

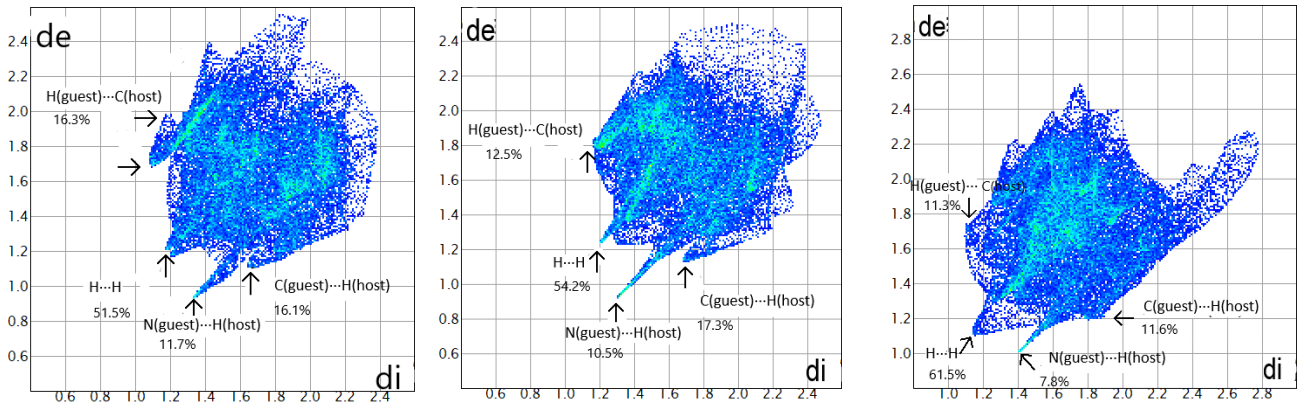

Figure S108. 2D fingerprint plots for complexes a) **H₂**·PYR [guest 1] b) **H₂**·PYR [guest 2] and c) **H₂**·4MP.

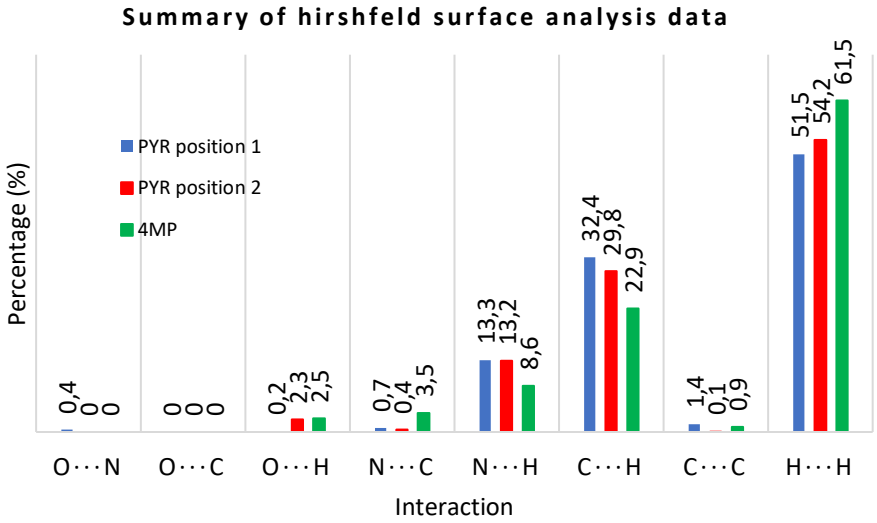

Figure S109. A graphical representation of the percentage and type of interactions in the complexes with PYR and 4MP.

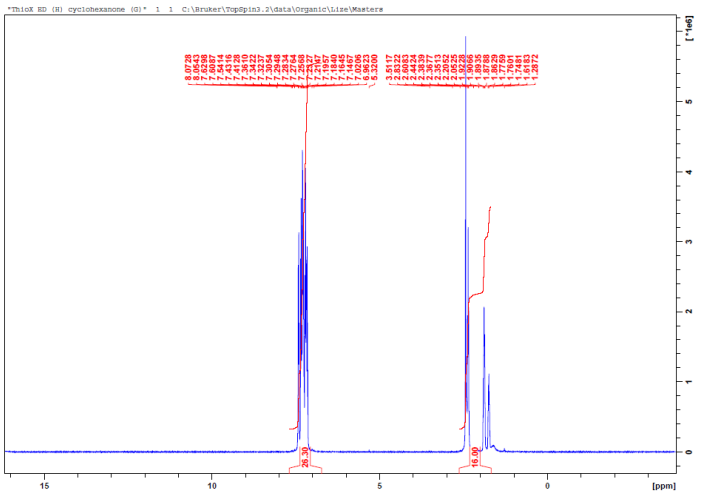

Figure S110. ^{1}H-NMR spectrum for **H₁**·CHN**.**

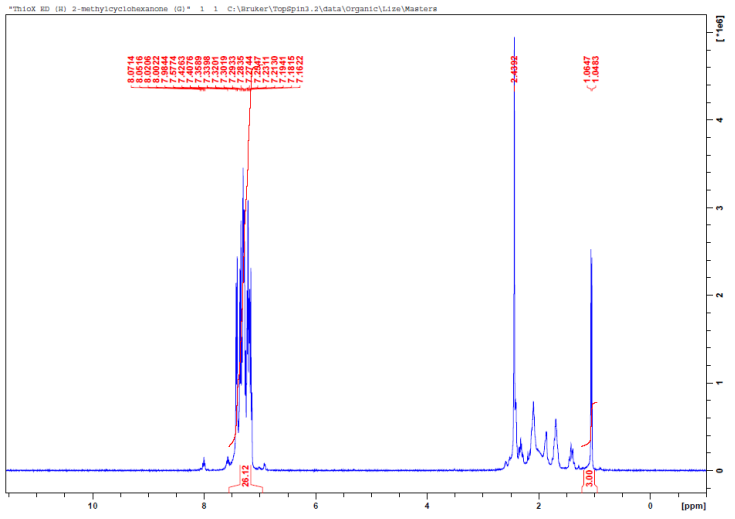

Figure S111. ^{1}H-NMR spectrum for **H$_1$**·2MCHN.

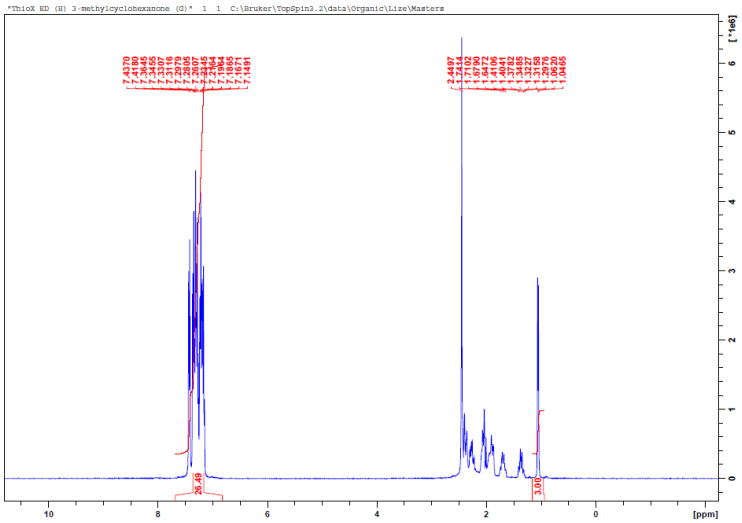

Figure S112. ^{1}H-NMR spectrum for **H$_1$**·3MCHN.

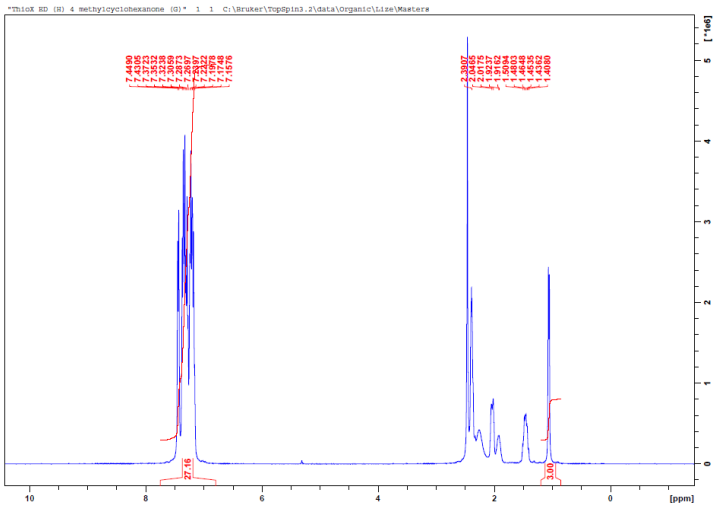

Figure S113. ^{1}H-NMR spectrum for **H$_1$**·4MCHN.

Table S114. Duplicate values for equimolar competition experiments of **H_1** with CHN, 2MCHN, 3MCHN and 4MCHN.

Guest:	Batch 1	Batch 2	Batch 3	Average	% e.s.d.s
CHN, 2MCHN	53.95:46.05	52.23:47.77	50.93:49.08	52.37:47.64	(1.24):(1.24)
CHN, 3MCHN	83.55:16.45	79.37:20.63	-	81.46:18.54	(2.09):(2.09)
CHN, 4MCHN	89.95:10.05	89.27:10.73	88.99:11.01	89.40:10.60	(0.40):(0.40)
2-, 3- MCHN	74.99:25.01	74.35:25.65	74.23:25.77	74.52: 25.48	(0.33):(0.33)
2-, 4- MCHN	84.00:16.00	84.29:15.71	81.83:18.17	83.37:16.63	(1.10):(1.10)
3-, 4- MCHN	69.59:30.41	71.62:28.38	-	70.60:29.40	(1.02):(1.02)
CHN, 2-, 3-MCHN	40.04:46.70: 13.26	38.59:47.86: 13.56	-	39.32:47.28: 13.41	(0.73):(0.58):(0.15)
CHN, 2-, 4-MCHN	41.65:49.58: 8.773	43.40:49.48: 7.12	-	42.53:49.53: 7.95	(0.88):(0.05):(0.85)
CHN, 3-, 4-MCHN	64.09:23.33: 12.59	65.76:22.56: 11.69	-	64.93:22.95: 12.14	(0.84):(0.39):(0.45)
2-, 3-, 4-MCHN	65.36:24.36: 10.28	69.76:21.93: 8.31	-	67.56:23.15: 9.30	(2.20):(1.22):(0.99)
CHN, 2-, 3-, 4-MCHN	39.40:41.96: 13.20:5.45	38.93:41.52: 13.71:5.84	-	39.17:41.74: 13.46:5.56	(0.24):(0.22):(0.26): (0.20)

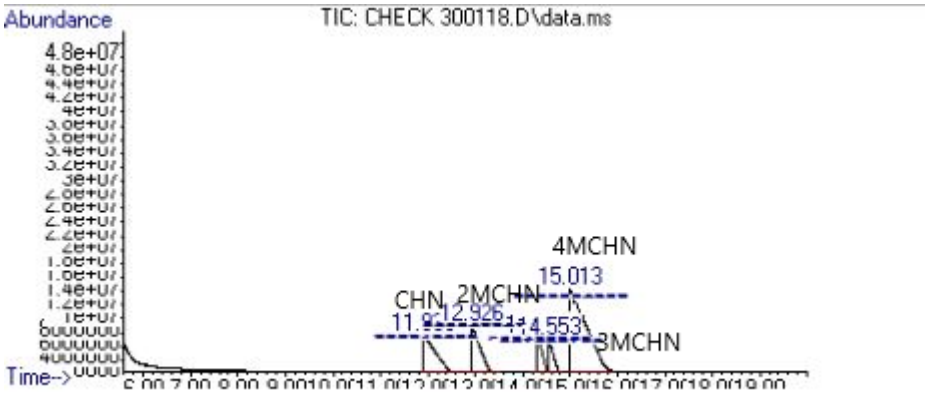

Figure S115. Chromatograph standard of pure CHN, 2MCHN, 3MCHN and 4MCHN.

Table S116. K values for competition experiment of CHN/2MCHN.[a,b]

CHN ml	CHN c	2MCHN ml	2MCHN c	K value
1	1	0	0	#DIV/0!
0,76	0,82	0,24	0,18	1,43859649
0,54	0,63	0,46	0,37	1,45045045
0,43	0,51	0,57	0,49	1,37968676
0,35	0,42	0,65	0,58	1,34482759
0,18	0,25	0,82	0,75	1,51851852
0	0	1	1	1,42641596

[a]Abbreviations in the table include ml (mother liquor) and c (crystal).
[b]The average K value is highlighted in yellow.

Table S117. K values for competition experiment of CHN/3MCHN.[a,b]

CHN ml	CHN c	3MCHN ml	3MCHN c	K value
1	1	0	0	#DIV/0!
0,76	0,93	0,24	0,07	4,19548872
0,54	0,88	0,46	0,12	6,24691358
0,45	0,81	0,55	0,19	5,21052632
0,35	0,73	0,65	0,27	5,02116402
0,17	0,47	0,83	0,53	4,32963374
0	0	1	1	5,00074528

[a]Abbreviations in the table include ml (mother liquor) and c (crystal).
[b]The average K value is highlighted in yellow.

Table S118. K values for competition experiment of CHN/4MCHN.[a,b]

CHN ml	CHN c	4MCHN ml	4MCHN c	K value
1	1	0	0	#DIV/0!
0,77	0,95	0,23	0,05	5,67532468
0,57	0,92	0,43	0,08	8,6754386
0,46	0,9	0,54	0,1	10,5652174
0,36	0,84	0,64	0,16	9,33333333
0,18	0,66	0,82	0,34	8,84313725
0	0	1	1	8,61849025

[a]Abbreviations in the table include ml (mother liquor) and c (crystal).
[b]The average K value is highlighted in yellow.

Table S119. K values for competition experiment of 2MCHN/3MCHN.[a,b]

2MCHN ml	2MCHN c	3MCHN ml	3MCHN c	K value
1	1	0	0	#DIV/0!
0,8	0,91	0,2	0,09	2,52777778
0,59	0,8	0,41	0,2	2,77966102
0,5	0,74	0,5	0,26	2,84615385
0,39	0,64	0,61	0,36	2,78062678
0,23	0,49	0,77	0,51	3,21653879
0	0	1	1	2,83015164

[a]Abbreviations in the table include ml (mother liquor) and c (crystal).
[b]The average K value is highlighted in yellow.

Table S120. K values for competition experiment of 2MCHN/4MCHN.[a,b]

2MCHN ml	2MCHN c	4MCHN ml	4MCHN c	K value
1	1	0	0	#DIV/0!
0,8	0,96	0,2	0,04	6
0,62	0,92	0,38	0,08	7,0483871
0,51	0,82	0,49	0,18	4,37690632
0,41	0,69	0,59	0,31	3,20298977
0	0	1	1	5,1570708

[a]Abbreviations in the table include ml (mother liquor) and c (crystal).
[b]The average K value is highlighted in yellow.

Table S121. K values for competition experiment of 3MCHN/4MCHN.[a,b]

3MCHN ml	3MCHN c	4MCHN ml	4MCHN c	K value
1	1	0	0	
0,80154	0,89545	0,19846	0,10455	2,120630925
0,63372	0,77345	0,36628	0,22655	1,973258441
0,535	0,71345	0,465	0,28655	2,164025133
0,47065	0,65229	0,52935	0,34771	2,109931685
0,26011	0,45585	0,73989	0,54415	2,382941793
0	0	1	1	2,150157595

[a]Abbreviations in the table include ml (mother liquor) and c (crystal).
[b]The average K value is highlighted in yellow.

Table S122. Summary of H···H interactions of inclusion compounds.[a]

Interactions	**H₁**·CHN	**H₁**·2MCHN	**H₁**·3MCHN	**H₁**·4MCHN
π···π	4.17–5.93 Å	4.22–5.80 Å	4.26–5.80 Å	4.41–5.53 Å
CH···π	2.69–2.99 Å, 132–148˚[2]	2.71–2.99 Å, 133–146˚[5]	2.73–2.98 Å, 134–146˚[3]	2.94 Å, 140˚[1]
Non-classical H-bonding	2.76–2.91 Å, 102–103˚[4]	2.76–2.90 Å, 102–103˚[4]	2.76–2.91 Å, 102–103˚[4]	2.75–3.40 Å, 102–154˚[5]
Other short contacts	2.88 Å, 149˚[1]	2.24–2.89 Å, 114–148˚[2]	2.79 Å, 115˚[1]	2.86–2.95 Å, 108–141˚[3]

[a]Number of H···H interactions are indicated in square parentheses.

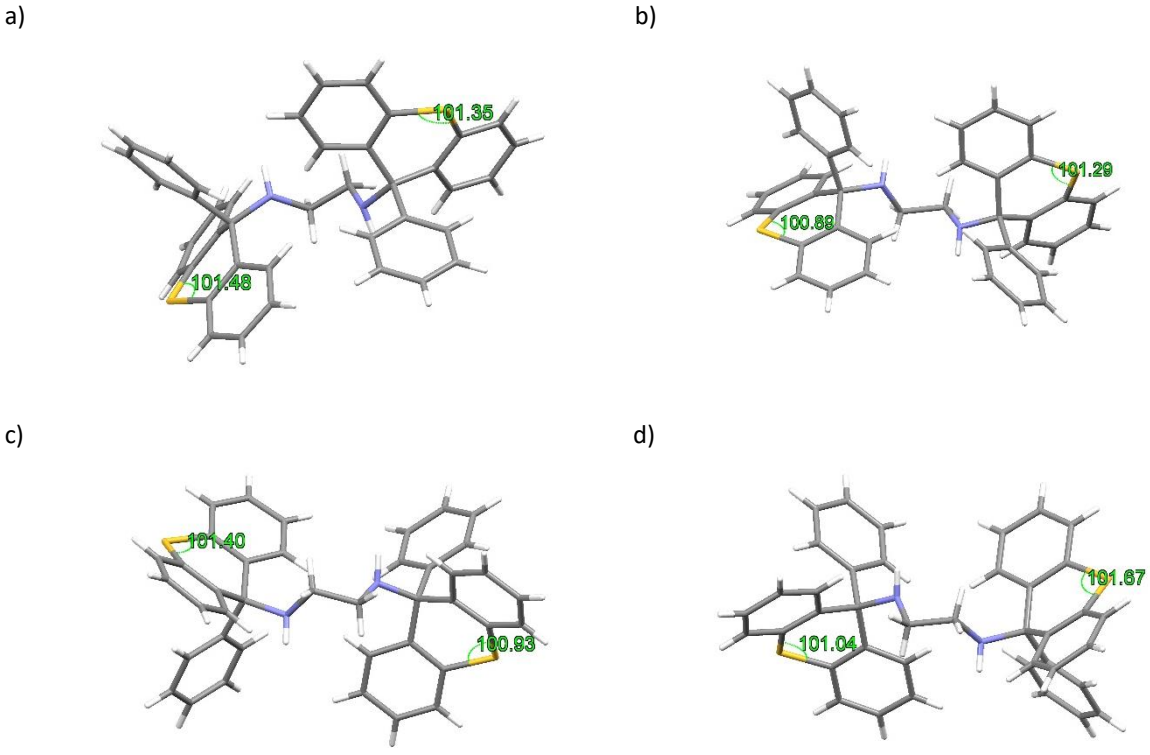

Figure S123. C–Ŝ–C angles in complexes a) **H₁**·CHN b) **H₁**·2MCHN, c) **H₁**·3MCHN and d) **H₁**·4MCHN, after guest removal.

a)

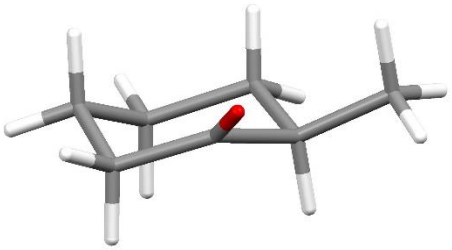

b)

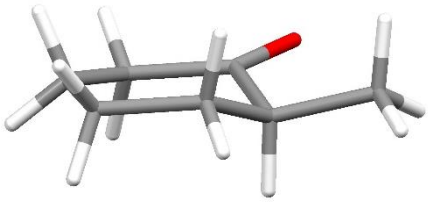

c)

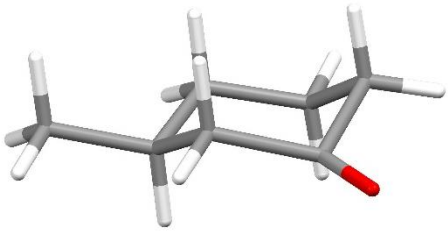

d)

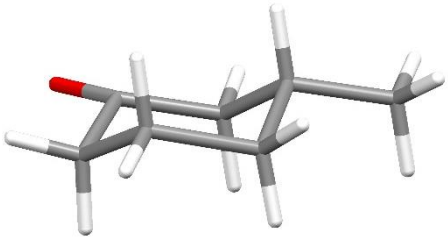

e)

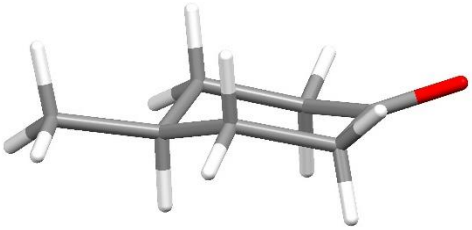

f)

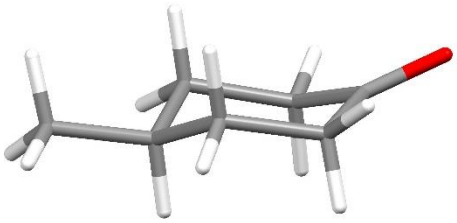

Figure S124. Guest geometry in complexes a) **H$_1$**·2MCHN [major component], b) **H$_1$**·2MCHN [minor component], c) **H$_1$**·3MCHN [major component], d) **H$_1$**·3MCHN [minor component], e) **H$_1$**·4MCHN [major component] and f) **H$_1$**·4MCHN [minor component].

a)

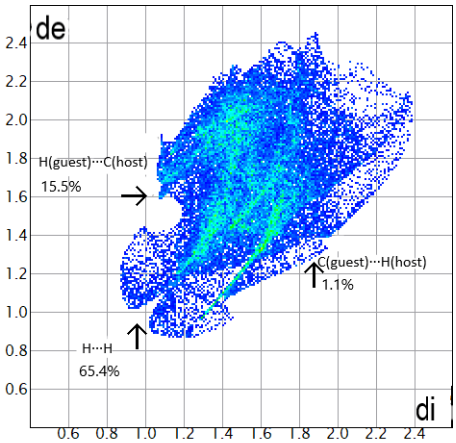

b)

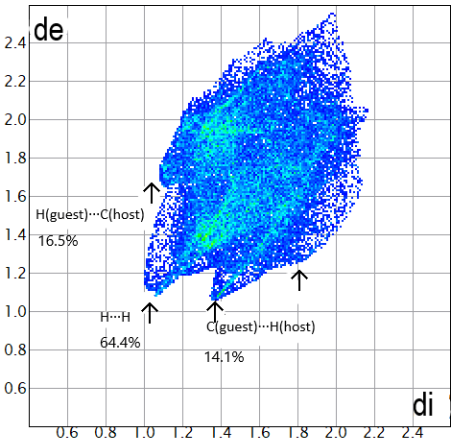

c)

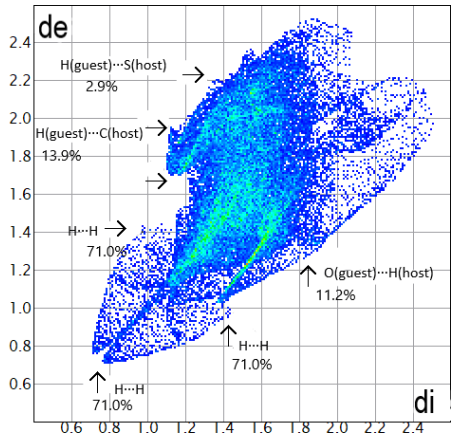

d)

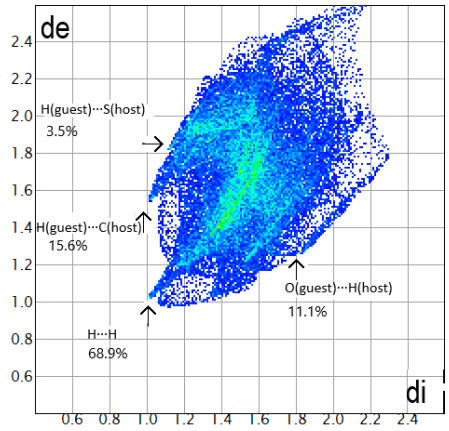

e)

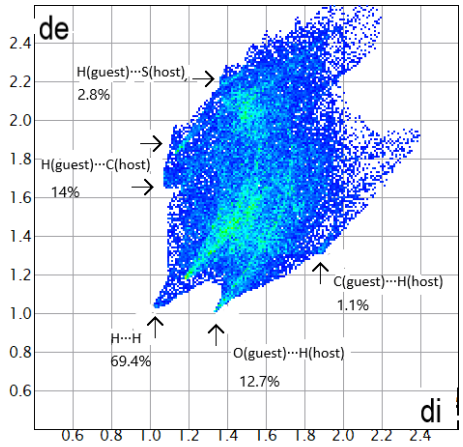

f)

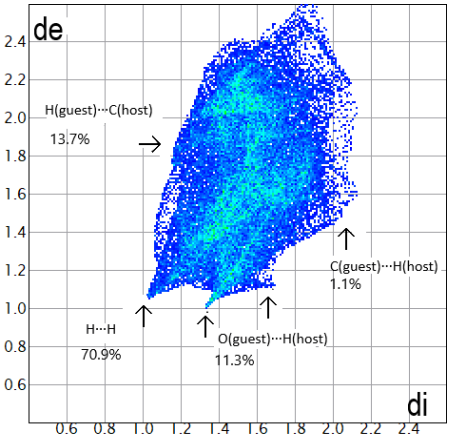

g)

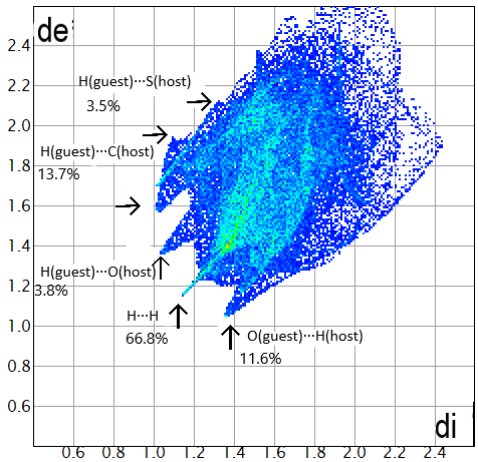

h)

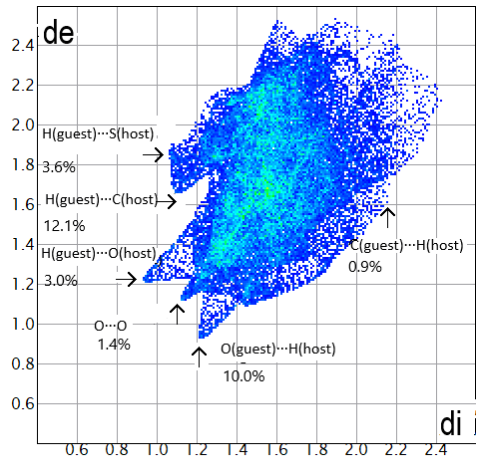

Figure S125. 2D fingerprint plots for complexes a) **H$_1$**·CHN [major component] b) **H$_1$**·CHN [minor component], c) **H$_1$**·2MCHN [major component], d) **H$_1$**·2MCHN [minor component], e) **H$_1$**·3MCHN [major component], f) **H$_1$**·3MCHN [minor component], g) **H$_1$**·4MCHN [major component] and h) **H$_1$**·4MCHN [minor component].

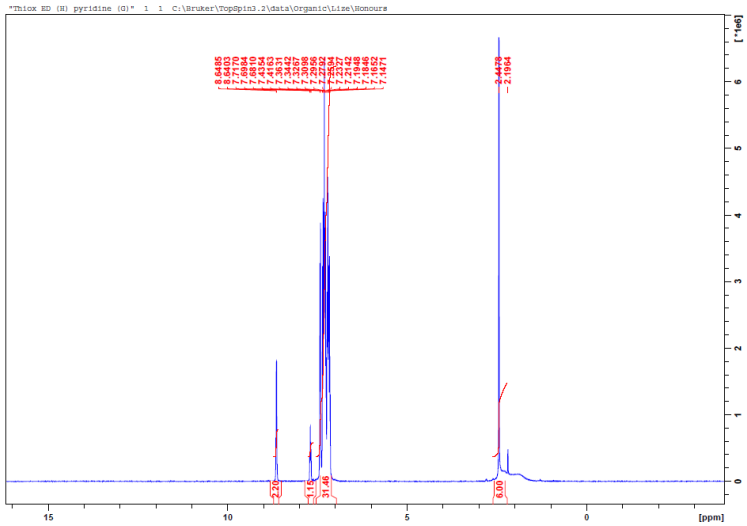

Figure S126. ^{1}H-NMR spectrum for **H$_1$**·PYR.

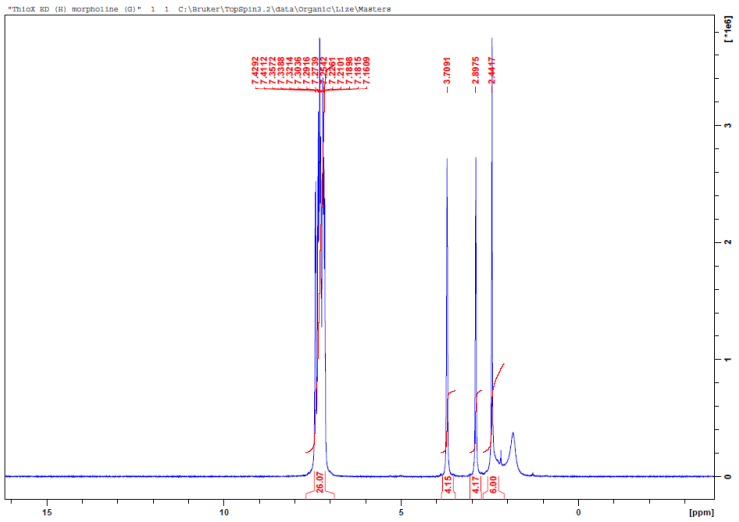

Figure S127. ^{1}H-NMR spectrum for **H$_1$**·MORPH**.**

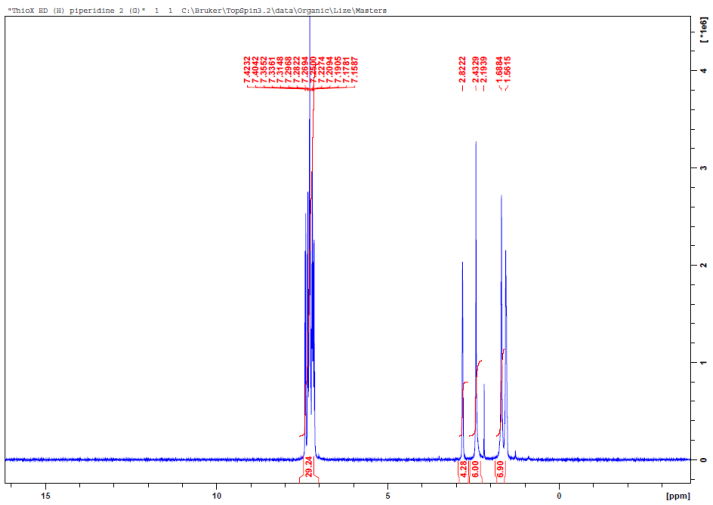

Figure S128. ^{1}H-NMR spectrum for **H$_1$**·PIP**.**

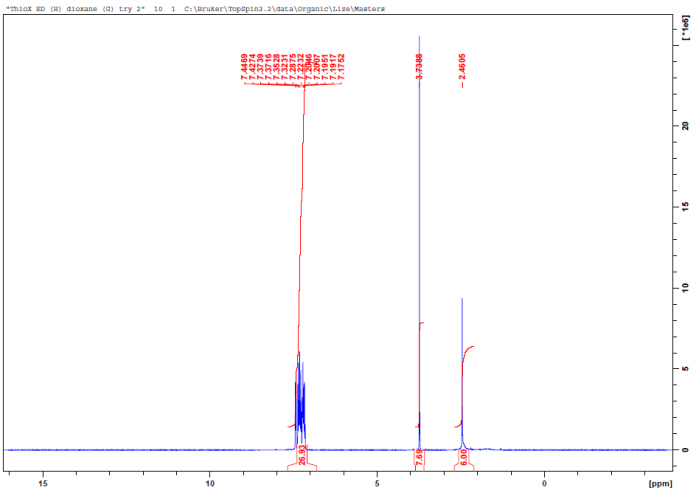

Figure S129. ^{1}H-NMR spectrum for **H_1**·DIOX**.**

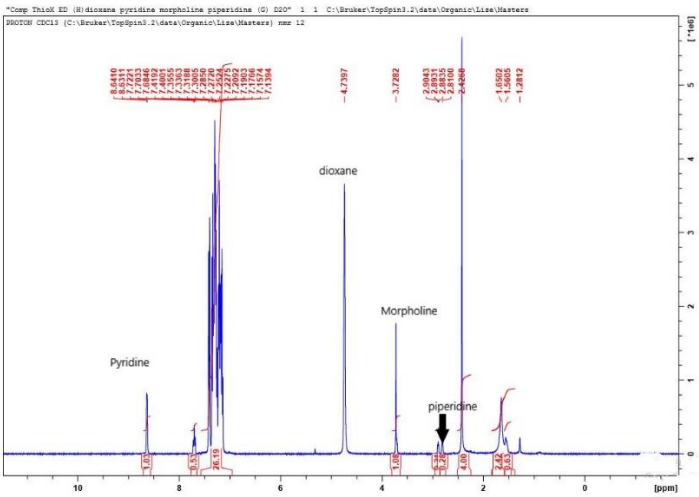

Figure 130. ^{1}H-NMR spectra of a mixed complex of the host and the four heterocyclic guests.

Table S131. Duplicate values for equimolar competition experiments of **H_1** with PYR, MORPH, PIP and DIOX.

Guests:	Batch 1	Batch 2	Average	% e.s.d.s
DIOX, PYR	18.92:81.08	17.48:82.52	18.20:81.80	(0.72):(0.72)
PYR, PIP	80.93:19.07	81.86:18.14	81.40: 18.61	(0.47):(0.47)
PYR, MORPH	76.70:23.30	74.51:25.49	75.61:23.89	(1.10):(1.10)
PIP, DIOX	54.72:45.28	52.93:47.07	53.83:46.18	(0.90):(0.90)
MORPH, DIOX	50.53:49.47	49.22:50.78	49.88:50.11	(0.66):(0.66)
MORPH, PIP	50.66:49.34	53.24:46.76	51.95:48.05	(1.29):(1.29)
PYR, PIP, MORPH	65.56:16.67:17.78	65.98:15.46:18.56	65.77:16.07:18.17	(0.21):(0.61):(0.39)
PYR, PIP, DIOX	69.70:16.16:14.14	69.05:17.31:13.64	69.38:16.74:13.89	(0.33):(0.58):(0.25)
PYR, MORPH, DIOX	60.95:17.14:21.90	61.73:16.69:21.58	61.34:16.92:21.75	(0.39):(0.23):(0.16)
DIOX, PIP, MORPH	33.00:34.62:32.38	31.94:33.88:34.18	32.47:34.25:33.28	(0.53):(0.37):(0.91)
PYR, DIOX, MORPH, PIP	57.12:12.37:15.89: 14.40	56.97:12.11:16.34: 14.58	57.04:12.24:16.12: 14.49	(0.08):(0.13):(0.23): (0.09)

Table S132. K values for competition experiment of PYR/PIP.[a,b]

PYR ml	PYR c	PIP ml	PIP c	K value
1	1	0	0	
0,79	0,93	0,21	0,07	3,53164557
0,58	0,86	0,42	0,14	4,44827586
0,49	0,82	0,51	0,18	4,7414966
0,38	0,78	0,62	0,22	5,784689
0,19	0,58	0,81	0,42	5,88721805
0	0	1	1	4,87866501

[a]Abbreviations in the table include ml (mother liquor) and c (crystal).
[b]The average K value is highlighted in yellow.

Table S133. K values for competition experiment of PYR/DIOX.[a,b]

PYR ml	PYR c	DIOX ml	DIOX c	K value
1	1	0	0	
0,79	0,95	0,21	0,05	5,05063291
0,58	0,88	0,42	0,12	5,31034483
0,48	0,84	0,52	0,16	5,6875
0,37	0,76	0,63	0,24	5,39189189
0,2	0,6	0,8	0,4	6
0	0	1	1	5,48807393

[a]Abbreviations in the table include ml (mother liquor) and c (crystal).
[b]The average K value is highlighted in yellow.

Table S134. K values for competition experiment of PYR/MORPH.[a,b]

PYR ml	PYR c	MORPH ml	MORPH c	K value
1	1	0	0	
0,79	0,92	0,21	0,08	3,05696203
0,58	0,82	0,42	0,18	3,29885057
0,48	0,74	0,52	0,26	3,08333333
0,38	0,68	0,62	0,32	3,46710526
0,19	0,53	0,81	0,47	4,80739082
0	0	1	1	3,5427284

[a]Abbreviations in the table include ml (mother liquor) and c (crystal).
[b]The average K value is highlighted in yellow.

Table S135. K values for competition experiment of MORPH/DIOX.[a,b]

MORPH ml	MORPH c	DIOX ml	DIOX c	K value
1	1	0	0	
0,8	0,8	0,2	0,2	1
0,61	0,6	0,39	0,4	1,042735043
0,52	0,5	0,48	0,5	1,083333333
0,4	0,4	0,6	0,6	1
0,2	0,2	0,8	0,8	1
0	0	1	1	1,025213675

[a]Abbreviations in the table include ml (mother liquor) and c (crystal).
[b]The average K value is highlighted in yellow.

Table S136. K values for competition experiment of PIP/MORPH.[a,b]

PIP ml	PIP c	MORPH ml	MORPH c	K value
1	1	0	0	
0,77	0,88	0,23	0,12	2,19047619
0,6	0,65	0,4	0,35	1,23809524
0,49	0,5	0,51	0,5	1,04081633
0,39	0,4	0,61	0,6	1,04273504
0,2	0,2	0,8	0,8	1
0	0	1	1	1,30242456

[a]Abbreviations in the table include ml (mother liquor) and c (crystal).
[b]The average K value is highlighted in yellow.

Table S137. K values for competition experiment of PIP/DIOX.[a,b]

PIP ml	PIP c	DIOX ml	DIOX c	K-value
1	1	0	0	
0,79	0,91	0,21	0,09	2,687763713
0,6	0,73	0,4	0,27	1,802469136
0,5	0,49	0,5	0,51	1,040816327
0,4	0,39	0,6	0,61	1,042735043
0,2	0,21	0,8	0,79	1,063291139
0	0	1	1	1,527415071

[a]Abbreviations in the table include ml (mother liquor) and c (crystal).
[b]The average K value is highlighted in yellow.

Table 138. Summary of H···H interactions of inclusion compounds.[a]

Interaction	**H$_1$**·PYR	**H$_1$**·PIP
π···π	4.30–5.98Å	4.39–5.97Å
CH···π	2.65–2.78Å, 135–151˚ [3]	2.73–2.99Å, 131–151˚ [3]
Non-classical H-bonding	2.77–3.44Å, 101–152˚ [5]	2.76–3.33Å, 102–143˚ [5]
Other short contacts	2.88Å, 153˚ [1]	2.39–2.79Å, 120–176˚ [2]

[a]Values in square brackets indicate the number of H···H interactions.

a) b)

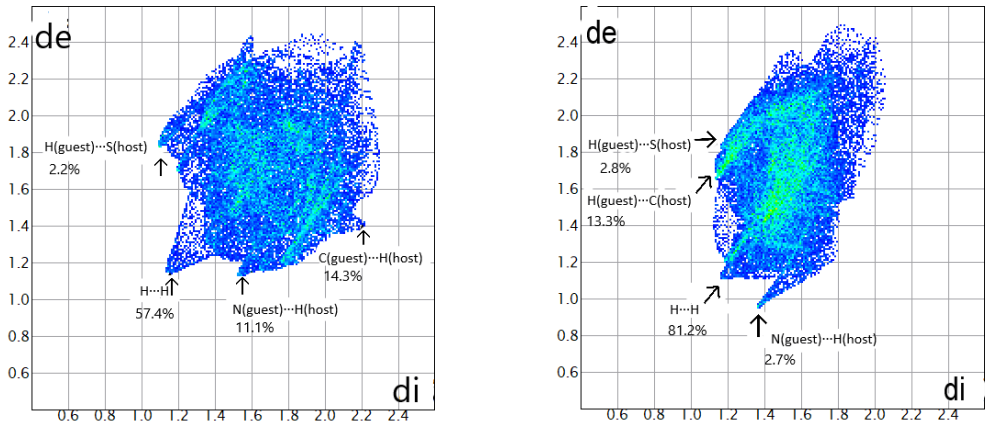

Figure 139. Hirshfeld surface analysis of a) **H₁**·PYR b) **H₁**·PIP.

a)

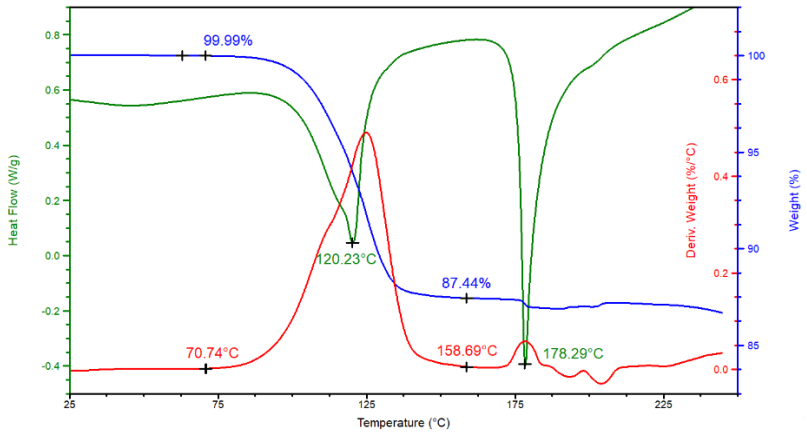

b)

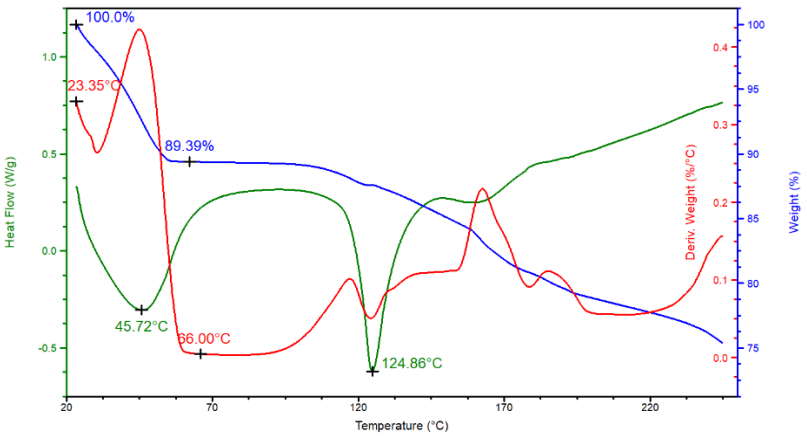

c)

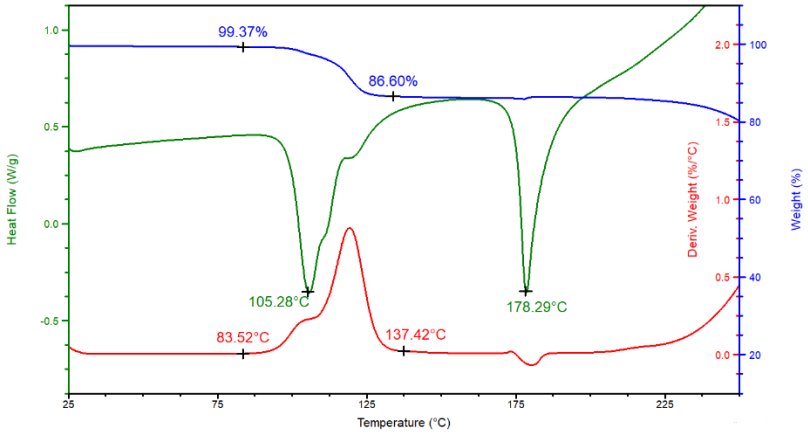

d)

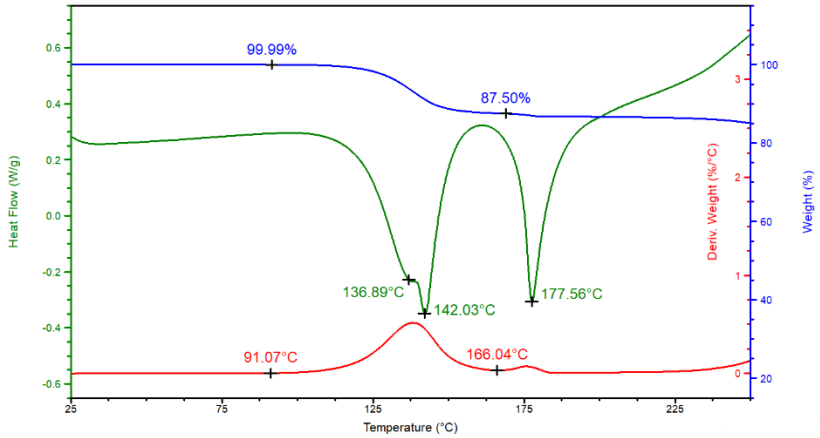

Figure 140. Overlaid TG, DTG and DSC thermograms for inclusion compounds with (a) DIOX, (b) MORPH, (c) PIP and (d) PYR.

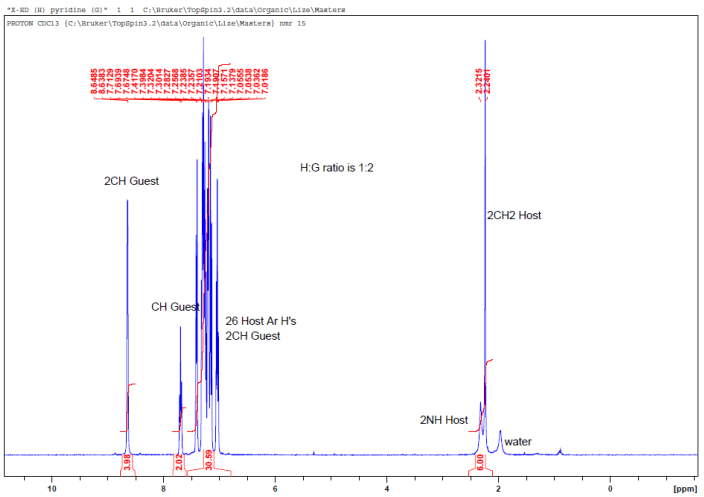

Figure S141. ^{1}H-NMR spectrum for **H₂**·PYR.

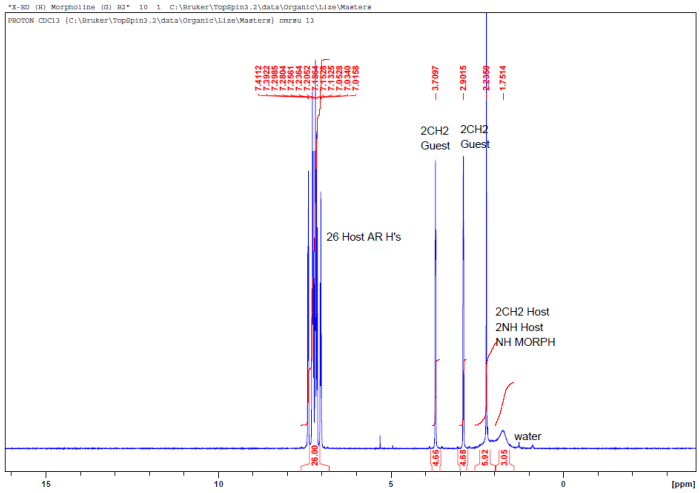

Figure S142. ^{1}H-NMR spectrum for **H₂**·MORPH.

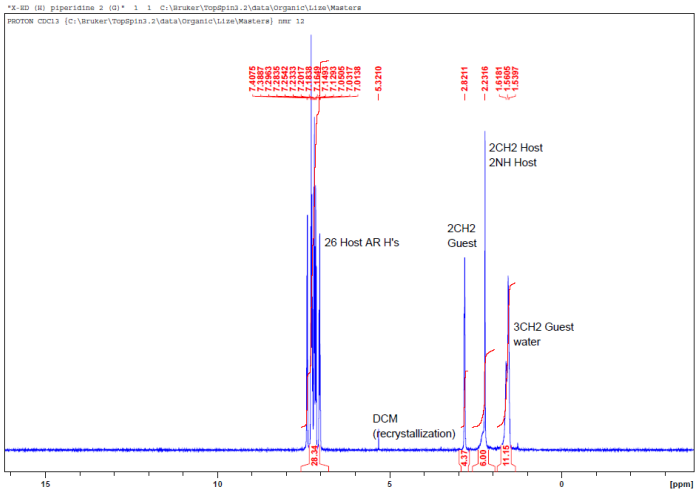

Figure S143. ^{1}H-NMR spectrum for **H₂**·PIP.

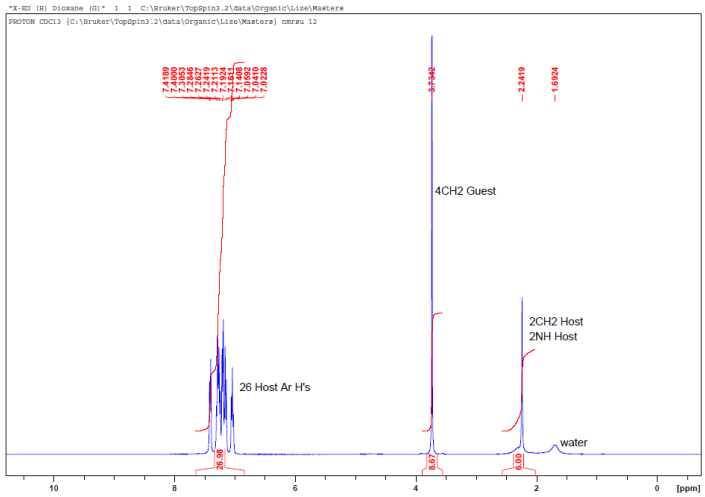

Figure S144. ^{1}H-NMR spectrum for **H₂**·DIOX.

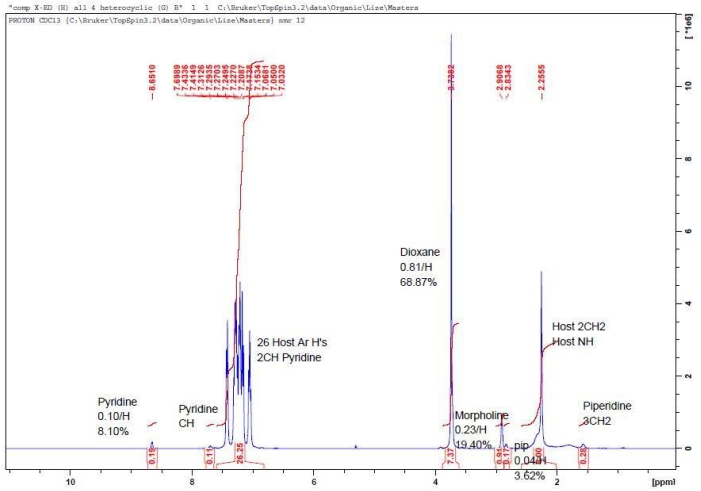

Figure 145. ^{1}H-NMR spectrum of a quaternary mixed inclusion compound with **H_2**.

Table S146. Duplicate values for equimolar competition experiments of **H_2** with PYR, MORPH, PIP and DIOX.

Guests:	Batch 1	Batch 2	Batch 3	Average	% e.s.d.s
DIOX, PYR	88.97:11.03	90.45:9.55	90.39:9.61	89.94:10.06	(0.68):(0.68)
PYR, PIP	-	-	-	5.00:95.00	-
PYR, MORPH	15.89:84.11	14.68:85.32	13.45:86.55	14.67:85.33	(1.00):(1.00)
PIP, DIOX	4.15:95.85	5.06:94.94	5.00:95.00	4.74:95.26	(0.42):(0.42)
MORPH, DIOX	30.53:69.47	30.47:69.53	28.48:71.52	29.83:70.17	(0.95):(0.95)
MORPH, PIP	95.52:4.48	95.66:4.34	91.36:8.64	94.18:5.82	(1.99):(1.99)
PYR, PIP, MORPH	7.86:7.64: 84.50	8.68:7.38:83.95	-	8.27:7.51: 84.23	(0.41):(0.13):(0.28)
PYR, PIP, DIOX	8.33:4.39: 87.28	7.61:2.91: 89.47	-	7.97:3.65: 88.34	(0.36):(0.74):(1.10)
PYR, MORPH, DIOX	11.45:21.95: 66.60	10.68:23.15: 66.17	-	11.07:22.55 :66.39	(0.39):(0.60):(0.22)
DIOX, PIP, MORPH	70.86:5.62: 23.52	73.98:4.41: 21.61	-	72.33:5.02: 22.57	(0.53):(0.37):(0.91)
PYR, DIOX, MORPH, PIP	8.10:68.87: 19.40:3.62	8.32:67.12: 20.60:3.95	-	8.21:68.00: 20.00:3.79	(0.11):(0.88):(0.60):(0.17)

[a]No crystallization occurred.

Table S147. K values for competition experiment of DIOX/MORPH.[a,b]

DIOX ml	DIOX c	MORPH ml	MORPH c	K value
79	91	21	9	2,68776371
60	81	40	19	2,84210526
52	81	48	19	3,93522267
40	65	60	35	2,78571429
18	46	82	54	3,88065844
				3,22629287

[a]Abbreviations in the table include ml (mother liquor) and c (crystal).

[b]The average K value is highlighted in yellow.

Table S148. K values for competition experiment of DIOX/PYR.[a,b]

DIOX ml	DIOX c	PYR ml	PYR c	K value
1	1	0	0	
0,81	0,97	0,19	0,03	7,58436214
0,61	0,9	0,39	0,1	5,75409836
0,5	0,89	0,5	0,11	8,09090909
0,42	0,88	0,58	0,12	10,1269841
0,2	0,86	0,8	0,14	24,5714286
0	0	1	1	11,2255565

[a]Abbreviations in the table include ml (mother liquor) and c (crystal).
[b]The average K value is highlighted in yellow.

Table S149. K values for competition experiment of DIOX/PIP.[a,b]

DIOX ml	DIOX c	PIP ml	PIP c	K value
1	1	0	0	
0,79	0,98	0,21	0,02	13,0253165
0,59	0,97	0,41	0,03	22,4689266
0,5	0,96	0,5	0,04	24
0,39	0,95	0,61	0,05	29,7179487
0,2	0,93	0,8	0,07	53,1428571
0	0	1	1	28,4710098

[a]Abbreviations in the table include ml (mother liquor) and c (crystal).
[b]The average K value is highlighted in yellow.

Table S150. K values for competition experiment of MORPH/PIP.[a,b]

MORPH ml	MORPH c	PIP ml	PIP c	K value
1	1	0	0	
0,79	0,92	0,21	0,08	3,05696203
0,58	0,91	0,42	0,09	7,32183908
0,49	0,89	0,51	0,11	8,42115028
0,4	0,78	0,6	0,22	5,31818182
0,21	0,75	0,79	0,25	11,2857143
0	0	1	1	7,0807695

[a]Abbreviations in the table include ml (mother liquor) and c (crystal).
[b]The average K value is highlighted in yellow.

Table S151. K values for competition experiment of MORPH/PYR.[a,b]

MORPH ml	MORPH c	PYR ml	PYR c	K value
1	1	0	0	
0,8	0,94	0,2	0,06	3,91666667
0,6	0,87	0,4	0,13	4,46153846
0,51	0,87	0,49	0,13	6,42986425
0,4	0,85	0,6	0,15	8,5
0,2	0,82	0,8	0,18	18,2222222
0	0	1	1	8,30605832

[a]Abbreviations in the table include ml (mother liquor) and c (crystal).
[b]The average K value is highlighted in yellow.

Table 152. Summary of H···H interactions of inclusion compounds with **H_2**.[a]

Interaction	**H_2**·2(PYR)	**H_2**·MORPH	**H_2**·PIP	**H_2**·DIOX
π···π	4.04–5.99Å	3.89–5.99Å	3.90–5.90Å	3.96-5.86Å
CH···π	2.65–2.86Å, 102–154˚ [4]	2.53–2.85Å, 85–106˚ [8]	2.55–2.82Å, 86–106˚ [4]	2.62-2.92Å, 85-114˚ [14]
Non-classical H-bonding	2.78–3.42Å, 101–155˚ [3]	2.79–3.45Å, 102–177˚ [8]	2.78–3.43Å, 101–171˚ [4]	2.78-3.52Å, 102-168˚ [5]
Other short contacts	2.36–2.89Å, 139–173˚ [3]	2.30–2.82Å, 150–177˚ [6]	2.46–2.86Å, 155–171˚ [3]	2.28-2.88Å, 129-174˚ [6]

[a]Values in square brackets indicate the number of H···G π···π interactions.

a)

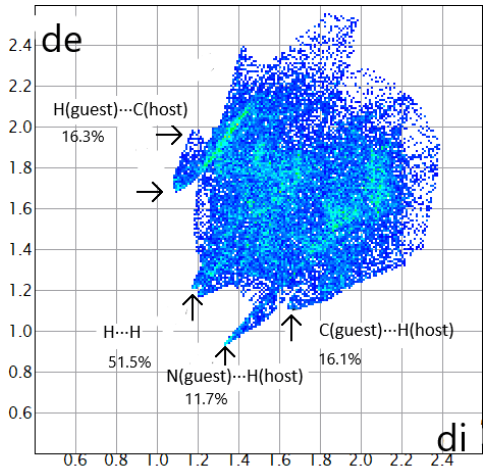

b)

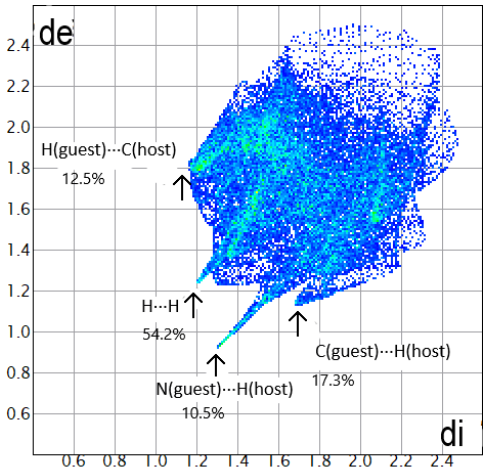

c)

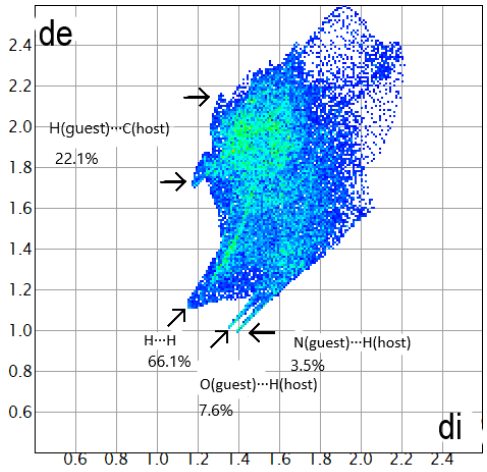

d)

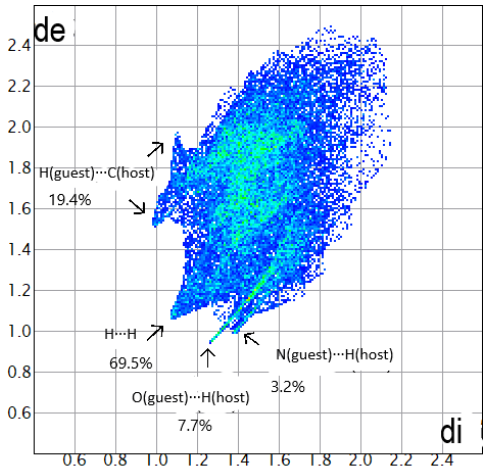

e)

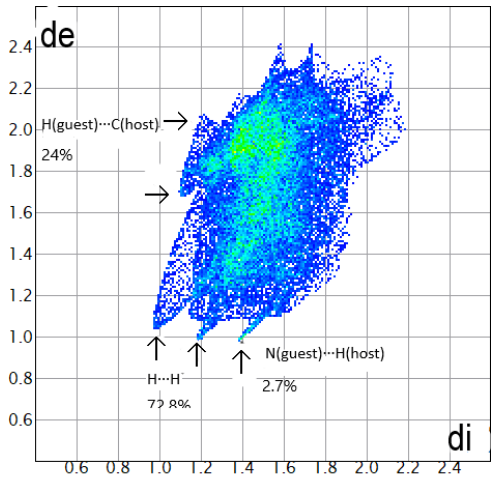

f)

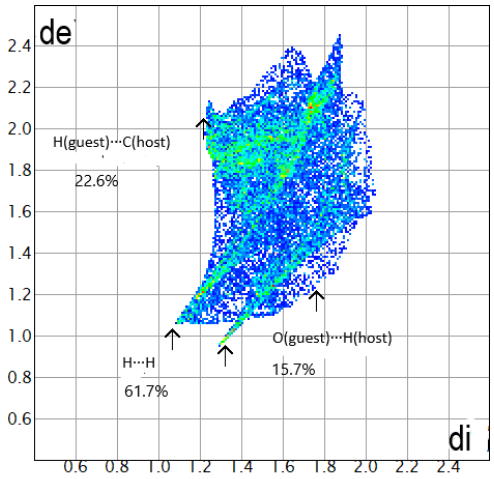

g)

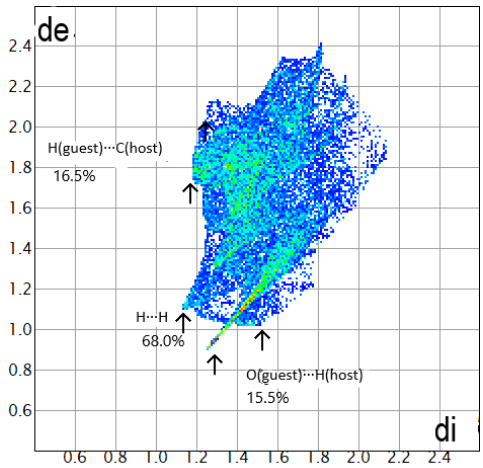

Figure 153. Includes 2D fingerprint plots for **H_2** with guests a) PYR guest 1, b) PYR guest 2, c) MORPH guest 1, d) MORPH guest 2, e) PIP, f) DIOX guest 1 and g) DIOX guest 2.

a)

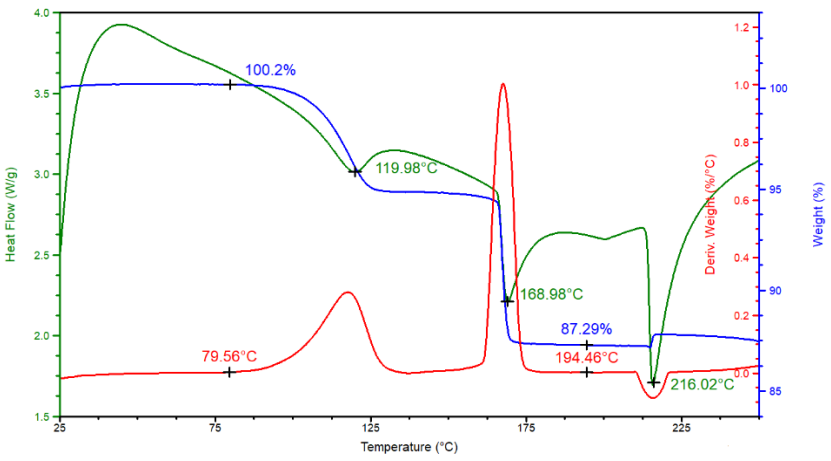

b)

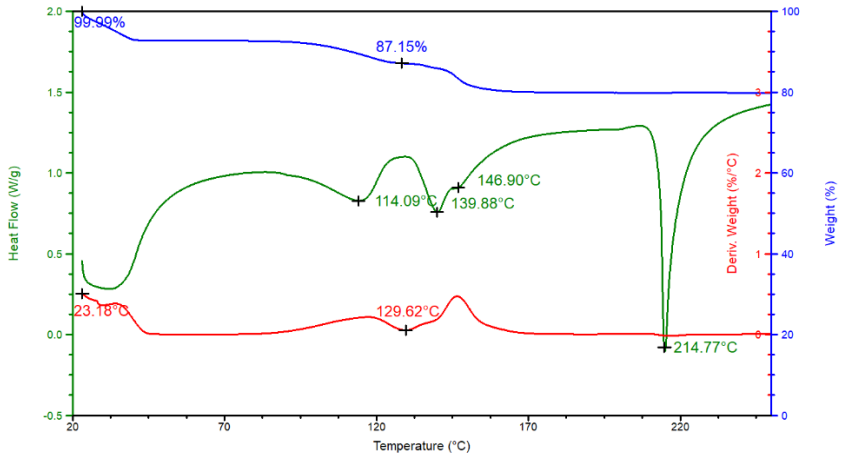

c)

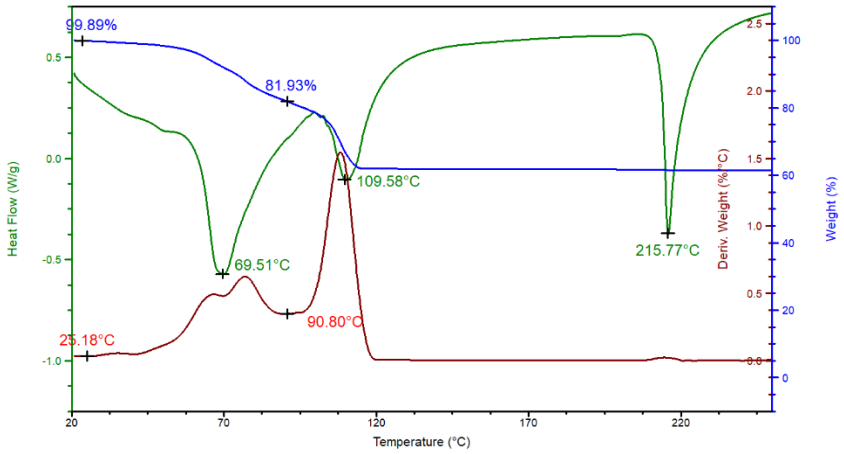

d)

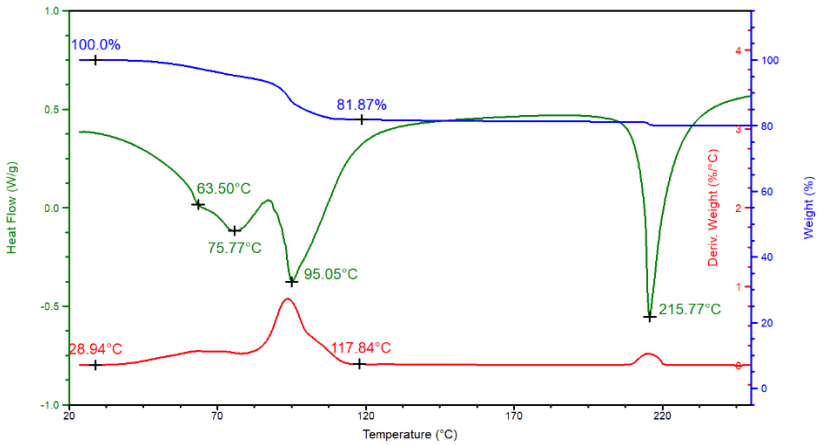

Figure 154. Includes overlaid TG, DTG and DSC thermograms for **H_2** with guests a) DIOX, b) MORPH, c) PIP and d) PYR.

Table S155. Selected structural parameters and relative energies[a] for **H₁** and **H₂** in their various crystal structures.

		E_{rel}/kJ.mol^{-1}			Torsion angles/°							Ring folding/°		Angle (O/S…C9–X)/°			
		MMFF94	B3LYP[b]	ωB97X-V[c]	*I*	*II*	*III*	*IV*	*V*	*VI*	*VII*	A	B	Ph_A	N_A	Ph_B	N_B
Apohost **2**	*anti* (*RS*)[a]	22.4	6.0	0.0	155	-173	-158	64	176	174	-159	3	19	127	125	109	143
2•(pyridine)-B	*anti* (*RS*)	13.2	0.0	10.6	156	-173	-173	180	173	173	-156	15	15	112	140	112	140
2•(dioxane)	*anti* (*RS*)	0.0	4.7	12.6	-172	-178	-171	-175	-177	-179	-173	3	0	121	130	126	125
2•(morpholine)-B	*anti* (*RS*)	0.4	4.6	13.2	175	-172	-174	180	174	172	-175	1	1	123	128	123	128
2•(piperidine)-*RR*	*syn* (*RR*)	11.7	9.0	15.4	179	-177	-167	-177	180	180	161	4	3	117	134	131	121
2•(pyridine)-A	*anti* (*RS*)	30.6	11.1	16.8	-177	79	-166	180	166	-79	177	20	20	144	106	144	106
2•(morpholine)-C	*anti* (*RS*)	7.4	11.4	18.1	-169	178	178	176	165	178	177	0	7	127	124	116	135
2•(morpholine)-A	*anti* (*RS*)	12.1	17.8	22.5	-173	-176	-162	180	162	176	173	3	3	120	130	120	130
2•(piperidine)-*RS*	*anti* (*RS*)	19.6	22.4	27.1	179	-177	-167	-177	180	180	161	4	3	117	134	131	121
3•(morpholine)	*syn* (*RR*)	36.7	0.97	0.00	121	-173	-165	79	-164	-171	118	36	37	93	161	91	164
3•(pyridine)	*syn* (*RR*)	39.8	2.90	0.32	118	-172	-162	80	-165	-173	117	37	37	91	164	93	162
3•(dioxane)	*syn* (*RR*)	35.6	0.00	0.34	121	-173	-165	79	-164	-171	119	36	37	93	161	91	163
3•(piperidine)	*syn* (*SS*)	29.0	1.31	1.21	-121	174	168	-75	159	173	-123	34	33	95	160	95	159
Apohost **3**	*anti* (*RS*)	0.0	2.16	3.31	162	-170	-156	67	170	175	-144	10	33	133	119	99	154

[a] *N*-configurations
[b] 6-31G* (geometry optimisation)
[c] 6-311+G(2df,2p) (single point)

ap/-*ap* *sc*/-*sc* *ac*/-*ac* *sp*/-*sp*

Pseudo axial
Pseudo equatorial

[a] ωB97X-V/6-311+G(2DF,2P) single point energies were calculated on ωB97X-D/6-31G* optimized geometries.

Table S156. Computed structural parameters for xanthene, thioxanthene and derivatives determined at the ωB97X-V/6-311+G(2df,2p) level.

	E_{rel}/kJ.mol^{-1}	Bond lengths/Å		Angles/°			
		C–X	C–CH_2	C–X–C	Tricyclic ring folding	X···C(9)–Ph	X···C(9)–N
Xanthene	–	1.37	1.51	119	0	127 (H)	–
9-Phenylxanthene	–	1.37	1.52	118	18	115	138 (H)
9-Aminoxanthene	0.00	1.37	1.51/1.52	119	14	137 (H)	117
	3.91	1.37	1.51	118	23	146 (H)	102
9-(*N*-Methylamino)xanthene	0.00	1.37	1.51/1.52	119	13	135 (H)	119
	3.10	1.37/1.38	1.51/1.52	118	24	146 (H)	107
9-Amino-9-phenylxanthene	0.00	1.37	1.53	119	6	132	119
	8.22	1.37	1.53	118	22	147	98
9-(*N*-Methylamino)-9-phenylxanthene	0.00	1.37	1.52/1.53	119	6	130	121
	5.26	1.37	1.53	119	26	147	103
Thioxanthene	–	1.77	1.51	99	48	82 (Ha) 171 (Hb)	–
9-Phenylthioxanthene	–	1.77	1.52	102	30	107	147 (H)
9-Aminothioxanthene	0.00	1.77	1.52/1.53	99	49	75 (H)	177
	0.03	1.77	1.51/1.52	100	41	161 (H)	92
9-(*N*-Methylamino)thioxanthene	0.00	1.77	1.51/1.52	100	42	162 (H)	91
	4.39	1.77	1.52/1.53	98	51	73 (H)	178
9-Amino-9-phenylthioxanthene	0.00	1.77	1.53/1.54	99	47	85	169
	4.95	1.76	1.54	101	40	161	89
9-(*N*-Methylamino)-9-phenylthioxanthene	0.00	1.76	1.54	101	42	162	87
	3.00	1.77	1.54	98	48	83	169
	3.00	1.76	1.54	103	13	135	115
Host **2***	–	1.36/1.37	1.52/1.53	119	4/5	130/132	122/119
Host **3***	–	1.77	1.53/1.55	104/100	1/39	128/162	123/83

Equilibrium conformer, ωB97X-D/6-31G optimized geometry

Figure S157. Selected conformations of xanthene and thioxanthene and C(9)-substituted derivatives.

Xanthene	Thioxanthene
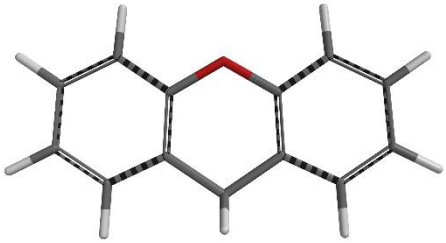	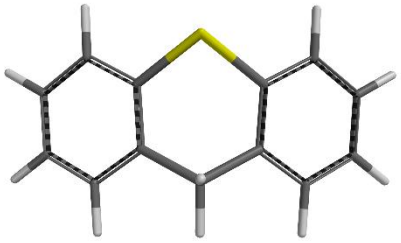
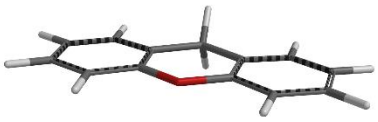	
9-Phenylxanthene	9-Phenylthioxanthene
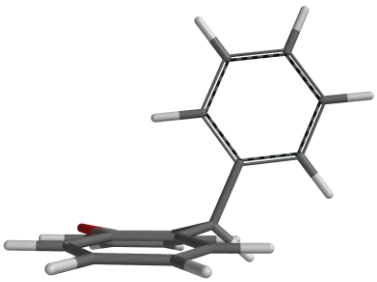	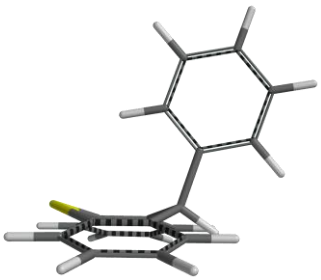
9-Aminoxanthene	9-Aminothioxanthene
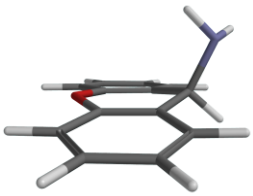	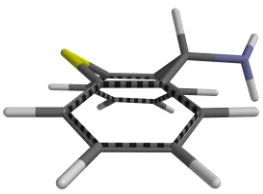
9-Amino-9-phenylxanthene	9-Amino-9-phenylthioxanthene
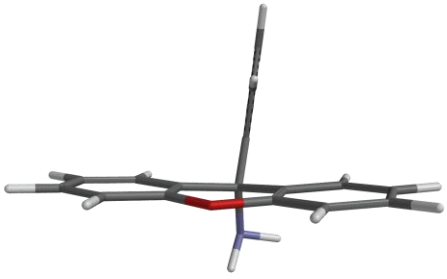	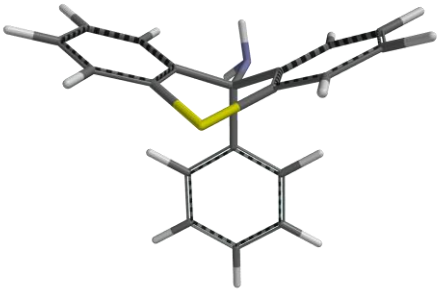
Conformer 1, E_{rel} = 0.00 kJ·mol^{-1}	Conformer 1, E_{rel} = 0.00 kJ·mol^{-1}

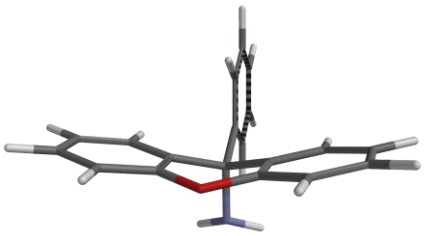	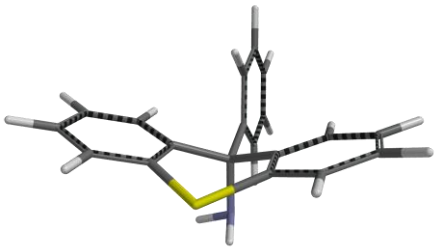
Conformer 2, E_{rel} = 8.22 kJ·mol^{-1}	Conformer 3, E_{rel} = 4.95 kJ·mol^{-1}
9-Methylamino-9-phenylxanthene	9-Methylamino-9-phenylthioxanthene
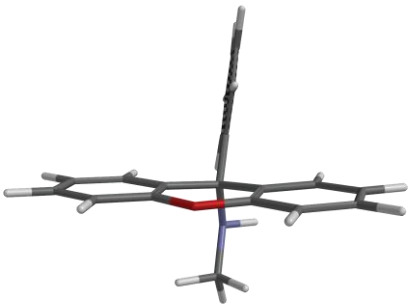	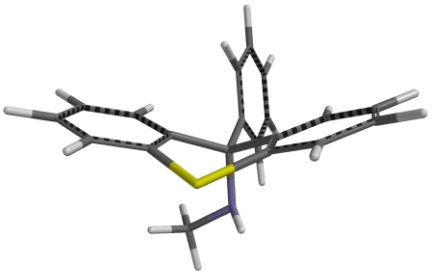
Conformer 1, E_{rel} = 0.00 kJ·mol^{-1}	Conformer 1, E_{rel} = 0.00 kJ·mol^{-1}
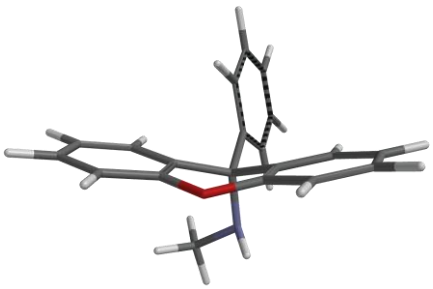	
Conformer 2, E_{rel} = 5.26 kJ·mol^{-1}	Conformer 2, E_{rel} = 2.90 kJ·mol^{-1}

Table S158. MMFF94 structural parameters for host compound **H_2** conformers.

		E_{rel}/kJ.mol^{-1}	Torsion angles/°							Ring folding/°		Angle (O···C9–X)/°			
			I	*II*	*III*	*IV*	*V*	*VI*	*VII*	A	B	Ph_A	N_A	Ph_B	N_B
2-I	*anti*	0.00	173	174	147	-50	-161	-174	-167	2	0	126	124	124	126
Apohost **2**-all_M	*anti*	0.00	167	174	162	50	-147	-174	-173	0	2	124	126	126	124
2-II	*syn*	6.53	-171	-180	178	41	178	-180	-171	0	0	124	126	124	126
2-III	*syn*	7.34	172	180	120	36	169	177	172	1	3	123	127	126	124
2-IV	*syn*	7.75	172	177	163	-40	-152	-178	171	1	2	125	126	122	128
2-V	*anti*	9.11	171	178	180	180	-180	-178	171	1	1	125	125	125	125
2-(piperidine)-*RS*-all_M	*anti*	9.11	171	178	180	180	-180	-178	-171	1	1	125	125	125	125
2-(morpholine)-C-all_M	*anti*	9.11	171	178	180	-180	-180	-178	-171	1	1	125	125	125	125
2-(dioxane)-all_M	*anti*	9.11	171	178	180	180	180	-178	-171	1	1	125	125	125	125
2-(morpholine)-B-all_M	*anti*	9.11	171	178	180	180	-180	-178	171	1	1	125	125	125	125
2-(morpholine)-A-all_M	*anti*	9.11	171	178	180	180	-180	-178	-171	1	1	125	125	125	125
2-(pyridine)-B-all_M	*anti*	9.11	171	178	-180	180	180	-178	-171	1	1	125	126	125	126
2-VI	*syn*	10.23	173	173	153	-73	153	173	173	3	3	127	123	127	123
2-VII	*anti*	11.48	171	177	176	-178	176	177	171	1	1	125	125	125	125
2-(piperidine)-*RR*-all_M	*syn*	11.48	171	177	176	-178	176	177	171	1	1	125	125	125	125
2-VIII	*syn*	12.71	172	164	64	171	168	175	172	0	1	123	128	125	125
2-IX	*anti*	13.59	-175	74	-174	47	-147	-176	-174	15	0	138	108	124	126
2-X	*anti*	15.86	175	162	83	40	149	176	-170	8	1	129	122	124	127
2-XI	*anti*	16.04	171	175	169	173	61	169	-165	0	4	125	125	120	131
2-XII	*syn*	16.22	166	-169	-61	-170	-167	-179	170	3	1	120	130	124	126
2-XIII	*anti*	16.39	170	-180	-170	-169	-65	-165	-172	0	0	124	126	123	128
2-XIV	*syn*	20.70	-172	71	-156	-36	157	176	173	15	0	138	108	124	126
2-XV	*anti*	22.57	168	175	169	41	-130	-65	179	1	17	125	125	140	106
2-XVI	*anti*	23.50	171	170	81	161	83	174	169	1	1	124	127	124	127
2-XVII	*anti*	24.59	177	-75	170	53	148	-174	-175	18	2	140	106	125	124
2-XVIII	*anti*	25.06	-177	76	97	17	159	177	-173	17	0	138	109	125	126
2-XIX	*anti*	25.88	175	163	81	44	162	-73	173	7	12	129	122	135	111
2-XX	*anti*	26.90	173	74	168	179	178	177	171	15	1	138	109	125	125
2-XXI	*syn*	27.38	-171	-178	178	178	168	-74	174	1	16	125	125	138	109
2-XXII	*syn*	28.19	-168	173	80	173	164	-72	173	1	15	124	127	138	109
2-XXIII	*anti*	28.33	173	-73	165	174	81	169	172	15	2	138	109	125	126
2-XXIV	*syn*	29.09	171	173	154	70	134	-63	171	2	16	126	124	138	107
2-XXV	*anti*	29.38	-173	66	112	68	-156	-171	-172	14	2	138	108	126	124
2-XXVI	*syn*	29.99	174	180	110	37	173	-77	180	0	17	124	126	139	107
2-XXVII	*syn*	31.03	175	-77	-172	47	124	-179	-170	17	1	139	108	124	127
2-XXVIII	*syn*	32.18	178	-73	166	-38	-163	-178	172	16	0	139	107	124	126
2-XXIX	*syn*	32.89	179	174	180	175	102	72	-176	4	19	127	124	141	106
2-XXX	*anti*	33.96	171	180	180	-173	-103	-70	175	3	18	126	124	140	106
2-XXXI	*syn*	34.67	-172	-165	-72	-167	169	-72	173	2	16	124	127	138	109
2-XXXII	*anti*	35.28	177	-74	167	-57	171	-179	-169	15	0	138	108	124	126
2-XXXIII	*syn*	35.35	180	72	108	54	-174	-176	-175	18	2	140	106	125	125
2-XXXIV	*anti*	35.40	166	169	-68	168	168	-71	173	2	15	121	130	137	109
2-XXXV	*anti*	36.62	171	179	-175	180	-168	75	-179	1	17	125	125	139	107
2-XXXVI	*anti*	37.12	172	174	172	-180	74	-85	169	4	20	128	122	142	105
2-XXXVII	*syn*	37.27	172	168	80	175	166	-74	178	2	17	124	126	139	107
2-XXXVIII	*syn*	37.94	171	180	172	178	74	84	168	3	19	127	123	141	106
2-XXXIX	*syn*	38.92	167	180	-158	59	-174	75	-174	3	14	122	128	137	110
2-XL	*anti*	40.04	-168	173	81	175	166	-74	178	1	17	124	127	139	107
2-XLI	*anti*	40.14	176	174	154	106	-87	-165	-172	2	0	125	125	122	129
2-XLII	*anti*	41.14	173	-65	-125	36	173	74	173	18	15	141	105	138	109
2-XLIII	*syn*	41.27	-170	-175	-171	178	-166	75	-178	1	17	125	125	139	107
2-XLIV	*syn*	42.17	174	-76	171	47	171	-76	174	16	16	138	109	138	109
2-XLV	*syn*	42.76	170	176	92	155	105	88	175	2	19	122	129	141	105
2-XLVI	*syn*	42.94	-170	-177	-106	117	109	-74	173	0	12	124	126	135	112
2-XLVII	*anti*	42.97	-174	74	-169	180	169	-74	174	15	15	138	109	138	109
2-(pyridine)-A-all_M	*anti*	42.97	-174	74	-169	180	169	-74	174	16	16	138	109	138	109
2-XLVIII	*anti*	43.63	177	176	99	24	96	78	176	4	19	126	124	142	104
2-XLIX	*anti*	44.96	-180	-73	-104	-179	177	-177	-172	20	3	141	105	126	124
2-(dioxane)-H_M	*anti*	44.99	-179	-178	-171	-175	-177	-179	-173	3	0	121	130	126	125
2-(morpholine)-B-H_M	*anti*	45.40	175	-172	-174	180	174	172	-175	1	1	123	128	123	128
2-L	*anti*	45.78	178	-74	167	-54	169	-73	175	15	15	138	108	137	108
2-LI	*syn*	46.53	-172	-162	-77	112	166	-76	174	3	11	124	126	134	113
2-LII	*anti*	46.54	-180	-72	-101	-168	-175	-178	170	19	2	141	105	125	125
2-LIII	*syn*	47.77	-174	75	173	-174	99	74	178	16	18	139	108	141	106
2-LIV	*syn*	48.38	-174	73	-162	-43	106	-73	176	15	16	138	108	138	107
2-LV	*anti*	48.82	172	167	66	161	-104	-70	176	1	18	124	127	140	106
2-LVI	*anti*	49.18	-166	169	67	164	-173	73	-177	2	17	121	130	139	107
2-LVII	*anti*	50.90	176	71	98	164	167	-80	175	19	16	141	105	139	109
2-LVIII	*anti*	51.86	171	179	-174	-179	-77	86	-173	3	19	127	123	140	105
2-(morpholine)-C-H_M	*anti*	52.40	-169	178	178	176	165	178	177	0	7	127	124	116	135
2-LIX	*syn*	52.66	172	-74	167	-69	167	-74	172	14	14	137	110	137	110
2-LX	*anti*	54.58	178	-75	168	-178	167	-74	173	17	15	139	107	138	109
2-LXI	*anti*	55.02	-167	-176	97	34	162	-76	178	4	16	127	124	139	108
2-LXII	*anti*	55.25	170	171	85	157	79	-84	168	4	20	121	130	140	106
2-LXIII	*anti*	55.48	-173	73	-180	-177	73	-89	172	16	22	139	108	143	104
2-LXIV	*syn*	55.60	169	-59	-135	65	-135	-59	169	13	13	136	109	136	109
2-LXV	*syn*	56.13	-175	75	-169	-178	171	-75	178	16	17	138	109	139	107
2-(piperidine)-*RR*-H_M	*syn*	56.71	179	-177	167	177	180	180	161	4	3	117	134	131	121
2-LXVI	*syn*	56.98	173	-78	172	171	77	-85	169	16	20	138	109	142	105
2-(morpholine)-A-H_M	*anti*	57.05	-173	-176	-162	180	162	176	173	3	3	120	130	120	130
2-LXVII	*syn*	57.86	-173	76	-178	-71	130	64	-172	19	20	141	106	141	104
2-(pyridine)-B-H_M	*anti*	58.17	156	-173	-173	180	173	173	156	15	15	112	140	112	140
2-LXVIII	*syn*	58.24	172	166	63	160	-106	-71	-179	1	19	123	127	141	105
2-LXIX	*syn*	60.54	-171	-171	-84	-167	77	-91	173	1	20	124	127	141	106
2-LXX	*syn*	60.61	179	74	97	163	167	-79	175	20	16	142	104	138	109
2-LXXI	*syn*	60.61	178	-75	174	-27	174	-75	178	16	16	139	107	139	107
2-LXXII	*anti*	60.83	179	-76	171	57	-175	-78	175	17	16	139	107	138	109
2-LXXIII	*anti*	63.32	-180	76	-171	180	171	-76	180	17	17	139	107	139	107
2-LXXIV	*syn*	63.99	179	-81	176	169	101	74	-177	17	20	138	108	142	105
2-LXXV	*syn*	64.55	-171	61	131	-70	174	-76	177	17	19	140	106	140	106
2-(piperidine)-*RS*-H_M	*anti*	64.59	179	-177	-167	-177	180	180	161	4	3	117	134	131	121
2-LXXVI	*anti*	65.95	-173	75	-166	64	178	-76	179	15	17	138	108	140	106
Apohost **2**-H_M	*anti*	67.40	155	-173	-158	64	176	174	-159	3	19	127	125	109	143
2-LXXVII	*syn*	69.33	-163	167	65	-95	-159	73	-175	7	12	117	135	135	111
2-LXXVIII	*anti*	70.52	178	-79	174	172	77	-86	170	17	21	139	107	142	104
2-LXXIX	*syn*	74.29	174	-68	106	180	77	-86	170	18	19	140	107	141	106
2-(pyridine)-A-H_M	*anti*	75.56	-177	79	-168	180	166	-79	177	20	20	144	106	144	106
2-LXXX	*syn*	81.06	179	-79	171	171	78	-88	174	17	20	139	107	142	104
2-LXXXI	*syn*	98.81	-173	88	-81	-179	77	-88	172	18	20	140	106	142	105

ap/ *ap*	*sc*/ *sc*	Pseudo axial	
ac/-*ac*	*sp*/-*sp*	Pseudo equatorial	

Figure S159. Host **H₂** in crystal structures and after DFT geometry optimization.

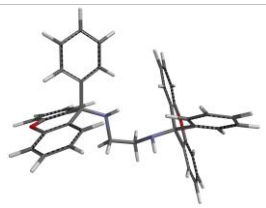	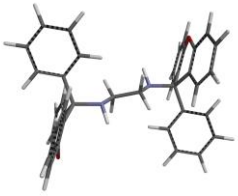	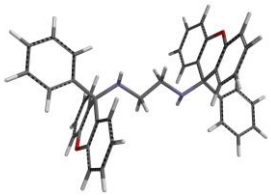	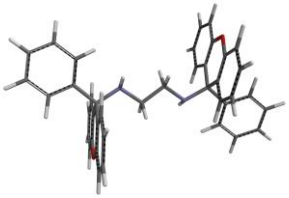
Apohost **H₂**	**H₂**·(pyridine)-A	**H₂**·(pyridine)-B	**H₂**·(dioxane)
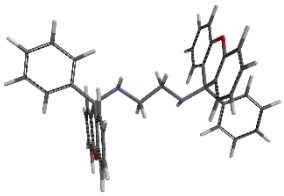	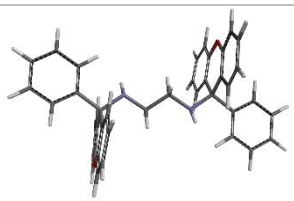	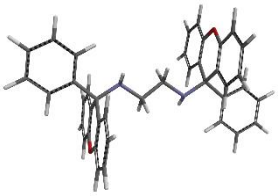	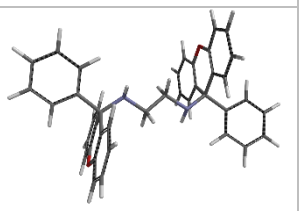
H₂·(piperidine)-*RS*	**H₂**·(morpholine)-A	**H₂**·(morpholine)-B	**H₂**·(morpholine)-C
Crystal structures			
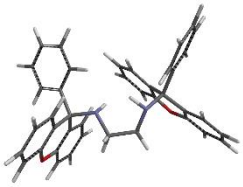	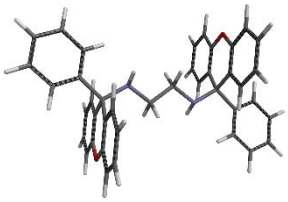	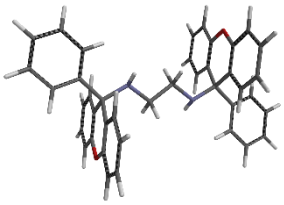	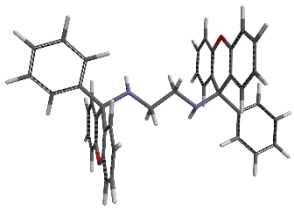
Apohost **H₂**	**H₂**·(piperidine)-*RS*[a]	**H₂**·(pyridine)-B	**H₂**·(piperidine)-*RS*
DFT optimised structures			

[a]Isostructural with **H₂**·(dioxane), **H₂**·(morpholine)-A, **H₂**·(morpholine)-B and **H₂**·(morpholine)-C.

Table S160. DFT structural parameters for host compound **H_2** conformers.

		E_{rel}/kJ.mol^{-1}	Torsion angles/°							Ring folding/°		Angle (O···C9–X)/°			
			I	*II*	*III*	*IV*	*V*	*VI*	*VII*	A	B	Ph_A	N_A	Ph_B	N_B
2-LXXXII	*anti*	0.00	-170	-178	-155	66	-153	-175	168	4	5	130	122	132	119
2-LXXXIII	*anti*	0.11	-168	-177	-155	67	-150	-174	168	3	9	130	122	135	116
2-LXXXIV	*syn*	3.10	-160	170	-115	-57	152	171	-163	3	0	124	129	126	125
2-LXXXV	*syn*	3.12	-173	-176	-143	75	-143	-176	-174	10	10	137	114	137	114
2-LXXXVI	*syn*	3.14	163	-172	-153	55	117	-170	159	1	5	127	124	122	130
2-LXXXVII	*anti*	3.33	-166	72	-162	-51	-63	-162	-172	4	9	131	119	132	119
2-LXXXVIII	*anti*	3.47	165	-176	-152	65	-147	-76	170	3	22	130	121	149	101
2-LXXXIX	*syn*	3.65	-170	-173	-161	61	107	-166	-172	5	15	129	122	139	112
2-XC	*anti*	4.35	168	-179	148	-60	150	66	-171	0	27	128	124	153	92
2-XCI	*anti*	4.45	166	-176	-86	-173	-131	-175	156	1	15	128	124	113	139
2-XCII	*anti*	5.61	157	-175	-138	-177	-74	-176	-165	16	3	112	139	124	128
Apohost **2**-all_D	*anti*	5.80	160	177	156	52	-139	-178	-169	3	7	124	128	134	117
2-XCIII	*anti*	6.23	-171	-162	-66	-49	143	-176	168	8	0	131	120	127	125
2-XCIV	*anti*	6.56	-168	-179	-143	53	-178	74	-171	0	17	128	123	143	106
2-XCV	*syn*	6.62	166	-175	-178	58	97	78	-174	5	18	129	123	145	105
2-XCVI	*syn*	6.64	171	-74	-130	71	-148	180	-165	17	1	141	108	128	123
2-XCVII	*anti*	6.84	168	180	143	-53	179	-74	170	1	16	128	123	142	107
2-XCVIII	*syn*	6.94	-167	-179	-167	-170	-55	-168	-170	2	1	126	125	126	125
2-XCIX	*anti*	7.20	173	162	67	38	97	69	-176	10	28	135	117	154	91
2-C	*syn*	7.33	167	-178	-93	-50	-173	78	-170	9	12	135	117	135	115
2-CI	*syn*	7.89	172	161	66	40	79	85	-176	10	27	134	117	150	99
2-CII	*syn*	8.03	-171	-173	-179	57	103	89	-177	9	25	131	120	151	94
2-CIII	*anti*	9.13	-168	-178	-160	-172	-63	-165	159	1	8	127	124	119	133
2-CIV	*anti*	9.52	179	-92	-79	-34	-165	79	-172	22	13	147	103	140	110
2-CV	*syn*	10.32	-165	173	85	177	159	-73	167	2	18	128	124	144	106
2-CVI	*anti*	10.71	169	-92	76	-170	170	178	171	25	12	150	99	139	112
2-CVII	*syn*	13.43	167	-175	-166	174	-77	87	-165	8	23	136	115	148	101
2-CVIII	*syn*	13.74	-169	75	134	-66	134	76	-170	14	13	142	108	141	108
2-CIX	*anti*	13.75	-154	171	150	163	82	84	-175	16	24	111	141	150	99
2-CX	*syn*	13.90	-173	78	95	62	-180	80	-171	16	17	142	107	142	107
2-CXI	*anti*	13.91	-169	66	-159	65	-139	-71	176	25	26	151	93	153	92
2-CXII	*anti*	13.92	174	-82	-84	-164	-157	-171	157	24	11	150	100	115	137
2-CXIII	*syn*	15.58	-154	-180	-148	-85	65	162	-149	12	18	115	136	108	145
2-CXIV	*syn*	15.82	-166	73	-169	-87	63	168	161	2	12	130	120	112	140
2-CXV	*syn*	15.83	-173	62	102	171	109	174	-155	26	18	152	93	110	142
2-CXVI	*syn*	15.96	-172	75	-162	67	-154	-176	133	17	27	144	106	105	148
2-CXVII	*anti*	16.27	-163	-166	-63	85	156	175	172	12	1	113	140	127	123
2-CXVIII	*syn*	16.43	-158	168	-123	-52	150	65	-173	9	30	118	134	154	90
2-CXIX	*syn*	17.17	-165	178	166	51	166	178	-165	0	0	126	125	126	125
2-CXX	*syn*	17.47	-151	170	145	166	93	71	-178	19	26	109	143	153	92
2-CXXI	*anti*	17.49	-170	76	-175	-56	164	-74	173	16	18	142	107	143	106
2-CXXII	*syn*	17.73	-151	162	59	-85	-157	62	-168	14	18	112	141	143	102
2-CXXIII	*syn*	18.08	167	172	71	176	158	-63	169	3	23	124	128	148	97
2-CXXIV	*syn*	18.10	169	-72	158	-71	157	-72	169	15	14	142	108	141	108
2-CXXV	*syn*	18.22	-172	77	91	175	-178	174	169	22	7	148	102	131	121
Apohost **2**-H_D	*anti*	18.33	155	-173	-158	64	176	174	-159	3	19	127	125	109	143
2-CXXVI	*anti*	18.63	-171	65	155	-173	-83	172	164	23	1	148	97	126	126
2-CXXVII	*syn*	18.83	-174	-173	99	77	-157	74	-175	16	23	142	109	148	97
2-CXXVIII	*anti*	18.91	-165	177	-98	-89	61	168	164	6	8	131	121	116	136
2-CXXIX	*syn*	19.48	-175	82	90	-151	-171	77	-170	23	13	147	103	139	111
2-CXXX	*syn*	19.76	169	-76	172	152	-90	-84	176	12	23	137	113	147	103
2-CXXXI	*syn*	19.87	170	177	169	-168	65	-81	171	12	25	139	112	150	93
2-CXXXII	*anti*	19.99	-167	179	176	-180	-176	-179	167	2	2	128	123	128	123
2-(piperidine)-*RS*-all_D	*anti*	20.01	167	-179	-175	180	175	179	-167	2	2	128	123	128	123
2-(morpholine)-A-all_D	*anti*	20.01	167	-179	-175	180	175	179	-167	2	2	128	123	128	123
2-(morpholine)-B-all_D	*anti*	20.01	167	-179	-175	180	175	179	-167	2	2	128	123	128	123
2-(morpholine)-C-all_D	*anti*	20.01	167	-179	-175	-180	175	179	-167	2	2	128	123	128	123
2-(dioxane)-all_D	*anti*	20.01	167	-179	-175	-180	175	179	-167	2	2	128	123	128	123
2-(pyridine)-B-all_D	*anti*	20.03	-167	179	175	180	-175	-179	167	2	2	128	123	128	123
2-CXXXIII	*syn*	20.10	167	179	-179	177	-179	179	167	3	3	129	122	129	122
2-CXXXIV	*anti*	20.16	-166	180	179	-178	-172	-177	165	2	0	128	123	126	125
2-(piperidine)-*RR*-all_D	*syn*	20.40	168	178	176	176	176	178	168	4	4	130	121	130	121
2-CXXXV	*syn*	20.40	-168	-178	-176	-176	-176	-178	-168	4	4	130	121	130	121
2-CXXXVI	*syn*	20.55	170	-75	165	52	167	178	-166	20	1	146	104	127	125
2-CXXXVII	*anti*	21.00	175	-67	-103	178	172	-177	-170	24	9	151	94	134	118
2-CXXXVIII	*anti*	21.41	169	174	179	178	102	64	-173	7	24	132	120	150	94
2-CXXXIX	*anti*	21.73	166	-177	-166	170	-67	78	-167	9	25	137	114	149	94
2-CXL	*syn*	23.37	-175	77	117	-80	162	-67	168	16	28	142	107	154	91
2-CXLI	*syn*	24.23	-168	-168	-60	-162	171	-73	168	0	17	124	128	142	108
2-CXLII	*anti*	24.28	171	169	58	143	-93	-76	175	5	23	131	121	147	103
2-CXLIII	*syn*	24.44	167	180	-178	179	-170	76	-170	3	19	129	123	144	106
2-CXLIV	*anti*	25.25	170	-76	167	180	179	-180	167	19	3	145	105	129	122
2-CXLV	*syn*	25.34	170	166	56	144	-106	-65	175	5	24	130	122	150	95
2-CXLVI	*anti*	25.38	-168	-180	179	-179	-168	76	-169	4	19	130	121	145	105
2-CXLVII	*syn*	26.78	169	-78	172	178	80	-87	165	19	23	144	106	148	101
2-CXLVIII	*anti*	28.76	-167	-177	112	-174	-174	-65	171	9	24	133	118	149	96
2-(pyridine)-B-H_D	*anti*	28.91	156	-173	-173	-180	173	173	-156	15	15	112	140	112	140
2-CXLIX	*anti*	30.69	-170	76	-169	180	169	-76	170	19	19	145	105	145	105
2-CL	*anti*	30.69	170	-76	169	180	-169	76	-170	19	19	145	105	145	105
2-(pyridine)-A-all_D	*anti*	30.69	170	-76	169	-180	-169	76	-170	19	19	145	105	145	105
2-(dioxane)-H_D	*anti*	30.90	-172	-178	-171	-175	-177	-179	-173	3	0	121	130	126	125
2-CLI	*syn*	31.12	170	-73	148	56	-159	64	-169	20	23	146	103	149	96
2-(morpholine)-B-H_D	*anti*	31.50	175	-172	-174	180	174	172	-175	1	1	123	128	123	128
2-CLII	*syn*	33.15	166	-178	-175	180	169	-66	171	2	23	128	123	148	97
2-(piperidine)-*RR*-H_D	*syn*	33.71	161	180	180	-177	-167	-177	179	3	4	131	121	117	134
2-CLIII	*syn*	34.37	179	-93	-77	-136	78	-109	177	21	27	146	103	151	98
2-(pyridine)-A-H_D	*anti*	35.08	177	-79	166	180	-166	79	-177	20	20	144	106	144	106
2-(morpholine)-C-H_D	*anti*	36.41	-169	178	178	176	165	178	177	0	7	127	124	116	135
2-CLIV	*syn*	37.42	-170	76	-171	176	167	-67	171	18	23	144	106	149	96
2-(morpholine)-A-H_D	*anti*	40.81	173	176	162	180	-162	-178	-173	3	3	120	130	120	130
2-CLV	*syn*	41.37	171	-68	170	176	67	-79	169	23	26	148	97	151	92
2-(piperidine)-*RS*-H_D	*anti*	45.40	161	180	180	-177	-167	-177	179	4	3	131	121	117	134
2-CLVI	*syn*	52.39	-169	84	-64	-152	79	-107	177	26	27	151	93	150	99

ap/-*ap*		*sc*/-*sc*	
ac/-*ac*		*sp*/-*sp*	

Pseudo axial
Pseudo equatorial

Table S161. MMFF94 structural parameters for host **H_1** conformers.

		E_{rel}/kJ.mol^{-1}	Torsion angles/°							Ring folding/°		Angle (S···C9–X)/°			
			I	*II*	*III*	*IV*	*V*	*VI*	*VII*	A	B	Ph_A	N_A	Ph_B	N_B
3-I	*anti*	0.00	176	174	149	-50	-160	-174	-171	4	1	127	123	125	126
Apohost **3**-all_M	*anti*	0.00	171	174	160	50	-149	-174	-176	1	4	125	126	127	123
3-II	*syn*	7.02	176	176	163	-42	-148	-179	173	4	4	127	123	122	129
3-III	*syn*	7.27	175	180	-177	-40	-177	180	175	2	2	125	125	125	125
3-IV	*syn*	7.70	175	-179	125	38	171	179	175	3	7	122	128	129	121
3•(morpholine)-all_M	*syn*	7.70	175	179	171	38	125	-179	175	7	3	129	121	122	128
3•(piperidine)-all_M	*syn*	7.70	-175	179	-125	-38	-171	-179	-175	3	7	122	128	129	121
3•(pyridine)-all_M	*syn*	7.70	175	179	171	38	125	-179	175	3	7	129	121	122	128
3•(dioxane)-all_M	*syn*	7.70	175	179	171	38	125	-179	175	7	3	129	121	122	128
3•(piperidine)-all_M	*syn*	7.70	175	-179	125	38	171	179	175	3	7	122	128	129	121
3-V	*syn*	8.86	175	173	154	-74	154	173	175	5	5	128	122	128	122
3-VI	*anti*	9.58	174	178	-180	180	180	-178	-174	3	3	126	124	126	124
3-VII	*syn*	10.83	175	171	84	172	175	178	174	4	2	126	125	125	125
3-VIII	*anti*	11.27	-178	77	-176	46	-147	-176	-176	34	1	153	95	125	125
3-IX	*syn*	12.11	174	177	176	-178	176	177	174	3	3	126	124	126	124
3-X	*syn*	13.70	173	-178	-167	-171	-59	-168	168	4	9	122	128	117	134
3-XI	*anti*	13.73	174	177	175	172	86	175	-173	2	5	125	125	126	125
3-XIV	*anti*	15.15	177	165	87	38	148	176	-174	13	1	131	119	123	127
3-XV	*syn*	19.61	176	177	156	-35	-157	75	-177	1	35	125	126	154	94
3-XVII	*syn*	21.13	-171	173	83	160	83	173	-171	5	5	120	131	120	131
3-XVIII	*syn*	21.86	-177	71	106	40	165	174	174	33	8	152	96	130	121
3-XIX	*syn*	23.25	173	172	85	160	85	172	173	5	5	121	130	121	130
3-XX	*anti*	23.48	173	171	83	160	84	174	-171	5	5	121	130	120	130
3-XXI	*anti*	25.41	173	179	-177	55	-169	-79	178	1	35	125	126	153	95
3-XXII	*anti*	27.06	-177	77	-169	179	-177	-178	-174	35	3	153	95	126	124
3-XXIII	*syn*	27.23	-178	77	-169	-178	-178	179	174	35	2	153	95	126	125
3-XXIV	*anti*	27.91	174	174	90	171	168	-77	177	2	35	125	126	153	95
3-XXV	*anti*	28.30	171	175	157	52	-140	-62	173	1	30	124	126	149	97
3-XXVI	*syn*	29.80	175	173	177	172	100	73	-178	9	36	130	121	154	94
3-XXVII	*anti*	31.10	-174	178	175	167	100	72	-177	6	37	128	123	154	93
3-XXVIII	*syn*	31.18	175	-178	-164	-38	167	-76	-179	1	33	125	125	152	95
3-XXIX	*anti*	32.56	174	-180	-103	-179	172	-79	178	8	36	130	121	154	95
3-XXX	*syn*	33.01	174	176	101	180	-172	80	-178	6	36	128	122	154	94
3-XXXI	*syn*	33.09	175	167	80	172	-171	78	-178	6	36	127	124	154	94
3-XXXII	*anti*	33.21	169	-167	-63	-173	172	-77	178	5	37	118	132	155	93
3-XXXIII	*anti*	35.04	173	-179	-163	58	-169	77	180	0	31	124	126	150	96
3-XXXIV	*anti*	35.06	-175	-176	-176	180	-74	88	-174	7	39	129	121	156	92
3-XXXVI	*syn*	36.48	177	179	-175	-53	-108	-67	178	8	31	129	121	151	96
3-XXXVII	*syn*	36.52	-179	-77	168	172	88	173	175	33	2	152	95	124	126
3-XXXVIII	*anti*	36.62	-173	87	-75	-178	-177	179	174	39	5	156	92	128	122
3-XXXIX	*syn*	37.65	-177	78	-177	58	-152	-179	171	33	5	152	96	121	129
3-XL	*anti*	38.37	177	-79	178	-47	132	63	-174	36	34	154	94	153	94
3-XLI	*anti*	38.72	173	-177	-91	-172	-169	78	179	4	33	126	125	151	96
3-XLII	*anti*	39.28	-179	-72	-103	-30	-88	-170	-178	33	10	153	94	129	121
3-XLIII	*syn*	40.65	-178	78	-172	-46	-172	78	-178	35	35	153	95	153	95
3-XLIV	*syn*	40.68	174	176	170	-178	166	-77	-180	3	33	126	124	152	95
3-XLV	*anti*	41.16	-178	77	-171	55	-173	-79	177	33	35	152	96	154	94
3-XLVI	*syn*	41.24	-177	70	100	153	83	174	173	37	5	155	92	120	131
3-XLVII	*anti*	41.57	-179	-73	-104	-177	178	-176	-175	35	8	153	94	129	122
3-XLVIII	*syn*	41.75	-177	77	-167	180	-167	77	-177	35	35	153	95	153	95
3-XLIX	*anti*	42.26	177	-77	170	180	-170	77	-177	35	35	153	95	153	95
3-L	*syn*	42.68	-178	74	101	-177	-172	78	-177	36	35	153	94	153	95
3-LI	*anti*	44.40	-179	76	-170	54	-169	77	-180	34	32	152	95	151	96
3-LII	*syn*	46.01	-179	-78	177	-169	-62	-168	169	35	6	153	94	118	133
3-LIII	*syn*	46.14	178	-90	77	180	174	176	175	35	7	153	93	129	121
3-LIV	*anti*	46.82	-178	82	-169	-164	-97	-74	178	34	37	152	96	155	93
3-LV	*syn*	47.25	180	-76	167	-44	-163	76	-178	32	35	151	95	154	94
3-LVI	*syn*	49.77	-178	75	167	38	112	68	-176	34	31	152	95	149	98
3-LVII	*anti*	49.87	174	178	-178	-179	-78	90	-177	6	35	129	121	153	94
3-LVIII	*syn*	50.34	-176	67	130	-67	-171	78	-176	37	36	155	92	155	94
3-LIX	*anti*	50.57	179	-76	168	49	-133	-65	175	35	34	154	93	152	95
Apohost **3**-H_M	*anti*	79.41	162	-170	-156	67	170	175	-144	10	33	133	119	99	154
3•(piperidine)-H_M	*syn*	108.38	-121	174	168	-75	159	173	-123	34	33	95	160	95	159
3•(dioxane)-H_M	*syn*	114.98	121	-173	-165	79	-164	-171	119	36	37	93	161	91	163
3•(morpholine)-H_M	*syn*	116.13	121	-173	-165	79	-164	-171	118	36	37	93	161	91	164
3•(pyridine)-H_M	*syn*	119.17	118	-172	-162	80	-165	-173	117	37	37	91	164	93	162

ap/-ap *sc/-sc*

ac/-ac *sp/-sp*

Pseudo axial

Pseudo equatorial

Table S162. DFT structural parameters for host **H_1** conformers.

		E_{rel} (kJ/mol)	Torsion angles/°							Ring folding/°		Angle (S···C9–X)/°			
			I	*II*	*III*	*IV*	*V*	*VI*	*VII*	A	B	Ph_A	N_A	Ph_B	N_B
3-LX	*anti*	0.00	173	180	145	-58	171	73	-176	1	39	128	123	162	83
3-LXI	*anti*	0.47	177	-68	-105	-42	-65	-164	-176	35	7	159	86	131	121
3-LXII	*anti*	1.21	177	173	-173	-55	-101	-65	175	24	37	142	109	161	85
3-LXIII	*anti*	1.37	170	-177	-147	63	-172	-82	175	10	38	135	116	161	89
3-LXIV	*anti*	1.55	170	-177	-145	63	-175	-82	174	10	39	136	116	162	88
3-LXV	*syn*	1.55	177	173	-173	-55	-101	-65	175	24	37	143	109	160	85
3-LXVI	*anti*	1.63	-176	80	179	54	-142	-177	-173	40	5	162	87	132	119
3-LXVII	*anti*	1.73	175	-64	-135	54	164	-84	174	36	41	158	87	163	87
3-LXVIII	*anti*	1.97	173	178	142	-53	179	-80	176	5	39	132	119	161	88
3-LXIX	*anti*	3.31	-132	171	137	165	83	80	-176	38	38	96	157	160	90
3-LXX	*anti*	3.89	173	177	137	-52	-150	177	-123	9	38	135	116	95	159
Apohost **3**-all_D	*anti*	3.89	123	-177	152	52	-137	-178	-173	38	9	95	160	135	116
3-LXXI	*anti*	4.99	-176	79	86	53	164	-170	-177	37	24	159	91	143	108
3-LXXII	*anti*	5.07	177	171	-164	-52	-85	-79	176	24	37	143	108	158	91
3-LXXIII	*anti*	5.33	178	-78	167	-54	178	84	-176	38	40	160	89	163	87
3-LXXIV	*syn*	5.43	-173	72	97	57	174	-179	173	37	23	159	91	143	109
3-LXXV	*anti*	5.51	-116	171	146	44	66	160	174	40	7	93	163	130	121
3-LXXVI	*anti*	5.62	-175	-161	-67	-43	-146	-171	116	8	40	131	121	93	163
3-LXXVII	*anti*	5.85	-177	77	-165	54	175	-84	176	39	40	160	89	163	87
3•(pyridine)-all_D	*syn*	6.33	169	-175	-146	48	132	-174	139	6	34	131	120	99	154
3-LXXVIII	*syn*	6.35	169	-176	-146	49	132	-173	138	7	34	132	119	99	154
3•(dioxane)-all_D	*syn*	6.38	169	-176	-146	48	133	-174	138	7	34	132	119	99	155
3•(morpholine)-all_D	*syn*	6.43	170	-176	-146	48	134	-174	138	7	34	132	119	99	155
3•(piperidine)-all_D	*syn*	6.70	-138	173	-134	-47	146	177	-170	34	9	99	155	133	118
3-LXXIX	*syn*	7.01	-178	80	-161	71	-157	-175	116	38	39	161	89	93	162
3-LXXX	*anti*	7.35	-173	82	-166	-166	-87	-79	177	39	39	162	89	160	90
3-LXXXI	*syn*	7.51	176	176	145	-75	145	176	176	12	12	137	114	137	114
3-LXXXII	*anti*	7.54	-175	178	-180	160	-75	96	-173	17	41	141	110	161	87
3-LXXXIII	*anti*	7.56	175	-178	-142	67	-162	67	-173	12	39	137	113	164	81
3-LXXXIV	*anti*	7.77	139	-173	-150	-173	-58	-170	-172	34	0	99	153	125	127
3-LXXXV	*syn*	8.14	176	-69	-93	-168	-136	-170	133	37	37	160	85	96	157
3-LXXXVI	*syn*	9.58	-176	78	94	178	-168	79	-174	39	40	159	91	160	90
3-LXXXVII	*anti*	9.66	171	179	86	175	168	-79	173	3	40	129	122	161	89
3-LXXXVIII	*syn*	9.66	175	171	162	-61	-107	165	175	8	19	130	121	141	110
3-LXXXIX	*syn*	9.87	-139	172	142	173	75	171	-167	33	6	99	153	123	128
3-XC	*syn*	10.95	-173	94	-77	164	-177	173	174	40	18	161	88	142	109
3-XCI	*anti*	11.45	-179	78	-164	55	-176	72	-175	39	38	160	88	163	83
3-XCII	*anti*	12.18	168	179	78	174	154	174	-136	15	35	118	133	98	154
3-XCIII	*anti*	12.29	137	-164	-44	174	-179	-82	175	35	41	98	155	163	87
3-XCIV	*syn*	12.92	-175	73	90	160	78	178	167	40	12	162	88	117	135
3-XCV	*syn*	12.97	174	176	-178	169	91	78	-176	17	39	137	114	160	90
3-XCVI	*syn*	13.94	-176	82	-162	-48	-162	82	-176	40	40	162	88	162	88
3-XCVII	*syn*	14.13	169	174	77	169	77	174	169	11	11	118	133	118	133
3-XCVIII	*syn*	14.34	-165	169	86	169	86	169	-165	14	14	115	136	115	136
3-XCIX	*syn*	14.34	169	173	74	169	89	171	-167	13	13	116	135	117	134
3-C	*syn*	14.83	-172	73	-140	-47	154	176	173	38	6	161	88	132	120
3-CI	*syn*	15.04	-173	79	169	61	100	70	-174	40	30	161	88	153	97
3-CII	*syn*	15.10	-172	73	-139	-48	152	176	173	38	5	160	88	130	120
3•(morpholine)-H_D	*syn*	15.15	121	-173	-165	79	-164	-171	118	36	37	93	161	91	164
3-CIII	*syn*	15.36	174	164	64	-179	-169	84	-177	5	42	127	124	163	87
3-CIV	*anti*	15.46	174	176	177	178	94	179	-173	10	19	130	120	140	111
3•(pyridine)-H_D	*syn*	15.46	118	-172	-162	80	-165	-173	117	37	37	91	164	93	162
3•(dioxane)-H_D	*syn*	15.49	121	-173	-165	79	-164	-171	119	36	37	93	161	91	163
3-CV	*syn*	15.88	174	164	61	174	-170	82	-176	4	42	126	125	162	88
3-CVI	*anti*	15.96	169	-179	169	178	57	166	-151	17	29	116	135	105	148
3•(piperidine)-H_D	*syn*	16.36	-121	174	168	-75	159	173	-123	34	33	95	160	95	159
3-CVII	*syn*	16.46	-175	78	-157	173	-157	78	-175	40	40	163	88	163	88
3-CVIII	*syn*	16.88	174	177	-178	-176	85	175	174	13	21	133	118	140	111
3-CIX	*anti*	17.96	176	-67	-102	-176	178	-175	-175	37	18	160	85	137	114
3-CX	*syn*	18.09	-175	78	-159	174	-152	-176	133	40	36	162	88	96	157
Apohost **3**-H_D	*anti*	18.46	162	-170	-156	67	170	175	-144	10	33	133	119	99	154
3-CXI	*anti*	18.72	175	-81	168	180	-168	81	-175	40	40	162	88	162	88
3-CXII	*syn*	18.96	174	-85	64	-157	179	-177	174	38	17	160	84	141	110
3-CXIII	*anti*	19.38	172	178	-92	-165	-159	71	-176	10	37	134	117	160	85
3-CXIV	*syn*	19.80	175	-68	165	171	81	178	171	36	2	159	86	125	126
3-CXV	*syn*	21.32	174	-68	160	-56	-148	78	-177	38	39	162	84	161	88
3-CXVI	*anti*	21.48	174	172	-177	162	-67	84	-174	17	38	141	110	160	84
3-CXVII	*anti*	22.97	-176	81	-165	-179	-179	-179	-173	40	12	162	88	135	116
3-CXVIII	*syn*	24.44	-173	179	168	50	168	179	-173	11	11	134	117	134	117
3-CXIX	*syn*	24.50	173	180	-168	-51	-168	180	173	12	12	135	116	135	116
3-CXX	*syn*	26.60	-173	-178	-180	179	-180	-178	-173	14	14	136	115	136	115
3-CXXI	*anti*	26.70	173	179	-177	-180	177	-179	-173	13	13	136	115	136	115
3-CXXII	*anti*	28.96	176	-69	161	-179	141	-179	-168	38	11	161	84	118	133
3-CXXIII	*syn*	32.24	173	178	179	178	165	-69	175	14	38	137	114	161	85

ap/-ap *sc/-sc*

ac/-ac *sp/-sp*

Pseudo axial

Pseudo equatorial

Figure S163. Host $\mathbf{H_1}$ in crystal structures and after DFT geometry optimization.

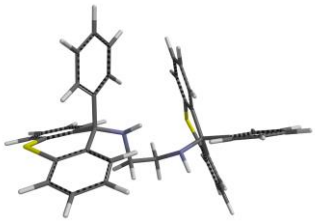	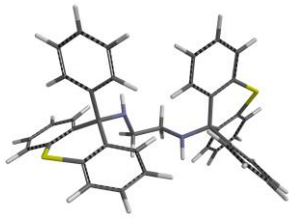	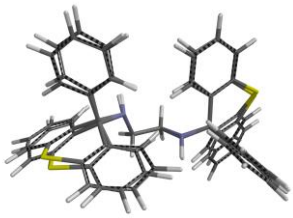
Apohost $\mathbf{H_1}$	$\mathbf{H_1}$·(dioxane)[a]	$\mathbf{H_1}$·(dioxane) and **3**·(piperidine) enantiomer
Crystal structures [a] Isostructural with **3**•(pyridine) and **3**•(morpholine)		
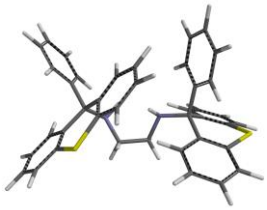	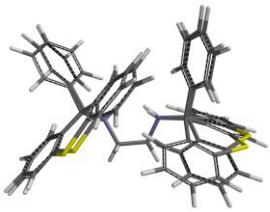	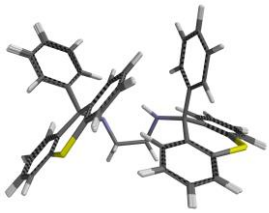
Apohost $\mathbf{H_1}$	Apohost $\mathbf{H_1}$ and $\mathbf{H_1}$·(dioxane)	$\mathbf{H_1}$·(dioxane), $\mathbf{H_1}$·(pyridine), $\mathbf{H_1}$·(morpholine) and $\mathbf{H_1}$·(piperidine) enantiomer
DFT optimized structures		

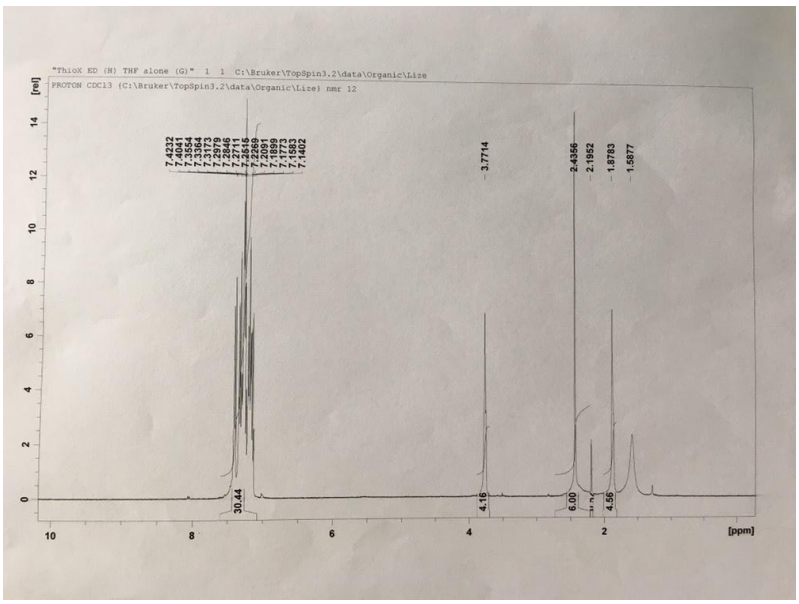

Figure S164. ^{1}H-NMR spectrum for $\mathbf{H_1}$·THF.

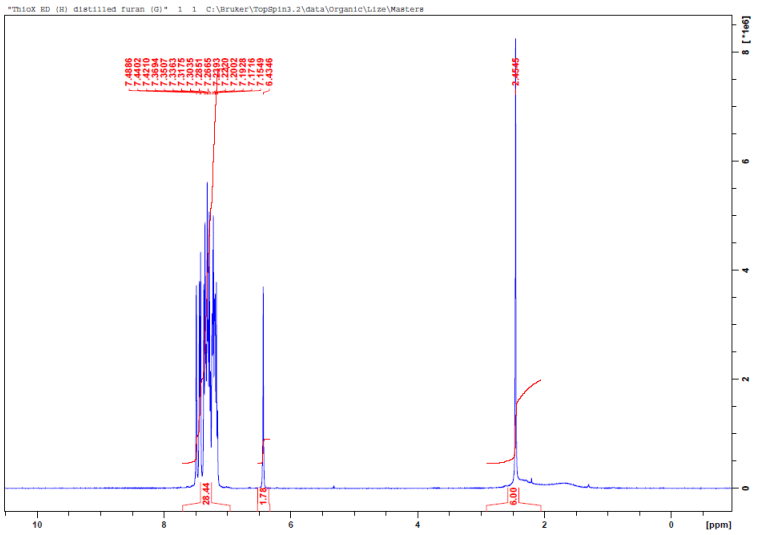

Figure S165. ^{1}H-NMR spectrum for **H$_1$**·Furan.

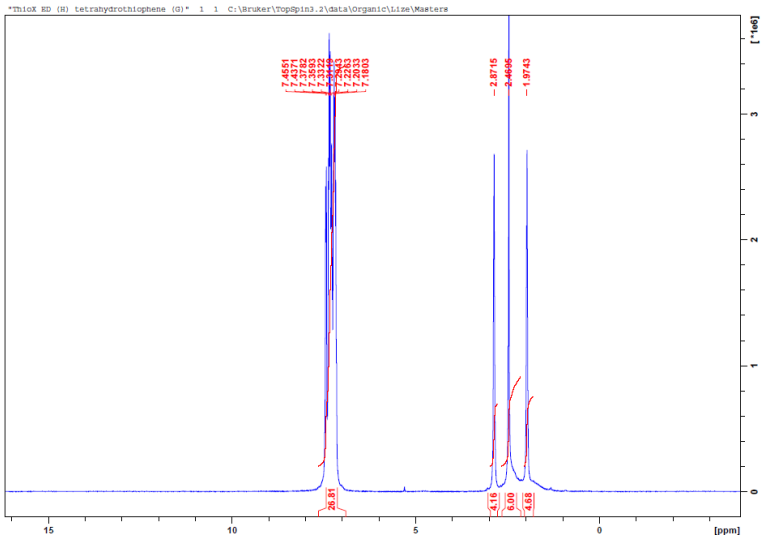

Figure S166. ^{1}H-NMR spectrum for **H$_1$**·THT.

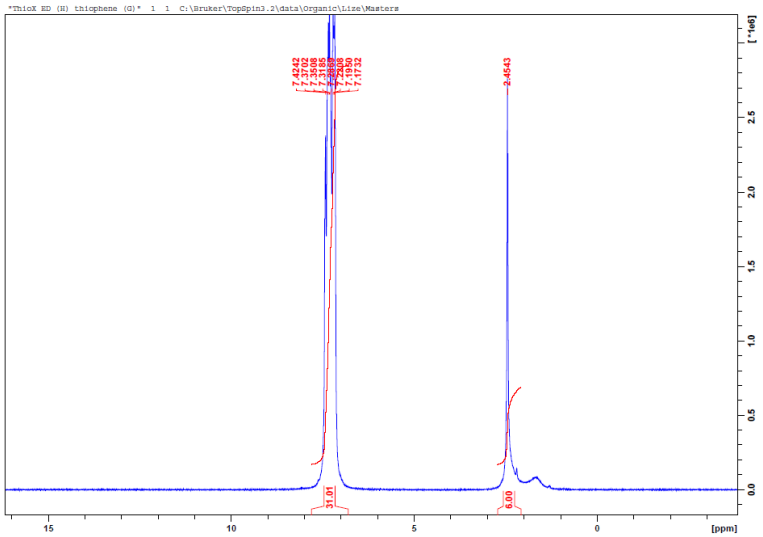

Figure S167. ^{1}H-NMR spectrum for **H$_1$**·Thiophene.

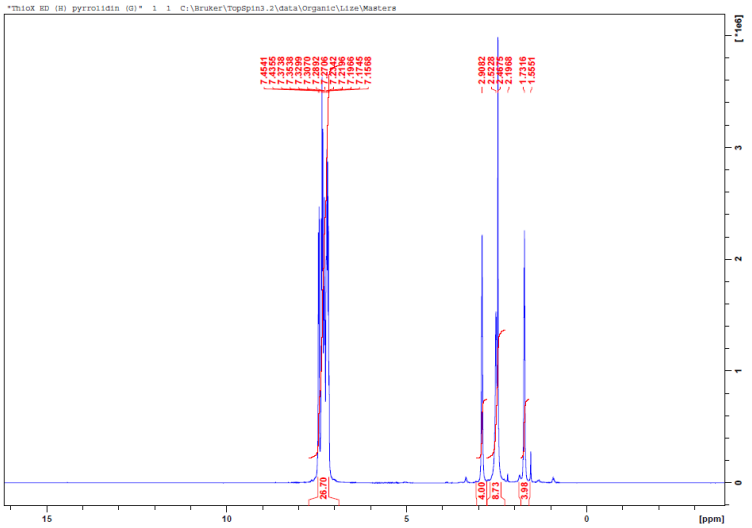

Figure S168. ^{1}H-NMR spectrum for **H$_1$**·Pyrrolidine.

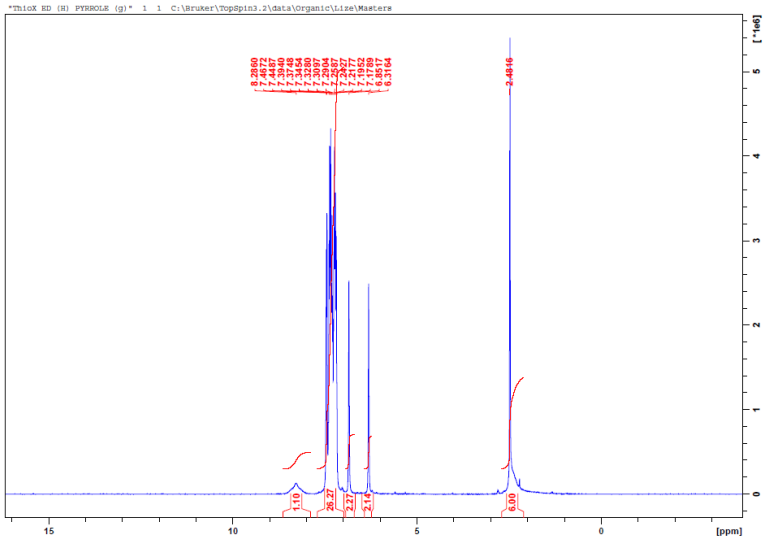

Figure S169. ^{1}H-NMR spectrum for **H$_1$**·Pyrrole.

Table S170. Duplicate values for equimolar competition experiments of **H$_1$**.

Guests:	Batch 1	Batch 2	Average	% e.s.d.s
THT, Thiophene	62.42:37.58	64.09:35.91	63.26:36.74	(0.84):(0.84)
THF, Furan	62.35:37.65	64.09:35.91	63.22:37.00	(0.87):(0.87)
Pyrrolidine, Pyrrole	50.00:50.00	50.99:49.01	50.50:49.50	(0.50):(0.50)
THT, THF	71.15:28.85	69.44:30.56	70.30:29.70	(0.86):(0.86)
THT, Pyrrolidine	79.69:20.31	77.12:22.88	78.40:21.60	(1.29):(1.29)
THF, Pyrrolidine	71.79:28.21	67.11:32.89	69.45:30.55	(2.34):(2.34)
Thiophene, Furan	76.50:23.50	73.50:26.50	75.00:25.00	(1.50):(1.50)
Thiophene, Pyrrole	85.57:14.43	85.22:14.78	85.40:14.60	(0.18):(0.18)
Furan, Pyrrole	66.20:33.80	66.35:33.65	66.28:33.72	(0.08):(0.08)

Table S171. K values for competition experiment of THF/Furan.[a,b]

THF ml	THF c	Furan ml	Furan c	K value
1	1	0	0	#DIV/0!
0,8	0,87	0,2	0,13	1,673076923
0,61	0,75	0,39	0,25	1,918032787
0,5	0,62	0,5	0,38	1,631578947
0,42	0,54	0,58	0,46	1,621118012
0,2	0,24	0,8	0,76	1,263157895
0	0	1	1	1,621392913

[a]Abbreviations in the table include ml (mother liquor) and c (crystal).
[b]The average K value is highlighted in yellow.

Table S172. K values for competition experiment of Furan/Pyrrole.[a,b]

Furan ml	Furan c	Pyrrole ml	Pyrrole c	K value
1	1	0	0	#DIV/0!
0,79	0,81	0,21	0,19	1,1332445
0,55	0,72	0,45	0,28	2,1038961
0,49	0,66	0,51	0,34	2,02040816
0,37	0,6	0,63	0,4	2,55405405
0,16	0,39	0,84	0,61	3,35655738
0	0	1	1	2,23363204

[a]Abbreviations in the table include ml (mother liquor) and c (crystal).
[b]The average K value is highlighted in yellow.

Table S173. K values for competition experiment of THF/Pyrrolidine.[a,b]

THF ml	THF c	Pyrrolidine ml	Pyrrolidine c	K value
1	1	0	0	#DIV/0!
0,8	0,85	0,2	0,15	1,41666667
0,62	0,75	0,38	0,25	1,83870968
0,51	0,67	0,49	0,33	1,9506833
0,43	0,66	0,57	0,34	2,57318741
0,25	0,47	0,75	0,53	2,66037736
0	0	1	1	2,08792488

[a]Abbreviations in the table include ml (mother liquor) and c (crystal).
[b]The average K value is highlighted in yellow.

Table S174. K values for competition experiment of Pyrrolidine/Pyrrole.[a,b]

pyrrolidine ml	pyrrolidine c	pyrrole ml	pyrrole c	K value
1	1	0	0	#DIV/0!
0,77	0,94	0,23	0,06	4,67965368
0,58	0,74	0,42	0,26	2,061007958
0,48	0,49	0,52	0,51	1,040849673
0,37	0,34	0,63	0,66	1,140056022
0,22	0,11	0,78	0,89	2,282051282
0	0	1	1	2,240723723

[a]Abbreviations in the table include ml (mother liquor) and c (crystal).
[b]The average K value is highlighted in yellow.

Table S175. K values for competition experiment of THT/THF.[a,b]

THT ml	THT c	THF ml	THF c	K value
1	1	0	0	#DIV/0!
0,74	0,84	0,26	0,16	1,84459459
0,55	0,74	0,45	0,26	2,32867133
0,53	0,71	0,47	0,29	2,17111256
0,38	0,59	0,62	0,41	2,3478819
0,2	0,4	0,8	0,6	2,66666667
0	0	1	1	2,27178541

[a]Abbreviations in the table include ml (mother liquor) and c (crystal).
[b]The average K value is highlighted in yellow.

Table S176. K values for competition experiment of THT/Pyrrolidine.[a,b]

THT ml	THT c	Pyrrolidine ml	Pyrrolidine c	K value
1	1	0	0	#DIV/0!
0,82	0,86	0,18	0,14	1,34843206
0,57	0,86	0,43	0,14	4,63408521
0,53	0,82	0,47	0,18	4,03983229
0,37	0,76	0,63	0,24	5,39189189
0,21	0,62	0,79	0,38	6,13784461
0	0	1	1	4,31041721

[a]Abbreviations in the table include ml (mother liquor) and c (crystal).
[b]The average K value is highlighted in yellow.

Table S177. K values for competition experiment of Thiophene/Pyrrole.[a,b]

Thiophene ml	Thiophene c	Pyrrole ml	Pyrrole c	K value
1	1	0	0	#DIV/0!
0,83	0,93	0,17	0,07	2,721170396
0,65	0,88	0,35	0,12	3,948717949
0,55	0,86	0,45	0,14	5,025974026
0,44	0,82	0,56	0,18	5,797979798
0,24	0,73	0,76	0,27	8,561728395
0	0	1	1	5,211114113

[a]Abbreviations in the table include ml (mother liquor) and c (crystal).
[b]The average K value is highlighted in yellow.

Table S178. K values for competition experiment of Thiophene/Furan.[a,b]

Thiophene ml	Thiophene c	Furan ml	Furan c	K value
1	1	0	0	#DIV/0!
0,78	0,87	0,22	0,13	1,887573964
0,58	0,78	0,42	0,22	2,567398119
0,5	0,73	0,5	0,27	2,703703704
0,48	0,7	0,52	0,3	2,527777778
0,19	0,28	0,81	0,72	1,657894737
0	0	1	1	2,26886966

[a]Abbreviations in the table include ml (mother liquor) and c (crystal).
[b]The average K value is highlighted in yellow.

Table S179. K values for competition experiment of THT/Thiophene.[a,b]

THT ml	THT c	thiophene ml	thiophene c	K value
1	1	0	0	#DIV/0!
0,83	0,88	0,17	0,12	1,50200803
0,66	0,73	0,34	0,27	1,39281706
0,57	0,64	0,43	0,36	1,3411306
0,44	0,51	0,56	0,49	1,32467532
0,24	0,26	0,76	0,74	1,11261261
0	0	1	1	1,33464873

[a]Abbreviations in the table include ml (mother liquor) and c (crystal).
[b]The average K value is highlighted in yellow.

a)

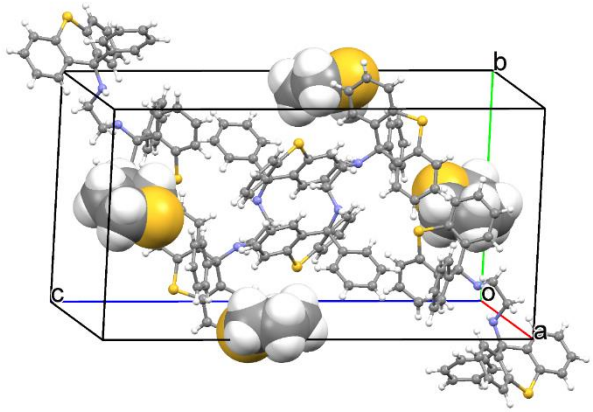

b)

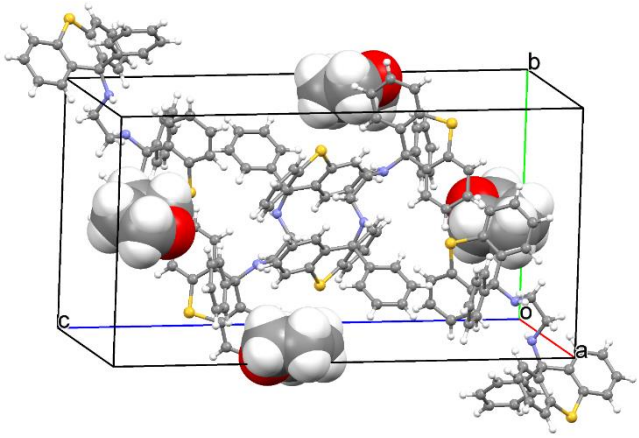

c)

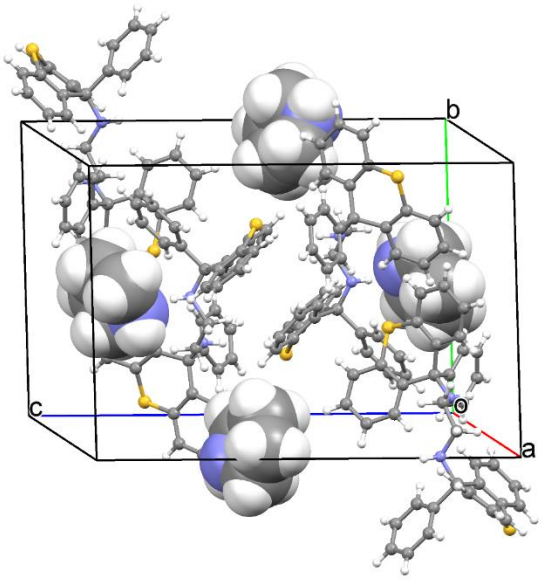

Figure S180. Units cell for complexes involving non-aromatic guests a) THT, b) THF and c) Pyrrolidine.

a)

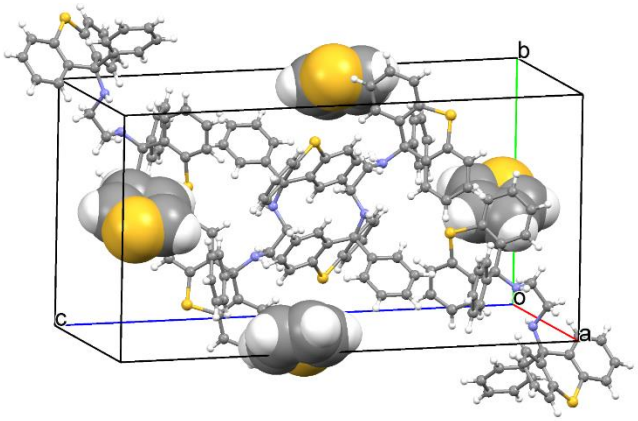

b)

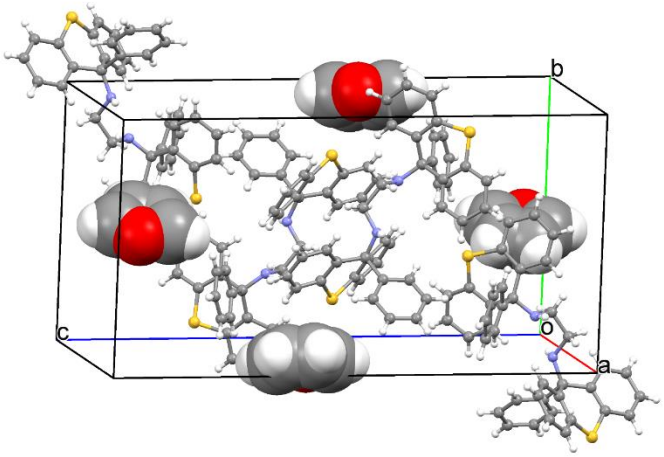

c)

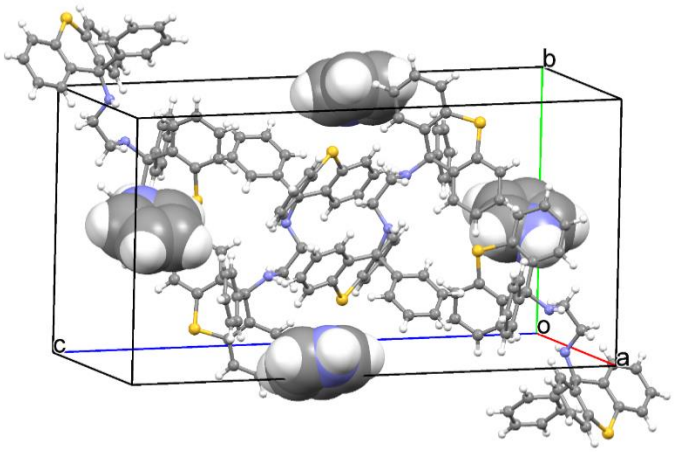

Figure S181. Units cell for complexes involving aromatic guests a) Furan, b) Thiophene and c) Pyrrole.

a)

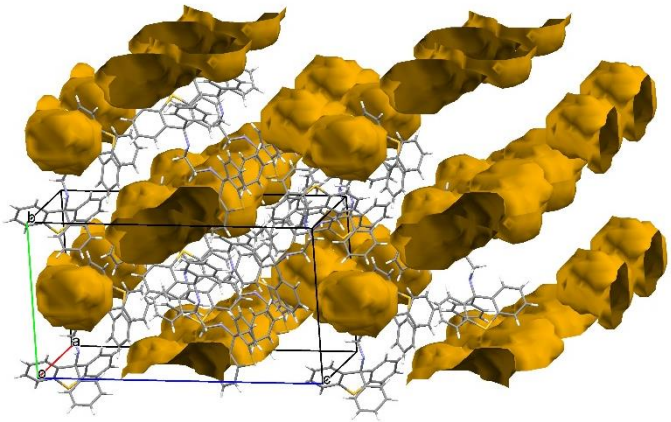

b)

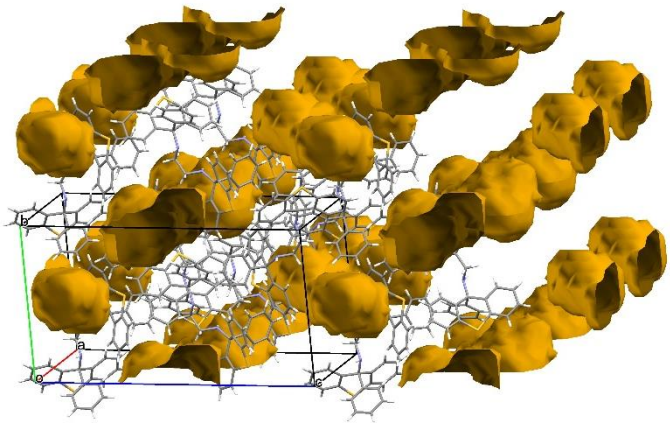

c)

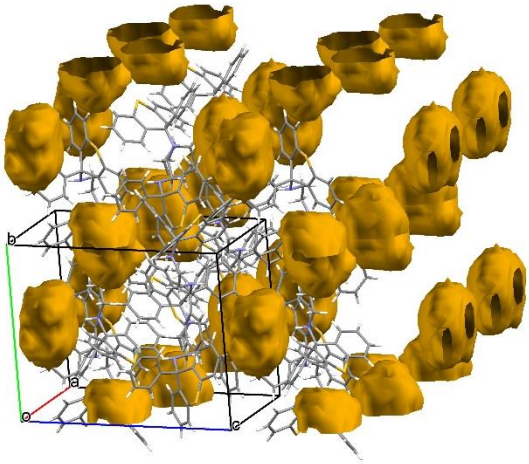

Figure S182. Guest accommodation of non-aromatic guests a) THF, b) THT and c) pyrrolidine.

a)

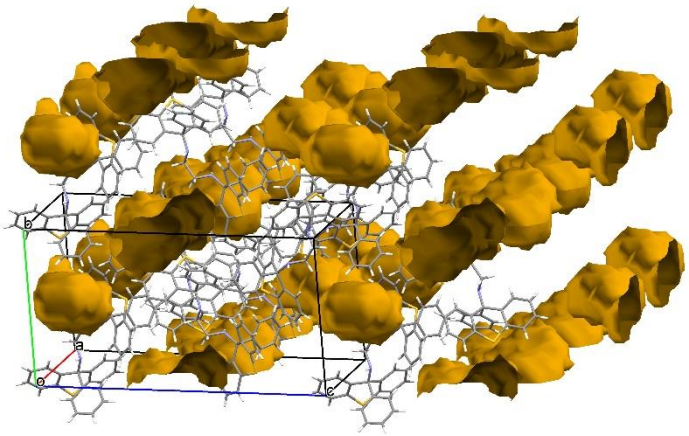

b)

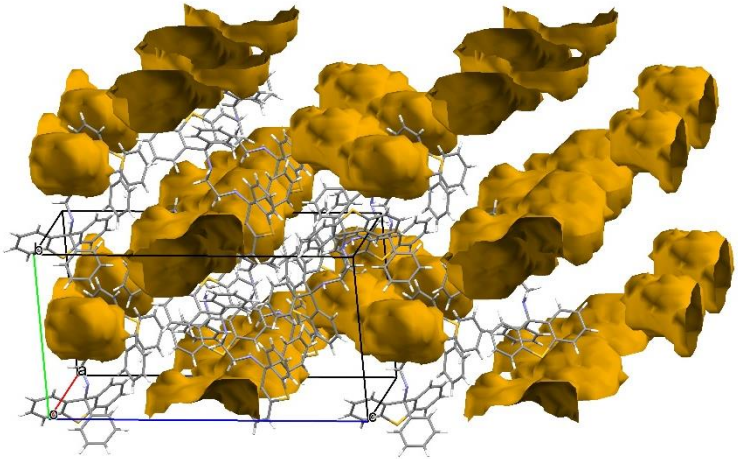

c)

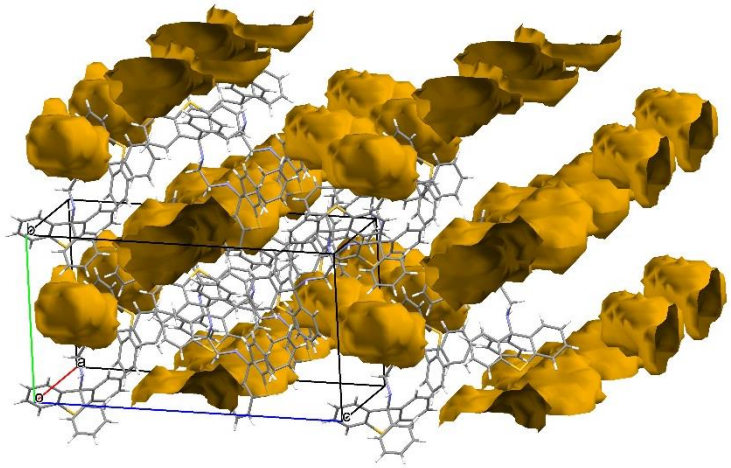

Figure S183. Guest accommodation of aromatic guests a) furan, b) thiophene and c) pyrrole.

Table S184. Interactions present in complexes of $\mathbf{H_1}$ with THF, THT and pyrrolidine.[a]

Non-covalent interaction	$\mathbf{H_1}$·THF	$\mathbf{H_1}$·THT	$\mathbf{H_1}$·pyrrolidine	Symmetry operation
π···π (H···H)	-	-	-	
CH···π (H···Cg, C–H···Cg)				
$C_{(H)}$–$H_{(H)}$···$Cg_{(H)}$				
$C_{(H)}$–$H_{(H)}$···$Cg_{(G2)}$	2.80 Å, 134°	2.79 Å, 134°		x, y, z
$C_{(H)}$–$H_{(H)}$···$Cg_{(H)}$	2.66 Å, 149°	2.68 Å, 149°	2.72 Å, 144°	3/2–x, –1/2+y, 1/2–z
$C_{(G1)}$–$H_{(G1)}$···$Cg_{(G1)}$	2.86 Å, 135°	2.91 Å, 136°	2.93 Å, 125°	x, 1+y, z
$C_{(H)}$–$H_{(H)}$···$Cg_{(H)}$	2.99 Å, 129°			3/2–x, –1/2+y, 1/2–z
	2.90 Å, 163°			3/2–x, –1/2+y, 1/2–z
$C_{(H)}$–$H_{(H)}$···$Cg_{(G2)}$				
$C_{(H)}$–$H_{(H)}$···$Cg_{(G1)}$			2.91 Å, 144°	1–x, 1–y, 1–z
$C_{(G1)}$–$H_{(G1)}$···$Cg_{(H)}$			2.79 Å, 154°	1/2–x, –1/2+y, 1/2–z
$C_{(G2)}$–$H_{(G2)}$···$Cg_{(H)}$			2.90 Å, 141°	x, y, z
			2.83 Å, 151°	x, y, z
H-bonding (D···A, D–H···A)	Non-classical	Non-classical	Non-classical	
$C_{(H)}$–$H_{(H)}$···$N_{(H)}$	2.77 Å, 103°	2.77 Å, 103°	2.91 Å, 102°	x, y, z
$C_{(H)}$–$H_{(H)}$···$N_{(H)}$	3.49 Å, 152°	3.47 Å, 152°		x, y, z
$C_{(H)}$–$H_{(H)}$···$N_{(H)}$	2.90 Å, 102°	2.91 Å, 102°	2.77 Å, 103°	x, y, z
$C_{(H)}$–$H_{(H)}$···$N_{(H)}$			3.34 Å, 144°	x, y, z
$C_{(H)}$–$H_{(H)}$···$N_{(H)}$	2.77 Å, 103°	2.77 Å, 103°	2.77 Å, 103°	x, y, z
$C_{(H)}$–$H_{(H)}$···$N_{(H)}$	2.90 Å, 102°	2.90 Å, 102°	2.91 Å, 102°	x, y, z
			Classical	
$N_{(H)}$–$H_{(H)}$···$N_{(G1)}$			2.42 Å, 167°	x, y, z
$N_{(H)}$–$H_{(H)}$···$N_{(G2)}$			2.33 Å, 158°	x, y, z
Short contacts (X···Z, X–Y···Z)				
$C_{(G1)}$–$H_{(G1)}$···$S_{(H)}$–$C_{(H)}$	2.93 Å, 145° (<)			–1/2+x, 1/2–y, –1/2+z
$C_{(G1)}$–$H_{(G1)}$···$C_{(H)}$–$S_{(H)}$	2.87 Å, 135° (<)			3/2–x, –1/2+y, 1/2–z
$C_{(G1)}$–$C_{(G1)}$···$S_{(H)}$–$C_{(H)}$		2.92 Å, 138° (<)		–1/2+x, 1/2–y, –1/2+z
$C_{(G2)}$–$H_{(G2)}$···$H_{(G2)}$–$C_{(G2)}$		2.27 Å, 108° (<)		1–x, 1–y, 1–z
$C_{(G2)}$–$H_{(G2)}$···$C_{(H)}$–$C_{(H)}$		2.68 Å, 157° (<<)		–1/2+x, 1/2–y, –1/2+z
$C_{(G2)}$–$H_{(G2)}$···$C_{(H)}$–$C_{(H)}$		2.88 Å, 152° (<)		3/2–x, –1/2-y, –1/2+z
$C_{(H)}$–$H_{(H)}$···$C_{(H)}$–$C_{(H)}$			2.76 Å, 122° (<)	1–x, 1–y, 1–z
$C_{(H)}$–$H_{(H)}$···$H_{(H)}$–$C_{(H)}$			2.30 Å, 175° (<)	1/2–x, 1/2+y, 1/2–z
$C_{(G2)}$–$H_{(G2)}$···$S_{(H)}$–$C_{(H)}$			2.94 Å, 121° (<)	1/2–x, 1/2+y, 1/2–z

[a]Distances denoted by < are contacts that measure less than the sum of the van der Waals radii of the atoms involved while those denoted by << is this sum minus 0.2 Å.

Table S185. Interactions present in complexes of **H$_1$** with furan, thiophene and pyrrole.[a]

Non-covalent interaction	**H$_1$**·furan	**H$_1$**·thiophene	**H$_1$**·pyrrole	Symmetry operation
π···π (H···H and H···G)	-	-	-	
CH···π (H···Cg, C–H···Cg)				
$C_{(H)}$–$H_{(H)}$···$Cg_{(H)}$	2.77 Å, 135°			x, y, z
$C_{(H)}$–$H_{(H)}$···$Cg_{(G2)}$	2.65 Å, 149°			3/2–x, –1/2+y, 1/2–z
$C_{(H)}$–$H_{(H)}$···$Cg_{(H)}$	2.79 Å, 136°			x, 1+y, z
$C_{(H)}$–$H_{(H)}$···$Cg_{(H)}$		2.75 Å, 135°		x, y, z
$C_{(H)}$–$H_{(H)}$···$Cg_{(G2)}$		2.67 Å, 148°		3/2–x, –1/2+y, 1/2–z
$C_{(H)}$–$H_{(H)}$···$Cg_{(H)}$		2.79 Å, 136°		x, 1+y, z
$C_{(H)}$–$H_{(H)}$···$Cg_{(H)}$			2.75 Å, 135°	x, y, z
$C_{(H)}$–$H_{(H)}$···$Cg_{(G2)}$			2.67 Å, 148°	3/2–x, –1/2+y, 1/2–z
$C_{(H)}$–$H_{(H)}$···$Cg_{(H)}$			2.76 Å, 136°	x, 1+y, z
H-bonding (D···A, D–H···A)	Non-classical	Non-classical	Non-classical	
$C_{(H)}$–$H_{(H)}$···$N_{(H)}$	2.76 Å, 103°	2.77 Å, 103°	2.77 Å, 103°	x, y, z
$C_{(H)}$–$H_{(H)}$···$N_{(H)}$	3.46 Å, 153°	3.43 Å, 152°	3.44 Å, 153°	x, y, z
$C_{(H)}$–$H_{(H)}$···$N_{(H)}$	2.91 Å, 102°	2.91 Å, 103°	2.91 Å, 103°	x, y, z
$C_{(H)}$–$H_{(H)}$···$N_{(H)}$	2.77 Å, 103°	2.77 Å, 103°	2.77 Å, 103°	x, y, z
$C_{(H)}$–$H_{(H)}$···$N_{(H)}$	2.89 Å, 102°	2.90 Å, 102°	2.90 Å, 102°	x, y, z
Short contacts (X···Z, X–Y···Z)				
$C_{(G2)}$–$H_{(G2)}$···$H_{(H)}$–$C_{(H)}$	2.36 Å, 126° (<)			x, y, z
		None		
			None	

[a]Distances denoted by < are contacts that measure less than the sum of the van der Waals radii of the atoms involved while those denoted by << is this sum minus 0.2 Å.

a)

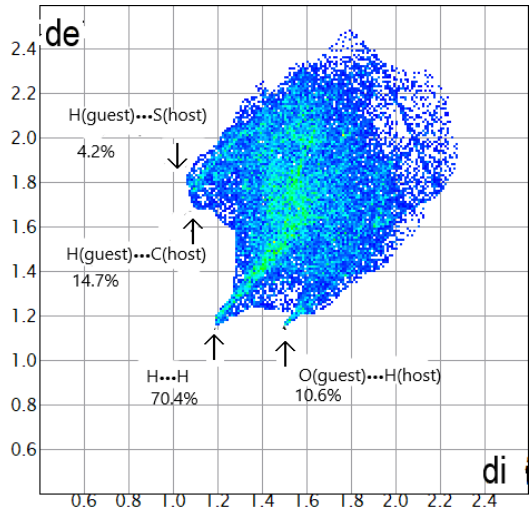

b)

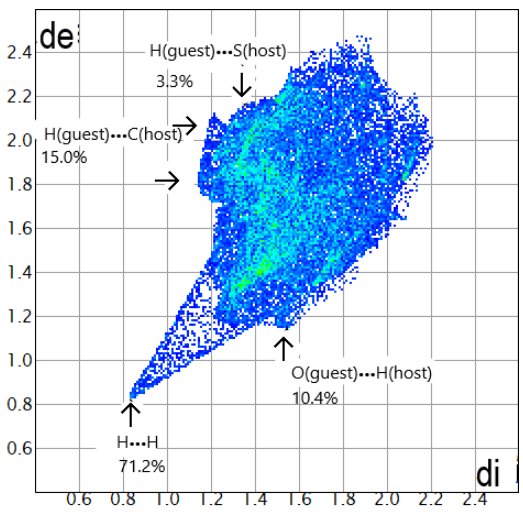

c)

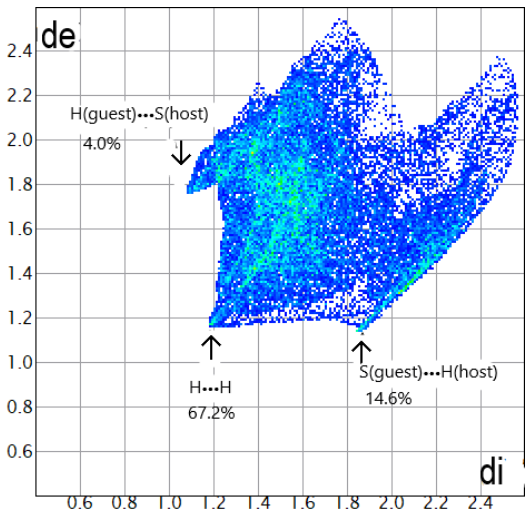
de
di
H(guest)···S(host)
4.0%
H···H
67.2%
S(guest)···H(host)
14.6%

d)

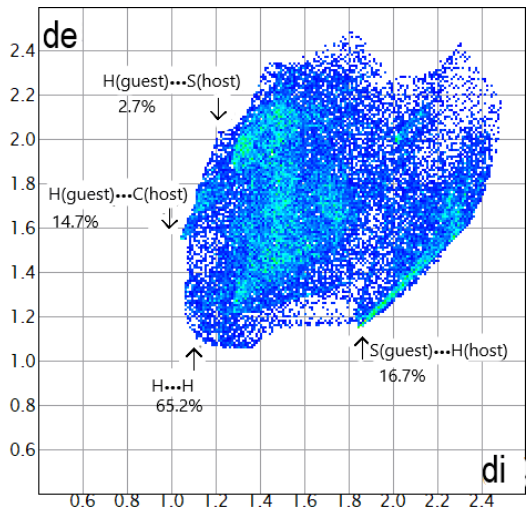
de
di
H(guest)···S(host)
2.7%
H(guest)···C(host)
14.7%
H···H
65.2%
S(guest)···H(host)
16.7%

e)

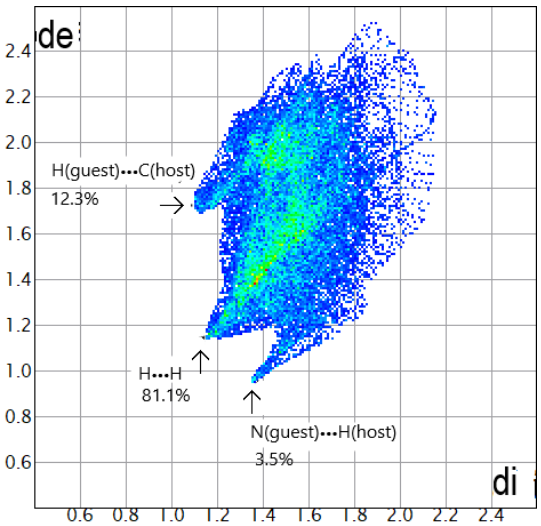
de
di
H(guest)···C(host)
12.3%
H···H
81.1%
N(guest)···H(host)
3.5%

f)

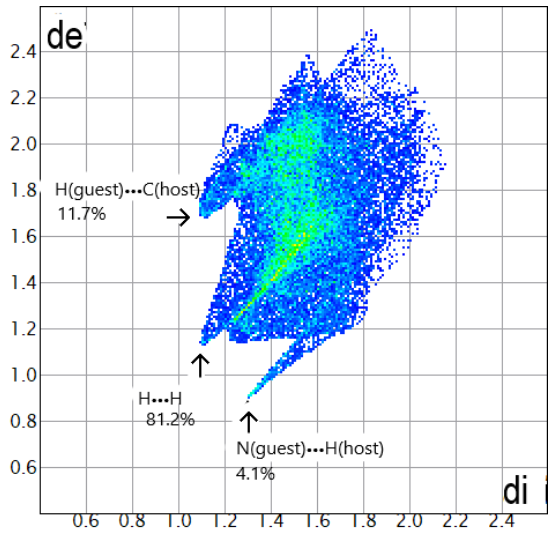
de
di
H(guest)···C(host)
11.7%
H···H
81.2%
N(guest)···H(host)
4.1%

g)

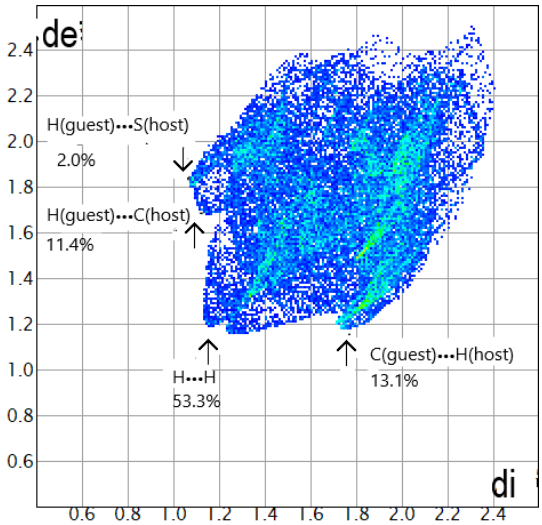
de
di
H(guest)···S(host)
2.0%
H(guest)···C(host)
11.4%
H···H
53.3%
C(guest)···H(host)
13.1%

h)

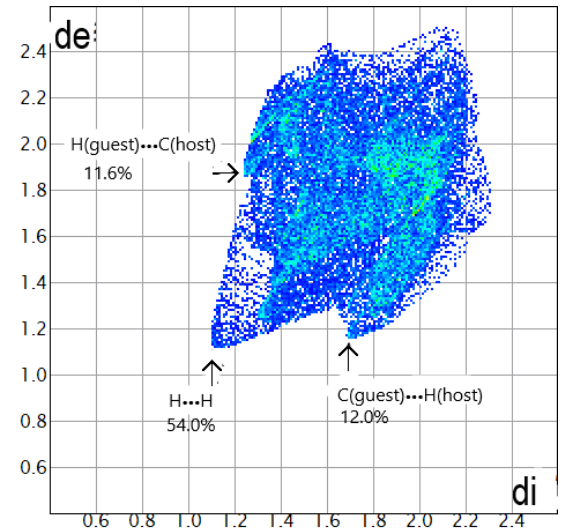
de
di
H(guest)···C(host)
11.6%
H···H
54.0%
C(guest)···H(host)
12.0%

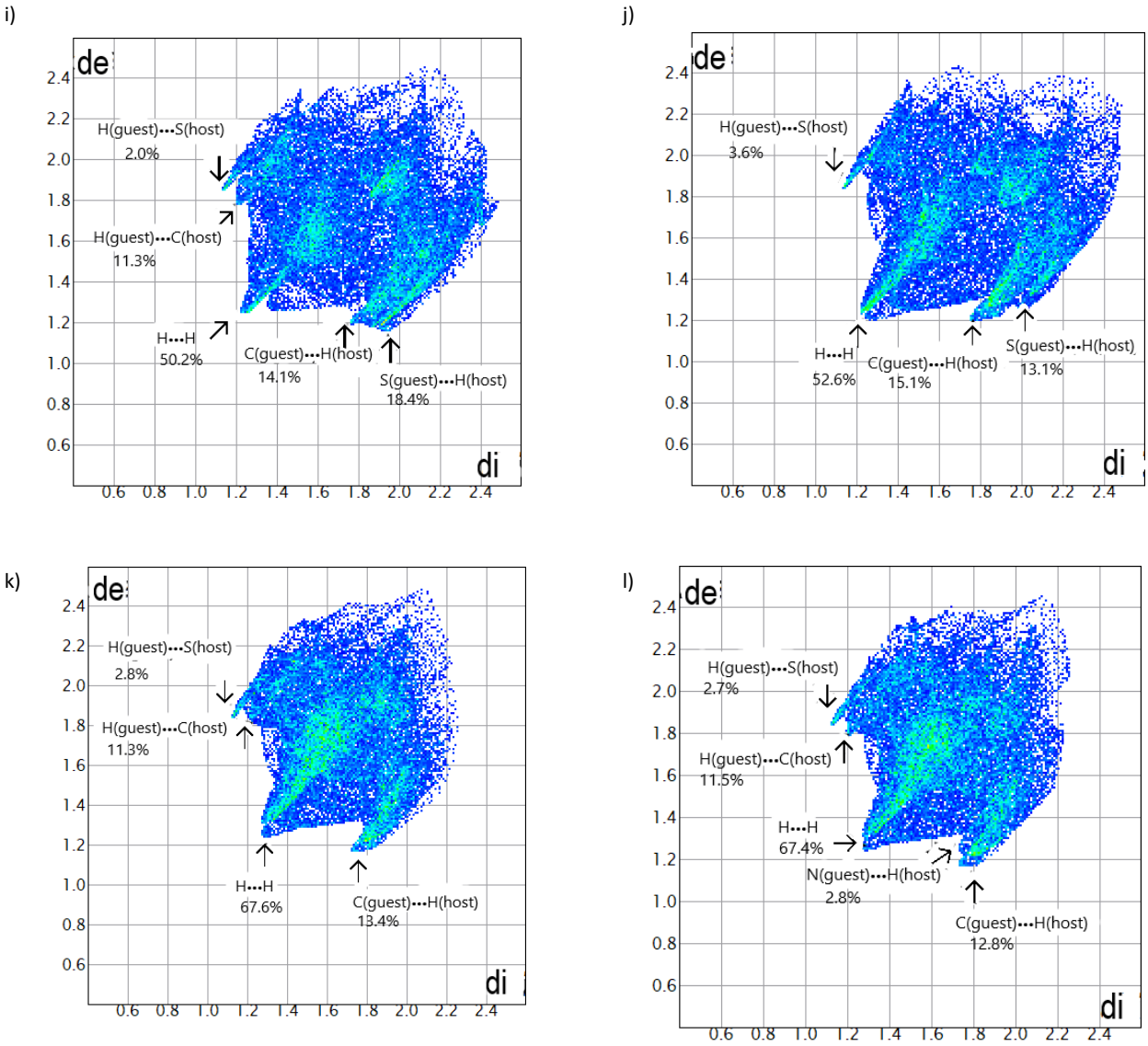

Figure S186. 2D Fingerprint plots for the inclusion compounds of **H_1** with guests a) THF (major component), b) THF (minor component), c) THT (major component), d) THT (minor component), e) pyrrolidine (major component), f) pyrrolidine (minor component), g) furan (major component), h) furan (minor component), i) thiophene (major component), j) thiophene (minor component), k) pyrrole (major component) and l) pyrrole (minor component).

a)

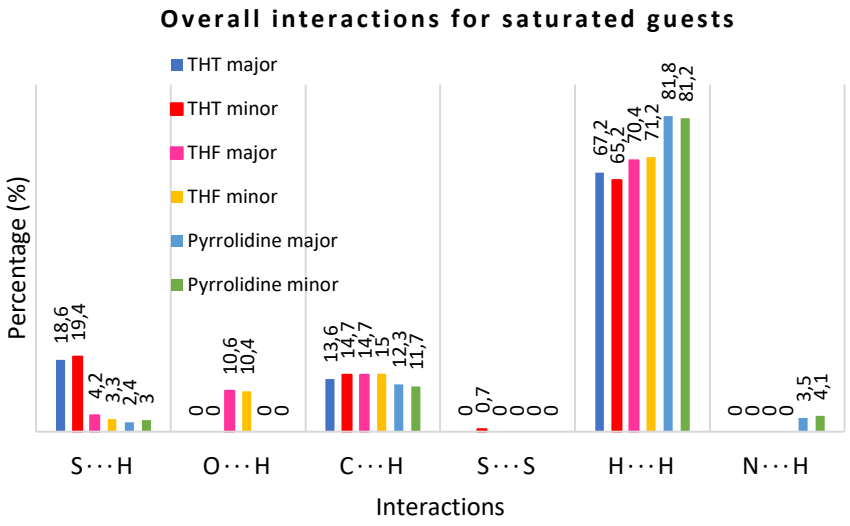

b)

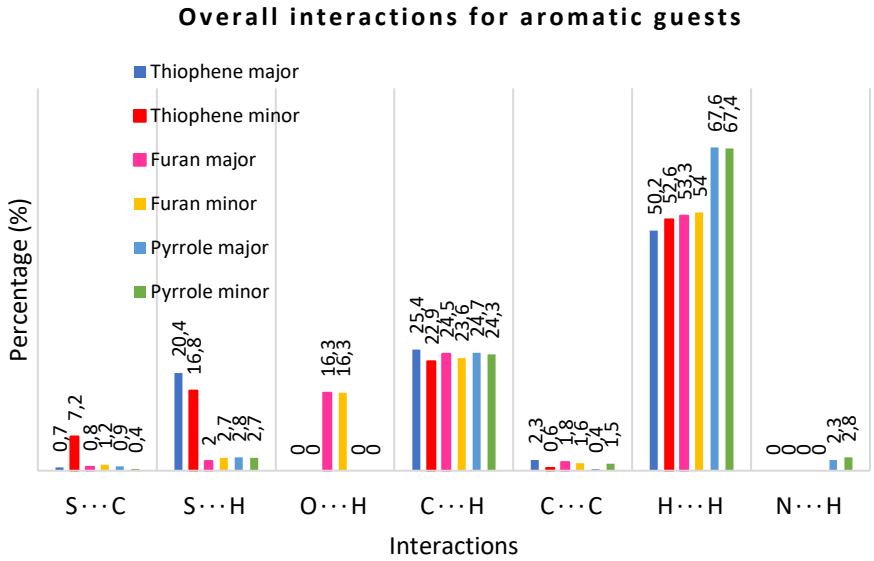

Figure S187. A graphical display emphasizing, quantitatively, the overall H···G/G···H interactions present in complexes of **H_1** with a) saturated guests and b) aromatic guests.

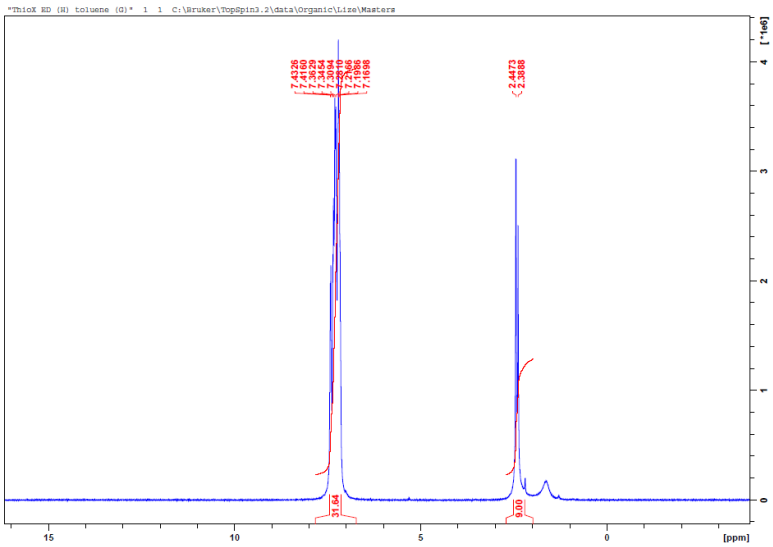

Figure S188. ^{1}H-NMR spectrum for **H$_1$**·TOL.

Table S189. Duplicate data for equimolar competition experiments of TOL, EB and CU with **H$_1$**

Comp:	Batch 1	Batch 2	Average	% e.s.d.s
TOL, EB	92.07:7.94	91.44:8.54	91.76:8.24	(0.31):(0.31)
TOL, CU	96.77:3.24	96.13:3.87	96.44:3.56	(0.32):(0.32)
EB, CU	62.09:37.91	63.70:36.30	62.90:37.10	(0.81):(0.81)
TOL, EB, CU	89.08:8.74:2.18	90.50:7.70:1.80	89.90:8.22:1.88	(0.71):(0.52):(0.19)

Table S190. K values for competition experiment of TOL/EB with **H$_1$**.[a,b]

TOL ml	TOL c	EB ml	EB c	K value
1	1	0	0	
0,74434	0,96978	0,25566	0,03022	11,0222483
0,55354	0,92547	0,44646	0,07453	10,0153186
0,43868	0,91253	0,56132	0,08747	13,3490607
0,34253	0,87077	0,65747	0,12923	12,9335409
0,18537	0,21562	0,81463	0,78438	1,20804602
0	0	1	1	9,70564289

[a]Abbreviations in the table include ml (mother liquor) and c (crystal).
[b]The average K value is highlighted in yellow.

Table S191. K values for competition experiment of TOL/CU with **H$_1$**.[a,b]

TOL ml	TOL c	CU ml	CU c	K value
1	1	0	0	
0,73171	0,98423	0,26829	0,01577	22,8839189
0,48083	0,9712	0,51917	0,0288	36,4111351
0,40474	0,96633	0,59526	0,03367	42,2097635
0,3137	0,94882	0,6863	0,05118	40,5586069
0,16365	0,51494	0,83635	0,48506	5,42541817
0	0	1	1	29,4977685

[a]Abbreviations in the table include ml (mother liquor) and c (crystal).
[b]The average K value is highlighted in yellow.

Table S192. K values for competition experiment of EB/CU with **H_1**.[a,b]

EB ml	EB c	CU ml	CU c	K value
1	1	0	0	
0,77593	0,87745	0,22407	0,12255	2,06761766
0,54517	0,70261	0,45483	0,29739	1,97108394
0,4639	0,63175	0,5361	0,36825	1,982549
0,35935	0,5158	0,64065	0,4842	1,89915204
0,18003	0,2538	0,81997	0,7462	1,54913567
0	0	1	1	1,89390766

[a]Abbreviations in the table include ml (mother liquor) and c (crystal).
[b]The average K value is highlighted in yellow.

Table S193. Crystallographic data for **H_1**·TOL and **H_1**·EB.[a]

Non-covalent interaction	**H_1**·TOL	**H_1**·EB	Symmetry
π···π (H···H and H···G)	4.361(1) – 5.919(1) Å 5.045(1) – 5.919(1) Å [8]	4.521(1) – 5.997(1) Å 4.999(1) – 5.997(1) Å [7]	
CH···π (H···H and H···G) (H···Cg, C–H···Cg) $C_{(H)}$–$H_{(H)}$···$Cg_{(H)}$ $C_{(H)}$–$H_{(H)}$···$Cg_{(H)}$ $C_{(H)}$–$H_{(H)}$···$Cg_{(H)}$ $C_{(G)}$–$H_{(G)}$···$Cg_{(H)}$ $C_{(H)}$–$H_{(H)}$···$Cg_{(H)}$ $C_{(G1)}$–$H_{(G1)}$···$Cg_{(H)}$ $C_{(G2)}$–$H_{(G2)}$···$Cg_{(H)}$	 2.80 Å, 134° 2.71 Å, 147° 2.84 Å, 138° 2.66 Å, 162°	 2.96 Å, 139° 2.99 Å, 155° 2.88 Å, 163°	 x, y, z 3/2–x, –1/2+y, 1/2–z x, 1+y, z 3/2–x, –1/2+y, 1/2–z x, y,1+z 1+x, y, –1+z 1+x, y, –1+z
H-bonding (intramolecular) (D···A, D–H···A) $C_{(H)}$–$H_{(H)}$···$N_{(H)}$ $C_{(H)}$–$H_{(H)}$···$N_{(H)}$ $C_{(H)}$–$H_{(H)}$···$N_{(H)}$ $C_{(H)}$–$H_{(H)}$···$N_{(H)}$ $C_{(H)}$–$H_{(H)}$···$N_{(H)}$ $C_{(H)}$–$H_{(H)}$···$N_{(H)}$	Non-classical 2.64(2) Å, 103° 3.443(2) Å, 152° 2.906(2) Å, 102° 2.766(2) Å, 103° 2.897(2) Å, 102°	Non-classical 2.761(2) Å, 103° 3.432(2) Å, 154° 2.904(2) Å, 102° 3.456(2) Å, 151° 2.764(2) Å, 103° 2.899(2) Å, 102°	 x, y, z x, y, z x, y, z x, y, z x, y, z x, y, z
Other short contacts (host/ guest and guest/guest) (X···Z, X–Y···Z) $C_{(H)}$–$H_{(H)}$···$H_{(G)}$–$C_{(G)}$ $C_{(H)}$–$H_{(H)}$···$H_{(G)}$–$C_{(G)}$ $C_{(H)}$–$H_{(H)}$···$C_{(H)}$–$C_{(H)}$ $C_{(G2)}$–$C_{(G2)}$···$H_{(G2)}$–$C_{(G2)}$	 2.35Å, 138°(<) 2.37Å, 129°(<)	 2.86 Å, 145° (<) 1.89 Å, 131° (<<)	 3/2–x, 1/2+y, 1/2–z x, y, z –x, 1–y, 1–z 2–x, 1–y, –z

[a]Distances denoted by < are contacts that measure less than the sum of the van der Waals radii of the atoms involved while those denoted by << is this sum minus 0.2 Å.

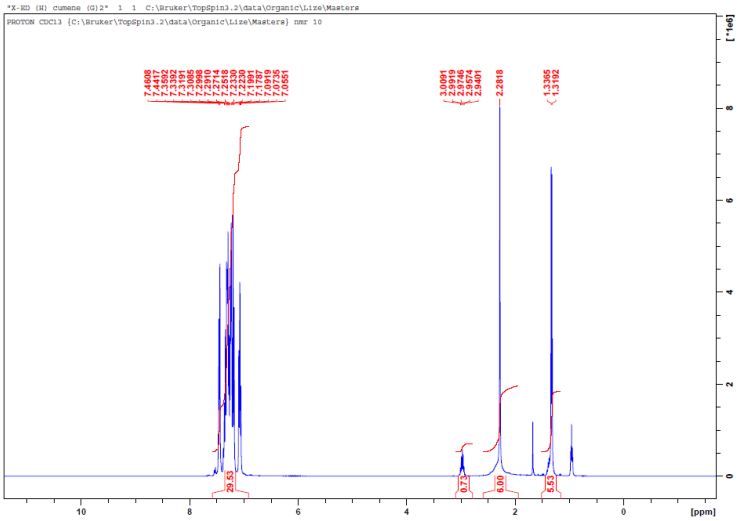

Figure S194. [1]H-NMR spectrum for **H₂**·CU.

Table S195. Duplicate data for equimolar competition experiments of TOL, EB and CU with **H₂**.

Guests:	Batch 1	Batch 2	Batch 3	Average	% e.s.d.s
TOL, EB	*a*	*a*	*a*	-	-
TOL, CU	*a*	*a*	*a*	-	-
EB, CU	49.19:50.81	46.51:53.50	49.98:50.02	48.56:51.44	(1.48):(1.48)
TOL, EB, CU	*a*	*a*	*a*	-	-

[a]No inclusion occurred

Table S196. K values for competition experiment of CU/EB with **H₂**.[a,b]

CU ml	CU c	EB ml	EB c	K value
1	1	0	0	
0,78946	0,8187	0,21054	0,1813	1,20429109
0,55886	0,62882	0,44114	0,37118	1,33725796
0,47916	0,50022	0,52084	0,49978	1,08794253
0,36782	0,35244	0,63218	0,64756	1,069028811
0,19814	0,15228	0,80186	0,84772	1,375571503
0	0	1	1	1,214818379

[a]Abbreviations in the table include ml (mother liquor) and c (crystal).

[b]The average K value is highlighted in yellow.

Table S197. Crystallographic data for **H_2**·CU.[a]

Non-covalent interaction	**H_2**·CU	Symmetry
π···π (H···H and H···G)	3.981(1)–5.977(1) Å	
CH···π (H···Cg, C–H···Cg)		
$C_{(H)}$–$H_{(H)}$···$Cg_{(H)}$	2.85 Å, 90°	x, y, z
$C_{(H)}$–$H_{(H)}$···$Cg_{(H)}$	2.96 Å, 84°	x, y, z
$C_{(H)}$–$H_{(H)}$···$Cg_{(H)}$	2.99 Å, 80°	x, y, z
$C_{(H)}$–$H_{(H)}$···$Cg_{(H)}$	2.74 Å, 94°	x, y, z
$C_{(H)}$–$H_{(H)}$···$Cg_{(H)}$	2.94 Å, 143°	x, –1+y, z
$C_{(H)}$–$H_{(H)}$···$Cg_{(G)}$	3.00 Å, 117°	–1+x, –1+y, z
$C_{(H)}$–$H_{(H)}$···$Cg_{(H)}$	2.68 Å, 105°	x, y, z
$C_{(H)}$–$H_{(H)}$···$Cg_{(H)}$	2.97 Å, 151°	1+x, y, z
$C_{(H)}$–$H_{(H)}$···$Cg_{(H)}$	2.77 Å, 104°	x, y, z
$C_{(H)}$–$H_{(H)}$···$Cg_{(H)}$	2.69 Å, 156°	1–x, 1–y, 1–z
H-bonding (intramolecular) (D···A, D–H···A)	Non-classical	
$C_{(H)}$–$H_{(H)}$···$N_{(H)}$	2.790(3) Å, 102°	x, y, z
$C_{(H)}$–$H_{(H)}$···$N_{(H)}$	2.758 (3) Å, 102°	x, y, z
Otherhort contacts (host/guest and guest/guest) (X···Z, X–Y···Z)		
$C_{(H)}$–$C_{(H)}$···$H_{(H)}$–$C_{(H)}$	2.87 Å, 112° (<)	–x, 1–y, 1–z
$C_{(H)}$–$C_{(H)}$···$C_{(G1)}$–$C_{(G1)}$	3.33 Å, 112° (<)	–1+x, –1+y, z
$C_{(H)}$–$H_{(H)}$···$H_{(H)}$–$C_{(H)}$	2.35 Å, 131° (<)	x, y, z
$C_{(H)}$–$H_{(H)}$···$C_{(G1)}$–$C_{(G1)}$	2.88 Å, 131° (<)	1–x, 1–y, –z
$C_{(H)}$–$H_{(H)}$···$H_{(H)}$–$C_{(H)}$	2.78 Å, 101° (<)	–1+x, y, z
$C_{(G1)}$–$H_{(G1)}$···$C_{(H)}$–$O_{(H)}$	2.83 Å, 169° (<)	1+x, y, z
$C_{(G2)}$–$H_{(G2)}$···$C_{(H)}$–$O_{(H)}$	2.72 Å, 150° (<)	1–x, 1–y, 1–z

[a]Distances denoted by < are contacts that measure less than the sum of the van der Waals radii of the atoms involved.

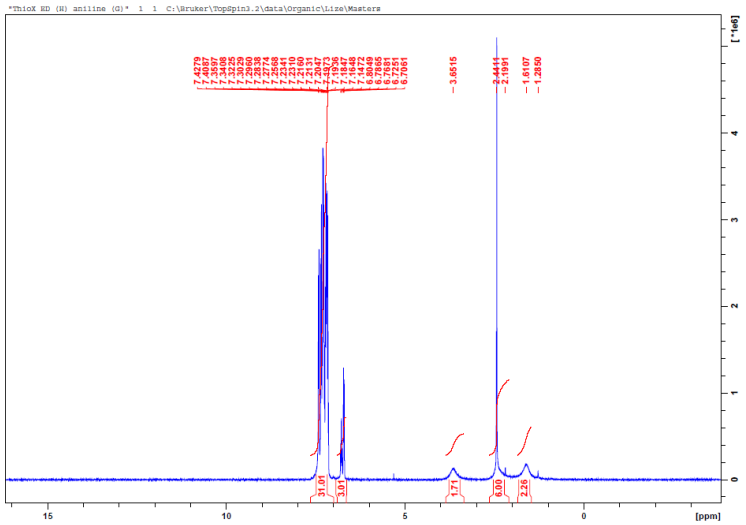

Figure S198. ^{1}H-NMR spectrum for **H_1**·ANL.

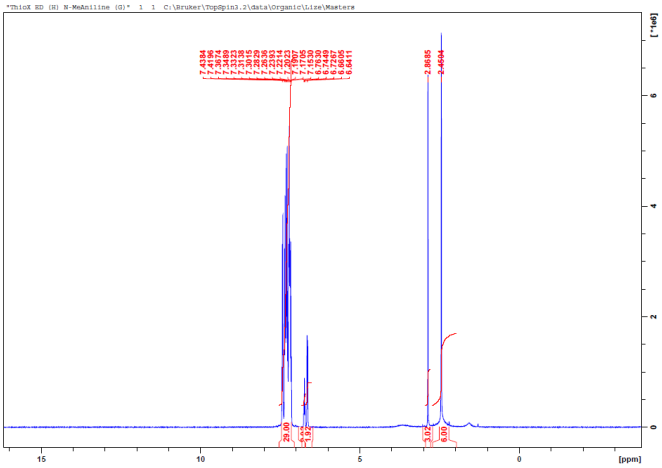

Figure S199. ^{1}H-NMR spectrum for **H$_1$**·NMA.

Table S200. Duplicate data for equimolar competition experiments of ANL, NMA and NNDMA with **H$_1$**.

Comp:	Batch 1	Batch 2	Average	% e.s.d.s
ANL, NMA	90.00:10.00	88.24:11.76	89.12:10.88	(0.88):(0.88)
ANL, NNDMA	93.77: 6.23	90.69:9.31	92.23:7.77	(1.54):(1.54)
NMA, NNDMA	[a]	[a]	-	-
ANL, NMA, NNDMA	89.50:5.73:4.78	88.90:5.91:5.20	89.20:5.82:4.98	(0.30):(0.09):(0.21)

[a]No inclusion occurred.

Table S201. K values for competition experiment of ANL/NMA with **H$_1$**.[a,b]

ANL ml	ANL c	NMA ml	NMA c	K values
1	1	0	0	
0,74531	0,92048	0,25469	0,07952	3,95560512
0,5402	0,94585	0,4598	0,05415	14,8675085
0,43038	0,91012	0,56962	0,08988	13,4019731
0,34044	0,90494	0,65956	0,09506	18,4431757
0,14723	0,02795	0,85277	0,97205	6,004421768
0	0	1	1	11,33453683

[a]Abbreviations in the table include ml (mother liquor) and c (crystal).
[b]The average K value is highlighted in yellow.

Table S202. K values for competition experiment of ANL/NNDMA with **H$_1$**.[a,b]

ANL ml	ANL c	NNDMA ml	NNDMA c	K values
1	1	0	0	
0,7598	0,93357	0,2402	0,06643	4,44279576
0,57566	0,90274	0,42434	0,09726	6,84189397
0,47608	0,91477	0,52392	0,08523	11,811484
0,34071	0,86149	0,65929	0,13851	12,0354053
0,22098	0,70008	0,77902	0,29992	8,22882605
0	0	1	1	8,67208101

[a]Abbreviations in the table include ml (mother liquor) and c (crystal).
[b]The average K value is highlighted in yellow.

Table S203. Crystallographic data for **H_1**·ANL and **H_1**·NMA.[a,b]

Non-covalent interaction	**H_1**·ANL	**H_1**·NMA	Symmetry
π···π (H···H and H···G) H···G major H···G minor	4.379(1) –5.935(3) Å 4.885(1) – 5.927(1) Å [7] 4.714(5) – 5.935(3) Å [8]	4.658(1) – 5.932(1) Å 4.935(1) – 5.893 (1) Å [7]	
CH···π (H···Cg, C–H···Cg)			
$C_{(H)}$–$H_{(H)}$···$Cg_{(H)}$	2.78 Å, 134°		x, y, z
$C_{(H)}$–$H_{(H)}$···$Cg_{(H)}$	2.71 Å, 149°		3/2–x, –1/2+y, 1/2–z
$C_{(H)}$–$H_{(H)}$···$Cg_{(H)}$	2.84 Å, 137°		x, 1+y, z
$C_{(H)}$–$H_{(H)}$···$Cg_{(H)}$	2.93 Å, 133°		x, y, z
$C_{(H)}$–$H_{(H)}$···$Cg_{(H)}$		2.94 Å, 139°	x, y, 1+z
$C_{(G)}$–$H_{(G)}$···$Cg_{(H)}$		2.93 Å, 140°	–x, 1–y, 1–z
X–Y···π (Y···Cg, X–Y···Cg)			
$C_{(guest)}$–$N_{(guest)}$···$Cg_{(host)}$	3.518 (4) Å, 109°		2–x, 1–y,1–z
H-bonding (D···A, D–H···A)	Non-classical	Non-classical	
$C_{(H)}$–$H_{(H)}$···$N_{(H)}$	2.766(2) Å, 103°	2.767(2) Å, 103°	x, y, z
$C_{(H)}$–$H_{(H)}$···$N_{(H)}$	3.436(2) Å, 152°	3.466(2) Å, 158°	x, y, z
$C_{(H)}$–$H_{(H)}$···$N_{(H)}$	2.913(2) Å, 102°	2.910(2) Å, 102°	x, y, z
$C_{(H)}$–$H_{(H)}$···$N_{(H)}$		3.454(2) Å, 148°	x, y, z
$C_{(H)}$–$H_{(H)}$···$N_{(H)}$	2.775(2) Å, 103°	2.768(2) Å, 103°	x, y, z
$C_{(H)}$–$H_{(H)}$···$N_{(H)}$	2.896(2) Å, 102°	2.900(2) Å, 102°	x, y, z
Other short contacts (host/ guest and guest/guest) (X···Z, X–Y···Z)			
$C_{(H)}$–$H_{(H)}$···$C_{(H)}$–$C_{(H)}$	2.89Å, 153°(<)		x, 1+y, z
$C_{(H)}$–$H_{(H)}$···$H_{(G1)}$–$C_{(G1)}$	2.34Å, 134°(<)		–1/2+x, ½-y, –1/2+z
$C_{(H)}$–$H_{(H)}$···$H_{(G2)}$–$C_{(G2)}$	2.30Å, 149°(<)		–1/2+x, 1/2–y, -1/2+z
$C_{(G2)}$–$N_{(G2)}$···$N_{(G2)}$–$C_{(G2)}$	2.3890Å, 125.1(6)°(<<)		2–x, –y, 1–z
$C_{(G2)}$–$H_{(G2)}$···$H_{(H)}$–$C_{(H)}$	2.35Å, 138°(<)		1–x, 1–y, 1-z
$C_{(G2)}$–$N_{(G2)}$···$C_{(H)}$–$C_{(H)}$	3.244Å, 105.5(2)°(<)		x, 1+y, z
$C_{(H)}$–$H_{(H)}$···$H_{(G1)}$–$C_{(G1)}$		2.37 Å, 143° (<)	x, 1+y, 1+z

[a]Number of H-G interactions indicated in parentheses.

[b]Distances denoted by < are contacts that measure less than the sum of the van der Waals radii of the atoms involved while those denoted by << is this sum minus 0.2 Å.

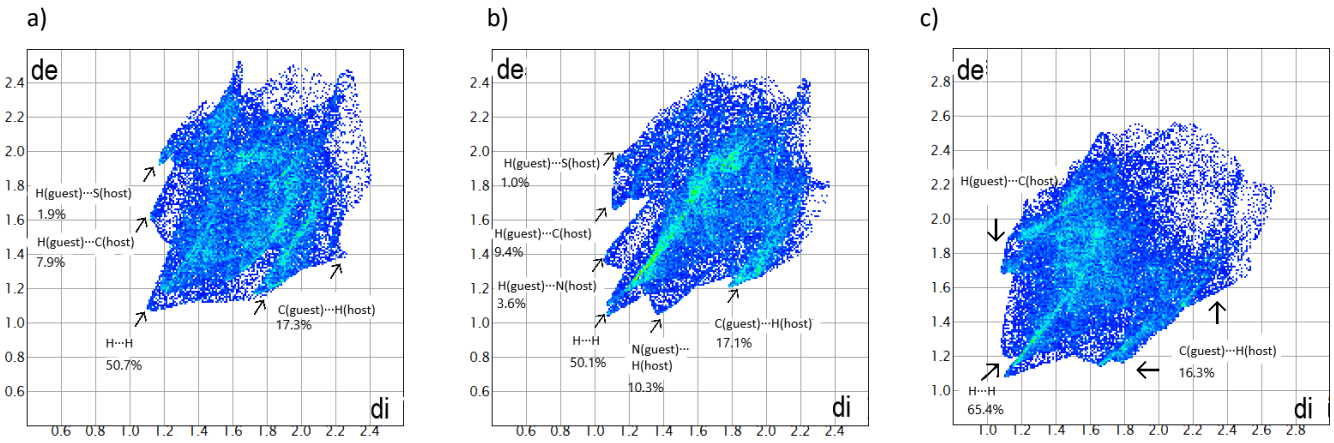

Figure S204. 2D Fingerprint plots for the inclusion compounds of **H_1** with guests a) ANL (major component), b) ANL (minor component) and c) NMA.

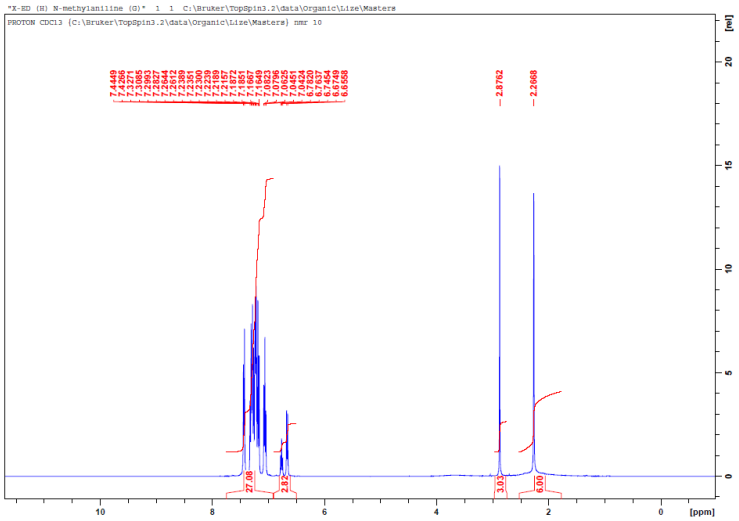

Figure S205. ^{1}H-NMR spectrum for **H_2**·NMA.

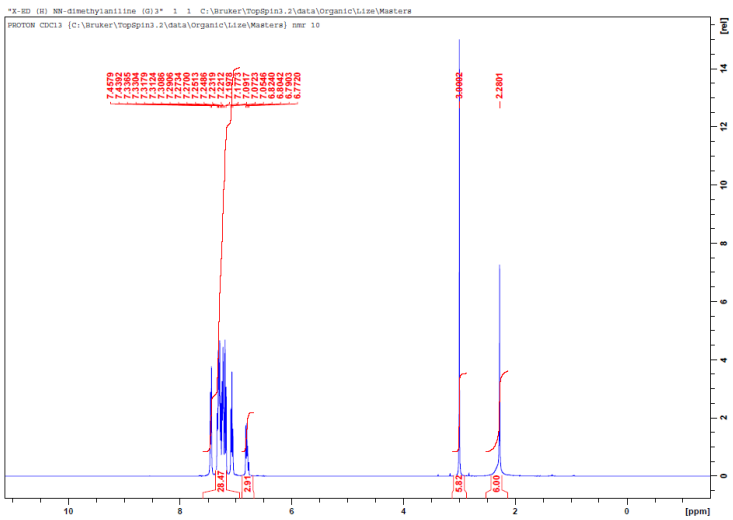

Figure S206. ^{1}H-NMR spectrum for **H_2**·NNDMA.

Table S207. Duplicate data for equimolar competition experiments of ANL, NMA and NNDMA with **H_2**.

Guests:	Batch 1	Batch 2	Average	% e.s.d.s
ANL, NMA	24.03:75.97	21.74:78,26	22.89:77.12	(1.15):(1.15)
ANL, NNDMA	1.35:98.65	1.28:98.72	1.32:98.69	(0.03):(0.03)
NMA, NNDMA	7.57:92.43	5.77:94.23	6.67:93.33	(0.90):(0.90)
ANL, NMA, NNDMA	1.99:5.99:92.01	5.38:6.17:88.46	3.69:6.08:90.24	(1.70):(0.09):(1.78)

Table S208. K values for competition experiment of ANL/NNDMA with **H_2**.[a,b]

NNDMA ml	NNDMA c	ANL ml	ANL c	K value
1	1	0	0	
0,84303	0,98557	0,15697	0,01443	12,7172958
0,63608	0,96269	0,36392	0,03731	14,7623465
0,56845	0,93178	0,43155	0,06822	10,369087
0,41709	0,94891	0,58291	0,05109	25,9573796
0,23338	0,60841	0,76662	0,39159	5,10365443
0	0	1	1	13,7819527

[a]Abbreviations in the table include ml (mother liquor) and c (crystal).
[b]The average K value is highlighted in yellow.

Table S209. K values for competition experiment of NMA/NNDMA with **H_2**.[a,b]

NNDMA ml	NNDMA c	NMA ml	NMA c	K value
1	1	0	0	
0,81391	0,96842	0,18609	0,03158	7,01129557
0,61555	0,93217	0,38445	0,06783	8,5832119
0,5	0,93524	0,5	0,06476	14,4416306
0,43407	0,43577	0,56593	0,56423	1,00694117
0,20745	0,04099	0,79255	0,95901	6,123954937
0	0	1	1	7,433406844

[a]Abbreviations in the table include ml (mother liquor) and c (crystal).
[b]The average K value is highlighted in yellow.

Table S210. K values for competition experiment of ANL/NMA with **H_2**.[a,b]

NMA ml	NMA c	ANL ml	ANL c	K value
1	1	0	0	
0,84382	0,94534	0,15618	0,05466	3,20106145
0,63729	0,80534	0,36271	0,19466	2,35464249
0,5147	0,79952	0,4853	0,20048	3,76022993
0,46543	0,75464	0,53457	0,24536	3,53253333
0,22835	0,18754	0,77165	0,81246	1,282002087
0	0	1	1	2,826093856

[a]Abbreviations in the table include ml (mother liquor) and c (crystal).
[b]The average K value is highlighted in yellow.

Table S211. Crystallographic data for **H_2**·NMA and **H_2**·NNDMA.[a]

Non-covalent interaction	**H_2**·NMA	**H_2**·NNDMA	Symmetry
π···π (H···H and H···G) H···G interactions	4.090(1)–5.930(1) Å 4.735(1)–5.930(1) Å [6]	3.919(2)–5.839(3) Å 4.977(3)–5.839(3) Å [8]	
CH···π (H···Cg, C–H···Cg)			
$C_{(H)}$–$H_{(H)}$···$Cg_{(H)}$	2.91 Å, 77°		x, y, z
$C_{(H)}$–$H_{(H}$ ···$Cg_{(H)}$	2.57 Å, 97°		x, y, z
$C_{(H)}$–$H_{(H)}$···$Cg_{(G)}$	2.95 Å, 127°		x, 1+y, z
$C_{(H)}$–$H_{(H)}$···$Cg_{(H)}$	2.61 Å, 163°		2–x, 2–y, 2–z
$C_{(H)}$–$H_{(H)}$···$Cg_{(H)}$	2.83 Å, 104°		x, y, z
$C_{(G)}$–$H_{(G)}$···$Cg_{(H)}$	2.89 Å, 139°		x, y, z
$C_{(H)}$–$H_{(H)}$···$Cg_{(H)}$		3.00 Å, 142°	x, –1+y, z
$C_{(H)}$–$H_{(H)}$···$Cg_{(H)}$		2.93 Å, 142°	1+x, y, z
$C_{(H)}$–$H_{(H)}$···$Cg_{(G)}$		2.95 Å, 141°	1–x, 1–y,1–z
$C_{(H)}$–$H_{(H)}$···$Cg_{(H)}$		2.90 Å, 141°	1–x, 2–y, -z
$C_{(H)}$–$H_{(H)}$···$Cg_{(H)}$		2.57 Å, 106°	x, y, z
H-bonding (D···A, D–H···A)	Non-classical	Non-classical	
$C_{(H)}$–$H_{(H)}$···$N_{(H)}$	2.804(1) Å, 102°	2.770(2) Å, 103°	x, y, z
Other short contacts (host/ guest and guest/guest) (X···Z, X–Y···Z)			
$C_{(H)}$–$H_{(H)}$···$H_{(G)}$–$C_{(G)}$	2.32 Å, 144° (<)		2-x, 1–y, 1–z
$C_{(H)}$–$H_{(H)}$···$O_{(H)}$–$C_{(H)}$	2.64 Å, 165° (<)		1+x, 1+y, z
$C_{(H)}$–$H_{(H)}$···$C_{(H)}$–$C_{(H)}$		2.81 Å, 136° (<)	1–x, 2–y, -z
$N_{(H)}$–$H_{(H)}$···$H_{(G)}$–$C_{(G)}$		2.26 Å, 168° (<)	–1+x, 1+y, z
$C_{(H)}$–$H_{(H)}$···$C_{(G)}$–$N_{(G)}$		2.75 Å, 146° (<)	1–x, 1–y, 1–z

[a]Distances denoted by < are contacts that measure less than the sum of the van der Waals radii of the atoms involved.

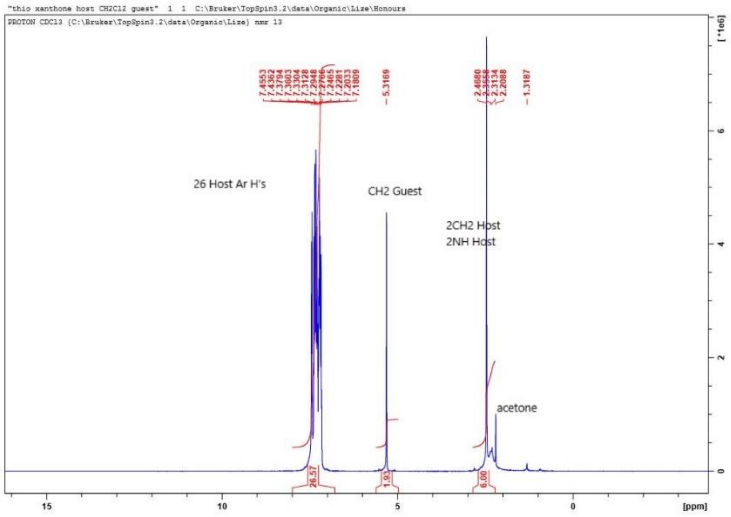

Figure S212. ^{1}H-NMR spectrum for **H$_1$**·DCM.

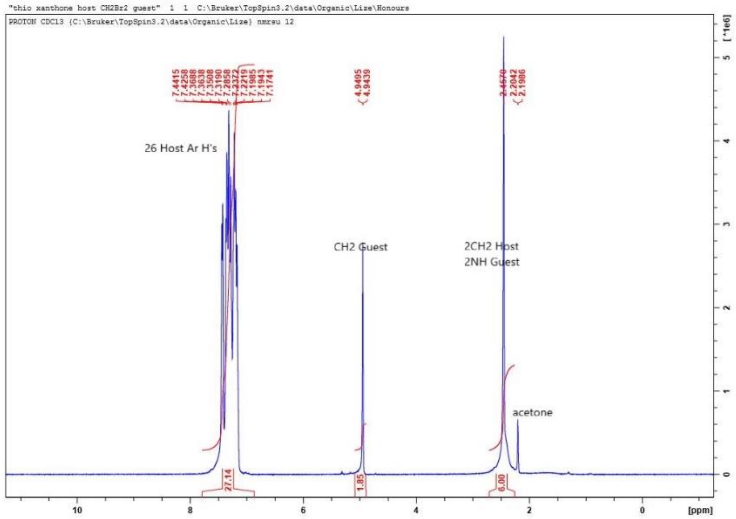

Figure S213. ^{1}H-NMR spectrum for **H$_1$**·DBM.

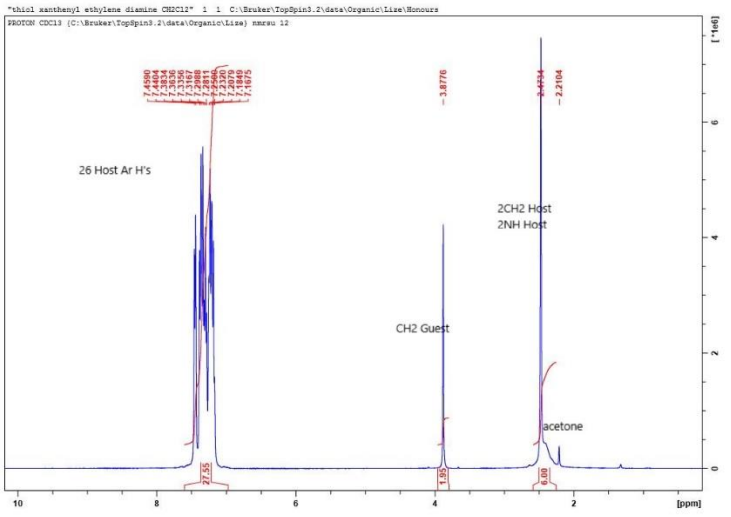

Figure S214. ^{1}H-NMR spectrum for **H$_1$**·DIM.

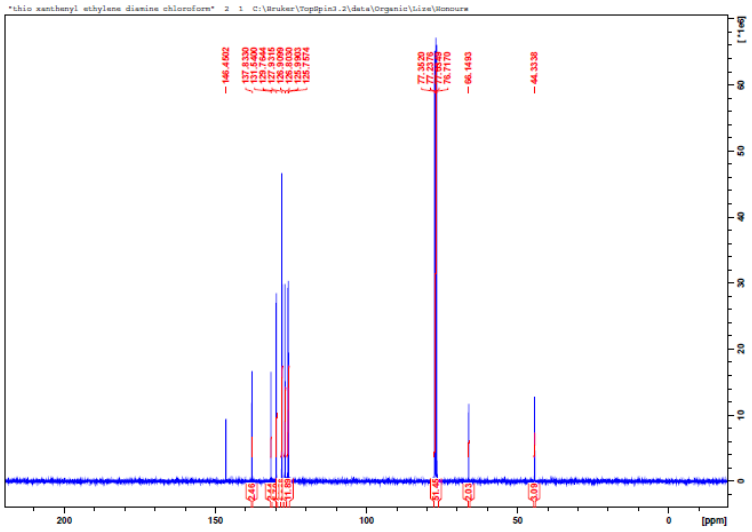

Figure S215. ^{1}H-NMR spectrum for **H$_1$**·chloroform.

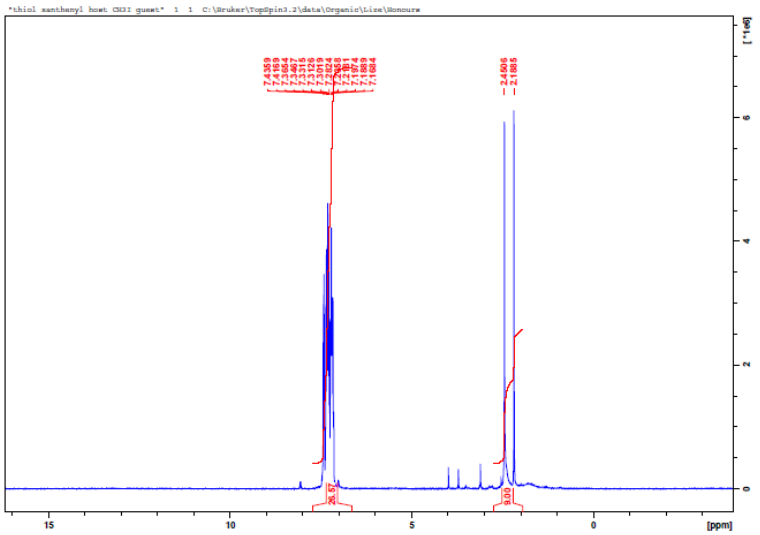

Figure S216. ^{1}H-NMR spectrum for **H$_1$**·iodomethane.

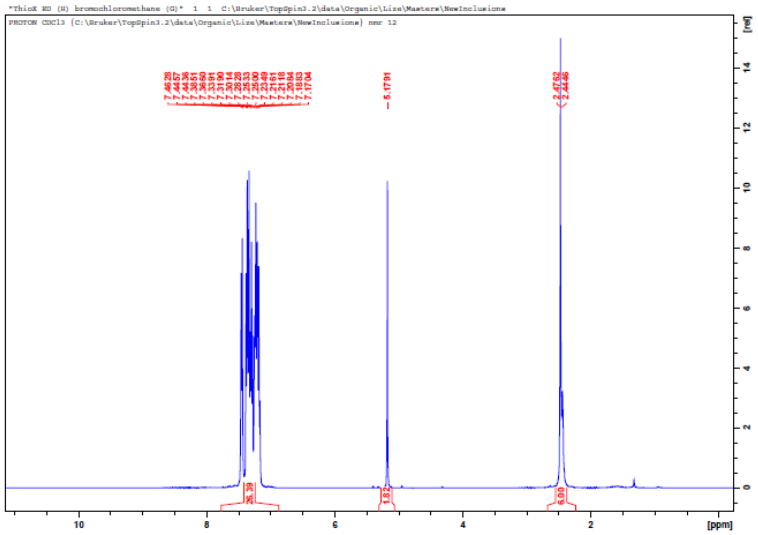

Figure S217. ^{1}H-NMR spectrum for **H$_1$**·bromochloromethane.

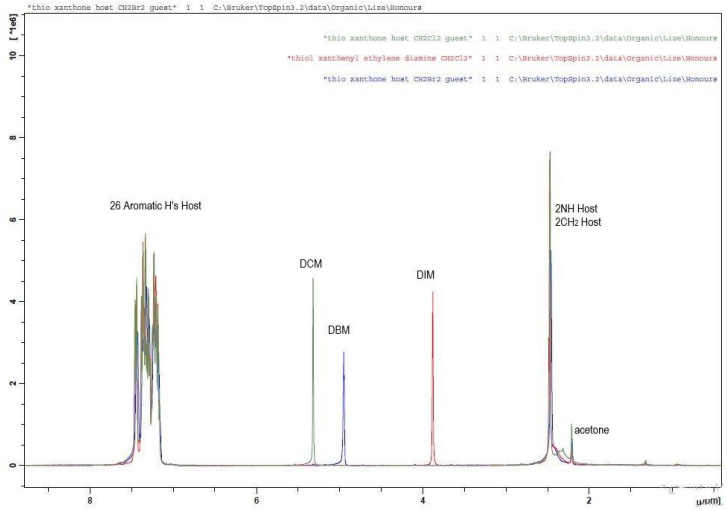

Figure S218. [1]H-NMR spectrum for mixed complex with all three dihaloalkane guests.

Table S219. Results of triplicate competition experiments using host and various equimolar mixtures of the guests[a,b]

Guests:	Batch 1	Batch 2	Batch 3	Average	e.s.d.s
DCM, DBM	22.80:77.20	28.02:71.98	26.83:73.17	22.35:77.65	(2.23):(2.23)
DCM, DIM	33.85:66.15	35.43:64.57	36.13:63.87	35.14:64.86	(0.95):(0.95)
DIM, DBM	36.27:63.73	36.90:63.10	35.45:64.55	35.94:64.06	(0.35):(0.35)
DCM, DBM, DIM	16.29:46.07:37.64	15.15:45.74:38.11	19.44:47.22:33.33	16.29:46.23:37.48	(1.42):(0.63):(1.77)

[a]Ratios determined using [1]H-NMR spectroscopy with $CDCl_3$ as solvent.
[b]Experiments were conducted in triplicate.

Table S220. K values for competition experiment of DIM/DCM with **H_1**.[a,b]

DIM ml	DIM c	DCM ml	DCM c	K-value
1	1	0	0	
0,86	0,76	0,14	0,24	1,939849624
0,69	0,68	0,31	0,32	1,04743833
0,66	0,66	0,34	0,34	1
0,5	0,59	0,5	0,41	1,43902439
0,28	0,44	0,72	0,56	2,020408163
0	0	1	1	1,489344102

[a]Abbreviations in the table include ml (mother liquor) and c (crystal).
[b]The average K value is highlighted in yellow.

Table S221. K values for competition experiment of DBM/DIM with **H_1**.[a,b]

DBM ml	DBM c	DIM ml	DIM c	K value
1	1	0	0	
0,7937	0,8449	0,2063	0,1551	1,41591232
0,6	0,7005	0,4	0,2995	1,55926544
0,5	0,6455	0,5	0,3545	1,82087447
0,3968	0,5531	0,6032	0,4469	1,88140794
0,1905	0,326	0,8095	0,674	2,05532061
0	0	1	1	1,74655616

[a]Abbreviations in the table include ml (mother liquor) and c (crystal).
[b]The average K value is highlighted in yellow.

Table S222. K values for competition experiment of DBM/DCM with **H₁**.[a,b]

DBM ml	DBM c	DCM ml	DCM c	K value
1	1	0	0	
0,8205	0,9071	0,1795	0,0929	2,1361184
0,75	0,8609	0,25	0,1391	2,0630242
0,5215	0,7317	0,4785	0,2683	2,50230366
0,4444	0,6541	0,5556	0,3459	2,36418672
0,3056	0,5269	0,6944	0,4731	2,53064725
0	0	1	1	2,31925605

[a]Abbreviations in the table include ml (mother liquor) and c (crystal).
[b]The average K value is highlighted in yellow.

Table S223. Summary of H···H interactions of inclusion compounds.[a]

Interaction	**H₁**·DCM	**H₁**·DBM	**H₁**·DIM
π···π	4.30–5.78Å [17]	4.27–5.79Å [17]	4.25–5.95Å [16]
CH···π	None	None	None
Non-classical H-bonding	2.76–3.47Å, 102-152˚ [5]	2.76–3.46Å, 102–152˚ [6]	2.76–3.68Å, 102–149˚ [6]
Other short contacts	2.79Å, 152˚ [1]	2.87Å, 148˚ [1]	2.83Å, 145˚ [1]

[a]The number of contacts are indicated in square brackets.

a)

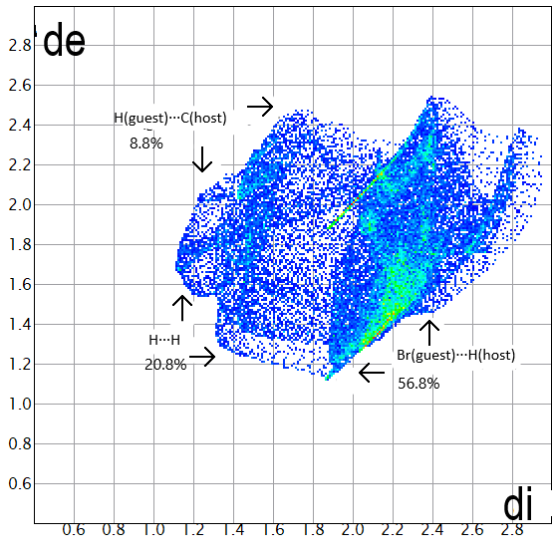

b)

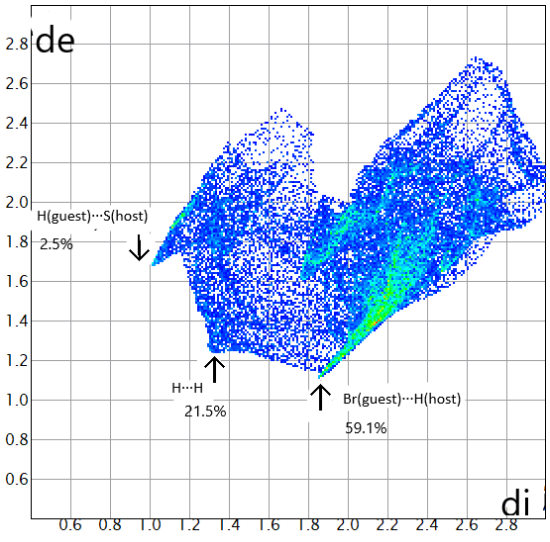

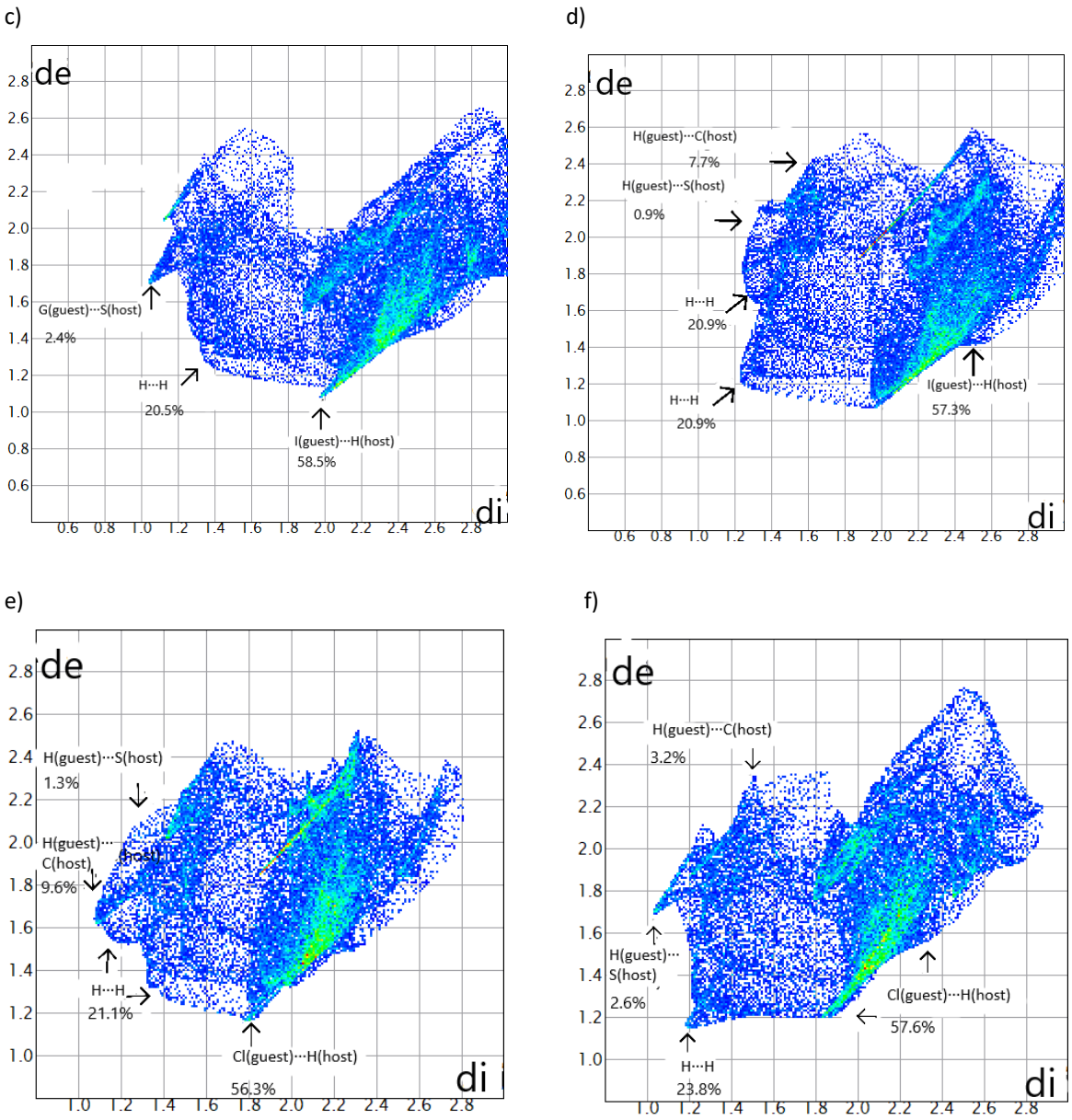

Figure 224. Includes 2D fingerprint for complexes with guests a) DBM major, b) DBM minor, c) DIM major, d) DIM minor, e) DCM major and f) DCM minor after Hirshfeld surface analyses.

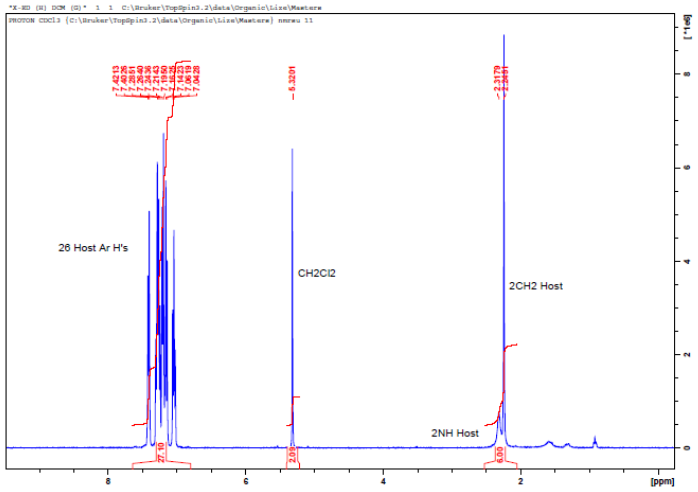

Figure S225. ^{1}H-NMR spectrum for **H₂**·2(DCM).

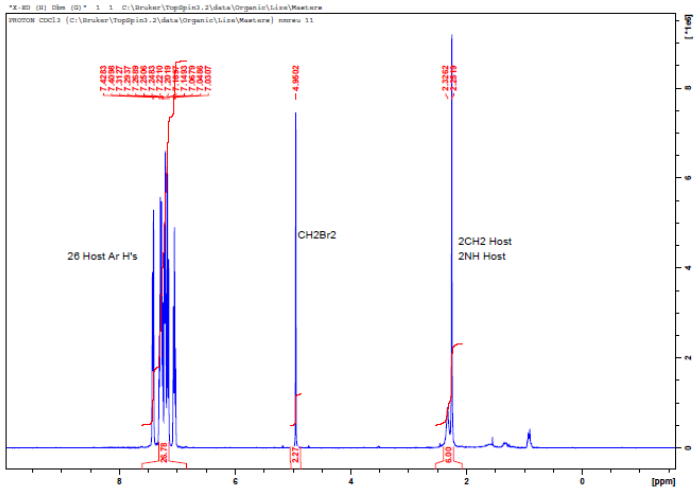

Figure S226. ^{1}H-NMR spectrum for **H₂**·2(DBM).

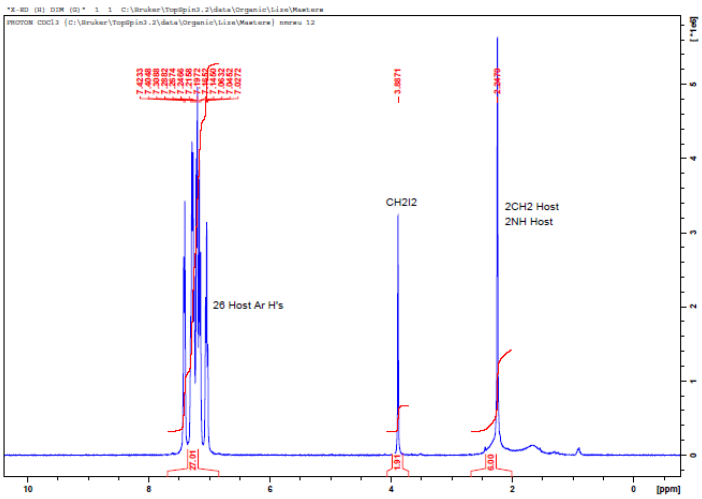

Figure S227. ^{1}H-NMR spectrum for **H₂**·DIM.

Table S228. Results of duplicate competition experiments using host and various equimolar mixtures of the guests[a,b]

Guests	Batch 1	Batch 2	Average	% e.s.d.s
DCM, DBM	36.44:63.56	40.48:59.52	38.46:61.54	(2.02):(2.02)
DCM, DIM	77.52:22.48	78.06:21.94	77.79:22.21	(0.27):(0.27)
DIM, DBM	15.70:84.30	15.98:84.02	15.84:84.16	(0.14):(0.14)
DCM, DBM, DIM	31.79:54.30:13.91	39.57:49.13:11.30	35.68:51.72:12.61	(3.89):(2.59):(1.31)

Table S229. K values for competition experiment of DBM/DIM with **H_2**.[a,b]

DBM ml	DBM c	DIM ml	DIM c	K value
1	1	0	0	
0,78	0,95	0,22	0,05	5,35897436
0,59	0,88	0,41	0,12	5,0960452
0,49	0,84	0,51	0,16	5,46428571
0,39	0,8	0,61	0,2	6,25641026
0,19	0,31	0,81	0,69	1,91533181
0	0	1	1	4,81820947

[a]Abbreviations in the table include ml (mother liquor) and c (crystal).
[b]The average K value is highlighted in yellow.

Table S230. K values for competition experiment of DBM/DCM with **H_2**.[a,b]

DBM ml	DBM c	DCM ml	DCM c	K value
1	1	0	0	
0,8	0,82	0,2	0,18	1,13888889
0,61	0,68	0,39	0,32	1,35860656
0,51	0,64	0,49	0,36	1,708061
0,41	0,53	0,59	0,47	1,62272963
0,21	0,37	0,79	0,63	2,20937264
0	0	1	1	1,60753174

[a]Abbreviations in the table include ml (mother liquor) and c (crystal).
[b]The average K value is highlighted in yellow.

Table S231. K values for competition experiment of DCM/DIM with **H_2**.[a,b]

DCM ml	DCM c	DIM ml	DIM c	K values
1	1	0	0	
0,81	0,88	0,19	0,12	1,72016461
0,55	0,86	0,45	0,14	5,02597403
0,46	0,78	0,54	0,22	4,16205534
0,35	0,66	0,65	0,34	3,60504202
0,21	0,25	0,79	0,75	1,25396825
0	0	1	1	3,15344085

[a]Abbreviations in the table include ml (mother liquor) and c (crystal).
[b]The average K value is highlighted in yellow.

a)

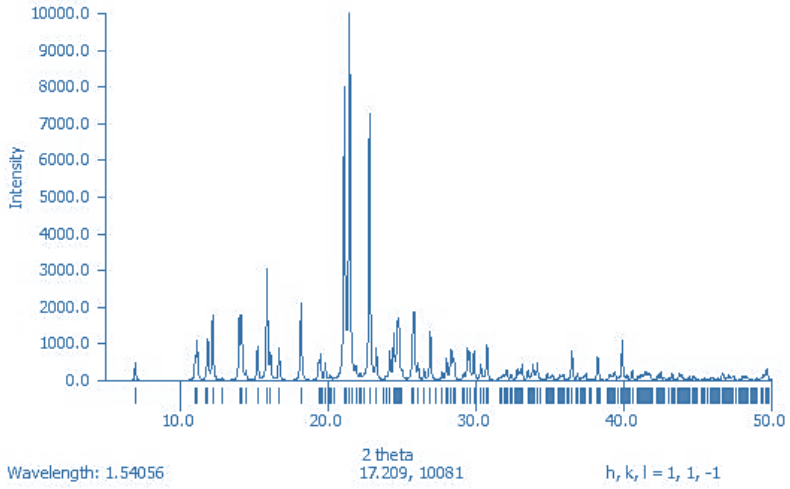

b)

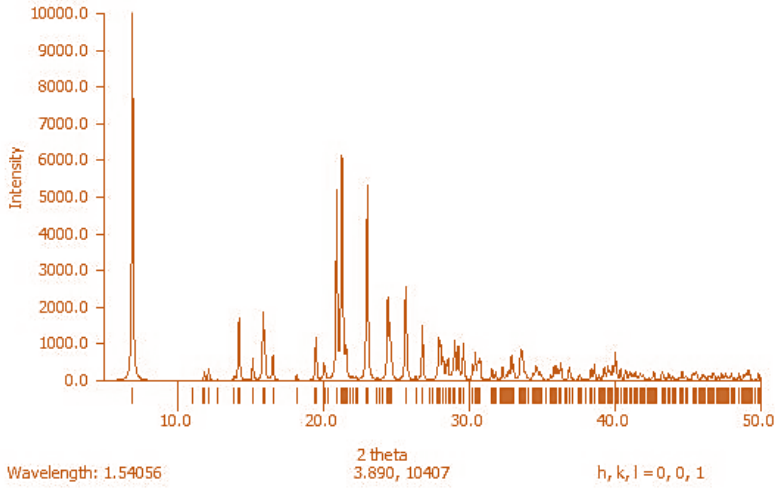

c)

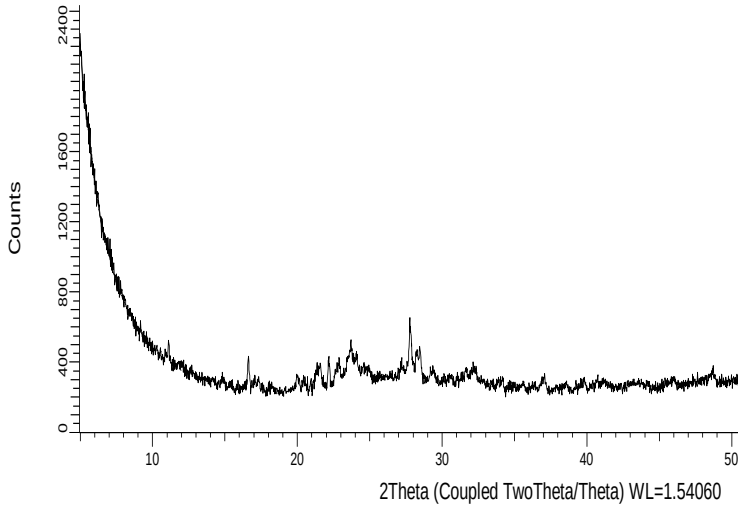

Cu tube with 1.54184 [Å] with a time/step of 0.4000

d)

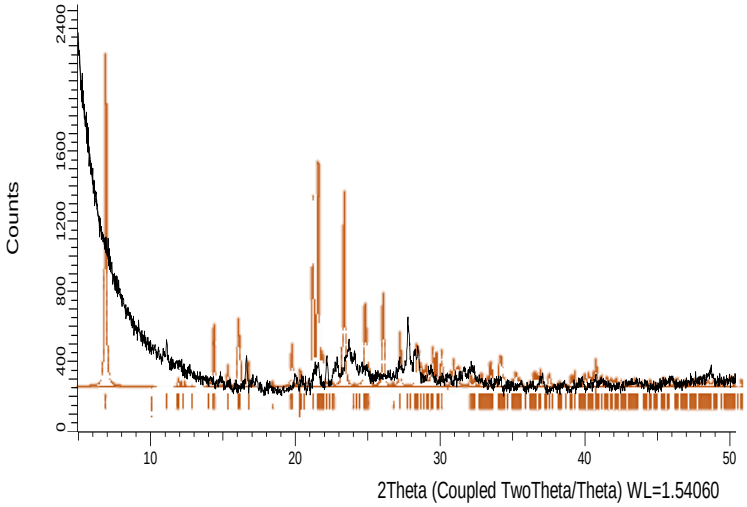

Figure S232. PXRD patterns of a) **H₂**·2(DCM), b) **H₂**·2(DBM) [which were generated using Mercury software], c) **H₂**·DIM and d) overlaid depiction of all three patterns.

Table S233. Summary of H···H interactions of inclusion compounds.[a]

Interaction	**H₂**·2(DCM)	**H₂**·2(DCM)
π-π	None	None
CH···π	2.62-2.82Å, 106-145˚ [2]	2.61-2.81Å, 106-143˚ [2]
Non-classical H-bonding	2.79-3.64Å, 102-156˚ [2]	2.78-3.72Å, 102-154˚ [2]
Short contacts	2.62Å, 140˚ [1]	2.70-2.87Å, 118-136˚ [3]

[a]The number of contacts are indicated in square brackets.

a)

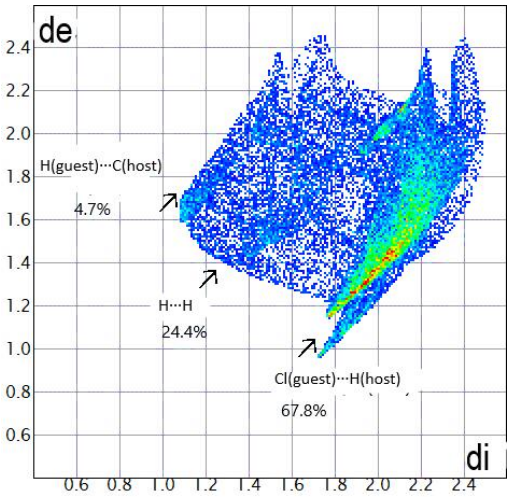

b)

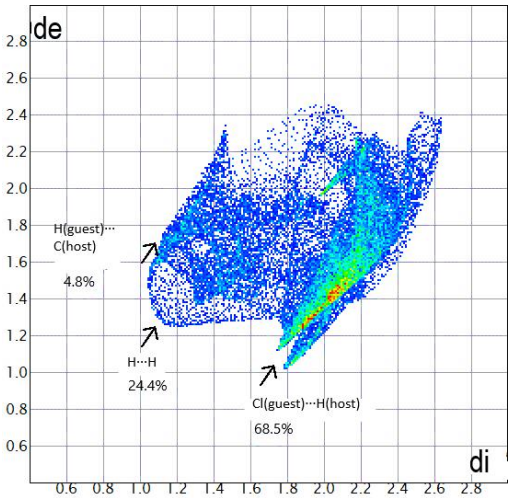

c)

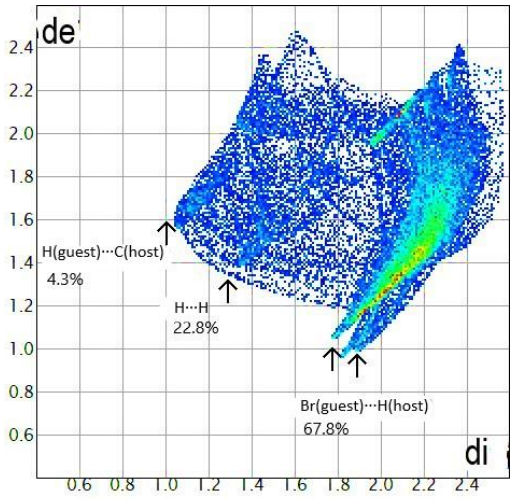

d)

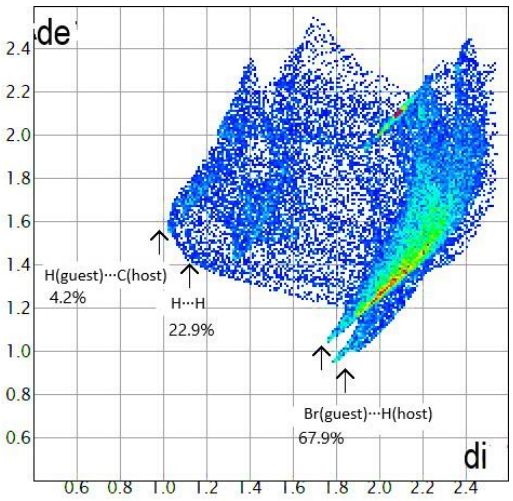

Figure S234. Include 2D fingerprint plots for complexes involving guests a) DCM major component, b) DCM minor component, c) DBM major component and (d) DBM minor component.

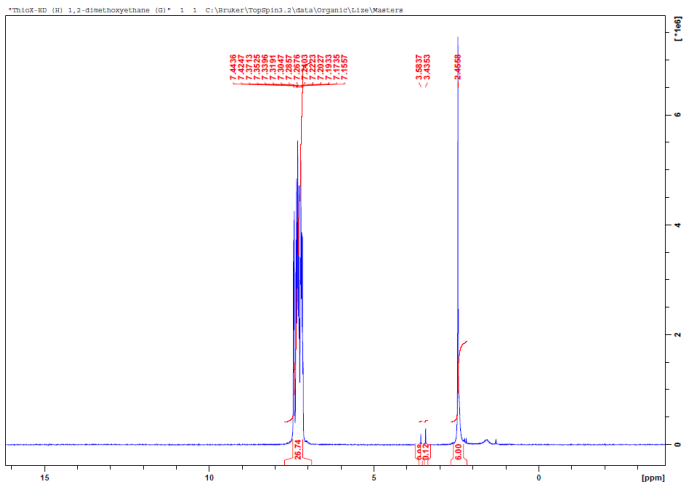

Figure S235. ^{1}H-NMR spectrum for **H$_1$**·1,2-dimethoxyethane.

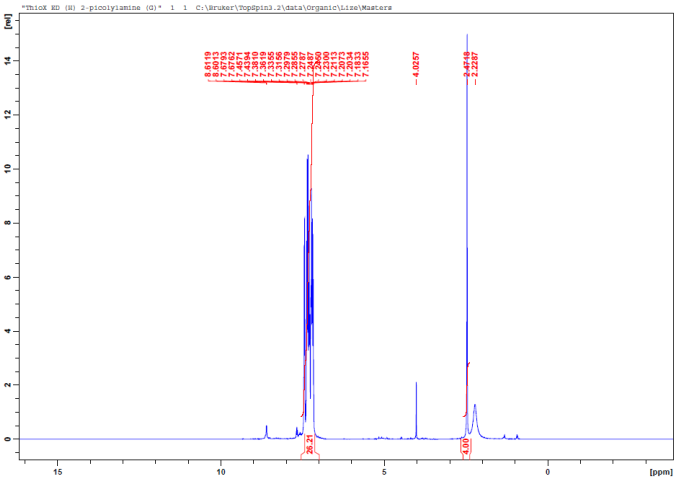

Figure S236. ^{1}H-NMR spectrum for **H$_1$**·2-picolylamine.

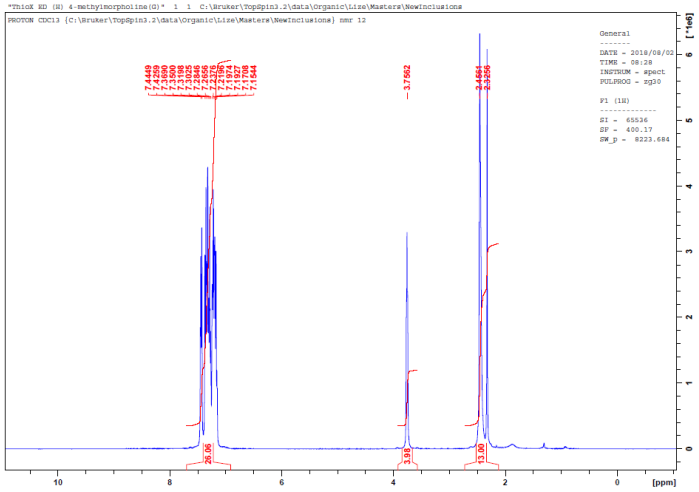

Figure S237. ^{1}H-NMR spectrum for **H$_1$**·4-methylmorpholine.

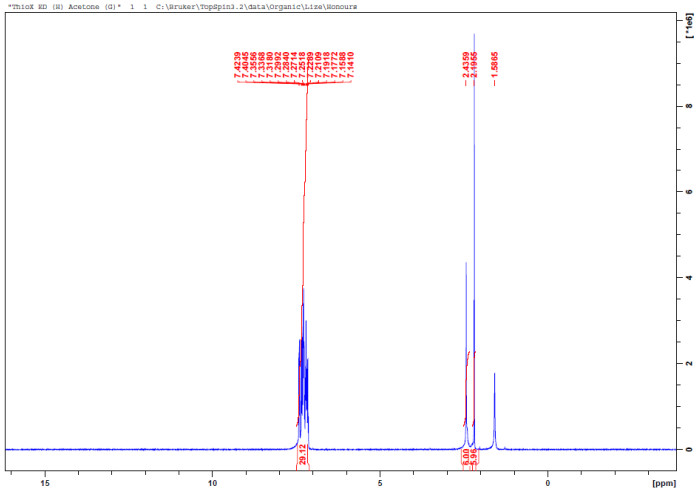

Figure S238. ^{1}H-NMR spectrum for **H$_1$**·acetone.

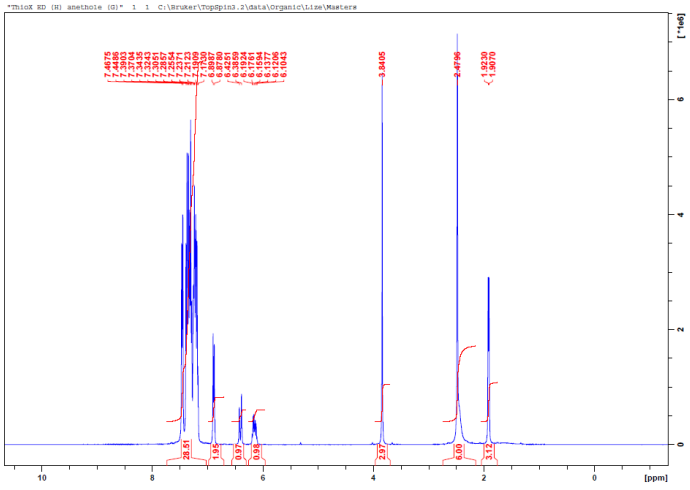

Figure S239. ^{1}H-NMR spectrum for **H$_1$**·anethole.

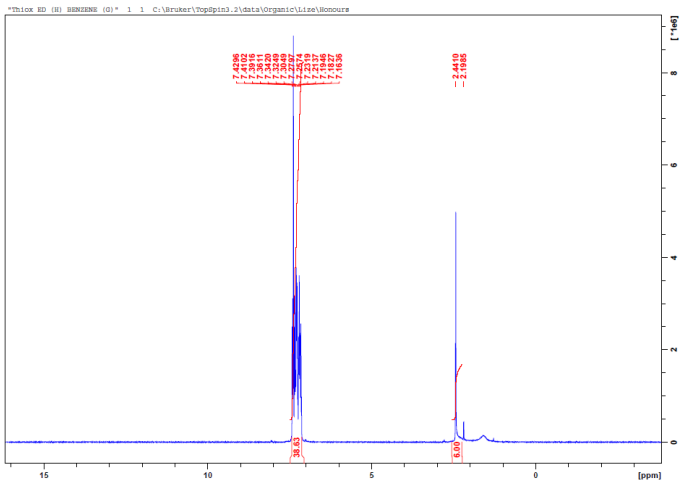

Figure S240. ^{1}H-NMR spectrum for **H$_1$**·benzene.

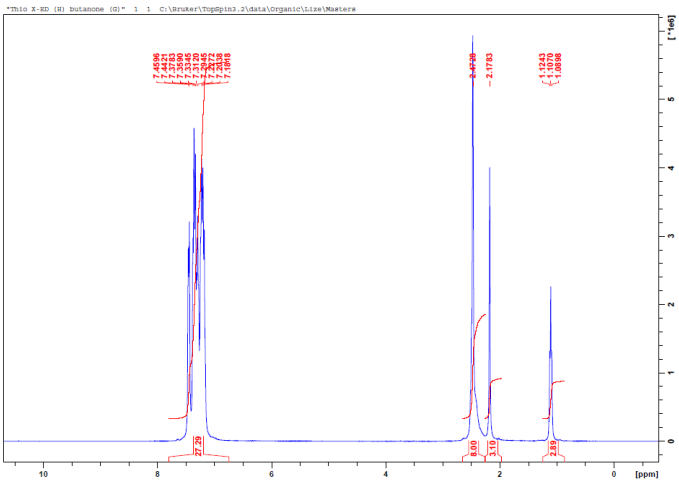

Figure S241. ^{1}H-NMR spectrum for **H$_1$**·butanone.

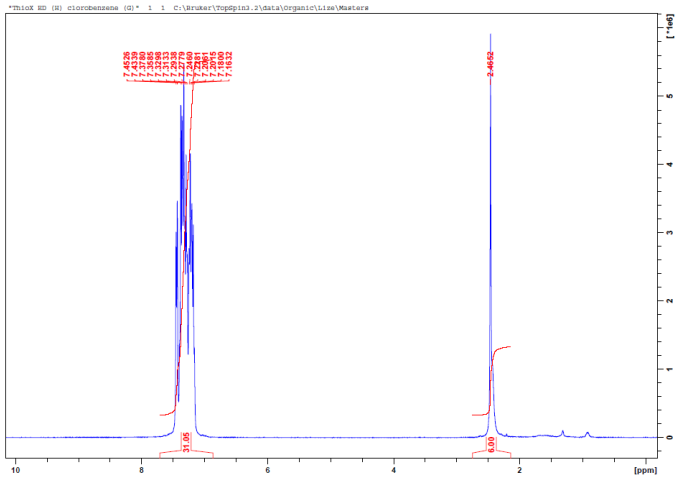

Figure S242. ^{1}H-NMR spectrum for **H$_1$**·chlorobenzene.

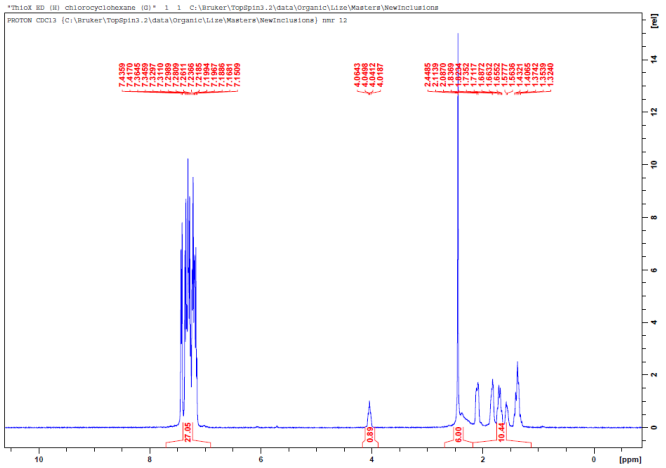

Figure S243. ^{1}H-NMR spectrum for **H$_1$**·chlorocyclohexane.

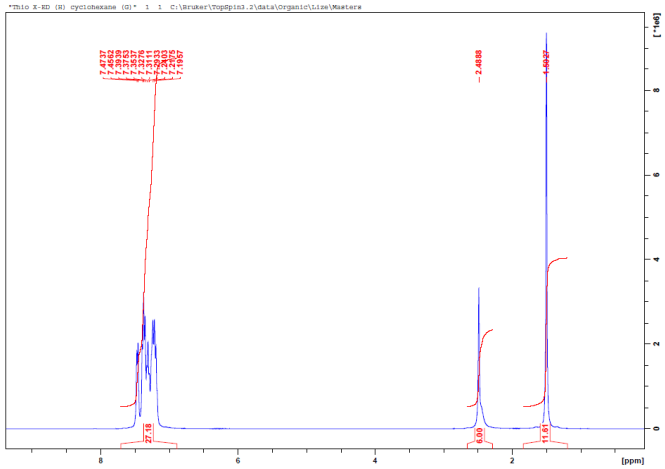

Figure S244. ^{1}H-NMR spectrum for **H$_1$**·cyclohexane.

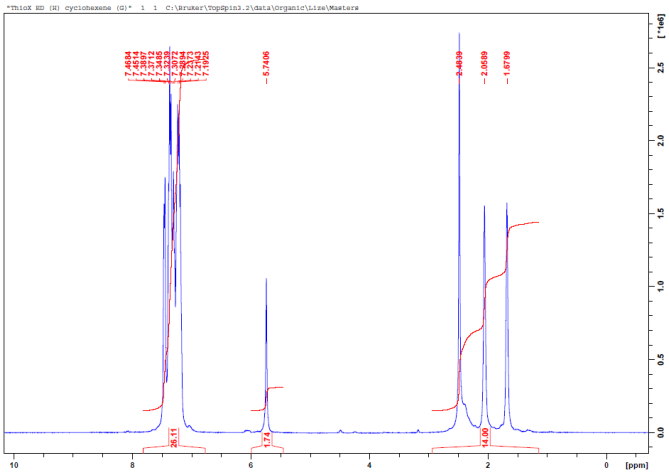

Figure S245. ^{1}H-NMR spectrum for **H$_1$**·cyclohexene.

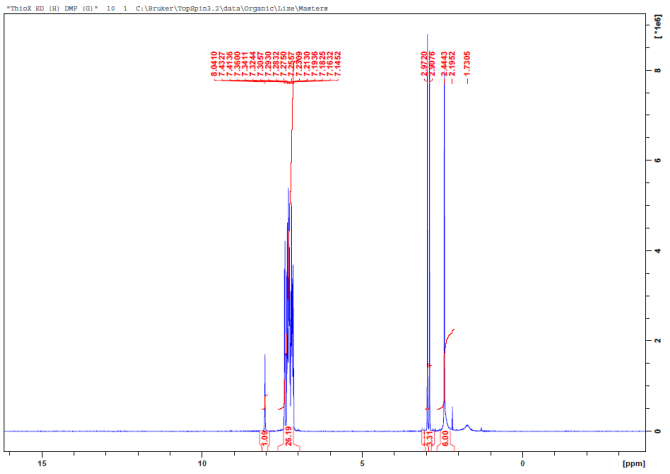

Figure S246. ^{1}H-NMR spectrum for **H$_1$**·DMF.

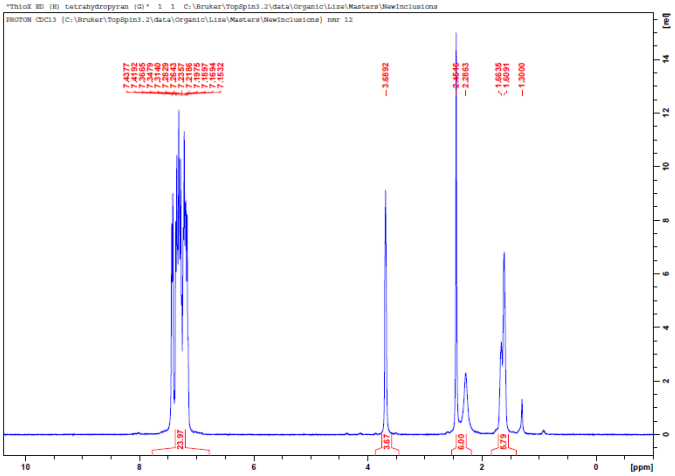

Figure S247. ^{1}H-NMR spectrum for **H$_1$**·tetrahydropyran.

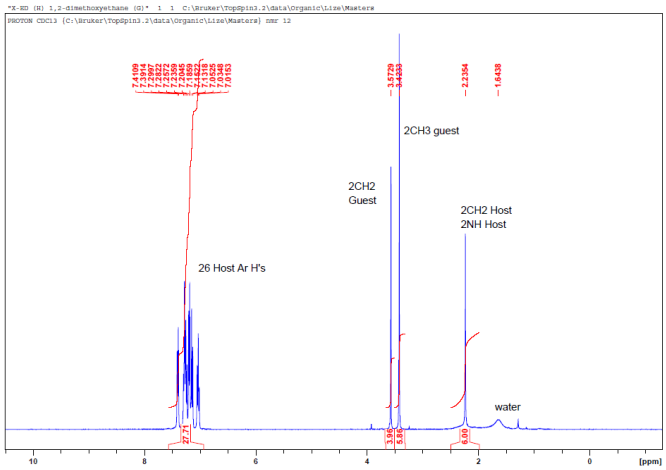

Figure S248. ^{1}H-NMR spectrum for **H$_2$**·1,2-dimethoxyethane.

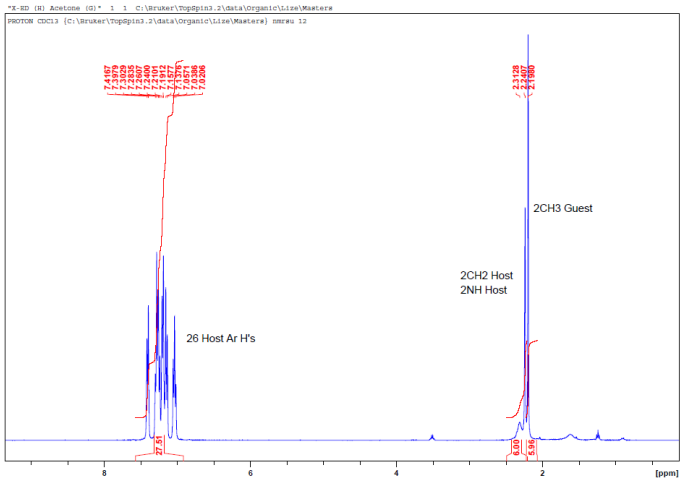

Figure S249. ^{1}H-NMR spectrum for **H₂**·acetone.

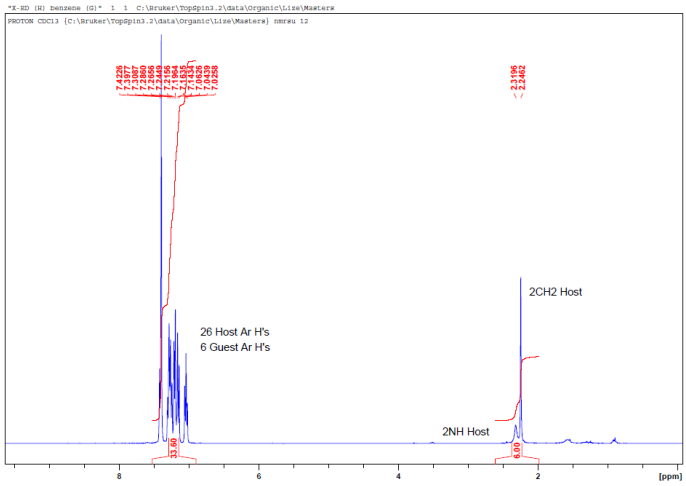

Figure S250. ^{1}H-NMR spectrum for **H₂**·benzene.

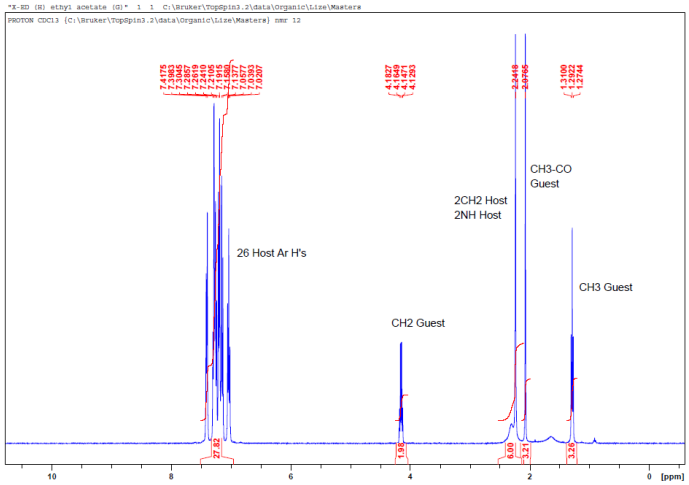

Figure S251. ^{1}H-NMR spectrum for **H₂**·ethyl acetate.

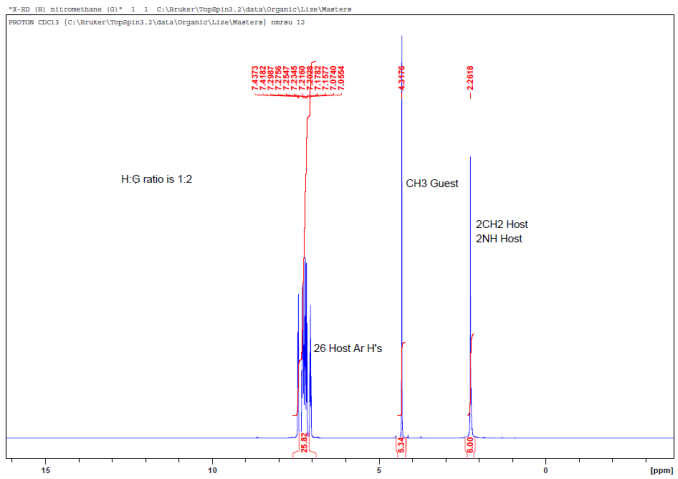

Figure S252. ^{1}H-NMR spectrum for **H$_2$**·2(nitromethane).

Table S253. Additional inclusion and solubility information for **H_1**.

Guest not included[a]	Solubility/crystallization issues
2,4,6-collidine	diethyl ether
2,4-dichloroaniline	1-butanol
2,6-lutidene	methanol
2-benzylpyridine	pentanol
2-nitrotoluene	formamide
2-picolylamine	paraldehyde
3,4-dichloroaniline	citronellol
3,5-dichloroaniline	decanol
3-aminopyridine	decanone
3-nitrotoluene	2,6-dimethoxycyclohexanone[b]
4-aminobenzoic acid	n-octane
4-aminopyridine	n-heptane
4-chloroaniline	n-pentane
4-picolylamine	iso-buteraldehyde[b]
acetamide	
acetonitrile	
bromoanisole	
catechol	
citral	
ethyl acetate	
hydrochinon	
imidazole	
iodobenzene	
limonene	
mesitylene	
m-toluidine	
nitromethane	
o-anisidine	
o-cresol	
o-toluidine	
p-anisidine	
p-cresol	
p-cymene	
phenanthrene	
phenetole	
phenol	
pinene	
p-tertiarybutylanisole	
p-toluidine	
pyrazole	
resorcinol	
1,4-dithiane	
veratrole	

[a]Crystals had formed but inclusion complex did not form.
[b]Gel formed.